

Trace minerals toughen
rodent teeth pp. 712 & 746

How hepatitis C virus copies
its genome p. 715 & 771

Plastic waste fouling
Earth's oceans p. 768

Science

\$10
13 FEBRUARY 2015
sciencemag.org

AAAS

Peopling Tibet

Genes and artifacts
trace the plateau's
first settlers p. 708



Editor-in-Chief Marcia McNutt

Executive Editor Monica M. Bradford **News Editor** Tim Appenzeller

Managing Editor, Research Journals Katrina L. Kelner

Deputy Editors Barbara R. Jasny, Andrew M. Sugden(UK), Valda J. Vinson, Jake S. Yeston

Research and Insights

SR. EDITORS Caroline Ash(UK), Gilbert J. Chin, Lisa D. Chong, Maria Cruz(UK), Julia Fahrenkamp-Uppenbrink(UK), Pamela J. Hines, Stella M. Hurtley(UK), Paula A. Kiberstis, Marc S. Lavine(Canada), Kristen L. Mueller, Ian S. Osborne(UK), Beverly A. Purnell, L. Bryan Ray, Guy Riddihough, H. Jesse Smith, Jelena Stajic, Peter Stern(UK), Phillip D. Szurmi, Brad Wible, Nicholas S. Wigginton, Laura M. Zahn **ASSOCIATE EDITORS** Brent Grocholski, Melissa R. McCartney, Margaret M. Moerchen, Sacha Vignieri **ASSOCIATE BOOK REVIEW EDITOR** Valerie B. Thompson **ASSOCIATE LETTERS EDITOR** Jennifer Sills **CHIEF CONTENT PRODUCTION EDITOR** Cara Tate **SR. CONTENT PRODUCTION EDITORS** Harry Jach, Trista Wagoner **CONTENT PRODUCTION EDITORS** Jeffrey E. Cook, Chris Filiatreau, Cynthia Howe, Lauren Kmec, Barbara P. Ordway **SR. EDITORIAL COORDINATORS** Carolyn Kyle, Beverly Shields **EDITORIAL COORDINATORS** Ramatoulaye Diop, Joi S. Granger, Lisa Johnson, Anita Wynn **PUBLICATIONS ASSISTANTS** Aneera Dobbins, Jeffrey Hearn, Dona Mathieu, Le-Toya Mayne Flood, Shannon McMahon, Scott Miller, Jerry Richardson, Rachel Roberts(UK), Alice Whaley(UK), Brian White **EXECUTIVE ASSISTANT** Anna Bashkirova **ADMINISTRATIVE SUPPORT** Janet Clements(UK), Michael Crabtree(UK, Intern), Lizanne Newton(UK), Maryrose Madrid, John Wood(UK)

News

NEWS MANAGING EDITOR John Travis **INTERNATIONAL EDITOR** Richard Stone **DEPUTY NEWS EDITORS** Daniel Clery(UK), Robert Coontz, Elizabeth Culotta, David Grimm, David Malakoff, Leslie Roberts **CONTRIBUTING EDITORS** Martin Enserink(Europe), Mara Hvistendahl **SR. CORRESPONDENTS** Jeffrey Mervis, Elizabeth Pennisi **NEWS WRITERS** Adrian Cho, Jon Cohen, Jennifer Couzin-Frankel, Carolyn Gramling, Eric Hand, Jocelyn Kaiser, Kelly Servick, Robert F. Service, Erik Stokstad(Cambridge, UK), Emily Underwood **INTERNS** Emily Conover, David Shultz, Jia You **CONTRIBUTING CORRESPONDENTS** Pallava Bagla(South Asia), Michael Balter(Paris), John Bohannon, Ann Gibbons, Sam Kean, Richard A. Kerr, Eli Kintisch, Kai Kupferschmidt(Berlin), Andrew Lawler, Christina Larson(Beijing), Mitch Leslie, Charles C. Mann, Eliot Marshall, Virginia Morell, Dennis Normile(Tokyo), Heather Pringle, Tania Rabesandratana(Brussels), Gretchen Vogel(Berlin), Lizzie Wade(Mexico City) **CAREERS** Jim Austin(Editor), Donisha Adams, Rachel Bernstein **COPY EDITORS** Kara Estelle, Nora Kelly, Jennifer Levin **ADMINISTRATIVE SUPPORT** Scherraine Mack

Executive Publisher Alan I. Leshner

Publisher Kent R. Anderson **Chief Digital Media Officer** Rob Covey

BUSINESS OPERATIONS AND ADMINISTRATION DIRECTOR Deborah Rivera-Wienhold **BUSINESS SYSTEMS AND FINANCIAL ANALYSIS DIRECTOR** Randy Yi **MANAGER OF FULFILLMENT SYSTEMS** Neal Hawkins **SYSTEMS ANALYST** Nicole Mehmedovich **ASSISTANT DIRECTOR, BUSINESS OPERATIONS** Eric Knott **MANAGER, BUSINESS OPERATIONS** Jessica Tierney **BUSINESS ANALYSTS** Cory Lipman, Cooper Tilton, Celeste Troxler **FINANCIAL ANALYST** Jeremy Clay **RIGHTS AND PERMISSIONS ASSISTANT DIRECTOR** Emilie David **PERMISSIONS ASSOCIATE** Elizabeth Sandler **RIGHTS, CONTRACTS, AND LICENSING ASSOCIATE** Lili Kiser

MARKETING DIRECTOR Ian King **MARKETING MANAGER** Julianne Wielga **MARKETING ASSOCIATE** Elizabeth Sattler **SR. MARKETING EXECUTIVE** Jennifer Reeves **SR. ART ASSOCIATE, PROJECT MANAGER** Izeitel Sorrosa **ART ASSOCIATE** Seil Lee **ASSISTANT COMMERCIAL EDITOR** Selby France **MARKETING PROJECT MANAGER** Angelissa McArthur **SR. WRITER** Bill Zimmer **PROGRAM DIRECTOR, AAAS MEMBER CENTRAL** Peggy Mihelich **FULFILLMENT SYSTEMS AND OPERATIONS** membership@aaas.org **MANAGER, MEMBER SERVICES** Pat Butler **SPECIALISTS** LaToya Casteel, Javia Flemmings, Latasha Russell **OPERATIONS, DATA ENTRY** Mickey Napoleoni **DATA ENTRY SPECIALISTS** JJ Regan, Jaimee Wise, Fiona Giblin

DIRECTOR, SITE LICENSING Tom Ryan **DIRECTOR, CORPORATE RELATIONS** Eileen Bernadette Moran **SR. PUBLISHER RELATIONS SPECIALIST** Kiki Forsythe **PUBLISHER RELATIONS MANAGER** Catherine Holland **PUBLISHER RELATIONS, EASTERN REGION** Keith Layson **PUBLISHER RELATIONS, WESTERN REGION** Ryan Rexroth **MANAGER, SITE LICENSE OPERATIONS** Iquo Edim **FULFILLMENT ANALYST** Lana Guz **ASSOCIATE DIRECTOR, MARKETING** Christina Schlecht **MARKETING ASSOCIATES** Thomas Landreth, Minah Kim

DIRECTOR OF WEB TECHNOLOGIES Ahmed Khadr **SR. DEVELOPER** Chris Coleman **DEVELOPERS** Dan Berger, Jimmy Marks **SR. PROJECT MANAGER** Trista Smith **SYSTEMS ENGINEER** Luke Johnson **PRODUCT MANAGER** Walter Jones

CREATIVE DIRECTOR, MULTIMEDIA Martyn Green **DIRECTOR OF ANALYTICS** Enrique Gonzales **SR. WEB PRODUCER** Sarah Crespi **WEB PRODUCER** Alison Crawford **VIDEO PRODUCER** Nguyen Nguyen **SOCIAL MEDIA PRODUCER** Meghna Sachdev

DIRECTOR OF OPERATIONS PRINT AND ONLINE Elizabeth Harman **DIGITAL/PRINT STRATEGY MANAGER** Jason Hillman **QUALITY TECHNICAL MANAGER** Marcus Spiegel **DIGITAL PRODUCTION MANAGER** Lisa Stanford **ASSISTANT MANAGER DIGITAL/PRINT** Rebecca Doshi **DIGITAL MEDIA SPECIALIST** Tara Kelly **SENIOR CONTENT SPECIALISTS** Steve Forrester, Antoinette Hodal, Lori Murphy, Anthony Rosen **CONTENT SPECIALISTS** Jacob Hedrick, Kimberley Oster

DESIGN DIRECTOR Beth Rakouskas **DESIGN EDITOR** Marcy Atarod **SENIOR SCIENTIFIC ILLUSTRATORS** Chris Bickel, Katharine Sutliff **SCIENTIFIC ILLUSTRATOR** Valerie Altounian **SENIOR ART ASSOCIATES** Holly Bishop, Preston Huey **SENIOR DESIGNER** Garvin Grullón **DESIGNER** Chrystal Smith **SENIOR PHOTO EDITOR** William Douthitt **PHOTO EDITOR** Leslie Blizard

DIRECTOR, GLOBAL COLLABORATION, CUSTOM PUBLICATIONS, ADVERTISING Bill Moran **EDITOR, CUSTOM PUBLISHING** Sean Sanders: 202-326-6430 **ASSISTANT EDITOR, CUSTOM PUBLISHING** Tianna Hicklin: 202-326-6463 **ADVERTISING MARKETING MANAGER** Justin Sawyers: 202-326-7061 **science_advertising@aaas.org** **ADVERTISING MARKETING ASSOCIATE** Javia Flemmings **ADVERTISING SUPPORT MANAGER** Karen Foote: 202-326-6740 **ADVERTISING PRODUCTION OPERATIONS MANAGER** Deborah Tompkins **SR. PRODUCTION SPECIALIST/GRAPHIC DESIGNER** Amy Hardcastle **PRODUCTION SPECIALIST** Yuse Lajiminmuhip **SR. TRAFFIC ASSOCIATE** Christine Hall **SALES COORDINATOR** Shirley Young **ASSOCIATE DIRECTOR, COLLABORATION, CUSTOM PUBLICATIONS/CHINA/TAIWAN/KOREA/SINGAPORE** Ruolei Wu: +86-186 0822 9345, rwu@aaas.org **COLLABORATION/CUSTOM PUBLICATIONS/JAPAN** Adarsh Sandhu + 81532-81-5142 asandhu@aaas.org **EAST COAST/Y.E. CANADA** Laurie Faraday: 508-747-9395, FAX 617-507-8199 **WEST COAST/W. CANADA** Lynne Stickrod: 415-931-9782, FAX 415-520-6940 **MIDWEST** Jeffrey Dembski: 847-498-4520 x3005, Steven Loerch: 847-498-4520 x3006 **UK EUROPE/ASIA** Roger Goncalves: TEL/FAX +41 43 243 1358 **JAPAN** Katsuyoshi Fukamizu(Tokyo): +81-3-3219-5777 fukamizu@aaas.org **CHINA/TAIWAN** Ruolei Wu: +186-0082-9345

WORLDWIDE ASSOCIATE DIRECTOR OF SCIENCE CAREERS Tracy Holmes: +44 (0) 1223 326525, FAX +44 (0) 1223 326532 tholmes@science-int.co.uk **CLASSIFIED** advertise@sciencecareers.org **U.S. SALES** Tina Burks: 202-326-6577 Nancy Toema: 202-326-6578 **SALES ADMINISTRATOR** Marci Gallun **EUROPE/ROW SALES** Axel Gesatzki, Sarah Lehard **SALES ASSISTANT** Kelly Grace **JAPAN** Hiroyuki Mashiki(Kyoto): +81-75-823-1109 hmashiki@aaas.org **CHINA/TAIWAN** Ruolei Wu: +86-186 0082 9345 rwu@aaas.org **MARKETING MANAGER** Allison Pritchard **MARKETING ASSOCIATE** Aimee Aponte

AAAS BOARD OF DIRECTORS **RETIRING PRESIDENT, CHAIR** Phillip A. Sharp **PRESIDENT** Gerald R. Fink **PRESIDENT-ELECT** Geraldine (Geri) Richmond **TREASURER** David Evans **SHAW CHIEF EXECUTIVE OFFICER** Alan I. Leshner **BOARD** Bonnie L. Bassler, May R. Berenbaum, Carlos J. Bustamante, Claire M. Fraser, Laura H. Greene, Elizabeth Loftus, Raymond Orbach, Inder M. Verma

SUBSCRIPTION SERVICES For change of address, missing issues, new orders and renewals, and payment questions: 866-434-AAAS (2227) or 202-326-6417, FAX 202-842-1065. Mailing addresses: AAAS, P.O. Box 96178, Washington, DC 20090-6178 or AAAS Member Services, 1200 New York Avenue, NW, Washington, DC 20005 **INSTITUTIONAL SITE LICENSES** 202-326-6755 **REPRINTS:** Author Inquiries 800-635-7181 **COMMERCIAL INQUIRIES** 803-359-4578 **PERMISSIONS** 202-326-6765, permissions@aaas.org **AAAS Member Services** 202-326-6417 or http://membercentral.aaas.org/discouints

Science serves as a forum for discussion of important issues related to the advancement of science by publishing material on which a consensus has been reached as well as including the presentation of minority of conflicting points of view. Accordingly, all articles published in Science—including editorials, news and comment, and books reviews—are signed and reflect the individual views of the authors and not official points of view adopted by AAAS or the institutions with which the authors are affiliated.

INFORMATION FOR AUTHORS See pages 678 and 679 of the 6 February 2015 issue or access www.sciencemag.org/about/authors

SENIOR EDITORIAL BOARD

A. Paul Alivisatos, Lawrence Berkeley Nat'l Laboratory, Ernst Fehr, U. of Zürich
Susan M. Rosenberg, Baylor College of Medicine, Ali Shalithard, Northwestern University
Feinberg School of Medicine, Michael S. Turner, U. of Chicago

BOARD OF REVIEWING EDITORS (Statistics board members indicated with \$)

Adriano Aguzzi, U. Hospital Zürich
Takuzo Aida, U. of Tokyo
Leslie Aiello, Wenner-Gren Foundation
Judith Allen, U. of Edinburgh
Sonia Altizer, U. of Georgia
Sebastian Amigorena, Institut Curie
Kathryn Anderson, Memorial Sloan-Kettering Cancer Center
Meinrat O. Andreae, Max-Planck Inst. Mainz
Paola Arlotta, Harvard U.
Johan Auwerx, EPFL
David Awschalom, U. of Chicago
Jordi Bascompte, Estación Biológica de Doñana CSIC
Facundo Batista, London Research Inst.
Ray H. Baughman, U. of Texas, Dallas
David Baum, U. of Wisconsin
Carlo Beenakker, Leiden U.
Kamran Behnia, ESPCI-ParisTech
Yasmine Belkaid, NIAID, NIH
Philip Benfey, Duke U.
Stephen J. Benkovic, Penn State U.
May Berenbaum, U. of Illinois
Gabriele Bergers, U. of California, San Francisco
Bradley Bernstein, Massachusetts General Hospital
Peer Bork, EMBL
Bernard Bourdon, Ecole Normale Supérieure de Lyon
Chris Bowler, Ecole Normale Supérieure
Ian Boyd, U. of St. Andrews
Emily Brodsky, U. of California, Santa Cruz
Ron Brookmeyer, U. of California Los Angeles (\$) **Christian Büchel**, U. Hamburg-Eppendorf
Joseph A. Burns, Cornell U.
Gyorgy Buzsaki, New York U. School of Medicine
Blanche Capel, Duke U.
Mats Carlsson, U. of Oslo
David Clapham, Children's Hospital Boston
David Clary, U. of Oxford
Joel Cohen, Rockefeller U., Columbia U.
Jonathan D. Cohen, Princeton U.
James Collins, Boston U.
Robert Cook-Deegan, Duke U.
Alan Cowman, Walter & Eliza Hall Inst.
Robert H. Crabtree, Yale U.
Roberta Croce, Vrije Universiteit
Janet Currie, Princeton U.
Jeff L. Dangl, U. of North Carolina
Tom Daniel, U. of Washington
Frans de Waal, Emory U.
Stanislas Dehaene, Collège de France
Robert Desimone, MIT
Claude Desplan, New York U.
Ap Dijksterhuis, Radboud U. of Nijmegen
Dennis Discher, U. of Pennsylvania
Gerald W. Dorn II, Washington U. School of Medicine
Jennifer A. Doudna, U. of California, Berkeley
Bruce Dunn, U. of California, Los Angeles
Christopher Dye, WHO
Todd Ehlers, U. of Tuebingen
David Ehrhardt, Carnegie Inst. of Washington
Tim Elston, U. of North Carolina at Chapel Hill
Gerhard Ertl, Fritz-Haber-Institut, Berlin
Barry Everitt, U. of Cambridge
Ernst Fehr, U. of Zurich
Anne C. Ferguson-Smith, U. of Cambridge
Michael Feuer, The George Washington U.
Kate Fitzgerald, U. of Massachusetts
Peter Fratzl, Max-Planck Inst.
Elaine Fuchs, Rockefeller U.
Daniel Geschwind, UCLA
Andrew Gewirth, U. of Illinois
Karl-Heinz Glassmeier, TU Braunschweig
Ramon Gonzalez, Rice U.
Julia R. Greer, Caltech
Elizabeth Grove, U. of Chicago
Nicolas Gruber, ETH Zurich
Kip Guy, St. Jude's Children's Research Hospital
Taekjip Ha, U. of Illinois at Urbana-Champaign
Christian Haass, Ludwig Maximilians U.
Steven Hahn, Fred Hutchinson Cancer Research Center
Michael Hasselmo, Boston U.
Martin Heimann, Max-Planck Inst. Jena
Yia Helariutta, U. of Cambridge
James A. Hendler, Rensselaer Polytechnic Inst.
Janet G. Hering, Swiss Fed. Inst. of Aquatic Science & Technology
Kai-Uwe Hinrichs, U. of Bremen
Kei Hirose, Tokyo Inst. of Technology
David Hodell, U. of Cambridge
David Holden, Imperial College
Lora Hooper, UT Southwestern Medical Ctr. at Dallas
Raymond Huey, U. of Washington
Steven Jacobsen, U. of California, Los Angeles
Kai Jonsson, EPFL Lausanne
Peter Jonas, Inst. of Science & Technology (IST) Austria
Matt Kaeblerlein, U. of Washington
William Kaelin Jr., Dana-Farber Cancer Inst.
Daniel Kahne, Harvard U.
Daniel Kammen, U. of California, Berkeley
Masashi Kawasaki, U. of Tokyo
Joel Kingsolver, U. of North Carolina at Chapel Hill
Robert Kingston, Harvard Medical School
Etienne Kochlin, Ecole Normale Supérieure
Alexander Koldkin, Johns Hopkins U.
Alberto R. Kornblitt, U. of Buenos Aires
Leonid Kruglyak, UCLA
Thomas Langer, U. of Cologne
Mitchell A. Lazar, U. of Pennsylvania
David Lazer, Harvard U.
Thomas Lecuit, IBDM
Virginia Lee, U. of Pennsylvania
Stanley Lemon, U. of North Carolina at Chapel Hill
Ottoline Leyser, Cambridge U.
Marcia C. Linn, U. of California, Berkeley
Jianguo Liu, Michigan State U.
Luis Liz-Marzan, CIC biomaGUNE
Jonathan Losos, Harvard U.
Ke Lu, Chinese Acad. of Sciences
Christian Lüscher, U. of Geneva
Laura Machesky, CRUK Beaton Inst. for Cancer Research
Aime Magurran, U. of St. Andrews
Oscar Marin, CSIC & U. Miguel Hernández
Charles Marshall, U. of California, Berkeley
C. Robertson McClung, Dartmouth College
Graham Medley, U. of Warwick
Yasushi Miyashita, U. of Tokyo
Mary Ann Moran, U. of Georgia
Richard Morris, U. of Edinburgh
Alison Motsinger-Reif, NC State U. (\$) **Sean Munro**, CSIC & U. of Molecular Biology
Thomas Murray, The Hastings Center
James Nelson, Stanford U. School of Med.
Daniel Neumark, U. of California, Berkeley
Timothy W. Nilsen, Case Western Reserve U.
Pär Nordlund, Karolinska Inst.
Heila Nowotny, European Research Advisory Board
Ben Oken, MIT
Joe Orenstein, U. of California
Berkeley & Lawrence Berkeley National Lab
Harry Orr, U. of Minnesota
Andrew Oswald, U. of Warwick
Steve Palumbi, Stanford U.
Jane Parker, Max-Planck Inst. of Plant Breeding Research
Giovanni Parmigiani, Dana-Farber Cancer Inst. (\$) **Donald R. Paul**, U. of Texas, Austin
John H. J. Petrini, Memorial Sloan-Kettering Cancer Center
Joshua Plotkin, U. of Pennsylvania
Alfred Polman, FOM Institute AMOLF
Philippe Poulin, CNRS
Jonathan Pritchard, Stanford U.
David Randall, Colorado State U.
Colin Renfrew, U. of Cambridge
Felix Rey, Institut Pasteur
Trevor Robbins, U. of Cambridge
Jim Roberts, Fred Hutchinson Cancer Research Ctr.
Barbara A. Romanowicz, U. of California, Berkeley
Jens Rostrup-Nielsen, Haldor Topsøe
Mike Ryan, U. of Texas, Austin
Mitsunori Saitou, Kyoto U.
Shimon Sakaguchi, Kyoto U.
Miquel Salmeron, Lawrence Berkeley National Lab
Jürgen Sandkühler, Medical U. of Vienna
Alexander Schier, Harvard U.
Randy Seeley, U. of Cincinnati
Vladimir Shalaev, Purdue U.
Robert Siliciano, Johns Hopkins School of Medicine
Joseph Silk, Institut d'Astrophysique de Paris
Denis Simion, Arizona State U.
Alison Smith, John Innes Centre
Richard Smith, U. of North Carolina (\$) **John Speakman**, U. of Aberdeen
Allan C. Spradling, Carnegie Institution of Washington
Jonathan Sprent, Garvan Inst. of Medical Research
Eric Steig, U. of Washington
Paula Stephan, Georgia State U. and National Bureau of Economic Research
Molly Stevens, Imperial College London
V. S. Subrahmanian, U. of Maryland
Ira Tabas, Columbia U.
Sarah Teichmann, Cambridge U.
John Thomas, North Carolina State U.
Shubha Tole, Tata Institute of Fundamental Research
Christopher Tyler-Smith, The Wellcome Trust Sanger Inst.
Herbert Virgin, Washington U.
Berth Vogelstein, Johns Hopkins U.
Cynthia Volkert, U. of Göttingen
Douglas Wallace, Dalhousie U.
David Wallace, Weizmann Inst. of Science
Ian Walsmsley, U. of Oxford
David A. Wardle, Swedish U. of Agric. Sciences
David Waxman, Fudan U.
Jonathan Weissman, U. of California, San Francisco
Chris Wickle, U. of Missouri (\$) **Ian A. Wilson**, The Scripps Res. Inst. (\$) **Timothy D. Wilson**, U. of Virginia
Rosemary Wyse, Johns Hopkins U.
Jan Zaenen, Leiden U.
Kenneth Zaret, U. of Pennsylvania School of Medicine
Jonathan Zehr, U. of California, Santa Cruz
Len Zon, Children's Hospital Boston
Maria Zuber, MIT

BOOK REVIEW BOARD

David Bloom, Harvard U. Samuel Bowring, MIT, Angela Creager, Princeton U., Richard Swedder, U. of Chicago, Ed Wasserman, DuPont

Give soils their due

We are not paying enough attention to the world's soils, a "nearly forgotten resource" and our "silent ally," 33% of which are in a state of degradation.* We can't breathe, eat, drink, or be healthy without sustainably managing soils. So in recognizing 2015 as the International Year of Soils, the United Nations (UN) is focusing global attention on the increasing pressures on soils and their ripple effect on other global challenges.

A major concern is whether soils will support the growing demand for food. Human activities have transformed soils, lands, and regions, with long-lasting effects that include desertification, decreased organic matter in soils, altered biodiversity, and changed biogeochemical and hydrological cycles. As a result, the land available for food production is shrinking, irreversibly in some cases. Converting cropland to biofuel systems and urban centers is having the same effect. Agricultural practices have increased soil erosion to rates much greater than those of soil formation (it can take up to 1000 years to form 1 cm of soil). The mismanagement of soil resources is exacerbating these assaults on the food supply.

The good news is that there is a mandate to improve soil management. With soil security now a priority, several Draft UN Sustainable Development Goals (2016 to 2030) directly and indirectly involve soils. Goals 2 and 15, for example, target sustainable food production and the use of lands. Nations also are addressing the major consequences of the misuse and mismanagement of soils through focused agendas: degraded land (UN Convention to Combat Desertification), loss of biodiversity and ecosystem services (UN Convention on Biological Diversity), and increased greenhouse gas emissions (UN Framework Convention on Climate Change). Further, the Global Soil Partnership—a voluntary partnership between national governments, concerned stakeholders (including universities, industry, and landowners), and nongovernment organizations—is facilitating collaborations among these

conventions. Its achievements are promising: An Inter-governmental Technical Panel on Soils is now advising on global soil issues.

Exploration of soil's unique habitats reveals numerous microbes and invertebrates that contribute to life-sustaining services such as cleansing water, regulating pests, and cycling nutrients. Connections between different soil biota can be severed through mismanagement of all lands: cities, forests, deserts, grasslands, and agricultural fields. Hence, this connectedness extends to bonds between soil biota and humans, and we must improve the functioning of soil biota as part of our long-term commitment to a sustainable future.

A holistic management approach to soils requires understanding that human health depends on nondegraded soils not only for food but for clean air and water. Air pollutants derived from disturbed soils include volatile organic compounds, greenhouse gases, dust, and biota. These are transported by wind for hundreds to thousands of miles. The impact of such mobility by potential pathogens such as parasitic worms on plants, animals, and humans is becoming clearer. Because soils are also one of the largest stores of carbon that is in direct exchange with the at-

mosphere, soil degradation negatively affects society via climate change feedbacks. The water we drink depends on maintaining soils that store, filter, and cleanse water. Although the soil-clean air-clean water-human health linkage has led to air and water regulations, they do not address the cause of the impacts: the mismanagement of soil.

The 2015 International Year of Soils is an occasion to celebrate and raise awareness of Earth's soil and its functions for humanity. As we pave fertile soils for cities, expand agriculture into marginal lands such as polar regions and deserts, and address climate change impacts of droughts and floods, we should consider the benefits that managing soils provides for multiple global environmental issues. As U.S. President Franklin D. Roosevelt said, "A nation that destroys its soils destroys itself."

— **Diana H. Wall and Johan Six**



Diana H. Wall is chair of the Global Biodiversity Initiative and a professor at the School of Global Environmental Sustainability and Department of Biology at Colorado State University, Fort Collins, CO, USA. E-mail: diana.wall@colostate.edu



Johan Six is a professor in the Department of Environmental Systems Science at the Swiss Federal Institute of Technology, ETH-Zurich, Switzerland. E-mail: jsix@ethz.ch



"We can't breathe, eat, drink, or be healthy without sustainably managing soils."

*www.fao.org/news/story/en/item/270812/icode/.

“It is one thing to debate the merits of a theory. It is quite another to impugn a person’s character with innuendos.”

A 5 February British Columbia Supreme Court ruling that Canada’s *National Post* defamed climate scientist Andrew Weaver and must retract several articles.

IN BRIEF



A little brown bat with white-nose syndrome hangs in Vermont’s Greeley Mine.

Fungus has decimated bat colonies

In just 7 years, a fungal disease known as white-nose syndrome has killed more than 5 million North American bats, nearly wiping out entire colonies. Initially identified by a white fungus growing on bats’ noses, the disease drains hibernating bats of their energy reserves. Now, a study in *Global Ecology and Biogeography* takes a closer look at how the size of a bat colony affects the likelihood of local extinction. They studied more than 1100 winter colonies of bats in North America, poring over 4 decades of population counts between 1976 and 2013. Since its discovery in North America in 2006, the disease has reduced populations of North American bats in the colonies by 60% to 98%, the researchers report. For five out of six species of hibernating bats studied in eastern North America, larger winter colonies helped insulate against local extinction—but for the sixth and most affected species, the northern long-eared bat, extinction risk was constant regardless of colony size. Resulting increases in mosquitoes and agricultural pests could lead to damaged crops and increased spread of human diseases.

AROUND THE WORLD

A new name for chronic fatigue

WASHINGTON, D.C. | A committee convened by the Institute of Medicine (IOM) has proposed a new name for a condition known as chronic fatigue syndrome or myalgic encephalomyelitis: systemic exertion intolerance disease (SEID). After reviewing thousands of studies, expert testimony, and public input, the committee concluded that “the name ‘chronic fatigue syndrome’ has done a disservice to many patients” as it was “stigmatizing and trivializing,” while myalgic encephalomyelitis “does not accurately describe the major features of the disease.” In a 235-page report released on 10 February, the committee also suggested diagnostic criteria for SEID that focus on “central symptoms”

such as reduced ability to work and study and “unrefreshing” sleep. Criteria used by the U.S. Centers for Disease Control and Prevention were deemed “overly inclusive, particularly of patients whose symptoms may be caused by a psychiatric disorder.” An estimated 836,000 to 2.5 million Americans have these disorders, but IOM notes that fewer people will meet the new, stricter criteria. <http://scim.ag/chronSEID>

New light source shines

UPTON, NEW YORK | On 6 February, Department of Energy (DOE) Secretary Ernest Moniz dedicated the new \$912 million National Synchrotron Light Source II (NSLS-II) at DOE’s Brookhaven National Laboratory in Upton, New York. The NSLS-II will be the brightest synchrotron

light source in the United States and—within a certain energy range—the world. NSLS-II research “will probe the fundamental structure of novel materials and help drive the development of low-cost, low-carbon energy technologies, spark advances in environmental science, and spur medical breakthroughs,” Moniz said. The NSLS-II, which will be 10,000 times as bright as its predecessor, will produce extremely intense beams of x-ray, ultraviolet, and infrared light. It will allow researchers to probe the properties of materials at resolutions approaching 10 nanometers. <http://scim.ag/NSLSII>

NIH old scientist award panned

BETHESDA, MARYLAND | An idea from the National Institutes of Health (NIH) to nudge

aging scientists to retire is being blasted in the blogosphere. The potential “emeritus award,” described in a 3 February notice and NIH’s Rock Talk blog, would allow senior investigators to wind down their labs or transfer the work to a junior colleague. Many of the more than 140 comments on the blog post argue that such an award is unnecessary and could take funding away from younger researchers. NIH Deputy Director for Extramural Research Sally Rockey says she’s not surprised by the negative responses: “In tight budget times, any proposed new award creates angst that it will have an impact on the rest of the pool” of investigators. Rockey encourages critics to submit formal comments. <http://scim.ag/oldsci>

Stem cell odd couple team up

SEOUL | Woo Suk Hwang, who fraudulently claimed to have created embryonic stem cells matched to human patients, and Shoukhrat Mitalipov, who really did it, will conduct joint research, reported South Korea’s *Dong-A Ilbo* newspaper this week. In 2006, Hwang retracted two papers published in *Science* and was later convicted for embezzling research funds and bioethics violations. Mitalipov, of the Oregon Health & Science University in Portland, reported in May 2013 that he had derived stem cells from cloned human embryos. Hwang told the newspaper that he, Mitalipov, and Xiaochun Xu, CEO of Boyalife Group in Wuxi, China, will jointly work on cloning mechanisms, with an eye to curing inherited mitochondrial disease. Boyalife, a Chinese regenerative medicine company, will put up about \$93 million. <http://scim.ag/stemodd>

DOE scraps carbon capture plant

WASHINGTON, D.C. | The U.S. Department of Energy (DOE) has again pulled out of FutureGen, the troubled project to create the first commercial-scale power plant in the United States that captures and sequesters CO₂ emissions. Originally conceived under President George W. Bush in 2003, the project was previously abandoned by the U.S. government in 2008 due to rising costs. In 2010, President Barack Obama earmarked \$1 billion for FutureGen 2.0, a \$1.7 billion revised version that would retrofit a coal-fired power plant in Illinois. The stimulus money would have to be spent by September 2015. However, permitting delays and legal challenges by environmental groups have slowed its progress, and on 3 February, FutureGen Alliance CEO Ken Humphreys announced that “the DOE has concluded that there is insufficient time to complete the project.”



Bolivia’s Potosí silver mine, shown here in 1884, produced significant air pollution.

Anthropocene started earlier in the Andes

Dust and metals preserved in an ice core from the Quelccaya Ice Cap high in the Peruvian Andes indicate that humans began polluting the region centuries before the industrial revolution arrived—and suggest that the Anthropocene, a geological epoch defined by humans’ influence on the planet, began at different times around the world. The ice core records centuries of South American air pollution from mining during precolonial times through 1989, researchers report online this week in the *Proceedings of the National Academy of Sciences*. Air pollution really took off when the Spanish colonized South America in the 16th century; one major culprit was likely a gigantic silver mine in Potosí, Bolivia. Lead levels in the ice core nearly doubled between 1450 C.E. and 1900 C.E. Although most of South America’s air pollution was released in the 20th century, colonial mines like Potosí had such a dramatic impact on the environment—240 years before the industrial revolution—that they should be considered the beginning of the Anthropocene in the region, the researchers say. <http://scim.ag/Andesmine>

BY THE NUMBERS

\$1.09 billion

Amount of money paid, as of 31 December 2014, to support the international response to the Ebola outbreak, or 37.7% of the \$2.89 billion pledged by donors.

250

Percent by which total energy used by consumer electronics rose in an average U.S. household from 1992 to 2007, according to a study in *Environmental Science & Technology*.

Shattered chromosome cure

BETHESDA, MARYLAND | A girl who grew up with a serious genetic immune disease was apparently cured in her 30s by one of her chromosomes shattering into pieces and reassembling. As a 9-year-old, the woman had the first known case of WHIM syndrome, which results in warts and frequent infections from low levels of certain white blood cells. Her two daughters developed the same rare disease through a fault in the *CXCR4* gene, but the woman, now 59, no longer has symptoms. National Institutes of Health (NIH) researchers traced her improvement to chromothripsis, a phenomenon discovered 4 years ago in which a chromosome somehow shatters during cell division, then reforms with the pieces scrambled. Although this can contribute to cancer, it seems to have cured the woman by deleting her flawed copy of *CXCR4* from a blood stem cell, the NIH team reported in *Cell*. <http://scim.ag/shatterchrom>



Push to protect farm animals

WASHINGTON, D.C. | The U.S. Congress last week proposed new protections for farm animals used in scientific research. The move comes in response to an exposé published in *The New York Times* last month, which documented numerous cases of animal suffering and death at a Department of Agriculture facility that has been trying to create larger and more fecund farm animals for several decades. Lawmakers from both parties are backing a bill—called the AWARE Act—that would expand the scope of the Animal Welfare Act, which governs the humane treatment of laboratory animals. Farm animals are currently excluded from the act, unless they're used in biomedical research or exhibition. The new law would require closer monitoring—and more inspections—of research involving cows, pigs, and other livestock. <http://scim.ag/farmani>

NEWSMAKERS

Head of FDA to step down

After serving nearly 6 years as head of the U.S. Food and Drug Administration (FDA), **Margaret Hamburg** revealed last week that she will step down at the end of March. Her e-mail announcement to FDA staff, later posted on the agency's website, provided little detail about the decision. The departure comes in the middle of a major overhaul of the agency's food safety oversight and as legislators prepare to propose key changes to its medical product review and approval process. FDA Chief Scientist Stephen Ostroff will fill her position until President Barack Obama appoints a new commissioner. Duke University cardiologist Robert Califf, who will step in as deputy commissioner later this month, is rumored to be a likely successor.



Rubble in L'Aquila, Italy, in April 2009, days after an earthquake killed more than 300 people.

Why Italian earthquake scientists were exonerated

Six scientists convicted of manslaughter in 2012 for advice they gave ahead of the deadly L'Aquila earthquake 3.5 years earlier were victims of "uncertain and fallacious" reasoning, found three judges who acquitted the experts in an appeal trial last November. The judges also reduced the sentence of a seventh defendant, a public official, from 6 years to 2 years. In a 389-page document deposited in court 6 February and since released to the public, the magistrates accepted the controversial idea that officially sanctioned reassurances were decisive in causing some of the quake victims to stay indoors—but ruled that those reassurances were the exclusive fault of the public official, at the time deputy head of Italy's Civil Protection Department, and no blame can be attributed to the scientists. <http://scim.ag/LAquilaapp>



BIOTECHNOLOGY

Agricultural researchers rattled by demands for documents

Group opposed to GM foods asks a dozen scientists to hand over letters, e-mails in probe of academic-industry ties

By Keith Kloor

The fierce public relations war over genetically modified (GM) food has a new front. A nonprofit group opposed to GM products filed a flurry of freedom of information requests late last month with at least four U.S. universities, asking administrators to turn over any correspondence between a dozen academic researchers and a handful of agricultural companies, trade groups, and PR firms. The scientists—many of whom have publicly supported agricultural biotechnologies—are debating how best to respond, and at least one university has already rejected the request.

"It seems like a fishing expedition to me," says geneticist Alison Van Eenennaam of the University of California (UC), Davis, one of six UC researchers targeted by the requests. "I am very worried [the correspondence] is going to be used to sully the reputations of scientists." The tactic is familiar in another controversial area, climate science, where researchers have faced an avalanche of document requests from climate change skeptics.

The group, U.S. Right to Know (USRTK) of

Oakland, California, says it has no vendetta. It has targeted only researchers who have written articles posted on GMO Answers, a website backed by food and biotechnology firms, and work in states with laws that require public institutions to share many internal documents on request, Executive Director Gary Ruskin told *Science*. USRTK is interested in documenting links between universities and business, he says, and is "especially looking to learn how these faculty members have been appropriated into the PR machine for the chemical-agro industry."

Ruskin is no stranger to the GM food debate. He helped manage an unsuccessful 2012 effort to pass a California ballot initiative requiring the labeling of food products containing GM ingredients. Late last year, he helped found USRTK, which works "to expose what the food industry doesn't want us to know. ... We stand up for the right to know what is in our food and how it affects our health." The group's three board members include Juliet Schor, a prominent economist at Boston College. USRTK's website says its sole major donor (more than \$5000) is the Organic Consumers Association, a nonprofit

GM food opponents, like these in Los Angeles, are adopting new strategies that put academics on the spot.

group based in Finland, Minnesota.

In the requests, Ruskin seeks all letters and e-mails exchanged after 2012 between the scientists and 14 companies and groups. The list includes Monsanto, Syngenta, DuPont, Dow, major biotech and grocery trade groups, and communications firms including FleishmanHillard and Ogilvy & Mather. "The records disclosed ... will be used in preparation of articles for dissemination to the public," states one request obtained by *Science*.

Many researchers are awaiting advice from university lawyers on how to respond. Kevin Folta, a biologist and biotech researcher at the University of Florida in Gainesville, would like to comply. But he anticipates trouble. "Unfortunately, when you skim through the 70,000 e-mails I have ... [USRTK] will find opportunities to pull out a sentence and use it against me," he predicts. "They will show I have 200 e-mails from big ag companies. While it is former students ... or chitchat about someone's kids, it won't matter. They'll report, 'Kevin Folta had 200 e-mails with Monsanto and Syngenta,' as a way to smear me."

USRTK has asked food allergy researcher Richard Goodman, a former Monsanto employee who has been at the University of Nebraska, Lincoln, since 2004, for any correspondence with his old firm related to a controversial study led by biologist Gilles-Eric Seralini of the University of Caen in France. The study, which claimed that foods caused health problems in rats, was published in *Food and Chemical Toxicology* in 2012 but was withdrawn in 2013, the same year Goodman became an associate editor of the journal.

Toxicologist Bruce Chassy, who retired in 2012 from the University of Illinois, Urbana-Champaign, understands why he is a target. "I suspect a disclosure would make me look bad," he says, noting he regularly interacts with firms that produce GM products and has urged them to do more to answer the technology's critics. But the school's lawyers rejected USRTK's request on 4 February, noting Chassy no longer works at the university.

USRTK says its requests are designed to promote transparency in a controversial research arena. But some researchers worry they will also have a chilling effect on academic freedom. "Your first inclination ... is to stop talking about the subject," Van Eenennaam says. "But that's what they want. And I don't want to be intimidated." ■

Keith Kloor is a freelance journalist living in New York City.

ENDANGERED SPECIES

Captive pandas succumb to killer virus

Deaths at breeding center in China have put scientists on edge

By Mara Hvistendahl

A fatal virus is felling pandas at a breeding center in China, raising questions about management of the iconic endangered species and prompting the State Forestry Administration (SFA) to institute strict quarantine and disease control measures.

The outbreak started with the death of an adult female at the Shaanxi Rare Wildlife Rescue and Breeding Research Center, near Xi'an, in early December. Chinese state media report that three more pandas have died—the latest on 4 February—and a fifth is stable. Officials are blaming canine distemper, a highly contagious virus often spread by dogs that in recent years has taken a heavy toll on lions, seals, and other mammals.

There is no sign that the virus has spread to other reserves or to the wild pandas on the other side of the Qin Mountains from the Shaanxi center, which housed 25 pandas before the outbreak. Still, the cases have rattled panda researchers at a time

when they are still waiting for the release of figures from China's fourth national panda survey, expected months ago. The deaths have also exposed concerns that China is overemphasizing captive breeding at the expense of conserving the animals' remaining wild habitat in the mountains of western China, where the last survey, in 2002, tallied some 1600 pandas.

It's unclear whether panda handling practices contributed to the outbreak in Xi'an. Chinese press reports suggest that the breeding center, which also houses other rare animals, is close to a residential area where villagers keep unvaccinated dogs. Although the virus can be deadly in animals—a 1994 outbreak killed an estimated 30% of all wild lions in Serengeti National Park—it is preventable in captive pandas, says Kati Loeffler, a veterinarian with the International Fund for Animal Welfare in Yarmouth Port, Massachusetts. Loeffler, who is the former director of animal health at the Chengdu Research Base of Giant Panda Breeding in China, says the

Chengdu center has used a recombinant canine distemper vaccine that worked well in pandas in the past. But it is unclear to what extent smaller centers like the Shaanxi one use the vaccine.

To avoid more deaths, the center's four remaining sick pandas and 17 others reportedly are in quarantine. Because people can carry distemper virus without showing symptoms, China's SFA on 9 January banned tourists from close contact with all endangered wildlife and instituted health checks for employees of breeding facilities. The authorities also ordered repairs on fences around breeding areas to prevent dogs and other animals from entering.

The deaths are a setback for China's booming breeding program, which generates income from tourism and loaning pandas to foreign zoos for large fees. In late December, China had 394 pandas in captivity, according to SFA—more than twice the number in 2003 and well above a target of 300 recommended by the International Union for Conservation of Nature for maintaining 90% of genetic diversity in the captive population for 100 years. (China's goal is now 500 animals.)

The rise in captive numbers has been achieved mainly through artificial insemination. International scientists have advised on the breeding process, even helping centers pair animals for optimal genetic health, but some practices that are frowned on at foreign zoos persist. For example, cubs in the wild stay with their mothers until about 18 months, but Chinese centers often separate them prematurely so that the mothers can breed year after year, Loeffler says. The breeding program is “completely geared toward producing numbers of cubs, with no regard for the overall well-being of individual animals,” she adds. “It's no different from your basic pig or chicken industry.”

David Wildt, head of the Center for Species Survival at the Smithsonian Conservation Biology In-

To halt the spread of distemper to pandas, China has banned encounters with tourists like this one at the Chengdu breeding center.



PHOTO: CHENGDU RESEARCH BASE

stitute in Front Royal, Virginia, disagrees. Although abuses may have happened at some Chinese breeding centers in the past, he says, there has been a “shift in philosophy” that has put “less focus on quantity of giant panda cubs and more on quality.”

But some outsiders are critical of another practice: taking female cubs from the wild to replenish breeding programs. Two of the females that died at the Shaanxi center had been taken into captivity as 1-year-olds. The center claims that the animals were injured, but Wang Dajun, a wildlife biologist with Peking University's School of Life Sciences in Beijing, says that this is often a pretext for replenishing breeding center populations with healthy cubs.

Larger centers have experimented with reintroducing captive-bred adults into the wild, targeting reserves with small, isolated panda populations. “This could increase genetic diversity and population size,” says Wei Fuwen, a conservation biologist with the Institute of Zoology in Beijing. Others say, however, that habitat conservation should be the top priority. Pandas migrate as the bamboo they eat matures or flowers, says Colby Loucks, deputy director of the wildlife conservation program at WWF in Washington, D.C. But because of human settlements on the lower elevations of the pandas' habitat, he says, “Pandas are somewhat boxed in at this point.”

The Chinese government has established habitat corridors connecting some of the 65 panda reserves, which cover 85% of the panda's natural habitat. “The wildlife habitat has been recovered a lot in the core area,” Wang says, though he adds that researchers don't yet know by exactly how much. But in China, as in other countries, some reserves are “paper parks,” says Sarah Bexell, director of conservation education at the Chengdu breeding center.

The fourth survey will shed light on the quality of the protected habitat, Wildt says. It includes data on the amount and types of bamboo on reserves, which should help scientists determine whether they can accommodate more reintroduced pandas.

Like the 2002 census, this one tallied the population by counting pieces of bamboo found in panda feces. The assumption is that individual pandas take bites of a characteristic size, allowing researchers to avoid duplicating animals in their count. This time around, the survey will also rely on analysis of fecal DNA to verify some of the findings, say scientists familiar with the effort.

It's unclear when the long-delayed results will be released; Chinese authorities now seem focused on getting the canine distemper outbreak under control. Says Bexell: “We're all sitting on the edge of our seats.” ■

The drug favipiravir is being tested at this Ebola treatment center in Guéckédou, Guinea.



INFECTIOUS DISEASES

Ebola drug trials lurch ahead

Changing epidemiology and hints of success alter studies of experimental treatments

By Kai Kupferschmidt and Jon Cohen

Even the researchers whose trial of a potential drug for Ebola made headlines last week worked hard to downplay the glimmer of efficacy it showed. “It is a weak signal in a nonrandomized trial,” Yves Levy, director of the French Institute of Health and Medical Research (INSERM) in Paris told *Science* about the data, which INSERM has not released. Weak or not, the report in *The New York Times* that favipiravir, a Japanese flu drug, had halved mortality in one group of Ebola patients in Guinea was one more piece of good news that is complicating prospects for trials of other Ebola drugs.

The Guinean government has already announced it wants to make favipiravir available to more people, and if the results hold up to greater scrutiny, they could force a change in the design of other clinical trials going forward. Meanwhile, the decline in new cases has investigators revamping trials at a time when manufacturers finally have enough supplies to test some of the most promising experimental drugs.

The toll of the outbreak ticked up last week, as Guinea, Liberia, and Sierra Leone—the three most affected countries—counted 124 confirmed cases, up from 99 cases the week before. As the World Health Organization's (WHO's) Bruce Aylward said at a press conference on 5 February: “The virus has told us this week, loud and clear, ‘I am not going to go away the way you're expecting me to.’” Yet the numbers represent a sharp drop from the height

of the epidemic in September when more than 700 cases were reported in a single week in West Africa.

Just last week, the Wellcome Trust, a charity in the United Kingdom that is funding several Ebola trials, announced that the Liberian trial of brincidofovir, an antiviral developed by Chimerix of Durham, North Carolina, would be canceled because the company withdrew support. “It was rather a surprise to us and a bit of a mystery,” says Peter Horby, an investigator at the University of Oxford in the United Kingdom who headed the study. Chimerix said it made the decision after discussions with the U.S. Food and Drug Administration (FDA), noting that the trial was also having trouble recruiting patients. Horby says his group was planning to open a second trial site in Sierra Leone, where new cases are far higher. Chimerix said it was concentrating on completing trials of the drug to treat other infections: cytomegalovirus and adenovirus. (FDA's Luciana Borio says Chimerix refused the agency's request to make public its correspondence with the company.)

Although one trial is canceled, others are about to go forward. Horby says his group hopes to start evaluating an RNA inhibitor called TKM-Ebola soon. The drug, made by Tekmira Pharmaceuticals of Burnaby, Canada, worked well in monkeys but has been in short supply.

Testing is also about to begin on the antibody cocktail ZMapp. Seen by many researchers as the best shot at treating Ebola because of promising monkey studies, ZMapp was used on nine patients last summer before the

company behind it, Mapp Biopharmaceutical of San Diego, California, announced it had no more supplies. Now there are enough doses to start a clinical trial in Liberia as early as this week. But there may be too few patients in that country for the experimental drug to prove its worth, says Clifford Lane, head of clinical research at the U.S. National Institute of Allergy and Infectious Diseases, which is launching the study in Monrovia with the Liberian Ministry of Health & Social Welfare.

So far, Guinea and Sierra Leone, where Ebola is still infecting dozens of people a week, have refused invitations to join the study. Their main stumbling block is trial design. ZMapp will be the first Ebola treatment that will be tested against a placebo control. “I think that’s the only way to tell whether these drugs are safe and effective,” Lane says.

The governments of Guinea and Sierra Leone, as well as Doctors Without Borders, which runs Ebola centers in those countries, have for ethical reasons been reluctant to participate in treatment trials that use a placebo. Jeremy Farrar, head of the Wellcome Trust, also objects to the randomized, controlled trial design for Ebola drugs, given the high mortality rate of the disease. “Given the data we have from animals and individual patients, I would not feel comfortable being randomized to ZMapp or a placebo,” he says.

Lane notes that the trial may not need many participants: If the drug is 100% effective and Ebola kills 50% of the people it infects, he says, as few as 30 people will need to receive ZMapp to determine whether it works. And even if there are not enough patients to provide a clear answer on efficacy, Lane says scientists might still get valuable data by looking at parameters like the blood levels of Ebola virus in those treated with the drug and those in the control arm.

The favipiravir study in Guinea illustrates

the complexity of discerning clear answers without a robust control. A researcher who had seen the data and asked not to be identified told *Science* that favipiravir did not help all of the 80 patients treated with it at two trial sites in Guinea. In a subset of trial participants who had low levels of Ebola virus in the blood, however, the mortality was just 15%. In similar patients who entered the centers earlier and did not receive favipiravir, mortality was 30%. Marie-Paule Kieny, an assistant director-general at WHO, says it is difficult to make sense of the data at this point. “You can say it doesn’t mean anything or you can say it is promising. More research is needed to find out what really happened.”

The INSERM researchers won’t make their data public until 25 February, at the Conference on Retroviruses and Opportunistic Infections in Seattle, Washington. “It is important to have a scientific debate about what these results really mean,” Levy says, noting that the meeting organizers insisted the data be embargoed. Meanwhile, the study in Guinea is continuing and has now enrolled more than 100 patients. “The final result may still be different,” Levy says. But the preliminary data have already led Guinean authorities to expand the numbers of sites where favipiravir is to be used.

Other trials could prove harder to organize and interpret if favipiravir is distributed widely. A study testing the use of convalescent serum started in Guinea this week. “If there is a decision now to use favipiravir everywhere, what happens with that trial?” Kieny asks. The ZMapp trial may also be affected. That trial is designed to compare ZMapp with the standard of care. “If the standard of care changes, so does the control used in the trial,” Lane says. But he has not seen any results, he says. “The only data I have seen from that study are what was in *The New York Times*.” ■

Ebola treatment trials, coming and going

One has stopped, others are starting.

TREATMENT	MECHANISM	TRIAL LOCATION	STATUS	SPONSORS
Brincidofovir	Nucleotide analog	Monrovia	Stopped	Chimerix, University of Oxford, Wellcome Trust, Liberian MoH
Favipiravir	Viral enzyme inhibitor	Guinea: Guéckédou, Nzérékoré, Macenta	Ongoing, signal of efficacy?	INSERM, Guinean MoH
Convalescent serum	Natural antibodies	Guéckédou, Guinea	Mid-February launch	Belgian Institute of Tropical Medicine
ZMapp	Ebola antibody cocktail	Monrovia	Mid-February launch	Liberian MoH, U.S. NIH, Mapp Bio



UNITED NATIONS

Sustainable goals from U.N. under fire

Scientific review labels development targets as vague, weak, or meaningless

By Erik Stokstad

A sk diplomats from 70 countries to chart a course for sustainable development and what do you get? A long wish list of vague aspirations, cynics say. The Sustainable Development Goals (SDGs), a major policy effort now in the works at the United Nations, “are fairy tales, dressed in the bureaucratized of intergovernmental narcissism,” fumed Richard Horton, editor of *The Lancet*, last year. Although that’s an extreme view, Horton and other critics have just gained some new ammunition.

In the most comprehensive analysis to date, a panel of scientists has reviewed the 169 draft targets included in the SDGs, which range from “equal access to justice” to ending poaching of wildlife. The report, conducted under the auspices of two international scientific organizations and released on 13 February, offers some tough love. Although supportive of the SDGs, it concludes that countries will struggle to achieve them unless the targets are clarified and quantified. The analysis is “one of the very few that’s taken a look at the whole agenda, in a careful way that’s science-based,” says Guido Schmidt-Traub, executive director of the Sustainable



Development Solutions Network, a nonprofit that advises the United Nations. “It is an impressive achievement,” adds Charles Kenny, a senior fellow at the Center for Global Development, a think tank in Washington, D.C.

The SDGs are a follow-up to a well-regarded U.N. initiative called the Millennium Campaign, which began in 2002 and helped bring attention and funding to development work around the world. The campaign’s eight goals caught on because they were concise (“End extreme poverty”) and included just 18 targets, for which progress was often measurable (“Halve, between 1990 and 2015, the proportion of people who suffer from hunger”), says Jan Vandemoortele, an independent scholar in Bruges, Belgium, who helped create the goals.

The world has made good progress toward those goals, according to a U.N. interim report last year. The percentage of children under the age of 5 who were stunted from poor nutrition, for example, dropped from 40% in 1990 to 25% in 2012. Child mortality has declined by almost half over the same period.

More needs to be done, and long before this year’s deadline for the Millennium Campaign’s goals, the United Nations was thinking about what would come next. In 2012, at the Rio+20 summit, nations agreed to create the SDGs to complete any unfinished work of the campaign, while adding an environmental focus to address concerns that economic development may further jeopardize the planet. A working group representing 70 countries spent a year and a half coming up with broad goals and targets meant to judge progress toward those

Scientists say U.N. targets should be specific, such as halving the number of people who lack enough water.

goals. By the time the draft was released last July, the list had expanded to 17 goals with 169 underlying targets.

One source of input to the working group was the International Council for Science (ICSU), a nonprofit based in Paris, which represents 121 national scientific organizations. ICSU has now decided to offer feedback as well. “We thought there was a need for a rigorous analysis from a science perspective,” says Anne-Sophie Stevance, a staff member, who coordinated the report. Teaming up with the International Social Science Council (ISSC), ICSU assembled more than 40 scientists from various fields who spent several months looking over the targets.

The overall findings: Only 29% of the 169 targets are well-defined and scientifically rigorous. The others lack specific endpoints and time frames, and some can’t be measured accurately, if at all. Many of the targets for water and sanitation, for ex-

ample, are ambiguous, not indicating what percentage of a population should experience improvements by 2030. “Unconvincing targets could deter donor agencies,” the authors warn. They suggest, for example, that “substantially reduce the number of people suffering from water scarcity”—a current target—be sharpened to halve the number.

Also vague are the targets under Goal 7: “Ensure access to affordable, reliable, sustainable, and modern energy for all.” The trouble is that access isn’t defined, nor is the level considered adequate. “Without being specific about this, the goal risks becoming weak and subject to loopholes,” the report says.

Another symptom of fuzziness is that some targets are expressed as activities rather than endpoints. The goal of reducing inequality within and between countries, for example, lists open-ended targets such as “improve regulation and monitoring of global financial markets.” The goal for peace, “Promote peaceful and inclusive societies for sustainable development,” is called out as “particularly vapid.” There should be concrete targets for reducing assaults, murder, and war, the review asserts.

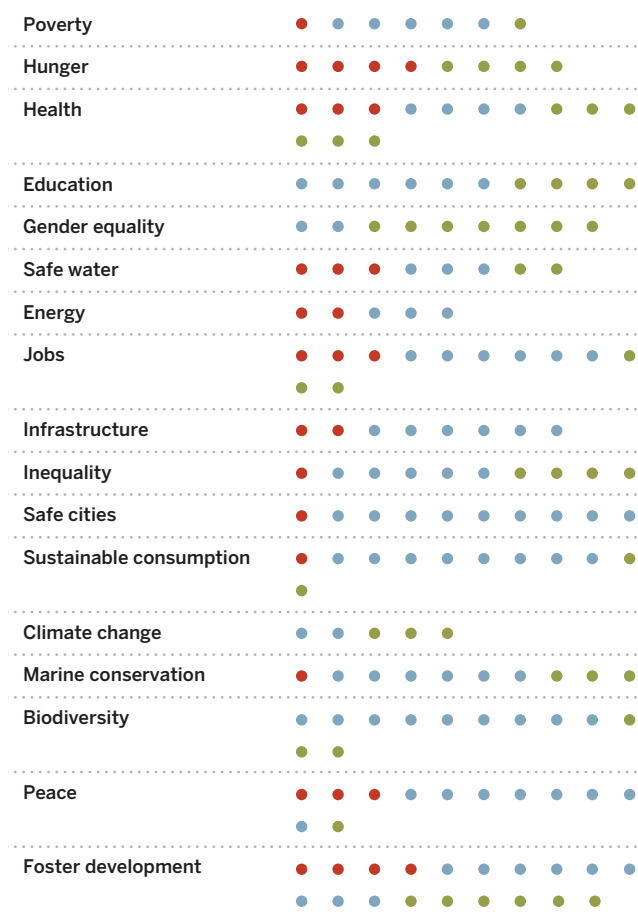
All told, 54% of the targets need to be strengthened, and 17% are weak or redundant and could be scrapped. The problem with vague goals, Vandemoortele says, is that they allow too much wiggle room in evaluating progress. “It leaves us at a low level of political debate,” he says. “It will all be based on ideology and self-interest.”

Yet the targets and goals, painstakingly negotiated among member states, may be hard to alter. “There’s a political concern, a fear that if you open any part of this, that the whole edifice might come crashing down,” Stevance says. Schmidt-Traub sees room for sharpening and condensing the targets over the coming weeks, but Vandemoortele is pessimistic about improvements beyond damage control. “We have passed the point of no return,” he says.

ICSU and ISSC will present the report next week in New York, while U.N. negotiators meet to discuss the overarching vision of the SDGs. After a technical review, the targets will be discussed by the full membership of the United Nations over the summer, with final goals and targets announced at a September summit. ■

Sustainable Development Goals off-target?

A report says only 29% of SDG’s targets are well-defined (●), while 54% need work (●), and 17% are weak or nonessential (●).





PHARMACEUTICALS

China's lakes of pig manure spawn antibiotic resistance

Researchers begin to size up a public health threat from burgeoning pork production

By **Christina Larson**, in Tongxiang and Xiamen, China

Everything about China's pork industry is outsized. The country raises and consumes roughly half the planet's pigs—about 500 million annually—as the middle class's appetite for pork grows. The pigs produce an estimated 618 billion kilograms of manure each year. And they consume and excrete tens of thousands of tons of antibiotics, added to their feed to keep them healthy and promote growth. Recent studies, including one due out soon, are documenting the predictable result: a proliferation in China's watercourses of bacteria containing genes for resistance to antibiotics.

It's a phenomenon familiar to other countries with industrialized meat systems, but on a whole new scale. "In China, every year, we use 150,000 tons to 200,000 tons of antibiotics—about 10 times the U.S. usage," says Ying Guangguo, an environmental chemist at the Chinese Academy of Sciences' (CAS's) State Key Laboratory of Organic Geochemistry in Guangzhou. About half goes to human use and half goes into feed, largely for pigs. In recent years, the Chinese government has taken steps to curtail overuse of antibiotics by people (*Science*, 18 May 2012, p. 795). But antibiotics in animal feed are still poorly regulated.

Zhu Yongguan, director of CAS's Institute of Urban Environment in Xiamen, hopes recent findings will prod the govern-

ment into action. In a 2013 study published in the *Proceedings of the National Academy of Sciences (PNAS)*, he and his colleagues found troublingly high levels of antibiotic resistance genes (ARGs) in manure from three large Chinese pig farms, with the most common ARGs present at levels hundreds or thousands of times higher than in control samples. The worry, Zhu says, is that the ARGs could "be transferred to pathogenic bacteria, and end up in clinical settings that have direct impact on humans—so-called superbugs."

Now, in what he says is China's "first study looking at ARGs in river water using high-throughput molecular tools," Zhu has shown that antibiotic-resistant bacteria are proliferating in the Jiulong River, which begins in the mountains of Fujian province in southern China and courses past rice paddies and swine farms. Zhu's team has 26 sampling sites along the river, allowing them to track where the ARGs enter it. In the study, which will soon appear in *Applied Microbiology and Biotechnology*, they report that the abundance of ARGs in water flowing through the city of Longyan, downstream of the farms, is "around a hundred times greater" than near the source.

The Jiulong River is hardly an isolated example. In December, a report on state broadcaster CCTV cast a public spotlight on antibiotic contamination in several major Chinese rivers—including the Yangtze, Pearl, and Huangpu, which flows through Shanghai. The report also alleged that Shandong

Antibiotic-resistant bacteria teem in the Jiulong River as it flows through the southern city of Longyan.

Lukang Pharmaceutical, a large drugmaker, was compounding the problem by illegally dumping antibiotics into rivers near its production facilities. (Company officials have admitted wrongdoing and pledged to clean up.)

Human overuse of antibiotics, which find their way into rivers through sewage treatment plants, contributes to the problem. But Zhu's lab can distinguish between the resistance genes for antibiotics administered only to animals in China, such as tetracycline, and those prescribed only for humans. He found that farms were a major source of the ARGs in the river.

Simple steps can reduce the presence of ARGs in runoff from swine farms, say researchers who have grappled with the problem elsewhere. "The key practical process ... is properly composting the manure," says James Tiedje, director of the National Science Foundation Center for Microbial Ecology at Michigan State University in East Lansing and a co-author of the *PNAS* paper. "Compost that reaches sufficiently high temperatures will kill a large proportion of bacteria." Zhu believes that Chinese farmers are beginning to adopt the practice.

Even better is to reduce antibiotic use. On U.S. farms, improvements in hygiene and separating pigs of different ages have cut the spread of disease, even while farmers reduce the use of antibiotics in feed. Animal growth doesn't suffer much. "We've started to reevaluate the use of antimicrobials and found that the responses are much lower in magnitude than earlier claims," says Steve Dritz, a swine nutrition specialist at the College of Veterinary Medicine of Kansas State University in Manhattan. Dutch farmers recently cut their use of antibiotics in half without seriously harming productivity.

Shen Jianping, an entrepreneur who in 2006 founded Tongxiang-based Zhejiang Huateng Animal Husbandry Ltd. Co., has found the same thing. His firm now sells about 40,000 metric tons of antibiotic-free pig feed annually and also raises about 5000 pigs on this diet. "The pigs grow more slowly," Shen says, "but can reach the same size."

His approach is still very much the exception, but Zhu found that it pays off. He took samples of pig manure from Shen's farm, analyzed them for ARGs, and compared the result with those from other Chinese farms. He has not yet published his findings but says the difference in diet "significantly reduces" ARGs in excrement and thus the risk of contaminating the soil and nearby waterways.

As Ying, the researcher in Guangzhou, puts it: "The simplest way to control ARGs in the environment is to reduce inputs." ■

CLIMATE SCIENCE

Fund climate intervention research, study says

U.S. needs more science to understand sun-blocking, carbon-removal technologies

By Eli Kintisch

The U.S. government should fund research in the contentious field of climate engineering, the National Research Council (NRC) declared this week. One tome of the hefty, two-volume report examines so-called albedo modification—concepts for cooling the planet by shading it, for example by spreading particles in the stratosphere or by making clouds more reflective. The other scrutinizes carbon dioxide removal techniques, which directly reduce the amount of greenhouse gas in the atmosphere, by using giant carbon-sucking machines, for instance.

Neither “intervention” is “a replacement for reducing carbon emissions” in combating climate change, the authors stressed in a statement. But they concluded that albedo modification—the more controversial of the options—requires a thorough look. And it’s “increasingly likely” that carbon removal and storage technologies will be needed “to avoid the worst impacts of climate change.” But any move to deploy them “should be informed by a far more substantive body of scientific research ... than is presently available.” To fill that gap, U.S. agencies need “coordinated” research plans, says the panel.

Researchers in the field welcomed the call to action. But given the field’s turbulent history, they wonder if NRC’s embrace will be enough to persuade skittish U.S. funding agencies to open their wallets. As early as 2006, geochemist and Nobel laureate Paul Crutzen urged a concerted research effort, and a number of scientific societies and advisory panels have repeated the call. The results have been meager: just a few million dollars in federal support and about \$8.5 million since 2007 from a fund supported by billionaire Bill Gates.

The new report, from a 16-member NRC panel led by geophysicist Marcia McNutt, the former head of the U.S. Geological

Survey and now editor-in-chief of *Science*, “might translate into government action,” says climate scientist David Keith of Harvard University. “It might be the ‘permission’ that [federal] program managers feel they need to move ahead.”

Previous funding initiatives have faltered. In 2001, a draft Department of Energy (DOE) plan called for creating a \$64 million research effort. But the agency squelched that proposal, former DOE official Aristides Patrinos said in 2009, because it didn’t match agency priorities. DOE also feared “adverse publicity, regardless of the merits of the research,” Patrinos noted. In Congress, says former Repre-

The report offers few specific guidelines for new funding. But it emphasizes that albedo modification potentially poses greater risks than carbon removal, because it involves large-scale changes to the atmosphere. The panel concludes that major experiments should not advance until the government establishes a “deliberative process” for weighing environmental risks. Both research areas should be managed by the cross-agency U.S. Global Change Research Program, it suggests, embedding such studies within mainstream climate science. Yet the authors warn that mixing albedo modification studies with basic atmospheric research could “have a chilling

effect” on funding such basic studies. Some scientists think a dedicated research program would be less likely to “contaminate” climate science.

Researchers are eager to see how the government responds. Keith leads a team that wants funding to release half a kilogram of sulfuric acid particles into the stratosphere to see how sulfate haze—a possible sunshade—would affect ozone (*Science*, 18 October 2013, p. 307). “The agencies say they’re waiting for guidance from OSTP [the White House Office of Science and

Technology Policy], but OSTP says the agencies can do what they want,” he says. (OSTP declined to address Keith’s comment.)

Some hope the report will end such gridlock—and help the United States avoid the controversies that have crippled climate engineering research elsewhere. In the United Kingdom, the Royal Society in 2009 recommended a decadelong, £100 million research program. Six years later, it has funded just three projects, and the first—which involved using a balloon to release water vapor 1000 meters up—died after controversy over patents and opposition from environmental groups. The lesson, says physicist Tim Kruger of the University of Oxford in the United Kingdom, is that “for any proposed technique to be deployable, it needs both to work technically and socially.” ■



A Canadian firm envisions carbon-sucking fans (artist's concept) that could help cool the planet.

sentative Bart Gordon (D-TN), who once led the House of Representatives science panel, the idea faced skeptics from both right and left—from conservative lawmakers who felt it addressed a nonexistent threat and from environmentalists worried that geoengineering would sap support for emissions cuts.

The field continued to get the cold shoulder under President Barack Obama. In 2009, after news reports suggested that White House science adviser John Holdren had put such studies in play, Holdren felt compelled to shoot down the idea. Among policymakers, the message was clear: The topic was taboo. It’s telling that the new report was originally requested by the CIA, although several research agencies, including DOE and NASA, ultimately helped pay for it.

MODELS

Models predict longer, deeper U.S. droughts

Future western “megadroughts” could be worse than ever

By Emily Underwood

The intricate sandstone ruins of Chaco Canyon, New Mexico—a once thriving settlement abandoned in the 13th century by the ancient Pueblo peoples during a decades-long “megadrought”—serve as a silent reminder to all who live in the arid regions: When water supplies dwindle, even sophisticated societies may not be able to adapt.

Now, new research suggests that the severe, 60-year drought that likely helped empty Chaco Canyon was a preview of longer, hotter dry spells to come as a result of climate change. The Chaco drought will look “quaint” compared with what computer models predict will hit the midwestern and southwestern United States over the next century, says Jason Smerdon, a climate scientist at Columbia University’s Lamont-Doherty Earth Observatory in Palisades, New York, and co-author of the new study, published this week in *Science Advances*.

Warnings that droughts will intensify as the climate warms are not new. But this forecast gains credibility, other researchers say, because Smerdon and colleagues developed detailed forecasts of soil moisture—a key drought measure—and put those predictions into historical perspective. The study is “the most sophisticated effort I’ve seen by far to connect records of ancient droughts with projections of future change,” says Jonathan Overpeck, a geologist and atmospheric scientist at the University of Arizona in Tucson.

How global warming will affect specific regions is one of the thorniest questions in climate science. Previous studies have suggested that, in a warming world, existing weather patterns will intensify, causing wet regions of North America to get wetter and dry regions drier, with the Southwest experiencing the worst droughts first. To add detail to that picture, the researchers used 17 state-of-the-art climate models to forecast three different measures of soil moisture over the next 100 years as the warming climate alters rainfall and speeds evaporation. The models also took into account variables such as wind speed and humidity.

The results were striking. In nearly every

climate model, the projections pointed to severe drying in the Southwest and Midwest by the end of the century if greenhouse gases continue to build up. “If models that are all constructed a bit differently all converge on the same answer, that gives us confidence that we are getting the right answer,” says co-author Benjamin Cook of the NASA Goddard Institute for Space Studies in New York City.

To compare projected droughts with those of the past, the team turned to a 1000-year reconstruction of past drought based on more than 1800 tree-ring chronologies collected across the continent. Tree-ring thickness decreases in dry years, allowing researchers to use changes in ring width to reconstruct drought histories using a metric called the Palmer Drought Severity Index (PDSI). A proxy for soil moisture, PDSI is used widely to assess drought because it can be calculated from precipitation and temperature measurements alone. But its relative simplicity has also raised doubts: There’s been “a lot of argument over how well PDSI represents” the real world, says Gregory Pederson of the U.S. Geological Survey in Bozeman, Montana.

To address that concern, the researchers took a careful look at the years between 1931

and 1990, an interval when historic tree-ring data is most complete. They compared tree-ring reconstructions of PDSI during that period with the models’ predictions of soil moisture over the same period and found that the two data sets were statistically indistinguishable. The results suggest that the PDSI is a more reliable measure of soil moisture than some have believed, Overpeck says.

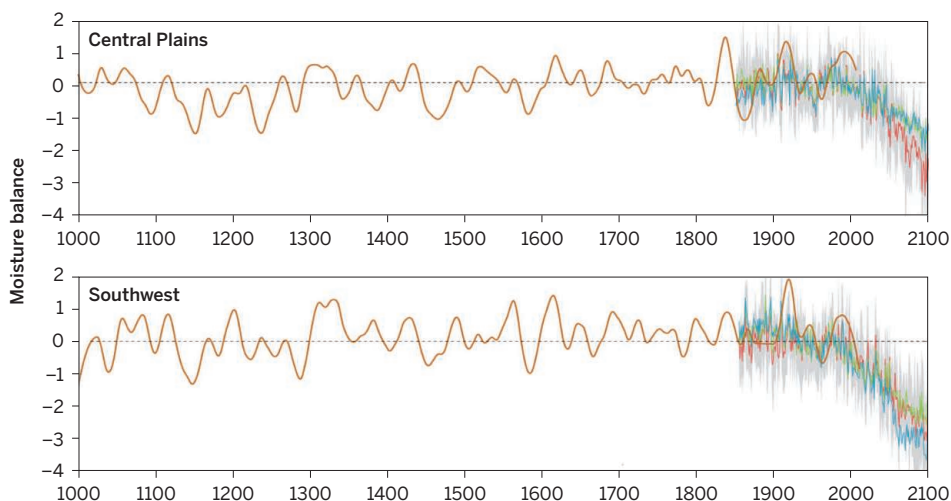
The findings also support previous studies suggesting that the 1000-year PDSI record accurately reflects past droughts, making it a valid benchmark for gauging the severity of future ones, Cook says. The projected drying trends “are really quite robust and in many cases scary when you compare them to even the severe megadroughts of the 1100s and 1200s.”

The models probably have weak spots, researchers say. Simulating summertime precipitation over the Southwest and Midwest, for example, has proved challenging. But the fact that the simulations all yielded similar trends is worrying, they say. Overpeck notes an 80% likelihood that at least one decades-long megadrought will hit the regions between 2050 and 2100. “The only difference is that future megadroughts will be hotter and more severe” than those seen in the past, he says.

Such prolonged dry spells would put tremendous pressure on surface and groundwater resources. And Overpeck worries that even big rivers, such as the Colorado, would at times “have a very good chance” of running dry. The question, he says, is whether drought will again drive people from their homes, as it did 800 years ago at Chaco Canyon. “There may come a time when the droughts are so bad we can’t manage them.” ■

A drought without respite

Soil moisture projections averaged across 17 climate models over the next century (green, red, and blue lines) compared with 1000-year drought history based on tree rings (brown).





The daily lives of early Tibetan farmers were preserved by the mud that swallowed their village 4000 years ago, but their origins are a mystery.

WHO ARE THE TIBETANS?

China and some scientists say they are Chinese. But others see a richer picture

By Jane Qiu

Even after 4000 years, the pose of the two skeletons, a woman and a child, is eloquent. Clutching the child to her breast, the woman looks to the sky as if seeking salvation. Nearby, a man lies on his stomach, his fractured legs folded backward. These and other poignant remains testify to the final moments 4000 years ago

of Lajia, a farming village at an altitude of about 1800 meters on the eastern edge of Tibet. Archaeologist Cai Linhai of the Qinghai Provincial Institute of Cultural Relics and Archaeology in Xining, who is excavating there, calls it “the Pompeii of the Tibetan Plateau.”

Lajia, on the upper reaches of the Yellow River, met its end when a mudflow engulfed it, perhaps triggered by an earthquake in the

seismically active region. But profound puzzles remain. Pottery and jade artifacts there appear to be derived from the Yangshao culture, widely considered the precursor of modern Chinese civilization. Were the victims of the apocalypse Han Chinese, or close kin? And what led their ancestors to settle on the harsh, low-oxygen “roof of the world”?

Like many questions of geography and migration, this one has political overtones. Seeking the high ground in disputes about Tibet’s historical relationship to China, the Chinese government has seized on recent findings that Tibetans and Han Chinese may have descended from a common ancestor, diverging only in the past several thousand years. “The Chinese government is keen to prove that Tibetans and Han Chinese are *tonggen tongyuan*—of the same roots and the same source—in order to justify its rule in Tibet,” says a Chinese archaeologist who requests anonymity for fear of political repercussions.

Some scholars say the evidence supports the government’s view. “Tibetans and Han Chinese are ultimately the same people, sharing a common ancestry that separated only very recently,” says Ren Xiaoyan, director of the Qinghai institute. Others disagree. “Tibet-

ans are not the result of a single ethnic group who moved to the plateau and subsequently became Tibetans,” says archaeologist Lü Hongliang of Sichuan University in Chengdu.

A spate of recent findings reveals that many different peoples sojournd on the great plateau. Archaeological evidence shows that nomads wandered up river valleys almost as soon as modern humans arrived in Asia. They came not just from the east—the Chinese heartland—but from the west and south as well. The Tibetan Plateau “may have been a surprisingly cosmopolitan place in prehistory—a melting pot for people from different directions,” says archaeologist Mark Aldenderfer of the University of California (UC), Merced. But which of those groups finally settled the plateau and became the present-day Tibetans?

Some genetic and archaeological studies support the idea that the people who met their doom at Lajia were recent arrivals from China. But other evidence points to a more complex and nuanced picture, suggesting that the nomads who ventured onto the plateau thousands of years earlier, from all across Asia, left a substantial genetic imprint on today's Tibetans.

FOUR TIMES THE SIZE OF TEXAS, with an average elevation of 4000 meters, the Tibetan Plateau is one of the most forbidding stretches of our planet. Yet the modern humans spreading across Asia 40,000 years ago and more were apparently not daunted. River valleys running deep into the plateau's heart “were probably quite a decent place to live,” even during the Last Glacial Maximum, a period of intense cold from about 28,000 to 17,000 years B.P., says Xu Baiqing, a climate and environmental scientist at the Institute of Tibetan Plateau Research of the Chinese Academy of Sciences (CAS) in Beijing. Game, wild barley, and other resources there “could have sustained small populations for a very long time.”

At Yushuiping, a site 2500 meters above sea level on the plateau's southeastern edge in present-day Yunnan province, archaeologist Dong Guanghui of Lanzhou University and colleagues recently excavated what may be the earliest evidence of humans in Tibet: stone tools and butchered animal bones dating to between 39,000 and 31,000 years B.P. The findings, which have not yet been submitted for publication, say nothing about where those early arrivals came from. But at sites on the opposite side of the plateau, in western Tibet, stone tools resemble those from Nepal dated to 25,000 to 20,000 years B.P. The implication, Aldenderfer says, is that “people could move onto the plateau from the southern Himalayas.”

They may have arrived from the west, too.

Stone tools from sites in western Tibet—some dated to 20,000 B.P.—are similar to ones found in the Altai Mountains, in southern Siberia. The Altai may have also been the source of a genetic adaptation that was key to later settlement at high altitudes. In a study in *Nature* last year, a team led by Wang Jun, director of BGI in Shenzhen, and population geneticist Rasmus Nielsen of UC Berkeley showed that *EPAS1*—a gene regulating the production of oxygen-carrying hemoglobin in the blood—might have originated in the Denisovans, an archaic hominin species whose fossil remains are found only in the Altai Mountains. They suspect that Denisovans and modern humans interbred near Tibet 50,000 to 20,000 years ago. The very earliest migrants might have carried the gene to Tibet, or it might have reached the plateau later, after spreading across Asia.

The early Tibetans would have been hunter-gatherers, chasing yaks and other game, as stone tools and animal fossils at the Yunnan site attest. Although some might have retreated to lower elevations in winter, other groups probably were year-round residents. “It simply would not be feasible for people to move up and down the plateau on a seasonal basis” if their settlements were in the heart of Tibet, Aldenderfer says. Prehistoric Tibetans “could seek refuge around the bountiful hot springs in western and central Tibet,” says archaeologist Hou Guangliang of Qinghai Normal University

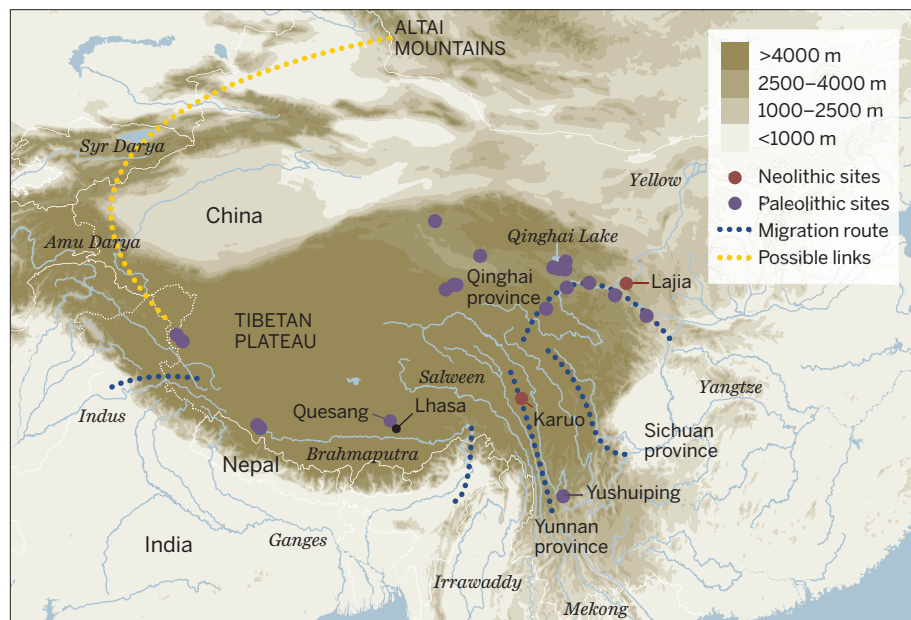
in Xining. They also warmed themselves at hearths; Hou and colleagues uncovered the oldest known fireplace on the plateau at Jiangxigou, a site on the southern edge of Qinghai Lake dating to 15,000 years B.P.

By 9000 to 6000 years ago, people probably lived year-round at Quesang, a newly excavated site near Lhasa, Tibet's capital, at a dizzying 4200 meters above sea level. Quesang's inhabitants would have had to travel at least 700 kilometers to descend from the plateau: too great a seasonal migration even for far-ranging hunter-gatherers, Aldenderfer says. Such sites indicate that people might have settled on the plateau—and began adapting genetically and culturally to the demands of life there—long before farming began, he says. “You don't have to live everywhere or stay at the same spot to have a year-round existence on the plateau.”

Over time, a hunter-gatherer lifestyle gave way to pastoralism: raising sheep and domesticated yaks. In *Quaternary Science Reviews* last year, ecologist Georg Miede of Philipps University of Marburg and colleagues suggested that the vegetation in Tibet began to change 8000 years ago as the herds multiplied. They cited several lines of evidence, including pollen from lake sediments, to show that the dominant grass species in Tibet emerged about 8000 years ago. They also documented charcoal in the ancient soil layers, along with a decline of forest pollen, suggesting that early colonizers of Tibet burned

The high frontier

Archaeological sites dot the Tibetan Plateau, showing that people arrived more than 30,000 years ago and may have been year-round residents by 6000 years ago. More than 3800 Neolithic sites (not shown) record the spread of farming.



forests to convert them to grasslands.

But sustaining larger settlements meant growing food: a daunting challenge on the parched, cold plateau. Paradoxically, an episode of global cooling may have triggered the key adaptations.

Today the high-altitude valleys of Tibet are carpeted with barley. But the first farmers grew a different crop: millet. At Karuo, a village at 3100 meters that is the oldest broadly accepted permanent settlement in Tibet, Sichuan University's Lü and colleagues recovered millet dating as far back as 5000 B.P. Karuo, on the upper reaches of the Mekong River, was a good spot for farming, Lü says—"a warmer and wetter part of the plateau."

Settling the colder and drier northern plateau, however, apparently required different crops. In a study published last month in *Science* (16 January, p. 248), Lanzhou University's Dong, archaeologist Zhang Dongju, and climate scientist Chen Fahu, along with colleagues, radiocarbon dated charred grains from 53 sites on the northeastern Tibetan Plateau. The dates showed that up until about 3600 B.P., people lived below 2500 meters and their crops were almost exclusively millet. But later settlers ventured higher onto the plateau and grew mostly barley and some wheat.

"This is counterintuitive," Dong says. "Barley and wheat need more time to mature than millet, and so would not seem to be a wise choice for the frigid high plateau where the growing season is short." Yet those grains are more resistant to frost than millet. Dong and colleagues think a global cooling beginning about 4500 B.P. and lasting for a

millennium may have driven a shift to these new cereals, imports from the Near East. They in turn allowed farmers to colonize to higher elevations. "Wheat and barley not only helped them survive the big chill," Chen says, "but expand their range to the heart of the plateau."

Conventional wisdom holds that people would have migrated onto the plateau en masse during a warming phase, when vegetation would have been lush. But the new proposal is gaining traction. "This strikes me as a very compelling scenario of why you'd get a rather late permanent colonization of the plateau," says P. Jeffrey Brantingham, an archaeologist at UC Los Angeles who was not involved in the study.

WHO WERE THESE PIONEER FARMERS?

Historical records only begin with the reign of Songtsan Gampo, a warrior who united Tibet's tribes in the 7th century C.E., while myths trace the origin of the Tibetans to the union of an ogress and monkey on the Gangpo Ri—a holy mountain 180 kilometers south of Lhasa. But lately, geneticists have started to pierce the haze.

"A hallmark of Tibetans that distinguishes them from other Asian populations is their ability to thrive in lofty mountains without getting altitude sickness," says Su Bing, a population geneticist at CAS's Kunming Institute of Zoology. Most Tibetans live above 3500 meters, where air contains 40% less oxygen than that at sea level and rates of low birth weight babies and infant mortality are several times higher. "You really need to have many generations of

people spending most of the year on the plateau to develop physiological adaptations and pass down adaptive genes," Su says.

To trace the history of those adaptations, a team led by BGI's Wang sequenced the coding region of 92% of the genes in 50 Tibetans and 40 Han Chinese. In at least 30 genes, they found, a variant common in Tibetans is rare in the Han. In the most extreme case, a variant of *EPAS1*—the gene linked to high-altitude adaptation—was present in 87% of Tibetans but only 9% of the Han. A group headed by UC Berkeley's Nielsen then tested various scenarios of population history—with different assumptions about population sizes, divergence time, and the amount of gene flow between peoples—to see which best explained Wang's results. "We found that a divergence time of 2750 years ago could best reproduce the pattern of genetic variations," says Nielsen, who with Wang and colleagues published their findings in *Science* in 2010 (2 July, p. 75).

That remarkably recent date has met deep skepticism. "It contradicts too many things we know about Tibet," Lü says, among them the evidence of farming settlements like Karuo, which dates from at least 2000 years earlier. Others take issue with the *Science* paper's methodology. "The sample size and population coverage are too small to tease out the complexity of the population history of Tibet," says Jin Li, a population geneticist at Fudan University in Shanghai. Nielsen's best fit scenario, which assumes a population of 288 Han Chinese and 22,642 Tibetans at the time of the split, also strikes many as implausible. "This simply can't be true," Su says.

"You can tweak the model to give you the pattern of genetic variations you want, but this doesn't necessarily mean that the scenario is realistic," Nielsen says. His team has revised its models and now thinks that Tibetans and Han Chinese probably separated 5000 to 3000 years ago.

Linguistics also suggests that the Tibetan and Chinese people share a common, but more distant, root. By comparing features such as sounds, dialects, and word order, William Shi-Yuan Wang, a linguist at City University of Hong Kong, constructed a family tree in 1998 that places the Tibetan-Chinese split at about 6000 years ago. George van Driem, an expert of Himalayan languages at the University of Bern, argues for a similar divergence time. After analyzing how the languages evolved over time—as new words emerged



Excavations at the 151 locality near Qinghai Lake have revealed elaborate wooden huts where early Tibetans may have sheltered themselves from the cold climate 9000 years ago.



Global cooling helped expand the range of cold-hardy barley, here being winnowed near Gyangtze in southern Tibet, to the high plateau 3600 years ago.

and old ones dropped out—he suggests that the first Tibetan speakers emerged in western Sichuan province, on the eastern edge of the Tibetan Plateau, about 7000 years ago.

But Su postulates a more complex and much earlier origin for Tibetans. In a series of papers in *Molecular Biology and Evolution* between 2011 and 2013, his team reported sequencing DNA from 6109 Tibetans from 41 villages across the Tibetan Plateau. They found Tibetan-specific sequences on the Y chromosome and in mitochondrial DNA that are absent or occur at very low frequencies in other Asian populations. Based on known mutation rates, Su suggests that the sequences began evolving 30,000 to 20,000 years ago, among early nomads who had settled on the plateau.

Sequence diversity can also track past population bottlenecks and expansions. In their DNA data, Su's team found signs that Tibet's population grew fourfold between 10,000 and 7000 years ago. Those arguing for a close kinship between the Tibetans and the Han may be at least partly right, Su says. "The data point to a second wave

of migration, probably of Han Chinese, into Tibet," he says. "The newcomers most likely bred with earlier settlers, giving rise to present-day Tibetans."

Existing genetic data won't be enough to sort out the puzzles. Researchers agree that they need more extensive archaeological data from the heart of the plateau, larger genetic studies, and clues from ancient DNA. "We are still looking for a good specific model of the history of Tibet," Nielsen says.

REGARDLESS OF THEIR ORIGINS, Tibetans never were isolated in their mountain fastness. They remained part of Eurasia's human melting pot, with new arrivals adding to the mix. "People normally see mountains as barriers," says Xinyi Liu, an archaeologist at Washington University in St. Louis. But in prehistory as today, he says, they entice people from the lowlands with their rich natural resources, such as plants and game, tool-making materials, firewood, and, most important, water.

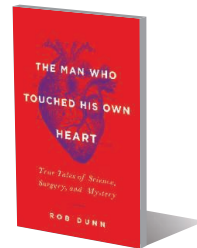
Over the past decade, archaeologists have documented numerous prehistoric settle-

ments along what archaeologist Michael Frachetti, also of Washington University, calls the Inner Asian Mountain Corridors, from Central Asia and the Himalayas to Tibet and the Altai Mountains. Around 5000 B.P., "you begin to see unquestionable connections" with clear signs of trade, he says.

These mountain corridors may well have been the precursors of the Silk Road, the overland trade routes linking China to South Asia, the Near East, Central Asia, and Europe starting around the first century B.C.E. The mountains were conduits for the exchange of genes, goods, and ideas, says Martin Jones, an archaeologist at the University of Cambridge in the United Kingdom.

Tibet was the heart of that cultural nexus. "It's been a magnet for peoples from different directions for tens of thousands of years," Aldenderfer says. If that's the case, today's Tibetans emerged from a prehistoric cosmopolitanism that, no matter which way the political winds blow, cannot be attributed to a single culture or ethnicity. ■

Jane Qiu is a science writer in Beijing.



PERSPECTIVES

BIOMINERALIZATION

Built for tough conditions

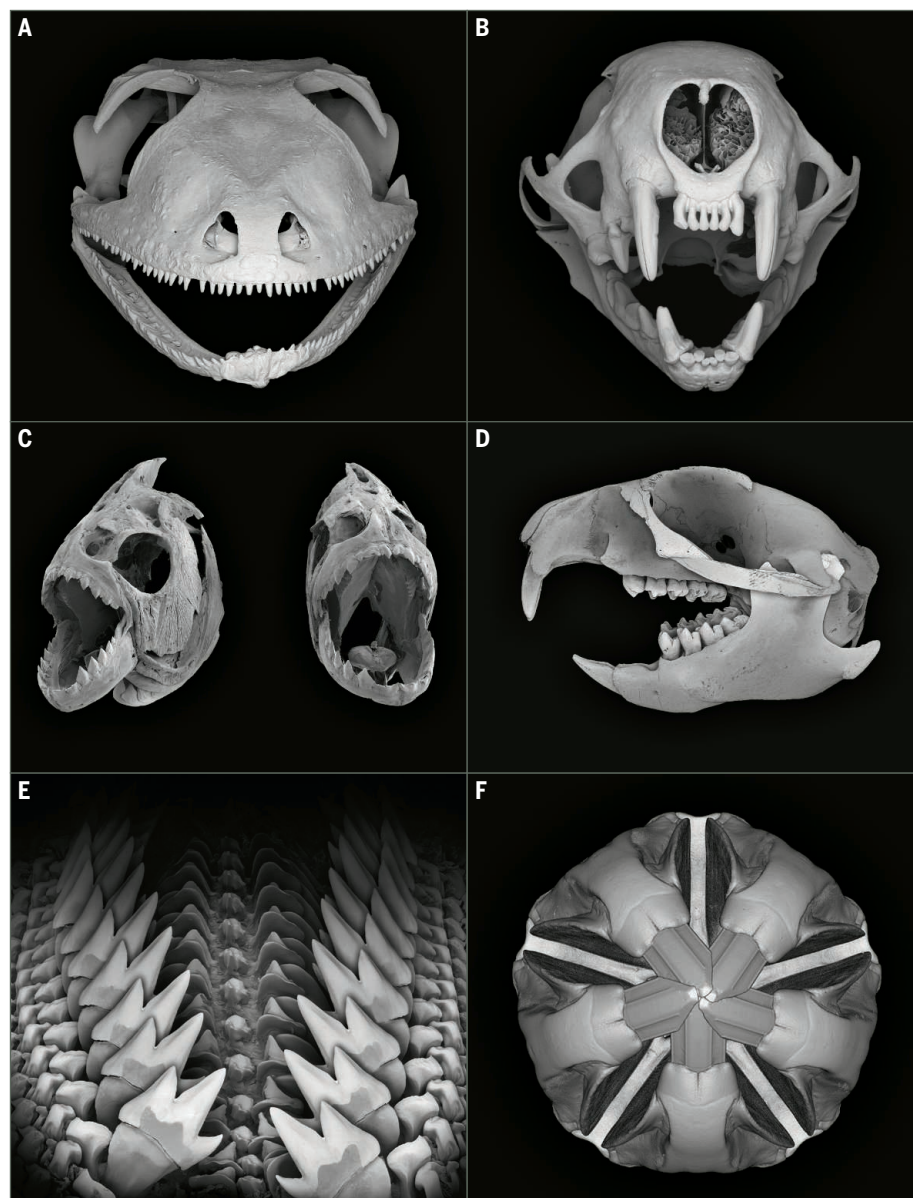
High-resolution structural data help to explain the mechanical properties of rodent teeth

By Yael Politi¹ and James C. Weaver²

To perform such mechanically demanding tasks as biting, chewing, or even rock-grinding, animal teeth have evolved into a wide range of morphologies, constructed from minerals as diverse as magnetite, calcium carbonate, and carbonated hydroxyapatite. Moreover, serial tooth replacement or continuously growing teeth with self-sharpening abilities have evolved in many vertebrates and invertebrates to counteract the effects of constant abrasion (see the figure). On page 746 of this issue, Gordon *et al.* (1) use rodent and rabbit tooth enamel as model systems, combining atomic resolution tomography and x-ray spectroscopy to elucidate the nanoscale architecture of this high-performance biological ceramic.

Teeth are routinely exposed to extremely high loads. Complex three-dimensional microstructures with finely tuned compositional gradients enable them to cope with these forces; interactions between the organic and inorganic building blocks largely govern the material's mechanical performance. Gordon *et al.* now map, at subnanometer resolution, the three-dimensional distribution of a highly doped interstitial amorphous mineral phase that surrounds the single-crystal fibers in dental enamel.

Tooth structural diversity in vertebrates and invertebrates. (A) Gecko, (B) weasel, (C) piranha, (D) squirrel, (E) chiton, and (F) sea urchin. Images (A) to (E) are scanning electron micrographs; image (F) is a three-dimensional reconstruction from microCT data. Inspired by the remarkable structural complexity of teeth such as those shown here, Gordon *et al.* elucidate subnanoscale variations in structure and composition of dental enamel in the continuously growing teeth of rabbits and beavers.



PHOTOS: JAMES C. WEAVER

Downloaded from www.sciencemag.org on February 12, 2015

The synthesis of many biominerals, including dental enamel (2), involves crystallization from a disordered precursor phase (2, 3). The amorphous layer in dental enamel described by Gordon *et al.* likely results from this process (2). Amorphous precursor phases were first found in the magnetite-containing teeth of chitons (see the figure, panel E) (3) and are known today in many other groups, including mollusks, echinoderms, vertebrates (2), and bacteria (3).

An amorphous precursor is advantageous for many reasons. It is a convenient way of transporting ions to the site of mineralization and permits molding of the mineral into complex shapes (4). These transformation mechanisms, though poorly understood, have a bearing on the nanoscale architecture and mechanical properties of the crystalline product (5).

“..beaver and rabbit incisors [are] excellent model systems for [...] investigating the complex structural hierarchies that have evolved to counteract repetitive high-energy loading events.”

Amorphous phases can accommodate more impurities than a crystal with well-defined lattice and symmetry restrictions. As a result, impurities from the amorphous phase may be trapped in the crystal lattice or excluded during crystallization. For example, biomacromolecules are often bound to specific atomic planes in the crystalline product, where they affect its texture and mechanical properties (4, 6, 7). It is unclear, however, when these molecules are introduced into the mineral and if or how they rearrange during the phase transformation.

Inorganic ions that can be accommodated by the emerging lattice during this phase transformation can persist in the final crystal and have a direct effect on the mineral's mechanical performance. In fact, using amorphous precursors, sea urchins can produce calcite with up to 45 mol% of Mg ions in the grinding tips of their continuously growing, self-sharpening teeth (8) (see the figure, panel F). If the impurities cannot be accommodated in the crystal lattice, they will be excluded by the crystallization front

and accumulate at grain boundaries, as seen by Gordon *et al.*

Most amorphous precursors are hydrated phases, whereas the crystalline forms are often anhydrous or contain less water than their disordered counterparts. During formation of the sea urchin larval skeleton, for example, this dehydration process precedes crystallization (9). Kababya *et al.* have suggested that water exclusion plays a key role in the atomic rearrangement of the amorphous phase (10).

The incorporation of some additives and the exclusion of others during the crystallization of amorphous precursors appear to be important features of various biomineralization processes. The excluded additives can concentrate at the crystal surface, resulting in a thin amorphous layer with altered composition. Such layers have been observed in mollusk nacre (11), sea urchins spines (12), and now vertebrate dental enamel (1). Gordon *et al.* show that this boundary layer may also critically affect the properties of the composite. In rabbit enamel, the Mg-rich amorphous calcium phosphate layer surrounding the carbonated hydroxyapatite fibers renders the enamel more soluble. In contrast, the iron-rich amorphous phase in pigmented beaver enamel is less soluble and exhibits increased hardness, as verified through nanoindentation measurements (1).

Both beaver and rabbit incisors grow continuously throughout the life of the animal. They are thus excellent model systems for investigating the real-time processes of tooth development and maturation, the mechanical consequences of wear and fatigue, and—as reported by Gordon *et al.*—the complex structural hierarchies that have evolved to counteract repetitive high energy loading events. The ultra-high resolution characterization techniques employed in the present study thus lay the groundwork for the exploration of similar structure-function relationships in human tooth enamel with potential implications for the prevention and treatment of dental caries. ■

REFERENCES

1. L. M. Gordon *et al.*, *Science* **347**, 746 (2015).
2. E. Beniash, R. A. Metzler, R. S. K. Lam, P. U. P. A. Gilbert, *J. Struct. Biol.* **166**, 133 (2009).
3. J. Baumgartner *et al.*, *Proc. Natl. Acad. Sci. U.S.A.* **110**, 14883 (2013).
4. L. Addadi, S. Weiner, *Phys. Scr.* **89**, 098003 (2014).
5. A. Gale *et al.*, *Adv. Funct. Mater.* **24**, 5420 (2014).
6. A. Berman *et al.*, *Science* **259**, 776 (1993).
7. B. Pokroy *et al.*, *Adv. Mater.* **18**, 2363 (2006).
8. R. Z. Wang, L. Addadi, S. Weiner, *Philos. Trans. R. Soc. Lond., B* **352**, 469 (1997).
9. Y. Politi *et al.*, *Proc. Natl. Acad. Sci. U.S.A.* **105**, 17362 (2008).
10. S. Kababya *et al.*, *J. Am. Chem. Soc.* **10.1021/ja511869g** (2015).
11. N. Nassif *et al.*, *Proc. Natl. Acad. Sci. U.S.A.* **102**, 12653 (2005).
12. J. Seto *et al.*, *Proc. Natl. Acad. Sci. U.S.A.* **109**, 3699 (2012).

¹Max-Planck-Institute of Colloids and Interfaces, 14424 Potsdam, Germany. ²Wyss Institute for Biologically Inspired Engineering, Harvard University, Cambridge, MA 02138, USA. E-mail: yael.politi@mpikg.mpg.de

DRUG DISCOVERY

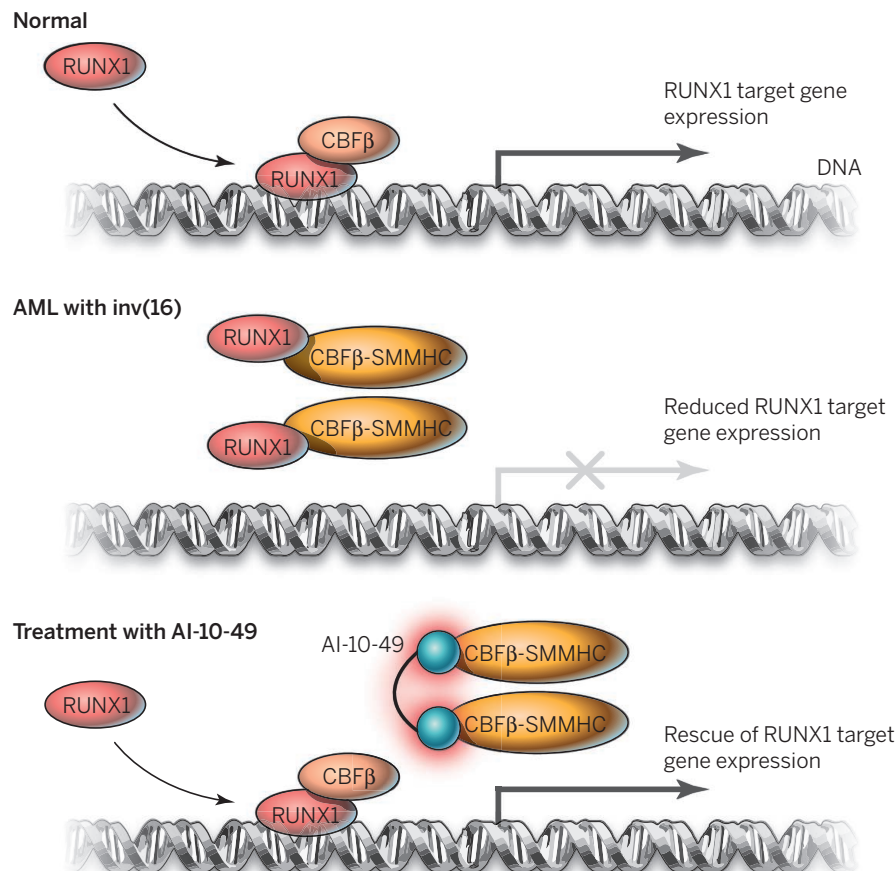
Tying up a transcription factor

A bivalent small molecule inhibits the activity of a rogue transcription factor in leukemia

By **Andrew Chen¹** and **Angela N. Koehler^{1,2}**

Transcription factors form multiprotein complexes that coordinate gene expression and regulate cellular responses (1). In cancer, aberrantly expressed transcription factors often alter gene expression programs, and although these transcription factors are promising targets for therapeutics (2), they remain largely untested. Deemed “undruggable” (3), their perturbation often requires specific disruption of protein-protein or protein-DNA interactions. To date, the discovery or design of small-molecule probes and drugs that specifically disrupt such interactions has proved challenging. On page 779 of this issue, Illendula *et al.* (4) describe the development of a small molecule that inhibits progression of a subtype of acute myeloid leukemia (AML). The compound binds to an oncogenic version of a transcription factor subunit called core binding factor β (CBF β), which arises from a chromosomal translocation. The strategy used to develop this drug may be applicable to other oncogenic proteins that arise from chromosomal translocation events.

AML is the most common form of adult leukemia, accounting for ~25% of such cases (5). The frontline treatment involves nonselective chemotherapy, leading to successful remission induction for most patients with newly diagnosed inv(16) AML. Despite this success, new therapeutic approaches are sorely needed, as there are few treatment options for patients with refractory disease or for older patients for whom intensive chemotherapy is less favorable (6, 7). In normal cells, CBF β binds to the transcription factor RUNX1 to promote DNA binding at RUNX1 target gene promoter sites, inducing their expression (8). AML cells with the chromosome inversion inv(16) produce a fusion protein consisting of CBF β and smooth-muscle myosin heavy chain (SMMHC). The fusion



protein has a higher affinity for RUNX1 than does CBFβ (9, 10). As a result, CBFβ-SMMHC sequesters RUNX1 from its target genes, deregulates RUNX1-mediated transcription, and induces AML.

Without definitive rules to guide rational design, large libraries of compounds are typically screened to identify candidate probes that modulate a given protein-protein or protein-nucleic acid interaction or that alter transcriptional readouts in cells (3, 11, 12). Despite a handful of successes—including antagonists of MDM2-p53 interaction and DNA-HIF-1 interaction (both complexes promote tumorigenesis) (13)—a systematic strategy for the intracellular modulation of transcription factor function in vitro or in vivo using small molecules has yet to be developed. Illendula *et al.* took advantage of the interaction between the oncogenic fusion protein CBFβ-SMMHC and RUNX1 to develop a small molecule capable of abrogating this association. The compound effectively sequesters the oncogenic fusion protein, thereby allowing RUNX1 to bind to normal CBFβ present in the cell and restore expression of RUNX1 target genes (see the figure).

Illendula *et al.* used a high-throughput fluorescence resonance energy transfer (FRET) assay (14) to identify a lead compound that blocked the interaction of the oncogenic fusion protein with the RUNX1 Runt domain. Because CBFβ-SMMHC is oligomeric in solution (whereas CBFβ is monomeric), the authors designed bivalent analogs of their lead compound with various polyethylene glycol linkers. Using the FRET-based assay and a cell viability assay, they found that a linker of seven atoms was optimal for potency and selectivity—that is, this iteration of the lead compound selectively inhibited the proliferation of a human AML cell line (ME-1) with the targeted chromosome inversion. The bivalent compound was further optimized through the introduction of trifluoromethoxy substitutions to increase its half-life in mouse plasma, resulting in the drug AI-10-49. This stable compound showed potent impairment of ME-1 cell viability as well as a high affinity for the oncogenic fusion protein. AI-10-49 specifically affected ME-1 out of a panel of normal bone marrow cells and 11 human leukemia cell lines (CBFβ-SMMHC was not present in the unaffected cells), and selectively bound the oncogenic fusion protein over CBFβ in experiments focused on monitoring dissociation of CBFβ-SMMHC and CBFβ from RUNX1 in response to drug

Potential treatment for leukemia. The polyvalent compound AI-10-49 allows the transcription factor RUNX1 to dissociate from the oncogenic fusion protein CBFβ-SMMHC, the underlying cause of inv(16) AML. This allows normal interaction of RUNX1 with its target genes. Treatment with AI-10-49 prolonged the survival of mice transplanted with leukemic cells expressing CBFβ-SMMHC.

treatment. Additionally, AI-10-49 treatment rescued target gene occupancy by RUNX1 and expression of RUNX1 target genes specifically in ME-1 cells.

In more clinically relevant experiments, AI-10-49 prolonged the survival of mice transplanted with leukemic cells without any observed toxic effects. The compound also reduced viability and colony formation (a readout for hematopoietic progenitor cell proliferation) in human primary inv(16) AML myeloid blasts (immature white blood cells), but not in AML cell samples without the chromosome inversion. Comparison of AI-10-49 to the monovalent version further validated the strategy of using a bivalent compound to selectively block the oncogenic fusion protein. The specificity of AI-10-49 for the oncogenic fusion protein CBFβ-SMMHC should enable targeted treatment of inv(16) AML that is unmatched by the few existing small molecules that directly bind to other transcription factors (3).

The polyvalent strategy may serve as a template for new drug discovery efforts focused on selective modulation of aberrant fusion proteins arising from chromosomal translocation events, particularly those that form homodimers. Although many transcription factors that are deranged in cancer may not benefit from this polyvalent strategy (because they do not form oligomers like CBFβ-SMMHC), the example of Illendula *et al.* serves as a proof of concept for targeted therapies aimed at dysregulated transcription and should inspire the development of additional directed approaches to control aberrant transcription factor function in cancer and other diseases. ■

REFERENCES

1. M. T. Marr 2nd, *et al.*, *Genes Dev.* **20**, 1458 (2006).
2. J. E. Darnell Jr., *Nat. Rev. Cancer* **2**, 740 (2002).
3. A. N. Koehler, *Curr. Opin. Chem. Biol.* **14**, 331 (2010).
4. A. Illendula *et al.*, *Science* **347**, 779 (2015).
5. C. C. Kumar, *Genes & Cancer* **2**, 95 (2011).
6. R. J. Orlowski, J. K. Mangan, S. M. Luger, *Curr. Opin. Hematol.* **10**, 1097/MOH.0000000000000115 (2015).
7. H. P. Erba, *Leuk. Res.* **39**, 183 (2015).
8. N. Adya *et al.*, *Semin. Cell Dev. Biol.* **11**, 361 (2000).
9. L. Zhang *et al.*, *Blood Cells Mol. Dis.* **30**, 147 (2003).
10. S. M. Lukasik *et al.*, *Nat. Struct. Biol.* **9**, 674 (2002).
11. C. Y. Majumdar, A. K. Mapp, *Curr. Opin. Chem. Biol.* **9**, 467 (2005).
12. T. Berg, *Curr. Opin. Chem. Biol.* **12**, 464 (2008).
13. D. Kong *et al.*, *Cancer Res.* **65**, 9047 (2005).
14. M. J. Gorczynski *et al.*, *Chem. Biol.* **14**, 1186 (2007).

¹Department of Biological Engineering, Koch Institute for Integrative Cancer Research, Massachusetts Institute of Technology, Cambridge, MA, USA. ²Broad Institute of MIT and Harvard, Cambridge, MA, USA. E-mail: koehler@mit.edu

Kickstarting a viral RNA polymerase

Hepatitis C virus RNA-dependent RNA polymerase primes synthesis of its RNA genome with an inbuilt proteinaceous primer

By **Stéphane Bressanelli**

RNA viruses are a ubiquitous class of pathogens that cause serious human, animal, and plant disease. To synthesize new viral genomes in infected hosts, RNA viruses encode special enzymes, RNA-dependent RNA polymerases (RdRps), which are thus prime targets for antiviral drug design. A case study is hepatitis C virus (HCV). HCV is a major human pathogen that chronically infects an estimated 170 million people worldwide, greatly increasing risk of developing life-threatening liver disease, including cirrhosis and cancer. New drugs against HCV have recently come to market that are extremely successful compared to the former standard of care and allow cure (that is, eradication of HCV from the patient) in over 95% of cases (1). Foremost among these new drugs is sofosbuvir, a nucleoside inhibitor targeting the active site of the HCV RdRp, NS5B. On page 771 of this issue, Appleby *et al.* describe

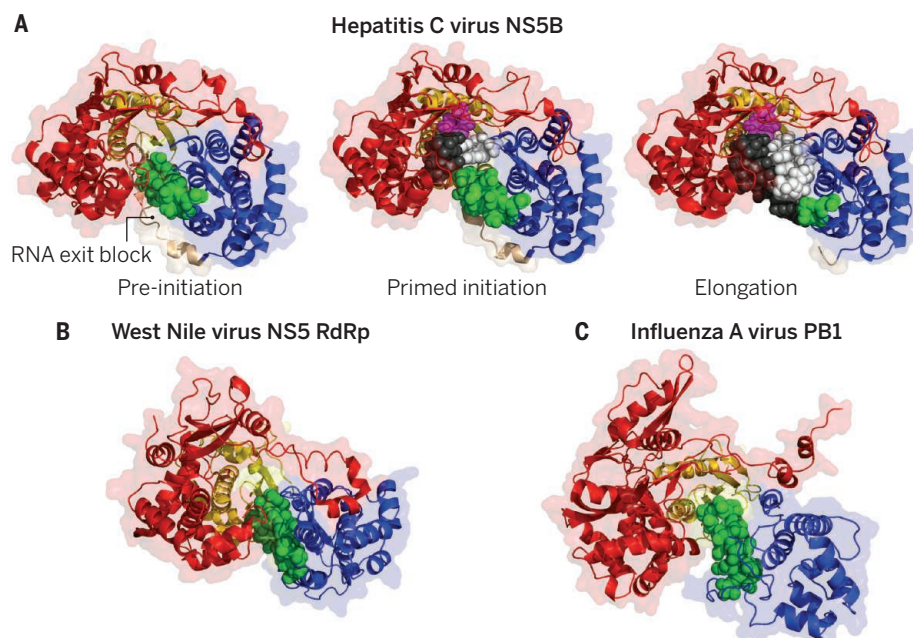
new crystal structures of HCV NS5B (2) that are a major advance both in our basic understanding of RdRp activity and in the way sofosbuvir can inhibit HCV replication.

When they synthesize a new nucleic acid, most RNA (and DNA) polymerases do not truly “start” synthesis of the strand complementary to a template strand. Instead, they only elongate an existing RNA (or DNA) primer molecule. There is an exception, though: A ubiquitous class of viral RdRps can initiate RNA synthesis *de novo*, in the absence of an RNA primer. The conundrum presented by these enzymes is that during initiation, they must provide themselves with a proteinaceous “priming platform” to buttress the priming ribonucleotide that in effect acts as a one-nucleotide primer. This platform must then be removed to allow for subsequent elongation of the *de novo* synthesized short RNA, resulting in a situation equivalent to primer-driven nucleic acid synthesis found in other polymerases (3). A mechanism by which this problem has been

solved was revealed by the x-ray crystal structure of the double-stranded RNA reovirus RdRp lambda3. In this case, the priming platform is a small, easily retracted protein loop, which allowed several rounds of RNA synthesis to be directly visualized (4).

In the case of HCV NS5B and other related RdRps, and unlike the case of reovirus lambda3, the exit path of the newly synthesized RNA is blocked by specific structural elements (in green and yellow in panel A of the figure, left) (5). Attempts to structurally characterize the mechanism by which the priming platform switches from its priming position to allow the transition to elongation of the RNA chain have long been unsuccessful. The main reason for this may seem paradoxical: In isolation, HCV NS5B is a self-inhibited RdRp with a low rate of initiation and a very poor transition to RNA chain elongation, a property clearly related to the block in the RNA exit path (6). This apparent “bug” in the system is actually a useful feature: In HCV-infected cells, a huge excess of NS5B is produced, almost all of which must be kept inactive.

How then did Appleby *et al.* catch HCV NS5B in the process of transitioning from initiation to elongation (panel A of the figure, middle)? The HCV community has produced an enormous amount of basic knowledge over 25 years of collaborative research from both academia and industry since the discovery of the main causative agent of “non-A, non-B hepatitis” (7). Appleby *et al.* cogently used this information and added several clever tricks of their own. Thus, they worked with an abnormal HCV strain, Japanese fulminant hepatitis 1 (JFH1), that caused a fulminant hepatitis instead of the usual slow course of HCV-related disease. This strain has extraordinary replicative capabilities (8) due to a much higher *de novo* RNA synthesis efficiency of its RdRp (9). In addition, they crafted an original combination of quasi-substrate and catalytic metal ion to lock JFH1 HCV NS5B in two successive steps of transition from initiation (panel A of the figure, middle and right). As usual with crystal structures, the new data provide a wealth of atomic-level



Priming the genome synthesis of an RNA virus. (A) Successive steps in RNA-dependent RNA polymerization by HCV NS5B. (Left) NS5B in its preinitiation conformation, with the RNA exit path blocked by the priming loop (in green) and carboxyl terminus (in yellow). (Middle and right) The new structures show how the primer loop recedes as NS5B opens, guiding the RNA along the opened path as successive nucleotides (in magenta) become incorporated in the growing RNA primer (in white) complementary to the template (in black). Among major pathogens, the flavivirus polymerase NS5 RdRp (from West Nile virus) (B) and the influenza virus RdRp catalytic subunit PB1 (C) also harbor an internal priming loop. For clarity, the PB1 carboxyl terminus is not displayed.

Institute for Integrative Biology of the Cell (I2BC), CEA, CNRS, Université Paris-Sud, 1 avenue de la terrasse, 91198 Gif-sur-Yvette, France. E-mail: stephane.bressanelli@i2bc.paris-saclay.fr

details that in one go both confirm, extend, and revise previous knowledge about HCV NS5B and related RdRps.

The new structures definitively establish the HCV NS5B priming platform as the “ β loop” (shown in green on panel A of the figure), an insertion in the “thumb” domain of viral RdRp. Such a priming loop, which had only been previously seen in HCV NS5B and its close RdRp relatives in the *Flaviviridae* family (5), has also recently been discovered in the influenza virus RdRp PB1 (10), extending the range of major pathogens to which Appleby *et al.*'s work is relevant. More importantly, Appleby *et al.* reveal the molecular mechanisms by which the β loop progressively recedes from the catalytic cleft of HCV NS5B, buttressing and guiding the nascent template-primer duplex along the RNA exit path right after initiation (panel A of the figure, middle).

Another major breakthrough is that, unlike in previous work of the same authors (11), the new structures are of so-called ternary complexes; that is, complexes with not only RNA but also the incoming, yet to-be-incorporated nucleotide at the catalytic site (in magenta on panel A of the figure, middle and right). The atomic details of incoming nucleotide recognition show unexpected features that explain how HCV NS5B may incorporate, and thus HCV replication be inhibited by, modified nucleosides such as sofosbuvir. As a final touch, the authors provide the structure of an actual ternary complex with incoming sofosbuvir.

Appleby *et al.*'s study is a technical tour de force providing much needed basic insights into viral RdRp structure and function, as well as the ways by which RdRp may be efficiently inhibited. The work was done with HCV NS5B (panel A of the figure), which was the first viral RdRp of known structure (5) and for which effective antiviral drugs now exist (1). But it also has far-reaching consequences for other major RNA viral pathogens for which new drugs are needed. These include West Nile virus (panel B of the figure) and Dengue virus in the same *Flaviviridae* family as HCV (5) but also more distantly related RNA viruses such as influenza viruses (panel C of the figure) (10). ■

REFERENCES

1. C. M. Rice, M. Saeed, *Nature* **510**, 43 (2014).
2. T. C. Appleby *et al.*, *Science* **347**, 771 (2015).
3. S. J. Butcher *et al.*, *Nature* **410**, 235 (2001).
4. Y. Tao *et al.*, *Cell* **111**, 733 (2002).
5. C. Caillet-Saguy *et al.*, *Antiviral Res.* **105**, 8 (2014).
6. D. Harrus *et al.*, *J. Biol. Chem.* **285**, 32906 (2010).
7. Q. L. Choo *et al.*, *Science* **244**, 359 (1989).
8. T. Wakita *et al.*, *Nat. Med.* **11**, 791 (2005).
9. P. Simister *et al.*, *J. Virol.* **83**, 11926 (2009).
10. A. Pflug *et al.*, *Nature* **516**, 355 (2014).
11. R. T. Mosley *et al.*, *J. Virol.* **86**, 6503 (2012).

10.1126/science.aaa5980

STRUCTURAL BIOLOGY

Breaking the intestinal barrier to deliver drugs

The structure of a tight junction protein bound to a disruptive toxin may guide drug delivery strategies

By Per Artursson¹ and Stefan D. Knight²

Many drugs must be absorbed into the circulation for medicinal effects to occur at the intended sites of action, and so a holy grail of drug delivery is to improve the passage of pharmaceuticals across tissue barriers. Most oral drugs are absorbed in the small intestine, where the lumen is lined with epithelial cells. Thus, new therapeutic strategies for efficient oral delivery can benefit from a better understanding of the protein complexes, such as the tight junction, that maintain the integrity of this epithelium. On page 775 of this issue, Saitoh *et al.* (1) report the structure of a tight junction constituent called claudin-19, bound to a bacterial toxin called *Clostridium perfringens* enterotoxin (CPE), an agent that disrupts tight junctions and is a major cause of foodborne illness by this pathogen. The structural information may be useful in developing specific claudin-targeted compounds that improve drug delivery across tissue barriers that currently limit drug absorption.

Tight junctions connect adjacent endothelial cells and control diffusion of solutes between them. In the skin, lungs, eyes, and gut, these junctions form epithelial barriers against harmful agents in the environment, and in brain capillaries they form the blood-brain barrier that protects the brain against leakage of toxic agents from the blood. Skin and blood-brain barrier tight junctions are largely impermeable, reflecting their essential barrier function in these tissues, whereas in the intestine and other epithelia that transport molecules, they display selective permeability for ions such as sodium, calcium, and magnesium (2). There is ample evidence that claudins—a 27-member family of transmembrane proteins—are responsible for the “paracellular barrier” functions in epithelia (3).

The claudins, which are expressed in tissue-specific combinations, form the extracellular compartment of the junctional complex together with other transmembrane barrier proteins such as occludin. Within an epithelial cell, claudins are linked to peripheral scaffolding proteins (e.g., ZO-1), that in

turn are linked to the cytoskeleton (actin and microtubules) through linker proteins (see the figure). Several of these intercellular proteins have phosphorylation sites that control assembly of the tight junction complex and hence the paracellular barrier. Tight junctions are dynamic structures in that they are sensitive to changes in the local environment—for example, those caused by proinflammatory cytokines and bacterial pathogens (2). Knowledge of how these junctions are regulated and affected by toxins such as CPE is essential for understanding tissue homeostasis and for tight junction-targeted drug development.

“...structural information may be useful in developing specific claudin-targeted compounds that improve drug delivery...”

The paracellular barrier function of tight junctions is attributed to several claudins, including the CPE-binding claudin-3, -4, and -19. However, a paracellular channel function has been suggested for others, including claudin-2 and -15. Disordering of the claudin structure may open either or both of two distinct channel populations of the tight junction: the pore pathway that routes small ions, and the leak pathway that allows the passage of drugs and macromolecules. In mice, ion pores in intestinal tight junctions provide the passage of sodium ions into the intestinal lumen, which is necessary for nutrient absorption (4). For drug delivery, claudin-targeted agents must open the leak pathway in a controlled, reversible manner that does not disturb ion transport and tissue homeostasis.

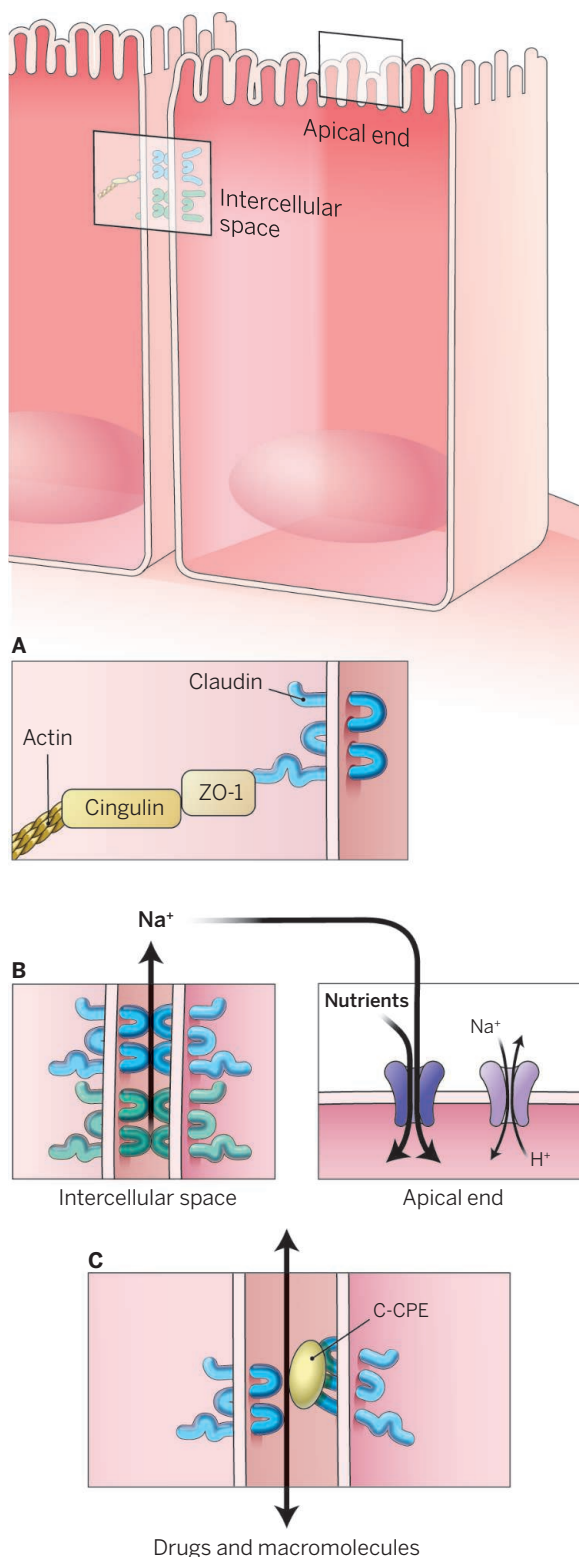
¹Department of Pharmacy and Science for Life Laboratories, Uppsala University, 751 23 Uppsala, Sweden. ²Department of Cell and Molecular Biology, Biomedical Center, Uppsala University, SE-751 24 Uppsala, Sweden. E-mail: per.artursson@farmaci.uu.se; stefan.knight@icm.uu.se

The crystal structure of claudin-15 (which does not bind the toxin CPE) revealed a five-stranded extracellular antiparallel β -sheet domain anchored to a transmembrane region consisting of a four-helix bundle (5). On the basis of this structure and mutagenesis data, a model for how claudins form tight junction strands in the membrane by assembling into antiparallel double rows has been proposed (5, 6). In this model, in-row interactions are maintained by conserved hydrophobic contacts between neighboring claudin molecules, while interactions across rows are mediated by β -strand pairing between adjacent edge strands of the extracellular β -sheet domains. Association between tight junction strands in adjacent cells via loops in the extracellular domain would result in the formation of ion-selective paracellular pores, ~ 10 Å in diameter, within pore-forming claudins (6).

The binding of CPE to the extracellular domain of target claudins through the toxin's C-terminal domain (C-CPE) leads to disassembly of tight junctions and aggregation of claudin-CPE complexes at the intestinal cell surface, as well as formation of a large transmembrane pore through oligomerization of CPE N-terminal domains. Calcium ion influx through this pore into epithelial cells leads to cell death. Saitoh *et al.* provide a first glimpse of how C-CPE causes tight junction disassembly in a crystal structure of claudin-19 bound to C-CPE. The observed interface between claudin-19 and C-CPE is predominantly hydrophobic, although there are also hydrogen-bond and ionic interactions that can provide specificity and thus may be useful in directing attempts to identify or design molecules that mimic the interaction between CPE and claudins.

Does the structure reported by Saitoh *et al.* explain how the binding of C-CPE to claudin-19

Intestinal epithelial cells



Exploiting disruption. (A) Tight junction assembly and dynamics are controlled by intercellular proteins associated with claudin. (B) Claudin-2 and -15 provide a pore pathway for maintaining sodium gradients that are essential for nutrient absorption from the intestinal lumen. (C) The molecule C-CPE binds to claudin, allowing passage of large molecules such as drugs, peptides, and proteins across the intestinal epithelium.

disrupts tight junctions? Unfortunately, no structure of claudin-19 without C-CPE bound is available, so direct observation of the effect of C-CPE binding is not possible. However, from comparison with a claudin-19 homology model that is based on the structure of claudin-15 (38% identical to claudin-19 by amino acid sequence), Saitoh *et al.* suggest that binding of C-CPE causes conformational changes in claudin-19 that would disrupt the tight junction in-row interactions. The modeling suggests that steric clashes between bound C-CPE and extracellular regions of neighboring claudin molecules would also contribute to tight junction disruption.

What are the prospects for using the new structural information for drug delivery and development? A variety of agents, including C-CPE, have been used to obtain more or less specific paracellular leaks, often without detailed mechanistic knowledge. Structural information provided by Saitoh *et al.* could potentially be used to develop safe and more specific claudin-targeted agents. Indeed, C-CPE, generally considered a nontoxic fragment of CPE, was recently shown to cause liver toxicity (7).

Improved understanding of C-CPE-mediated disintegration of the tight junction may also assist in the design of compounds that target these junctions with higher affinity than C-CPE; these could be delivered to tumors that overexpress claudins, such as prostate cancer (8). Conversely, compounds that mimic the binding site(s) in the extracellular domain of claudin may be developed to block CPE-induced fluid accumulation and tissue damage caused by *C. perfringens* infection (9). Targeted suppression of claudin-5, resulting in size-selective modulation of the blood-brain barrier, alleviates brain edema after traumatic brain injury in mice and provides proof of the concept that controlled modulation of tight junctions is possible (10). A remaining challenge is to resolve the extent to which the different claudins interact through homologous subdomains or through heterogeneous interactions to form tissue-specific tight junction barriers. Perhaps the key to more specific interactions can be found in the latter. ■

REFERENCES

1. Y. Saitoh *et al.*, *Science* **347**, 775 (2015).
2. J. R. Turner, M. M. Buschmann, I. Romero-Calvo, A. Sailer, L. Shen, *Semin. Cell Dev. Biol.* **36**, 204 (2014).
3. A. Tamura, S. Tsukita, *Semin. Cell Dev. Biol.* **36**, 177 (2014).
4. M. Wada, A. Tamura, N. Takahashi, S. Tsukita, *Gastroenterology* **144**, 369 (2013).
5. H. Suzuki *et al.*, *Science* **344**, 304 (2014).
6. H. Suzuki *et al.*, *J. Mol. Biol.* **427**, 291 (2015).
7. X. Li *et al.*, *Eur. J. Pharm. Sci.* **52**, 132 (2014).
8. V. Romanov *et al.*, *Cancer Lett.* **351**, 260 (2014).
9. A. Shrestha *et al.*, *Infect. Immun.* **82**, 4778 (2014).
10. M. Campbell *et al.*, *Nat. Commun.* **3**, 849 (2012).

ATMOSPHERIC CHEMISTRY

Just add water dimers

Fast reaction with water dimers may limit the impact of the simplest Criegee intermediate on atmospheric chemistry

By **Mitchio Okumura**

Alkenes constitute a large fraction of the natural and human-made volatile organic compounds (VOCs) that are emitted into the troposphere. Their oxidation products degrade air quality and contribute to climate warming. Alkene oxidation is thought to involve Criegee intermediates (CIs), highly reactive molecules that form when ozone reacts with alkenes. However, the impact of CIs may be limited if they react rapidly with water. Modelers have found it difficult to quantify the effect of CIs on atmospheric composition, because laboratory data on CI reactions with water have been contradictory. On page 751 of this issue, Chao *et al.* (1) show that the simplest CI, formaldehyde oxide (CH_2OO), reacts rapidly with the water dimer, $(\text{H}_2\text{O})_2$. Similar results are reported by Lewis *et al.* (2).

Alkene ozonolysis is a common reaction in organic chemistry (see the figure) (3). Alkenes colliding with ozone initially form a primary ozonide, which rapidly dissociates to produce a stable ketone or aldehyde and a carbonyl oxide: the Criegee intermediate. This highly unusual molecule is both very reactive and highly polar. During ozonolysis, some CIs are formed hot and decay or react immediately, but a sizable fraction becomes stabilized. Scientists have long sought to determine the yields of stabilized CIs as well as their reactivity (4, 5), but the measurements were hampered by an inability to directly detect the elusive intermediate in the gas phase.

In 2008, Taatjes *et al.* reported the successful detection of a CI—formaldehyde oxide, CH_2OO —in the gas phase with photoionization spectroscopy using vacuum ultraviolet synchrotron radiation (6). In 2012, they showed that relatively high concentrations of CIs could be generated in a short pulse by photolyzing diiodomethane, CH_2I_2 , to form CH_2I , which reacts with O_2 to form CH_2OO in a gentle, nearly thermoneutral reaction (7). These two discoveries led to a rapidly growing literature that includes detection of larger CIs, discovery of a strong ultraviolet absorption band, and determination

of a number of reaction rate coefficients (8, 9).

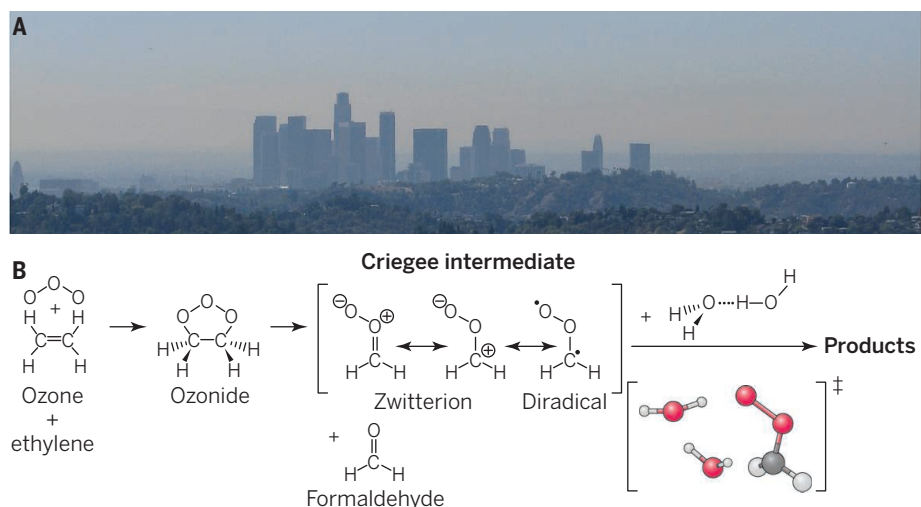
Experiments that directly observed CIs found far higher reaction rates with atmospheric species such as NO_2 , SO_2 , and organic acids than did earlier studies. The fast reaction with SO_2 , which oxidizes very slowly in the atmosphere, led modelers to propose that CIs contribute substantially to sulfate aerosol formation in the troposphere (10).

The evidence for the reaction of CIs with water has been contradictory. End-product studies done over a decade ago concluded that CIs are lost with high yields at high relative humidities in environmental chambers. These experiments led atmospheric chemists to assume that CIs are rapidly lost at moderate to high relative humidities. However, more recent laboratory experiments found that CIs react slowly, if at all, with water molecules (7, 11, 12).

lar transition states (see the figure), an effect well known from water cluster studies.

Experimental support for enhanced reactivity of the water dimer with CIs comes from experiments reported in 2014. Berndt *et al.* used a relative rate approach to show that CH_2OO reacts with water dimers at a fast rate that depends quadratically on relative humidity (14). However, their rates exceeded upper bounds set in two experiments that used CH_2I_2 chemistry (11, 12).

Chao *et al.* and Lewis *et al.* have now succeeded in measuring the reaction rate of the simplest CI, CH_2OO , with water vapor over a wide range of relative humidities. Both groups use the CH_2I_2 chemistry and take advantage of the strong UV absorption spectrum discovered by Beames *et al.* (9) to follow the decay of CH_2OO in real time at much higher pressures and larger relative humidities than is possible with photoionization detection. Both groups find that the decay rate depends quadratically on the water vapor concentration—evidence that the CIs are reacting with the water dimer. By using the known equilibrium constant for the water dimer, they arrive at similar rate coefficients for the bimolecular reaction of CH_2OO with $(\text{H}_2\text{O})_2$. Chao *et al.* recorded more precise data over a wider range of relative humidity,



Alkene oxidation. (A) Alkenes such as ethylene, emitted by both plants and human sources, are oxidized in the atmosphere through reaction with ozone, degrading air quality. (B) During ethylene ozonolysis, a cyclic primary ozonide decomposes to form the simplest Criegee intermediate (formaldehyde oxide, CH_2OO) and formaldehyde. Two studies (1, 2) show that CH_2OO reacts rapidly with water dimers. The molecular model shows the predicted transition state (13).

In 2004, Ryzhkov and Ariya proposed that CIs react not with isolated water molecules but rather with water dimers (13). On the basis of quantum chemistry and statistical rate calculations, they predicted that the water dimer would react 3.5×10^5 times as quickly as the monomer. The enhancement stems from the cooperativity of cyclic hydrogen-bonded structures, which preferentially stabilize po-

although systematic errors may arise from estimated water concentration or missing secondary reactions.

The new studies (1, 2) validate the observation of rapid water dimer reaction by Berndt *et al.* (14), although the new rate constants are smaller by a factor of 1.5 to 2. The results are consistent with the upper bound found by photoionization detection

Arthur Amos Noyes Laboratory of Chemical Physics, California Institute of Technology, Pasadena, CA 91125, USA. E-mail: mo@caltech.edu

(7) at very low water concentrations, but lie well above the upper bounds set by the two other experiments that used CH_2I_2 chemistry (10, 11). The latter measurements inferred CI concentrations by monitoring secondary products as proxies, which might lead to erroneous results if other reactions form the same products.

The observed rates are so fast that, in the troposphere, reaction with the water dimer will be the largest sink for CH_2OO and will limit its steady-state concentration. Of course, even small concentrations could conceivably still oxidize very stable species such as SO_2 . Previous simulations, such as those by Vereecken *et al.* (15), have assumed that water reactions are important but have been hampered by the large uncertainties in the rate coefficients. The atmospheric impact of this simplest of CIs can now be quantitatively addressed in model calculations.

Perhaps the most critical remaining issue concerns the reaction rates of larger CIs with water dimers. Quantum chemistry calculations predict that larger CIs react more slowly than CH_2OO , at least with one water molecule. Vereecken *et al.*, among others, have predicted that the larger CIs could influence atmospheric composition, for example, by causing a substantial increase in sulfate aerosol loading (8, 10, 15). However, the estimated rates could be off by orders of magnitude. Fortunately, the same approach used in the current papers can be applied to the larger CIs; indeed, Chao *et al.* present preliminary data that clearly reveal at least one conformer of acetaldehyde oxide, CH_3CHOO , reacting quickly with water dimers (1). The impact of the full range of CIs on atmospheric composition remains an open question, but one that experiments can now address. ■

REFERENCES

- W. Chao, J.-T. Hsieh, C.-H. Chang, J. J.-M. Lin, *Science* **347**, 751 (2015).
- T. R. Lewis, M. A. Blitz, D. E. Heard, P. W. Seakins, *Phys. Chem. Chem. Phys.* **10**, 1039/C4CP04750H (2015).
- R. Criegee, *Angew. Chem. Int. Ed. Engl.* **14**, 745 (1975).
- D. Johnson, G. Marston, *Chem. Soc. Rev.* **37**, 699 (2008).
- N. M. Donahue, G. T. Drozd, S. A. Epstein, A. A. Presto, J. H. Kroll, *Phys. Chem. Chem. Phys.* **13**, 10848 (2011).
- C. A. Taatjes *et al.*, *J. Am. Chem. Soc.* **130**, 11883 (2008).
- O. Welz *et al.*, *Science* **335**, 204 (2012).
- C. A. Taatjes, D. E. Shallcross, C. J. Percival, *Phys. Chem. Chem. Phys.* **16**, 1704 (2014).
- J. M. Beames, F. Liu, L. Lu, M. I. Lester, *J. Am. Chem. Soc.* **134**, 20045 (2012).
- C. J. Percival *et al.*, *Faraday Dis.* **165**, 45 (2013).
- B. Ouyang, M. W. McLeod, R. L. Jones, W. J. Bloss, *Phys. Chem. Chem. Phys.* **15**, 17070 (2013).
- D. Stone, M. Blitz, L. Daubney, N. U. M. Howes, P. Seakins, *Phys. Chem. Chem. Phys.* **16**, 1139 (2014).
- A. B. Ryzhkov, P. A. Ariya, *Phys. Chem. Chem. Phys.* **6**, 5042 (2004).
- T. Berndt *et al.*, *Phys. Chem. Chem. Phys.* **16**, 19130 (2014).
- L. Vereecken, H. Harder, A. Novelli, *Phys. Chem. Chem. Phys.* **16**, 4039 (2014).

ACKNOWLEDGMENTS

Supported by NSF grant CHE-1413712.

10.1126/science.aaa5506

ORGANIC CHEMISTRY

Harnessing weak interactions for enantioselective catalysis

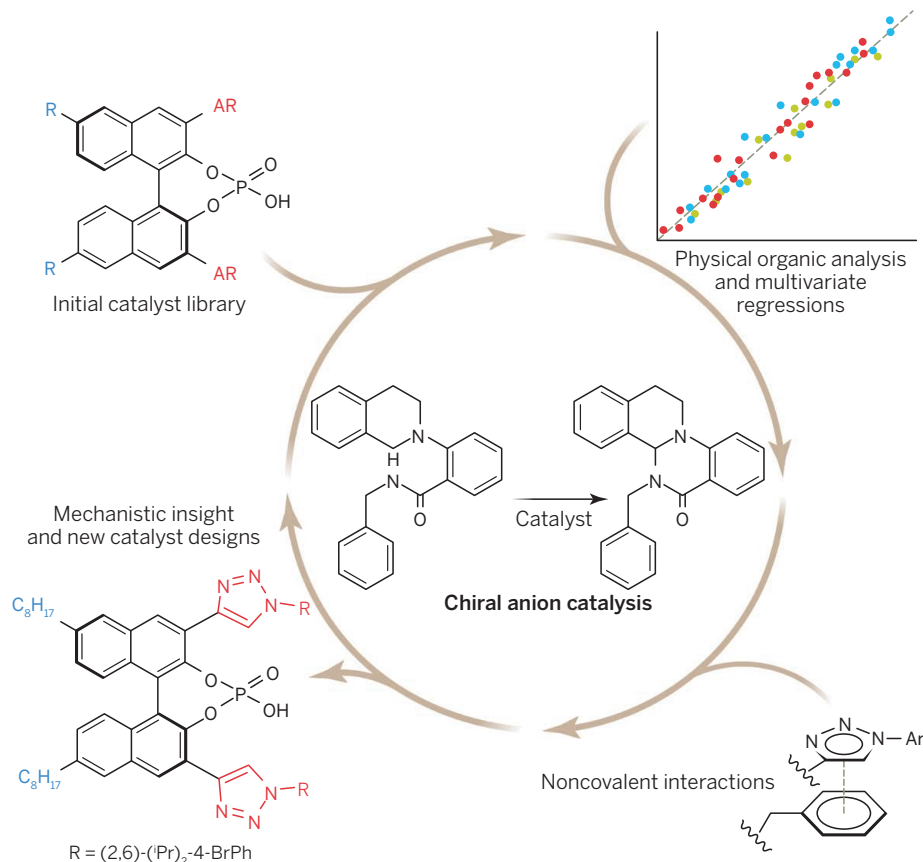
The traditional tools of physical organic chemistry benefit from modern data analysis techniques

By Tongxiang Lu and Steven E. Wheeler

Elucidating catalytic reaction mechanisms is often a challenge, and these difficulties are compounded in the case of enantioselective catalysts. The ability of a catalyst to preferentially form one enantiomer over the other often hinges on the balance of many attractive and repulsive nonbonded interactions that occur in competing transition states. On page 737 of this issue, Milo *et al.* (1) combine physical organic and computational quantum chemistry with modern data analysis techniques to identify these interactions. Their predictive mathematical models elucidate the underlying reac-

tion mechanism and the role of nonbonded interactions in these enantioselective reactions, facilitating the rational design of more effective catalysts.

Enantioselectivity typically arises from a difference in free energy between competing transition states that lead to two possible enantiomeric products. Traditionally, such free-energy differences were rationalized by the destabilization of the pathway leading to the undesired product by repulsive steric interactions. However, there has been recent emphasis on the role of favorable noncovalent interactions in enantioselective reactions (2), and more effective catalysts can be designed by preferentially stabilizing one pathway over other, un-



Catalytic design cycle. Screening of an initial catalyst library yields extensive data sets, which are then distilled into predictive mathematical models through multivariate regressions. These models yield new mechanistic insights and lead to improved catalyst designs. Abbreviations: ⁱPr, isopropyl; Ph, phenyl.

desired pathways (3). The benefit of such an approach, which is typical of enzyme catalysts, is that it should lead to greater overall catalytic activity while retaining selectivity. Moreover, recent advances in our understanding of noncovalent interactions, including π -stacking and cation- π interactions, appear to have laid the groundwork for the exploitation of these interactions in rational catalyst design (4).

However, harnessing the power of noncovalent interactions for enantioselective catalysis has proved difficult. Chief among the reasons is the relatively weak, nondirectional nature of these interactions, necessitating the introduction of numerous

dicting enantioselectivities based on simple molecular descriptors (such as vibrational frequencies and dipole moments) that characterize the reactants (7). These data are easily obtained, obviating the need to compute all possible transition states for each catalyst-substrate combination. Moreover, they showed that classical physical organic techniques can be effectively combined with modern data analysis tools to yield insights into the mechanisms of catalyzed reactions and the role of noncovalent interactions in enantioselectivity.

To demonstrate the power of their approach, Milo *et al.* tackled a particular example of chiral anion catalysis, in which enantioselectivity is induced by the noncovalent association of a cationic intermediate with a chiral, anionic catalyst (see the figure) (8, 9). To understand these reactions, they synthesized and tested a library of catalysts exhibiting a broad range of enantioselectivities. These experiments provided a wealth of data regarding the impact of steric and electronic factors on enantioselectivity, which was then distilled into predictive mathematical models through multivariate regressions. These models unveiled subtle factors that control the enantioselectivity of these reactions and, ultimately, lead to the design of better catalysts.

By embracing modern data analysis techniques to enhance the more traditional tools of physical organic chemistry, Milo *et al.* have provided a way to harness the power of noncovalent interactions for the design of enantioselective catalysts. Importantly, their approach is general and should be applicable to a wide range of catalytic reactions. This expands the power of the simple linear free-energy relations that have long been the workhorse of physical organic chemistry, and provides a key step toward a future in which big data can be used to design small catalysts. ■

REFERENCES

1. A. Milo, A. J. Neel, F. D. Toste, M. S. Sigman, *Science* **347**, 737 (2015).
2. E. H. Krenske, K. N. Houk, *Acc. Chem. Res.* **46**, 979 (2013).
3. R. R. Knowles, E. N. Jacobsen, *Proc. Natl. Acad. Sci. U.S.A.* **107**, 20678 (2010).
4. S. E. Wheeler, J. W. G. Bloom, *J. Phys. Chem. A* **118**, 6133 (2014).
5. K. N. Houk, P. H.-Y. Cheong, *Nature* **455**, 309 (2008).
6. K. N. Houk, P. Liu, *Daedalus* **143**, 49 (2014).
7. A. Milo, E. N. Bess, M. S. Sigman, *Nature* **507**, 210 (2014).
8. M. Mahlau, B. List, *Angew. Chem. Int. Ed.* **52**, 518 (2013).
9. A. J. Neel, J. P. Hehn, P. F. Tripet, F. D. Toste, *J. Am. Chem. Soc.* **135**, 14044 (2013).

“To demonstrate the power of their approach, Milo et al. tackled a particular example of chiral anion catalysis, in which enantioselectivity is induced by the noncovalent association of a cationic intermediate with a chiral, anionic catalyst.”

interactions that must operate in concert to effectively stabilize the desired reaction pathway (3). Rationally designing catalysts that achieve such coordinated effects is fraught with difficulties. Indeed, even identifying the noncovalent interactions responsible for selectivity in existing catalytic reactions, which is a prerequisite for rational catalyst design, is often not straightforward based only on experimental data.

Computational quantum chemistry, in which quantum mechanics is used to predict molecular properties by describing the electronic motion, has proved invaluable for understanding chemical reactions and even designing catalysts (5, 6). It is routinely used to understand enantioselectivities by predicting the structures and energies of the operative transition states, while also quantifying the impact of noncovalent interactions on these structures. Unfortunately, for many catalytic reactions, there are simply too many potential transition-state structures (possibly hundreds) for such analyses to be practical. For example, in noncovalent catalysis, the catalyst and substrate can interact in a myriad of ways, and many such transformations are not amenable to computational study with this direct approach.

Milo *et al.* have effectively circumvented this problem by providing a means of pre-

HEALTH CARE POLICY

Randomize evaluations to improve health care delivery

Administrative data and experimental designs lead the way

By Amy Finkelstein^{1,2,3*}
and Sarah Taubman²

The medical profession has long recognized the importance of randomized evaluations; such designs are commonly used to evaluate the safety and efficacy of medical innovations such as drugs and devices. Unfortunately, innovations in how health care is delivered (e.g., health insurance structures, interventions to encourage the use of appropriate care, and care coordination approaches) are rarely evaluated using randomization. We consider barriers to conducting randomized trials in this setting and suggest ways for overcoming them. Randomized evaluations of fundamental issues in health care policy and delivery should be—and can be—closer to the norm than the exception.

There is particular interest in improving delivery of health care in the United States, where the health care sector accounts for almost one-fifth of the economy. The newly created Patient-Centered Outcomes Research Institute is providing an estimated \$3.5 billion in research grants, and the latest round of Center for Medicare and Medicaid Innovation Health Care Innovation Awards provides about \$1 billion in research grants—much of it aimed at improving the delivery of U.S. health care.

Studies of U.S. health care delivery typically rely on a range of observational and quasi-experimental methods. These can be extremely valuable for learning as much as possible from existing historical data and for studying questions that are not amenable to randomized designs. For prospective evaluation of new interventions, however, it is often possible to use a randomized design without adding substantially to the cost or difficulty

of the study. When feasible, randomized designs have an unparalleled ability to provide credible evidence on an intervention's impact. This can be seen in the outsized and enduring influence of the 1970s RAND Health Insurance Experiment, a randomized evaluation of the impact of health insurance in the United States (1, 2). More recently, the attention paid to the 2008 Oregon Health Insurance Experiment (OHIE), a randomized evaluation of the impact of Medicaid (3–6), underscores the continued power and influence of such randomized evaluations in both the academy and public discourse.

To explore how commonly randomization is used in health care delivery studies, we examined papers published in a limited set of top journals in medicine, economics, and health services between 2009 and 2013 [see (7) for details on data and methods]. We included papers designed to study causal effects of an intervention (using either randomized or other methods). We focused on a handful of top journals to capture an illustrative set of high-profile studies; the picture may be different across all published (and unpublished) studies. We did, however, observe similar patterns in reviews of trials registered with clinicaltrials.gov and of reports from major contract research organizations (7).

On average, 18% of studies of U.S. health care delivery interventions used randomization (see the table). By comparison, 79% of studies of U.S. medical interventions were randomized (P -value for comparison < 0.001). Medical studies involving drugs were very likely to be randomized (86%), but randomization was also common in nondrug medical studies (66%).

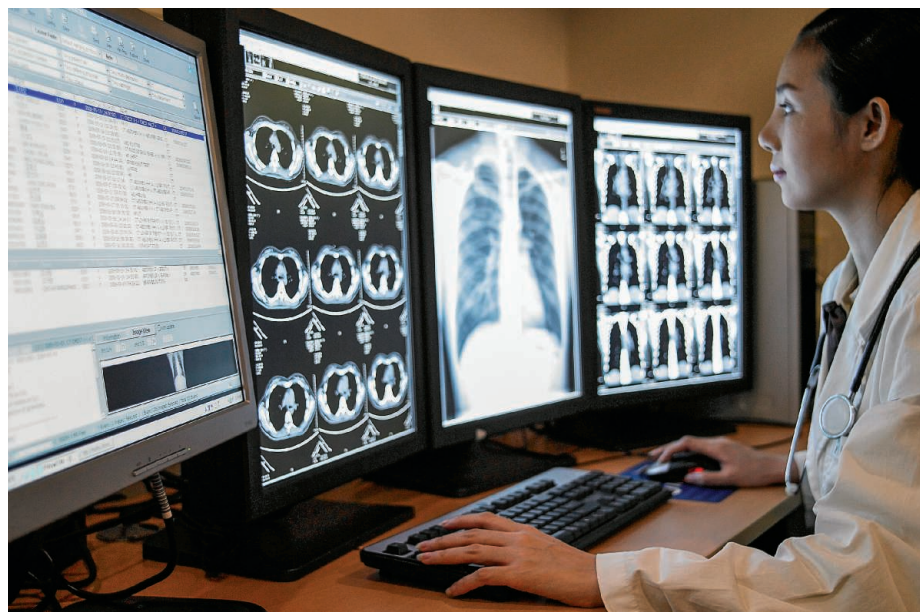
Of course, regulatory and funding environments in medicine are quite different from those in the social sciences. However, we found several areas of social science where randomization is used far more than in health care delivery. In U.S. education studies in top economics journals, 36% were randomized (P -value for comparison = 0.028). More notably, 46% of international development studies in top economics journals were randomized ($P < 0.001$). Even within health care delivery, there appears to be more use of randomization internationally than within the United States. Looking across the same journals in medicine, economics, and health services as above, 41% of health care delivery studies conducted outside of the United States were randomized, compared with 18% in the United States ($P < 0.001$).

DATA AND DESIGN. To understand why randomized trials in U.S. health care delivery have been rare, we turn to some of the challenges in conducting such studies. We then propose practical approaches to managing these challenges.

We begin with potential ethical considerations. For medical innovations, randomized trials are considered essential in determining both safety and efficacy. In health care delivery, safety concerns tend to be less strong. However, there is often equipoise regarding effectiveness. Moreover, it is common in health care delivery for promising programs to reach only a small fraction of the individuals who might benefit. Where

A corollary of this labor-intensive approach is that randomized evaluations frequently focus on very specific patient populations. Of the 31 randomized health care delivery studies from top medical journals included in the table, 77% were convenience samples (for example, patients at a single hospital). This raises important concerns about their generalizability.

This expensive, time-consuming, and convenience-sample approach may be necessary in most medical trials, where there are often real risks to participants. However, in most health care delivery interventions, there is usually only minimal risk of harm to participants. As a result, an alternative ap-



there are capacity constraints, random assignment can be the most equitable way to allocate limited slots. Indeed, the random selection used in the OHIE was designed by the state in conjunction with stakeholders specifically to address fairness concerns (8).

Another common concern is that randomized evaluations are prohibitively costly, but this does not have to be the case. It is true that the typical model for randomized controlled trials in medicine is expensive and time-consuming. Screening, recruiting, and obtaining informed consent from individual patients before randomization and then collecting follow-up data for the purposes of the study is labor-intensive and difficult. Historically, most randomized trials of health care delivery innovations have followed this model. Our review of randomized studies of U.S. health care delivery published between 2009 and 2013 in top medical journals (7) found that 80% recruited and requested consent from individuals and 85% collected primary data.

proach to randomization can produce valid causal estimates at substantially reduced cost. Randomization is done, with a waiver of informed consent, on a set of potentially eligible individuals, and those who are randomized into the treatment group are offered the intervention. All individuals included in the random assignment—including those who do not accept the offer of the intervention—are followed. Low take-up of the program (adherence to the assigned protocol) does not interfere with obtaining consistent estimates of the program's causal effects (9). This type of randomization design was used in the OHIE; those randomly selected were offered Medicaid applications, which allowed us to study the impact of Medicaid coverage.

Although this approach reduces the statistical power of the study, it is compatible with running large trials and trials with more representative samples, because it does not require individual recruitment, and individuals can be followed passively in administrative data. Data collected, used, and stored for

¹Department of Economics, Massachusetts Institute of Technology, Cambridge, MA 02139, USA. ²J-PAL North America, Massachusetts Institute of Technology, Cambridge, MA 02139, USA. ³National Bureau of Economic Research, Cambridge, MA 02138, USA. *E-mail: afink@mit.edu

TOPIC	NUMBER OF STUDIES	NUMBER RANDOMIZED	PERCENT RANDOMIZED
U.S. health care delivery			
Top medical journals (subsample)	62	31	50
Top economics journals	13	2	15
Top health services journals	405	13	3
Adjusted average*			18
Comparison to medical innovations in top medical journals			
Medical treatment (U.S. based)	176	139	79
Medical treatment (international)	177	136	77
Comparison to other topics in top economics journals**			
All other U.S.-based	192	14	7
Public finance	50	4	8
Industrial organization	48	0	0
Labor	31	2	6
Education	22	8	36
Other	57	4	7
International development	37	17	46
Health care delivery studies conducted outside of the U.S.A.			
Top medical journals (subsample)	30	19	63
Top economics journals	4	1	25
Top health services journals	53	2	4
Adjusted average*			41

Use of randomization by study topic. The table includes all empirical papers designed to study causal effects of an intervention and published in top journals in three fields. Medical: four randomly selected months per year 2009–2013 for *New England Journal of Medicine*, *Journal of the American Medical Association*, *Annals of Internal Medicine*, and *PLOS Medicine*. We excluded *BMJ* and *Lancet* after a preliminary investigation of 4 months of publications found no studies of U.S. health care delivery in either journal. Economics: 2009–2013 in the *American Economic Review*, *Quarterly Journal of Economics*, *Journal of Political Economy*, and *Econometrica*. Health services: 2009–2013 in *Health Affairs*, *Medical Care*, and *Milbank Quarterly*. *The average adjusts for the fact that we reviewed only 20 out of 60 months of medical journals but all issues of economics and health services journals. Medical journals typically published more frequently and provided ample articles to provide a good estimate, which was then upweighted in the total. **Economics papers may be coded as having more than one topic and would contribute to each. See (7) for details.

reasons other than the study—such as from insurance claims, hospital discharges, electronic medical records, employment records, and mortality records—often include a virtual census of the relevant individuals. These data allow researchers to examine a wide range of impacts at substantially lower cost than primary data collection.

Compared with surveys, such administrative data offer several additional advantages besides lower cost. They are less likely to suffer from bias due to differential nonresponse or attrition. They can provide close-to-real-time results on the impact of an intervention. They can also be used for following up on long-term outcomes of the intervention [e.g., the impact of kindergarten classes on adult earnings in the Project STAR study (10)]. By combining the alternative randomization approach with follow-up in administrative data, randomized evaluations can be made no more costly than the prospective observational evaluations that are commonly done in U.S. health care delivery.

A final set of challenges revolves around the ways individuals and systems interact. Some of the most promising ideas for U.S. health care delivery interventions involve reforms to entire systems of care. Cluster-randomized designs can be a useful tool here. Some system-level or comprehensive interventions may even be amenable to patient-level randomization. For example, innovations such as including bundling payments for episodes of care and creating shared saving contracts—major themes in current health policy discussions—are often held up as examples of something hard to study through randomized evaluation. Yet as these payment mechanisms expand to take on new groups of patients, randomizing which individuals are included may be possible.

Of course, some interventions—including individual-level interventions—can have system-wide effects if implemented on a large scale. Consider the expansion of insurance coverage. A randomized study like the OHIE allows us to detect effects of covering a given

individual with insurance, while holding the general health care environment constant. However, capacity constraints in the health care system may limit effects of market-wide expansions, particularly in the short run; alternatively, as suggested by quasi-experimental work (11), provider responses to a market-wide insurance expansion—such as adoption of new medical technology and changes in practice style—may amplify effects of market-wide expansions. In some cases, it is possible to design studies that look at these broader effects, by randomizing the proportion of individuals within the relevant unit who are assigned the treatment, as well as randomizing which individuals within the unit are assigned the treatment (12). In other cases, however, such approaches are not practical or feasible, and we need to draw on other methods.

More generally, this discussion highlights the value of experiments that are actively designed by researchers to shed light on specific mechanisms. The OHIE was not prospectively designed by researchers (8) and, as a result, leaves much to be debated, such as whether an alternatively designed Medicaid program could achieve most of the benefits but at lower cost [see, e.g., (13)]. By contrast, the RAND Health Insurance Experiment was prospectively designed by researchers to shed light on tradeoffs involved in cost-sharing. It used multiple arms to randomly vary cost-sharing features of health insurance that individuals received. It has been widely used in policy and academic discussions of optimal cost-sharing designs.

Governments, insurers, employers, and health care providers are experimenting with a wide variety of innovations intended to improve health and reduce costs. Increased use of randomized evaluations offers a feasible way to more rigorously measure their efficacy and accelerate the pace at which we improve the health care delivery system. ■

REFERENCES AND NOTES

1. J. P. Newhouse, the Insurance Experiment Group, *Free for All? Lessons from the RAND Health Insurance Experiment* (Harvard Univ. Press, Cambridge, 1993).
2. A. Aron-Dine et al., *J. Econ. Perspect.* **27**, 197 (2013).
3. K. Baicker et al., *N. Engl. J. Med.* **368**, 1713 (2013).
4. K. Baicker et al., *Am. Econ. Rev.* **104**, 322 (2014).
5. A. Finkelstein et al., *Q. J. Econ.* **127**, 1057 (2012).
6. S. L. Taubman et al., *Science* **343**, 263 (2014).
7. A. Finkelstein, S. Taubman, "Using randomized evaluations to improve the efficiency of US healthcare delivery" (J-PAL North America, Cambridge, MA, 2014); www.povertyactionlab.org/node/10558.
8. H. Allen et al., *J. Health Polit. Policy Law* **38**, 1183 (2013).
9. J. Angrist et al., *J. Am. Stat. Assoc.* **91**, 444 (1996).
10. R. Chetty et al., *Q. J. Econ.* **126**, 1593 (2011).
11. A. Finkelstein, *Q. J. Econ.* **122**, 1 (2007).
12. B. Crepon et al., *Q. J. Econ.* **128**, 531 (2013).
13. R. Douthat, *New York Times*, 5 May 2013.

ACKNOWLEDGMENTS

We acknowledge funding from the Laura and John Arnold Foundation.

10.1126/science.aaa2362

sciencemag.org **SCIENCE**

BOOKS *et al.*

BOTANY

Botanical brilliance

Are plants decision-makers or elaborate fakers?



By Andrew G. Zink* and Zheng-Hui He

In *Plant Behaviour and Intelligence*, Anthony Trewavas challenges us to leave behind our prejudices and view the world from a plant's perspective. Plants, he argues, behave on their own time scale, with their own unique physiology, and solve problems that are equally as complex as those confronting animals. This book represents a treasure trove of fascinating case studies and has the potential to serve as an important resource for plant physiologists and behavioral ecologists alike.

Behavioral ecologists have long recognized the possibility of applying their models of animal behavior to the plant kingdom. The journal *Behavioral Ecology* has invited papers on plant behavior since its inception in 1990, but it took more than

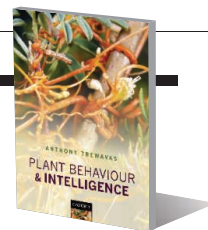
two decades for the first (and only) paper on plant behavior to be published (1). The journal *Plant Signaling and Behavior* was created in 2006 to bridge this plant-animal divide, but so far it has focused almost entirely on specific mechanisms rather than evolutionary adaptations.

Bridging the worlds of plant and animal behavior remains a conceptual (and political) challenge. Trewavas has been persistent and courageous in his defense of plant behavior for many years and maintains his position in this book, reasonably asserting that any "response of an organism to a specific stimulus" can be defined as a behavior, especially if it is tied to survival and reproduction.

The scale of plant behaviors described in this book ranges from individual cells to tissues and organs to entire plants. This is likely to surprise (and possibly disori-

Plant Behaviour and Intelligence

Anthony Trewavas
Oxford University Press,
2014. 303 pp.



ent) many behavioral ecologists, who tend to reserve the term "behavior" for entire organisms. Although Trewavas's analogies would have been much simpler to comprehend if he had focused exclusively on whole plants, some of his best are drawn between the behaviors of animals and those of plant organs. Such unexpected comparisons force us to reconsider our very notion of individuality.

In one example, Trewavas proposes that leaves "behave" when responding to quantities and qualities of light. In another example, he proposes that roots "behave" when they forage along key environmental gradients such as gravity, water, and mineral nutrients. But in both of these cases, as well as in the many similar analogies, we were left wondering if the entire plant is "behaving" by guiding a peripheral tissue or if these plant tissues are operating as autonomous behavioral entities. If the latter is true, how might disagreements among plant tissues be resolved, and how might this translate into what Trewavas calls "intelligent" behavior by the whole plant?

Most philosophers would be quite skeptical of Trewavas's claim that plants have true intelligence and would have even stronger objections to the claim that plants exhibit a form of consciousness, as he suggests in the book's final chapters. But Trewavas views intelligence as an emergent phenomenon of the entire plant, arising from coordinated behaviors of individual tissues. He argues that this is analogous to problem-solving by social insect colonies through coordination among workers. This is where this book becomes the most challenging but also the most exciting in terms of generating new ideas.

In Chapter 11, for example, Trewavas purports to show that the cambium layer of a tree acts as an "integration assessor," quantifying the productivity of individual branches in a way that is similar to how a honeybee colony integrates information from various waggle dances by worker bees. He views this as a competitive process in which the cambium layer preferentially distributes resources to the most productive branches. We would point out that this

The reviewers are in the Department of Biology, San Francisco State University, San Francisco, CA 94132, USA.

*Corresponding author. E-mail: zink@sfsu.edu

cooperation among plant tissues is likely facilitated by the absence of genetic conflicts that are much more common in social insect colonies. One notable exception to this would be the phenomenon of multiple paternity of seeds in a single plant. In Chapter 17, Trewavas suggests that game theory could be used to address seed competition; one can easily imagine seeds within and across fruits competing for resources, much like chicks in a nest begging for food.

Although admirable in scope and ambition, there are a few places in which Trewavas's analogies fall short. For example, individual workers within social insect colonies can easily change tasks and move their positions within the colony. Plant cells and tissues are static due to their cell walls. Therefore, any decision-making behavior by the whole plant can only occur through growth and decay. This unique constraint found in plants is what leads Trewavas to claim, "Behaviour in plants is most easily seen as changes in form." We were left asking whether plant "behavior" is simply prolonged developmental plasticity or if judicial self-pruning and regeneration represent a true strategy.

As we read this book, we wondered whether the series of analogies with animal behaviors sidelined the unique and astonishing ability of plants to exhibit behaviors (e.g., regeneration) that most animals could never achieve. Because plants cannot run away from danger, for example, they have evolved defenses against pathogens and herbivores that rival and even exceed the sophistication of many animal immune systems. One gets the sense that Trewavas, too, is frustrated that animal biologists have neglected the unique sophistication and problem-solving abilities of plants, but it is possible that his animal-centric analogies may play an unintended role in perpetuating this bias.

There is no doubt that using terminology from the field of animal behavior to describe plant behavior may to some degree downgrade the amazingly unique things that only plants can do. However, we believe that applying the rich theoretical perspectives of behavioral ecology to plants can only help scientists to appreciate and better understand the evolutionary significance of plant behavior. And at the very least, this book will likely inspire a bit more respect for a kingdom of master problem-solvers who happen to march to the beat of their own (very slow) drum.

REFERENCES

1. M. Gagliano, *Behavioral Ecology* **24**, 789 (2013).

10.1126/science.aaa2412

MEDICINE

Stories from the heart

A history of cardiac research and therapies

By Yevgeniya Nusinovich

Since prehistoric times, people have known that the heart is critical for sustaining life, but its true function was not well understood until recently. The roles traditionally ascribed to the heart included being the seat of the mind, the organ of love, and the location of the soul. An understanding of the heart's true role in the circulatory system took much longer to emerge. In *The Man Who Touched His Own Heart*, evolutionary biologist Rob Dunn takes readers on a meandering journey through the evolution of human knowledge about this mystical organ and ways to treat its many maladies.

Dunn uses his own mother's recent cardiac problems to set the scene for the story and, presumably, explain his own sudden interest in matters of the heart. From there, he begins with the improbable story of the first documented heart surgery, performed by an African American doctor in an understaffed and underfunded hospital in Chicago in 1893, before going back to the time of Galen, a prominent Greek physician and philosopher who was among the first to attempt to understand the heart's function in the ancient world.

Subsequent events are discussed more or less chronologically, with the exception of those that occurred in the 20th century, when so much was being learned and done in parallel. The majority of the book is devoted to the events that led to the development of cardiac imaging, medical treatments for atherosclerosis, and, of course, heart surgery itself.

Among these stories is the tale of the German physician Werner Forssmann, who inspired the book's title. Forssmann's bold experiment on his own heart, which I won't spoil here, paved the way for a number of new diagnostics and interventions and ultimately earned him the Nobel Prize in Medicine.

The reviewer is on staff at Science Translational Medicine, AAAS, Washington, DC 20005, USA. E-mail: ynusinov@aaas.org

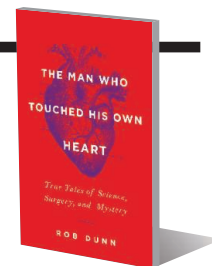
The Man Who Touched His Own Heart

True Tales of Science, Surgery, and Mystery

Rob Dunn

Little, Brown, 2015.

384 pp.



The writing in this book is clear and understandable, without unnecessary use of medical jargon and with detailed explanations of all relevant terms. However, it does occasionally stray into the overly lyrical and cutesy—for example, when Dunn describes the heart as “the Mount Everest of the body” or “that bloody engine.” Additionally, the heavy use of foreshadowing for some of the more dramatic events in the story

sometimes makes the book feel like a television drama; however, on the whole this should not detract much from the reader's enjoyment. Even when I already knew how everything was going to turn out (both from personal knowledge and from the foreshadowing), I found the stories to be well told and compelling.

The best part of the book, in my opinion, and

the one that's likely to be the least familiar to the majority of readers, deals with the evolution of the circulatory system across a range of species, from sea sponges to humans. This seems to be the author's favorite topic area, and he writes about it without the dramatic flair of his surgical stories but with clear love for the subject.

Despite having been written for a general audience, this book would make great reading for medical professionals, as it features an extensive collection of medical anecdotes and fascinating history (including the occasional bar fight, which is apparently a common way for someone to end up needing emergency heart surgery). I would recommend it to anyone who is interested in the heart, in medical history, or in dramatic and improbable stories from the field of medicine.

10.1126/science.aaa1413

LETTERS

Edited by Jennifer Sills

Cancer risk: Role of environment

THE REPORT “VARIATION in cancer risk among tissues can be explained by the number of stem cell divisions” (C. Tomasetti and B. Vogelstein, 2 January, p. 78) is dangerously misleading because it understates the role of prevention in cancer causation. It is widely acknowledged that many cancers can be explained by a two-step process: initiation by one or a series of mutations, followed by the promotion of the genetic “mistake” to a recognizable tumor or blood disease (1). The observation that replication of the mistake may proceed at different rates in different tissues is no doubt correct. However, some mutations are initiated by chemical or viral exposures, and others occur without a known cause.

Promotion of DNA damage to recognizable disease occurs in both cases. The conclusion that “stochastic effects of DNA replication can be...distinguished from external environmental factors” is an inaccurate statement that rests on a false dichotomy. An environmental influence can in fact create a DNA change which, if present when the DNA is copied, is subsequently “fixed” into the genome as a permanent change. The more replications, the less time there is for DNA repair to take place before the next copying/fixation event. Thus, the correlation between frequency of copying events and lifetime cancer risks among tissues does not imply that environmental influences play a lesser role in the causation of those same mutations. The fact that age-adjusted cancer rates for different tissues vary substantially among countries where statistics are kept, and between workplaces or communities that differ in environmental exposures, demonstrates that a large fraction of cancers are influenced by environmental factors (2).

What the authors’ work suggests is that stochastic differences in effects of DNA replication on cancer occurrence in different tissues can be distinguished from effects of external environmental factors. This distinction is far from trivial. Furthermore, the conclusion that “[t]he concept underlying the current work is that many genomic changes occur simply by chance during DNA replication rather than as a result of carcinogenic factors” ignores the fact that

an initiation event must have taken place for a mutation to be replicated. The paper obscures the distinction between differences in cancer incidence and differences in occurrence of initiating events leading to cancer.

**Nicholas A. Ashford,^{1*} Patricia Bauman,²
Halina S. Brown,³ Richard W. Clapp,^{4,5}
Adam M. Finkel,^{6,7} David Gee,⁸ Dale B.
Hattis,⁹ Marco Martuzzi,¹⁰ Annie J. Sasco,¹¹
Jennifer B. Sass^{12,13}**

¹Sociotechnical Systems Research Center, Massachusetts Institute of Technology, Cambridge, MA 02139, USA. ²Bauman Foundation, Washington, DC 20009, USA. ³Department of International Development, Community, and Environment, Clark University, Worcester, MA 01610, USA. ⁴Boston University School of Public Health, Boston, MA 02118, USA. ⁵University of Massachusetts, Lowell, MA 01854, USA. ⁶Penn Program on Regulation, University of Pennsylvania Law School, Philadelphia, PA 19104, USA. ⁷Department of Environmental Health Sciences, University of Michigan School of Public Health, Ann Arbor, MI 48109, USA. ⁸Institute of Environment, Health, and Societies, Brunel University, London, SW11 6HT, UK. ⁹The George Perkins Marsh Institute, Clark University, Worcester, MA 01610, USA. ¹⁰World Health Organization—Regional Office for Europe, European Centre for Environment and Health, 53113 Bonn, Germany. ¹¹Epidemiology for Cancer Prevention, Team on HIV, Cancer and Global Health, Inserm U 897—Epidemiology and Biostatistics, Bordeaux Segalen University, 33076 Bordeaux, France. ¹²Natural Resources Defense Council, Washington, DC 20005, USA. ¹³George Washington University, Washington, DC 20037, USA.

*Corresponding author. E-mail: nashford@mit.edu

REFERENCES

1. D. Hanahan, R. A. Weinberg, *Cell* **144**, 646 (2011).
2. IARC, *Cancer Incidence in Five Continents, Vol. X* (International Agency for Research on Cancer, Lyon, France, 2013).

Cancer risk: Tumors excluded

IN THEIR REPORT “Variation in cancer risk among tissues can be explained by the number of stem cell divisions” (2 January, p. 78), C. Tomasetti and B. Vogelstein discuss an interesting correlation (0.804) between estimated lifetime stem cell division number in 31 tissue types and corresponding cancer incidence rates in the United States. However, their assertion that only 35% of cancer risk variation is due to environmental or genetic factors is problematic.

The correlation analysis excluded many cancers (such as stomach, breast, prostate, cervix, kidney, endometrium, bladder, and lymphoma) that are common in the United States or worldwide, so no statement about overall cancer rate variation that is “explained” by stem cell divisions can be made. Furthermore, the correlation was anchored by five data points for osteosarcoma and included tumor subtypes having genetic (colorectal) and environmental influences (lung), but stem cell division rates were not estimated separately for organ subtypes. There are strong time trends in cancer incidence rates and large incidence-rate variations internationally for nearly all cancer types [for example, the rate of squamous esophagus cancer among men with the high-

est incidence (Jiashan County in China and African Americans in South Carolina) is more than 100 times the rate among men with the lowest incidence (Algeria) (1)]. If international rates were added to Figure 1, a much smaller fraction of incidence rate variation would be explained by stem cell divisions. Moreover, as the authors note, “The total number

of stem cells in an organ and their proliferation rate may of course be influenced by genetic and environmental factors,” so that stem cell division numbers could serve, substantially, as a mediator of genetic and environmental influences, rather than a distinct etiologic factor.

Finally, high values of the authors’ extra risk score (ERS) are described as arising when “there is high cancer risk relative to the number of stem cell divisions,” but ERS is calculated not as the ratio, but as the product, of cancer incidence rates and stem cell division number. Hence the resulting classification into D and R tumors does not seem interpretable and, regardless, could aim only to identify tumors that have etiologic mechanisms other than stem cell division number.

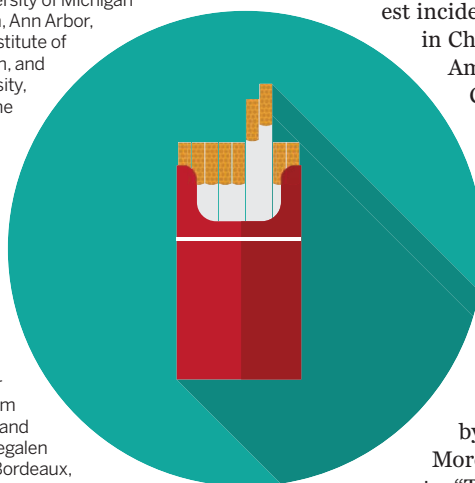
John D. Potter* and Ross L. Prentice

Division of Public Health Sciences, Fred Hutchinson Cancer Research Center, Seattle, WA 98109, USA.

*Corresponding author. E-mail: jpotter@fredhutch.org

REFERENCE

1. M. P. Curado et al., *Cancer Incidence in Five Continents, Volume IX* (International Agency for Research on Cancer Scientific Publications, No. 160, Lyon, France, 2007).



Cancer risk: Role of chance overstated

THE RECENT ASSERTION from C. Tomasetti and B. Vogelstein that most variation in cancer risk among tissues is due to “bad luck” demands close consideration, especially as they go on to argue for increased focus on early detection (“Variation in cancer risk among tissues can be explained by the number of stem cell divisions,” Reports, 2 January, p. 78). Observations from cancer epidemiology and limitations in their analysis argue strongly against this conclusion. Most cancers show considerable differences in incidence rates between distinct populations. Rates change over time, and migrants soon exhibit incidence rates similar to their host country. Each of these is consistent with a major etiologic role for environment and lifestyle. Consequently, a majority of cancers are preventable, with primary prevention achieving notable successes and promising more (1).

In their analysis, the authors correlate total stem cell divisions in selected organs or sites, and lifetime risk of a particular cancer at those sites. There is much uncertainty in the estimates of total stem cell divisions for each cancer site, and the vast age-related fluctuations in cell division for some tissues are overlooked. Of greater concern is the lifetime risk of cancers. Their analysis excludes frequent cancers with major environmental causes (such as stomach, breast, and cervix) and oversamples cancers rare in all populations (such as osteosarcomas, small intestine, and medulloblastoma). Overall, the cancer sites included account for only 34% of the cancer cases in the United States (2). The choice of the U.S. population is also arbitrary. A different population with different cancer patterns would have provided different results.

We also take issue with the statistical analysis. Despite the reported correlation of 0.81, stem cell replication is a poor predictor of incidence rates at any given cancer site. The residual standard deviation of the log rates is 0.75, so the 95% confidence limits for the log rate of any

cancer site are given by the linear predictor ± 1.47 (i.e., 1.96×0.75). Converting from a log10 scale to an absolute scale gives an error factor of $10^{1.47} = 29.4$; i.e., the incidence rate may be 30 times higher or 30 times lower than the value predicted by stem cell division rates alone. This residual variation is consistent with large effects of environmental and lifestyle factors.

The role of chance underlying the onset of any individual cancer has long been recognized (3). However, although important for the individual, chance has little to say about the incidence rate in a population, or differences between populations. These are far better explained by exposure to environmental and lifestyle factors, allowing important opportunities for, and supporting implementation of, primary prevention.

Christopher Wild,* Paul Brennan, Martyn Plummer, Freddie Bray, Kurt Straif, Jiri Zavadil

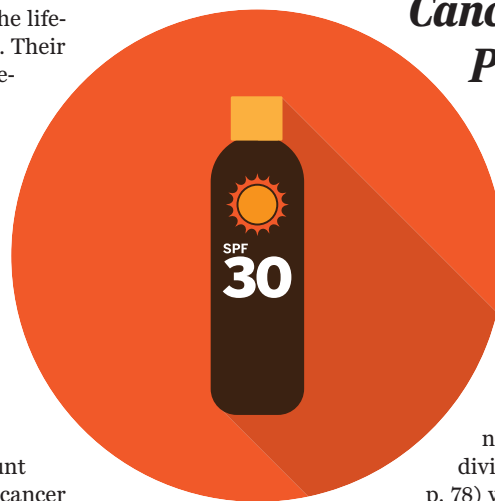
International Agency for Research on Cancer, Lyon, 69008, France.

*Corresponding author. E-mail: director@iarc.fr

REFERENCES

1. *World Cancer Report 2014*. B. W. Stewart, C. P. Wild, Eds. (IARC, Lyon, France, 2014).
2. National Cancer Institute, Surveillance Epidemiology and End Results Program (www.seer.cancer.gov).
3. P. Armitage, R. Doll, *Br. J. Cancer* **8**, 1 (1954).

Cancer risk: Prevention is crucial



AS CANCER prevention scientists, we read C. Tomasetti and B. Vogelstein's Report “Variation in cancer risk among tissues can be explained by the number of stem cell divisions” (2 January, p. 78) with considerable interest. Many of the findings

support previous research: Cancers vary in preventability, and the cancers that cause the most mortality in developed countries (lung and colon) are highly preventable (1). However, other findings in the Report do not reflect the current evidence.

For example, many of the “R-tumor” type cancers that the authors hypothesize to be unlikely to be preventable have well-known modifiable risk factors, such as tobacco and alcohol use for esophageal

and head and neck cancers, radon exposure for lung cancer in nonsmokers, and ultraviolet light exposure for melanoma (1). There is also well-documented variation in cancer incidence rates for these and other cancers, globally and due to migration, as well as over time (1). These kinds of changes do not seem to be compatible with the theory that these cancers originate primarily from random stem cell mutations.

Tomasetti and Vogelstein found an interesting statistical relationship between rates of stem cell division and cancer rates in selected tissues, but they overinterpret the results by implying a causal relation. Emerging evidence suggests that stem cell division rates, and errors in division, are not simply a product of time and chance; they vary due to many external influences, including obesity, environmental pollution, infections, and inflammation (2, 3).

Carolyn Gotay,* Trevor Dummer,¹ John Spinelli^{2,1}

¹School of Population and Public Health, University of British Columbia, Vancouver, BC, V6T1Z3, Canada. ²Cancer Control Research, British Columbia Cancer Agency, Vancouver, BC, V5Z1L3, Canada.

*Corresponding author. E-mail: carolyn.gotay@ubc.ca

REFERENCES

1. D. Schottenfeld, J. F. Fraumeni Jr., Eds., *Cancer Epidemiology and Prevention* (Oxford Univ. Press, New York, ed. 3, 2006).
2. J. Doles, M. Storer, L. Cozzuto, G. Roma, W. M. Keyes, *Genes Dev.* **26**, 2144 (2012).
3. L. Wu, B. O. Diekmann, D. Jain, F. Guilak, *Int. J. Obes. London* **37**, 1079 (2013); published online 20 November 2012.

Cancer risk: Many factors contribute

IN THEIR REPORT “Variation in cancer risk among tissues can be explained by the number of stem cell divisions” (2 January, p. 78), C. Tomasetti and B. Vogelstein found a high correlation between the number of lifetime stem cell divisions of a given tissue and the lifetime risk of cancer in that tissue. Based on the finding that 65% of the variation in cancer risk among different tissues can be explained by the number of stem cell divisions in those tissues, the authors concluded that “these results suggest that only a third of the variation in cancer risk among tissues is attributable to environmental factors or inherited predispositions.” This conclusion presumes that the total contribution of different components to variation in cancer risk among tissues adds up to 100%. However,

most cancers are caused by multiple overlapping factors, and the attributable fractions for individual factors can add up to more than 100%. Furthermore, Tomasetti and Vogelstein suggest using the extra risk score (ERS) to direct allocation of primary versus secondary prevention for different cancers. However, although the ERS indicates how important the stochastic effects of DNA replication are for the variation in cancer rates across organs, it does not inform about the preventability of a certain cancer in the population. As shown in Figure 1 in the Report, a wide variation in cancer rates exists even within highly proliferative tissues, indicating a substantial role of non-stochastic factors in carcinogenesis (such as sun exposure for melanoma, tobacco for lung cancer, viruses and obesity for hepatocellular carcinoma, and obesity and tobacco for pancreatic ductal adenocarcinoma) and an enormous potential for primary prevention. The proportion of cancer cases that can be potentially prevented by environmental (mainly lifestyle) modification should be estimated on the basis of the comparison of cancer rates across populations with different risk factor profiles (1, 2), rather than the comparison of cancer rates across tissues within individuals.

Mingyang Song¹ and Edward L. Giovannucci^{1,2*}

¹Departments of Nutrition and Epidemiology, Harvard T.H. Chan School of Public Health, Boston, MA 02115, USA. ²Channing Division of Network Medicine, Department of Medicine, Harvard Medical School, Brigham and Women's Hospital, Boston, MA 02115, USA.

*Corresponding author. E-mail: egiovann@hsph.harvard.edu

REFERENCES

1. R. Doll, R. Peto, *J. Natl. Cancer Inst.* **66**, 1191 (1981).
2. G. Danaei, S. Vander Hoorn, A. D. Lopez, C. J. Murray, M. Ezzati, *Lancet* **366**, 1784 (2005).

Cancer risk: Accuracy of literature

WE READ WITH INTEREST the recent cancer etiology Report "Variation in cancer risk among tissues can be explained by the number of stem cell divisions" (2 January, p. 78), in which C. Tomasetti and B. Vogelstein claim that most cancer risk can be explained by chance mutations. However, the selection criteria used for cancer types included in the study are not robust. First, the authors report using an "extensive literature search" to identify eligible tissue types. There is no evidence that a systematic literature review was conducted. Second, the assessment of

literature quality and subsequent inclusion criteria is not clear. According to the authors, "Other cancer types could not be assessed, largely because details about the normal stem cells maintaining the tissue in homeostasis have not yet been agreed upon or accurately quantified." There have been volumes written about the necessity of systematic literature reviews and subsequent appraisal as a critical component of obtaining accurate and unbiased research results (1).

The method used by Tomasetti and Vogelstein leads to the exclusion of breast and prostate cancer, together accounting for ~25% of all newly diagnosed cancers (2). No doubt other cancer types are excluded as well. Breast and prostate cancer have been closely studied, in many cases to a much greater extent than those cancers that the authors select. Lack of agreement regarding accurate quantification of these cell types should be addressed by sensitivity analysis rather than exclusion. Large bodies of literature will invariably contain disagreement between authors. This is hardly justification for exclusion.

Michael O'Callaghan

Department of Urology, SA Health, Daw Park, SA 5041, Australia. E-mail: michael.ocallaghan@health.sa.gov.au

REFERENCES

1. J. P. T. Higgins, S. Green, *Cochrane Handbook for Systematic Reviews of Interventions* Version 5.1.0 [updated March 2011] (The Cochrane Collaboration, 2011); www.cochrane-handbook.org.
2. Australian Institute of Health and Welfare, "Cancer in Australia: An overview 2014" (AIHW, Canberra, Cancer series No. 90, Cat. no. CAN 88, 2014).

Response

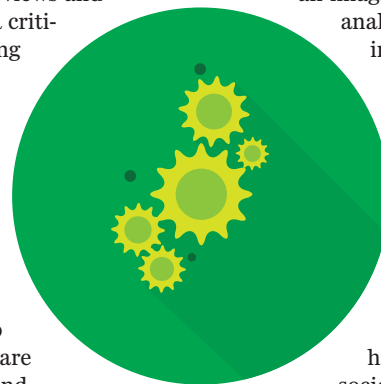
THESE LETTERS CONTINUE the healthy and intelligent debate among scientists and the public about the root causes of cancer and the best way to reduce cancer deaths. The debate hinges on the following question: What causes the mutations that are responsible for cancer? Two causes—environmental and hereditary factors—have long been recognized. A third cause—mutations that arise during normal stem cell divisions in the absence of exogenous factors—was also known, but there had been no way to measure the relative importance of these mutations in cancers and compare them to the other causes. Our analysis enabled such a measurement, and we found evidence for a surprisingly

large role of these mutations, henceforth called replicative mutations.

Suppose we had discovered a mutagenic, industrial agent that was present in human tissues at concentrations that were very highly correlated with cancer incidence. The implications of this discovery would be obvious. But such an imaginary discovery is highly analogous to the one reported in our paper. The difference is that the "agent" is not exogenous. Replicative mutations are unavoidable. They are in a sense a side-effect of evolution, which cannot proceed without them. That they play a larger role in cancer than previously believed has important scientific and societal implications.

At least three reactions to our paper have emerged. To some, the idea that we cannot completely control our cancer destinies by living a perfect lifestyle in a perfect environment, even when we have no hereditary predisposition to cancer, has proved unsettling. To others, our paper had a completely different message. That a child has cancer is bad enough; that a parent may feel guilty for failing to avoid a certain life-style or environment, and thereby "causing" that cancer, is agonizing. We chose to use the word "bad luck" particularly because we were aware of the unjustified guilt felt by many patients and their families about cancers that were beyond their control. The third reaction is fear that recognition of a major role for "bad luck" in cancer could lead individuals to conclude that all types of cancer are unpreventable and there is nothing they can do to avert any of them. We and many others, including those who have written Letters to *Science*, have vigorously campaigned against this mistaken belief (1, 2).

Ashford *et al.* state that "some mutations are initiated by chemical or viral exposures, and others occur without a known cause," leaving open the possibility that other mutations are caused by chemical or viral exposures that have not yet been identified. The views of Ashford *et al.* stem from influential studies carried out in 1947 in which mice were treated topically with a single dose of a strong mutagen (i.e., initiator), followed by repeated topical doses of croton oil (i.e., promoter) (3). Ashford *et al.* thus state that our study "ignores that fact that an initiation event must have taken place for a mutation to be replicated." In contrast,



our view is that no exposure to an exogenous agent is required for tumor initiation. Replicative mutations can be responsible for either initiating the process of tumorigenesis or for driving tumor progression.

Potter and Prentice and Wild *et al.* suggest that if we had

been able to include other cancer types, particularly common cancer types such as those of the prostate and breast, we might have concluded that less than two-thirds of the variation in cancer risk across tissues is ascribable to replicative mutations.

We stated in our Report that we could only include cancers in which normal stem cells had been well-characterized, and agree that this was a limitation of our study. However, Cancer Research UK estimates that no cases of prostate cancer and only 27% of breast cancers are preventable (4). Therefore, once adequate research on the stem cells in these organs is performed, we expect that the inclusion of these cancers will not significantly affect the correlation coefficient we observed [see (5) for more details].

We agree with Potter and Prentice and Wild *et al.* that the evaluation of data from other countries in the same way will be valuable. However, those data will not affect our conclusion that “stochastic effects associated with DNA replication contribute in a substantial way to human cancer incidence in the United States.” Although replicative mutations are expected to vary little among populations, inherited mutations and environmentally based mutations are known to vary considerably. For example, in a country where everyone smokes and is obese, the correlation between stem cell divisions and cancer rates will be far lower than 0.80 because avoidable factors play a greater role.

Potter and Prentice criticize our multiplication of two logarithms to derive extra risk score (ERS). It may seem unintuitive to multiply rather than add logarithms, but both are valid mathematical operations to apply, with different interpretations. A detailed explanation of the mathematical basis of the ERS was provided in the Supplementary Materials and is expanded upon in our Technical Report (5).

Potter and Prentice and Gotay *et al.* state that genetic and environmental influences could influence the total number of stem

cell divisions. We agree, which is why we defined replicative mutations to exclude such effects. Replicative errors occur at rates that can be measured in totally normal cells in vitro in the absence of

any carcinogens. Carcinogens and hereditary factors

add extra mutations to the baseline level established by the unavoidable replicative mutations.

Wild *et al.* state that “a majority of cancers are preventable.” The Centers for Disease Control (CDC) estimates that 21% of cancer deaths are potentially preventable in the United States (6). The most recent estimate from Cancer Research UK is that

42% of cancers in the UK are preventable (4). These two organizations, as well as the World Health Organization Wild *et al.* represent, are committed to cancer prevention efforts and to identifying and implementing strategies to reduce cancer risk. Nothing in our study contradicts their estimates of potentially preventable cancers. To the contrary, our data provide a mechanism to help understand the molecular basis for the CDC’s estimate (as noted above, our cancer incidence data were derived from a U.S. population).

Wild *et al.* also state that “although important for the individual, chance has little to say about the incidence rate in a population” and comment about prediction of “incidence rates at any given cancer site.” Our results specifically demonstrate that chance plays an important role in the incidence rate in a population. Our approach explains variation in cancer incidence across tissues, rather than providing prediction at any particular cancer type.

Wild *et al.* support their claim that “the role of chance...has long been recognized” with a reference to the classic studies of Armitage and Doll (7). This claim illustrates that the role of replicative mutations in cancer is not adequately appreciated, even today. Armitage and Doll’s work was directed to understanding “carcinogenesis” considering “the ages at which the subjects are exposed” to various carcinogens. There are no such exposures

required for replicative mutations.

Song and Giovannucci state that the “attributable fractions for individual factors could add up to more than 100%.” The potential causes of mutations, and therefore cancer, can be partitioned in two subsets: factors related to the number of stem cell divisions and factors unrelated to those divisions. Thus, by assumption, these two causes add up to explain exactly 100% of the variation in risk.

We agree with Song and Giovannucci that the preventability of specific cancer types is more precisely estimated by epidemiologic evaluations than by ERS. The ERS provides a rough idea of the potential preventability of individual cancer types, but only in relation to other cancer types rather than in absolute terms (5). At the same time, our work provides a way to calculate the evidence for such extra risks that is free from all assumptions used previously. The idea that two-thirds of the relative variation in cancer risk can be explained (correlation coefficient of 0.80), and the relative environmental or hereditary influences roughly estimated, from a single biological feature (number of stem cell divisions) is unprecedented.

With respect to comments of O’Callaghan, our study was not intended to be a meta-analysis such as that used to evaluate clinical interventions. We used PubMed to find all the references we could and used our judgment to select 146 that we considered among the most reliable.

However, we did not have complete trust in our judgment, nor complete trust in

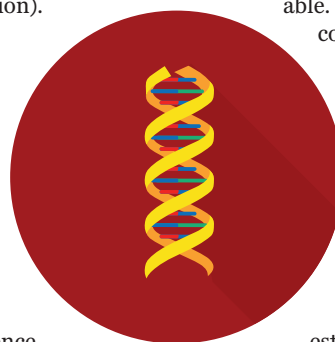
the estimates made in the original references. We therefore performed rigorous tests for robustness of the conclusions based on these estimates. For example, statistical significance persisted even when we allowed the reported estimates of stem cell divisions to vary by ~100-fold in either

direction [see our Report, Supplementary Materials]. Few meta-analyses would survive robustness tests like these.

Cristian Tomasetti¹ and Bert Vogelstein²

¹Division of Biostatistics and Bioinformatics, Department of Oncology, Sidney Kimmel Cancer Center, Johns Hopkins University School of Medicine and Department of Biostatistics, Johns Hopkins Bloomberg School of Public Health, Baltimore, MD 21205, USA. ²Ludwig Center for Cancer Genetics and Therapeutics and Howard Hughes Medical Institute, Johns Hopkins Kimmel Cancer Center, Baltimore, MD 21205, USA.

*Corresponding author. E-mail: ctomasetti@jhu.edu (C.T.); vogelbe@jhmi.edu (B.V.)



REFERENCES

1. B. Vogelstein *et al.*, *Science* **339**, 1546 (2013).
2. Johns Hopkins Medicine, "Bad luck of random mutations plays predominant role in cancer, study shows" (www.hopkinsmedicine.org/news/media/releases/bad_luck_of_random_mutations_plays_predominant_role_in_cancer_study_shows).
3. I. Berenblum, P. Shubik, *Br. J. Cancer* **1**, 383 (1947).
4. Cancer Research UK, Statistics on Preventable Cancers (www.cancerresearchuk.org/cancer-info/cancerstats/causes/preventable).
5. C. Tomasetti, B. Vogelstein, "Technical Report: Musings on the theory that variation in cancer risk among tissues is explained by the number of divisions of the normal stem cells" (<http://arxiv.org/abs/1501.05035>).
6. CDC, Potentially Preventable Deaths from the Five Leading Causes of Death—United States, 2008–2010 (www.cdc.gov/mmwr/preview/mmwrhtml/mm6317a1.htm).
7. P. Armitage, R. Doll, *Br. J. Cancer* **8**, 1 (1954).

TECHNICAL COMMENT ABSTRACTS

Comment on "Using ecological thresholds to evaluate the costs and benefits of set-asides in a biodiversity hotspot"

Christopher Finney

Banks-Leite *et al.* (Reports, 29 August 2014, p. 1041) conclude that a large-scale program to restore the Brazilian Atlantic Forest using payments for environmental services (PES) is economically feasible. They do not analyze transaction costs, which are quantified infrequently and incompletely in the literature. Transaction costs can exceed 20% of total project costs and should be included in future research.

Full text at <http://dx.doi.org/10.1126/science.aaa0916>

Response to Comment on "Using ecological thresholds to evaluate the costs and benefits of set-asides in a biodiversity hotspot"

Cristina Banks-Leite, Renata Pardini, Leandro R. Tambosi, William D. Pearse, Adriana A. Bueno, Roberta T. Bruscagin, Thais H. Condez, Marianna Dixo, Alexandre T. Igari, Alexandre C. Martensen, Jean Paul Metzger

Finney claims that we did not include transaction costs while assessing the economic costs of a set-aside program in Brazil and that accounting for them could potentially render large payments for environmental services (PES) projects unfeasible. We agree with the need for a better understanding of transaction costs but provide evidence that they do not alter the feasibility of the set-aside scheme we proposed.

Full text at <http://dx.doi.org/10.1126/science.aaa1602>

TECHNICAL RESPONSE

CONSERVATION ECONOMICS

Response to Comment on “Using ecological thresholds to evaluate the costs and benefits of set-asides in a biodiversity hotspot”

Cristina Banks-Leite,^{1,2*} Renata Pardini,³ Leandro R. Tambosi,² William D. Pearse,⁴ Adriana A. Bueno,⁵ Roberta T. Bruscagin,² Thais H. Condez,⁶ Marianna Dixo,² Alexandre T. Igari,⁷ Alexandre C. Martensen,⁸ Jean Paul Metzger²

Finney claims that we did not include transaction costs while assessing the economic costs of a set-aside program in Brazil and that accounting for them could potentially render large payments for environmental services (PES) projects unfeasible. We agree with the need for a better understanding of transaction costs but provide evidence that they do not alter the feasibility of the set-aside scheme we proposed.

As Finney points out (1), transaction costs are rarely quantified and/or reported in the payments for environmental services (PES) literature, and this is particularly true for the Atlantic Forest. Finney correctly suggests that transaction costs were ignored in Banks-Leite *et al.* (2) due to a lack of existing data and proposes four questions that should be answered before we can understand the actual feasibility of PES projects. The questions posed by Finney should certainly be used to guide future research on the feasibility of PES at large scales, but their answers require collecting additional data. In the absence of those data, we here focus on whether including transaction costs would change the main conclusion reported in Banks-Leite *et al.* (2). Specifically, we ask whether the set-aside program would become prohibitively expensive if transactions costs are explicitly accounted for, and discuss ways in which transaction costs could be curtailed.

Finney provides data to show that transaction costs vary widely and mentions one specific case study where transaction costs were shown to be comparable to PES costs. This suggests that the PES estimates reported by Banks-Leite *et al.* (2) were roughly half of the real cost of paying for set-asides in the Atlantic Forest. We have reanalyzed the data provided in Banks-Leite *et al.* (2) by doubling our previous estimates of US\$56.3 million per year for paying landowners to set aside 424,000 ha of private land for restoration. In our new estimates, US\$112.6 million would be needed to cover PES and transaction costs, which, added to the active restoration costs of US\$141.3 million, gives a total sum of US\$253.9 million per year for the biome-wide set-aside program. This estimate accounts for 0.0118% of Brazil's GDP (previous calculated as 0.009%) and 8.3% of Brazil's annual expenditure on agricultural subsidies (previous calculated as 6.5%). The new figures are obviously higher but still show the feasibility of the set-aside program advocated in Banks-Leite *et al.* (2) and suggest that even greater transaction costs would still be feasible.

The data reported by Finney in table 1 (1) show that 55% of transaction costs consist of general assessment, property mapping, and monitoring, but we believe that the costs of these measures can be reduced. First, the Brazilian government is now implementing a new program called CAR (Cadastro Ambiental Rural), for which it will buy high-resolution satellite images for the whole country every year and will restrict the endowment of rural credits just to landowners who submit to the national database a detailed map of their properties (including native vegetation, production areas, legal reserves, and

potential areas for restoration). This would reduce the costs of general assessment and property mapping by improving the database of potential areas for restoration.

Second, remote sensing techniques are often underused in pilot projects, such as the ones mentioned by Finney, and their efficiency and cost-effectiveness dramatically increase with scale. For instance, monitoring the recovery of biodiversity and ecological processes depends on expensive and time-consuming field work. However, field monitoring can be replaced by remote sensing and appropriate landscape indicators for a fraction of the costs (3), thus reducing the need for a more complete and detailed field assessment to just a subset of the restored sites.

It is also appropriate to further explore another advantage of the set-aside program advocated by Banks-Leite *et al.* (2). Although we propose the restoration of 424,000 ha of Atlantic Forest, the initial area can be increased or reduced according to an existing budget, and more areas can be added to the program once active restoration is no longer needed. For instance, using Banks-Leite's *et al.* (2) original estimates, let's consider that only \$100 million can be committed each year, which halves the amount of area that can be set aside for restoration. When active restoration practices are no longer needed after 3 years, the overall costs of the program would drop to US\$28.5 million, which means that US\$71.5 million would become available for restoring a further 153,500 ha of priority landscapes. The addition of new areas to the program after the active-restoration period can be iterated many times and could potentially restore up to 750,000 ha within 30 years with a limited budget of US\$100 million per year. If the whole budget of US\$200 million is available, the effect of this program would be much wider and larger and it would deliver outcomes much faster.

In conclusion, although Finney raises a very important issue that we indeed had not dealt with in Banks-Leite *et al.* (2), we believe that even reasonably high transaction costs would not be an impediment to the proposed PES scheme and that our approach is still robust and cost-efficient. A biome-wide set-aside program is also still more realistic than creating protected areas, and it can be easily adapted to protecting watersheds or other discontinuous areas.

REFERENCES AND NOTES

1. C. Finney, *Science* **347**, 731 (2015).
2. C. Banks-Leite *et al.*, *Science* **345**, 1041–1045 (2014).
3. C. Banks-Leite, R. M. Ewers, V. Kapos, A. C. Martensen, J. P. Metzger, *J. Appl. Ecol.* **48**, 706–714 (2011).

ACKNOWLEDGMENTS

This article is a contribution to Imperial College's Grand Challenges in Ecosystems and the Environment initiative.

14 November 2014; accepted 13 January 2015
10.1126/science.aaa1602

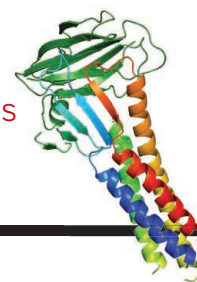
¹Grand Challenges in the Ecosystems and Environment, Department of Life Sciences, Imperial College London, Silwood Park Campus, Ascot, SL5 7PY, UK. ²Departamento de Ecologia, Instituto de Biociências, Universidade de São Paulo, Rua do Matão, 321, Travessa 14, 05508-090, São Paulo, SP, Brazil. ³Departamento de Zoologia, Instituto de Biociências, Universidade de São Paulo, Rua do Matão, 321, Travessa 14, 05508-090, São Paulo, SP, Brazil. ⁴Department of Ecology, Evolution, and Behavior, University of Minnesota, 215 Ecology Building, 1987 Upper Buford Circle, Saint Paul, MN 55108, USA. ⁵Fundação Florestal, Rua do Horto, 931, 02377-000, São Paulo, SP, Brazil. ⁶Departamento de Zoologia, Instituto de Biociências, Universidade Estadual Paulista, Caixa Postal 199, 13506-900, Rio Claro, SP, Brazil. ⁷Curso de Gestão Ambiental, Escola de Artes, Ciências e Humanidades, Universidade de São Paulo, Avenida Arlindo Bettio, 1000, 03828-000, São Paulo, SP, Brazil. ⁸Department of Ecology and Evolutionary Biology, University of Toronto, 25 Willcocks Street, Toronto, ON M5S 3B2, Canada.

*Corresponding author. E-mail: c.banks@imperial.ac.uk

RESEARCH

How a food poisoning toxin interferes with tight junctions

Saitoh et al., p. 775



IN SCIENCE JOURNALS

Edited by Stella Hurtley

DENTAL MATERIALS

Key trace minerals greatly strengthen teeth

The outer layers of teeth are made up of nanowires of enamel that are prone to decay. Gordon *et al.* analyzed the composition of tooth enamel from a variety of rodents at the nanometer scale (see the Perspective by Politi). In regular and pigmented enamel, which contain different trace elements at varying boundary regions, two intergranular phases—magnesium amorphous calcium phosphate or a mixed-phase iron oxide—control the rates of enamel demineralization. This suggests that there may be alternative options to fluoridation for strengthening teeth against decay. — MSL

Science, this issue p. 746; see also p. 712

Rodent skull shows pigmented and regular tooth enamel



MARINE POLLUTION

Dumping lots of plastics into our oceans

Considerable progress has been made in determining the amount and location of plastic debris in our seas, but how much plastic actually enters them in the first place is more uncertain. Jambeck *et al.* combine available data on solid waste with a model that uses population density and economic status to estimate the amount of land-based plastic waste entering the ocean. Unless waste management practices are improved, the flux of plastics to the oceans could increase by an order of magnitude within the next decade. — HJS

Science, this issue p. 768

CANCER

A PET approach to imaging brain tumors

Cancers are readily visible with positron emission tomography, or PET, an imaging method in which a radioactively labeled tracer accumulates in the tumor. Labeled glucose is often used as a tracer because tumor cells tend to require large amounts of glucose. PET cannot be used to image brain tumors, however, because normal brain cells are also highly dependent on glucose. Now Venneti *et al.* show that radiolabeled glutamine, which is also taken up by tumor cells, yields clear images of brain tumors in mice and humans. With the glutamine label, cancer cells can be distinguished from normal brain cells and even from tumors that are no longer growing. — YN

Sci. Transl. Med. **7**, 274ra17 (2015).

SUPERCONDUCTIVITY

Light switch for superconductivity

The conducting properties of materials sensitively depend on the available carrier concentration. Physicists can vary this concentration by inducing carriers in the material; for example, by placing it next to an ionic liquid in an electric field. Suda *et al.* instead used a layer of the molecule spiropyran, which changes from a non-ionic to an ionic form when it is irradiated by ultraviolet (UV) light. The authors placed the layer on top of a thin crystal

of an organic material. When they shone UV light on the spiropyran, the adjacent material became superconducting, thanks to the carriers induced at the interface. — JS

Science, this issue p. 743

MAMMALIAN EVOLUTION

Taking advantage of new neighborhoods

Mammals are one of the most morphologically diverse organisms, with adaptation to unique ecological conditions creating a wide array of forms, from mice to

whales. Two new basal mammals from the mid-Jurassic period suggest that this diversification was well under way millions of years earlier than previously thought. Luo *et al.* describe a burrowing species with limb and digit modifications similar to those of current burrowers and identify the likely genes and developmental pathways involved. Meng *et al.* describe an arboreal species with modifications for climbing and that possessed teeth clearly adapted for a herbivorous diet, including the consumption of sap. — SNV

Science, this issue p. 760, p. 764

HUMORAL IMMUNITY

For a single B cell, many roads to take

To successfully fight a pathogen, immunological B cells must wage a multipronged attack: They can differentiate into antibody-secreting plasma cells or become T cell–helping germinal center cells, or even long-lived memory cells. But can a single B cell acquire all of these different fates? To find out, Taylor *et al.* tracked the responses of single B cells in mice. Although some B cells acquired only one fate, others differentiated into all three. The authors linked the ability of B cells to differentiate into multiple subsets to their ability to proliferate and resist cell death, and the affinity of their antigen receptor. — KLM

Science, this issue p. 784

NEURAL CIRCUITS

Taking a snapshot of active brain circuitry

Neuroscientists now have a method to mark active populations of neurons in vivo to study circuit activity in the behaving animal. Fosque *et al.* designed and thoroughly validated a fluorescent protein–based reagent that allows permanent marking of active cells over short time scales. This indicator, termed CaMPARI, switches from its



Active neuronal circuits revealed in zebrafish

native green to a red fluorescent state by simultaneous illumination with violet light and exposure to increased levels of intracellular calcium. CaMPARI successfully marked active nerve cells in *Drosophila*, zebrafish, and mouse brains. — PRS

Science, this issue p. 755

VIRAL REPLICATION

A view of the HCV polymerase at work

More than 3% of the world's population is infected with hepatitis C virus (HCV), a predisposing factor for life-threatening liver diseases such as cirrhosis and cancer. HCV encodes a polymerase called NS5B that catalyzes replication of the viral RNA genome. Drugs inhibiting NS5B have shown impressive antiviral activity in recent clinical trials. Appleby *et al.* (see the Perspective by Bressanelli) reveal the inner workings of HCV RNA replication by analyzing crystal structures of stalled NS5B polymerase ternary complexes during the initiation and elongation of RNA synthesis. They also define the way in which sofosbuvir, a drug with potent clinical efficacy, interacts with the NS5B active site. — PAK

Science, this issue p. 771; see also p. 715

SENSORY PERCEPTION

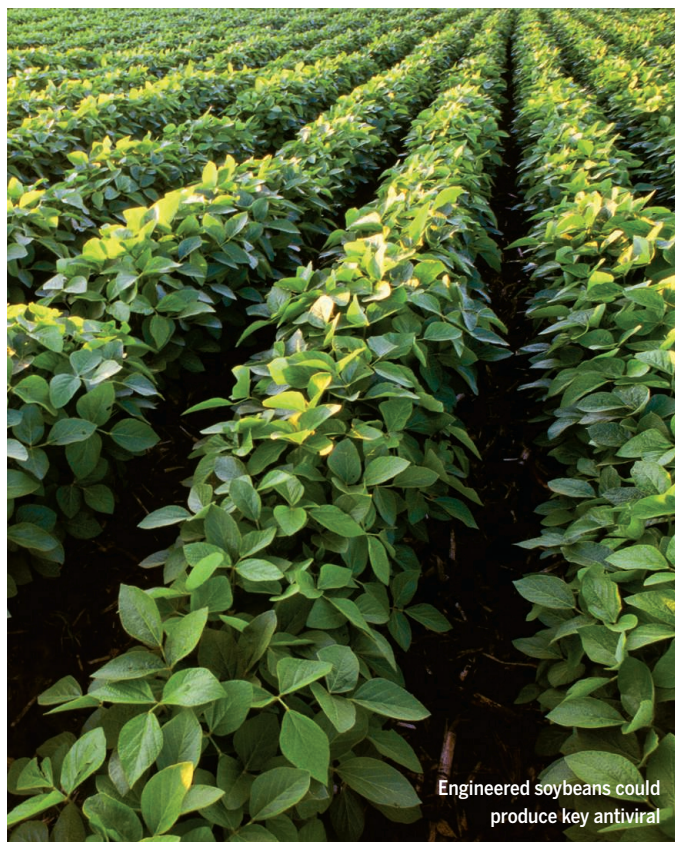
How capsaicin channels pain relief

Ion channels are essential in sensing pain and pressure. The chemical in chilies that makes them hot is capsaicin, which activates the calcium-permeable channel TRPV1. Seemingly paradoxically, this chemical is also used as a topical analgesic. Borbiero *et al.* found that activation of TRPV1 by capsaicin inhibited the mechanosensitive Piezo channels by depleting specific phosphoinositides in the plasma membrane (see the Focus by Altier). These results may explain some of the analgesic effects of capsaicin. — NRG

Sci. Signal. **8**, ra15 and fs3 (2015).

IN OTHER JOURNALS

Edited by **Kristen Mueller**
and **Jesse Smith**



Engineered soybeans could produce key antiviral

PLANT SCIENCE

HIV antivirals from engineered soybeans

Affordable antivirals used as vaginal microbicides could have a substantial impact on the HIV epidemic, particularly in the developing world. One potential candidate is cyanovirin-N, a protein produced by a cyanobacterium that prevents viral entry in preclinical studies. Large-scale production of cyanovirin-N, however, is prohibitively expensive. To get around this, O'Keefe *et al.* genetically engineered soybean seeds to make cyanovirin-N. The seeds produced large quantities of the antiviral and it survived the normal industrial processing systems already in place for soybeans. By rough estimate, one greenhouse growing engineered soybeans could provide enough cyanovirin-N to protect a woman for 90 years. — PJH

Plant Biotech. J. 10.1111/pbi.12309 (2015).

NEUROSCIENCE

Brain activity predicts later recollection

When people remember details about a specific event (a process referred to as “recollection”), a part of their brain called the core

recollection network is highly active. To better understand the underlying connectivity of different brain regions involved in recollection, King *et al.* scanned the brains of people while they were retrieving earlier memories. Memory retrieval led to

ALSO IN SCIENCE JOURNALS

Edited by Stella Hurtley

ENVIRONMENTAL SCIENCE

Changing tastes in marine microbe food webs

Protists are single-celled organisms complete with nuclei, organelles, and symbionts, and possess a multiplicity of physiological talents. They are ubiquitous, abundant, and often neglected by science. Worden *et al.* review the challenges of understanding the role protists play in geochemical cycling in the oceans. These organisms can photosynthesize like plants, graze on bacteria and archaea, parasitize each other and bigger creatures, have sex, and sometimes do all these things serially as conditions change. Their activities may have a significant influence on carbon cycling, and research efforts need to be amplified to understand their functional importance in marine ecosystems. — CA

Science, this issue p. 735

SUSTAINABILITY

Crossing the boundaries in global sustainability

The planetary boundary (PB) concept, introduced in 2009, aimed to define the environmental limits within which humanity can safely operate. This approach has proved influential in global sustainability policy development. Steffen *et al.* provide an updated and extended analysis of the PB framework. Of the original nine proposed boundaries, they identify three (including climate change) that might push the Earth system into a new state if crossed and that also have a pervasive influence on the remaining boundaries. They also develop the PB framework so that it can be applied usefully in a regional context. — AMS

Science, this issue p. 736

ORGANIC CHEMISTRY

Optimizing a catalyst many ways at once

Optimization strategies are often likened to hikes in a hilly landscape. If your goal is to get to the top of the highest hill, and you only take steps toward higher ground, you might never find a peak on a route that requires a preliminary descent. So it is in chemistry, where optimizing each structural feature of a catalyst consecutively might gloss over subtle tradeoffs that in combination offer the best performance. Milo *et al.* use multidimensional analysis techniques to generate a predictive model of how selectivity depends on multiple characteristics of the catalyst and substrate in a C-N bond-forming reaction (see the Perspective by Lu). They then apply this model to improve the catalyst globally. — JSY

Science, this issue p. 737;
see also p. 719

ATMOSPHERIC CHEMISTRY

Double trouble for Criegee intermediates

Atmospheric ozone reacts with unsaturated hydrocarbons to form unstable compounds called Criegee intermediates. Only recently did a reliable method emerge to make and study these compounds in the laboratory, and they didn't seem to react with water. Now, Chao *et al.* show that the simplest Criegee intermediate, CH₂OO, does in fact react very rapidly with pairs of water molecules (see the Perspective by Okumura). Earlier studies may have missed this result because they were conducted at low pressure, where water dimers are scarce, or because they monitored downstream processes. The

new rate measurements imply that reactivity with atmospheric water pairs is a major decay channel for Criegees. — JSY

Science, this issue p. 751;
see also p. 718

TIGHT JUNCTIONS

How a toxin makes epithelial sheets leaky

The entire human body and its many compartments are shielded from their external environments by the barrier function of epithelial cell sheets. The paracellular barrier function of tight junctions (TJs) is critical for maintaining homeostasis in any multicellular organism, especially in the skin and internal organs and at the blood-brain barrier. One of the major components of TJs is a family of adhesive membrane proteins known as claudins. Several members of the claudin family are receptors for the bacterial toxin *Clostridium perfringens* enterotoxin. This toxin often causes food-borne illness both in humans and animals. Saitoh *et al.* crystallized a complex between the toxin and a claudin that reveals just how the toxin damages epithelial barriers (see the Perspective by Artursson and Knight). — SMH

Science, this issue p. 775;
see also p. 716

CHEMICAL BIOLOGY

Toward drugging the undruggable in cancer

Many human cancers are characterized by inappropriate activity of transcription factors. These proteins are attractive drug targets in principle, but normalizing their function requires drugs that modulate specific protein-protein interactions,

a goal that has been challenging. In acute myeloid leukemia, a chromosomal translocation creates an aberrant form of the transcription factor CBF-beta, which outcompetes "normal" CBF-beta for binding to another transcription factor called RUNX1, thereby deregulating its activity. Illendula *et al.* identified and chemically optimized a small molecule that selectively disrupts the interaction between the aberrant CBF-beta and RUNX1 (see the Perspective by Koehler and Chen). This molecule restored normal gene expression patterns and delayed leukemia progression in mice. Thus, transcription factors may not be as undruggable as once thought. — PAK

Science, this issue p. 779;
see also p. 713

CENTROMERES

The α -satellite arrays of human centromeres

Centromeres link sister chromatids and are central to chromosome segregation. Centromeres are found within the tandemly repetitive α -satellite DNA sequences. It has been difficult to define the molecular processes involved in the formation of centromeres. Henikoff *et al.* identified two sets of human α -satellite dimer sequences that are consistently associated with particular centromere-associated nucleosomes—the proteinaceous structures around which chromosomal DNA is wrapped. This finding may help to identify other tandem repeat arrays within the centromeres of other eukaryotes and should allow for a better molecular understanding of centromere evolution and function. — ASH

Science Advances 10.1126/sciadv.00234 (2015).

Ingested algae pitch in
to prevent starvation



SYMBIOSIS

Plastid thieves escape starvation

Green sea slugs feed on algae, and in the process they take up photosynthetic plastids from the algae. The plastids stay intact in the slug's gut cells for months, and the slugs benefit nutritionally from ongoing photosynthesis. So much so that some scientists think that the plastids can prevent slugs from dying of starvation. But photosynthesis and starvation can also produce toxic products that cause the slugs to die. de Vries *et al.* found one species of slug that does not rely on photosynthesis to keep it going during hard times. This slug resists death by ramping up mechanisms to remove damaged plastids and toxins. — CA

Proc. R. Soc. B 10.1098/rspb.2014.2519 (2015).

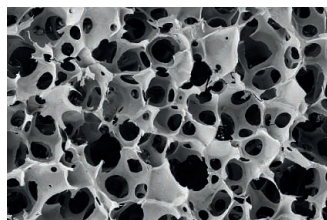
increased activity in specific areas of their brains, both in the core recollection network and in other regions. By analyzing the active areas in different people, areas of functional connectivity emerged. More accurate recollections correlated with greater connectivity among these different regions. — PRS

J. Neurosci. **35**, 1763 (2015).

BIOMATERIALS

Better bone patching with hydrogel foam

Bone grafts are currently the clinical standard for replacing larger bone defects caused by trauma, infections, or tumors. Degradable biomaterials are not sufficient for regenerating bone without the addition of peptides or growth factors to attract and direct the needed cells. Neffe *et al.* devised a one-step process for creating



Pore structure of a 3D architected hydrogel (ArcGel)

hydrogels through a foaming process using gelatin and lysine connected by urea junctions. The gels form an open porous structure that allows cells to invade and provides support for their adhesion, as well as offering tailorable local environments and mechanical properties and controlled and rapid degradation. In vivo testing for the regeneration of 5-mm femoral defects in rats showed healing capacity comparable to that of bone grafts after 6 weeks. — MSL

Adv. Mater. 10.1002/adma.201404787 (2015).

BIOMECHANICS

Measuring the forces that shape tissues

During development, intracellular molecular motors generate forces that cause cells to change shape and remodel their contacts with other cells. But exactly how these forces change cell shape is largely unknown. Bambardekar *et al.* used light-sheet microscopy and optical tweezers to image a developing fruit fly embryo and directly measure the tension at cell-cell junctions. As morphogenesis progressed, the tension increased and became anisotropic (directional) across the embryo. On

the basis of these measurements and by monitoring the effect of cell deformations on neighboring cells, the authors then created a model that predicts how local deformations propagate through the tissue. — VV

Proc. Natl. Acad. Sci. U.S.A. 10.1073/pnas.1418732112 (2015).

ENVIRONMENTAL SCIENCE

Energy and wastewater treatment, too

Treating wastewater removes organic matter that would otherwise harm the environment when released back into waterways. New bioelectrochemical systems provide the added benefit of using this organic matter as a fuel for bacteria to generate hydrogen gas or electricity during wastewater treatment. However, concerns remain about whether the other functions of wastewater treatment, including reducing the amount of trace organic compounds released back into the environment, will be lost. Werner *et al.* tested the breakdown of low levels of pharmaceuticals, pesticides, and antibiotics in microbial fuel cells and microbial electrolysis cells. Although some of these contaminants persisted after passing through the microbial

reactors, the breakdown efficiency was similar to that of most modern wastewater treatment methods. — NW

Water Res. 10.1016/j.watres.2015.01.013 (2015).

OPTICS

A temperature probe for the ultracold

The temperature of an everyday macroscopic object is well understood and easy to measure. The concept of temperature, however, becomes blurry when the number of particles in a system becomes so small that the ensemble breaks down into a number of individual components, such as for atoms or molecules trapped in an optical lattice and cooled to ultralow temperatures. McDonald *et al.* demonstrate a spectroscopic technique that uses the line shift and change in the line shape of an atomic or molecular transition to determine the temperature of trapped atoms or molecules down to nanokelvin temperatures. This technique should prove useful in a range of applications, including metrology and probing the energetic dynamics of ultracold chemical reactions. — ISO

Phys. Rev. Lett. **114**, 23001 (2015).

CANCER RESEARCH

Lifetime risk of cancer goes up

More than 50% of people born in the U.K. since 1960 will develop cancer in their lifetimes, finds a new study. Combining actual cancer rates from 1951 to 2012 with projected rates for 2013 through 2060, Ahmad *et al.* estimated lifetime risks for men and women born in 1930 with those for men and women born from 1931 to 1960. For men, the risk increased from 38.5% for those born in 1930 to 53.5% for those born in 1960; for women, risk increased from 36.7% to 47.5%. Increasing life expectancy was the primary reason for the risk increase. —CG

Br. J. Cancer. 10.1038/bjc.2014.606 (2014).

REVIEW SUMMARY

ENVIRONMENTAL SCIENCE

Rethinking the marine carbon cycle: Factoring in the multifarious lifestyles of microbes

Alexandra Z. Worden,* Michael J. Follows, Stephen J. Giovannoni, Susanne Wilken, Amy E. Zimmerman, Patrick J. Keeling

BACKGROUND: Marine ecosystems are composed of a diverse array of life forms, the majority of which are unicellular—archaea, bacteria, and eukaryotes. The power of these microbes to process carbon, shape Earth's atmosphere, and fuel marine food webs has been established over the past 40 years. The marine biosphere is responsible for approximately half of global primary production, rivaling that of land plants. Unicellular eukaryotes (protists) are major contributors to this ocean productivity. In addition to photosynthetic growth, protists exhibit a range of other trophic modes, including predation, mixotrophy (a combina-

tion of photosynthetic and predatory-based nutrition), parasitism, symbiosis, osmotrophy, and saprotrophy (wherein extracellular enzymes break down organic matter to smaller compounds that are then transported into the cell by osmotrophy).

ADVANCES: Sensitive field approaches have illuminated the enormous diversity of protistan life (much of it uncultured) and, coupled with activity measurements, are leading to hypotheses about their ecological roles. In parallel, large-scale sequencing projects are providing fundamental advances in knowledge of

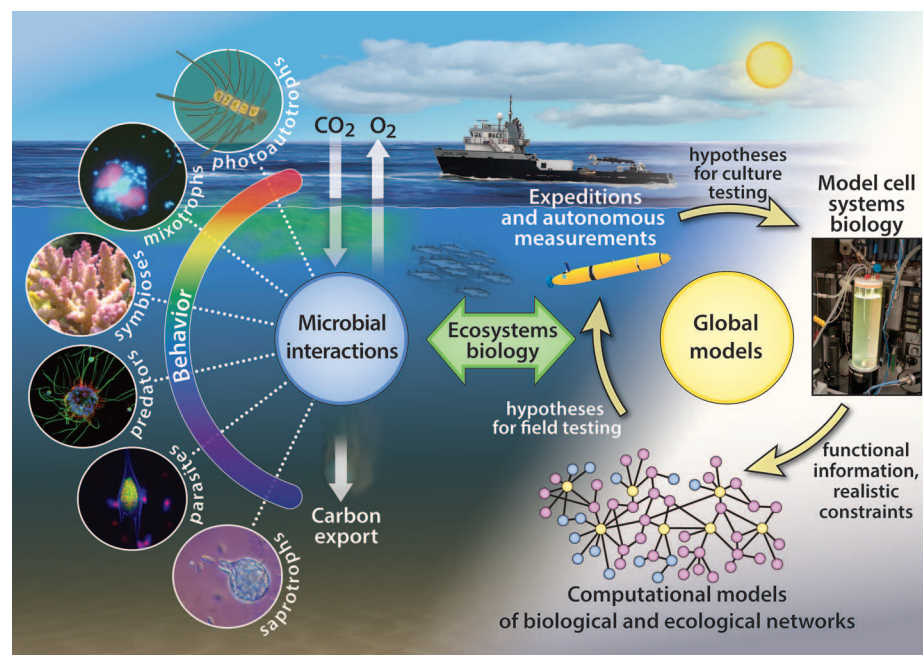
genome/gene composition, especially among photosynthetic lineages, many of which are complex amalgams derived from multiple endosymbiotic mergers. Marine protists have yielded insight into basic biology, evolution,

ON OUR WEB SITE

Read the full article at <http://dx.doi.org/10.1126/science.1257594>

and molecular machine-ries that control organismal responses to the environment. These studies reveal tightly controlled signaling and transcriptional regulation as well as responses to limitation of resources such as iron, nitrogen, and vitamins, and offer understanding of animal and plant evolution. With the formulation of better computational approaches, hypotheses about interactions and trophic exchanges are becoming more exact and modelers more assertive at integrating different data types. At the same time, the impacts of climate change are being reported in multiple systems, of which polar environments are the touchstone of change.

OUTLOOK: Driven by the need to translate the biology of cells into processes at global scales, researchers must bring the conceptual framework of systems biology into bigger “ecosystems biology” models that broadly capture the geochemical activities of interacting plankton networks. Existing data show that protists are major components of marine food webs, but deducing and quantifying their ecosystem linkages and the resulting influences on carbon cycling is difficult. Genome-based functional predictions are complicated by the importance of cellular structures and flexible behaviors in protists, which are inherently more difficult to infer than the biochemical pathways typically studied in prokaryotes. Alongside the plethora of genes of unknown function, manipulable genetic systems are rare for marine protists. The development of genetic systems and gene editing for diverse, ecologically important lineages, as well as innovative tools for preserving microbe-microbe interactions during sampling, for visual observation, and for quantifying biogeochemical transformations, are critical but attainable goals. These must be implemented in both field work and laboratory physiology studies that examine multiple environmental factors. Expanding genome functional predictions to identify the molecular underpinnings of protistan trophic modes and realistically constrain metabolism will position the field to build reliable cell systems biology models and link these to field studies. By factoring in true complexities, we can capture key elements of protistan interactions for assimilation into more predictive global carbon cycle models. ■



Global biogeochemical and ecological models rely on understanding organismal biology and the interactions occurring in marine microbial food webs. Protists have multifarious roles from the sunlit surface ocean to leagues below. Understanding of protistan behaviors and adaptability lags far behind knowledge of evolutionary processes that have shaped their genomes. As such, microbial mediation of carbon fluxes and specific interactions remain ill-resolved and predictive capabilities are still weak. Strategies to narrow this gap involve iteration between experimental and observational field studies, controlled laboratory experiments, systems biology approaches that preserve cellular structures and behaviors using relevant model taxa, and computational approaches.

The list of author affiliations is available in the full article online.

*Corresponding author. E-mail: azworden@mbari.org

Cite this article as A. Z. Worden et al., *Science* **347**, 1257594 (2015). DOI: 10.1126/science.1257594

REVIEW

ENVIRONMENTAL SCIENCE

Rethinking the marine carbon cycle: Factoring in the multifarious lifestyles of microbes

Alexandra Z. Worden,^{1,2,3*} Michael J. Follows,⁴ Stephen J. Giovannoni,⁵ Susanne Wilken,¹ Amy E. Zimmerman,¹ Patrick J. Keeling^{3,6}

The profound influence of marine plankton on the global carbon cycle has been recognized for decades, particularly for photosynthetic microbes that form the base of ocean food chains. However, a comprehensive model of the carbon cycle is challenged by unicellular eukaryotes (protists) having evolved complex behavioral strategies and organismal interactions that extend far beyond photosynthetic lifestyles. As is also true for multicellular eukaryotes, these strategies and their associated physiological changes are difficult to deduce from genome sequences or gene repertoires—a problem compounded by numerous unknown function proteins. Here, we explore protistan trophic modes in marine food webs and broader biogeochemical influences. We also evaluate approaches that could resolve their activities, link them to biotic and abiotic factors, and integrate them into an ecosystems biology framework.

The marine carbon cycle plays a critical role in Earth's habitability for humans and other large fauna. At the core of the cycle are interconversions of inorganic and organic carbon forms, which lead to major ecosystem services. Protistan (unicellular eukaryotic) phytoplankton have long been recognized as foundational to fisheries and export of atmospheric CO₂ to the deep ocean (1–3). Protists convert CO₂ to organic carbon via photosynthesis, simultaneously altering cycles of other elements linked to carbon by the stoichiometry of cellular composition. Thus, the carbon cycle interacts with biogeochemical cycles of nitrogen, silica, and many other elements (4–6). How air-sea exchanges of CO₂, primary productivity, and carbon sequestration to the deep sea will be altered as climate change affects these and other microbes (7) is poorly understood. Here, we review current understanding of the diverse functionality and lifestyles of marine protists and how they participate in the carbon cycle.

During the 1970s and 1980s, ideas emerged about microbial connectivity in ocean food webs (8) and the microbial loop (9), which formalized the importance of bacteria and archaea as hubs of metabolic diversity. The classical diatom-

copepod-fish food chain view of ocean productivity was thus revolutionized by the understanding that diverse forms of dissolved organic matter (DOM) derived from algae were a major energy source for heterotrophic bacterial growth (Fig. 1). In turn, predatory protists consumed the bacteria and were themselves preyed upon by larger zooplankton. In this framework, algal primary production had multiple routes to higher trophic levels. The microbial loop was the most inefficient route in terms of respiratory carbon losses (conversion of organic carbon to CO₂) because as algal DOM and particulate organic matter (POM) pass through heterotrophic bacteria and archaea, respiration losses occur alongside important nutrient remineralization. Viral lysis of bacteria was subsequently recognized as another potentially substantial source of DOM (10). Protists are now often represented as either photoautotrophs (typically diatoms and coccolithophores) or heterotrophic predators (Fig. 1).

Global-scale simulations of ocean ecosystems and biogeochemical cycles, overlain on circulation models, have become a common tool for carbon cycle and climate sensitivity studies, including Intergovernmental Panel on Climate Change assessments. Such models focus on simulating biogeochemical cycles rather than the organisms that mediate them, and build on the seminal studies of Riley and colleagues (11). Plankton populations are described by partial differential equations that represent physical transport, growth, death, and interactions at broad levels. Today, such models resolve a few broad “functional types” of photoautotrophic microbes (e.g., all small phytoplankton described by a single set of parameters) and two predator groups: protistan and metazoan consumers of algae, or “grazers” (12–14). If het-

erotrophic bacteria are included, it is as one homogeneous population. Population growth rates are described using highly idealized relationships to external resources (15) or internal stores (16), without representation of the highly flexible and adaptive physiology of the organisms concerned. In part, the current parameterization of microbial physiology in models reflects computational limitations, but it also reflects a lag in assimilation of new data and understanding of microbial cell biology. Determining the level of granularity required to accurately simulate and interpret ocean ecosystems, the type of baseline information that would be adequate to assess change, and how to integrate organismal diversity, dynamics, and interactions into large-scale models are not easy tasks.

As reviewed here, protistan biology comprises diverse lifestyles that shape the carbon cycle through elaborate but poorly appreciated food web connections. A repertoire of phagotrophic modes and a penchant for symbioses have led to the evolution of cell architectures that can be orders of magnitude larger and more complex than those of prokaryotes (17). Size matters, in part because larger cells (such as the largest coccolithophores) sink faster, altering export of carbon and other elements to the deep ocean on massive scales (17–20). Marine microbiologists and modelers alike are becoming acutely aware that phenotypic variation in protistan physiology and behavior is critical to assessing their broader ecosystem roles and future ocean productivity.

Complex factors govern protistan primary production: Phytoplankton

Marine algae account for about 50 Pg C year⁻¹ of primary production, rivaling that of terrestrial plants (1). In addition to the roles played by larger photosynthetic protists, understanding of the importance of picoplanktonic taxa (diameter <2 μm) is growing (21–23). In the 1950s, the picoeukaryote *Micromonas pusilla* was shown to dominate in the English Channel (23), and subsequent discoveries of the abundant (non-eukaryotic) cyanobacteria *Synechococcus* (24) and *Prochlorococcus* (25) confirmed the importance of very small phytoplankton to marine systems. However, while larger algae such as diatoms have clear food chain roles and fast, quantifiable sinking rates that result in carbon export to the deep sea, similar knowledge is limited for eukaryotic and prokaryotic picoplankton (20, 26). Moreover, photosynthetic protists are extremely diverse; many are difficult to quantify in nature, many remain uncultured, and we lack baseline information on wild populations. “New” algal lineages are still being discovered (27, 28). Additionally, picoplanktonic eukaryotes, including uncultured groups, are unexpectedly important contributors to CO₂ fixation in environments where cyanobacteria dominate numerically (29–32).

Eukaryotic phytoplankton have evolved from heterotrophic ancestors on multiple independent occasions, resulting in marked differences in genome content and functional capabilities, from which they continue to diversify (Box 1 and Fig. 2). Comparing the cell wall composition of four

¹Monterey Bay Aquarium Research Institute, Moss Landing, CA 95039, USA. ²Department of Ocean Sciences, University of California, Santa Cruz, CA 95064, USA. ³Integrated Microbial Biodiversity Program, Canadian Institute for Advanced Research, Toronto, Ontario M5G 1Z8, Canada. ⁴Department of Earth Atmospheric and Planetary Sciences, Massachusetts Institute of Technology, Cambridge, MA 02139, USA. ⁵Department of Microbiology, Oregon State University, Corvallis, OR 97331, USA. ⁶Department of Botany, University of British Columbia, Vancouver, British Columbia V6T 1Z4, Canada.

*Corresponding author. E-mail: azworden@mbari.org

common algal lineages illustrates this diversity and its influence on ocean biogeochemistry: Some stramenopiles have silicate frustules of nanoscale precision (diatoms), whereas others are naked; haptophytes can be covered in ornate calcium carbonate plates (coccolithophores), whereas many picoplanktonic species are naked or have organic scales; dinoflagellates can possess intracellular cellulose plates or be naked; and among the prasinophytes, a few species are naked but most are enveloped by organic scales (4, 33, 34). Consequently, the growth of these algae depends on different elements' input sources, remineralization rates, and crystal structures (e.g., calcium carbonate in the form of aragonite or calcite) and will have correspondingly distinct responses to decreasing pH caused by climate change (35).

Analysis of algae in the context of genomic information is advancing understanding of their physiology. These studies often focus on diatoms or prasinophytes, underscoring highly differentiated responses to iron and nitrogen availability, tightly controlled gene regulatory

programs, and signaling systems conserved with land plants [e.g., (36–41)]. Genomes are available for other marine phytoplankton as well (42–44). Complex relationships between resource availability and adaptive strategies are also being identified using genomes from cultured strains as contextual information and innovative approaches to unraveling interactive effects in the field (45, 46). For example, diatoms in a Pacific Ocean study were highly responsive to iron fertilization, but metatranscriptome analyses suggested continued dependence on iron-free photosynthetic proteins rather than a switch to iron-containing functional equivalents present in their gene repertoire (45). This is hypothesized to allow newly available iron to be used for resource acquisition (rather than for photosynthetic machinery), contributing to frequent diatom success under iron fertilization. These findings would be difficult to deduce in laboratory experiments, because they would not capture the sharp contrasts between diatom responses and those of the broader algal community.

Nonetheless, many aspects of algal physiology remain unclear. This knowledge gap is becoming critical as climate change influences marine food webs and carbon sequestration (47–49). Perturbations typically influence multiple environmental parameters simultaneously, and algal responses appear to be highly regionalized. For example, in the Canadian Arctic, larger photosynthetic protists such as diatoms are reportedly being replaced by photosynthetic picoeukaryotes (50), and similar shifts are expected in other regions as a result of stratification-related causes, altering both the food web and carbon export. In contrast, massive amounts of algal carbon, primarily from diatoms, are sinking to the eastern central Arctic sea floor (51). The interactive effects of perturbations are extensive [e.g., climate-influenced CO_2 , pH, and temperature changes; reviewed in (52)], but most laboratory experiments fail to capture their complexity. Cell systems biology experiments involving the controlled study of model organisms in culture are essential for designing field studies that gauge the

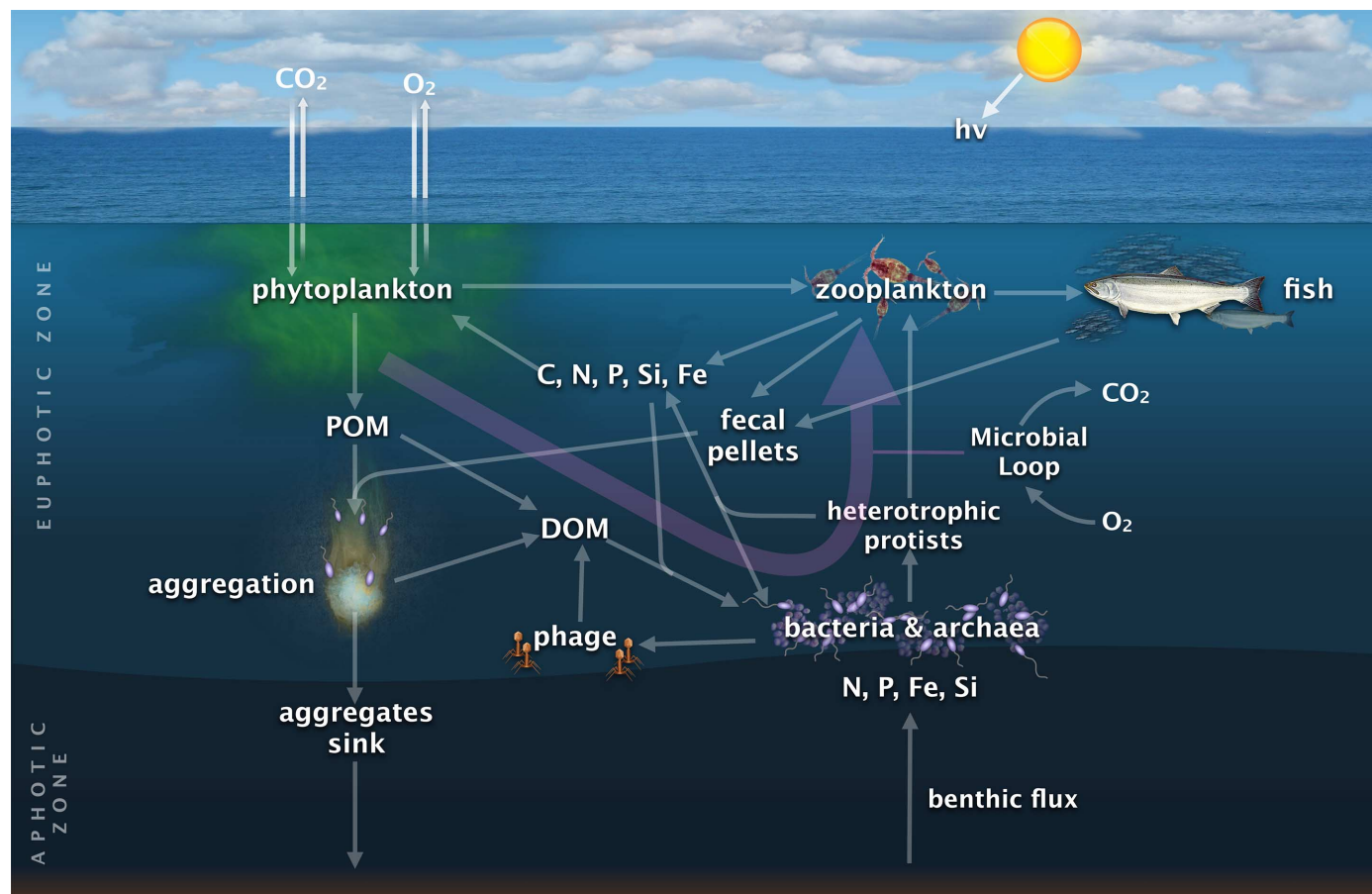


Fig. 1. A common depiction of marine microbial food webs. Dissolved and particulate organic matter (DOM and POM, respectively) from phytoplankton form a basic resource for bacteria and archaea, which respire CO_2 (via the microbial loop, purple arrow), thereby modifying the flow of carbon expected in earlier diatom-copepod-fish food chains (diatoms are algae within the stramenopile lineage, and copepods are multicellular zooplankton in the opisthokont lineage). Most such schemas do not differentiate phytoplankton in different size fractions, although size influences food

web linkages. Inorganic nutrients are also important factors shaping community composition. By necessity, processes in the euphotic zone, where photosynthesis occurs, are differentiated from those in the aphotic zone, where sunlight is unavailable. Anthropogenic impacts (not depicted) include acidification, coastal eutrophication, and changes to water column structure induced by warming, such as stronger stratification and reduced nutrient flux into surface waters, as well as increased exposure to high light intensities (7). [Adapted from (105)]

impacts of individual taxa on higher ecosystem-level processes.

Carbon in the balance: Predation, osmotrophy, and parasitism

Carbon cycling and sequestration depend on carbon oxidation rates as much as on photosynthesis. This balance pivots on the wide-ranging nutritional strategies of heterotrophic organisms (Fig. 3). The best-studied heterotrophic mode of marine protists is predation. On average, micro- and nano-zooplankton (<200 μm) consume 62% of daily algal production, albeit with high regional and temporal variability (53). These predators are largely protistan, but grazing measurements generally reflect bulk rates without group-specific information. This is problematic because the protists involved are diverse. In productive environments, dinoflagellates can be major grazers of diatom blooms, whereas in more oligotrophic regions, ciliates and diverse flagellates are important consumers of picophytoplankton and bacteria (32, 54–56). Structurally complex choanoflagellates, amoebozoans, dinoflagellates, and rhizarians can also be regionally important predators (57–59). Members of the latter group, which includes Acantharia (part of what used to be called “Radiolaria”) and Foraminifera, also feed extensively on hetero-

trophs, including on multicellular zooplankton such as copepods (58). The identity of the taxa responsible for most predation is not known, particularly for heterotrophic flagellates. Novel marine stramenopiles (MASTs) are presumed to dominate predatory flagellates (21), but most MASTs are uncultured (60–62) and correct assignment of trophic modes is complicated because the stramenopiles include algae, saprotrophs, predators, and mixotrophs (Box 2). Some MASTs clearly consume bacteria and picophytoplankton (55, 56), but single-cell and colony isolation studies indicate that more complex associations also exist. For example, the MAST *Solenicola setigera* grows on frustules of the diatom *Leptocylindrus mediterraneus*, sometimes alongside *Synechococcus*, upon which it may also feed (60). These discoveries show the difficulties in discerning the nature of associations in the wild.

The huge variation in protistan predation strategies is not represented in current marine biogeochemical and ecological models because the bases for prey selection, feeding rates, and alternate strategies are not known. Generally predators are larger than their prey; however, protists can ingest prey of equal or larger size than themselves. Examples include the haptophyte *Prymnesium parvum* (63) and the dinoflagellate *Karlodinium armiger*, which immobilizes cope-

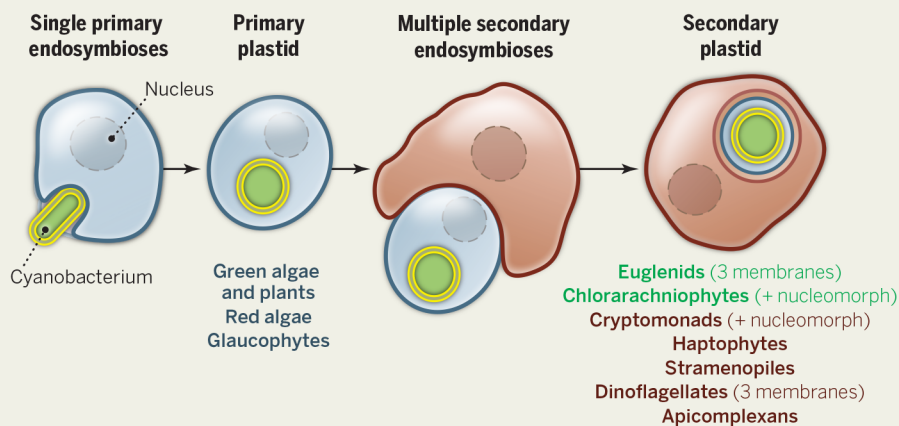
pods that are 50 times its size before consuming them (64). As a consequence, organism size does not necessarily increase with trophic level, allowing for a longer food chain and comparatively greater carbon losses. Although cell size may play a role in prey selection, so too does prey quality, relative abundance, and extracellular characteristics (21, 65–67), which thereby influence the flow of carbon through specific populations. Assimilation efficiencies vary among predators and prey types, as well as with prey quality and quantity. Growth and carbon assimilation by the predatory stramenopile *Picophagus flagellatus* (<2 μm) is very different when fed *Prochlorococcus* versus *Synechococcus*, resulting in differing carbon flows between trophic compartments (65). Additionally, trophic cascades are strengthened at higher temperatures, including grazing control of primary producers, but in a nutrient-dependent fashion (68, 69). The metabolic processes underlying heterotrophy appear to respond more strongly to temperature than does primary production, so that increased temperature results in a shift to more heterotrophic ecosystem metabolism (70).

Predatory activities also contribute to pools of DOM and POM. The marine DOM carbon pool is nearly equal to atmospheric CO_2 and about 200 times that in living marine biomass (71). Both DOM and POM are complex amalgams spanning a gradient of sizes and levels of recalcitrance. The operational definition of DOM—material passing through a 0.2- μm filter—means that it ranges from small molecules that can be transported directly into cells (osmotrophy) to large macromolecules or colloids that may require extracellular digestion (saprotrophy) prior to osmotrophic utilization. Labile forms of organic matter are quickly respired or assimilated by bacteria and protists into living POM (72, 73). Thus, labile DOM accounts for <0.2 Pg C of the 662 Pg C of measurable marine DOM in a recent global survey, and most of the organic carbon pool is resistant to oxidation on time scales from months to millennia (71).

The diversity of marine organic carbon compounds necessitates an elaborate network of heterotrophic strategies to decompose it. Most ocean models assume that DOM and POM are oxidized by a homogeneous class of prokaryotic heterotrophs that live largely by chemistry transacted at the cell surface via enzymes that modify, transport, and/or remineralize organic molecules (i.e., chemoheterotrophs). Ironically, although fungi are considered central to terrestrial decomposition, eukaryotic saprotrophs are not represented in ocean ecosystem models, despite growing evidence of diverse marine fungi (74, 75). Recent reports indicate that correlations exist between fungal populations and total organic carbon, nitrate, sulfide, and dissolved inorganic carbon, in anoxic marine pelagic environments and especially at the sea floor (76, 77). If fungi do contribute to marine organic matter degradation—an idea that has not yet been formally tested—it will be important to learn how flexible they are in this role. To what extent do they and other eukaryotes that function as marine saprotrophs compete for the same substrates? Labyrinthulids and thraustochytrids

Box 1. Evolutionary history of algal endosymbiosis and putative plastid losses.

Mitochondria and plastids both arose from the endosymbiotic uptake of a bacterium (an alphaproteobacterium and a cyanobacterium, respectively), but the subsequent evolution of plastids has been complicated by additional endosymbiosis events. The original or “primary” plastid that descended directly from the cyanobacterial endosymbiont is still found in the archaeplastids (glaucophytes, red algae, green algae, and plants). But green and red algae have themselves been taken up by other eukaryotic lineages, resulting in “secondary” plastids characterized by the additional membranes and more complex protein-targeting systems present in euglenids, chlorarachniophytes, cryptophytes, haptophytes (also referred to herein as prymnesiophytes), stramenopiles, dinoflagellates, and apicomplexans. Some members of these groups are mixotrophic, and others are purely heterotrophic (predatory, saprotrophic, or even parasitic) because photosynthesis or plastids have been lost. Although green algae are common in marine environments (e.g., picoprasinophytes such as *Bathycoccus*, *Ostreococcus*, and *Micromonas*), lineages resulting from secondary endosymbiotic partnerships include many other important marine primary producers (e.g., diatoms, pelagophytes, prymnesiophytes, and dinoflagellates) and represent incredible metabolic versatility. It is interesting to speculate that the redundancy and reshuffling of characteristics resulting from mergers of distinct eukaryotic lineages favors new combinations of traits with strong ecological potential.



are stramenopiles hypothesized to primarily use terrestrial organic matter present in coastal marine habitats, but they have also been reported in oligotrophic waters (78). Preliminary experiments suggest competition with prokaryotes (79), but to what extent is this true in nature? Are the activities of eukaryotic saprotrophs largely restricted to sediments, or do they operate in the water column as well?

Eukaryotes also use endocytosis to ingest high-molecular weight and colloidal DOM, rich sources of trace metals (80). The Picozoa ingest, then process marine colloids of <150 nm diameter in a vacuole (81). These colloids are similar in size to many marine eukaryotic viruses. Interestingly, virus sequences were detected in association with a sorted picozoan cell (82) potentially from an

infecting virus or food. Regardless, the discovery of colloid-sized particle ingestion by picozoans has important implications for remineralization rates, because intracellular processing is presumably more efficient than extracellular mechanisms.

Another means by which heterotrophic protists acquire nutrition is parasitism, an efficient strategy once the host is encountered. If life in oceans is anything like that on land, then for every marine animal species there are likely several parasite species. Infective life stages (Fig. 3, inset) allow more constant access to higher concentrations of organic material than are encountered by most free-living microbes. The most abundant sequences in marine protistan diversity surveys are novel uncultured marine alveolates (MALVs) that belong to the Syndiniales (21, 83).

Several Syndiniales groups are known to be parasitic and can control blooms of other marine dinoflagellates or infect ciliates, other protists, and animals (83–85). The interplay between the life cycles of one such parasite, *Amoebophrya*, and its dinoflagellate host is complicated, with infection speeding up host cyst formation in a response hypothesized to promote resistance to infection (84). Currently, direct evidence that most MALV clades are parasitic is lacking. Associations observed between uncharacterized MALVs and radiolarians (86) are equally consistent with a symbiotic relationship, and environmental factors could potentially shift a relationship from commensal to pathogenic. For MALVs that are parasitic, what taxa do they infect and by what mechanism? Is the outcome of infection benign

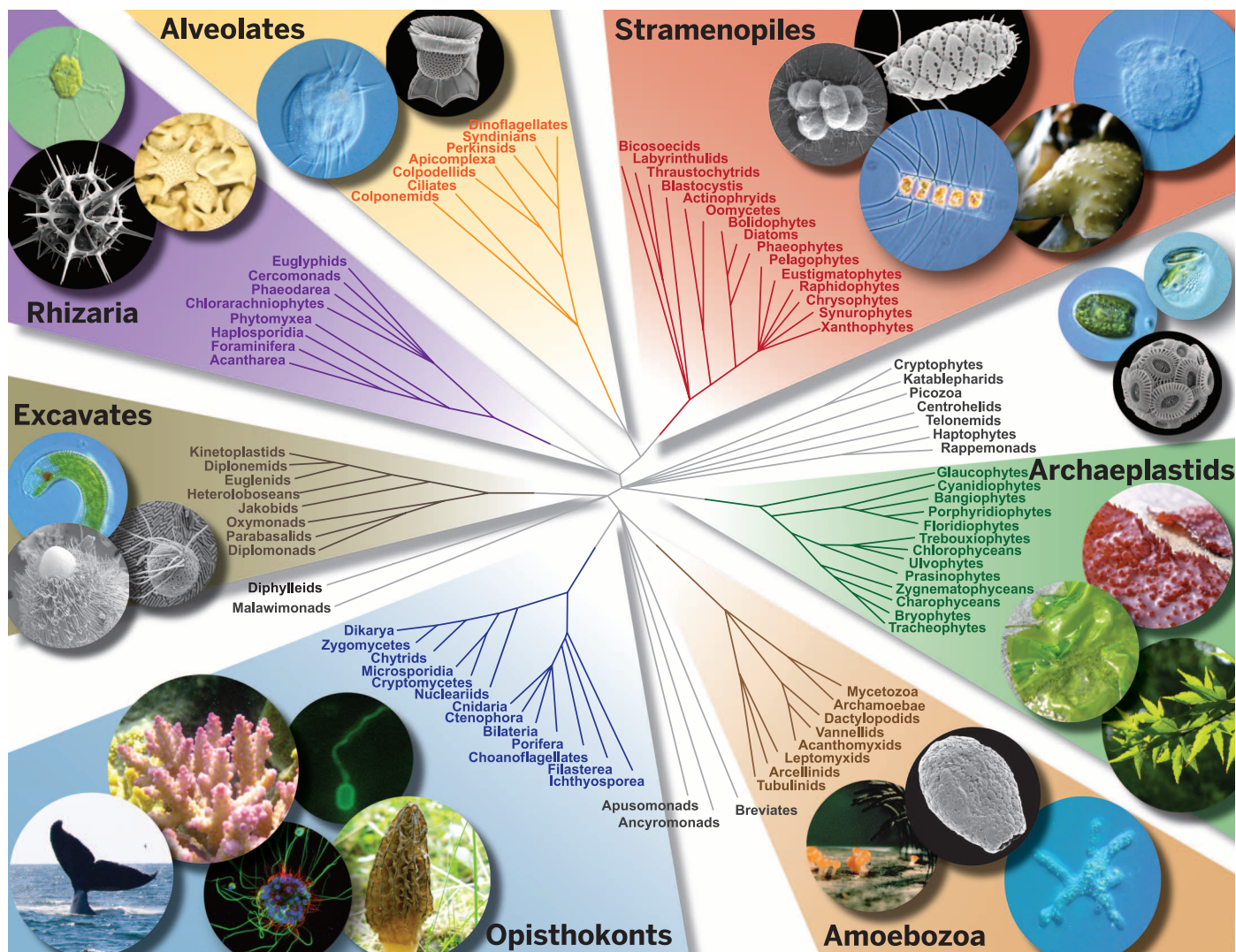


Fig. 2. Protists constitute the majority of lineages across the eukaryotic tree of life. This schematic represents a synthesis of information on morphology, phylogenetic analyses (based on a few genes from a large diversity of organisms), as well as phylogenomic analyses (of many genes from representatives of major lineages). Seven “supergroups” are indicated by colored wedges, all of which contain multiple marine protistan lineages. Relationships of groups listed outside the supergroups remain contentious. Peripheral pictures highlight eukaryotic diversity, both microbial and multicellular. Clockwise

from right: archaeplastids (rhodophyte, chlorophyte, streptophyte); amoebozoa (tubulinid, arcellinid, mycetozoa); opisthokonts (fungus, microsporidian, choanoflagellate, cnidarian, bilaterian); excavates (parabasalid, oxymonad, euglenid); rhizaria (acantharian, foraminiferan, chlorarachniophyte); alveolates (ciliate, dinoflagellate); stramenopiles (labyrinthulid, synurophyte, diatom, phaeophyte, actinophryid); unassigned [cryptomonad, katablepharid, haptophyte (referred to here as prymnesiophytes, and to which coccolithophores belong)]. [Phylogenomic analyses adapted from (158)]

or pathogenic? Do they have complex life cycles, reservoir species, or active free-living stages?

Parasitism presents challenges for ecosystem modeling, even if it is an easily interpretable nutritional mode. Thus, parasites, like protistan saprotrophs, have not been incorporated into ecosystem and carbon cycle models. What are the tradeoffs between protection against predation, resource acquisition strategies, and costs leveraged by high abundance that increase encounters with parasites and viruses? Some parasites also consume bacteria by phagocytosis. For example, the human parasite *Trichomonas vaginalis* has a predatory mode that remains “unseen” in its genome (87). Hence, the complexity of protistan trophic modes underscores the importance of study-

ing organisms in natural or near-natural milieus where sundry interaction possibilities are maintained.

Diverse metabolic pathways facilitate organic matter processing in all domains of life, but in eukaryotes the evolution of phagotrophy and parasitism, in addition to osmotrophy and saprotrophy, renders several carbon oxidation modes difficult to identify (Fig. 3). Phototrophy is easily recognized by huge, highly conserved macromolecular complexes that are found in plastids, the semi-autonomous organelles of photosynthetic protists (Box 1). In contrast, heterotrophy is a diverse amalgam of pathways that overlaps with widely distributed anaplerotic pathways that form intermediates used in both autotrophic and heterotrophic metabolisms. Moreover, the specific

mechanics of most types of protistan heterotrophy are shadowy. Genomic and proteomic studies could provide candidate genes for cell surface properties related to prey sensing (88) or host sensing by parasites. Although all aspects of these processes are doubtless driven by proteins encoded in nuclear genomes, these are likely to be among the ~50% of proteins in any given genome that have unknown functions (89). Because eukaryotic mechanisms relating to heterotrophy may have evolved in parallel (in contrast to shared ancestry of photosynthetic systems; Box 2), a master list of genes relating to feeding in one predator might have limited predictive power for other predatory lineages. As a result, we lack a catalog of genes responsible for the cellular components

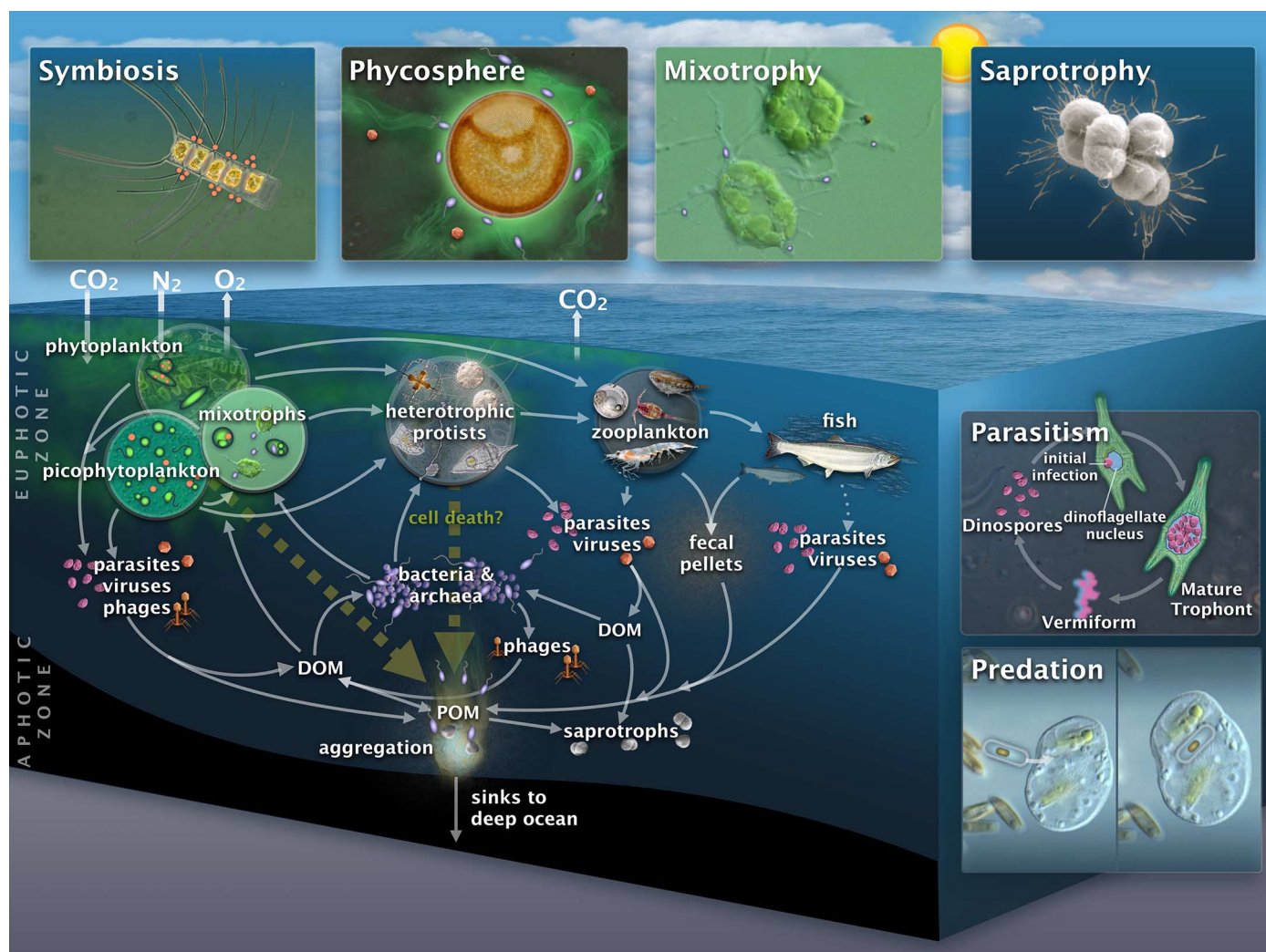


Fig. 3. Microbes from the three domains of life interact to structure ocean ecosystems and the carbon cycle. CO₂ fixation into organic matter is performed by diverse photosynthetic eukaryotes, as well as cyanobacteria, that have different food web linkages. Eukaryotes are involved in many interactions, as depicted in inset boxes. Some widespread phytoplankton consume other microbes (mixotrophs; see Box 2). Eukaryotic parasites are another force of mortality that presumably affects many types of eukaryotes (with host specificity), as do viral infections. Death by parasite or viral infection results in release of a continuum of nondissolvable organic matter (i.e., POM) and DOM, a complex suite of polymers and molecules. Programmed cell death

of protists (apoptosis; background arrow) has also been proposed. Microbes contribute to CO₂ respiration (e.g., archaea, heterotrophic bacteria, saprotrophs, parasites, mixotrophs, and even photosynthetic taxa at night), which can result in CO₂ release to the atmosphere and reduces organic carbon export to the deep ocean. Some eukaryotes grow in low-nitrogen regions by using symbiotic relationships with N₂-fixing bacteria (upper left box). The majority of protistan roles and linkages are not represented in ecosystem and carbon cycle models, and most have not yet been rigorously quantified. Inorganic nutrients and direct release of CO₂ depicted in Fig. 1 have been removed for simplification purposes. [Parasite life cycle adapted from (159)]

involved in protistan heterotrophy, such as feeding apparatuses, receptors for specific host or prey recognition factors, or signaling pathways that govern predatory behavior and trophic mode shifts.

Shifting boundaries between trophic modes: Mixotrophy

In addition to the oversimplification inherent in the convenient categories of “producers” (algae) and “consumers” (heterotrophs), a larger problem is that many protists do not even stick to one or the other role. Recognition that mixotrophy—a fusion of phototrophy and heterotrophy—is important arose in 1986, when seminal research on freshwater plankton showed that “...at least some natural phytoplankton are phagotrophic and apparently obtain a substantial fraction of their energy and nutrients by ingesting bacteria at rates very similar to those measured for nonphotosynthetic microflagellates” (90). This publication was quickly followed by reports on mixotrophic marine algae (91), and more recent shipboard experiments demonstrated that small algae perform 37 to 95% of total bacterivory in the Atlantic Ocean (32).

Phagotrophic capabilities in otherwise photosynthetic organisms have exciting ecological implications. Prey ingestion may serve as a source of energy and carbon when photosynthesis is limited by light availability (e.g., deep in the water column or under ice) (92). However, in oligotrophic euphotic waters where uncultured mixotrophic prymnesiophytes and chrysophytes (stramenopiles) are prominent (31, 93, 94), acquisition of nutrients needed for photosynthetic growth, not carbon, is considered the feeding trigger (32). Through prey digestion, demand for scarce inorganic nutrients is lessened because particulate nutrients (from the prey cell) support primary production,

thereby lowering release of remineralized nutrients relative to heterotrophic predation. In primarily heterotrophic mixotrophs, respiratory carbon needs can be met by photosynthesis, making high assimilation efficiencies possible (95). If group-specific predation (and photosynthetic inputs to growth) can be accurately estimated, the influences of dissolved inorganic nutrients and remineralization rates can be better assessed.

Little is known about how biotic and abiotic factors influence where a protist resides along the spectrum between heterotrophic and photoautotrophic growth at any given time, or species-level variability. Experiments are difficult, in part because most cultured predators, mixotrophic and otherwise, reside with prey communities and symbionts (if present) that restrict defined experimentation. Moreover, many groups are not represented in culture. Uncultured prymnesiophytes contribute significantly to open-ocean primary production (30, 31, 94). Some of these same prymnesiophytes are mixotrophic (93, 94) and consume *Prochlorococcus*, the most abundant photosynthetic organism on the planet (and presumably prey upon other picoplankton as well). If such organisms shift trophic modes opportunistically—perhaps to capture resources through predation when that strategy becomes more favorable—then the environmental triggers behind such a shift fundamentally reshape their ecosystem roles and food web dynamics.

Predatory protists, whether mixotrophic or strictly heterotrophic, will likely be affected by ocean change through direct temperature effects and by altered composition of prey. The mixotrophic chrysophyte *Ochromonas* switches to more heterotrophic nutrition under elevated temperatures, although it remains unknown whether higher CO₂ availability reverses this effect (96). A shift toward smaller phytoplankton, as observed

with warming in the Arctic and in ocean acidification experiments, favors nanoflagellate grazers over larger predators (50, 97). Altered phytoplankton stoichiometry (due to increased CO₂ availability) also affects copepod consumption rates, modifying growth and the fraction of organic carbon converted to CO₂ or excreted as DOM (98).

There are multiple further complications. For example, not all phototrophs rely on canonical oxidative photosynthesis. The light-driven proton pump proteorhodopsin, known from some marine bacteria (99), occurs in photosynthetic and heterotrophic eukaryotes (100). Its distribution and function are still poorly understood, but new copies are being found in additional lineages. Marine proteorhodopsins derived from eukaryotes were recovered in metagenomic surveys but were misinterpreted as being bacterially derived, until they were found and characterized in cultivated protists (100). This highlights the power of meta-omic approaches as well as the important role of reference data from cultured taxa in the process of extrapolating function from metagenomic data.

The role of behavior: Ecological capabilities beyond carbon processing

Typically, bacterial and archaeal diversity is manifested at the level of metabolism, whereas eukaryotic diversity is strongly influenced by their cellular structures and, by extension, behavior (101, 102). Bacteria and archaea do use sensing and motility (chemotaxis) to optimize their location and communicate by means of pheromones (103). Nonetheless, our view of how prokaryotes contribute to the marine carbon cycle (and food webs in general) is dominated by analyzing the sum of the enzymes and biochemical pathways they express, even when microscale heterogeneity (itself influenced by eukaryotic cells' activities, death, and aggregation) is taken into account (104–106). Comparative methods can be used to extrapolate these enzymes and pathways from genomic and metagenomic data reasonably well, which in turn allows hypotheses to be generated on their ecological roles, to be generated largely from sequence data.

For eukaryotes, the balance between metabolism and behavior is tipped in the opposite direction: Metabolism may be diverse, but environmental interactions are strongly guided by cellular structures and the behaviors they underpin. Protists can build traps and feeding apparatuses; they not only move about but often actively hunt down specific prey (57, 107). They also take actions to evade hunters or to build defenses against them. Protists actively capture other cells, take them up, and digest them or domesticate them (see below). These characteristics emerge from protein functions and interactions that are several degrees further removed from genomic sequence data than are enzymatic pathways. As a result, we are far less adept at reconstructing cellular structures and behavior from sequence data—or, by extension, the role of diverse eukaryotic microbes in the marine carbon cycle.

Of course there are exceptions; many eukaryotes take advantage of metabolic versatility much

Box 2. Lifestyles and specialized interaction zones.

- (i) Primary producer: Generates organic carbon by photosynthesis and CO₂ fixation (the role traditionally played by phytoplankton).
- (ii) Osmotrophy: Cells take up organic material from the external environment as small molecules or macromolecules.
- (iii) Saprotrophy: A mode of osmotrophy whereby extracellular digestion is involved in processing or recycling organic matter, also often referred to as chemoheterotrophy.
- (iv) Predation: Consumption of prey cells, often by phagocytosis.
- (v) Mixotrophic predation: A combination of phototrophic and heterotrophic metabolism. In some cases, mixotrophs may alternate between trophic mechanisms (e.g., predation, which can result in release of CO₂, and photosynthesis, resulting in capture of CO₂).
- (vi) Parasitism: Defined here as one organism existing in association with another to the detriment of that partner (Fig. 3 inset shows a dinoflagellate infected by *Amoebophrya*).
- (vii) Phycosphere: A region surrounding phytoplankton cells that results from the basic physics of the diffusive boundary layer and has a higher concentrations of organic matter (produced by the eukaryote) than local waters. This zone attracts free-living prokaryotes, some of which may attach (and could also include other eukaryotes). The zone of influence in the fluid medium is disproportionately greater for larger phytoplankton cells and is considered akin to the rhizosphere (Fig. 3 inset depicts a diatom phycosphere containing bacteria).
- (viii) Symbioses: Defined here as mutualistic relationships where one species lives on or within another species (Fig. 3 inset shows a diatom with N₂-fixing cyanobacteria on its spines).

as bacteria do (e.g., fungi), and some ecologically important activities are readily interpreted from genomic data (e.g., photosynthesis). But, as we have seen above, we lack the catalog of gene functions needed to recognize many trophic behaviors, or the mechanisms that control shifts between trophic modes. This problem is particularly acute for free-living protistan heterotrophs and mixotrophs, many of which are the most structurally complex but least investigated microbial cells.

Complexity through associations: Phycosphere, symbioses, and viruses

Heterogeneities in carbon pools will also be affected by physical associations, some of which are mutualistic. Bacteria (and potentially archaea and protists) actively detect and take up exuded extracellular products in the zone around phytoplankton known as the phycosphere (Box 2 and Fig. 3) (106, 108–110). The associated bacteria can be attached, or motile and unattached, but so far phycosphere interactions and the molecules exchanged have proven difficult to discern.

Symbiotic associations involving protists are also well known, although overlooked in microbial food web dynamics. Many involve metabolite exchanges, sometimes where the protist is a symbiont within an animal (e.g., algae in corals), or where heterotrophic protists play host to bacterial or eukaryotic algal symbionts, or algal organelles retained by kleptoplastidy (111–114). Thus, mixotrophy is not restricted to phytoplankton capable of phagocytosis, but is also widespread among heterotrophic ciliates, dinoflagellates, foraminifera, and acantharians (59, 115). Obligate N_2 -fixing cyanobacterial symbionts are present in some diatoms, dinoflagellates, and prymnesiophytes (116–118), although destructive sampling of the latter initially led to the mistaken conclusion that the symbionts were free-living cells, thus emphasizing the value of visual observation. These symbioses allow goods exchanges, including newly fixed N , that represent alternative resource acquisition strategies for the hosts. They thereby stimulate productivity and influence overall nitrogen availability (119).

Viruses play important but unquantified roles in structuring microbial communities and interrupt flows of carbon and nutrients through the microbial loop (10, 120–122). Labile DOM generated through viral-mediated cell lysis can be rapidly assimilated and remineralized by microbes, promoting nutrient retention in the euphotic zone and potentially decreasing the efficiency of carbon export to the deep sea (121–123). However, infection of photosynthetic protists can also enhance production of exudates, which stimulate particle aggregation and facilitate export (123, 124). Notably, viruses can influence predator populations directly by infection and lysis or by reducing prey availability (122, 125). Indirect effects involve increased bacterial growth on released DOM and POM, resulting in community changes. Moreover, viruses themselves may serve as food particles.

Like their hosts, fundamental differences between eukaryotic viruses and phages necessitate

separate empirical methods for characterization and explicit inclusion in marine food webs (Fig. 3). Some eukaryotic viruses appear to exploit mechanisms of programmed cell death during lysis (124), and some may promote sexual cycling in species where ploidy level determines viral susceptibility (126), but this and other resistance mechanisms are not well understood (127). An extreme example of how marine eukaryotic viruses differ from phages is the giant virus that infects a predatory stramenopile alongside a smaller “virophage” that parasitizes the giant virus (128). The diversity of protists and their viruses may preclude broad commonalities for several aspects of interactions (121). Challenges moving forward include linking natural viruses (and viral sequences) to actual hosts, examining viruses as food particles, and incorporating the nuances of species-specific viral interactions in ecosystem models.

Diverse data for a complex problem

An overwhelming volume of sequence data is being collected and analyzed from marine microbes. Its value for characterizing protistan contributions to autotrophic and heterotrophic functionality, and teasing apart their interactions with other microbes and consequent influences on biogeochemical cycles, will be maximized by tools and approaches tailored to the unique biology of protists. Statistical approaches that detect interactions between organisms using co-occurrence networks can help development of hypotheses about the ecology of eukaryotic plankton (129, 130). Massive sequencing of marker genes (or even metagenomic and metatranscriptomic sequences) provides such data, with the caveat that for success large numbers of samples are needed, as are experimental designs that adequately cover key environmental variables and involve rate measurements.

Although rare, studies designed to capture physical associations between cells provide critical avenues for validating ecological interaction networks. For example, genome reconstruction can help to identify traded services, the hallmark of symbioses. Thus, “single cell” sequencing with enough coverage to highlight key metabolic pathways absent from one but present in the other partner can provide evidence of symbiosis. A robust example with relevance to global geochemical models is N_2 fixation by symbionts (116–118). However, in cases involving new and unknown interactions, sequencing alone may not resolve the true nature of interactions, but rather can lead to (mis)interpretation as symbiosis, contamination, predation, presence of osmotrophically degraded material, infection, or even a horizontal gene transfer (131).

A few “rules” that have ensured success in meta-omic studies are not as readily met by protists. These are (i) having a reference genome to help recruit relevant sequences [not the case for most marine protists because only ~20 genomes are available]; (ii) having a small genome and sufficient sequencing depth [genome sizes from free-living protists vary from ~10 MB to much

larger than the human genome]; and (iii) having low system diversity (i.e., few taxa present)—a situation sometimes true in extreme environments, but not commonly so. Eukaryotes present other types of genome complexity as well, such as regions of widely varied composition that complicate binning without a reference genome (89) and “mosaic” phylogenetic signals that require deciphering complex evolutionary histories (2, 31, 43, 44, 132). Transcriptome sequencing and assembly has improved protistan reference databases while minimizing genome structural complexity issues (133). Another strategy used to sidestep such issues for wild planktonic protists is cell sorting based on optical signatures, which raises coverage of target organisms by suppressing diversity, making genome assembly more likely (26, 31, 62, 82, 134–136). Microfluidic approaches that sort cells by imaging and thereby link genomes to morphology will further surmount these problems (136). Higher-throughput applications of these technologies are needed to expand genomic representation of protistan complexity.

Biology has much to gain from expanded genomic coverage of protistan diversity, especially as a broader range of trophic strategy variants is investigated. Marine protistan genomes sequenced thus far have resulted in massive strides in understanding the origins of multicellularity (137, 138), intron evolution (139, 140), genome integration and control (43), and even fundamental aspects of methylation, nucleosome positioning, and chromatin compaction (141). Major gains will also be made for marine phytoplankton, given that the evolutionary distance between the two genome-sequenced diatom genera (*Thalassiosira* and *Phaeodactylum*) is greater than that between humans and fish (132), and marker analysis of different clades within the prasinophyte genus *Micromonas* shows divergence equivalent to the separation between corn and rice (139, 142).

Still, genomics has limits. So, as questions about the carbon cycling activities of protists are formulated in greater detail, we need to ask: Where are new strategies needed? One such area involves functional studies on ecologically important model organisms in environmentally relevant conditions. For example, omic data facilitated the discovery that microbes previously considered dependent on exogenous vitamin B_1 grow in its absence, but only after pathway gap theory (143) was implemented together with experiments on cultured species (144, 145). What was thought to represent (incomplete) pathways in the evolutionary process of reduction is actually a noncanonical vitamin pathway dependent on the import of a precursor that can be more abundant in seawater than the vitamin itself. Once understood in a few cultured organisms, the B_1 (thiamine) metabolism of diverse planktonic bacteria and eukaryotic phytoplankton could be reinterpreted (144, 145). These discoveries change “facts” regarding phytoplankton bloom controls and reveal the likely involvement of several proteins of unknown function in thiamine biosynthesis. Such studies illustrate that the power of comparative approaches is contingent on reference data, but more importantly that

the greatest gain is harvested from omic data sets when paired with detailed studies on the biology of strategically chosen marine taxa.

One of the biggest obstacles to interpreting protistan genomes is the dearth of information about the evolution of proteins that control behaviors such as mixotrophy, predation, and parasitism, as well as regulatory strategies—for example, those that control energy allocation (146) to optimize growth. The recent discovery of extensive oxidative metabolism for one-carbon and methylated compounds in the hyperabundant Pelagibacterales clade of marine bacteria illustrates how geochemically important information lay within plain view in genomes for a decade before being deciphered (147). This discovery focused attention on a neglected but apparently important sector of the carbon cycle: methylated and volatile compounds. This brings us to a second answer to the “Where are new strategies needed?” question. A great deal can be garnered from pathway gap theory, but in the end, studies that infer higher-order function from genomes are founded on experimental proof of protein functions. One of the biggest impediments to systems biology and ecosystems biology (104, 148) approaches is that the majority of important marine protistan groups (even algae) lack representatives with established genetic systems. Robust but relatively low-efficiency manipulation systems exist for two algae with limited marine distributions: the diminutive piceoeukaryote *Ostreococcus tauri* (149) and the diatom *Phaeodactylum tricornutum* (150). New knowledge on marine protistan diversity and distributions calls for concerted initiatives to develop genetic systems that target ecologically relevant lineages from across the eukaryotic tree, and to develop parallel technologies such as CRISPR (clustered regularly interspaced short palindromic repeat) and TALEN (transcription activator–like effector nuclease)–based gene editing. These, as well as sampling that preserves microbe–microbe interactions, improved visualization, and experiments in advanced bioreactors that allow testing of multifactorial impacts, precise modulation of CO₂, light, and nutrients, and real-time measurements of physiological parameters, are key steps forward.

Ecological and biogeochemical modeling

Rapidly advancing bioinformatic and statistical approaches must be complemented by mechanistic models that encapsulate and synthesize understanding of complex systems at cellular, community, and global scales. Marine protistan diversity presents challenges for theory and modeling: Can we understand the rich and flexible ecology of these functionally diverse organisms to interpret and simulate it with mathematical and numerical models? What facets of their biology affect carbon flow and sequestration sufficiently to warrant inclusion in climate and carbon cycle models? Consider mixotrophy: Now that field studies show its prevalence [e.g., (32, 94)], should global carbon cycle models that currently only separate autotrophy and heterotrophy capture this complexity? To date, the costs and ben-

efits of mixotrophic predation have been addressed by few studies (151–153). This emphasizes the need to evaluate trophic strategies with data and modeling, explore their biogeochemical importance and food web impacts, and assess how they modify predictions by global models.

Modeling paradigms generally resolve a few coarse phytoplankton phenotypes with highly simplified carbon and nutrient flows between them. Currently, diversity within a few functional types related to cell size or temperature adaptations can also be resolved (14). Yet many chemical exchanges occur between protists and their neighbors; are these simplified descriptions sufficient to describe the system? Of particular interest is how diversity and connectivity affect system stability—a question long debated in the context of food webs (154). The ability to predict how plankton populations and their biogeochemical roles respond to a changing environment is tightly linked to this question. For example, in a recent five-box model, the relative abundance of fast- and slow-growing phytoplankton taxa controlled community elemental composition and new nitrogen import rates (155). In another study, inclusion of contributions from various system members (including microbes) helped to reconcile aphotic zone flux terms that were long out of balance (156). These studies highlight the need for improved input data (even relating to the basic elemental stoichiometry of different algae), but also demonstrate that idealized models can be tools for exploring how complex networks behave and for generating hypotheses that can be tested in the lab and field.

The black-box descriptions of physiology used in current ecosystem models neglect the powerful constraints of redox and energy balance that become explicit once cellular metabolism is resolved. Environmental engineers have exploited these constraints using schematic metabolic networks. Flux balance analysis (157), a tool from systems biology, extends this approach to provide mechanistic, quantitative predictions of growth rates and efficiencies rooted in genome-scale metabolic reconstructions. Such a goal requires considerable advances in protein function annotations, as well as rigorous testing with model organisms. However, looking forward, the application of flux balance analysis in models of marine ecosystems will enable a vastly richer repertoire of applications and will bring empirical and theoretical perspectives together with a common language.

Conclusions

The complexity of protistan behaviors will test the perspective that mechanistic models of cell functions can be merged with global models to understand marine ecosystems. How scientists will winnow this complexity to find those kernels of protistan biology most important for ocean ecosystem-level processes and carbon cycling remains to be seen. The diverse biology of protists is not yet understood well enough to fully evaluate their whole impact on biogeochemical models, but enough is known to say their roles must be reevaluated. Protistan genomes and behaviors

are innately challenging to decipher but are essential to dissecting trophic connections. Technologies that overcome scale-related issues of sequencing and proteome analyses are helping, as is the application of network theory and modeling to identify ecological links and generate testable hypotheses. As hypothetical links are identified, the challenge is to validate them by characterizing the underlying mechanisms, constrain them by empirical measurements, and parameterize them into global biogeochemical models. The most direct source of data on trophic modes and interactions will come from studying cells at multiple levels, integrating cell and structural biology, physiology, and behavior. Combining investigations of cellular systems with a broader sampling of eukaryotic diversity will empower comparative approaches with the promise of substantial progress in quantifying activities of protists and their impacts on the global carbon cycle.

REFERENCES AND NOTES

- C. B. Field, M. J. Behrenfeld, J. T. Randerson, P. Falkowski, Primary production of the biosphere: Integrating terrestrial and oceanic components. *Science* **281**, 237–240 (1998). doi: [10.1126/science.281.5374.237](https://doi.org/10.1126/science.281.5374.237); pmid: [9657713](https://pubmed.ncbi.nlm.nih.gov/9657713/)
- E. V. Armbrust, The life of diatoms in the world's oceans. *Nature* **459**, 185–192 (2009). doi: [10.1038/nature08057](https://doi.org/10.1038/nature08057); pmid: [19444204](https://pubmed.ncbi.nlm.nih.gov/19444204/)
- M. B. Higgins, R. S. Robinson, J. M. Husson, S. J. Carter, A. Pearson, Dominant eukaryotic export production during ocean anoxic events reflects the importance of recycled NH₄⁺. *Proc. Natl. Acad. Sci. U.S.A.* **109**, 2269–2274 (2012). doi: [10.1073/pnas.1104313109](https://doi.org/10.1073/pnas.1104313109); pmid: [22315397](https://pubmed.ncbi.nlm.nih.gov/22315397/)
- P. J. Tréguer, C. L. De La Rocha, The world ocean silica cycle. *Annu. Rev. Mar. Sci.* **5**, 477–501 (2013). doi: [10.1146/annurev-marine-121211-172346](https://doi.org/10.1146/annurev-marine-121211-172346)
- K. R. Hendry, M. A. Brzezinski, Using silicon isotopes to understand the role of the Southern Ocean in modern and ancient biogeochemistry and climate. *Quat. Sci. Rev.* **89**, 13–26 (2014). doi: [10.1016/j.quascirev.2014.01.019](https://doi.org/10.1016/j.quascirev.2014.01.019)
- J. P. Zehr, R. M. Kudela, Nitrogen cycle of the open ocean: From genes to ecosystems. *Annu. Rev. Mar. Sci.* **3**, 197–225 (2011). doi: [10.1146/annurev-marine-120709-142819](https://doi.org/10.1146/annurev-marine-120709-142819)
- S. C. Doney et al., Climate change impacts on marine ecosystems. *Annu. Rev. Mar. Sci.* **4**, 11–37 (2012). doi: [10.1146/annurev-marine-041911-111611](https://doi.org/10.1146/annurev-marine-041911-111611)
- L. Pomeroy, The ocean's food web, a changing paradigm. *Bioscience* **24**, 499–504 (1974). doi: [10.2307/1296885](https://doi.org/10.2307/1296885)
- F. Azam et al., The ecological role of water-column microbes in the sea. *Mar. Ecol. Prog. Ser.* **10**, 257–263 (1983). doi: [10.3354/meps010257](https://doi.org/10.3354/meps010257)
- M. Breitbart, Marine viruses: Truth or dare. *Annu. Rev. Mar. Sci.* **4**, 425–448 (2012). doi: [10.1146/annurev-marine-120709-142805](https://doi.org/10.1146/annurev-marine-120709-142805)
- G. A. Riley, Factors controlling phytoplankton populations on Georges Bank. *J. Mar. Res.* **6**, 54–73 (1946).
- C. Le Quéré et al., Ecosystem dynamics based on plankton functional types for global ocean biogeochemistry models. *Global Change Biol.* **11**, 2016–2040 (2005).
- J. K. Moore, S. C. Doney, K. Lindsay, Upper ocean ecosystem dynamics and iron cycling in a global three-dimensional model. *Global Biogeochem. Cycles* **18**, GB4028 (2004). doi: [10.1029/2004GB002220](https://doi.org/10.1029/2004GB002220)
- M. J. Follows, S. Dutkiewicz, S. Grant, S. W. Chisholm, Emergent biogeography of microbial communities in a model ocean. *Science* **315**, 1843–1846 (2007). pmid: [17395828](https://pubmed.ncbi.nlm.nih.gov/17395828/)
- J. Monod, The growth of bacterial cultures. *Annu. Rev. Microbiol.* **3**, 371–394 (1949). doi: [10.1146/annurev.mi.03.100149.002103](https://doi.org/10.1146/annurev.mi.03.100149.002103)
- M. R. Droop, Vitamin B₁₂ and marine ecology. IV. The kinetics of uptake, growth and inhibition in *Monochrysis lutheri*. *J. Mar. Biol. Assoc. U.K.* **48**, 689–733 (1968). doi: [10.1017/S0025315400019238](https://doi.org/10.1017/S0025315400019238)
- D. A. Caron, A. Z. Worden, P. D. Countway, E. Demir, K. B. Heidelberg, Protists are microbes too: A perspective. *ISME J.* **3**, 4–12 (2009). doi: [10.1038/ismej.2008.101](https://doi.org/10.1038/ismej.2008.101); pmid: [19005497](https://pubmed.ncbi.nlm.nih.gov/19005497/)
- P. Ziveri, B. de Bernardi, K. H. Baumann, H. M. Stoll, P. G. Mortyn, Sinking of coccolith carbonate and potential contribution to organic carbon ballasting in the deep ocean. *Deep Sea Res. II* **54**, 659–675 (2007). doi: [10.1016/j.dsr.2.2007.01.006](https://doi.org/10.1016/j.dsr.2.2007.01.006)

19. B. A. Ward, S. Dutkiewicz, O. Jahn, M. J. Follows, A size-structured food-web model for the global ocean. *Limnol. Oceanogr.* **57**, 1877–1891 (2012). doi: [10.4319/lo.2012.57.6.1877](https://doi.org/10.4319/lo.2012.57.6.1877)
20. T. L. Richardson, G. A. Jackson, Small phytoplankton and carbon export from the surface ocean. *Science* **315**, 838–840 (2007). doi: [10.1126/science.1133471](https://doi.org/10.1126/science.1133471); pmid: 17289995
21. R. Massana, Eukaryotic picoplankton in surface oceans. *Annu. Rev. Microbiol.* **65**, 91–110 (2011). doi: [10.1146/annurev-micro-090110-102903](https://doi.org/10.1146/annurev-micro-090110-102903); pmid: 21639789
22. D. A. Caron, P. D. Countway, A. C. Jones, D. Y. Kim, A. Schnetzer, Marine protistan diversity. *Annu. Rev. Mar. Sci.* **4**, 467–493 (2012). doi: [10.1146/annurev-marine-120709-142802](https://doi.org/10.1146/annurev-marine-120709-142802)
23. E. W. Knight-Jones, P. R. Walne, *Chromulina pusilla* Butcher; a dominant member of the ultraplankton. *Nature* **167**, 445–446 (1951). doi: [10.1038/167445a0](https://doi.org/10.1038/167445a0); pmid: 14826795
24. J. B. Waterbury, S. W. Watson, R. R. L. Guillard, L. E. Brand, Widespread occurrence of a unicellular, marine, planktonic, cyanobacterium. *Nature* **277**, 293–294 (1979). doi: [10.1038/277293a0](https://doi.org/10.1038/277293a0)
25. S. W. Chisholm et al., A novel free-living prochlorophyte abundant in the oceanic euphotic zone. *Nature* **334**, 340–343 (1988). doi: [10.1038/334340a0](https://doi.org/10.1038/334340a0)
26. A. Z. Worden et al., Global distribution of a wild alga revealed by targeted metagenomics. *Curr. Biol.* **22**, R675–R677 (2012). doi: [10.1016/j.cub.2012.07.054](https://doi.org/10.1016/j.cub.2012.07.054); pmid: 22974991
27. E. Kim et al., Newly identified and diverse plastid-bearing branch on the eukaryotic tree of life. *Proc. Natl. Acad. Sci. U.S.A.* **108**, 1496–1500 (2011). doi: [10.1073/pnas.101337108](https://doi.org/10.1073/pnas.101337108); pmid: 21205890
28. J. Janouskovec, A. Horák, K. L. Barott, F. L. Rohwer, P. J. Keeling, Global analysis of plastid diversity reveals apicomplexan-related lineages in coral reefs. *Curr. Biol.* **22**, R518–R519 (2012). doi: [10.1016/j.cub.2012.04.047](https://doi.org/10.1016/j.cub.2012.04.047); pmid: 22789997
29. A. Z. Worden, J. K. Nolan, B. Palenik, Assessing the dynamics and ecology of marine picophytoplankton: The importance of the eukaryotic component. *Limnol. Oceanogr.* **49**, 168–179 (2004). doi: [10.4319/lo.2004.49.1.0168](https://doi.org/10.4319/lo.2004.49.1.0168)
30. L. Jardillier, M. V. Zubkov, J. Pearman, D. J. Scanlan, Significant CO₂ fixation by small prymnesiophytes in the subtropical and tropical northeast Atlantic Ocean. *ISME J.* **4**, 1180–1192 (2010). doi: [10.1038/ismej.2010.36](https://doi.org/10.1038/ismej.2010.36); pmid: 20393575
31. M. L. Cuvelier et al., Targeted metagenomics and ecology of globally important uncultured eukaryotic phytoplankton. *Proc. Natl. Acad. Sci. U.S.A.* **107**, 14679–14684 (2010). doi: [10.1073/pnas.1001665107](https://doi.org/10.1073/pnas.1001665107); pmid: 20668244
32. M. Hartmann et al., Mixotrophic basis of Atlantic oligotrophic ecosystems. *Proc. Natl. Acad. Sci. U.S.A.* **109**, 5756–5760 (2012). doi: [10.1073/pnas.1118179109](https://doi.org/10.1073/pnas.1118179109); pmid: 22451938
33. S. M. Adl et al., The revised classification of eukaryotes. *J. Eukaryot. Microbiol.* **59**, 429–514 (2012). doi: [10.1111/j.1550-7408.2012.00644.x](https://doi.org/10.1111/j.1550-7408.2012.00644.x); pmid: 23020233
34. L. Beaufort et al., Sensitivity of coccolithophores to carbonate chemistry and ocean acidification. *Nature* **476**, 80–83 (2011). doi: [10.1038/nature10295](https://doi.org/10.1038/nature10295); pmid: 21814280
35. S. C. Doney, V. J. Fabry, R. A. Feely, J. A. Kleypas, Ocean acidification: The other CO₂ problem. *Annu. Rev. Mar. Sci.* **1**, 169–192 (2009). doi: [10.1146/annurev.marine.010908.163834](https://doi.org/10.1146/annurev.marine.010908.163834)
36. A. Monnier et al., Orchestrated transcription of biological processes in the marine picoeukaryote *Ostreococcus* exposed to light/dark cycles. *BMC Genomics* **11**, 192 (2010). doi: [10.1186/1471-2164-11-192](https://doi.org/10.1186/1471-2164-11-192); pmid: 20307298
37. A. E. Allen et al., Evolution and metabolic significance of the urea cycle in photosynthetic diatoms. *Nature* **473**, 203–207 (2011). doi: [10.1038/nature10074](https://doi.org/10.1038/nature10074); pmid: 21562560
38. M. Lommer et al., Genome and low-iron response of an oceanic diatom adapted to chronic iron limitation. *Genome Biol.* **13**, R66 (2012). doi: [10.1186/gb-2012-13-7-r66](https://doi.org/10.1186/gb-2012-13-7-r66); pmid: 22835381
39. J. Ashworth et al., Genome-wide diel growth state transitions in the diatom *Thalassiosira pseudonana*. *Proc. Natl. Acad. Sci. U.S.A.* **110**, 7518–7523 (2013). doi: [10.1073/pnas.1300962110](https://doi.org/10.1073/pnas.1300962110); pmid: 23596211
40. D. Duanmu et al., Marine algae and land plants share conserved phytochrome signaling systems. *Proc. Natl. Acad. Sci. U.S.A.* **111**, 15827–15832 (2014). doi: [10.1073/pnas.1416751111](https://doi.org/10.1073/pnas.1416751111)
41. S. J. Bender, C. A. Durkin, C. T. Berthiaume, R. L. Morales, E. V. Armbrust, Transcriptional responses of three model diatoms to nitrate limitation of growth. *Front. Mar. Sci.* **1**, article 3 (2014). doi: [10.3389/fmars.2014.00003](https://doi.org/10.3389/fmars.2014.00003)
42. C. J. Gobler et al., Niche of harmful alga *Aureococcus anophagefferens* revealed through ecogenomics. *Proc. Natl. Acad. Sci. U.S.A.* **108**, 4352–4357 (2011). doi: [10.1073/pnas.1016106108](https://doi.org/10.1073/pnas.1016106108); pmid: 21368207
43. B. A. Curtis et al., Algal genomes reveal evolutionary mosaicism and the fate of nucleomorphs. *Nature* **492**, 59–65 (2012). doi: [10.1038/nature11681](https://doi.org/10.1038/nature11681); pmid: 23201678
44. B. A. Read et al., Pan genome of the phytoplankton *Emiliania* underpins its global distribution. *Nature* **499**, 209–213 (2013). doi: [10.1038/nature12221](https://doi.org/10.1038/nature12221); pmid: 23760476
45. A. Marchetti et al., Comparative metatranscriptomics identifies molecular bases for the physiological responses of phytoplankton to varying iron availability. *Proc. Natl. Acad. Sci. U.S.A.* **109**, E317–E325 (2012). doi: [10.1073/pnas.1118408109](https://doi.org/10.1073/pnas.1118408109); pmid: 22380424
46. E. M. Bertrand et al., Influence of cobalamin scarcity on diatom molecular physiology and identification of a cobalamin acquisition protein. *Proc. Natl. Acad. Sci. U.S.A.* **109**, E1762–E1771 (2012). doi: [10.1073/pnas.1201731109](https://doi.org/10.1073/pnas.1201731109); pmid: 22652568
47. P. W. Boyd et al., Marine phytoplankton temperature versus growth responses from polar to tropical waters—outcome of a scientific community-wide study. *PLOS ONE* **8**, e63091 (2013). doi: [10.1371/journal.pone.0063091](https://doi.org/10.1371/journal.pone.0063091); pmid: 23704890
48. J. Beardall, S. Stojkovic, S. Larsen, Living in a high CO₂ world: Impacts of global climate change on marine phytoplankton. *Plant Ecol. Divers.* **2**, 191–205 (2009). doi: [10.1080/17550870903271363](https://doi.org/10.1080/17550870903271363)
49. U. Riebesell, A. Körtzinger, A. Oschlies, Sensitivities of marine carbon fluxes to ocean change. *Proc. Natl. Acad. Sci. U.S.A.* **106**, 20602–20609 (2009). doi: [10.1073/pnas.0813291106](https://doi.org/10.1073/pnas.0813291106); pmid: 19959581
50. W. K. W. Li, F. A. McLaughlin, C. Lovejoy, E. C. Carmack, Smallest algae thrive as the Arctic Ocean freshens. *Science* **326**, 539 (2009). doi: [10.1126/science.1179798](https://doi.org/10.1126/science.1179798); pmid: 19900890
51. A. Boetius et al., Export of algal biomass from the melting Arctic sea ice. *Science* **339**, 1430–1432 (2013). doi: [10.1126/science.1231346](https://doi.org/10.1126/science.1231346); pmid: 23413190
52. P. W. Boyd, D. A. Hutchins, Understanding the responses of ocean biota to a complex matrix of cumulative anthropogenic change. *Mar. Ecol. Prog. Ser.* **470**, 125–135 (2012). doi: [10.3354/meps10121](https://doi.org/10.3354/meps10121)
53. C. Schmoker, S. Hernandez-Leon, A. Calbet, Microzooplankton grazing in the oceans: Impacts, data variability, knowledge gaps and future directions. *J. Plankton Res.* **35**, 691–706 (2013). doi: [10.1093/plankt/fbt023](https://doi.org/10.1093/plankt/fbt023)
54. E. B. Sherr, B. F. Sherr, C. Ross, Deep-Sea Res. **94**, 57–67 (2013).
55. R. Massana et al., Grazing rates and functional diversity of uncultured heterotrophic flagellates. *ISME J.* **3**, 588–596 (2009). doi: [10.1038/ismej.2008.130](https://doi.org/10.1038/ismej.2008.130); pmid: 19129862
56. Y. C. Lin et al., Distribution patterns and phylogeny of marine stramenopiles in the north Pacific Ocean. *Appl. Environ. Microbiol.* **78**, 3387–3399 (2012). doi: [10.1128/AEM.06952-11](https://doi.org/10.1128/AEM.06952-11); pmid: 22344659
57. M. J. Dayel, N. King, Prey capture and phagocytosis in the choanoflagellate *Salpingoeca rosetta*. *PLOS ONE* **9**, e95577 (2014). doi: [10.1371/journal.pone.0095577](https://doi.org/10.1371/journal.pone.0095577); pmid: 24806026
58. N. R. Swanberg, D. A. Caron, Patterns of sarcodine feeding in epipelagic oceanic plankton. *J. Plankton Res.* **13**, 287–312 (1991). doi: [10.1093/plankt/13.2.287](https://doi.org/10.1093/plankt/13.2.287)
59. J. Decelle et al., An original mode of symbiosis in open ocean plankton. *Proc. Natl. Acad. Sci. U.S.A.* **109**, 18000–18005 (2012). doi: [10.1073/pnas.1212303109](https://doi.org/10.1073/pnas.1212303109); pmid: 23071304
60. F. Gómez, D. Moreira, K. Benzerara, P. López-García, *Solenicola setigera* is the first characterized member of the abundant and cosmopolitan uncultured marine stramenopile group MAST-3. *Environ. Microbiol.* **13**, 193–202 (2011). doi: [10.1111/j.1462-2920.2010.02320.x](https://doi.org/10.1111/j.1462-2920.2010.02320.x); pmid: 20722698
61. R. Massana, J. del Campo, M. E. Sieracki, S. Audic, R. Logares, Exploring the uncultured microeukaryote majority in the oceans: Reevaluation of ribogroups within stramenopiles. *ISME J.* **8**, 854–866 (2014). doi: [10.1038/ismej.2013.204](https://doi.org/10.1038/ismej.2013.204); pmid: 24196325
62. R. S. Roy et al., Single cell genome analysis of an uncultured heterotrophic stramenopile. *Sci. Rep.* **4**, 4780 (2014). doi: [10.1038/srep04780](https://doi.org/10.1038/srep04780); pmid: 24759094
63. U. Tillmann, Phagotrophy by a plastidic haptophyte, *Prymnesium patelliferum*. *Aquat. Microb. Ecol.* **14**, 155–160 (1998). doi: [10.3354/ame014155](https://doi.org/10.3354/ame014155)
64. T. Berge, L. K. Poulsen, M. Moldrup, N. Daugbjerg, P. Juel Hansen, Marine microalgae attack and feed on metazoans. *ISME J.* **6**, 1926–1936 (2012). doi: [10.1038/ismej.2012.29](https://doi.org/10.1038/ismej.2012.29); pmid: 22513533
65. L. Guillou, S. Jacquet, M. Chretiennot-Dinet, D. Vault, Grazing impact of two small heterotrophic flagellates on *Prochlorococcus* and *Synechococcus*. *Aquat. Microb. Ecol.* **26**, 201–207 (2001). doi: [10.3354/ame026201](https://doi.org/10.3354/ame026201)
66. A. Z. Worden, B. J. Binder, Application of dilution experiments for measuring growth and mortality rates among *Prochlorococcus* and *Synechococcus* populations in oligotrophic environments. *Aquat. Microb. Ecol.* **30**, 159–174 (2003). doi: [10.3354/ame030159](https://doi.org/10.3354/ame030159)
67. E. Sherr, B. Sherr, D. Caron, D. Vault, A. Worden, Oceanic protists. *Oceanography* **20**, 130–134 (2007). doi: [10.5670/oceanog.2007.57](https://doi.org/10.5670/oceanog.2007.57)
68. A. M. Lewandowska et al., Effects of sea surface warming on marine plankton. *Ecol. Lett.* **17**, 614–623 (2014). doi: [10.1111/ele.12265](https://doi.org/10.1111/ele.12265); pmid: 24575918
69. M. I. O'Connor, M. F. Piehler, D. M. Leech, A. Anton, J. F. Bruno, Warming and resource availability shift food web structure and metabolism. *PLOS Biol.* **7**, e1000178 (2009). doi: [10.1371/journal.pbio.1000178](https://doi.org/10.1371/journal.pbio.1000178); pmid: 19707271
70. J. Wohlers et al., Changes in biogenic carbon flow in response to sea surface warming. *Proc. Natl. Acad. Sci. U.S.A.* **106**, 7067–7072 (2009). doi: [10.1073/pnas.0812743106](https://doi.org/10.1073/pnas.0812743106); pmid: 19359482
71. D. A. Hansell, Recalcitrant dissolved organic carbon fractions. *Annu. Rev. Mar. Sci.* **5**, 421–445 (2013). doi: [10.1146/annurev-marine-120710-100757](https://doi.org/10.1146/annurev-marine-120710-100757)
72. S. Dyhrman, Ectoenzymes in *Prorocentrum minimum*. *Harmful Algae* **4**, 619–627 (2005). doi: [10.1016/j.jhal.2004.08.011](https://doi.org/10.1016/j.jhal.2004.08.011)
73. D. K. Stoecker, D. E. Gustafson Jr., Cell-surface proteolytic activity of photosynthetic dinoflagellates. *Aquat. Microb. Ecol.* **30**, 175–183 (2003). doi: [10.3354/ame030175](https://doi.org/10.3354/ame030175)
74. T. Stoeck et al., Living at the limits: Evidence for microbial eukaryotes thriving under pressure in deep anoxic, hypersaline habitats. *Adv. Ecol.* **2014**, 532687 (2014). doi: [10.1155/2014/532687](https://doi.org/10.1155/2014/532687)
75. T. A. Richards, M. D. Jones, G. Leonard, D. Bass, Marine fungi: Their ecology and molecular diversity. *Annu. Rev. Mar. Sci.* **4**, 495–522 (2012). doi: [10.1146/annurev-marine-120710-100802](https://doi.org/10.1146/annurev-marine-120710-100802)
76. W. Orsi, J. F. Biddle, V. Edgcomb, Deep sequencing of subsurface eukaryotic rRNA reveals active Fungi across marine subsurface provinces. *PLOS ONE* **8**, e56335 (2013). doi: [10.1371/journal.pone.0056335](https://doi.org/10.1371/journal.pone.0056335); pmid: 23418566
77. W. D. Orsi, V. P. Edgcomb, G. D. Christman, J. F. Biddle, Gene expression in the deep biosphere. *Nature* **499**, 205–208 (2013). doi: [10.1038/nature12230](https://doi.org/10.1038/nature12230); pmid: 23760485
78. Q. Li, X. Wang, X. Liu, N. Jiao, G. Wang, Abundance and novel lineages of thaustochytrids in Hawaiian waters. *Microb. Ecol.* **66**, 823–830 (2013). doi: [10.1007/s00248-013-0275-3](https://doi.org/10.1007/s00248-013-0275-3); pmid: 23942794
79. S. Raghukumar, V. S. Damare, Increasing evidence for the important role of Labyrinthulomycetes in marine ecosystems. *Bot. Mar.* **54**, 3–11 (2011). doi: [10.1515/bot.2011.008](https://doi.org/10.1515/bot.2011.008)
80. M. L. Wells, in *Biogeochemistry of Marine Dissolved Organic Matter*, D. A. Hansell, C. A. Carlson, Eds. (Academic Press, New York, 2002), pp. 367–404.
81. R. Seenivasan, N. Sausen, L. K. Medlin, M. Melkonian, *Picozonas jadrakae* gen. et sp. nov.: The first identified member of the Picozoa phylum nov., a widespread group of picoeukaryotes, formerly known as 'picobiliphytes'. *PLOS ONE* **8**, e59565 (2013). doi: [10.1371/journal.pone.0059565](https://doi.org/10.1371/journal.pone.0059565); pmid: 23551060
82. H. S. Yoon et al., Single-cell genomics reveals organismal interactions in uncultivated marine protists. *Science* **332**, 714–717 (2011). doi: [10.1126/science.1203163](https://doi.org/10.1126/science.1203163); pmid: 21551060
83. L. Guillou et al., Widespread occurrence and genetic diversity of marine parasitoids belonging to Syndiniales (Alveolata). *Environ. Microbiol.* **10**, 3349–3365 (2008). doi: [10.1111/j.1462-2920.2008.01731.x](https://doi.org/10.1111/j.1462-2920.2008.01731.x); pmid: 18771501
84. A. Chambouvet et al., Interplay between the parasite *Amoebohypha* sp. (Alveolata) and the cyst formation of the red tide dinoflagellate *Scripsiella trochoidea*. *Protist* **162**, 637–649 (2011). doi: [10.1016/j.protis.2010.12.001](https://doi.org/10.1016/j.protis.2010.12.001); pmid: 21349764
85. T. R. Bachvaroff, S. Kim, L. Guillou, C. F. Delwiche, D. W. Coats, Molecular diversity of the syndinean genus *Euduboscquella* based on single-cell PCR analysis. *Appl. Environ. Microbiol.* **78**, 334–345 (2012). doi: [10.1128/AEM.06678-11](https://doi.org/10.1128/AEM.06678-11); pmid: 22081578
86. J. Bråte et al., Radiolaria associated with large diversity of marine alveolates. *Protist* **163**, 767–777 (2012). doi: [10.1016/j.protis.2012.04.004](https://doi.org/10.1016/j.protis.2012.04.004); pmid: 22658831
87. J. G. Rendón-Maldonado, M. Espinosa-Cantellano, A. González-Robles, A. Martínez-Palomó, *Trichomonas vaginalis*: In vitro phagocytosis of lactobacilli, vaginal epithelial cells, leukocytes, and erythrocytes. *Exp. Parasitol.* **89**, 241–250 (1998). doi: [10.1006/expr.1998.4297](https://doi.org/10.1006/expr.1998.4297); pmid: 9635448
88. E. C. Roberts, C. Legrand, M. Steinke, E. C. Wootton, Mechanisms underlying chemical interactions between predatory planktonic protists and their prey. *J. Plankton Res.* **33**, 833–841 (2011). doi: [10.1093/plankt/fbr005](https://doi.org/10.1093/plankt/fbr005)
89. A. Z. Worden, A. E. Allen, The voyage of the microbial eukaryote. *Curr. Opin. Microbiol.* **13**, 652–660 (2010). doi: [10.1016/j.mib.2010.08.001](https://doi.org/10.1016/j.mib.2010.08.001); pmid: 20832353
90. D. F. Bird, J. Kalf, Bacterial grazing by planktonic lake algae. *Science* **231**, 493–495 (1986). doi: [10.1126/science.231.4737.493](https://doi.org/10.1126/science.231.4737.493); pmid: 17776022
91. K. W. Estep, P. G. Davis, M. D. Keller, J. M. Sieburth, How important are oceanic algal nanoflagellates in bacterivory? *Limnol. Oceanogr.* **31**, 646–650 (1986). doi: [10.4319/lo.1986.31.3.0646](https://doi.org/10.4319/lo.1986.31.3.0646)

92. S. Flöder, T. Hansen, R. Ptacnik, Energy-dependent bacteriivory in *Ochromonas minima*—a strategy promoting the use of substitutable resources and survival at insufficient light supply. *Protist* **157**, 291–302 (2006). doi: [10.1016/j.protis.2006.05.002](#); pmid: [16843063](#)
93. J. Frias-Lopez, A. Thompson, J. Waldbauer, S. W. Chisholm, Use of stable isotope-labelled cells to identify active grazers of picocyanobacteria in ocean surface waters. *Environ. Microbiol.* **11**, 512–525 (2009). doi: [10.1111/j.1462-2920.2008.01793.x](#); pmid: [19196281](#)
94. F. Unrein, J. M. Gasol, F. Not, I. Forn, R. Massana, Mixotrophic haptophytes are key bacterial grazers in oligotrophic coastal waters. *ISME J.* **8**, 164–176 (2014). doi: [10.1038/ismej.2013.132](#); pmid: [23924785](#)
95. J. Tittel et al., Mixotrophs combine resource use to outcompete specialists: Implications for aquatic food webs. *Proc. Natl. Acad. Sci. U.S.A.* **100**, 12776–12781 (2003). doi: [10.1073/pnas.2130696100](#); pmid: [14569026](#)
96. S. Wilken, J. Huisman, S. Naus-Wiezer, E. Van Donk, Mixotrophic organisms become more heterotrophic with rising temperature. *Ecol. Lett.* **16**, 225–233 (2013). doi: [10.1111/ele.12033](#); pmid: [23173644](#)
97. C. P. D. Brussaard et al., Arctic microbial community dynamics influenced by elevated CO₂ levels. *Biogeosciences* **10**, 719–731 (2013). doi: [10.5194/bg-10-719-2013](#)
98. K. L. Schoo, A. M. Malzahn, E. Krause, M. Boersma, Increased carbon dioxide availability alters phytoplankton stoichiometry and affects carbon cycling and growth of a marine planktonic herbivore. *Mar. Biol.* **160**, 2145–2155 (2013). doi: [10.1007/s00227-012-2121-4](#)
99. O. Béjà et al., Bacterial rhodospin: Evidence for a new type of phototrophy in the sea. *Science* **289**, 1902–1906 (2000). doi: [10.1126/science.289.5486.1902](#); pmid: [10988064](#)
100. C. H. Slamovits, N. Okamoto, L. Burri, E. R. James, P. J. Keeling, A bacterial proteorhodopsin proton pump in marine eukaryotes. *Nat. Commun.* **2**, 183 (2011). doi: [10.1038/ncomms1188](#); pmid: [21304512](#)
101. P. J. Keeling, Crystal ball-2013. *Environ. Microbiol. Rep.* **5**, 4–5 (2013). doi: [10.1111/1758-2229.12021](#)
102. J. S. Guasto, R. Rusconi, R. Stocker, Fluid mechanics of planktonic microorganisms. *Annu. Rev. Fluid Mech.* **44**, 373–400 (2012). doi: [10.1146/annurev-fluid-120710-101156](#)
103. S. A. West, S. P. Diggle, A. Buckling, A. Gardner, A. S. Griffin, The social lives of microbes. *Annu. Rev. Ecol. Syst.* **38**, 53–77 (2007). doi: [10.1146/annurev.ecolsys.38.091206.095740](#)
104. F. Azam, A. Z. Worden, Microbes, molecules, and marine ecosystems. *Science* **303**, 1622–1624 (2004). doi: [10.1126/science.1093892](#); pmid: [15016987](#)
105. F. Azam, F. Malfatti, Microbial structuring of marine ecosystems. *Nat. Rev. Microbiol.* **5**, 782–791 (2007). doi: [10.1038/nrmicro1747](#); pmid: [17853906](#)
106. S. A. Amin, M. S. Parker, E. V. Armbrust, Interactions between diatoms and bacteria. *Microbiol. Mol. Biol. Rev.* **76**, 667–684 (2012). doi: [10.1128/MMBR.00007-12](#); pmid: [22933565](#)
107. H. A. Blossom, N. Daugbjerg, P. J. Hansen, Toxic mucus traps: A novel mechanism that mediates prey uptake in the mixotrophic dinoflagellate *Alexandrium pseudogonyaulax*. *Harmful Algae* **17**, 40–53 (2012). doi: [10.1016/j.hal.2012.02.010](#)
108. M. Sapp et al., Species-specific bacterial communities in the phycosphere of microalgae? *Microb. Ecol.* **53**, 683–699 (2007). doi: [10.1007/s00244-006-9162-5](#); pmid: [17264999](#)
109. S. Jasti, M. E. Sieracki, N. J. Poulton, M. W. Giewat, J. N. Rooney-Varga, Phylogenetic diversity and specificity of bacteria closely associated with *Alexandrium* spp. and other phytoplankton. *Appl. Environ. Microbiol.* **71**, 3483–3494 (2005). doi: [10.1128/AEM.71.7.3483-3494.2005](#); pmid: [16000752](#)
110. R. Stocker, Marine microbes see a sea of gradients. *Science* **338**, 628–633 (2012). doi: [10.1126/science.1208929](#); pmid: [23118182](#)
111. J. P. McCutcheon, C. D. von Dohlen, An interdependent metabolic pathwork in the nested symbiosis of mealybugs. *Curr. Biol.* **21**, 1366–1372 (2011). doi: [10.1016/j.cub.2011.06.051](#); pmid: [21835622](#)
112. M. Kleiner et al., Metaproteomics of a gutless marine worm and its symbiotic microbial community reveal unusual pathways for carbon and energy use. *Proc. Natl. Acad. Sci. U.S.A.* **109**, E1173–E1182 (2012). doi: [10.1073/pnas.1221198109](#); pmid: [22517752](#)
113. D. K. Stoecker, M. D. Johnson, C. de Vargas, F. Not, Acquired phototrophy in aquatic protists. *Aquat. Microb. Ecol.* **57**, 279–310 (2009). doi: [10.3354/ame01340](#)
114. E. Meyer, V. M. Weis, Study of cnidarian-algal symbiosis in the “omics” age. *Biol. Bull.* **223**, 44–65 (2012). pmid: [22983032](#)
115. K. J. Flynn et al., Misuse of the phytoplankton-zooplankton dichotomy: The need to assign organisms as mixotrophs within plankton functional types. *J. Plankton Res.* **35**, 3–11 (2013). doi: [10.1093/plankt/fbs062](#)
116. R. A. Foster et al., Nitrogen fixation and transfer in open ocean diatom-cyanobacterial symbioses. *ISME J.* **5**, 1484–1493 (2011). doi: [10.1038/ismej.2011.26](#); pmid: [21451586](#)
117. J. A. Hilton et al., Genomic deletions disrupt nitrogen metabolism pathways of a cyanobacterial diatom symbiont. *Nat. Commun.* **4**, 1767 (2013). doi: [10.1038/ncomms2748](#); pmid: [23612308](#)
118. A. W. Thompson et al., Unicellular cyanobacterium symbiotic with a single-celled eukaryotic alga. *Science* **337**, 1546–1550 (2012). pmid: [22997339](#)
119. D. M. Karl, M. J. Church, J. E. Dore, R. M. Letelier, C. Mahaffey, Predictable and efficient carbon sequestration in the North Pacific Ocean supported by symbiotic nitrogen fixation. *Proc. Natl. Acad. Sci. U.S.A.* **109**, 1842–1849 (2012). doi: [10.1073/pnas.1120312109](#); pmid: [22308450](#)
120. Y. Lehahn et al., Decoupling physical from biological processes to assess the impact of viruses on a mesoscale algal bloom. *Curr. Biol.* **24**, 2041–2046 (2014). doi: [10.1016/j.cub.2014.07.046](#)
121. S. M. Short, The ecology of viruses that infect eukaryotic algae. *Environ. Microbiol.* **14**, 2253–2271 (2012). doi: [10.1111/j.1462-2920.2012.02706.x](#); pmid: [22360532](#)
122. J. Haaber, M. Middelboe, Viral lysis of *Phaeocystis pouchetii*: Implications for algal population dynamics and heterotrophic C, N and P cycling. *ISME J.* **3**, 430–441 (2009). doi: [10.1038/ismej.2008.125](#); pmid: [19129863](#)
123. A. R. Sheik et al., Responses of the coastal bacterial community to viral infection of the algae *Phaeocystis globosa*. *ISME J.* **8**, 212–225 (2014). doi: [10.1038/ismej.2013.135](#); pmid: [23949664](#)
124. A. Vardi et al., Host-virus dynamics and subcellular controls of cell fate in a natural coccolithophore population. *Proc. Natl. Acad. Sci. U.S.A.* **109**, 19327–19332 (2012). doi: [10.1073/pnas.1208895109](#); pmid: [23134731](#)
125. C. Evans, W. H. Wilson, Preferential grazing of *Oxyrrhis marina* on virus infected *Emiliania huxleyi*. *Limnol. Oceanogr.* **53**, 2035–2040 (2008). doi: [10.4319/lo.2008.53.5.2035](#)
126. M. Frada, I. Probert, M. J. Allen, W. H. Wilson, C. de Vargas, The “Cheshire Cat” escape strategy of the coccolithophore *Emiliania huxleyi* in response to viral infection. *Proc. Natl. Acad. Sci. U.S.A.* **105**, 15944–15949 (2008). doi: [10.1073/pnas.0807707105](#); pmid: [18824682](#)
127. R. Thomas, S. Jacquet, N. Grimsley, H. Moreau, Strategies and mechanisms of resistance to viruses in photosynthetic aquatic microorganisms. *Adv. Oceanogr. Limnol.* **3**, 1–15 (2012). doi: [10.1080/19475721.2012.672338](#)
128. M. G. Fischer, C. A. Suttle, A viroplage at the origin of large DNA transposons. *Science* **332**, 231–234 (2011). doi: [10.1126/science.1199412](#); pmid: [21385722](#)
129. K. Faust, J. Raes, Microbial interactions: From networks to models. *Nat. Rev. Microbiol.* **10**, 538–550 (2012). doi: [10.1038/nrmicro2832](#); pmid: [22796884](#)
130. J. A. Steele et al., Marine bacterial, archaeal and protistan association networks reveal ecological linkages. *ISME J.* **5**, 1414–1425 (2011). doi: [10.1038/ismej.2011.24](#); pmid: [21430787](#)
131. P. Deschamps, D. Moreira, Reevaluating the green contribution to diatom genomes. *Genome Biol. Evol.* **4**, 683–688 (2012). doi: [10.1093/gbe/evs053](#); pmid: [22684208](#)
132. C. Bowler, A. Vardi, A. E. Allen, Oceanographic and biogeochemical insights from diatom genomes. *Annu. Rev. Mar. Sci.* **2**, 429–461 (2010). doi: [10.1146/annurev-marine-120308-081051](#)
133. P. J. Keeling et al., The Marine Microbial Eukaryote Transcriptome Sequencing Project (MMETSP): Illuminating the functional diversity of eukaryotic life in the oceans through transcriptome sequencing. *PLOS Biol.* **12**, e1001889 (2014). doi: [10.1371/journal.pbio.1001889](#); pmid: [24959919](#)
134. A. Monier, S. Sudek, N. M. Fast, A. Z. Worden, Gene invasion in distant eukaryotic lineages: discovery of mutually exclusive genetic elements reveals marine biodiversity. *ISME J.* **7**, 1764–1774 (2013). doi: [10.1038/ismej.2013.70](#)
135. D. Vaulot et al., Metagenomes of the picoplankton *Bathycoccus* from the Chile coastal upwelling. *PLOS ONE* **7**, e39648 (2012). doi: [10.1371/journal.pone.0039648](#)
136. Z. C. Landry, S. J. Giovannoni, S. R. Quake, P. C. Blainey, Optofluidic cell selection from complex microbial communities for single-genome analysis. *Methods Enzymol.* **531**, 61–90 (2013). doi: [10.1016/B978-0-12-407863-5.00004-6](#); pmid: [24060116](#)
137. R. A. Alegado, N. King, Bacterial influences on animal origins. *Cold Spring Harb. Perspect. Biol.* **6**, a016162 (2014). doi: [10.1101/cshperspect.a016162](#)
138. N. King et al., The genome of the choanoflagellate *Monosiga brevicollis* and the origin of metazoans. *Nature* **451**, 783–788 (2008). doi: [10.1038/nature06617](#); pmid: [18273011](#)
139. A. Z. Worden et al., Green evolution and dynamic adaptations revealed by genomes of the marine picoeukaryotes *Micromonas*. *Science* **324**, 268–272 (2009). doi: [10.1126/science.1167222](#); pmid: [19359590](#)
140. B. Verhelst, Y. Van de Peer, P. Rouzé, The complex intron landscape and massive intron invasion in a picoeukaryote provides insights into intron evolution. *Genome Biol. Evol.* **5**, 2393–2401 (2013). doi: [10.1093/gbe/evt189](#); pmid: [24273312](#)
141. J. T. Huff, D. Zilberman, Dnm1-independent CG methylation contributes to nucleosome positioning in diverse eukaryotes. *Cell* **156**, 1286–1297 (2014). doi: [10.1016/j.cell.2014.01.029](#); pmid: [24630728](#)
142. J. Slapeta, P. López-García, D. Moreira, Global dispersal and ancient cryptic species in the smallest marine eukaryotes. *Mol. Biol. Evol.* **23**, 23–29 (2006). doi: [10.1093/molbev/msj001](#); pmid: [16120798](#)
143. A. Osterman, R. Overbeek, Missing genes in metabolic pathways: A comparative genomics approach. *Curr. Opin. Chem. Biol.* **7**, 238–251 (2003). doi: [10.1016/S1367-5931\(03\)00027-9](#); pmid: [12714058](#)
144. P. Carini et al., Discovery of a SAR11 growth requirement for thiamin’s pyrimidine precursor and its distribution in the Sargasso Sea. *ISME J.* **8**, 1727–1738 (2014). doi: [10.1038/ismej.2014.61](#)
145. D. McRose et al., Alternatives to vitamin B1 uptake revealed with discovery of riboswitches in multiple marine eukaryotic lineages. *ISME J.* **8**, 2517–2529 (2014). doi: [10.1038/ismej.2014.146](#)
146. K. H. Halsey, B. M. Jones, Phytoplankton strategies for photosynthetic energy allocation. *Annu. Rev. Mar. Sci.* **7**, 265–297 (2015). doi: [10.1146/annurev-marine-010814-015813](#)
147. J. Sun et al., One carbon metabolism in SAR11 pelagic marine bacteria. *PLOS ONE* **6**, e23973 (2011). doi: [10.1371/journal.pone.0023973](#); pmid: [21886845](#)
148. J. Raes, P. Bork, Molecular eco-systems biology: Towards an understanding of community function. *Nat. Rev. Microbiol.* **6**, 693–699 (2008). doi: [10.1038/nrmicro1935](#); pmid: [18587409](#)
149. G. van Ooijen, K. Knox, K. Kis, F. Y. Bouget, A. J. Millar, Genomic transformation of the picoeukaryote *Ostreococcus tauri*. *J. Vis. Exp.* **XX**, e4074 (2012). pmid: [22825291](#)
150. V. De Riso et al., Gene silencing in the marine diatom *Phaeodactylum tricornutum*. *Nucleic Acids Res.* **37**, e96 (2009). doi: [10.1093/nar/gkp448](#); pmid: [19487243](#)
151. S. Våge, M. Castellani, J. Giske, T. F. Thingstad, Successful strategies in size structured mixotrophic food webs. *Aquat. Ecol.* **47**, 329–347 (2013). doi: [10.1007/s10452-013-9447-y](#)
152. T. A. Troost, B. W. Kooi, S. A. Kooijman, When do mixotrophs specialize? Adaptive dynamics theory applied to a dynamic energy budget model. *Math. Biosci.* **193**, 159–182 (2005). doi: [10.1016/j.mbs.2004.06.010](#); pmid: [15748728](#)
153. A. Mitra et al., The role of mixotrophic protists in the biological carbon pump. *Biogeosciences* **11**, 995–1005 (2014). doi: [10.5194/bg-11-995-2014](#)
154. N. Rooney, K. S. McCann, Integrating food web diversity, structure and stability. *Trends Ecol. Evol.* **27**, 40–46 (2012). doi: [10.1016/j.tree.2011.09.001](#); pmid: [21944861](#)
155. M. M. Mills, K. R. Arrigo, Magnitude of oceanic nitrogen fixation influenced by the nutrient uptake ratio of phytoplankton. *Nat. Geosci.* **3**, 412–416 (2010). doi: [10.1038/ngeo856](#)
156. S. L. Giering et al., Reconciliation of the carbon budget in the ocean’s twilight zone. *Nature* **507**, 480–483 (2014). doi: [10.1038/nature13123](#); pmid: [24670767](#)
157. B. O. Palsson, *Systems Biology: Deconstruction of Reconstructed Networks* (Cambridge Univ. Press, Cambridge, 2006).
158. F. Burki, P. J. Keeling, Rhizaria. *Curr. Biol.* **24**, R103–R107 (2014). doi: [10.1016/j.cub.2013.12.025](#); pmid: [24502779](#)
159. L. Guillou, C. Alves-de-Souza, R. Siano, H. González, *Microbiol. Today* **37**, 92–94 (2010).

ACKNOWLEDGMENTS

We thank C. Bachy, F. Burki, S. Haddock, R. Harbeitner, and L. Klosterman for comments and criticism; T. A. Richards and A. Santoro for discussions; C. Alves-de-Souza, P. Burkhardt, K. Carpenter, J. Decelle, J. Fell, T. Heger, N. King, D. Klimov, C. Leander, K. K. Newell, N. Okamoto, F. Spiegel, T. Walsh, L. Weiss, and N. Yubuki for a subset of the images used here; and A. Gough, M. Salisbury, H. Hadaway, M. Stoermer, and D. Firstein. Supported by a Guggenheim Fellowship and Tula Foundation award (P.J.K.), by NSF OCE-1436865 (S.J.G.), GBMF3305 (A.E.Z./A.Z.W.), GBMF3307 (S.W./A.Z.W.), and by Moore Marine Microbiology Investigator awards GBMF3788 and GBMF3778 (A.Z.W. and M.J.F., respectively).

10.1126/science.1257594

RESEARCH ARTICLE SUMMARY

SUSTAINABILITY

Planetary boundaries: Guiding human development on a changing planet

Will Steffen,* Katherine Richardson, Johan Rockström, Sarah E. Cornell, Ingo Fetzer, Elena M. Bennett, Reinette Biggs, Stephen R. Carpenter, Wim de Vries, Cynthia A. de Wit, Carl Folke, Dieter Gerten, Jens Heinke, Georgina M. Mace, Linn M. Persson, Veerabhadran Ramanathan, Belinda Meyers, Sverker Sörlin

INTRODUCTION: There is an urgent need for a new paradigm that integrates the continued development of human societies and the maintenance of the Earth system (ES) in a resilient and accommodating state. The planetary boundary (PB) framework contributes to such a paradigm by providing a science-based analysis of the risk that human perturbations will destabilize the ES at the planetary scale. Here, the scientific underpinnings of the PB framework are updated and strengthened.

RATIONALE: The relatively stable, 11,700-year-long Holocene epoch is the only state of the ES

that we know for certain can support contemporary human societies. There is increasing evidence that human activities are affecting ES functioning to a degree that threatens the resilience of the ES—its ability to persist in a Holocene-like state in the face of increasing human pressures and shocks. The PB framework is based on critical processes that regulate ES functioning. By combining improved scientific understanding of ES functioning with the precautionary principle, the PB framework identifies levels of anthropogenic perturbations below which the risk of destabilization of the ES is likely to remain low—a “safe operating

space” for global societal development. A zone of uncertainty for each PB highlights the area of increasing risk. The current level of anthropogenic impact on the ES, and thus the risk to the stability of the ES, is assessed by comparison with the proposed PB (see the figure).

RESULTS: Three of the PBs (climate change, stratospheric ozone depletion, and ocean acidification) remain essentially unchanged from the earlier analysis. Regional-level boundaries as well as globally aggregated PBs have now been developed for biosphere integrity (earlier “biodiversity loss”), biogeochemical flows, land-system change, and freshwater use. At present, only one regional boundary (south Asian monsoon) can be established for atmospheric aerosol loading. Although we cannot identify a single PB

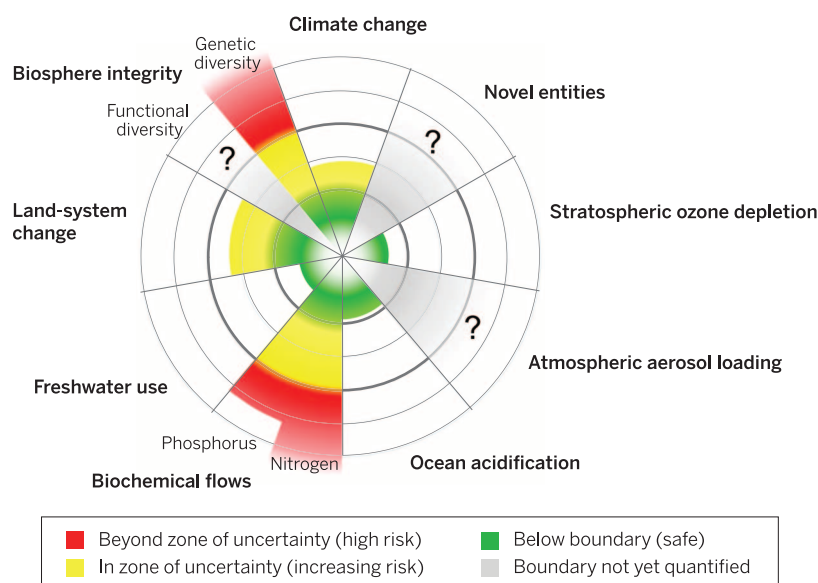
ON OUR WEB SITE

Read the full article at <http://dx.doi.org/10.1126/science.1259855>

for novel entities (here defined as new substances, new forms of existing substances, and modified life forms that have the potential for unwanted geophysical and/or biological

effects), they are included in the PB framework, given their potential to change the state of the ES. Two of the PBs—climate change and biosphere integrity—are recognized as “core” PBs based on their fundamental importance for the ES. The climate system is a manifestation of the amount, distribution, and net balance of energy at Earth’s surface; the biosphere regulates material and energy flows in the ES and increases its resilience to abrupt and gradual change. Anthropogenic perturbation levels of four of the ES processes/features (climate change, biosphere integrity, biogeochemical flows, and land-system change) exceed the proposed PB (see the figure).

CONCLUSIONS: PBs are scientifically based levels of human perturbation of the ES beyond which ES functioning may be substantially altered. Transgression of the PBs thus creates substantial risk of destabilizing the Holocene state of the ES in which modern societies have evolved. The PB framework does not dictate how societies should develop. These are political decisions that must include consideration of the human dimensions, including equity, not incorporated in the PB framework. Nevertheless, by identifying a safe operating space for humanity on Earth, the PB framework can make a valuable contribution to decision-makers in charting desirable courses for societal development. ■



Current status of the control variables for seven of the planetary boundaries. The green zone is the safe operating space, the yellow represents the zone of uncertainty (increasing risk), and the red is a high-risk zone. The planetary boundary itself lies at the intersection of the green and yellow zones. The control variables have been normalized for the zone of uncertainty; the center of the figure therefore does not represent values of 0 for the control variables. The control variable shown for climate change is atmospheric CO₂ concentration. Processes for which global-level boundaries cannot yet be quantified are represented by gray wedges; these are atmospheric aerosol loading, novel entities, and the functional role of biosphere integrity.

The list of author affiliations is available in the full article online.

*Corresponding author. E-mail: will.steffen@anu.edu.au
Cite this article as W. Steffen et al., *Science* 347, 1259855 (2015). DOI: 10.1126/science.1259855

RESEARCH ARTICLE

SUSTAINABILITY

Planetary boundaries: Guiding human development on a changing planet

Will Steffen,^{1,2*} Katherine Richardson,³ Johan Rockström,¹ Sarah E. Cornell,¹ Ingo Fetzer,¹ Elena M. Bennett,⁴ Reinette Biggs,^{1,5} Stephen R. Carpenter,⁶ Wim de Vries,^{7,8} Cynthia A. de Wit,⁹ Carl Folke,^{1,10} Dieter Gerten,¹¹ Jens Heinke,^{11,12,13} Georgina M. Mace,¹⁴ Linn M. Persson,¹⁵ Veerabhadran Ramanathan,^{16,17} Belinda Reyers,^{1,18} Sverker Sörlin¹⁹

The planetary boundaries framework defines a safe operating space for humanity based on the intrinsic biophysical processes that regulate the stability of the Earth system. Here, we revise and update the planetary boundary framework, with a focus on the underpinning biophysical science, based on targeted input from expert research communities and on more general scientific advances over the past 5 years. Several of the boundaries now have a two-tier approach, reflecting the importance of cross-scale interactions and the regional-level heterogeneity of the processes that underpin the boundaries. Two core boundaries—climate change and biosphere integrity—have been identified, each of which has the potential on its own to drive the Earth system into a new state should they be substantially and persistently transgressed.

The planetary boundary (PB) approach (1, 2) aims to define a safe operating space for human societies to develop and thrive, based on our evolving understanding of the functioning and resilience of the Earth system. Since its introduction, the framework has been subject to scientific scrutiny [e.g., (3–7)] and has attracted considerable interest and discussions within the policy, governance, and business sectors as an approach to inform efforts toward global sustainability (8–10).

In this analysis, we further develop the basic PB framework by (i) introducing a two-tier approach for several of the boundaries to account for regional-level heterogeneity; (ii) updating the quantification of most of the PBs; (iii) identifying two core boundaries; and (iv) proposing a regional-level quantitative boundary for one of the two that were not quantified earlier (1).

The basic framework: Defining a safe operating space

Throughout history, humanity has faced environmental constraints at local and regional levels, with some societies dealing with these challenges more effectively than others (11, 12). More recently, early industrial societies often used local waterways and airsheds as dumping grounds for their waste and effluent from industrial processes. This eroded local and regional environmental quality and stability, threatening to undermine the progress made through industrialization by damaging human health and degrading ecosystems. Eventually, this led to the introduction of local or regional boundaries or constraints on what

could be emitted to and extracted from the environment (e.g., chemicals that pollute airsheds or waterways) and on how much the environment could be changed by direct human modification (land-use/cover change in natural ecosystems) (13). The regulation of some human impacts on the environment—for example, the introduction of chemical contaminants—is often framed in the context of “safe limits” (14).

These issues remain, but in addition we now face constraints at the planetary level, where the magnitude of the challenge is vastly different. The human enterprise has grown so dramatically since the mid-20th century (15) that the relatively stable, 11,700-year-long Holocene epoch, the only state of the planet that we know for certain can support contemporary human societies, is now being destabilized (figs. S1 and S2) (16–18). In fact, a new geological epoch, the Anthropocene, has been proposed (19).

The precautionary principle suggests that human societies would be unwise to drive the Earth system substantially away from a Holocene-like condition. A continuing trajectory away from the Holocene could lead, with an uncomfortably high probability, to a very different state of the Earth system, one that is likely to be much less hospitable to the development of human societies (17, 18, 20). The PB framework aims to help guide human societies away from such a trajectory by defining a “safe operating space” in which we can continue to develop and thrive. It does this by proposing boundaries for anthropogenic perturbation of critical Earth-system processes. Respecting these boundaries would greatly reduce the

risk that anthropogenic activities could inadvertently drive the Earth system to a much less hospitable state.

Nine processes, each of which is clearly being modified by human actions, were originally suggested to form the basis of the PB framework (1). Although these processes are fundamental to Earth-system functioning, there are many other ways that Earth-system functioning could be described, including potentially valuable metrics for quantifying the human imprint on it. These alternative approaches [e.g., (4)] often represent ways to explore and quantify interactions among the boundaries. They can provide a valuable complement to the original approach (1) and further enrich the broader PB concept as it continues to evolve.

The planetary boundary framework: Thresholds, feedbacks, resilience, uncertainties

A planetary boundary as originally defined (1) is not equivalent to a global threshold or tipping point. As Fig. 1 shows, even when a global- or continental/ocean basin-level threshold in an Earth-system process is likely to exist [e.g., (20, 21)], the proposed planetary boundary is not placed at the position of the biophysical threshold but rather upstream of it—i.e., well before reaching the threshold. This buffer between the boundary (the end of the safe operating space, the green zone in Fig. 1) and the threshold not only accounts for uncertainty in the precise position of the threshold with respect to the control variable

¹Stockholm Resilience Centre, Stockholm University, 10691 Stockholm, Sweden. ²Fenner School of Environment and Society, The Australian National University, Canberra, ACT 2601, Australia. ³Center for Macroecology, Evolution, and Climate, University of Copenhagen, Natural History Museum of Denmark, Universitetsparken 15, Building 3, 2100 Copenhagen, Denmark. ⁴Department of Natural Resource Sciences and McGill School of Environment, McGill University, 21, 111 Lakeshore Road, Ste-Anne-de-Bellevue, QC H9X 3V9, Canada. ⁵Centre for Studies in Complexity, Stellenbosch University, Private Bag X1, Stellenbosch 7602, South Africa. ⁶Center for Limnology, University of Wisconsin, 680 North Park Street, Madison WI 53706 USA. ⁷Alterra Wageningen University and Research Centre, P.O. Box 47, 6700AA Wageningen, Netherlands. ⁸Environmental Systems Analysis Group, Wageningen University, P.O. Box 47, 6700 AA Wageningen, Netherlands. ⁹Department of Environmental Science and Analytical Chemistry, Stockholm University, 10691 Stockholm, Sweden. ¹⁰Beijing Institute of Ecological Economics, Royal Swedish Academy of Sciences, SE-10405 Stockholm, Sweden. ¹¹Research Domain Earth System Analysis, Potsdam Institute for Climate Impact Research (PIK), Telegraphenberg A62, 14473 Potsdam, Germany. ¹²International Livestock Research Institute, P.O. Box 30709, Nairobi, 00100 Kenya. ¹³CSIRO (Commonwealth Scientific and Industrial Research Organization), St. Lucia, QLD 4067, Australia. ¹⁴Centre for Biodiversity and Environment Research (CBER), Department of Genetics, Evolution and Environment, University College London, Gower Street, London WC1E 6BT, UK. ¹⁵Stockholm Environment Institute, Linnégatan 87D, SE-10451 Stockholm, Sweden. ¹⁶Scripps Institution of Oceanography, University of California at San Diego, 8622 Kennel Way, La Jolla, CA 92037 USA. ¹⁷TERI (The Energy and Resources Institute) University, 10 Institutional Area, Vasant Kunj, New Delhi, Delhi 110070, India. ¹⁸Natural Resources and the Environment, CSIR, P.O. Box 320, Stellenbosch 7599, South Africa. ¹⁹Division of History of Science, Technology and Environment, KTH Royal Institute of Technology, SE-10044 Stockholm, Sweden.
*Corresponding author. E-mail: will.steffen@anu.edu.au

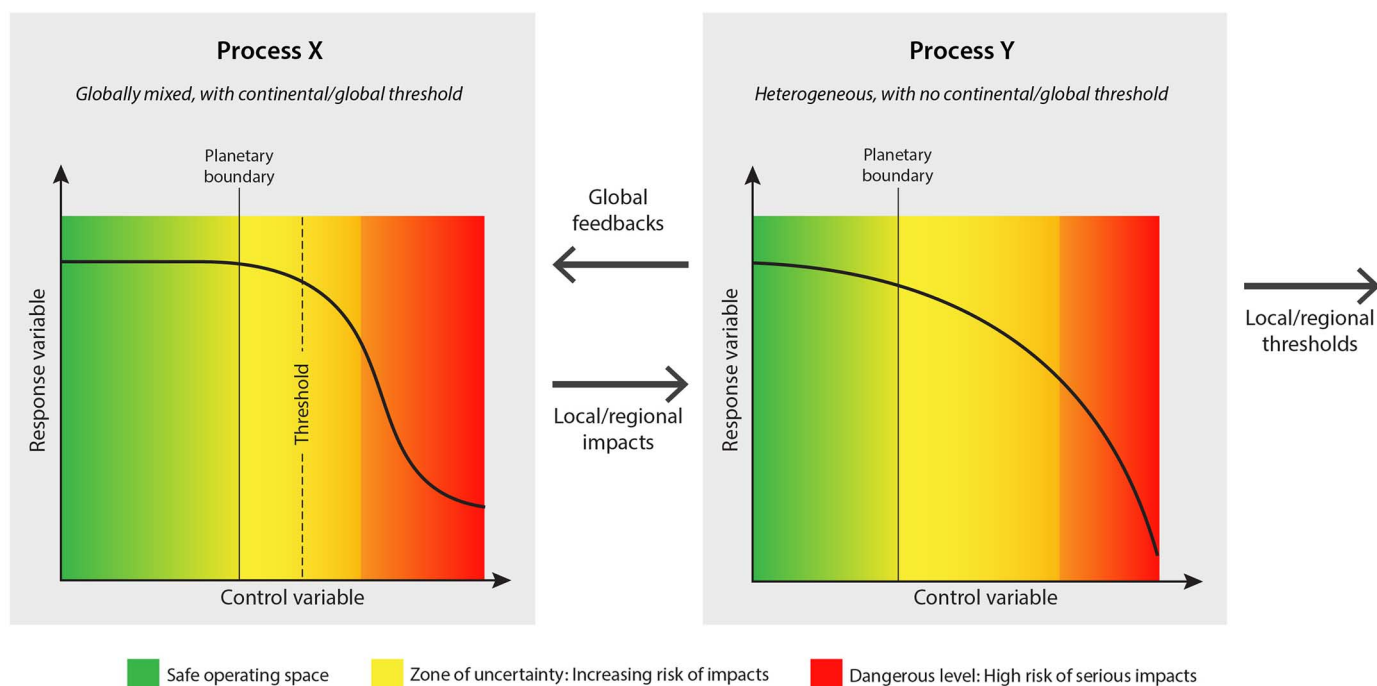


Fig. 1. The conceptual framework for the planetary boundary approach, showing the safe operating space, the zone of uncertainty, the position of the threshold (where one is likely to exist), and the area of high risk. Modified from (1).

but also allows society time to react to early warning signs that it may be approaching a threshold and consequent abrupt or risky change.

The developing science of early-warning signs can warn of an approaching threshold or a decrease in the capability of a system to persist under changing conditions. Examples include “critical slowing down” in a process (22), increasing variance (23), and flickering between states of the system (24–26). However, for such science to be useful in a policy context, it must provide enough time for society to respond in order to steer away from an impending threshold before it is crossed (27, 28). The problem of system inertia—for example, in the climate system (18)—needs to be taken into account in assessing the time needed for society to react to early-warning signs.

Not all Earth-system processes included in the PB approach have singular thresholds at the global/continental/ocean basin level (1). Nevertheless, it is important that boundaries be established for these processes. They affect the capacity of the Earth system to persist in a Holocene-like state under changing conditions (henceforth “resilience”) by regulating biogeochemical flows (e.g., the terrestrial and marine biological carbon sinks) or by providing the capacity for ecosystems to tolerate perturbations and shocks and to continue functioning under changing abiotic conditions (29, 30). Examples of such processes are land-system change, freshwater use, change in biosphere integrity [rate of biodiversity loss in (1, 2)], and changes in other biogeochemical flows in addition to carbon (e.g., nitrogen and phosphorus). Placing boundaries for these processes is more

difficult than for those with known large-scale thresholds (21) but is nevertheless important for maintaining the resilience of the Earth system as a whole. As indicated in Fig. 1, these processes, many of which show threshold behavior at local and regional scales, can generate feedbacks to the processes that do have large-scale thresholds. The classic example is the possible weakening of natural carbon sinks, which could further destabilize the climate system and push it closer to large thresholds [e.g., loss of the Greenland ice sheet (18)]. An interesting research question of relevance to the PB framework is how small-scale regime shifts can propagate across scales and possibly lead to global-level transitions (31, 32).

A zone of uncertainty, sometimes large, is associated with each of the boundaries (yellow zone in Fig. 1). This zone encapsulates both gaps and weaknesses in the scientific knowledge base and intrinsic uncertainties in the functioning of the Earth system. At the “safe” end of the zone of uncertainty, current scientific knowledge suggests that there is very low probability of crossing a critical threshold or substantially eroding the resilience of the Earth system. Beyond the “danger” end of the zone of uncertainty, current knowledge suggests a much higher probability of a change to the functioning of the Earth system that could potentially be devastating for human societies. Application of the precautionary principle dictates that the planetary boundary is set at the “safe” end of the zone of uncertainty. This does not mean that transgressing a boundary will instantly lead to an unwanted outcome but that the farther the boundary is transgressed, the higher the risk of regime shifts, destabilized sys-

tem processes, or erosion of resilience and the fewer the opportunities to prepare for such changes. Observations of the climate system show this principle in action by the influence of increasing atmospheric greenhouse gas concentrations on the frequency and intensity of many extreme weather events (17, 18).

Linking global and regional scales

PB processes operate across scales, from ocean basins/biomes or sources/sinks to the level of the Earth system as a whole. Here, we address the subglobal aspects of the PB framework. Rockström *et al.* (1) estimated global boundaries only, acknowledging that the control variables for many processes are spatially heterogeneous. That is, changes in control variables at the subglobal level can influence functioning at the Earth-system level, which indicates the need to define subglobal boundaries that are compatible with the global-level boundary definition. Avoiding the transgression of subglobal boundaries would thus contribute to an aggregate outcome within a planetary-level safe operating space.

We focus on the five PBs that have strong regional operating scales: biosphere integrity, biogeochemical flows [earlier termed “phosphorus (P) and nitrogen (N) cycles” (1, 2)], land-system change, freshwater use, and atmospheric aerosol loading. Table S1 describes how transgression of any of the proposed boundaries at the subglobal level affects the Earth system at the global level.

For those processes where subglobal dynamics potentially play a critical role in global dynamics, the operational challenge is to capture the importance of subglobal change for the functioning

of the Earth system. To do this, we propose the development of a two-level set of control variables and boundaries. The subglobal-level units of analysis for these six boundaries are not identical; they vary according to the role that the processes play in the Earth system: (i) changes in biosphere integrity occur at the level of land-based biomes, large freshwater ecosystems, or major marine ecosystems as the largest subglobal unit; (ii) the role of direct, human-driven land-system change in biophysical climate regulation is primarily related to changes in forest biomes; (iii) freshwater flows and use occur at the largest subglobal level in the major river basins around the world; and (iv) changes in biogeochemical flows, exemplified by phosphorus and nitrogen cycling, aggregate from relatively localized but very severe perturbations in intensive agricultural zones to affect global flows of nutrients. We recognize these as critical regions for Earth-system functioning. Where appropriate, the updates of the individual boundaries (see below) (33) now contain both the globally aggregated boundary value of the control variable and its regional distribution function. Figure 2 shows the distributions and current status of the control variables for three of the boundaries where subglobal dynamics are crit-

ical: biogeochemical cycles, land-system change, and freshwater use.

We emphasize that our subglobal-level focus is based on the necessity to consider this level to understand the functioning of the Earth system as a whole. The PB framework is therefore meant to complement, not replace or supersede, efforts to address local and regional environmental issues.

Updates of the individual boundaries

Brief updates of all nine of the PBs are given in this section, and more detailed descriptions of the updates for three of the PBs that have undergone more extensive revision can be found in (33). The geographical distribution issues discussed above are particularly important for five of the PBs, and their control variables and boundaries have been revised accordingly (Table 1). Figure 3 shows the current status of the seven boundaries that can be quantified at the global level.

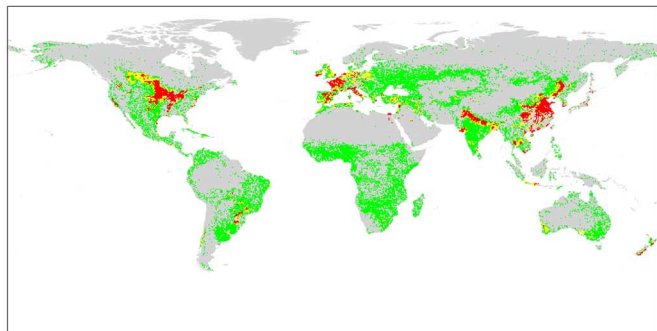
Climate change

We retain the control variables and boundaries originally proposed—i.e., an atmospheric CO₂ concentration of 350 parts per million (ppm) and an increase in top-of-atmosphere radiative forcing of +1.0 W m⁻² relative to preindustrial levels (1). The radiative forcing control variable is the more

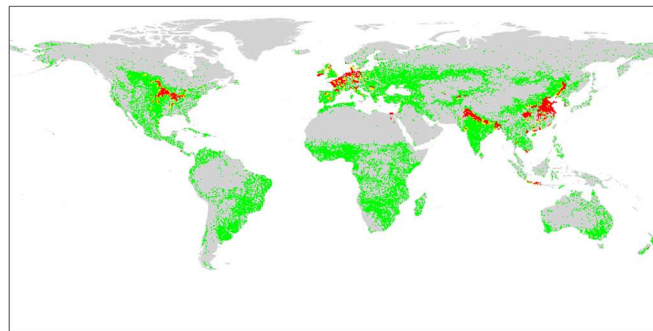
inclusive and fundamental, although CO₂ is important because of its long lifetime in the atmosphere and the very large human emissions. Human-driven changes to radiative forcing include all anthropogenic factors: CO₂, other greenhouse gases, aerosols, and other factors that affect the energy balance (18). Radiative forcing is generally the more stringent of the two boundaries, although the relationship between it and CO₂ can vary through time with changes in the relative importance of the individual radiative forcing factors.

Evidence has accumulated to suggest that the zone of uncertainty for the CO₂ control variable should be narrowed from 350 to 550 ppm to 350 to 450 ppm CO₂ (17, 18), while retaining the current zone of uncertainty for radiative forcing of +1.0 to 1.5 W m⁻² relative to preindustrial levels. Current values of the control variables are 399 ppm CO₂ (annual average concentration for 2014) (34) and +2.3 W m⁻² (1.1 to 3.3 W m⁻²) in 2011 relative to 1750 (18). Observed changes in climate at current levels of the control variables confirm the original choice of the boundary values and the narrowing of the zone of uncertainty for CO₂. For example, there has already been an increase in the intensity, frequency, and duration of heat waves globally (35); the number of heavy rainfall

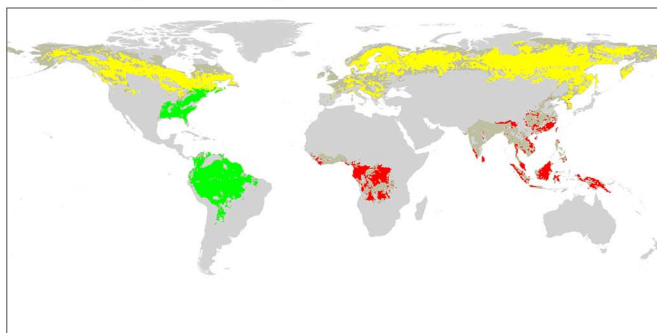
A Phosphorus



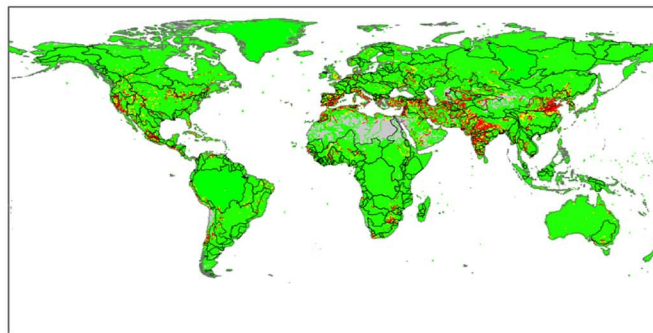
B Nitrogen



C Land-system change



D Freshwater use



■ Beyond zone of uncertainty (high risk) ■ In zone of uncertainty (increasing risk) ■ Below boundary (safe)

Fig. 2. The subglobal distributions and current status of the control variables for (A) biogeochemical flows of P; (B) biogeochemical flows of N; (C) land-system change; and (D) freshwater use. In each panel, green areas are within the boundary (safe), yellow areas are within the zone of uncertainty (increasing risk), and red areas are beyond the zone of uncertainty (high risk). Gray areas in (A) and (B) are areas where P and N fertilizers are not applied; in (C), they are areas not covered by major forest biomes; and in (D), they are areas where river flow is very low so that environmental flows are not allocated. See Table 1 for values of the boundaries and their zones of uncertainty and (33) for more details on methods and results.

Table 1. The updated control variables and their current values, along with the proposed boundaries and zones of uncertainty, for all nine planetary boundaries. In the first column, the name for the Earth-system process used in the original PB publication (R2009, reference 1) is given for comparison.

Earth-system process	Control variable(s)	Planetary boundary (zone of uncertainty)	Current value of control variable
Climate change (R2009: same)	Atmospheric CO ₂ concentration, ppm	350 ppm CO ₂ (350–450 ppm)	398.5 ppm CO ₂
	Energy imbalance at top-of-atmosphere, W m ⁻²	+1.0 W m ⁻² (+1.0–1.5 W m ⁻²)	2.3 W m ⁻² (1.1–3.3 W m ⁻²)
Change in biosphere integrity (R2009: Rate of biodiversity loss)	<i>Genetic diversity:</i> Extinction rate	< 10 E/MSY (10–100 E/MSY) but with an aspirational goal of ca. 1 E/MSY (the background rate of extinction loss). E/MSY = extinctions per million species-years	100–1000 E/MSY
	<i>Functional diversity:</i> Biodiversity Intactness Index (BII)	Maintain BII at 90% (90–30%) or above, assessed geographically by biomes/large regional areas (e.g. southern Africa), major marine ecosystems (e.g., coral reefs) or by large functional groups	84%, applied to southern Africa only
	Note: These are interim control variables until more appropriate ones are developed		
Stratospheric ozone depletion (R2009: same)	Stratospheric O ₃ concentration, DU	<5% reduction from pre-industrial level of 290 DU (5%–10%), assessed by latitude	Only transgressed over Antarctica in Austral spring (~200 DU)
Ocean acidification (R2009: same)	Carbonate ion concentration, average global surface ocean saturation state with respect to aragonite (Ω_{arag})	≥80% of the pre-industrial aragonite saturation state of mean surface ocean, including natural diel and seasonal variability (≥80%– ≥70%)	~84% of the pre-industrial aragonite saturation state
Biogeochemical flows: (P and N cycles) (R2009: Biogeochemical flows: (interference with P and N cycles))	<i>P Global:</i> P flow from freshwater systems into the ocean	11 Tg P yr ⁻¹ (11–100 Tg P yr ⁻¹)	~22 Tg P yr ⁻¹
	<i>P Regional:</i> P flow from fertilizers to erodible soils	6.2 Tg yr ⁻¹ mined and applied to erodible (agricultural) soils (6.2–11.2 Tg yr ⁻¹). Boundary is a global average but regional distribution is critical for impacts.	~14 Tg P yr ⁻¹
	<i>N Global:</i> Industrial and intentional biological fixation of N	62 Tg N yr ⁻¹ (62–82 Tg N yr ⁻¹). Boundary acts as a global 'valve' limiting introduction of new reactive N to Earth System, but regional distribution of fertilizer N is critical for impacts.	~150 Tg N yr ⁻¹

Earth-system process	Control variable(s)	Planetary boundary (zone of uncertainty)	Current value of control variable
Land-system change (R2009: same)	<i>Global:</i> Area of forested land as % of original forest cover	<i>Global:</i> 75% (75–54%) Values are a weighted average of the three individual biome boundaries and their uncertainty zones	62%
	<i>Biome:</i> Area of forested land as % of potential forest	<i>Biome:</i> Tropical: 85% (85–60%) Temperate: 50% (50–30%) Boreal: 85% (85–60%)	
Freshwater use (R2009: Global freshwater use)	<i>Global:</i> Maximum amount of consumptive blue water use (km ³ yr ^{–1})	<i>Global:</i> 4000 km ³ yr ^{–1} (4000–6000 km ³ yr ^{–1})	~2600 km ³ yr ^{–1}
	<i>Basin:</i> Blue water withdrawal as % of mean monthly river flow	<i>Basin:</i> Maximum monthly withdrawal as a percentage of mean monthly river flow. For low-flow months: 25% (25–55%); for intermediate-flow months: 30% (30–60%); for high-flow months: 55% (55–85%)	
Atmospheric aerosol loading (R2009: same)	<i>Global:</i> Aerosol Optical Depth (AOD), but much regional variation		0.30 AOD, over South Asian region
	<i>Regional:</i> AOD as a seasonal average over a region. South Asian Monsoon used as a case study	<i>Regional:</i> (South Asian Monsoon as a case study): anthropogenic total (absorbing and scattering) AOD over Indian subcontinent of 0.25 (0.25–0.50); absorbing (warming) AOD less than 10% of total AOD	
Introduction of novel entities (R2009: Chemical pollution)	No control variable currently defined	No boundary currently identified, but see boundary for stratospheric ozone for an example of a boundary related to a novel entity (CFCs)	

events in many regions of the world is increasing (17); changes in atmospheric circulation patterns have increased drought in some regions of the world (17); and the rate of combined mass loss from the Greenland and Antarctic ice sheets is increasing (36).

Changes in biosphere integrity

We propose a two-component approach, addressing two key roles of the biosphere in the Earth system. The first captures the role of genetically unique material as the “information bank” that ultimately determines the potential for life to

continue to coevolve with the abiotic component of the Earth system in the most resilient way possible. Genetic diversity provides the long-term capacity of the biosphere to persist under and adapt to abrupt and gradual abiotic change. The second captures the role of the biosphere in Earth-system functioning through the value, range, distribution, and relative abundance of the functional traits of the organisms present in an ecosystem or biota (7).

For the first role, the concept of phylogenetic species variability (PSV) (7, 33, 37) would be an appropriate control variable. However, because

global data are not yet available for PSV, we retain the global extinction rate as an interim control variable, although it is measured inaccurately and with a time lag. There may be a considerable risk in using extinction rate as a control variable, because phylogenetic (and functional) diversity may be more sensitive to human pressures than species-level diversity (38). In principle, the boundary should be set at a rate of loss of PSV no greater than the rate of evolution of new PSV during the Holocene. Because that is unknown, we must fall back on the (imperfectly) known extinction rate of well-studied organisms over the past several

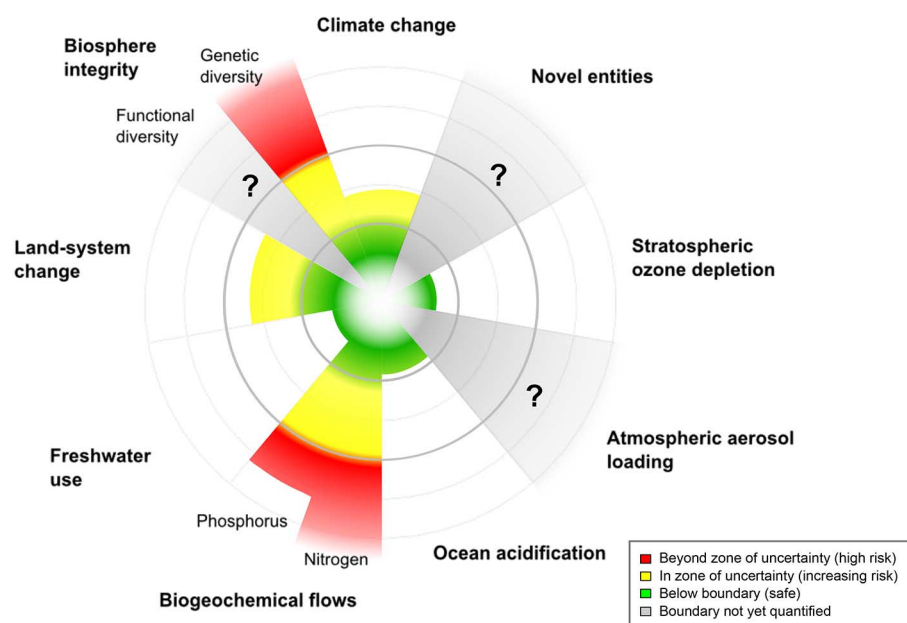


Fig. 3. The current status of the control variables for seven of the nine planetary boundaries. The green zone is the safe operating space (below the boundary), yellow represents the zone of uncertainty (increasing risk), and red is the high-risk zone. The planetary boundary itself lies at the inner heavy circle. The control variables have been normalized for the zone of uncertainty (between the two heavy circles); the center of the figure therefore does not represent values of 0 for the control variables. The control variable shown for climate change is atmospheric CO₂ concentration. Processes for which global-level boundaries cannot yet be quantified are represented by gray wedges; these are atmospheric aerosol loading, novel entities, and the functional role of biosphere integrity. Modified from (1).

million years—about 1 per million species-years (39)—and add a large uncertainty bound, raising the boundary to 10 per million species-years. The risk is that, although the Earth system can tolerate a higher-than-background level of extinctions for a time, we do not know what levels of, or types of, biodiversity loss may possibly trigger nonlinear or irreversible changes to the Earth system.

The second control variable aims to capture the role of the biosphere in Earth-system functioning and measures loss of biodiversity components at both global and biome/large ecosystem levels. Although several variables have been developed at local scales for measuring functional diversity [e.g., (40)], finding an appropriate control variable at regional or global levels is challenging. For the present, we propose an interim control variable, the Biodiversity Intactness Index (BII) (41). BII assesses change in population abundance as a result of human impacts, such as land or resource use, across a wide range of taxa and functional groups at a biome or ecosystem level using pre-industrial era abundance as a reference point. The index typically ranges from 100% (abundances across all functional groups at preindustrial levels) to lower values that reflect the extent and degree of human modification of populations of plants and animals. BII values for particular functional groups can go above 100% if human modifications to ecosystems lead to increases in the abundance of those species.

Due to a lack of evidence on the relationship between BII and Earth-system responses, we pro-

pose a preliminary boundary at 90% of the BII but with a very large uncertainty range (90 to 30%) that reflects the large gaps in our knowledge about the BII–Earth-system functioning relationship (42, 43). BII has been so far applied to southern Africa's terrestrial biomes only (see fig. S3 for an estimation of aggregated human pressures on the terrestrial biosphere globally), where the index (not yet disaggregated to functional groups) was estimated to be 84%. BII ranged from 69 to 91% for the seven countries where it has been applied (41). Observations across these countries suggest that decreases in BII adequately capture increasing levels of ecosystem degradation, defined as land uses that do not alter the land-cover type but lead to a persistent loss in ecosystem productivity (41).

In addition to further work on functional measures such as BII, in the longer term the concept of biome integrity—the functioning and persistence of biomes at broad scales (7)—offers a promising approach and, with further research, could provide a set of operational control variables (one per biome) that is appropriate, robust, and scientifically based.

Stratospheric ozone depletion

We retain the original control variable [O₃ concentration in DU (Dobson units)] and boundary (275 DU). This boundary is only transgressed over Antarctica in the austral spring, when O₃ concentration drops to about 200 DU (44). However, the minimum O₃ concentration has been

steady for about 15 years and is expected to rise over the coming decades as the ozone hole is repaired after the phasing out of ozone-depleting substances. This is an example in which, after a boundary has been transgressed regionally, humanity has taken effective action to return the process back to within the boundary.

Ocean acidification

This boundary is intimately linked with one of the control variables, CO₂, for the climate change PB. The concentration of free H⁺ ions in the surface ocean has increased by about 30% over the past 200 years due to the increase in atmospheric CO₂ (45). This, in turn, influences carbonate chemistry in surface ocean waters. Specifically, it lowers the saturation state of aragonite (Ω_{arag}), a form of calcium carbonate formed by many marine organisms. At $\Omega_{\text{arag}} < 1$, aragonite will dissolve. No new evidence has emerged to suggest that the originally proposed boundary ($\geq 80\%$ of the pre-industrial average annual global Ω_{arag}) should be adjusted, although geographical heterogeneity in Ω_{arag} is important in monitoring the state of the boundary around the world's oceans (fig. S4). Currently, Ω_{arag} is approximately equal to 84% of the preindustrial value (46). This boundary would not be transgressed if the climate-change boundary of 350 ppm CO₂ were to be respected.

Biogeochemical flows

The original boundary was formulated for phosphorus (P) and nitrogen (N) only, but we now propose a more generic PB to encompass human influence on biogeochemical flows in general. Although the carbon cycle is covered in the climate-change boundary, other elements, such as silicon (47, 48), are also important for Earth-system functioning. Furthermore, there is increasing evidence that ratios between elements in the environment may have impacts on biodiversity on land and in the sea (49–51). Thus, we may ultimately need to develop PBs for other elements and their ratios, although for now we focus on P and N only.

A two-level approach is now proposed for the P component of the biogeochemical flows boundary (see also the supplementary materials). The original global-level boundary, based on the prevention of a large-scale ocean anoxic event, is retained, with the proposed boundary set at a sustained flow of 11 Tg P year⁻¹ from freshwater systems into the ocean. Based on the analysis of Carpenter and Bennett (3), we now propose an additional regional-level P boundary, designed to avert widespread eutrophication of freshwater systems, at a flow of 6.2 Tg P year⁻¹ from fertilizers (mined P) to erodible soils.

Given that the addition of P to regional watersheds is almost entirely from fertilizers, the regional-level boundary applies primarily to the world's croplands. The current global rate of application of P in fertilizers to croplands is 14.2 Tg P year⁻¹ (52, 53). Observations point toward a few agricultural regions of very high P application rates as the main contributors to the transgression of this boundary (Fig. 2 and fig. S5A) and suggest that a redistribution of P from areas

where it is currently in excess to areas where the soil is naturally P-poor may simultaneously boost global crop production and reduce the transgression of the regional-level P boundary (3, 52, 54).

The N boundary has been taken from the comprehensive analysis of de Vries *et al.* (5), which proposed a PB for eutrophication of aquatic ecosystems of 62 Tg N year⁻¹ from industrial and intentional biological N fixation, using the most stringent water quality criterion. As for the P boundary, a few agricultural regions of very high N application rates are the main contributors to the transgression of this boundary (Fig. 2 and fig. S5B). This suggests that a redistribution of N could simultaneously boost global crop production and reduce the transgression of the regional-level boundary.

Because the major anthropogenic perturbation of both the N and P cycles arises from fertilizer application, we can analyze the links between the independently determined N and P boundaries in an integrated way based on the N:P ratio in the growing plant tissue of agricultural crops. Applying this ratio, which is on average 11.8 (55), to the P boundary (6.2 Tg P year⁻¹) gives an N boundary of 73 Tg N year⁻¹. Conversely, applying the ratio to the N boundary (62 Tg N year⁻¹) gives a P boundary of 5.3 Tg P year⁻¹. The small differences between the boundaries derived using the N:P ratio and those calculated independently, which are likely nonsignificant differences given the precision of the data available for the calculations, show the internal consistency in our approach to the biogeochemical boundaries.

More detail on the development of the P and N boundaries is given in (33), where we also emphasize that the proposed P and N boundaries may be larger for an optimal allocation of N (and P) over the globe.

Land-system change

The updated biosphere integrity boundary provides a considerable constraint on the amount and pattern of land-system change in all terrestrial biomes: forests, woodlands, savannas, grasslands, shrublands, tundra, and so on. The land-system change boundary is now focused more tightly on a specific constraint: the biogeophysical processes in land systems that directly regulate climate—exchange of energy, water, and momentum between the land surface and the atmosphere. The control variable has been changed from the amount of cropland to the amount of forest cover remaining, as the three major forest biomes—tropical, temperate and boreal—play a stronger role in land surface–climate coupling than other biomes (56, 57). In particular, we focus on those land-system changes that can influence the climate in regions beyond the region where the land-system change occurred.

Of the forest biomes, tropical forests have substantial feedbacks to climate through changes in evapotranspiration when they are converted to nonforested systems, and changes in the distribution of boreal forests affect the albedo of the land surface and hence regional energy exchange. Both have strong regional and global teleconnections.

The biome-level boundary for these two types of forest have been set at 85% (Table 1 and the supplementary materials), and the boundary for temperate forests has been proposed at 50% of potential forest cover, because changes to temperate forests are estimated to have weaker influences on the climate system at the global level than changes to the other two major forest biomes (56). These boundaries would almost surely be met if the proposed biosphere integrity boundary of 90% BII were respected.

Estimates of the current status of the land-system change boundary are given in Figs. 2 and 3 and fig. S6 and in (58).

Freshwater use

The revised freshwater use boundary has retained consumptive use of blue water [from rivers, lakes, reservoirs, and renewable groundwater stores (59)] as the global-level control variable and 4000 km³/year as the value of the boundary. This PB may be somewhat higher or lower depending on rivers' ecological flow requirements (6). Therefore, we report here a new assessment to complement the PB with a basin-scale boundary for the maximum rate of blue water withdrawal along rivers, based on the amount of water required in the river system to avoid regime shifts in the functioning of flow-dependent ecosystems. We base our control variable on the concept of environmental water flows (EWF), which defines the level of river flows for different hydrological characteristics of river basins adequate to maintain a fair-to-good ecosystem state (60–62).

The variable monthly flow (VMF) method (33, 63) was used to calculate the basin-scale boundary for water. This method takes account of intra-annual variability by classifying flow regimes into high-, intermediate-, and low-flow months and allocating EWF as a percentage of the mean monthly flow (MMF). Based on this analysis, the zones of uncertainty for the river-basin scale water boundary were set at 25 to 55% of MMF for the low-flow regime, 40 to 70% for the intermediate-flow regime, and 55 to 85% for the high-flow regime (table S2). The boundaries were set at the lower end of the uncertainty ranges that encompass average monthly EWF. Our new estimates of the current status of the water use boundary—computed based on grid cell-specific estimates of agricultural, industrial, and domestic water withdrawals—are shown in Figs. 2 and 3, with details in figs. S7 and S8.

Atmospheric aerosol loading

Aerosols have well-known, serious human health effects, leading to about 7.2 million deaths per year (64). They also affect the functioning of the Earth system in many ways (65) (fig. S9). Here, we focus on the effect of aerosols on regional ocean-atmosphere circulation as the rationale for a separate aerosols boundary. We adopt aerosol optical depth (AOD) (33) as the control variable and use the south Asian monsoon as a case study, based on the potential of widespread aerosol loading over the Indian subcontinent to switch the monsoon system to a drier state.

The background AOD over south Asia is ~0.15 and can be as high as 0.4 during volcanic events (66). Emissions of black carbon and organic carbon from cooking and heating with biofuels and from diesel transportation, and emission of sulfates and nitrates from fossil fuel combustion, can increase seasonal mean AODs to as high as 0.4 (larger during volcanic periods), leading to decreases of 10 to 15% of incident solar radiation at the surface (fig. S9). A substantial decrease in monsoon activity is likely around an AOD of 0.50, an increase of 0.35 above the background (67). Taking a precautionary approach toward uncertainties surrounding the position of the tipping point, we propose a boundary at an AOD of 0.25 (an increase due to human activities of 0.1), with a zone of uncertainty of 0.25 to 0.50. The annual mean AOD is currently about 0.3 (66), within the zone of uncertainty.

Introduction of novel entities

We define novel entities as new substances, new forms of existing substances, and modified life forms that have the potential for unwanted geophysical and/or biological effects. Anthropogenic introduction of novel entities to the environment is of concern at the global level when these entities exhibit (i) persistence, (ii) mobility across scales with consequent widespread distributions, and (iii) potential impacts on vital Earth-system processes or subsystems. These potentially include chemicals and other new types of engineered materials or organisms [e.g., (68–71)] not previously known to the Earth system, as well as naturally occurring elements (for example, heavy metals) mobilized by anthropogenic activities. The risks associated with the introduction of novel entities into the Earth system are exemplified by the release of CFCs (chlorofluorocarbons), which are very useful synthetic chemicals that were thought to be harmless but had unexpected, dramatic impacts on the stratospheric ozone layer. In effect, humanity is repeatedly running such global-scale experiments but not yet applying the insights from previous experience to new applications (72, 73).

Today there are more than 100,000 substances in global commerce (74). If nanomaterials and plastic polymers that degrade to microplastics are included, the list is even longer. There is also a “chemical intensification” due to the rapidly increasing global production of chemicals, the expanding worldwide distribution as chemical products or in consumer goods, and the extensive global trade in chemical wastes (75).

In recent years, there has been a growing debate about the global-scale effects of chemical pollution, leading to calls for the definition of criteria to identify the kinds of chemical substances that are likely to be globally problematic (76, 77). Persson *et al.* (73) proposed that there are three conditions that need to be fulfilled for a chemical to pose a threat to the Earth system: (i) the chemical has an unknown disruptive effect on a vital Earth-system process; (ii) the disruptive effect is not discovered until it is a problem at the global scale; and (iii) the effect is not readily

reversible. The challenge to the research community is to develop the knowledge base that allows the screening of chemicals, before they are released into the environment, for properties that may predispose them toward becoming global problems.

As a first step toward meeting this challenge, the three conditions outlined above have been used as the basis for identifying scenarios of chemical pollution that fulfill the conditions and as a next step for pinpointing chemical profiles that fit the scenarios (28). This proposal constitutes a first attempt at adding the Earth-system perspective when assessing hazard and risk of chemicals and offers a vision for a systematic approach to a complex management situation with many unknowns.

Despite this progress in developing an Earth-system-oriented approach, there is not yet an aggregate, global-level analysis of chemical pollution on which to base a control variable or a boundary value. It may also serve little purpose to define boundary values and control variables for a planetary boundary of this complexity. Nevertheless, there is a potential threat from novel entities to disrupt the functioning of the Earth-system and society needs to learn how to mitigate these unknown risks and manage chemicals under uncertainty (28, 73).

Some precautionary and preventive actions can be considered. These may include a stronger focus on green chemistry (78), finding synergies with risk-reducing interventions in other fields such as occupational health (79), paying more attention to learning from earlier mistakes (80, 81), and investing in science to better understand and monitor vital Earth-system processes in order to be able to detect disruptive effects from novel entities as early as possible.

Hierarchy of boundaries

An analysis of the many interactions among the boundaries (table S3 and fig. S10) suggests that two of them—climate change and biosphere integrity—are highly integrated, emergent system-level phenomena that are connected to all of the other PBs. They operate at the level of the whole Earth system (7) and have coevolved for nearly 4 billion years (82). They are regulated by the other boundaries and, on the other hand, provide the planetary-level overarching systems within which the other boundary processes operate. Furthermore, large changes in the climate or in biosphere integrity would likely, on their own, push the Earth system out of the Holocene state. In fact, transitions between time periods in Earth history have often been delineated by substantial shifts in climate, the biosphere, or both (82, 83).

These observations suggest a two-level hierarchy of boundaries, in which climate change and biosphere integrity should be recognized as core planetary boundaries through which the other boundaries operate. The crossing of one or more of the other boundaries may seriously affect human well-being and may predispose the transgression of a core boundary(ies) but does not by itself lead to a new state of the Earth system. This

hierarchical approach to classifying the boundaries becomes clearer by examining in more detail the roles of climate and biosphere integrity in the functioning of the Earth system.

The climate system is a manifestation of the amount, distribution, and net balance of energy at Earth's surface. The total amount of energy sets the overall conditions for life. In Earth's current climate, a range of global surface temperatures and atmospheric pressures allows the three phases of water to be present simultaneously, with ice and water vapor playing critical roles in the physical feedbacks of the climate system. The distribution of energy by latitude, over the land and sea surfaces, and within the ocean plays a major role in the circulation of the two great fluids, the ocean and the atmosphere. These systemic physical characteristics are key spatial determinants of the distribution of the biota and the structure and functioning of ecosystems and are controllers of biogeochemical flows.

Biosphere integrity is also crucial to Earth-system functioning, where the biosphere is defined as the totality of all ecosystems (terrestrial, freshwater, and marine) on Earth and their biota (32). These ecosystems and biota play a critical role in determining the state of the Earth system, regulating its material and energy flows and its responses to abrupt and gradual change (7). Diversity in the biosphere provides resilience to terrestrial and marine ecosystems (83, 84). The biosphere not only interacts with the other planetary boundaries but also increases the capacity of the Earth system to persist in a given state under changes in these other boundaries. The ultimate basis for the many roles that the biosphere plays in Earth-system dynamics is the genetic code of the biota, the basic information bank that defines the biosphere's functional role and its capacity to innovate and persist into the future.

Planetary boundaries in a societal context

A proposed approach for sustainable development goals (SDGs) (85) argues that the stable functioning of the Earth system is a prerequisite for thriving societies around the world. This approach implies that the PB framework, or something like it, will need to be implemented alongside the achievement of targets aimed at more immediate human needs, such as provision of clean, affordable, and accessible energy and the adequate supply of food. World development within the biophysical limits of a stable Earth system has always been a necessity [e.g., (86, 87)]. However, only recently, for a number of reasons, has it become possible to identify, evaluate, and quantify risks of abrupt planetary- and biome-level shifts due to overshoot of key Earth-system parameters: (i) the emergence of global-change thinking and Earth-system thinking (88); (ii) the rise of “the Planetary” as a relevant level of complex system understanding (89–92); and (iii) observable effects of the rapid increase in human pressures on the planet (16).

The PB approach is embedded in this emerging social context, but it does not suggest how to

maneuver within the safe operating space in the quest for global sustainability. For example, the PB framework does not as yet account for the regional distribution of the impact or its historical patterns. Nor does the PB framework take into account the deeper issues of equity and causation. The current levels of the boundary processes, and the transgressions of boundaries that have already occurred, are unevenly caused by different human societies and different social groups. The wealth benefits that these transgressions have brought are also unevenly distributed socially and geographically. It is easy to foresee that uneven distribution of causation and benefits will continue, and these differentials must surely be addressed for a Holocene-like Earth-system state to be successfully legitimated and maintained. However, the PB framework as currently construed provides no guidance as to how this may be achieved [although some potential synergies have been noted (54)], and it cannot readily be used to make choices between pathways for piecemeal maneuvering within the safe operating space or more radical shifts of global governance (93).

The nature of the PB framework implies that two important cautions should be observed when application of the framework to policy or management is proposed: boundary interactions and scale.

Boundary interactions

The planetary boundaries framework arises from the scientific evidence that Earth is a single, complex, integrated system—that is, the boundaries operate as an interdependent set [e.g., (94)] (table S1 and fig. S10). Although a systematic, quantitative analysis of interactions among all of the processes for which boundaries are proposed remains beyond the scope of current modeling and observational capacity, the Earth system clearly operates in well-defined states in which these processes and their interactions can create stabilizing or destabilizing feedbacks (16, 90, 95). This has profound implications for global sustainability, because it emphasizes the need to address multiple interacting environmental processes simultaneously (e.g., stabilizing the climate system requires sustainable forest management and stable ocean ecosystems).

Scale

The PB framework is not designed to be “downscaled” or “disaggregated” to smaller levels, such as nations or local communities. That said, the PB framework recognizes the importance of changes at the level of subsystems in the Earth system (e.g., biomes or large river basins) on the functioning of the Earth system as a whole. Also, there are strong arguments for an integrated approach coupling boundary definitions at regional and global levels with development goals to enable the application of “PB thinking” at levels (nations, basins, and regions) where policy action most commonly occurs [e.g., (85, 96)].

This update of the PB framework is one step on a longer-term evolution of scientific knowledge to

inform and support global sustainability goals and pathways. This evolution is needed more than ever before; there are severe implementation gaps in many global environmental policies relating to the PB issues, where problematic trends are not being halted or reversed despite international consensus about the urgency of the problems. The prospect of tighter resource constraints and rising environmental hazards is also unavoidably turning the focus onto global social equity and the planetary stewardship of Earth's life-support system. There is a need for a truly global evidence base, with much greater integration among issues, in order to respond to these global challenges. New research initiatives [e.g., Future Earth (www.futureearth.org)] provide evidence that science can respond to this need by applying Earth-system research to advance a new generation of integrated global analyses and to explore options for transformations toward sustainability. This is a clear sign that, as the risks of the Anthropocene to human well-being become clearer, research is maturing to a point where a systemic step-change is possible—and necessary—in exploring and defining a safe and just planetary operating space for the further development of human societies.

Methods summary

Our approach to building the planetary boundaries framework is described above. We have implemented the framework through an expert assessment and synthesis of the scientific knowledge of intrinsic biophysical processes that regulate the stability of the Earth system. Our precautionary approach is based on the maintenance of a Holocene-like state of the Earth system and on an assessment of the level of human-driven change that would risk destabilizing this state. For the climate change PB, there is already much literature on which to base such an assessment. For others, such as stratospheric ozone, ocean acidification, extinction rates, and P and N cycles, we have used estimates of preindustrial values of the control variable as a Holocene baseline. Where large, undesirable thresholds exist and have been studied (e.g., polar ice sheets, Amazon rainforest, aragonite dissolution, atmospheric aerosols, and the south Asian monsoon), quantitative boundaries can be readily proposed. For others, where the focus is on erosion of Earth-system resilience, the boundaries are more difficult (but not impossible) to quantify, as reflected in larger uncertainty zones.

We used large-scale assessments of the impacts of human activities on Earth-system functioning [e.g., Intergovernmental Panel on Climate Change (17, 18), the International Geosphere-Biosphere Programme synthesis (16), and chemicals (75, 80)] as sources of community-level understanding on which to propose PBs. Our update has also relied on post-2009 assessments of individual boundaries by the relevant expert research communities; examples include phosphorus (3), nitrogen (5), biosphere integrity (7), freshwater use (5, 63), and novel entities [with a focus on chemicals (28, 73)]. Finally, some new analyses have

been undertaken specifically for this paper: (i) a freshwater-use PB based on the EWF approach (33, 63); (ii) the linkage of the phosphorus and nitrogen boundaries via the N:P ratio in growing crop tissue (33); and (iii) the use of major forest biomes as the basis for the land-system change PB (33).

REFERENCES AND NOTES

1. J. Rockström *et al.*, Planetary boundaries: Exploring the safe operating space for humanity. *Ecol. Soc.* **14**, 32 (2009). <http://www.ecologyandsociety.org/vol14/iss2/art32/>
2. J. Rockström *et al.*, A safe operating space for humanity. *Nature* **461**, 472–475 (2009). doi: [10.1038/461472a](https://doi.org/10.1038/461472a); pmid: 19779433
3. S. R. Carpenter, E. M. Bennett, Reconsideration of the planetary boundary for phosphorus. *Environ. Res. Lett.* **6**, 014009 (2011). doi: [10.1088/1748-9326/6/1/014009](https://doi.org/10.1088/1748-9326/6/1/014009)
4. S. W. Running, Ecology. A measurable planetary boundary for the biosphere. *Science* **337**, 1458–1459 (2012). doi: [10.1126/science.1227620](https://doi.org/10.1126/science.1227620); pmid: 22997311
5. W. de Vries, J. Kros, C. Kroeze, S. P. Seitzinger, Assessing planetary and regional nitrogen boundaries related to food security and adverse environmental impacts. *Curr. Opin. Environ. Sust.* **5**, 392–402 (2013). doi: [10.1016/j.cosust.2013.07.004](https://doi.org/10.1016/j.cosust.2013.07.004)
6. D. Gerten *et al.*, Towards a revised planetary boundary for consumptive freshwater use: Role of environmental flow requirements. *Curr. Opin. Environ. Sust.* **5**, 551–558 (2013). doi: [10.1016/j.cosust.2013.11.001](https://doi.org/10.1016/j.cosust.2013.11.001)
7. G. M. Mace *et al.*, Approaches to defining a planetary boundary for biodiversity. *Glob. Environ. Change* **28**, 289–297 (2014). doi: [10.1016/j.gloenvcha.2014.07.009](https://doi.org/10.1016/j.gloenvcha.2014.07.009)
8. V. Galaz, *Global Environmental Governance, Technology and Politics: The Anthropocene Gap*. (Edward Elgar, Cheltenham, UK, 2014).
9. UN GSP (UN High-Level Panel on Global Sustainability). *Resilient People, Resilient Planet: A Future Worth Choosing* (Report for the 2012 Rio+20 Earth Summit, United Nations, New York, 2012).
10. WBCSD (World Business Council on Sustainable Development). *Action 2020 Overview* (WBCSD, Geneva, Switzerland, <http://action2020.org>, accessed 18 June 2014).
11. R. Costanza, L. Graumlich, W. Steffen, Eds., *Integrated History and Future of People on Earth* (MIT Press, Cambridge, MA USA, 2006).
12. S. Sörlin, P. Warde, in *Nature's End: History and the Environment*, S. Sörlin, P. Warde, Eds. (Palgrave MacMillan, London, 2009), pp. 1–19.
13. R. C. Bishop, Endangered species and uncertainty: The economics of a safe minimum standard. *Am. J. Agric. Econ.* **61**, 10–18 (1978). doi: [10.2307/1240156](https://doi.org/10.2307/1240156)
14. T. M. Crowards, Safe minimum standards: Costs and opportunities. *Ecol. Econ.* **25**, 303–314 (1998). doi: [10.1016/S0921-8009\(97\)00041-4](https://doi.org/10.1016/S0921-8009(97)00041-4)
15. W. Steffen, J. Crutzen, J. R. McNeill, The Anthropocene: Are humans now overwhelming the great forces of Nature? *Ambio* **36**, 614–621 (2007). doi: [10.1579/0044-7447\(2007\)36\[614:TAHNO\]2.0.CO;2](https://doi.org/10.1579/0044-7447(2007)36[614:TAHNO]2.0.CO;2); pmid: 18240674
16. W. Steffen *et al.*, *Global Change and the Earth System: A Planet Under Pressure* (The IGBP Book Series, Springer-Verlag, Berlin, Heidelberg, New York, 2004).
17. IPCC (Intergovernmental Panel on Climate Change), *Managing the risks of extreme events and disasters to advance climate change adaptation. A special report of Working Groups I and II of the IPCC*. C.B. Field *et al.*, Eds. (Cambridge University Press, Cambridge, UK (2012). doi: [10.1017/CBO9781139177245](https://doi.org/10.1017/CBO9781139177245)
18. IPCC (Intergovernmental Panel on Climate Change), *Climate Change 2013: The Physical Science Basis. Summary for Policymakers*, L. Alexander *et al.*, Eds. (IPCC Secretariat, Geneva, Switzerland, 2013). doi: [10.1017/CBO9781107415324](https://doi.org/10.1017/CBO9781107415324)
19. P. J. Crutzen, Geology of mankind. *Nature* **415**, 23 (2002). doi: [10.1038/415023a](https://doi.org/10.1038/415023a); pmid: 11780095
20. K. Richardson, W. Steffen, D. Liverman, *Climate Change: Global Risks, Challenges and Decisions* (Cambridge Univ. Press, Cambridge, UK, 2011).
21. T. M. Lenton *et al.*, Tipping elements in the Earth's climate system. *Proc. Natl. Acad. Sci. U.S.A.* **105**, 1786–1793 (2008). doi: [10.1073/pnas.0705414105](https://doi.org/10.1073/pnas.0705414105); pmid: 18258748
22. M. Scheffer *et al.*, Early-warning signals for critical transitions. *Nature* **461**, 53–59 (2009). doi: [10.1038/nature08227](https://doi.org/10.1038/nature08227); pmid: 19727193
23. S. R. Carpenter, W. A. Brock, Rising variance: A leading indicator of ecological transition. *Ecol. Lett.* **9**, 311–318 (2006). doi: [10.1111/j.1461-0248.2005.00877.x](https://doi.org/10.1111/j.1461-0248.2005.00877.x); pmid: 16958897
24. J. Bakke *et al.*, Rapid oceanic and atmospheric changes during the Younger Dryas cold period. *Nat. Geosci.* **2**, 202–205 (2009). doi: [10.1038/ngeo439](https://doi.org/10.1038/ngeo439)
25. M. Scheffer *et al.*, Anticipating critical transitions. *Science* **338**, 344–348 (2012). doi: [10.1126/science.1225244](https://doi.org/10.1126/science.1225244); pmid: 23087241
26. R. Wang *et al.*, Flickering gives early warning signals of a critical transition to a eutrophic lake state. *Nature* **492**, 419–422 (2012). doi: [10.1038/nature11655](https://doi.org/10.1038/nature11655); pmid: 23160492
27. R. Biggs, S. R. Carpenter, W. A. Brock, Turning back from the brink: Detecting an impending regime shift in time to avert it. *Proc. Natl. Acad. Sci. U.S.A.* **106**, 826–831 (2009). doi: [10.1073/pnas.0811729106](https://doi.org/10.1073/pnas.0811729106); pmid: 19124774
28. M. MacLeod *et al.*, Identifying chemicals that are planetary boundary threats. *Environ. Sci. Technol.* **48**, 11057–11063 (2014). doi: [10.1021/es501893m](https://doi.org/10.1021/es501893m); pmid: 25181298
29. C. S. Holling, Resilience and stability of ecological systems. *Annu. Rev. Ecol. Syst.* **4**, 1–23 (1973). doi: [10.1146/annurev.es.04.110173.000245](https://doi.org/10.1146/annurev.es.04.110173.000245)
30. C. Folke *et al.*, Resilience thinking: Integrating resilience, adaptability and transformability. *Ecol. Soc.* **15**, 20 (2010). www.ecologyandsociety.org/vol15/iss4/art20
31. T. P. Hughes, S. Carpenter, J. Rockström, M. Scheffer, B. Walker, Multiscale regime shifts and planetary boundaries. *Trends Ecol. Evol.* **28**, 389–395 (2013). doi: [10.1016/j.tree.2013.05.019](https://doi.org/10.1016/j.tree.2013.05.019); pmid: 23769417
32. T. M. Lenton, H. T. P. Williams, On the origin of planetary-scale tipping points. *Trends Ecol. Evol.* **28**, 380–382 (2013). doi: [10.1016/j.tree.2013.06.001](https://doi.org/10.1016/j.tree.2013.06.001); pmid: 23777818
33. Supplementary text, figures, and tables are available on Science Online.
34. NOAA (National Oceanic and Atmospheric Administration), NOAA-ESRL Annual CO₂ Data, accessed at: <http://co2now.org/Current-CO2/CO2-Now/annual-co2.html> (2014).
35. S. E. Perkins, L. V. Alexander, J. Nairn, Increasing frequency, intensity and duration of observed global heat waves and warm spells. *Geophys. Res. Lett.* **39**, L20714 (2012). doi: [10.1029/2012GL053361](https://doi.org/10.1029/2012GL053361)
36. A. Shepherd *et al.*, A reconciled estimate of ice-sheet mass balance. *Science* **338**, 1183–1189 (2012). doi: [10.1126/science.1228102](https://doi.org/10.1126/science.1228102); pmid: 23197528
37. M. R. Helmus, T. J. Bland, C. K. Williams, A. R. Ives, Phylogenetic measures of biodiversity. *Am. Nat.* **169**, E68–E83 (2007). doi: [10.1086/511334](https://doi.org/10.1086/511334); pmid: 17230400
38. S. D'agata *et al.*, Human-mediated loss of phylogenetic and functional diversity in coral reef fishes. *Curr. Biol.* **24**, 555–560 (2014). doi: [10.1016/j.cub.2014.01.049](https://doi.org/10.1016/j.cub.2014.01.049); pmid: 24560574
39. A. D. Barnosky *et al.*, Has the Earth's sixth mass extinction already arrived? *Nature* **471**, 51–57 (2011). doi: [10.1038/nature09678](https://doi.org/10.1038/nature09678); pmid: 21368823
40. N. W. Mason, F. de Bello, D. Mouillot, S. Pavoine, S. Dray, A guide for using functional diversity indices to reveal changes in assembly processes along ecological gradients. *J. Veg. Sci.* **24**, 794–806 (2013). doi: [10.1111/jvs.12013](https://doi.org/10.1111/jvs.12013)
41. R. J. Scholes, R. Biggs, A biodiversity intactness index. *Nature* **434**, 45–49 (2005). doi: [10.1038/nature03289](https://doi.org/10.1038/nature03289); pmid: 15744293
42. B. Cardinale, Ecology. Impacts of biodiversity loss. *Science* **336**, 552–553 (2012). doi: [10.1126/science.1222102](https://doi.org/10.1126/science.1222102); pmid: 22556243
43. D. U. Hooper *et al.*, A global synthesis reveals biodiversity loss as a major driver of ecosystem change. *Nature* **486**, 105–108 (2012). doi: [10.1038/nature11118](https://doi.org/10.1038/nature11118); pmid: 22678289
44. BAS (British Antarctic Survey), "Antarctic ozone" www.antarctica.ac.uk/met/jds/ozone/index.html#data, J. Shanklin, British Antarctic Survey (2013).
45. Royal Society, *Ocean Acidification Due to Increasing Atmospheric Carbon Dioxide*. Policy Document 12/05 (The Royal Society, London, 2005).
46. J. M. Guinotte, V. J. Fabry, Ocean acidification and its potential effects on marine ecosystems. *Ann. N. Y. Acad. Sci.* **1134**, 320–342 (2008). doi: [10.1196/annals.1439.013](https://doi.org/10.1196/annals.1439.013); pmid: 18566099
47. D. J. Conley, Terrestrial ecosystems and the global biogeochemical silica cycle. *Global Biogeochem. Cycles* **16**, 681–688 (2002). doi: [10.1029/2002GB001894](https://doi.org/10.1029/2002GB001894)

48. F. Vandevenne, E. Struyf, W. Clymans, P. Meire, Agricultural silica harvest: Have humans created a new loop in the global silica cycle? *Front. Ecol. Environ* **10**, 243–248 (2012). doi: [10.1890/110046](https://doi.org/10.1890/110046)
49. S. E. Gress, T. D. Nichols, C. C. Northcraft, W. T. Peterjohn, Nutrient limitation in soils exhibiting differing nitrogen availabilities: What lies beyond nitrogen saturation? *Ecol.* **88**, 119–130 (2007). doi: [10.1890/0012-9658\(2007\)88\[119:NUSED\]2.0.CO;2](https://doi.org/10.1890/0012-9658(2007)88[119:NUSED]2.0.CO;2); pmid: [17489460](https://pubmed.ncbi.nlm.nih.gov/17489460/)
50. H. Hillebrand, V. Lehmppuhl, Resource stoichiometry and consumers control the biodiversity-productivity relationship in pelagic metacommunities. *Am. Nat.* **178**, 171–181 (2011). doi: [10.1086/660831](https://doi.org/10.1086/660831); pmid: [21750381](https://pubmed.ncbi.nlm.nih.gov/21750381/)
51. C. M. Moore *et al.*, Processes and patterns of oceanic nutrient limitation. *Nat. Geosci.* **6**, 701–710 (2013). doi: [10.1038/ngeo1765](https://doi.org/10.1038/ngeo1765)
52. G. K. MacDonald, E. M. Bennett, P. A. Potter, N. Ramankutty, Agronomic phosphorus imbalances across the world's croplands. *Proc. Natl. Acad. Sci. U.S.A.* **108**, 3086–3091 (2011). doi: [10.1073/pnas.1010808108](https://doi.org/10.1073/pnas.1010808108); pmid: [21282605](https://pubmed.ncbi.nlm.nih.gov/21282605/)
53. L. Bouwman *et al.*, Exploring global changes in nitrogen and phosphorus cycles in agriculture induced by livestock production over the 1900–2050 period. *Proc. Natl. Acad. Sci. U.S.A.* **110**, 20882–20887 (2013). doi: [10.1073/pnas.1012878108](https://doi.org/10.1073/pnas.1012878108); pmid: [21576477](https://pubmed.ncbi.nlm.nih.gov/21576477/)
54. W. Steffen, M. Stafford Smith, Planetary boundaries, equity and global sustainability: Why wealthy countries could benefit from more equity. *Curr. Opin. Environ. Sust.* **5**, 403–408 (2013). doi: [10.1016/j.cosust.2013.04.007](https://doi.org/10.1016/j.cosust.2013.04.007)
55. D. J. Greenwood *et al.*, A unifying concept for the dependence of whole-crop N : P ratio on biomass: theory and experiment. *Ann. Bot. (Lond.)* **102**, 967–977 (2008). doi: [10.1093/aob/mcn188](https://doi.org/10.1093/aob/mcn188); pmid: [18840873](https://pubmed.ncbi.nlm.nih.gov/18840873/)
56. P. K. Snyder, C. Delire, J. A. Foley, Evaluating the influence of different vegetation biomes on the global climate. *Clim. Dyn.* **23**, 279–302 (2004). doi: [10.1007/s00382-004-0430-0](https://doi.org/10.1007/s00382-004-0430-0)
57. P. C. West, G. T. Narisma, C. C. Barford, C. J. Kucharik, J. A. Foley, An alternative approach for quantifying climate regulation by ecosystems. *Front. Ecol. Environ* **9**, 126–133 (2010). doi: [10.1890/0900015](https://doi.org/10.1890/0900015)
58. EPI (Earth Policy Institute), "Forest cover" www.earthpolicy.org/indicators/C56/forests_2012_ (2014).
59. M. Falkenmark, Meeting water requirements of an expanding world population. *Philos. Trans. R. Soc. Lond. B Biol. Sci.* **352**, 929–936 (1997). doi: [10.1098/rstb.1997.0072](https://doi.org/10.1098/rstb.1997.0072)
60. J. S. Wallace, M. C. Acreman, C. A. Sullivan, The sharing of water between society and ecosystems: From conflict to catchment-based co-management. *Philos. Trans. R. Soc. Lond. B Biol. Sci.* **358**, 2011–2026 (2003). doi: [10.1098/rstb.2003.1383](https://doi.org/10.1098/rstb.2003.1383); pmid: [14728795](https://pubmed.ncbi.nlm.nih.gov/14728795/)
61. N. L. Poff *et al.*, The natural flow regime: A paradigm for river conservation and restoration. *BioSci.* **47**, 769–784 (1997). doi: [10.2307/1313099](https://doi.org/10.2307/1313099)
62. N. L. Poff, J. K. H. Zimmerman, Ecological responses to altered flow regimes: A literature review to inform the science and management of environmental flows. *Biol.* **55**, 194–205 (2010). doi: [10.1111/j.1365-2427.2009.02272.x](https://doi.org/10.1111/j.1365-2427.2009.02272.x)
63. A. V. Pastor, F. Ludwig, H. Biemans, H. Hoff, P. Kabat, Accounting for environmental flow requirements in global water assessments. *Hydrol. Earth Syst. Sci.* **18**, 5041–5059 (2014). doi: [10.5194/hess-18-5041-2014](https://doi.org/10.5194/hess-18-5041-2014)
64. WHO (World Health Organization), *Burden of Disease from the Joint Effects of Household and Ambient Air Pollution for 2012* (www.who.int/phe/health_topics/outdoorair/databases/FINAL_HAP_AAP_BoD24March2014.pdf, accessed 23 June 2014; http://www.who.int/phe/health_topics/outdoorair/databases/en)
65. O. Boucher *et al.*, in *Climate Change 2013: The Physical Science Basis*. IPCC AR5 WGI report, T. Stocker *et al.*, Eds. (Cambridge Univ. Press, Cambridge, UK, 2013), chap. 7, pp. 571–657.
66. M. Chin *et al.*, Multi-decadal aerosol variations from 1980 to 2009: A perspective from observations and a global model. *Atmos. Chem. Phys.* **14**, 3657–3690 (2014). doi: [10.5194/acp-14-3657-2014](https://doi.org/10.5194/acp-14-3657-2014)
67. V. Ramanathan *et al.*, Atmospheric brown clouds: Impacts on South Asian climate and hydrological cycle. *Proc. Natl. Acad. Sci. U.S.A.* **102**, 5326–5333 (2005). doi: [10.1073/pnas.0500656102](https://doi.org/10.1073/pnas.0500656102); pmid: [15749818](https://pubmed.ncbi.nlm.nih.gov/15749818/)
68. M. Cole, P. Lindeque, C. Halsband, T. S. Galloway, Microplastics as contaminants in the marine environment: A review. *Mar. Pollut. Bull.* **62**, 2588–2597 (2011). doi: [10.1016/j.marpolbul.2011.09.025](https://doi.org/10.1016/j.marpolbul.2011.09.025); pmid: [22001295](https://pubmed.ncbi.nlm.nih.gov/22001295/)
69. EEA (European Environment Agency), *Genetically Modified Organisms (GMOs): The Significance of Gene Flow Through Pollen Transfer* (Environmental Issue Report 28, European Environment Agency, Copenhagen, Denmark, 2002).
70. J. A. Ivar do Sul, M. F. Costa, The present and future of microplastic pollution in the marine environment. *Environ. Pollut.* **185**, 352–364 (2014). doi: [10.1016/j.envpol.2013.10.036](https://doi.org/10.1016/j.envpol.2013.10.036); pmid: [24275078](https://pubmed.ncbi.nlm.nih.gov/24275078/)
71. R. Kessler, Engineered nanoparticles in consumer products: Understanding a new ingredient. *Environ. Health Perspect.* **119**, a120–a125 (2011). doi: [10.1289/ehp.119-a120](https://doi.org/10.1289/ehp.119-a120); pmid: [21356630](https://pubmed.ncbi.nlm.nih.gov/21356630/)
72. M. Rees, *Our Final Century. Will Civilisation Survive the Twenty-first Century?* (Arrow Books, London, 2003).
73. L. M. Persson *et al.*, Confronting unknown planetary boundary threats from chemical pollution. *Environ. Sci. Technol.* **47**, 12619–12622 (2013). doi: [10.1021/es402501c](https://doi.org/10.1021/es402501c); pmid: [23980998](https://pubmed.ncbi.nlm.nih.gov/23980998/)
74. P. P. Egeghy *et al.*, The exposure data landscape for manufactured chemicals. *Sci. Total Environ.* **414**, 159–166 (2012). doi: [10.1016/j.scitotenv.2011.10.046](https://doi.org/10.1016/j.scitotenv.2011.10.046); pmid: [22104386](https://pubmed.ncbi.nlm.nih.gov/22104386/)
75. UNEP (United Nations Environment Programme), *GCO Global Chemicals Outlook: Towards Sound Management of Chemicals* (United Nations Environment Programme, Nairobi, Kenya, 2013).
76. S. Stempel, M. Scheringer, C. A. Ng, K. Hungerbühler, Screening for PBT chemicals among the "existing" and "new" chemicals of the EU. *Environ. Sci. Technol.* **46**, 5680–5687 (2012). doi: [10.1021/es3002713](https://doi.org/10.1021/es3002713); pmid: [22494215](https://pubmed.ncbi.nlm.nih.gov/22494215/)
77. M. Scheringer *et al.*, How many persistent organic pollutants should we expect? *Atmos. Poll. Res.* **3**, 383–391 (2012). doi: [10.5094/APR.2012.044](https://doi.org/10.5094/APR.2012.044)
78. K. Sanderson, Chemistry: It's not easy being green. *Nature* **469**, 18–20 (2011). doi: [10.1038/469018a](https://doi.org/10.1038/469018a); pmid: [21209638](https://pubmed.ncbi.nlm.nih.gov/21209638/)
79. P. A. Schulte *et al.*, Occupational safety and health, green chemistry, and sustainability: A review of areas of convergence. *Environ. Health* **12**, 31 (2013). doi: [10.1186/1476-069X-12-31](https://doi.org/10.1186/1476-069X-12-31); pmid: [23587312](https://pubmed.ncbi.nlm.nih.gov/23587312/)
80. EEA (European Environment Agency), *Late Lessons from Early Warnings: The Precautionary Principle 1896-2000* (Environmental Issue Report 22/2001, Copenhagen, Denmark, 2001).
81. D. Gee, Late lessons from early warnings: Toward realism and precaution with endocrine-disrupting substances. *Environ. Health Perspect.* **114** (suppl. 1), 152–160 (2006). doi: [10.1289/ehp.8134](https://doi.org/10.1289/ehp.8134); pmid: [16818262](https://pubmed.ncbi.nlm.nih.gov/16818262/)
82. T. Lenton, A. Watson, A., *Revolutions That Made the Earth* (Oxford Univ. Press, Oxford UK, 2011).
83. R. Biggs *et al.*, Toward principles for enhancing the resilience of ecosystem services. *Annu. Rev. Environ. Resour.* **37**, 421–448 (2012). doi: [10.1146/annurev-environ-051211-123836](https://doi.org/10.1146/annurev-environ-051211-123836)
84. G. S. Cumming, P. Olsson, F. S. Chapin III, C. S. Holling, Resilience, experimentation and scale mismatches in social-ecological systems. *Landscape Ecol.* **28**, 1139–1150 (2013). doi: [10.1007/s10980-012-9725-4](https://doi.org/10.1007/s10980-012-9725-4)
85. D. Griggs *et al.*, Policy: Sustainable development goals for people and planet. *Nature* **495**, 305–307 (2013). doi: [10.1038/495305a](https://doi.org/10.1038/495305a); pmid: [23518546](https://pubmed.ncbi.nlm.nih.gov/23518546/)
86. R. Costanza, Ed., *Ecological Economics: The Science and Management of Sustainability* (Columbia Univ. Press, New York, 1991).
87. C. Folke, in *Linking the Natural Environment and the Economy: Essays from the Eco-Eco Group*, C. Folke, T. Kåberger, Eds. (Kluwer Academic Publishers, Dordrecht, Netherlands, 1991), pp. 77–94.
88. L. Robin, S. Sörlin, P. Warde, Eds., *The Future of Nature: Documents of Global Change* (Yale Univ. Press, New Haven, CT, 2013).
89. U. Heise, *Sense of Place and Sense of Planet: The Environmental Imagination of the Global* (Oxford Univ. Press, Oxford, 2008).
90. M. Scheffer, *Critical Transitions in Nature and Society* (Princeton Univ. Press, Princeton, NJ, 2009).
91. J. Masco, Bad weather: On planetary crisis. *Soc. Stud. Sci.* **40**, 7–40 (2010). doi: [10.1177/0306312709341598](https://doi.org/10.1177/0306312709341598)
92. G. Pálsson *et al.*, Reconceptualizing the 'Anthropos' in the Anthropocene: Integrating the social sciences and humanities in global environmental change research. *Environ. Sci. Policy* **28**, 4 (2013). doi: [10.1016/j.envsci.2012.11.004](https://doi.org/10.1016/j.envsci.2012.11.004)
93. N. Castree *et al.*, Changing the intellectual climate. *Nature Clim. Change* **4**, 763–768 (2014). doi: [10.1038/nclimate2339](https://doi.org/10.1038/nclimate2339)
94. J. M. Anderies, S. R. Carpenter, W. Steffen, J. Rockström, The topology of non-linear global carbon dynamics: From tipping points to planetary boundaries. *Environ. Res. Lett.* **8**, 044048 (2013). doi: [10.1088/1748-9326/8/4/044048](https://doi.org/10.1088/1748-9326/8/4/044048)
95. S. E. Cornell, I. C. Prentice, J. I. House, C. J. Downy, *Understanding the Earth System. Global Change Science for Application* (Cambridge Univ. Press, Cambridge, 2012).
96. J. A. Dearing *et al.*, Safe and just operating spaces for regional social-ecological systems. *Glob. Environ. Change* **28**, 227–238 (2014). doi: [10.1016/j.gloenvcha.2014.06.012](https://doi.org/10.1016/j.gloenvcha.2014.06.012)

ACKNOWLEDGMENTS

We thank J. Foley and N. Ramankutty for contributions to the land-system change boundary; A. Pastor for analytical work on the PB for freshwater; B. Armstrong, C. Butler, T. McMichael, and A. Woodward for contributions to the novel entities boundary; and B. Scholes for comments on an earlier version of the manuscript. Data associated with the paper are located at the Stockholm Resilience Centre, Sweden (<http://www.stockholmresilience.org/21/research/research-programmes/planetary-boundaries.html>). The planetary boundaries research at the Stockholm Resilience Centre is made possible through a core grant from MISTRA (Swedish Foundation for Strategic Environmental Research). S.E.C. is supported by the Swedish Research Council, E.M.B. is supported by the Natural Sciences and Engineering Research Council of Canada and by the Trottier Institute for Science and Public Policy, R.B. is supported by a Branco Weiss Fellowship, C.F. is supported by the Family Erling Persson Academy Programme on Global Economic Dynamics and the Biosphere, I.F. is supported by the Stordalen Foundation (Norway), S.S. is supported by the Riksbankens Jubileumsfond and the Institute for Advanced Study, Princeton NJ, and S.R.C. and V.R. are supported by the U.S. National Science Foundation.

SUPPLEMENTARY MATERIALS

www.sciencemag.org/content/347/6223/1259855/suppl/DC1
Methods
Figs. S1 to S10
Tables S1 to S3
References (97–158)

11 August 2014; accepted 8 January 2015
Published online 15 January 2015;
[10.1126/science.1259855](https://doi.org/10.1126/science.1259855)

RESEARCH ARTICLE

ORGANIC CHEMISTRY

A data-intensive approach to mechanistic elucidation applied to chiral anion catalysis

Anat Milo,^{1*} Andrew J. Neel,^{2*} F. Dean Toste,^{2†} Matthew S. Sigman^{1†}

Knowledge of chemical reaction mechanisms can facilitate catalyst optimization, but extracting that knowledge from a complex system is often challenging. Here, we present a data-intensive method for deriving and then predictively applying a mechanistic model of an enantioselective organic reaction. As a validating case study, we selected an intramolecular dehydrogenative C-N coupling reaction, catalyzed by chiral phosphoric acid derivatives, in which catalyst-substrate association involves weak, noncovalent interactions. Little was previously understood regarding the structural origin of enantioselectivity in this system. Catalyst and substrate substituent effects were probed by means of systematic physical organic trend analysis. Plausible interactions between the substrate and catalyst that govern enantioselectivity were identified and supported experimentally, indicating that such an approach can afford an efficient means of leveraging mechanistic insight so as to optimize catalyst design.

Catalyst discovery and development often rely on empirical observations gained through the laborious evaluation of multiple potential reaction variables (*1*). Although high-throughput methods can streamline this process (*1–9*), the ability to rationally design catalysts that affect chemical reactions in a predictable manner would be a transformative step forward. In catalysis, the principal challenge lies in inferring how catalyst structural features affect the mechanistic aspects of a given chemical reaction, including those that govern selectivity when multiple products are possible (*10–12*). Although mechanistic studies are able to guide the rational design of catalytic systems, traditional approaches are not often suited to address the complexity of modern catalytic transformations. This limitation is especially apparent in cases in which selectivity is affected by subtle catalyst and substrate structural features (*13*), and/or the product-determining step of the reaction occurs after the rate-determining step. In order to address such systems, we envisioned a strategy for mechanistic study involving the application of modern data analysis techniques. This approach relies on the generation of mathematical correlations between quantifiable properties describing the interacting reaction partners' molecular structures (molecular descriptors) and a measurable outcome of the reaction {for example, enantioselectivity,

which is represented as the energy difference between transition states leading to either enantiomer $\Delta\Delta G^\ddagger = -RT\ln[(S)/(R)]$, kilocalories/mole} (*14*). Combining appropriate experimental design, data organization, and trend analysis techniques provides the basis to distinguish causal relations, producing testable hypotheses regarding the structural origin of the reaction outcome. New catalysts can be designed, and the ability of the models to predict new experimental outcomes can be used as validation of the mechanistic hypotheses. Here, we demonstrate that this approach enables in-depth mechanistic analysis of interactions that govern enantioselectivity, affording nonintuitive insight into the origin of asymmetric induction and guiding rational catalyst design.

Choice of case study

To assess the applicability of this data-driven approach toward mechanistic analysis, a system was sought with a poorly understood mechanism that would be difficult to probe by using standard techniques. Accordingly, the field of chiral anion catalysis was appealing because diverse catalyst-substrate interactions contribute to enantioselectivity, but their distinctive effects are difficult to deconvolute. Particularly, the oxoammonium salt (**3**)-mediated enantioselective cross dehydrogenative coupling (CDC) catalyzed by chiral 1,1'-Bi-2-naphthol (BINOL)-based phosphoric acids (PAs) (Fig. 1, **1**) bearing triazoles at the 3 and 3' positions reported in 2013 by Toste and coworkers (*15*) was identified as a prototypical example. This type of reaction could benefit from such an analysis because of the following challenges. First, high levels of enantioselectivity were necessarily predicated on the oxidant's (*16–19*) insolubility under the reaction condi-

tions, precluding rigorous kinetic analyses. Second, the enantioselectivity trends with respect to both catalyst and substrate were not obvious, with even modest structural modifications resulting in substantial differences (Fig. 1C). Last, we hypothesized that enantioselectivity was governed by attractive noncovalent interactions (*15*). These subtle interactions are ubiquitous in biological and catalytic systems (*13*) but are difficult to study or apply toward rational catalyst design, especially if several such interactions are involved in determining reaction outcomes.

The distinct mechanistic features of triazole-PA catalysts are highlighted by the observation that they result in opposite and enhanced enantioselectivities (Fig. 1A) relative to more conventional PAs such as C₈-TRIP (**5**) and TCYP (**6**), which are representative of BINOL-based PAs that have seen the most extensive use (*20–22*). Additionally, electronically distinct pyrazolyl (**pyr-1e**) and imidazolyl (**imid-1e**) PAs afford products with significantly reduced enantioselectivities relative to the parent triazolyl (Fig. 1A, **1e**), despite having nearly identical steric profiles. Although these data allude to selectivity determination via attractive, noncovalent interactions between the catalyst and substrate, such interactions are difficult to further characterize. This limitation is not uncommon in enantioselective catalysis. Thus, our goal was to develop a general, data-driven technique for the evaluation of how subtle structural features affect selectivity, using this reaction as a challenging case study.

Kinetic isotope effects

Before any mechanistic study focused on the origins of selectivity, we sought to establish the enantioselectivity-imparting step (or steps) in the catalytic cycle. Bearing in mind the aim of mathematically relating structural features of the reacting components to enantioselectivity, this knowledge would reveal the elementary step that is being represented by the catalyst and substrate molecular descriptors (vide infra). With respect to the general mechanism in Fig. 1B, we sought to distinguish two scenarios: (i) Enantioselectivity is determined during oxidation of substrate **2**, or (ii) enantioselectivity is determined during the cyclization of an oxidized intermediate (Fig. 2A, **A**). With respect to the former scenario, it was conceivable that although the stereogenic center is formally set in the cyclization from the oxidized intermediate (**A**), the interactions between the substrate and catalyst during the oxidation event may preorganize the system for effective enantioselection.

To distinguish between these possibilities, a set of kinetic isotope (KIE) experiments was performed by using **2a-d₁** [90% D incorporation, 74:26 enantiomeric ratio (er)]. We expected that if the chiral phosphate were involved in substrate oxidation, different KIEs would be observed for the formation of **4a-d₁** when using enantiomeric catalysts. Indeed, (*R*)- and (*S*)-**1e** promoted the reaction with KIEs of 3.42 and 1.08 respectively, suggesting the involvement of the catalyst in the

¹Department of Chemistry, University of Utah, 315 South 1400 East, Salt Lake City, UT 84112, USA. ²Chemical Sciences Division, Lawrence Berkeley National Laboratory, and Department of Chemistry, University of California, Berkeley, CA 94720, USA.

*These authors contributed equally to this work. †Corresponding author. E-mail: sigman@chem.utah.edu (M.S.S.); fdtoste@berkeley.edu (F.D.T.)

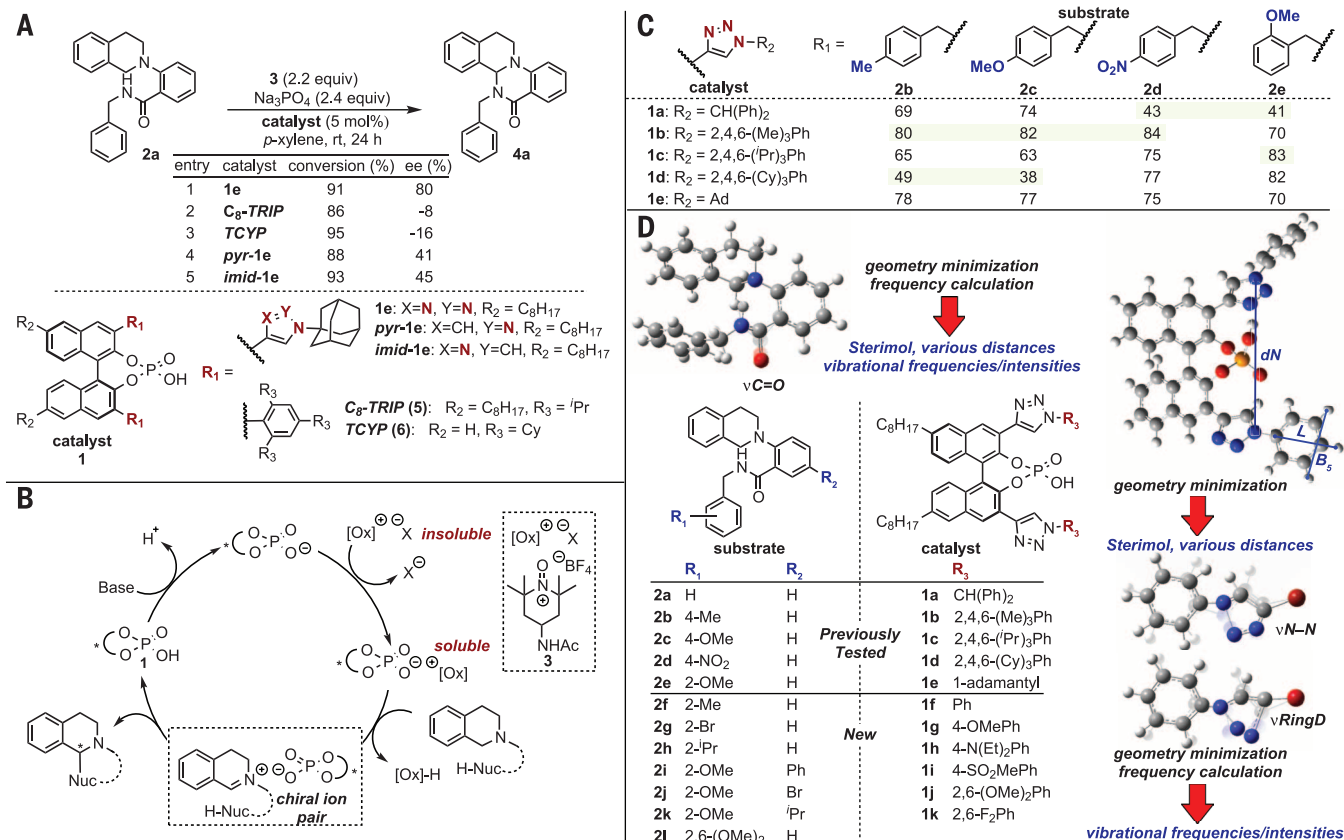


Fig. 1. System under study: asymmetric C-N dehydrogenative coupling. (A) BINOL-based phosphoric acid scaffold, enantioselective cross dehydrogenative coupling reaction scheme, and nitrogen-deletion experiment. (B) Proposed mechanism involving a chiral phosphate-substrate ion pair. (C) Enantiomeric excess (ee) values obtained by using various substrate/catalyst combinations. (D) Library design and parameter identification strategy.

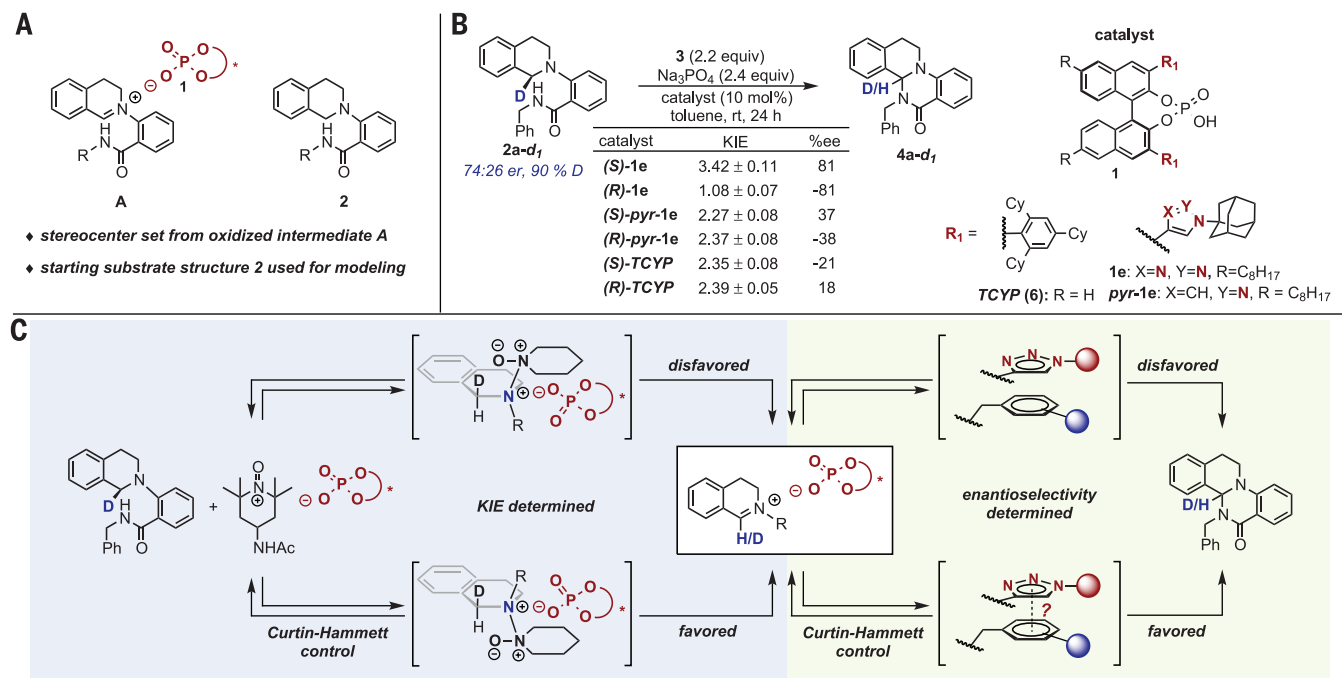


Fig. 2. Kinetic isotope effect studies and mechanistic implications. (A) Considerations regarding the origin of enantioselectivity. (B) KIEs of deuterated enantiomerically enriched substrate 2a-d₁ with (R) and (S) PA catalysts: adamantyl-substituted triazolyl (1e) and pyrazolyl (pyr-1e), and TCYP (6). (C) Revised mechanism of enantioselectivity determination.

oxidation (Fig. 2B). If enantioselectivity were also established in this step, different enantiomeric excess (ee) values would be expected when using the enantiomeric catalysts. The observation that the final products exhibited equal but opposite levels of enantioselectivity is consistent with enantioselection occurring during the bond-forming event from an oxidized intermediate such as **A**. This result indicated that the two key steps of this reaction (oxidation and cyclization) proceed under independent Curtin-Hammett control (10, 11), with similar interactions presumably governing selectivity in both cases (Fig. 2C). The KIE values resulting from the less-selective catalysts **pyr-1e** and **6** (Figs. 1A and 2B) do not display the same enantiomer-dependency as those from **1e**. This effect is consistent with the assertion that similar catalyst-substrate interactions are involved throughout the mechanism, as well as the triazole substituent's superior ability to interact with substrate **2**. However, the specific nature of this interaction remained undefined. To this end, a thorough analysis of an extensive data set containing structural perturbations to the catalyst and substrate could serve to illuminate these enantioselectivity-directing interactions.

Experimental design and analysis

The collection and organization of diverse data sets is at the foundation of data-driven analysis strategies (23). Therefore, an effective experimental library should include rational changes to various structural features that affect the reaction outcome of interest. To this end, substrates (**2**) were modified at positions hypothesized to influence enantioselectivity (at the 2-, 4-, and 6-positions of the benzyl ring and the distal aryl ring) (Fig. 1D), using substituents with varied electronic and steric properties (according to their Hammett σ_{para} and Sterimol B_1 values, respectively; additional details are provided in the supplementary materials, p4-8). Similarly, catalysts (**1**) were modified at the 2-, 4-, and 6-positions of the aryl ring attached to the triazole. Adamantyl-substituted catalysts **1e**, **pyr-1e**, and **imid-1e** were also included to explore the effect of changes to the heterocyclic ring. In total, 12 substrates and 11 triazolyl catalysts were selected (Fig. 1D). These libraries were then synthesized, and the enantioselectivity of each catalyst-substrate combination was obtained. Simultaneously, a diverse array of molecular descriptor values was collected to describe the structural features of each catalyst and substrate, including Sterimol parameters (24), length measurements from geometry optimized structures, and computationally derived vibrational frequencies and intensities (details are provided in the supplementary materials, p4-8) (Fig. 1D) (25). Linear regression algorithms were then applied to various subsets of the data to identify correlations between molecular structure and the experimentally determined enantioselectivity. Subsequently, analysis and refinement of the resulting models were used to produce explicit mechanistic hypotheses that were then tested and validated experimentally.

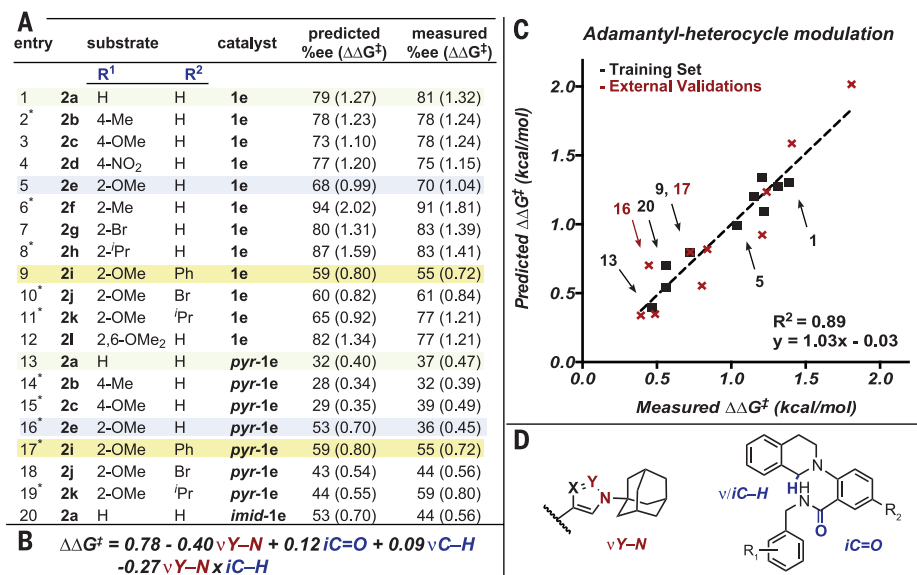


Fig. 3. Impact of heterocyclic catalyst substituent on enantioselectivity. (A) Predicted and measured enantioselectivities for various substrates with adamantyl-substituted triazolyl (**1e**), pyrazolyl (**pyr-1e**), and imidazolyl (**imid-1e**) PAs. Values identified with an asterisk are external validations. (B) Mathematical correlation of normalized catalyst and substrate vibrational parameters to enantioselectivity. (C) Predicted versus measured $\Delta\Delta G^\ddagger$ plot. (D) Illustration of the structural features implicated by the identified parameters.

Modeling catalyst heterocyclic rings

Given the clear importance of the catalyst heterocyclic ring in enantioselectivity determination (vide supra), we initially sought to understand the subset of results obtained by using catalysts **1e**, **pyr-1e**, and **imid-1e**. Accordingly, by using linear regression techniques the correlation depicted in Fig. 3B was identified from a training set of 10 different substrate-catalyst combinations (Fig. 3, A and C, black squares). Of the large number of steric (26) and vibrational (25) terms initially investigated as molecular descriptors, four discrete vibrational parameters were sufficient to produce a correlation with enantioselectivity: one catalyst descriptor ($\nu\text{Y-N}$, a stretching frequency on the heterocyclic ring), and two substrate descriptors (the stretching frequency of the amide C=O bond, $\nu\text{C=O}$, and stretching frequency/intensity of the C-H bond undergoing oxidation, $\nu\text{iC-H}$) (Fig. 3, B and D). A cross-term between the catalyst and substrate descriptors improves the overall quality of the model ($\nu\text{Y-N} \times \text{iC-H}$), suggesting a synergistic structural effect. The model was evaluated by plotting measured versus predicted $\Delta\Delta G^\ddagger$ values (Fig. 3C), and as a validation of its robustness, the enantioselectivities of 10 catalyst-substrate combinations not included in the training set were well-predicted (Fig. 3, A and C, red crosses). A slope approaching unity and intercept approaching zero over the training and validation sets indicate an accurate and predictive model, and the R^2 value of 0.90 demonstrates a high degree of precision. The largest coefficient in this normalized model belongs to the heterocyclic ring vibrational frequency, signifying its substantial role in the quantification of enantioselectivity.

This model is capable of predicting results whose origins are not obvious upon inspection. For example, comparison of the reaction outcomes using **1e** and **pyr-1e** with substrate **2a** (Fig. 3, entries 1 versus 13) may lead to the conclusion that **pyr-1e** generally affords inferior selectivity. Indeed, experimental results for several additional substrates support this notion and are accurately predicted by the model (for example, 2-OMe benzyl substrate **2e**, entries 5 versus 16). However, with substrate **2i** ($R_1 = 2\text{-OMe}$, $R_2 = \text{Ph}$, entries 9 versus 17), the triazolyl and pyrazolyl PAs afford the product with similar levels of enantioselectivity. This counterintuitive result is precisely predicted, indicating that the divergent enantioselectivity displayed by **1e**, as compared with **pyr-1e** and **imid-1e**, is adequately addressed by the model.

Trend analysis

Although the model in Fig. 3B establishes the capacity of the chosen parameters to describe subtle aspects of this system, the ultimate goal of this approach was to discern underlying mechanistic phenomena. This objective could not be achieved by using merely the above correlation because it was produced by using a small subset of data, in which the catalyst heterocyclic rings bore the same substituent (adamantyl). We hypothesized that the complete data set contained invaluable information to this end because it was produced by using strategically modified catalysts and substrates with substituents intentionally introduced to probe subtle effects, resulting in 132 enantioselectivities between -54 and 94% ee, which corresponds to a $\Delta\Delta G^\ddagger$ range of 2.8 kcal/mol. In accordance with

a data-intensive strategy, none of these measured values was discarded because even low enantioselectivity carries information regarding the catalyst-substrate interactions at the origin of asymmetric induction.

Yet before producing a global, predictive model, we considered that a series of focused correlations, coupled with an evaluation of overall trends, might serve to reveal fundamental features of the system. To this end, for each individual substrate a correlation was produced relating its observed enantioselectivity values for the entire set of catalysts, with parameters describing the catalyst structure (**2a-2l**, 12 models in total) (fig. S3). The same strategy was applied to all aryl-substituted triazole catalysts by using parameters describing the substrate structure (**1b-1d**, **1f-1k**, 9 models total) (table S7). This organizational scheme was viewed as a means to facilitate the identification of catalyst features that affect particular substrate types (and vice versa). Substrates or catalysts with similar structures behave analogously not only in a qualitative manner, but also in terms of the molecular descriptors that effectively serve to predict their enantioselectivities (individual substrate and catalyst measured versus predicted $\Delta\Delta G^\ddagger$ plots and equations are available in figs. S2, S3, and S4 and table S7). These quantitative correlations, together with systematically organized trends of experimental outcomes, can guide the development of testable mechanistic hypotheses.

To simultaneously inspect multiple aspects of large and intricate data sets, a communicative

visualization of data is crucial (27). Thus, we elected to present information gained from these focused mathematical models, alongside multiple observed enantioselectivity results, organized according to trends in catalyst or substrate structural features. Demonstrating this visualization technique, the enantioselectivity trend for each catalyst (in Fig. 4, each line represents a catalyst) was plotted as a function of the substrates (in Fig. 4, each x axis tick-line represents a substrate), and vice versa (Fig. 5). To afford a quantitative trend analysis, the plots were arranged according to which positions were modified on the catalyst or substrate structures, and the corresponding R_1 or R_2 substituent's Sterimol B_1 value (additional visualizations are provided in figs. S5 and S6) (24). For example, in the purple frame in Fig. 4, 2-substituted benzyl substrates are displayed from the largest to smallest substituent. The catalyst molecular descriptors required for correlating each subset of substrates are also depicted (Fig. 4), along with the substrate descriptors for each subset of catalysts (Fig. 5). For example, the catalyst molecular descriptors used as parameters for the correlation of enantioselectivity obtained for 2-substituted benzyl substrates are presented below the blue frame in Fig. 4 ($vN-N$, \angle_{tor}).

Analysis of this systematic data arrangement reveals that in general, catalyst performance correlates with the aryl substitution pattern in the order 2,4,6 > 2,6 > 4 (Fig. 5, gray, orange, and blue frames, respectively). Additionally, by juxtaposing Figs. 4 and 5, it appears that the reaction is mainly under catalyst control because catalyst

features affect enantioselectivity in a more considerable and systematic manner (Fig. 5), whereas for each substrate, the spread of observed enantioselectivity is broader (Fig. 4). All substrates bearing a 2-substituted benzyl group—even those with substitution at R_2 (Fig. 4, purple and blue frames, respectively)—can be modeled by using the torsion angle between the triazole and its substituent, and a triazole vibration frequency (\angle_{tor} , $vN-N$) (individual models are provided in table S7). The torsion angle represents a steric effect yet also contains information concerning the conjugation between the triazole ring and its substituent. The vibration frequency can serve as a correction to both of these effects because it takes into account nonadditive features of the substituents' charge and mass distribution (25).

The models for substrates with 4-benzyl substitution (Fig. 4, green frame) contain the same two terms (\angle_{tor} , $vN-N$) and an additional steric descriptor (the catalyst aryl ring minimal width, B_1). Similar interactions with the triazole ring should still be present for these 4-benzyl substrates, but the presence of a B_1 term suggests an additional steric interaction between the substrate and catalyst substituents, which is avoided in the case of hydrogen at the 4-benzyl position. This claim is supported by the lower enantioselectivities observed for substrates with larger 4-benzyl substituents, especially when using catalysts with larger 2,6-groups. Thus, the lack of the catalyst B_1 term in the models describing 2- relative to 4-benzyl substrates, and their overall higher

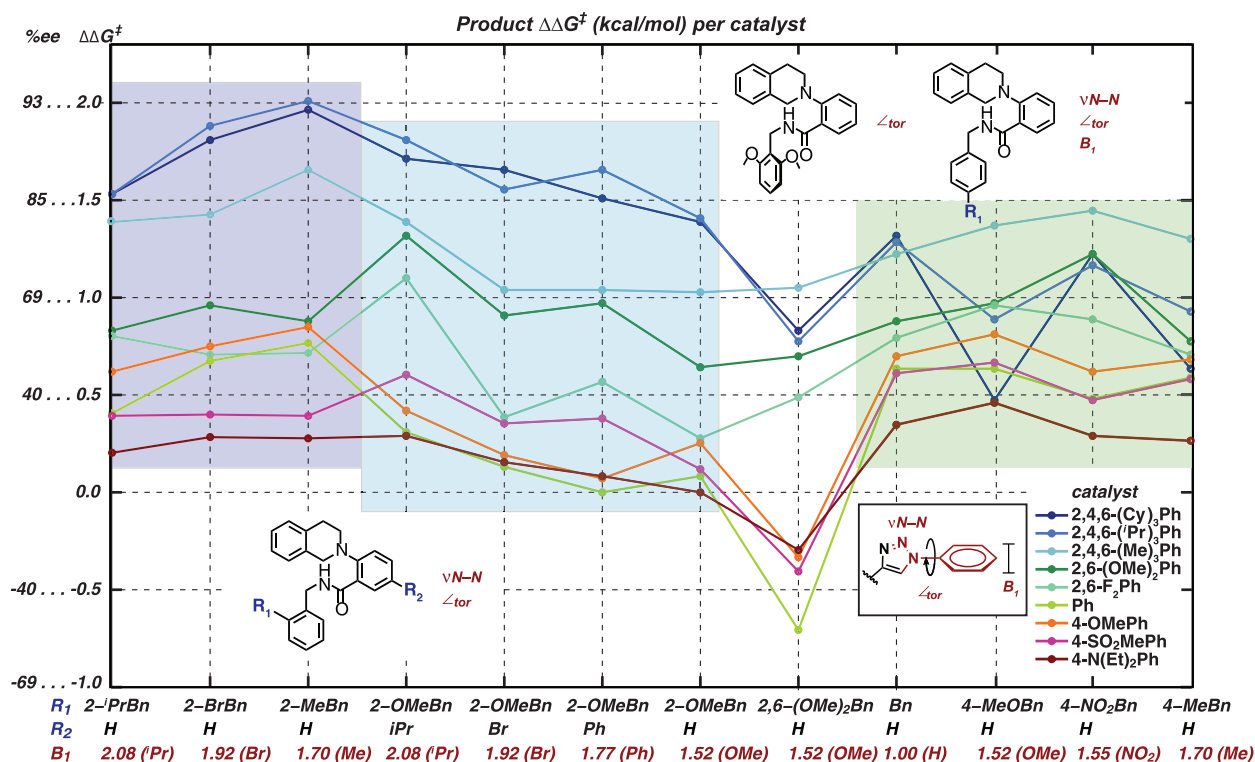


Fig. 4. Graphical representation of catalyst structure-selectivity trends as a function of substrate. Enantioselectivity trends for every catalyst against all substrates. Each trend line represents a catalyst, and each x axis tick-line represents a substrate.

enantioselectivities, are thought to arise from a better accommodation of the former substrates' shapes in the catalyst active site.

The individual catalyst trends and models carry complementary information, revealing the substrate descriptors relevant to each catalyst subset (Fig. 5). The parameters that correlate with 4-substituted aryl catalysts' enantioselectivity (Fig. 5, blue frame) include the substrate carbonyl-stretching vibrational frequency and intensity ($\nu(\text{C}=\text{O})$), the amide N-H vibrational frequency ($\nu(\text{N}-\text{H})$), and a cross-term between the two ($\nu(\text{C}=\text{O}) \times \nu(\text{N}-\text{H})$). These values vary in response to substitution on the substrate benzyl ring or the distal aryl ring, with the former having a greater effect (table S2). These same parameters effectively correlate with the enantioselectivity observed for 2,6-disubstituted aryl catalysts (Fig. 5, orange frame), along with an additional vibrational term ($\nu(\text{Bn})$) describing a benzyl ring stretch. The enantioselectivity spread of catalysts with larger substituents at the 2,4,6-position [for example, 38 to 93% ee for 2,4,6-(Cy)₃-Ph catalyst **1d** (Fig. 5, gray frame)] can be described by using two terms associated with the benzyl ring ($\nu(\text{Bn})$, $\text{iN}-\text{H}$), stressing this ring's role in determining enantioselectivity.

Trend interpretation

Collectively, these results suggest that a π interaction is established between the triazole ring and substrate during the enantioselectivity determining step, the strength of which is modulated by local steric and electronic structural features of both interacting partners (13, 28–34). Furthermore, π interactions are often strengthened

by heteroatoms (35–37), which could explain the reduced enantioselectivity values obtained by using **imid-1e**, **pyr-1e**, and TCYP catalysts compared with **1e** (Fig. 1A), as well as the similar KIE values obtained when using both the (*R*)- and (*S*)-enantiomers of **pyr-1e** and TCYP as catalysts, compared with the divergent ones displayed by (*R*)- and (*S*)-**1e** (Fig. 2B). In relation to the substrate, participation of both the benzyl group and the distal aryl group in putative π interactions are supported by the presence of molecular descriptors that are sensitive to substitution on these rings in every catalyst model ($\nu(\text{C}=\text{O})$, $\text{iC}=\text{O}$, $\nu(\text{N}-\text{H})$, and $\nu(\text{Bn})$) (Fig. 5 and table S2).

The energy stabilization gained from π interactions is affected by the distance and geometry of the rings involved (13, 30–37). If a π interaction between the substrate and triazole is at the origin of enantioselectivity determination, the directionality of the triazole—represented by the torsion angle between the triazole and its substituent—is expected to directly affect enantioselectivity. In agreement with this hypothesis, catalysts with more pronounced torsional effects lead to higher enantioselectivity values for substrates with relatively small substituents at the benzyl 4-position. The torsion angle approaches perpendicularity (90°) owing to larger 2,6-substituents on the catalyst aryl ring connected to the triazole (Fig. 4, purple and blue frames, blue lines). Moreover, large catalyst 2,6-aryl substituents are presumed to serve as a steric barrier, docking the substrate in place for an improved overlap with the catalyst triazole

ring. Correspondingly, substrates with elongated 4-substituents ($R = \text{Me}$, OMe) lead to lower enantioselectivities by using catalysts with large substituents at the 2,6-position (Fig. 4, green frame, blue lines). For these substrates, the steric repulsion exerted by the large 2,6-substituents affords a weaker or less directing π interaction and, subsequently, lower enantioselectivity. Thus, the importance of the torsion angle and vibration parameters for correlating enantioselectivity in the individual models and overall trends (Fig. 4, fig. S2, and table S7) is proposed to reflect the angle at which the triazole engages the substrate and the steric role of the catalyst aryl group. Lending further credence to this proposal, catalysts with reduced torsion angles (such as catalysts with triazole *R* substituents: Ph, 4-NO₂Ph, 4-OMePh, or 4-SO₂MePh) that do not introduce the proposed directional and steric effects lead to diminished enantioselectivities overall (Fig. 5).

Comprehensive model and probes of mechanistic hypotheses

On the basis of these hypotheses, we set out to design a series of new catalysts to specifically probe putative interactions. To facilitate catalyst development, a predictive model (Fig. 6) was generated for the entire substrate set with the aryl-substituted catalysts (**1b-1d** and **1f-1k**). This model contains 108 combinations (9 catalysts times 12 substrates) from the initial library of experiments, where half were used as a training set (Fig. 6B, black squares) and the other half as external validations (Fig. 6B, red crosses). New catalysts were proposed to address hypotheses

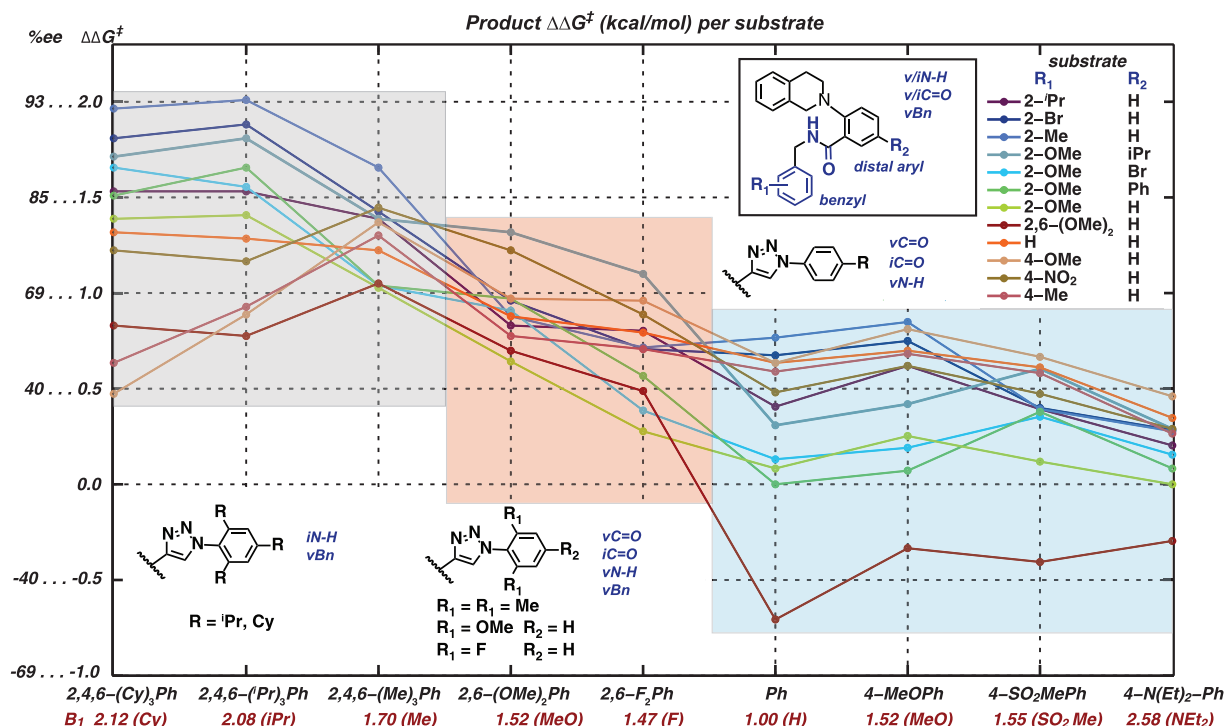


Fig. 5. Graphical representation of substrate structure-selectivity trends as a function of catalyst. Enantioselectivity trends for every substrate against all catalysts. Each trend line represents a substrate, and each x axis tick-line represents a catalyst.

raised by the focused models and trend analysis, and their enantioselectivity was predicted before synthesis by the comprehensive model (Fig. 6).

First, to probe whether the aryl substituent on the triazole ring plays a primarily steric role, rather than directly engaging the substrate in a π interaction, perfluorophenyl catalyst **1l** was designed and evaluated. Substituent local sterics and charge distribution have been shown to strongly affect noncovalent π interactions (28–30, 32–39). Therefore, we expected that if enantioselectivity were predominantly dependent on the aryl substituent directly engaging as a partner in a π interaction (as opposed to taking an ancillary role in π interactions involving the triazole), perfluorophenyl catalyst **1l** would deviate significantly from its Ad (**1e**), 2,6-(F)₂-Ph (**1k**) or 2,6-(MeO)₂-Ph (**1j**) counterparts. However, all four catalysts behave similarly with respect to the magnitude and sign of enantioselectivity (Fig. 6C, entries 1 to 9 and 24 to 26). This result is well predicted by the model (Fig. 6B) and is consistent with the hypothesis that the main function of the aryl substituent is steric.

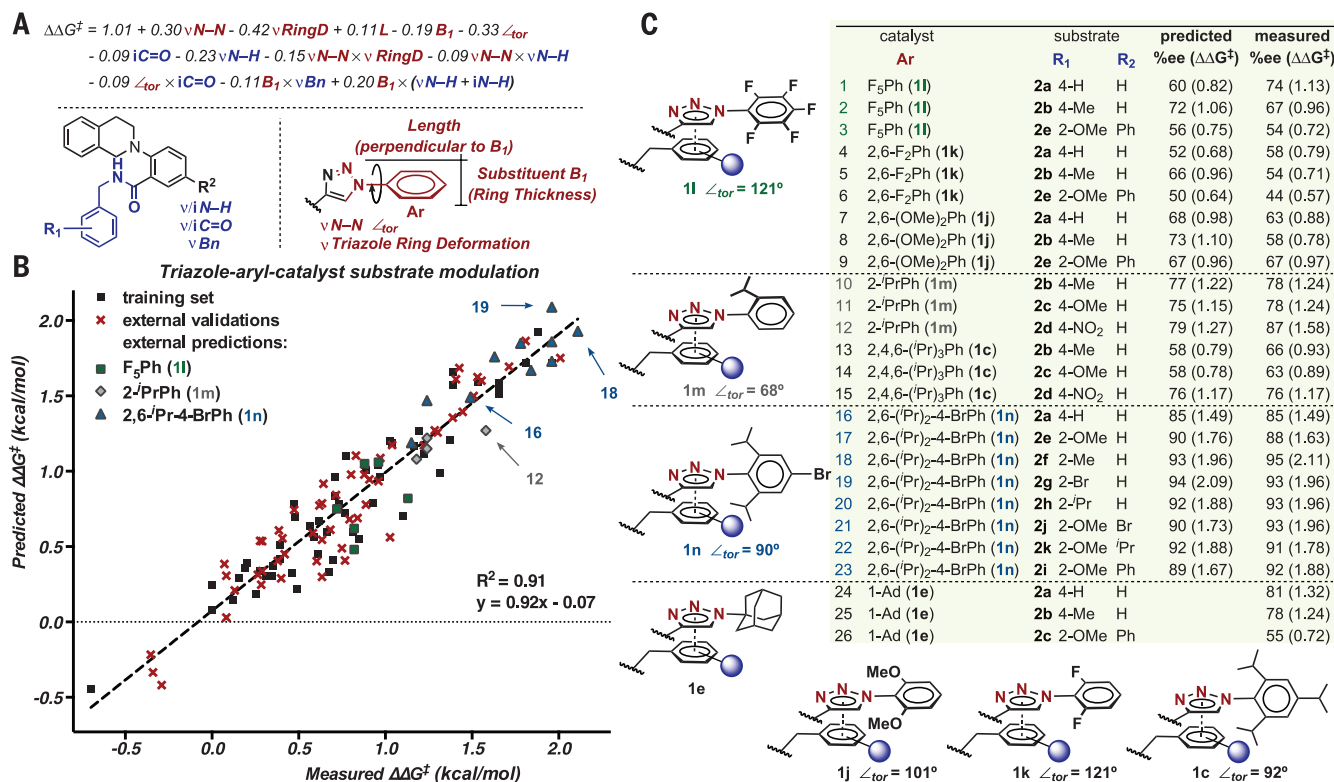
Next, catalyst **1m**, bearing a single isopropyl group at the 2-position of the triazole aryl substituent, was prepared to probe the hypothesis that steric repulsion exists between larger catalyst 2,6-substituents and elongated substrate 4-substituents. We anticipated that an isopropyl group would induce the torsion necessary to enforce the proposed benzyl-triazole π interac-

tion, while avoiding a direct steric interaction between the substrate benzyl 4-position and the catalyst aryl 2,6-substituents. Indeed, for all 4-substituted substrates tested (Fig. 6C, entries 10 to 12), **1m** provided the corresponding product in higher enantioselectivity than that of **1c**, which bears isopropyl groups at both ortho positions of the triazole aryl substituent (Fig. 6C, entries 13 to 15). For 4-NO₂-Bn substrate **2d**, the 2-*i*Pr catalyst **1m** resulted in the highest enantioselectivity observed to date (Fig. 6, B and C, entry 12), as predicted by the model.

Last, in order to evaluate the capacity to obtain improved enantioselectivity as a result of a data-intensive approach, and the hypothesis that torsion leads to enhanced enantioselectivity for the 2-substituted substrates, several proposed catalysts were evaluated by using the model in Fig. 6. Catalyst **1n** was selected because it is synthetically feasible, accommodates a torsion angle close to 90°, and was predicted to give improved enantioselectivity for all substrates bearing hydrogen at the 4-benzyl position. This prediction was verified in practice for all eight substrates evaluated, affording the highest enantioselectivities observed to date (Fig. 6C, entries 16 to 23). These results confirm that a perpendicular geometry of the triazole and the aryl ring can indeed lead to higher enantioselectivities, supporting the premise that the orientation of the triazole ring coupled with its R group's steric constraints control triazole π interactions.

The overall analysis of the triazole-PA case study demonstrates the complementary manner in which classical physical organic techniques and modern data analysis strategies can be merged toward a more complete mechanistic assessment (40). This approach is based on the use of empirical data, which is often a prerequisite for a rational reaction optimization process, to concomitantly conduct a mechanistic investigation. Information of this sort that could be used for an in-depth analysis is often omitted from reports in the field of catalysis because only results leading to the desired outcomes are generally presented and pursued. Yet because high-throughput (2, 4, 8), automated (7) methods for reaction development are now common, data analysis strategies could be applied in parallel to optimization procedures, allowing for simultaneous mechanistic and structural analysis.

Creatively collecting and organizing data to examine proposed hypotheses affords improved generalizations, particularly as data sets become larger and more complex (23). This idea holds true for the analysis of reaction trends by parameters that reflect structural modification. Indeed, the focused catalyst and substrate models—and their organization according to fundamental, quantitative, physical-organic trends—provided nonintuitive insights regarding interactions involved in enantioselectivity determination. Although this approach is general for the prediction and study of chemical reaction outcomes, this case



study was chosen as a stringent benchmark because it uses weak, noncovalent interactions for asymmetric induction. These interactions are typically in the energy range required to distinguish a highly enantioselective reaction from its racemate forming counterpart (2 to 3 kcal/mol) (*12*, *13*, *32*, *37*), providing seemingly endless approaches to rational catalyst design. However, controlling noncovalent interactions represents a notable challenge in the design of catalytic systems because of multiple energetically accessible orientations (*13*). Complemented with rigorous experimental analysis, the disclosed data-intensive approach is suited to addressing such intricacies and holds potential for the analysis of increasingly complicated catalytic systems streamlining both reaction and catalyst development.

REFERENCES AND NOTES

- K. D. Collins, T. Gensch, F. Glorius, *Nat. Chem.* **6**, 859–871 (2014).
- M. T. Reetz, *Angew. Chem. Int. Ed. Engl.* **41**, 1335–1338 (2002).
- D. W. Robbins, J. F. Hartwig, *Science* **333**, 1423–1427 (2011).
- A. McNally, C. K. Prier, D. W. C. MacMillan, *Science* **334**, 1114–1117 (2011).
- J. R. Schmink, A. Bellomo, S. Berritt, *Aldrichim Acta* **46**, 71–80 (2013).
- M. R. Friedfeld et al., *Science* **342**, 1076–1080 (2013).
- P. L. Heider et al., *Org. Process Res. Dev.* **18**, 402–409 (2014).
- P. Metola, S. M. Nichols, B. Kahr, E. V. Anslyn, *Chem. Sci.* **5**, 4278–4282 (2014).
- A. Buitrago Santanilla et al., *Science* **347**, 49–53 (2015).
- D. Y. Curtin, *Rec. Chem. Prog.* **15**, 110–128 (1954).
- J. Halpern, *Science* **217**, 401–407 (1982).
- E. V. Anslyn, D. A. Dougherty, *Modern Physical Organic Chemistry* (University-Science Books, Herndon, VA, 2006).
- R. R. Knowles, E. N. Jacobsen, *Proc. Natl. Acad. Sci. U.S.A.* **107**, 20678–20685 (2010).
- K. C. Harper, M. S. Sigman, *Proc. Natl. Acad. Sci. U.S.A.* **108**, 2179–2183 (2011).
- A. J. Neel, J. P. Hehn, P. F. Tripet, F. D. Toste, *J. Am. Chem. Soc.* **135**, 14044–14047 (2013).
- J. M. Bobbitt, C. Brückner, N. Merbouh, in *Organic Reactions* (John Wiley & Sons, New York, 2004).
- C.-J. Li, *Acc. Chem. Res.* **42**, 335–344 (2009).
- C. S. Yeung, V. M. Dong, *Chem. Rev.* **111**, 1215–1292 (2011).
- O. García Mancheño, T. Stopka, *Synthesis* **45**, 1602–1611 (2013).
- T. Akiyama, *Chem. Rev.* **107**, 5744–5758 (2007).
- M. Terada, *Synthesis* **2010**, 1929–1982 (2010).
- D. Parmar, E. Sugiono, S. Raja, M. Rueping, *Chem. Rev.* **114**, 9047–9153 (2014).
- N. Silver, *The Signal and the Noise: Why so Many Predictions Fail—But Some Don't* (Penguin Press, New York, 2012).
- A. Verloop, J. Tipker, *Pharmacochem. Libr.* **2**, 63–81 (1977).
- A. Milo, E. N. Bess, M. S. Sigman, *Nature* **507**, 210–214 (2014).
- K. C. Harper, E. N. Bess, M. S. Sigman, *Nat. Chem.* **4**, 366–374 (2012).
- M. Lima, *Visual Complexity: Mapping Patterns of Information* (Princeton Architectural Press, New York, 2013).
- C. A. Hunter, J. K. M. Sanders, *J. Am. Chem. Soc.* **112**, 5525–5534 (1990).
- F. Cozzi, M. Cinquini, R. Annunziata, T. Dwyer, J. S. Siegel, *J. Am. Chem. Soc.* **114**, 5729–5733 (1992).
- C. R. Martinez, B. L. Iverson, *Chem. Sci.* **3**, 2191 (2012).
- E. H. Krenske, K. N. Houk, *Acc. Chem. Res.* **46**, 979–989 (2013).
- K. E. Riley, P. Hobza, *Acc. Chem. Res.* **46**, 927–936 (2013).
- C. D. Sherrill, *Acc. Chem. Res.* **46**, 1020–1028 (2013).
- R. M. Parrish, C. D. Sherrill, *J. Am. Chem. Soc.* **136**, 17386–17389 (2014).
- E. G. Hohenstein, C. D. Sherrill, *J. Phys. Chem. A* **113**, 878–886 (2009).
- S. E. Wheeler, *Acc. Chem. Res.* **46**, 1029–1038 (2013).
- B. F. Shchegolev, M. L. McKee, A. V. Zhuravlev, E. V. Savvateeva-Popova, *Biofizika* **58**, 461–467 (2013).
- S. E. Wheeler, K. N. Houk, *J. Am. Chem. Soc.* **130**, 10854–10855 (2008).
- D. O'Hagan, *Chem. Soc. Rev.* **37**, 308–319 (2008).
- T. T. Tidwell, Z. Rappoport, C. L. Perrin, Eds., *Pure Appl. Chem.* **69**, 1–76 (1997).

ACKNOWLEDGMENTS

We thank the NSF (CHE-0749506 and CHE-1361296) and the National Institute of General Medical Sciences (R01 GM104534) for partial support of this work. The support and resources from the Center for High Performance Computing at the University of Utah

are gratefully acknowledged. A.J.N. gratefully acknowledges an Amgen Fellowship in Organic Chemistry for funding and Jörg Hehn for early contributions to this work.

SUPPLEMENTARY MATERIALS

www.sciencemag.org/content/347/6223/737/suppl/DC1
Materials and Methods
SupplementaryText
Figs. S1 to S7
Tables S1 to S6
References (41–53)

9 September 2014; accepted 13 January 2015
10.1126/science.1261043

REPORTS

SUPERCONDUCTIVITY

Light-induced superconductivity using a photoactive electric double layer

Masayuki Suda,^{1,2*} Reizo Kato,² Hiroshi M. Yamamoto^{1,2*}

Electric double layers (EDLs) of ionic liquids have been used in superconducting field-effect transistors as nanogap capacitors. Because of the freezing of the ionic motion below ~200 kelvin, modulations of the carrier density have been limited to the high-temperature regime. Here we observe carrier-doping–induced superconductivity in an organic Mott insulator with a photoinduced EDL based on a photochromic spiropyran monolayer. Because the spiropyran can isomerize reversibly between nonionic and zwitterionic isomers through photochemical processes, two distinct built-in electric fields can modulate the carrier density even at cryogenic conditions.

The electric potential difference that usually exists across a phase boundary creates two layers of space charges of different signs, the so-called electric double layer (EDL) (*1*, *2*). In recent years, EDL transistors with ionic liquids or electrolytes as gate dielectrics have been used increasingly (*3*, *4*). Under an applied gate voltage, ions are driven to the surface of the channel materials, forming an EDL that acts as a nanogap capacitor. Using this method to accumulate a large numbers of carriers (~10¹⁴ cm⁻²) (*5–9*), field-induced superconductivity has been realized in various materials. However, modulations of the carrier density in EDL transistors have been limited to the high-temperature regime because the ionic motions of ionic liquids or electrolytes are frozen below ~200 K.

Here we observe field-induced superconductivity even at low temperatures by using a photoactive EDL system, a spiropyran monolayer. Spiropyran is a photochromic molecule that can photoisomerize

reversibly between the nonionic spiropyran (SP) form and the zwitterionic merocyanine (MC) form upon ultraviolet (UV) (forward reaction) or visible light irradiation (reverse reaction) (fig. S1) (*10*, *11*). Therefore, an EDL-like large electric field across the film can be induced or be eliminated by UV light or visible light irradiation, respectively. The advantage of the photochromic EDL system over the conventional one is that it retains the modulation capability even at low temperatures, because these photochromic reactions proceed with photon-energy dissipation under nonequilibrium conditions. Hence, a highly aligned SP monolayer is a promising candidate for a photoinduced EDL system that can directly switch superconductivity only by photoirradiation. Although there have been attempts to tune the conductivity and even superconductivity using photochromic layers (*12–17*), photoinduced phase transitions (including superconducting transitions) have not been realized yet.

We fabricated a photoactive superconducting device by laminating a thin single crystal of κ -(BEDT-TTF)₂Cu[N(CN)₂]Br (κ -Br) [BEDT-TTF: bis(ethylenedithio)tetrathiafulvalene] on top of an Al₂O₃ (or HfO₂)/Nb:SrTiO₃ substrate covered with a self-assembled monolayer of spiropyran

¹Research Center of Integrative Molecular Systems (CiMoS), Institute for Molecular Science, Okazaki, Aichi 444-8585 Japan. ²RIKEN, Wako, Saitama 351-0198 Japan.

*Corresponding author. E-mail: msuda@ims.ac.jp (M.S.); yhiroschi@ims.ac.jp (H.M.Y.)

derivatives (SP-SAM) (Fig. 1). The device also has a bottom-gate structure for electrostatic carrier doping to finely modulate the carrier density accumulated as a result of photoirradiation. We chose κ -Br as a target material because κ -type BEDT-TTF is a strongly correlated molecular conductor (18) that has a relatively low half-filled carrier density ($\sim 2 \times 10^{14}/\text{cm}^2$) (19). We recently demonstrated a field-induced superconductivity in a thin single crystal of κ -Br (20).

The surface density of SP-SAM estimated by the comparison of absorption spectra between a monolayer film and a solution (fig. S2) was $\sim 1.8 \times 10^{14}$ molecules/ cm^2 . The surface density for the close-packed model (2.0×10^{14} molecules/ cm^2) was already reported (13), indicating that we have obtained a high-coverage SP-SAM. The photoisomerization of SP-SAM at room temperature was monitored by UV-visible absorption spectroscopy (fig. S3). The spectrum of the initial state has a weak absorption peak at 580 nm that is ascribed to the π - π^* transition in the MC form. This means that the initial state of SP-SAM is in a SP state-dominant mixed state. After UV irradiation for 5 min, the absorption peak was enhanced, indicating SP-to-MC photoisomerization. After a subsequent irradiation with visible light, the peak almost vanished, indicating MC-to-SP back photoisomerization. SP-to-MC-to-SP photoisomerization was then repeated without any attenuation of the area between the absorption curves. These reversible spectral changes clearly demonstrated reversible photoisomerization of spiropyrans, even after the SAM formation.

Subsequently, we investigated the effects of photoirradiation of UV and visible light on the four-probe resistance of κ -Br devices. Figure 2A shows a time trace of the resistance for the device at 5 K. After brief resistance measurements in the dark, the device was irradiated with UV light. During the UV irradiation, the resistance value drastically decreased and the final state persisted even after the irradiation was stopped. Furthermore, this reduced resistance value recovered to nearly the initial value by visible light irradiation, which also lasted even after the irradiation was stopped (Fig. 2B), showing reversible switching capability. The resistance switching was repeated several times, with negligible attenuation (Fig. 2C). To rule out that the response was caused by photo-thermal effects, we also conducted control experiments on the κ -Br device without the photochromic layer. We found almost no resistance change during UV and visible light irradiation. Therefore, the reversible resistance switching must be caused by the reversible photoisomerization of SP-SAM.

Figure 3A shows the temperature dependence of the resistance after various UV irradiation times at 5 K. In the initial state, the κ -Br device exhibited Mott insulating behavior at low temperature; this behavior is contrary to the superconducting character of the bulk crystal and caused by the tensile strain from the substrate (20–22) (details are described in fig. S4). The resistance value decreased with increasing the irradiation time, and when the irradiation time

reached 180 s, the device showed an abrupt resistance drop around 7.3 K; the drop was suppressed by a magnetic field of 7 T (fig. S5). This behavior indicates that the system showed a photoinduced phase transition from a Mott insulating phase to a partially superconducting phase.

The photoinduced superconducting transition was also confirmed by magnetic susceptibility measurements (Fig. 3B). In the initial state, small

shielding and Meissner effects were observed below ~ 10 K in zero-field-cooled and field-cooled measurements. After UV light irradiation, the zero-field-cooled curve was strongly enhanced, implying an increase in the superconducting fraction. The superconducting fraction created by UV light irradiation can be estimated by comparing the diamagnetic value of the κ -Br device with that of bulk κ -Br. From this estimation, $\sim 5\%$

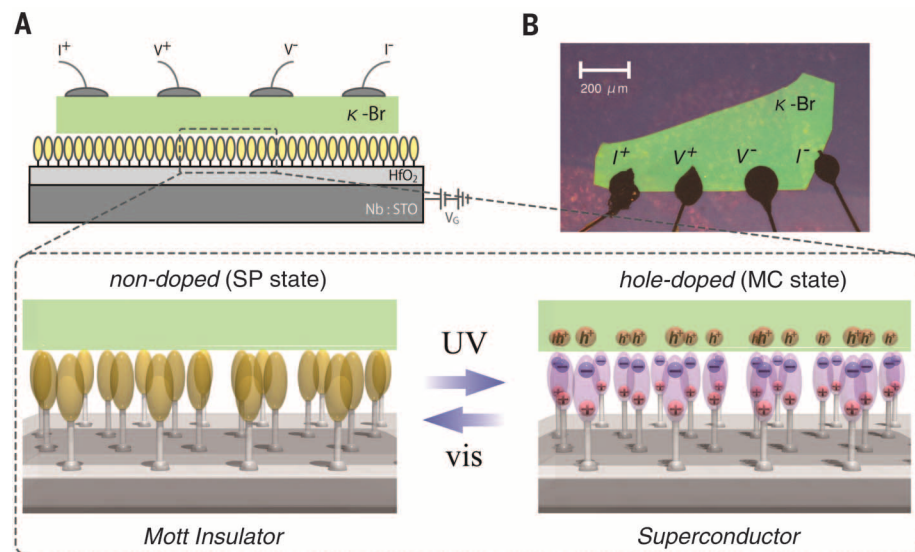


Fig. 1. Configuration of the κ -Br device. (A) Schematic cross section of the device; the spiropyran (SP) monolayer can isomerize reversibly by UV and visible light irradiation at the interface (fig. S1). (B) Optical microscope image of the κ -Br single crystal laminated on the substrate. Gold wires were attached to the crystal with carbon paste for standard four-probe measurement. Scale bar, 200 μm .

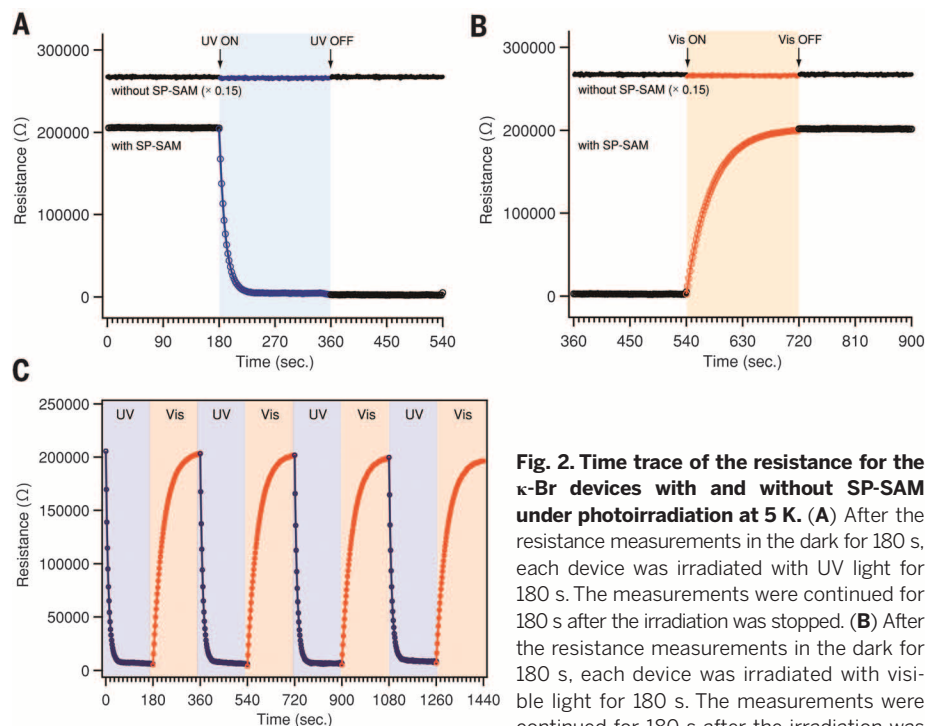


Fig. 2. Time trace of the resistance for the κ -Br devices with and without SP-SAM under photoirradiation at 5 K. (A) After the resistance measurements in the dark for 180 s, each device was irradiated with UV light for 180 s. The measurements were continued for 180 s after the irradiation was stopped. (B) After the resistance measurements in the dark for 180 s, each device was irradiated with visible light for 180 s. The measurements were continued for 180 s after the irradiation was stopped. (C) Time trace of the resistance for the κ -Br device with alternate photoirradiation of UV and visible light.

of the volume fraction seems to be caused by UV light irradiation, suggesting that the superconducting transition occurs not only at the interface layer but also in the bulk of the device,

because the volume fraction of the interface layer (monolayer) is only $\sim 0.3\%$ (the thickness of the κ -Br crystal used for the magnetic measurements was 600 nm, which corresponds to ~ 300 layers).

Because the carriers injected at the interface are unlikely to diffuse into the layers far from the interface, such a bulk phase transition should originate from an interlayer dielectric screening of the Coulomb interaction, where effective repulsion among Mott insulating carriers in the bulk of the device is screened by the mobile superconducting carriers at the interface (23). A similar bulk phase transition has been also observed for the field-induced superconductivity in a single-crystal field-effect transistor (FET) of κ -Br (20).

We now turn to the study of the photoswitching mechanism. κ -Br has been shown to turn superconducting as a result of electrostatic carrier doping (20). It is therefore reasonable to assume that the photoinduced phenomena presented here are also caused by carrier doping by the photoisomerization of SP-SAM. It has been found that, when organic molecules with sizable dipole moments are organized as a SAM, a co-operative effect of charge transfer occurs between the monolayer and the substrate (24, 25). The electric field produced by such a monolayer dipole can exceed the field that can be applied across the gate dielectric in a standard FET configuration. We can calculate the expected

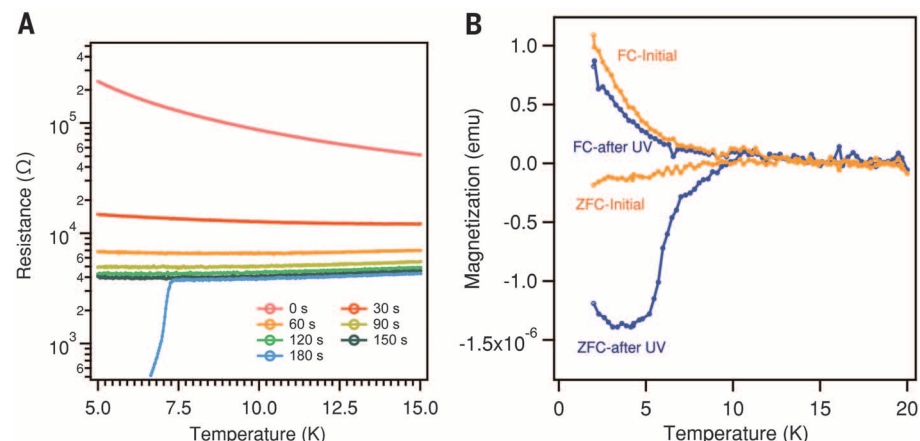


Fig. 3. Temperature dependence of the resistance and the magnetization for the κ -Br device. (A) Resistance versus temperature for the κ -Br device after various times of irradiation with UV light. (B) Magnetic susceptibility [zero-field-cooled (ZFC) and field-cooled (FC) measurements] for device 4 in the initial state and UV-irradiated state under a field of 100 Oe.

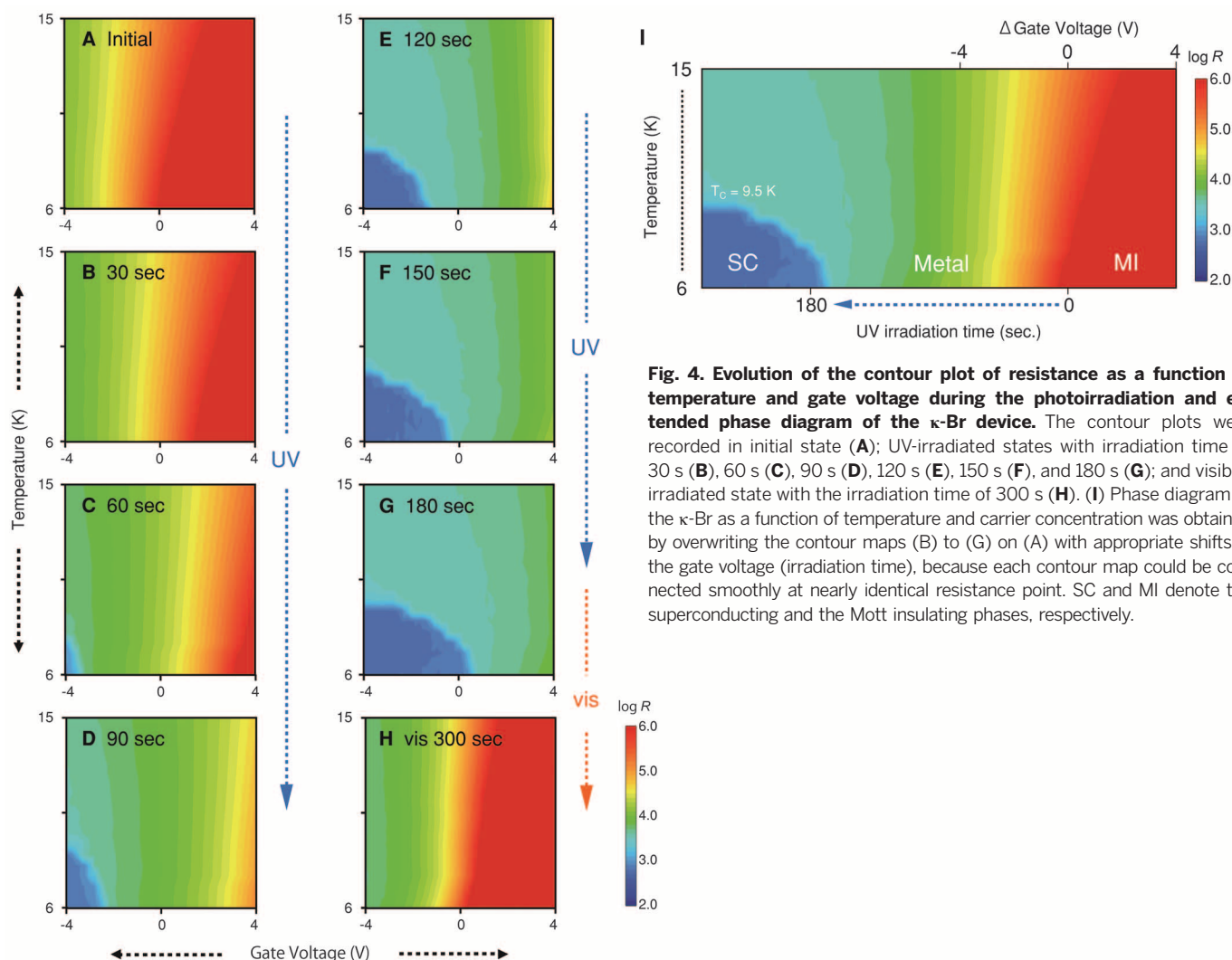


Fig. 4. Evolution of the contour plot of resistance as a function of temperature and gate voltage during the photoirradiation and extended phase diagram of the κ -Br device. The contour plots were recorded in initial state (A); UV-irradiated states with irradiation time of 30 s (B), 60 s (C), 90 s (D), 120 s (E), 150 s (F), and 180 s (G); and visible-irradiated state with the irradiation time of 300 s (H). (I) Phase diagram of the κ -Br as a function of temperature and carrier concentration was obtained by overwriting the contour maps (B) to (G) on (A) with appropriate shifts in the gate voltage (irradiation time), because each contour map could be connected smoothly at nearly identical resistance point. SC and MI denote the superconducting and the Mott insulating phases, respectively.

electric field inside a SAM through the following relationship

$$E_{\text{in}} = N(\mu_{\text{mol}}/\epsilon d_{\text{mol}}) \quad (1)$$

where N , d_{mol} and ϵ are, respectively, the surface density, the height of the molecules, and the effective dielectric constant inside the monolayer (26, 27). For our SP-SAM, we assumed that N is 1.8×10^{14} molecules/cm², ϵ is between 2 and 3, μ_{mol} is 6.4 D for the SP state and 13.9 D for the MC state, and d_{mol} is 2.2 nm (13); conversion efficiency from SP-to-MC state is ~66%. Using these values, we can estimate the difference in the electric fields (E_{in}) between the SP and MC states as 5.0 ~ 7.5 MV/cm, which is much larger than the electric fields that can be produced by applying a gate voltage using the bottom-gate structure.

To confirm this hypothesis, we performed gate voltage sweeps using the bottom-gate structure with various irradiation times. Figure 4 shows the contour plots of the resistance as a function of temperature and gate voltage for increasing times of UV light irradiation, which was performed at 5 K. The irradiation was stopped during the gate-sweep mode electrical measurement. The κ -Br device without SP-SAM was not affected by UV or visible light irradiation (fig. S9). For κ -Br devices with SP-SAM, the contour plot shifted in the positive voltage direction with elapsed UV-light irradiation time, reflecting a gradual progress of the hole carrier injection, as expected from Eq. 1. After the irradiation time of 60 s, a sudden resistance drop appeared at negative gate voltage ($V_G \approx -4$ V), showing the (field-effect assisted) photoinduced superconducting transition. When the irradiation time reached 180 s, a superconducting phase could be observed even without gate voltage. The observed voltage shift after 180 s is ~9 V, which leads to the difference in the built-in potential of 4.3 MV/cm. This value is somewhat smaller than the results obtained theoretically by Eq. 1 (5.4 ~ 8.1 MV/cm). One reason for this discrepancy is a decline of the conversion efficiency of SP-to-MC photoisomerization because of the lamination of the crystal; it is well known that the free volume around spiropyrans has an effect on the photochromic response (28).

Finally, a phase diagram of the κ -Br as a function of temperature and irradiation time (with applied gate voltage) was obtained by superimposing Fig. 4, A to G, as shown in Fig. 4I. We found continuous shift of the contour plots in Fig. 4, A to G, without noticeable color gradation difference in the overlapping areas. In addition, we observed a portion of a superconducting dome resembling that of the superconducting cuprates (29) and the κ -Br with conventional FET configuration (20). These results indicate that the photoinduced effect was caused not by thermal heating or interface chemical reactions but rather by the (hole) carrier doping. Furthermore, the field-induced carriers and the photoinduced carriers were working as the same type of carriers that are indistinguishable from one another in the κ -Br crystals. This means that SP-SAM EDL can expand the limit of electrostatic carrier doping beyond the density that can be

accumulated only by means of a normal FET configuration.

REFERENCES AND NOTES

- W. Schmickler, *Chem. Rev.* **96**, 3177–3200 (1996).
- P. Simon, Y. Gogotsi, *Nat. Mater.* **7**, 845–854 (2008).
- S. Ono, K. Miwa, S. Seki, J. Takeya, *Appl. Phys. Lett.* **94**, 063301 (2009).
- T. Fujimoto, K. Awaga, *Phys. Chem. Chem. Phys.* **15**, 8983–9006 (2013).
- K. Ueno et al., *Nat. Mater.* **7**, 855–858 (2008).
- J. T. Ye et al., *Nat. Mater.* **9**, 125–128 (2010).
- A. T. Bollinger et al., *Nature* **472**, 458–460 (2011).
- K. Ueno et al., *Nat. Nanotechnol.* **6**, 408–412 (2011).
- J. T. Ye et al., *Science* **338**, 1193–1196 (2012).
- V. I. Minkin, *Chem. Rev.* **104**, 2751–2776 (2004).
- N. Tamai, H. Miyasaka, *Chem. Rev.* **100**, 1875–1890 (2000).
- E. Orgiu, P. Samorì, *Adv. Mater.* **26**, 1827–1845 (2014).
- H. Zhang et al., *Nano Lett.* **11**, 4939–4946 (2011).
- A. R. Jang et al., *ACS Nano* **6**, 9207–9213 (2012).
- M. Kim, N. S. Safran, C. Huang, M. S. Arnold, P. Gopalan, *Nano Lett.* **12**, 182–187 (2012).
- A. Ikegami, M. Suda, T. Watanabe, Y. Einaga, *Angew. Chem. Int. Ed.* **49**, 372–374 (2010).
- I. Carmeli et al., *Angew. Chem. Int. Ed.* **51**, 7162–7165 (2012).
- K. Kanoda, *J. Phys. Soc. Jpn.* **75**, 051007 (2006).
- R. Kato et al., *Chem. Lett.* **16**, 507–510 (1987).
- H. M. Yamamoto et al., *Nat. Commun.* **4**, 2379–2385 (2013).
- Y. Kawasaki et al., *Appl. Phys. Lett.* **92**, 243508 (2008).
- Y. Kawasaki et al., *Phys. Rev. Lett.* **103**, 116801 (2009).
- H. Shinaoka, T. Misawa, K. Nakamura, M. Imada, *J. Phys. Soc. Jpn.* **81**, 034701 (2012).
- H. Ishii, K. Sugiyama, E. Ito, K. Seki, *Adv. Mater.* **11**, 605–625 (1999).
- D. Cahen, R. Naaman, Z. Vager, *Adv. Funct. Mater.* **15**, 1571–1578 (2005).
- G. Ashkenasy, D. Cahen, R. Cohen, A. Shanzer, A. Vilan, *Acc. Chem. Res.* **35**, 121–128 (2002).
- I. H. Campbell et al., *Appl. Phys. Lett.* **71**, 3528–3530 (1997).
- M. Suzuki, T. Asahi, H. Masuhara, *Phys. Chem. Chem. Phys.* **4**, 185–192 (2002).
- N. Doiron-Leyraud et al., *Nature* **447**, 565–568 (2007).

ACKNOWLEDGMENTS

Financial support for this work was provided by Grants-in-Aid for Scientific Research (S) (no. 22224006) from the Japan Society for the Promotion of Science (JSPS).

SUPPLEMENTARY MATERIALS

www.sciencemag.org/content/347/6223/743/suppl/DC1
Materials and Methods
Figs. S1 to S9

2 June 2014; accepted 14 January 2015
10.1126/science.1256783

DENTAL MATERIALS

Amorphous intergranular phases control the properties of rodent tooth enamel

Lyle M. Gordon,^{1*} Michael J. Cohen,¹ Keith W. MacRenaris,² Jill D. Pasteris,³ Takele Seda,⁴ Derk Joester^{1†}

Dental enamel, a hierarchical material composed primarily of hydroxylapatite nanowires, is susceptible to degradation by plaque biofilm-derived acids. The solubility of enamel strongly depends on the presence of Mg²⁺, F[−], and CO₃^{2−}. However, determining the distribution of these minor ions is challenging. We show—using atom probe tomography, x-ray absorption spectroscopy, and correlative techniques—that in unpigmented rodent enamel, Mg²⁺ is predominantly present at grain boundaries as an intergranular phase of Mg-substituted amorphous calcium phosphate (Mg-ACP). In the pigmented enamel, a mixture of ferrihydrite and amorphous iron-calcium phosphate replaces the more soluble Mg-ACP, rendering it both harder and more resistant to acid attack. These results demonstrate the presence of enduring amorphous phases with a dramatic influence on the physical and chemical properties of the mature mineralized tissue.

Tooth enamel has evolved to resist the most grueling conditions of mechanical stress, fatigue, and wear (1). In addition, it is exposed to chemical attack in the corrosive environment of the oral cavity. Caries, or tooth decay, commonly begins with the de-

mineralization of enamel because of production of acid by oral bacteria (2, 3). Caries has an extremely high relative incidence of disease, with nearly 100% of adults worldwide having or having had caries (4). Although drinking water fluoridation is credited with reducing caries by an impressive 25% across all age groups, current dental expenditure in 2012 has been hovering at ~\$110 billion in the United States alone (5). As the most prevalent chronic disease, caries thus remains an important public health problem. A substantial challenge encountered in characterizing structure and chemistry of enamel is its complex, hierarchical, and graded architecture with substantial heterogeneity in structure and composition. Closing this gap in our knowledge will aid development of quantitative models

¹Northwestern University, Materials Science and Engineering, 2220 Campus Drive, Evanston, IL 60208, USA.

²Northwestern University, Quantitative Bioelemental Imaging Center (QBIC), 2170 Campus Drive, Evanston, IL 60208, USA.

³Washington University, Department of Earth and Planetary Sciences, Campus Box 1169, St. Louis, MO 63130, USA.

⁴Western Washington University, Department of Physics and Astronomy, Bellingham, WA 98225, USA.

*Present address: Environmental Molecular Sciences Laboratory, Pacific Northwest National Laboratory, Post Office Box 999, Mail Stop K8-93, 3335 Innovation Boulevard, Richland, WA 99354, USA.
†Corresponding author. E-mail: d-joester@northwestern.edu

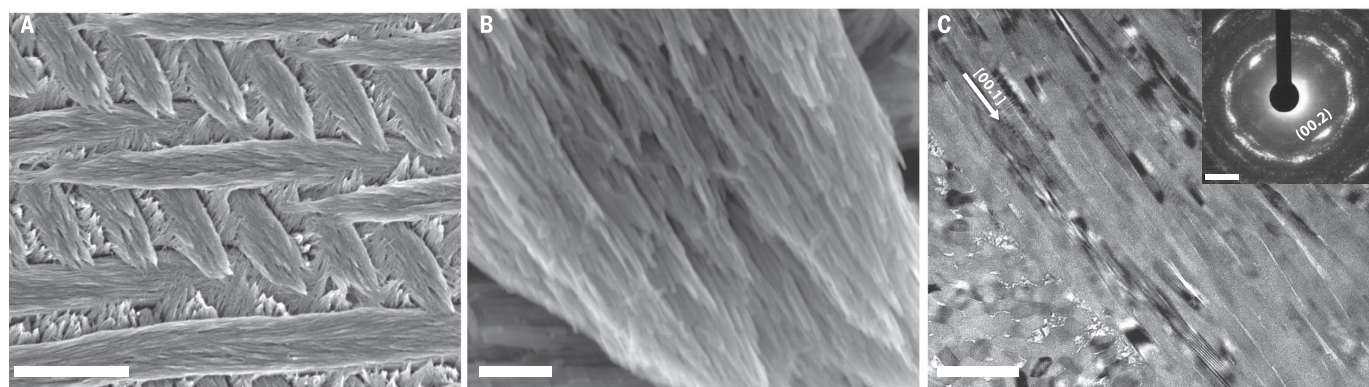


Fig. 1. Overview of mouse incisor enamel structure. (A and B) SEM images of a lactic acid-etched cross-section. (C) In this bright-field TEM image of a FIB-prepared thin section and (inset) selected-area diffraction pattern (SAED) of the edge of one enamel rod, alignment of nanowires parallel to the crystallographic *c* axis of the apatite lattice is apparent. Scale bars, 5 μm (A); 250 nm (B); 200 nm (C); and 2 nm^{-1} (inset).

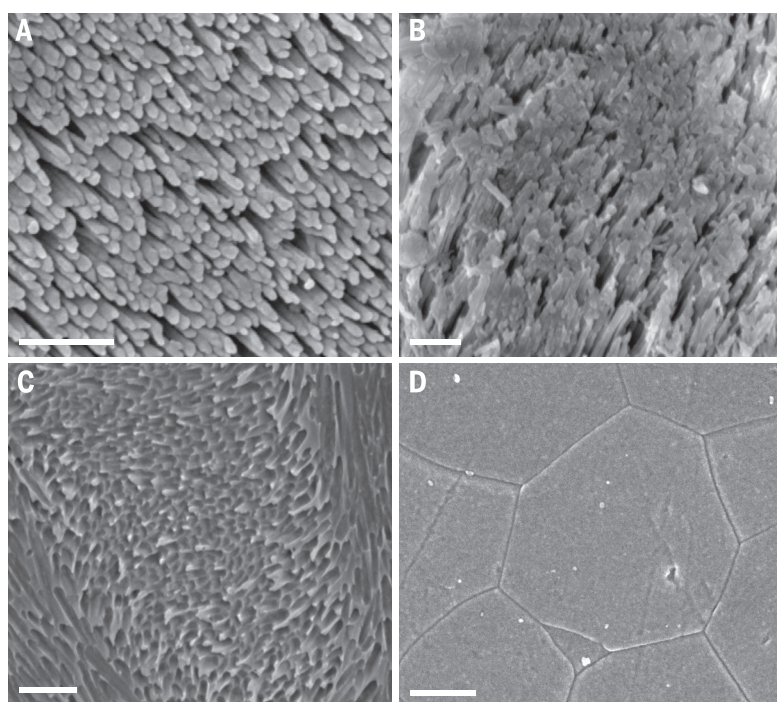


Fig. 2. SEM images of lactic acid-etched rodent enamel and sintered OHAp cross-sections. (A) Mouse (*Mus musculus*) incisor inner enamel. A comparison of sections before and after etching is provided in fig. S12. (B) Fluoride-treated mouse inner enamel. (C) Rat (*Rattus norvegicus*) pigmented enamel. (D) Sintered synthetic OHAp. Scale bars, 250 nm.

of enamel mechanical properties, connect the tissue-level etiology of caries to the underlying material structure and properties, and help innovate prophylaxis, early detection, and minimally invasive intervention.

Enamel is composed of single-crystal hydroxylapatite [OHAp, $\text{Ca}_{10}(\text{PO}_4)_6(\text{OH})_2$] nanowires that have a rhombohedral shape with typical cross-sectional edge lengths of 25 to 50 nm (Fig. 1) (6, 7). Nanowires are elongated parallel to the crystallographic [00.1] direction and have very large aspect ratios. On the order of 10^4 nanowires are bundled in rods. Rods are arranged in a dense three-dimensional (3D) weave interspersed with interrod enamel; this arrangement serves to deflect and arrest cracks (8). Spe-

cific features depend, among others, on location within the enamel layer of a given tooth. In the inner enamel of rodent incisors, rods are arranged in decussating layers (Fig. 1). In outer enamel, rods are packed in parallel instead and reach the enamel surface at a characteristic angle. Superimposed on the hierarchical structure, however, is a level of chemical heterogeneity that has been much more difficult to capture.

Enamel is highly mineralized at 96 weight percent (wt %) mineral, ~3 wt % water, and only ~1 wt % residual biomacromolecules (6). However, even small amounts of substituting ions such as magnesium (0.2 to 0.5 wt % Mg^{2+}), carbonate (2 to 4 wt % CO_3^{2-}), and fluoride (F⁻)

strongly affect its properties (9). This is commonly ascribed to substitutional defects in the OHAp lattice. For example, Mg^{2+} substitution for Ca^{2+} or CO_3^{2-} substitution for either PO_4^{3-} or OH^- results in increased solubility (10). Given the low solubility of fluorapatite, F⁻ substituting for OH^- is thought to decrease enamel susceptibility to acid attack and enhance remineralization. The concentration of these ions typically is graded over tens to hundreds of micrometers, with Mg^{2+} and CO_3^{2-} concentration increasing from the enamel surface to the dentino-enamel junction (3). Little is known about the distribution of ions at the length scale of rods or individual nanowires and the interfaces between them.

We used a comparative approach to understand the interplay between susceptibility to acid attack, mechanical properties, and nano-scale structure and chemistry. Rodent enamel is a generally accepted model system for human enamel (11). We therefore compared unpigmented “regular” rodent enamel with pigmented rodent enamel. Pigmented enamel is a reddish-brown, iron-rich type of outer enamel frequently found as an outermost layer on the incisors of rodents, shrews, and a few other species (12). Typically only 10 to 15 μm thick, its structural organization, but not its chemistry, is similar to that of the regular outer enamel directly underneath.

The susceptibility of enamel to dissolution in acidic environments was evaluated qualitatively by means of acid etching (13). Under conditions designed to approximate the intra-oral environment during carious attack, we observed that etching is highly anisotropic even at the level of individual rods (Fig. 2). In regular mouse inner enamel, etching results in a “forest” of aligned nanowires, indicating that dissolution along the boundaries between {hk.0} facets is much more rapid than at the (00.1) face. When regular enamel is topically treated with fluoride before etching, dissolution along the grain boundaries is still the prevalent mode, but the extent is reduced. Although evidence in the literature led us to expect increased resistance of pigmented enamel to acid attack (14), we were surprised by the dramatic effect that indicates a change in mechanism. Specifically, etching parallel to the

grain boundaries is strongly suppressed, and slight dissolution of the nanowires on the (00.1) face leads to a characteristic honeycomb appearance in etched pigmented enamel. In contrast, etching of randomly oriented, polycrystalline OHAp with very low impurity levels is only mildly anisotropic. At comparable times of exposure to acid, only minor corrosion at the OHAp grain boundaries was observed, and there was little to no evidence of bulk dissolution or a strong dependence of etch rate on grain orientation.

We confirmed these observations through quantitative assessment of the rate at which enamel is etched. Because of their larger size, incisors from the European rabbit (*Oryctolagus cuniculus*) were used as a model for regular enamel, and from the North American beaver (*Castor canadensis*) as a model for pigmented rodent enamel. Although these organisms belong to different orders—the beaver is a rodent, and the rabbit is a lagomorph—recent evidence puts them in a monophyletic clade (Glires), and the structure of their outer enamel is similar (15). An additional advantage of beaver incisor is that the outer enamel is much thicker (>100 μm) than, for example, in the rat, with no noticeable structural difference in the arrangement of ap-

atite nanowires between the outermost 10 to 15 μm of pigmented enamel and the underlying regular outer enamel (fig. S1).

A known area, typically 10 to 20 mm^2 in size, of the enamel surface was exposed to a lactic acid solution (250 mM, initial pH = 4.0, 37°C). The concentration of relevant ions in the etchant was monitored over time by using inductively coupled plasma mass spectrometry (ICP-MS) (fig. S14). The average loss of enamel mass per unit time and area was determined from time-concentration data, assuming a linear dependency, which is reasonable at short etching times. Consistent with electron microscopy and earlier qualitative observations (14), pigmented beaver enamel etches at a much lower rate ($115 \pm 15 \text{ ng mm}^{-2} \text{ min}^{-1}$, $n = 3$ incisor segments) than that of regular rabbit enamel ($655 \pm 60 \text{ ng mm}^{-2} \text{ min}^{-1}$, $n = 3$ incisor segments). At least some of this difference could in principle arise from slight structural or chemical differences in the outer enamel between the two species. However, when the regular outer enamel of the beaver was exposed with the careful mechanical removal of the pigmented layer, the etching rate was comparable with that of rabbit enamel ($695 \pm 60 \text{ ng mm}^{-2} \text{ min}^{-1}$, $n = 3$ xxxxx).

Topical treatment of the enamel so exposed with fluoride at neutral pH reduced etching rates substantially ($205 \pm 35 \text{ ng mm}^{-2} \text{ min}^{-1}$, $n = 3$ incisor segments). However, the etch rate of fluoridated enamel is still about twice faster than that of pigmented enamel, indicating that pigmentation affords better protection against acid attack. However, remineralization in the presence of fluoride, at different pH, and over longer time periods may give different results. Taken together, the electron microscopy of etched enamel surfaces and quantitative measurement of etch rates is strong evidence that the composition of enamel is heterogeneous across the diameter of individual nanowires and that this heterogeneity affects the anisotropic etching of grain boundaries and the overall susceptibility of enamel to corrosion.

Beyond the impact on acid etching, enamel composition also affects the mechanical properties. We systematically determined enamel hardness as a function of the distance from the enamel surface using nanoindentation (fig. S2). Pigmented outer enamel of beavers and rats is harder (5 to 6 GPa, $n = 3$ incisors, 170 indents) than the underlying nonpigmented outer (4 to 5 GPa, $n = 3$ incisors, 386 indents) and inner

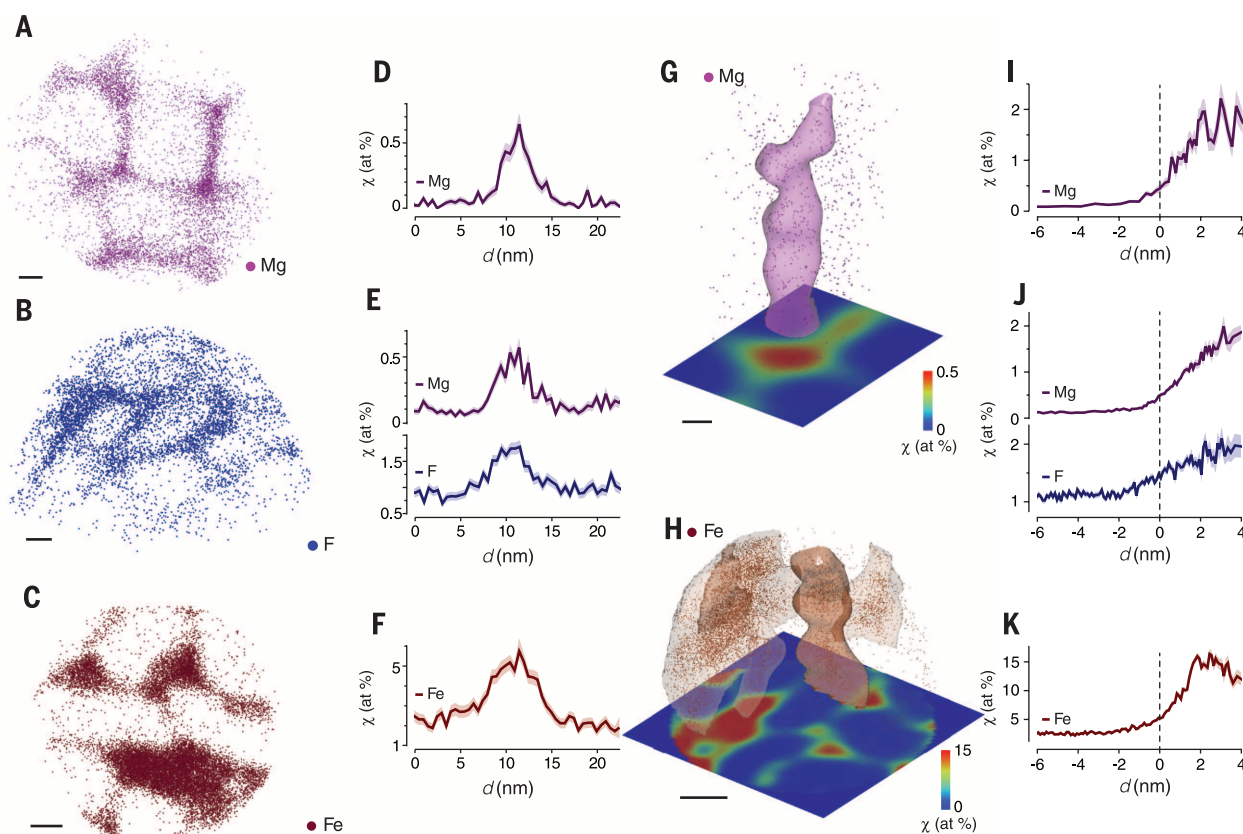


Fig. 3. APT reconstructions and compositional profiles. (A) Mg ($^{24}\text{Mg}^{2+}$) ion positions in mouse outer enamel. (B) F ($^{40}\text{Ca}^{19}\text{F}^{+}$) ion positions in fluoride-treated mouse inner enamel. (C) Fe ($^{56}\text{Fe}^{2+}$) ions in pigmented rat enamel. Scale bars, 10 nm. The view direction is parallel to the long axis of the nanowires. (D to F) Representative concentration profiles across grain boundaries. (G) Isosurface (0.5 atomic %) surrounding Mg-rich multiple grain boundary in

(A). (H) Isosurface (5 atomic %) enveloping Fe-rich multiple grain boundary in (C). Scale bars in (G) and (H), 5 nm. (I to K) Representative proxigrams of multiple grain boundaries in (I) mouse outer enamel, (J) fluoride-treated outer mouse enamel, and (K) pigmented rat enamel. The distance d is relative to the isosurface. In concentration profiles and proxigrams, the solid line represents the mean and the shaded area the mean \pm SD, based on counting statistics.

enamel (4.5 GPa, $n = 3$ incisors, 18 indents). The hardness does not change abruptly but rather decreases gradually from the pigmented enamel surface toward the nonpigmented outer enamel. The concentration of iron is graded in the same direction (fig. S2). In rat enamel, a structural transition between the outer and inner enamel may contribute to the gradient in mechanical properties (12, 14). In beaver enamel, no such transition is apparent. Furthermore, in both rat and beaver, hardness is nearly constant across the unpigmented outer enamel of the extreme mesial and distal aspect of the incisor (fig. S2). Clearly, the presence of iron has a substantial impact on enamel hardness. A likely function of the hardness gradient is to maintain a sharp edge on the continuously growing incisor (15).

Thus, iron not only protects enamel against acid attack but also increases mechanical hardness. Etching indicates that there are compositional differences across grain boundaries between nanowires. Atom probe tomography (APT) is a technique suited to compositional mapping at such length scales (16, 17). The recent introduction of ultraviolet laser-pulsed APT has enabled the investigation of the chemical nanostructure of mineralized tissues such as the chiton tooth, bone, and dentin (16, 17). During APT, single atoms or small clusters on the surface of a very sharp specimen are field-evaporated after a laser pulse. The resulting ions are projected onto an imaging detector and identified by their time of flight. The identity and position of each ion are used to create 3D reconstructions of the sample, with a spatial resolution typically better than 0.2 nm. Because of its unbiased sensitivity across the periodic table, APT is particularly powerful for samples with low-atomic-number components.

We prepared samples of inner and outer enamel from ground and polished tooth sections

by means of focused ion beam (FIB) milling (18). APT spectra show the typical features of OHAp and a range of minor constituents, including Mg and Na in regular enamel, and Fe in pigmented enamel (fig. S3) (17). In 3D reconstructions, the cross sections of faceted nanowires are apparent from the distribution of minor ions (Fig. 3, A to C). At grain boundaries in regular enamel, Mg^{2+} is enriched ~20 times over the apparent solubility limit of ~0.03 atomic % in the bulk of the nanowire (table S1). This peripheral enrichment confirms earlier in vitro experiments, showing that Mg^{2+} is not readily incorporated into the apatite crystal lattice (10, 19). In pigmented enamel, Fe is almost completely excluded from the interior of the nanowires (< 0.2 atomic %). No Fe was detected in regular enamel, and only trace amounts of Mg were present in pigmented enamel (table S1). Concentration profiles across the grain boundaries (Fig. 3, D to F) reveal that the concentration of minor ions is sharply elevated over a narrow region. The absolute concentration and total amount of Mg or Fe atoms at grain boundaries varies considerably, even between the boundaries on one nanowire and its neighbors. This variability may result from differences in surface energy of the particular facets but is likely also dependent on the kinetics of crystallite growth.

A convenient way to visualize the 3D distribution of impurities at multiple grain boundaries is by way of an isoconcentration surface (isosurface) (Fig. 3, G and H) that encloses a volume in which the concentration of a given ion is higher than a threshold. Proximity histograms (proxigrams) (Fig. 3, I to K) report the average mole fraction of ions as a function of distance to this surface (20). The physical dimensions and the exceptionally high concentration of trace ions in the associated proxigrams—~60 times the apparent solubility limit for Mg and at least 80

times the solubility limit for Fe—are strong indications that an intergranular phase that is chemically and structurally distinct from apatite is present. In regular enamel treated topically with fluoride, there is colocalization of F and Mg (Fig. 3, E and J, and fig. S13), indicating that grain boundaries and grain edges serve as short-circuit diffusion pathways. Thus, an understanding of the fundamental processes of tooth decay must account for transport along grain boundaries and the participation of the Mg-rich intergranular phase (21). Intergranular phases are known to strongly affect mechanical properties of ceramic materials (22); the increased hardness of pigmented enamel is likely a result of the structural and compositional difference of the interphase.

Although the existence of Mg-rich phases in enamel—in particular, dolomite [$\text{CaMg}(\text{CO}_3)_2$], huntite [$\text{Mg}_3\text{Ca}(\text{CO}_3)_4$], and whitlockite $\text{Ca}_3\text{Mg}(\text{PO}_4)_3(\text{PO}_3\text{OH})$ —has been proposed previously, these phases have not been observed experimentally (19). The strong enrichment of Mg^{2+} at interfaces and in the intergranular phase (~90% of total Mg) observed by APT allows us to use x-ray absorption spectroscopy to probe its structure. The position and intensity of transitions in Mg *K*-edge x-ray absorption near-edge structure (XANES) spectra are sensitive to the coordination number, geometry, bond length, and order at intermediate range. Many Mg-containing minerals can be identified by their spectral fingerprints (23). Spectra of enamel lack the pre-A, D, and E peaks that are characteristic for crystalline dolomite, huntite, and whitlockite (Fig. 4, A and B). However, the Mg-rich intergranular phase shows a striking similarity to spectra of synthetic Mg-substituted amorphous calcium phosphate (Mg-ACP), Mg/phosphate rich amorphous calcium carbonate (ACC) in the lobster cuticle, and Mg-silicate glasses (23, 24). The dominant feature in spectra of these

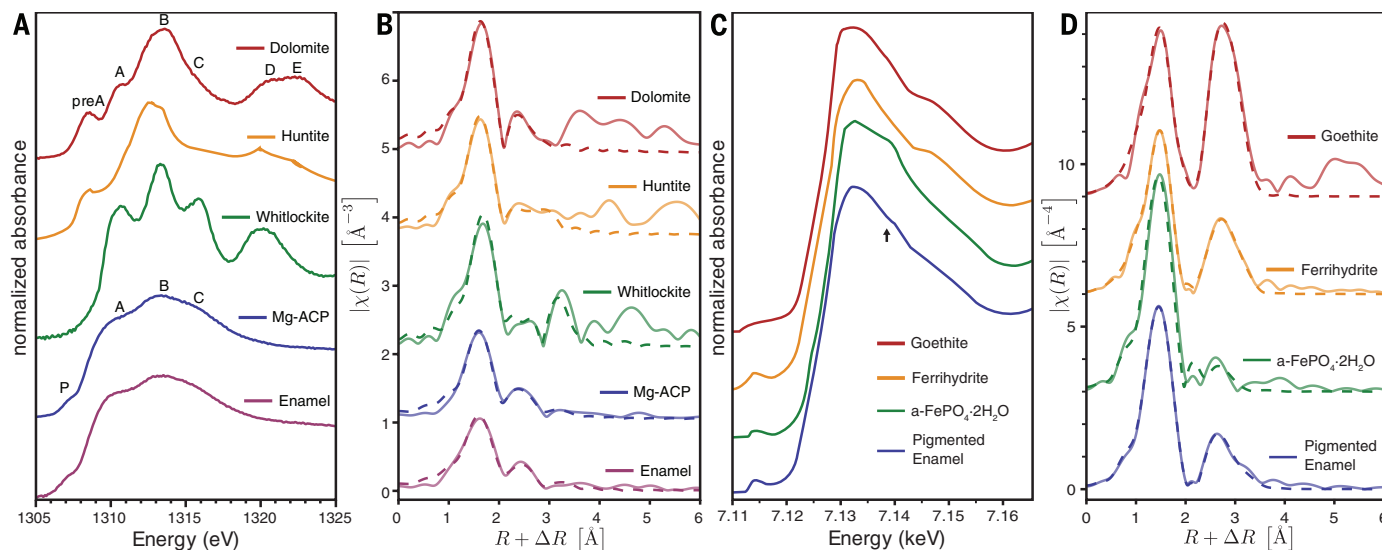


Fig. 4. X-ray absorption spectra. (A) Mg *K*-edge XANES and (B) k^2 -weighted EXAFS spectra. (C) Fe *K*-edge XANES and (D) k^3 -weighted EXAFS spectra. A post-edge shoulder at ~7138 eV (black arrow) appears in pigmented enamel and amorphous $\text{FePO}_4 \cdot 2\text{H}_2\text{O}$. In EXAFS spectra, fits (dashed lined) are overlaid on experimental data (solid lines).

amorphous materials is the transition associated with the first coordination sphere (feature B), with little or no features that depend on order beyond the first shell. At the same time, the lower-edge energy is indicative of a lower coordination number and Mg-O bond distance consistent with amorphous materials.

Confirming this assessment, the Mg K-edge extended x-ray absorption fine structure (EXAFS) of enamel is nearly indistinguishable from that of synthetic Mg-ACP (Fig. 4, A and B, and fig. S4). In sharp contrast to the crystalline reference compounds, in which numerous scattering features from more distant shells are apparent, spectra of enamel and Mg-ACP are dominated by the nearest neighbor shell. Analysis of the local environment around Mg by fitting EXAFS spectra with theoretical scattering paths (table S2) reveals that the nearest-neighbor Mg-O bond lengths in enamel (2.03 Å) and Mg-ACP (2.02 Å) are notably shorter than Ca-O bonds in OHAp (2.40 Å) and ACP (2.36 Å) and also shorter than the Mg-O bonds in the crystalline reference compounds (2.08 to 2.11 Å) (25, 26). However, Mg-O bonds in enamel are similar in length to Mg-O bonds observed in Mg-substituted ACC (24). In enamel and Mg-ACP, this shortening is accompanied by a reduction in the coordination number from 6 to ~4, which is indicative of an amorphous material and/or the presence of water in the first coordination sphere (23, 24). We conclude that the environment of the majority of Mg^{2+} in enamel exhibits only short- to medium-range order, with dramatic Mg-O bond shortening, a reduction in coordination number, and the possibility of water or hydroxyl ions in the first shell, similar to the environment of Ca in ACP (25). Although we favor the interpretation that Mg-ACP is present as an interphase, an alternate hypothesis is that Mg^{2+} occupies disordered Ca[II] sites in apatite (27). In either case, the disordered environment around Mg is likely to greatly increase the solubility at the periphery of OHAp nanowires and result in anisotropic etching.

Qualitative comparison of Fe K-edge XANES and EXAFS spectra of pigmented beaver enamel and reference standards suggests that iron is present in a ferrihydrite-like material (Fig. 4, C and D, fig. S5, and table S2). Quantitative analysis of EXAFS along with Mössbauer (fig. S6) and Raman (fig. S7) spectroscopy confirms the presence of poorly crystalline ferrihydrite (Fh) (28). Because the presence of phosphate is known to inhibit growth of crystalline iron oxyhydroxides, we would expect that metastable Fh forms from any Fe(II) secreted by ameloblasts, through oxidation to Fe(III) and subsequent hydrolysis (29). The presence of Fh in pigmented beaver enamel is in agreement with results from nutria (*Myocastor coypus*) (30) but differs from the “nearly amorphous magnetite” postulated for pigmented enamel of the shrew *Blarina brevicauda*, in which pigmented enamel may have arisen through convergent evolution (32).

However, with both Ca^{2+} (7 to 19 atomic % Ca) and PO_4^{3-} (8 to 13 atomic % P) present in APT reconstructions of the Fe-rich intergranular

phase, the material cannot be simply pure Fh. Furthermore, the stability of the intergranular phase against transformation upon heating is much greater than that of bulk Fh and leads to different products (fig. S8) (31). Analysis of the pre-edge region (fig. S9) reveals that the ligand field-splitting energy of pigmented enamel ($10Dq = 1.13$ eV) is larger than that of pure ferrihydrite (0.96 eV) and a small post-edge shoulder (Fig. 4C). Both are consistent with the presence of hydrated amorphous iron phosphate (a- $\text{FePO}_4 \cdot 2\text{H}_2\text{O}$, $10Dq = 1.19$ eV). According to linear combination analysis of EXAFS spectra, as much as 42% of the iron may be present in this form (fig. S10). Unlike the corresponding crystalline phases, amorphous phases can be very accommodating of substituents. The iron-rich interphase may thus be best described as a mixture of Fh and amorphous iron-calcium phosphate. Indeed, we observed that the interphase is strongly graded, ranging in composition from calcium-rich (Fe/Ca = 0.2) at the periphery to iron-rich (Fe/Ca = 4) in the center. Given the corrosion resistance of iron phosphates, replacing Mg-ACP with iron phosphate likely hardens pigmented enamel against acid attack (32).

We find that Mg^{2+} segregates at grain boundaries in regular rodent enamel, as does Fe^{3+} in pigmented enamel. We present evidence for the presence of Mg-ACP as an intergranular phase in regular enamel and of a mixture of Fh and amorphous iron-calcium phosphate in pigmented enamel. Last, we link interphase structure and composition to the resistance of pigmented enamel against acid attack and its improved hardness. In addition to the recent recognition of amorphous phases in biomineralization as transient precursors (33, 34), these results demonstrate enduring amorphous phases with a dramatic influence on the physical and chemical properties of the mineralized tissue.

REFERENCES AND NOTES

- J. L. Cuy, A. B. Mann, K. J. Livi, M. F. Teaford, T. P. Weihs, *Arch. Oral Biol.* **47**, 281–291 (2002).
- M. A. Taubman, D. A. Nash, *Nat. Rev. Immunol.* **6**, 555–563 (2006).
- C. Robinson et al., *Crit. Rev. Oral Biol. Med.* **11**, 481–495 (2000).
- World Health Organization, “Oral health,” fact sheet (World Health Organization Media Centre, Geneva, Switzerland, 2012).
- American Dental Association, “U.S. Dental Spending Remains Flat Through 2012,” research brief (American Dental Association Health Policy Institute, 2014).
- A. Nanci, *Ten Cate’s Oral Histology: Development, Structure, and Function* (C. V. Mosby, Maryland Heights, MO, ed. 8, 2012).
- C. B. Moench, S. P. Lyngstadaas, S. Risnes, *J. Anat.* **189**, 325–333 (1996).
- S. Bechtel, S. Habelitz, A. Klocke, T. Fett, G. A. Schneider, *Biomaterials* **31**, 375–384 (2010).
- J. D. Featherstone, S. Doméjean, *Adv. Dent. Res.* **24**, 28–31 (2012).
- R. Z. Legros, T. Sakae, C. Bautista, M. Retino, J. P. LeGeros, *Adv. Dent. Res.* **10**, 225–231 (1996).
- W. H. Bowen, *Odontology* **101**, 9–14 (2013).
- M. Dumont, T. Tütken, A. Kostka, M. J. Duarte, S. Borodin, *J. Struct. Biol.* **186**, 38–48 (2014).
- L. M. Silverstone, C. A. Saxton, I. L. Dogon, O. Fejerskov, *Caries Res.* **9**, 373–387 (1975).
- P. Vogel, *Rev. Suisse Zool.* **91**, 699–708 (1984).
- T. Martin, *Zoosystemat. Evol.* **75**, 257–273 (1999).
- L. M. Gordon, D. Joester, *Nature* **469**, 194–197 (2011).
- L. M. Gordon, L. Tran, D. Joester, *ACS Nano* **6**, 10667–10675 (2012).
- K. Thompson et al., *Ultramicroscopy* **107**, 131–139 (2007).

- R. A. Terpstra, F. C. Driessens, *Calcif. Tissue Int.* **39**, 348–354 (1986).
- O. C. Hellman, J. A. Vandenbroucke, J. Rüsing, D. Isheim, D. N. Seidman, *Microsc. Microanal.* **6**, 437–444 (2000).
- G. S. Ingram, *J. Dent. Res.* **69**, 581–586, discussion 634–636 (1990).
- D. R. Clarke, *J. Am. Ceram. Soc.* **70**, 15–22 (1987).
- L. Dien, P. Mingsheng, T. Murata, *Can. Mineral.* **37**, 199–206 (1999).
- Y. Politi et al., *Chem. Mater.* **22**, 161–166 (2009).
- C. Holt et al., *J. Cryst. Growth* **92**, 239–252 (1988).
- J. M. Hughes, M. Cameron, K. D. Crowley, *Am. Mineral.* **74**, 870–876 (1989).
- D. Laurencin et al., *Biomaterials* **32**, 1826–1837 (2011).
- J. Zhao, F. E. Huggins, Z. Feng, G. P. Huffman, *Clays Clay Miner.* **42**, 737–746 (1994).
- J. Rose, A.-M. Flank, A. Mason, J.-Y. Bottero, P. Elmerich, *Langmuir* **13**, 1827–1834 (1997).
- M. B. Madsen, S. Mørup, C. J. Koch, G. Lindemann, *Hyperfine Interact.* **29**, 1431–1434 (1986).
- F. M. Michel et al., *Proc. Natl. Acad. Sci. U.S.A.* **107**, 2787–2792 (2010).
- G. Görecki, *Corrosion* **48**, 613–616 (1992).
- L. Addadi, S. Raz, S. Weiner, *Adv. Mater.* **15**, 959–970 (2003).
- L. Addadi, N. Vidavsky, S. Weiner, *Z. Kristallogr.* **227**, 711–717 (2012).

ACKNOWLEDGMENTS

The National Science Foundation (NSF DMR-0805313, DMR-1106208, and DMR-1341391), the Northwestern University Materials Research Center [NSF–Materials Research and Engineering Center (MRSEC) DMR-1121262], the International Institute for Nanotechnology, the Institute for Sustainability and Energy at Northwestern (ISEN), and the Petroleum Research Fund of the ACS in part supported this work. The Canadian National Sciences and Engineering Research Council in part supported L.M.G. The NIH predoctoral Biotechnology Training Grant T32GM008449 in part supported M.J.C. Portions of this work were performed at the DuPont-Northwestern-Dow Collaborative Access Team (DND-CAT) and the Canadian Light Source (CLS). DND-CAT is located at Sector 5 of the Advanced Photon Source (APS), an Office of Science User Facility operated for the U.S. Department of Energy (DOE) Office of Science by Argonne National Laboratory supported by the U.S. DOE under contract DE-AC02-06CH11357. E. I. DuPont de Nemours & Co., The Dow Chemical Company, and Northwestern University support DND-CAT. The Natural Sciences and Engineering Research Council of Canada, the National Research Council of Canada, the Canadian Institutes of Health Research, the Province of Saskatchewan, Western Economic Diversification Canada, and the University of Saskatchewan support CLS. This work made use of the Northwestern University Center for Atom Probe Tomography (NUCAPT) supported by NSF-MRI (DMR-0420532) and ONR-DURIP (N00014-0400798, N00014-0610539, N00014-0910781); the Optical Microscopy and Metallography Facility; the J. B. Cohen X-Ray Diffraction Facility supported by the NSF-MRSEC (DMR-1121262); the Northwestern University Quantitative Bioelemental Imaging Center supported by NASA Ames Research Center NNA06CB93G; the Northwestern University Atomic and Nanoscale Characterization and Experimental Center (NUANCE), Electron Probe Instrumentation Center (EPIC), and the Northwestern Nanoscale Integrated Fabrication, Testing, and Instrumentation Facility (NIFTI) supported by NSF-NSEC (EEC-0118025/003), NSF-MRSEC (DMR-1121262), the Keck Foundation, the State of Illinois, and Northwestern University. We thank Q. Ma and T. Regier for assistance with x-ray absorption spectroscopy; B. Myers for assistance with TEM sample preparation; C. Phatak for performing correlative TEM of APT samples; C. Whyne and M. Akens for supplying rat incisors; and C. Newcomb, S. Sur, and A. Deymier-Black for supplying mouse incisors. The supplementary materials contain additional data. L.M.G., J.D.P., and D.J. designed experiments, analyzed the data, and prepared the manuscript. L.M.G., M.J.C., K.W.M., J.D.P., and T.S. performed experiments.

SUPPLEMENTARY MATERIALS

www.sciencemag.org/content/347/6223/746/suppl/DC1
Materials and Methods
Figs. S1 to S14
Tables S1 to S3
References (35–56)

18 July 2014; accepted 19 December 2014
10.1126/science.1258950

ATMOSPHERIC CHEMISTRY

Direct kinetic measurement of the reaction of the simplest Criegee intermediate with water vapor

Wen Chao,^{1,2} Jun-Ting Hsieh,^{1,3} Chun-Hung Chang,¹ Jim Jr-Min Lin^{1,2,4*}

Carbonyl oxides, or Criegee intermediates, are important transient species formed in the reactions of unsaturated hydrocarbons with ozone. Although direct detection of Criegee intermediates has recently been realized, the main atmospheric sink of Criegee intermediates remains unclear. We report ultraviolet absorption spectroscopic measurements of the lifetime of the simplest Criegee intermediate, CH₂OO, at various relative humidity levels up to 85% at 298 kelvin. An extremely fast decay rate of CH₂OO was observed at high humidity. The observed quadratic dependence of the decay rate on water concentration implied a predominant reaction with water dimer. On the basis of the water dimer equilibrium constant, the effective rate coefficient of the CH₂OO + (H₂O)₂ reaction was determined to be $6.5 (\pm 0.8) \times 10^{-12}$ cubic centimeters per second. This work would help modelers to better constrain the atmospheric concentrations of CH₂OO.

Criegee intermediates (CIs) have long been implicated in atmospheric reactions of ozone with unsaturated hydrocarbons, but only recently were simple CIs detected via their preparation through the reactions of α -iodoalkyl radicals with O₂ (1). The reaction rate coefficients of simple CIs with atmospheric trace gases, including SO₂, NO₂, and carboxylic acids, could then be measured directly using vacuum ultraviolet photoionization mass spectrometry (VUV-PIMS) (1–3). These measurements indicated that the previously reported rate coefficients derived from indirect ozonolysis experiments had been underestimated by factors of 50 to 10,000 (1–3). Because CIs are important in the oxidative capacity of the atmosphere, as well as radical generation and aerosol formation there (4–6), the higher rate coefficients implied a greater role of CIs in atmospheric chemistry than previously assumed. However, the precise kinetics of CI reactions with water vapor have not yet been determined, even though these water reactions may control the atmospheric fate of CIs by virtue of the comparatively high abundance of water vapor.

Welz *et al.* (1) investigated the kinetics of the simplest Criegee intermediate, CH₂OO, by using VUV-PIMS to monitor CH₂OO concentration. Although the rate coefficients of CH₂OO reactions with SO₂ and NO₂ were determined, the authors did not observe any detectable reaction of CH₂OO with water (reaction 1) and set an upper bound for the rate coefficient k_1 of 4×10^{-15} cm³ s^{−1} (1). Using a similar technique, Taatjes *et al.* mea-

sured the rate coefficient of the reaction of *anti*-CH₃CHOO with water to be $1.0 (\pm 0.4) \times 10^{-14}$ cm³ s^{−1}, but still could not observe the reactions of water with CH₂OO and *syn*-CH₃CHOO (2). Stone *et al.* reported $k_1 < 9 \times 10^{-17}$ cm³ s^{−1} by measuring the laser-induced fluorescence of H₂CO, a product in the CH₂OO reaction system (7). Ouyang *et al.* reported $k_1 = 2.5 (\pm 1) \times 10^{-17}$ cm³ s^{−1}, determined in a relative rate experiment monitoring NO₃ production (8).

Evidence for substantial reactivity of CH₂OO with water has been reported in C₂H₄ ozonolysis experiments (9, 10), despite a large scatter in the reported rate coefficient (10^{-17} to 10^{-12} cm³ s^{−1}) (11–13). Berndt *et al.* (14) investigated H₂SO₄ formation from SO₂ oxidation in C₂H₄ ozonolysis at various relative humidities (H_R) up to 50%. Through analysis of the H₂SO₄ yields, the authors implied a preferred reaction of CH₂OO with water dimer, as suggested by the theoretical works of Ryzhkov and Ariya (15).

Berndt *et al.* (14) further pointed out that their result, as well as a series of earlier studies (9–13) using C₂H₄ ozonolysis for CH₂OO formation, indicates that the CH₂OO reaction with water vapor is predominant under near-atmospheric conditions. However, this conclusion was not supported by other recent studies (1, 2, 7, 8) that applied the CH₂I₂-O₂ photolysis technique (CH₂I₂ + $h\nu \rightarrow$ CH₂I + I; CH₂I + O₂ \rightarrow CH₂OO + I). This discrepancy is puzzling, especially when detailed spectroscopic investigations in the VUV (1), UV (16–18), infrared (19), and microwave (20) spectral regions have confirmed that CH₂OO is the predominant isomer formed in the CH₂I₂-O₂ photolysis process. In addition, the kinetics of ozonolysis experiments are inherently complex: Reliable data for individual CI reactions can be difficult to obtain under such conditions, as other oxidants (ozone and/or ozonides) are likely involved in complicated side reactions that may

obscure the rate determinations (1–5). In particular, the rate coefficients of CI reactions with SO₂, NO₂, and carboxylic acids are found to be much faster in the direct determinations (1–3) than in the ozonolysis analyses (6, 21, 22), suggesting the need for reinterpretation of earlier ozonolysis measurements (3, 4).

To clarify the kinetics of CI reactions with water, which is ubiquitous in the atmosphere, we performed direct rate measurements at multiple humidity levels. CH₂OO was synthesized by CH₂I₂-O₂ photolysis and probed via its strong UV absorption (16). The decay of CH₂OO was detected with two complementary methods: One recorded the transient difference absorption spectra (280 to 600 nm) with an image-intensified charge-coupled device (iCCD) spectrometer at various delay times after the photolysis laser pulse (16, 23); the other recorded full time traces of absorption change at 335 to 345 nm using a bandpass filter and a balanced photodiode detector (24).

Typical transient absorption spectra of the CH₂I₂-O₂ photolysis system are shown in Fig. 1. The strong UV absorption band of CH₂OO can be seen at a delay time of 15 μ s. CH₂OO is quite reactive; it decays at longer delay times, and depletion of CH₂I₂ and formation of IO can also be clearly observed. The transient absorption spectra can be decomposed into absorbance bands attributable to CH₂I₂ (depletion), CH₂OO, and IO using their reported spectra (16, 25) (Fig. 1C). The corresponding number densities can be found in fig. S4. Detailed kinetic analysis of the CH₂I₂-O₂ photolysis system (without water) has been published (26). When water vapor was introduced (Fig. 1B), the CH₂OO absorption band was found to decrease much faster, indicating CH₂OO reaction with water vapor.

Selective detection of CH₂OO could be performed by choosing a wavelength window of 335 to 345 nm (Fig. 1), where CH₂OO absorbs much more strongly than CH₂I₂ and IO (their cross sections are 1.21×10^{-17} cm², 8.58×10^{-19} cm², and 2.67×10^{-19} cm², respectively, averaged over 335 to 345 nm) (16, 25).

Other species, such as H₂CO and ICH₂OO, may also be formed in the reaction cell. The absorption of H₂CO is rather weak, but the UV spectrum of ICH₂OO is uncertain (26). Fortunately, the CH₂OO spectrum has characteristic vibronic structures on the long-wavelength side (355 to 405 nm) (16). Ting *et al.* (26) made use of this feature to show that the absorption band of ICH₂OO does not overlap with that of CH₂OO and hence would not interfere with the concentration determination of CH₂OO via its UV absorption.

Figure 2 shows typical temporal profiles of CH₂OO concentration, [CH₂OO], which decays much faster at higher humidity. The resultant decay rates are consistent with those from the iCCD measurements (24). Figure 3A shows the decay rate coefficient (k_{obs}) of CH₂OO as a function of H_R . Remarkably, k_{obs} depends on the relative humidity quadratically. Figure 3B plots

¹Institute of Atomic and Molecular Sciences, Academia Sinica, Taipei 10617, Taiwan. ²Department of Chemistry, National Taiwan University, Taipei 10617, Taiwan. ³Stanford University, Stanford, CA 94305, USA. ⁴Department of Applied Chemistry, National Chiao Tung University, Hsinchu 30010, Taiwan.

*Corresponding author. E-mail: jimlin@gate.sinica.edu.tw

k_{obs} against the concentration of water dimer estimated with the reported equilibrium constant (27). The linear behavior of k_{obs} versus $[(\text{H}_2\text{O})_2]$ indicates that the reaction of CH_2OO with water dimer (reaction 2) predominates.

Even under the dry condition, CH_2OO has a finite lifetime, mainly due to the reactions with itself and with other radical species (26). We assume that the overall decay rate of CH_2OO is the sum of the dry decay rate, $k_0[\text{CH}_2\text{OO}]$, and the rate due to reaction with water, $k'_w[\text{CH}_2\text{OO}]$:

$$-\frac{d[\text{CH}_2\text{OO}]}{dt} = k_0[\text{CH}_2\text{OO}] + k'_w[\text{CH}_2\text{OO}]$$

$$= k_{\text{obs}}[\text{CH}_2\text{OO}] \quad (1)$$

where k'_w is the effective first-order rate coefficient of the CH_2OO reaction with water vapor. The observed k'_w , plotted as a function of H_R in Fig. 4 and in figs. S5 to S8, can be well fitted with Eq. 2, regardless of different total pressures, initial concentrations, and buffer gases, indicating a quadratic rate dependence on water:

$$k'_w = k_H \left(\frac{H_R}{100\%} \right)^2 \quad (2)$$

where k_H is a proportional constant.

Because not only CH_2OO but also other radical species (I, OH, etc.) are formed in the $\text{CH}_2\text{I}_2\text{-O}_2$ photolysis system, we need to test the effect of other radical species. We varied the radical concentrations by a factor of 4 and found that the concentrations of radical species (including CH_2OO) greatly affect the CH_2OO lifetime under the dry condition (26) but do not affect the rate due to the CH_2OO reaction with water vapor (table S1 and fig. S2), indicating the validity of Eq. 1. In addition, we have tested the effect of OH radicals by adding 5 torr of propane, an efficient OH scavenger, to the reaction system. We found that addition of propane makes no difference for the rates of CH_2OO reaction with water vapor (fig. S3), indicating that OH radicals do not interfere with our rate determination.

The water dimer concentration $[(\text{H}_2\text{O})_2]$ can be estimated with Eq. 3, which takes into account the reported equilibrium constant $K_p = 0.0501 \text{ bar}^{-1}$ at 298 K (27) and the ideal gas law:

$$[(\text{H}_2\text{O})_2] = N_A \frac{K_p}{RT} \left(\frac{H_R}{100\%} P_{\text{sat}} \right)^2$$

$$= 1.23 \times 10^{15} \left(\frac{H_R}{100\%} \right)^2 \text{ cm}^{-3} \quad (3)$$

where N_A is Avogadro's number and P_{sat} is the saturation water vapor pressure (23.8 torr at 298 K). Because k'_w scales quadratically with respect to H_R and linearly with respect to $[(\text{H}_2\text{O})_2]$, as demonstrated in Figs. 3 and 4, we have $k'_w = k_2[(\text{H}_2\text{O})_2]$.

Our k_H value of 7968 s^{-1} corresponds to $k_2 = 6.5 \times 10^{-12} \text{ cm}^3 \text{ s}^{-1}$. The manufacturer-specified uncertainty of our relative humidity sensor is 3.5% (we have verified this by using a few saturated salt solutions), which translates to 7% error in k_H . The vapor pressure of water has a consider-

able temperature dependence, about 7% per kelvin, which corresponds to 5% uncertainty in $[\text{H}_2\text{O}]$ for our temperature stability of 0.7 K. The uncertainty in the dimer equilibrium constant is 3.2% with a negative temperature dependence of -2% per kelvin (27). Then the overall percentage

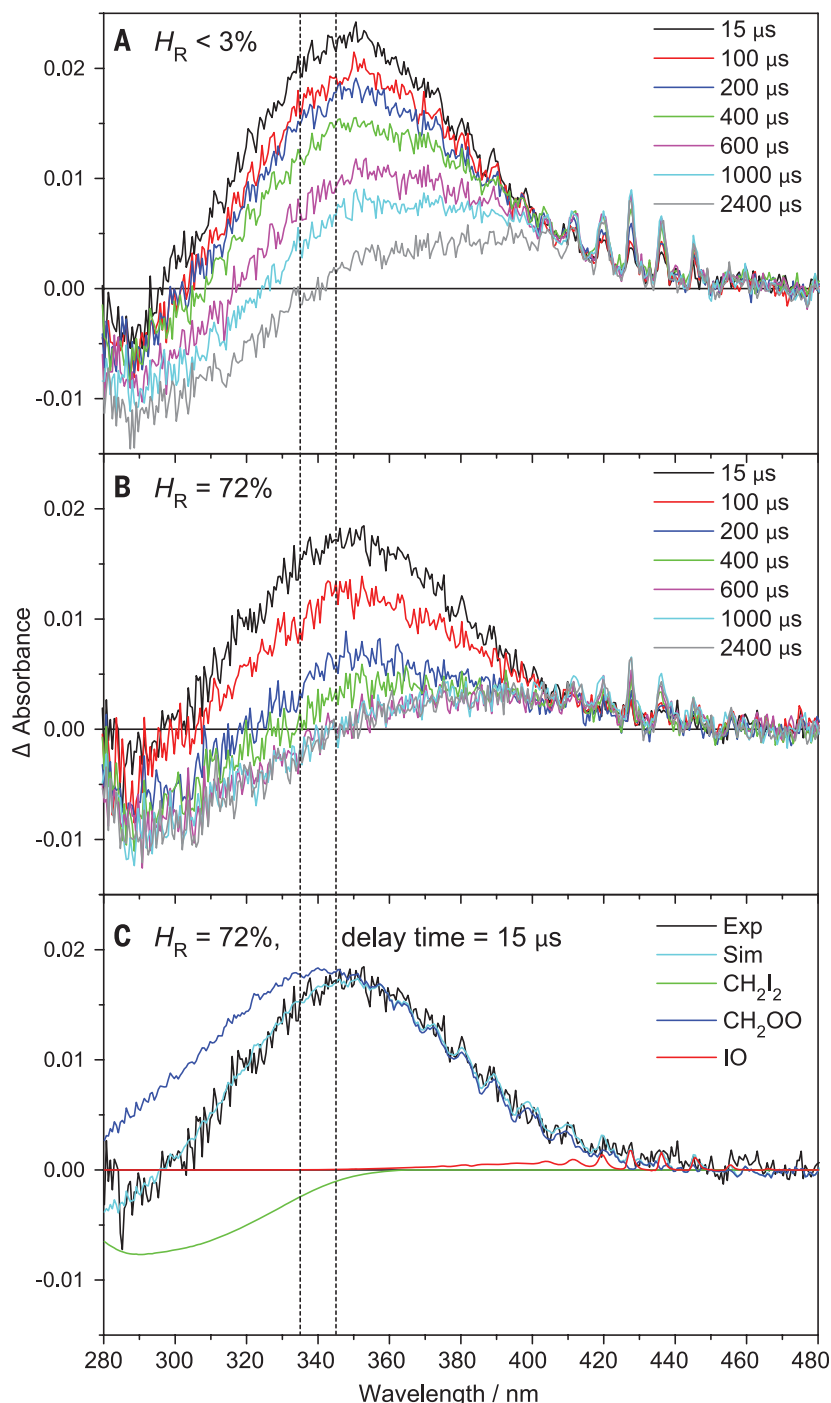


Fig. 1. Difference transient absorption spectra recorded in the $\text{CH}_2\text{I}_2\text{-O}_2$ photolysis. (A and B) Spectra are shown at selected delay times after the photolysis laser pulse under dry conditions ($H_R < 3\%$) (A) and wet conditions ($H_R = 72\%$) (B). (C) Experimental transient absorption spectra were decomposed into bands assigned to CH_2I_2 (depletion), CH_2OO , and IO using their reported spectra (16, 25). (See fig. S4 for details). The vertical dashed lines indicate the detection window of the balanced photodiode detector (335 to 345 nm).

uncertainty in $[(\text{H}_2\text{O})_2]$ can be estimated as $[(7\%)^2 + (2 \times 5\% - 0.7 \times 2\%)^2 + (3.2\%)^2]^{0.5} = 12\%$. Thus, we report $k_2 = 6.5 (\pm 0.8) \times 10^{-12} \text{ cm}^3 \text{ s}^{-1}$ at 298 K.

Including the water monomer reaction in the decay kinetics of CH_2OO does not improve the fit to the experimental data. Considering

our experimental error bars, the upper limit of k_1 is estimated to be $1.5 \times 10^{-15} \text{ cm}^3 \text{ s}^{-1}$.

Our data demonstrate that two water molecules are required for the reaction that consumes CH_2OO . We cannot distinguish, merely by the experimental data, whether it is due to the reaction of $\text{CH}_2\text{OO} + (\text{H}_2\text{O})_2$ or a reaction such as $\text{CH}_2\text{OO}(\text{H}_2\text{O}) + \text{H}_2\text{O}$. Therefore, the reported k_2 should be regarded as an effective rate coefficient. Note that the pre-reactive complexes, $\text{CH}_2\text{OO}(\text{H}_2\text{O})$ and $\text{CH}_2\text{OO}(\text{H}_2\text{O})_2$, would not affect the detection of CH_2OO because of their low equilibrium concentrations (15).

Previous direct kinetic measurements of CI reactions with water vapor were performed by using the VUV-PIMS techniques (1, 2). Although VUV-PIMS is a powerful tool that can selectively detect a conformer or isomer on the basis of their different ionization thresholds, the total pressure of the reactor is limited to only a few torr. As a result, the water pressure used was 1 torr or less ($[\text{H}_2\text{O}] \leq 3.2 \times 10^{16} \text{ cm}^{-3}$), and $[(\text{H}_2\text{O})_2]$ would be too low ($\leq 2 \times 10^{12} \text{ cm}^{-3}$ at 298 K) to affect the decay rates of CIs.

Using the same $\text{CH}_2\text{I}_2\text{-O}_2$ photolysis source, Stone *et al.* (7) and Ouyang *et al.* (8) investigated the reaction at higher $P_{\text{H}_2\text{O}}$ —up to 5 and 21 torr, respectively—but with indirect detection (detecting the effect of humidity on the CH_2OO reaction with a third reagent). Both groups did not observe any reaction of CH_2OO with water dimer, however. The discrepancy might be explained by the following: Stone *et al.* detected the laser-induced fluorescence of H_2CO , one likely product in the CH_2OO reaction system (for example, $\text{CH}_2\text{OO} + \text{X} \rightarrow \text{XO} + \text{H}_2\text{CO}$, where X denotes a radical); Ouyang *et al.* measured the yield of NO_3 in the reaction of CH_2OO with NO_2 ($\text{CH}_2\text{OO} + \text{NO}_2 \rightarrow \text{NO}_3 + \text{H}_2\text{CO}$). If the products of the CH_2OO reaction with water dimer also end up forming the same detected product [H_2CO for (7), NO_3 for (8)], the effect of adding water might not be very obvious in their experimental observations. The fluorescence signal of H_2CO is also quenched by water, further complicating the situation of Stone *et al.* As a result, the rate coefficient of the water dimer reaction with CH_2OO might be underestimated in their analyses using complicated but incomplete reaction mechanisms.

The above assumption is partly supported by the theoretical work of Ryzhkov and Ariya (15). They have proposed that the products of $\text{CH}_2\text{OO} + (\text{H}_2\text{O})_2$ are likely hydroxymethyl hydroperoxide (HMHP; HOCH_2OOH) and H_2O ; this reaction is quite exothermic, and some of the internally excited HMHP may decompose to HOOH and H_2CO with H_2O acting as a catalyst (15).

Berndt *et al.* (14) investigated the competitive kinetics for CH_2OO reactions with SO_2 (reaction 3) and with water vapor by measuring the H_2SO_4 product yield at $P_{\text{H}_2\text{O}} \leq 12$ torr in a C_2H_4 ozonolysis experiment. They found considerable reduction in the H_2SO_4 product yield at high humidity and suggested $k_2/k_3 = 0.29 \pm 0.01$ at 293 K; that is, $k_2 = 1.2 \times 10^{-11} \text{ cm}^3 \text{ s}^{-1}$, assuming $k_3 = 4 \times 10^{-11} \text{ cm}^3 \text{ s}^{-1}$ (1). This value of k_2 is about twice our value. The discrepancy may arise from

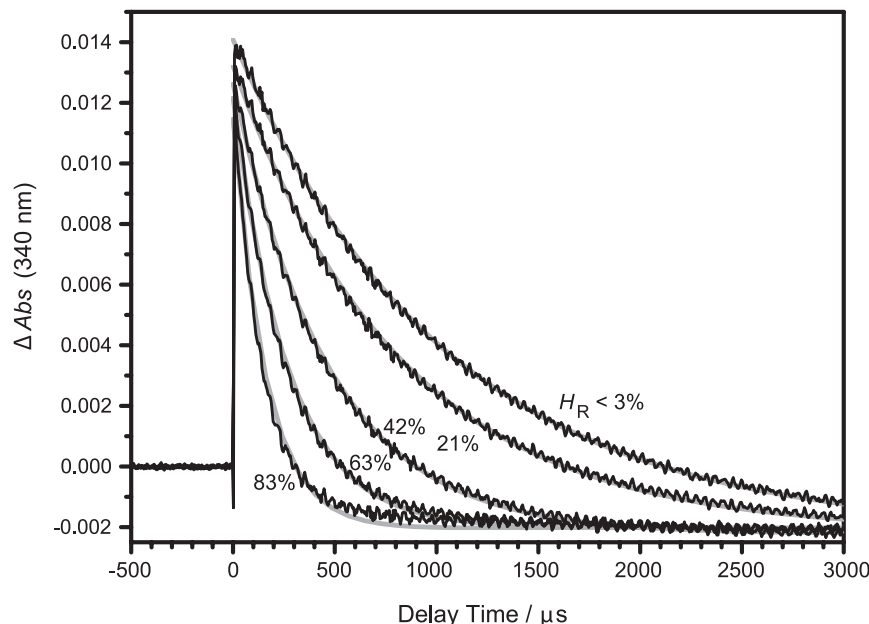
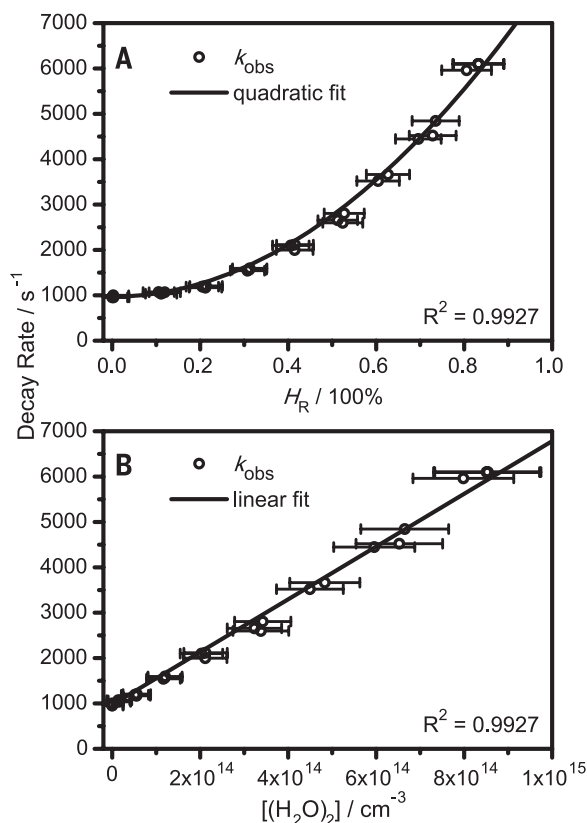


Fig. 2. Typical temporal profiles of the absorbance change near the peak of the CH_2OO band.

Absorption was monitored with a balanced photodiode detector and a bandpass filter (335 to 345 nm) at various relative humidity levels ($H_R = 0$ to 83%). The smooth lines are single-exponential fits to the experimental data, which were averaged for 60 to 120 laser shots (experiment 3) (24). Because IO absorbs rather weakly in this wavelength window and the depletion of CH_2I_2 is constant after the photolysis (causing negative baselines at long times), these temporal profiles mainly represent changes in $[\text{CH}_2\text{OO}]$.

Fig. 3. Dependence of CH_2OO decay rate coefficient on water monomer and dimer concentrations.

(A) The decay rate coefficient of CH_2OO (k_{obs}) measured under various relative humidity levels H_R (experiment 3). k_{obs} is obtained from single-exponential fit to the time traces measured with the balanced photodiode detector. (B) The same rate data as in (A), but plotted against the estimated concentration of water dimer. The horizontal error bar includes the uncertainties in the relative humidity and temperature (see text). The vertical error bar is the error in the exponential fitting (see table S3) but is too small to be seen.



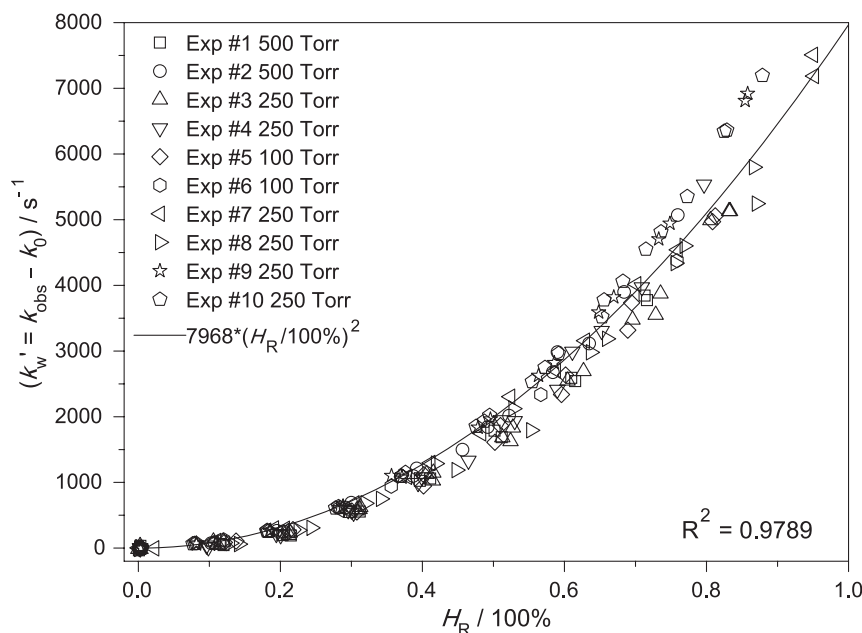


Fig. 4. Effective first-order rate coefficient of CH_2OO reaction with water vapor k'_w plotted as a function of relative humidity H_R . There are total 188 measurements at 298 K with buffer gases of N_2 (experiments 1 to 6), O_2 (experiment 7), SF_6 (experiment 8), N_2 (experiment 9, the reference experiment for 10), and $\text{N}_2 + \text{C}_3\text{H}_8$ (experiment 10). A different humidity sensor was used for experiments 9 and 10, which caused some deviation of the data points, but they are within the error bars of the humidity sensors (24). The total pressures are also listed in the figure. The quadratic fit to all data points yields $k_H = 7968 \text{ s}^{-1}$.

Table 1. Estimation of the effective first-order rate coefficients k_{eff} for CH_2OO reactions with water vapor and atmospheric key species.

Co-reactant	k_{reaction} ($\text{cm}^3 \text{ s}^{-1}$)	Assumed concentration [§]	Number density [§] (cm^{-3})	k_{eff} (s^{-1})
$(\text{H}_2\text{O})_2$	$6.5 \times 10^{-12*}$	$H_R \geq 36\%$	$\geq 1.6 \times 10^{14}$	≥ 1000
SO_2	$4 \times 10^{-11\dagger}$	50 ppb	1.2×10^{12}	50
NO_2	$7 \times 10^{-12\dagger}$	50 ppb	1.2×10^{12}	9
Carboxylic acids	$1 \times 10^{-10\dagger}$	5 ppb	1.2×10^{11}	12

*This work. †(1). ‡(3). §At 298 K and 760 torr.

the complexity of the ozonolysis reaction relative to individual CI reactions. For example, with similar H_2SO_4 detection, the rate coefficients of simple CI reactions with SO_2 in ozonolysis experiments were reported to be on the order of $10^{-13} \text{ cm}^3 \text{ s}^{-1}$ (22), much slower than those (2.4×10^{-11} to $6.7 \times 10^{-11} \text{ cm}^3 \text{ s}^{-1}$) obtained from the direct determinations (2).

Ryzhkov and Ariya (15) have performed quantum chemistry calculations on the reaction of CH_2OO with water dimer and estimated the effective rate coefficient at various H_R levels and temperatures. At 298 K, their estimated effective rate coefficient [figure 5 of (15)] is of the same order of magnitude as our experimental values.

Even in a relatively dry atmosphere ($H_R \approx 35\%$), the decay of CH_2OO due to water is much faster than other CH_2OO reactions with SO_2 , NO_2 , and carboxylic acids (Table 1). Recent direct kinetic measurements of CI reactions with carboxylic

acids suggest that the reaction with carboxylic acids is a substantially more important loss process for CIs than is previously assumed (3). But Welz *et al.* (3) used a value of k_2 derived from (7) that is smaller than this new determination by a factor of 20, leading to underestimation of the effect of the water dimer reaction with CH_2OO .

Theoretical calculations (15, 28, 29) and investigations of alkene ozonolysis (14, 22, 30) indicate that the reactivity of CIs toward water depends on their structures. For example, *anti*- CH_3CHOO was found to be more reactive to water than *syn*- CH_3CHOO (2); the above data show that water dimer is much more reactive than water monomer for CH_2OO . Furthermore, our preliminary investigation of CH_3CHOO suggests that the *syn* form reacts with water much more slowly than the *anti* form; the latter also reacts quickly with water dimer (see fig. S13). The role of water and water dimer in the at-

mospheric chemistry of CIs surely demands further investigation. The method demonstrated in this work opens a door to direct kinetic measurements of CIs under near-atmospheric conditions.

REFERENCES AND NOTES

1. O. Welz *et al.*, *Science* **335**, 204–207 (2012).
2. C. A. Taatjes *et al.*, *Science* **340**, 177–180 (2013).
3. O. Welz *et al.*, *Angew. Chem. Int. Ed.* **53**, 4547–4550 (2014).
4. C. A. Taatjes, D. E. Shallcross, C. J. Percival, *Phys. Chem. Chem. Phys.* **16**, 1704–1718 (2014).
5. L. Vereecken, *Science* **340**, 154–155 (2013).
6. D. Johnson, G. Marston, *Chem. Soc. Rev.* **37**, 699–716 (2008).
7. D. Stone, M. Blitz, L. Daubney, N. U. Howes, P. Seakins, *Phys. Chem. Chem. Phys.* **16**, 1139–1149 (2014).
8. B. Ouyang, M. W. McLeod, R. L. Jones, W. J. Bloss, *Phys. Chem. Chem. Phys.* **15**, 17070–17075 (2013).
9. P. Neeb, F. Sauer, O. Horie, G. K. Moortgat, *Atmos. Environ.* **31**, 1417–1423 (1997).
10. A. S. Hasson, G. Orzechowska, S. E. Paulson, *J. Geophys. Res.* **106** (D24), 34131–34142 (2001).
11. M. Suto, E. R. Manzanares, L. C. Lee, *Environ. Sci. Technol.* **19**, 815–820 (1985).
12. K. H. Becker, J. Bechara, K. J. Brockmann, *Atmos. Environ.* **27**, 57–61 (1993).
13. K. E. Leather *et al.*, *Atmos. Chem. Phys.* **12**, 469–479 (2012).
14. T. Berndt *et al.*, *Phys. Chem. Chem. Phys.* **16**, 19130–19136 (2014).
15. A. B. Ryzhkov, P. A. Ariya, *Phys. Chem. Chem. Phys.* **6**, 5042–5050 (2004).
16. W.-L. Ting, Y. H. Chen, W. Chao, M. C. Smith, J. J. Lin, *Phys. Chem. Chem. Phys.* **16**, 10438–10443 (2014).
17. J. M. Beames, F. Liu, L. Lu, M. I. Lester, *J. Am. Chem. Soc.* **134**, 20045–20048 (2012).
18. J. H. Lehman, H. Li, J. M. Beames, M. I. Lester, *J. Chem. Phys.* **139**, 141103 (2013).
19. Y.-T. Su, Y.-H. Huang, H. A. Witek, Y.-P. Lee, *Science* **340**, 174–176 (2013).
20. M. Nakajima, Y. Endo, *J. Chem. Phys.* **139**, 101103 (2013).
21. D. Johnson, A. G. Lewin, G. Marston, *J. Phys. Chem. A* **105**, 2933–2935 (2001).
22. T. Berndt *et al.*, *J. Phys. Chem. Lett.* **3**, 2892–2896 (2012).
23. M. C. Smith *et al.*, *J. Chem. Phys.* **141**, 074302 (2014).
24. See supplementary materials on Science Online.
25. S. P. Sander *et al.*, *Chemical Kinetics and Photochemical Data for Use in Atmospheric Studies. Evaluation Number 17*, JPL Publication 10-6 (Jet Propulsion Laboratory, Pasadena, CA, 2011).
26. W.-L. Ting *et al.*, *J. Chem. Phys.* **141**, 104308 (2014).
27. B. Ruscic, *J. Phys. Chem. A* **117**, 11940–11953 (2013).
28. J. M. Anglada, J. González, M. Torrent-Sucarrat, *Phys. Chem. Chem. Phys.* **13**, 13034–13045 (2011).
29. L. Vereecken, H. Harder, A. Novelli, *Phys. Chem. Chem. Phys.* **16**, 4039–4049 (2014).
30. T. Berndt *et al.*, *Atmos. Environ.* **89**, 603–612 (2014).

ACKNOWLEDGMENTS

Materials and methods and more kinetic data are presented in the supplementary materials. Supported by Academia Sinica and Ministry of Science and Technology, Taiwan, grants MOST103-2113-M-001-019-MY3 and MOST103-2815-C-001-001-M. We thank Y. T. Lee for discussion.

SUPPLEMENTARY MATERIALS

www.sciencemag.org/content/347/6223/751/suppl/DC1
Materials and Methods
Supplementary Text
Figs. S1 to S13
Tables S1 to S3

21 September 2014; accepted 16 December 2014
Published online 1 January 2015;
10.1126/science.1261549

NEURAL CIRCUITS

Labeling of active neural circuits in vivo with designed calcium integrators

Benjamin F. Fosque,^{*†} Yi Sun,^{*} Hod Dana,^{*} Chao-Tsung Yang, Tomoko Ohyama, Michael R. Tadross, Ronak Patel, Marta Zlatić, Douglas S. Kim, Misha B. Ahrens, Vivek Jayaraman, Loren L. Looger, Eric R. Schreiter[†]

The identification of active neurons and circuits in vivo is a fundamental challenge in understanding the neural basis of behavior. Genetically encoded calcium (Ca^{2+}) indicators (GECIs) enable quantitative monitoring of cellular-resolution activity during behavior. However, such indicators require online monitoring within a limited field of view. Alternatively, post hoc staining of immediate early genes (IEGs) indicates highly active cells within the entire brain, albeit with poor temporal resolution. We designed a fluorescent sensor, CaMPARI, that combines the genetic targetability and quantitative link to neural activity of GECIs with the permanent, large-scale labeling of IEGs, allowing a temporally precise “activity snapshot” of a large tissue volume. CaMPARI undergoes efficient and irreversible green-to-red conversion only when elevated intracellular Ca^{2+} and experimenter-controlled illumination coincide. We demonstrate the utility of CaMPARI in freely moving larvae of zebrafish and flies, and in head-fixed mice and adult flies.

Brain function relies on patterns of synaptic input and action potential firing, which are accompanied by transient changes in free intracellular calcium (Ca^{2+}) concentration ($[\text{Ca}^{2+}]$) (1, 2). Genetically encoded calcium indicators (GECIs) are useful for monitoring the activity of populations of neurons and synapses in behaving organisms (3–6). However, the transient nature of GECI responses following $[\text{Ca}^{2+}]$ rises requires continuous monitoring during behavior using sophisticated imaging equipment with limited fields of view, and often physical restraint to prevent brain movement. Alternatively, expression of immediate early genes (IEGs) such as *Arc* and *cFos* can be measured following free behavior (7) within several hours, but is only weakly correlated with neural electrical activity (8, 9) and is constrained neither by genetic cell type nor by a precise temporal window. The creation of molecular tools to allow genetic targeting of direct reporters of neural activity that can be rendered permanent for post hoc analysis across entire brains, and that only mark neurons active during short, user-defined behavioral epochs, would be transformative (10, 11).

The GCaMP calcium indicator reports changes in free $[\text{Ca}^{2+}]$ [rise and decay times <1 s (12)] through mechanisms that modulate the environment of the 488-nm-absorbing, fluorescent 4-(*p*-hydroxybenzylidene)-5-imidazolinone chromophore of circularly permuted green fluorescent protein (cpGFP) (13). The photoconvertible

fluorescent protein (FP) EosFP is a bright green FP that irreversibly converts to a bright red fluorescent species {backbone cleavage produces 2-[(1E)-2-(5-imidazolyl)ethenyl]-4-(*p*-hydroxybenzylidene)-5-imidazolinone} upon illumination with violet light (14). Previously, circular permutation of a photoconvertible FP and attachment to the Ca^{2+} -binding protein calmodulin (CaM) and its associated M13 peptide (M13) gave rise to a photoconvertible GECI that produced GCaMP-like rises in fluorescent intensity both in the unconverted, green state and in the converted, red state (15). We reasoned that related constructs would undergo Ca^{2+} -dependent allosteric modulation of the chromophore photoconvertibility. Such a protein species would convert from green to red only in the simultaneous presence of high $[\text{Ca}^{2+}]$ and user-supplied violet light (Fig. 1A). By combining library screening and structure-guided mutagenesis (16) we produced such a protein, which we named CaMPARI (calcium-modulated photoactivatable ratiometric integrator).

CaMPARI has the primary structure depicted in Fig. 1B and fig. S1, and includes a nuclear export signal (NES) to exclude it from the nucleus when expressed in eukaryotic cells. CaMPARI exhibits 60 and 40% of the green and red fluorescence brightness of mEos2, respectively, and photoconverts to the red form 21 times as fast in the presence of calcium (Fig. 1C and table S1). Photoconversion (PC) of the calcium-bound and calcium-free states of CaMPARI occurs three times and one-seventh as fast, respectively, as that of the parent EosFP variant (fig. S2). No effect of calcium on PC of the parent EosFP variant was observed (fig. S2).

Measuring the PC rate while titrating calcium gave an apparent dissociation constant (K_d) of 128 ± 6 nM (Fig. 1D). We modified the

affinity of CaMPARI for calcium via mutagenesis at the CaM/M13 interface (fig. S3), thus increasing dynamic range in cells with a wide range of baseline and peak calcium concentrations. In addition to a calcium-dependent green-to-red PC rate, the fluorescence of both green and red CaMPARI states is also calcium-dependent, decreasing by a factor of 9 and 23, respectively, upon calcium binding (Fig. 1E, fig. S4, and table S1).

After initial characterization in cultured HeLa cells (fig. S5), we expressed CaMPARI in primary cultured rat hippocampal neurons. Whereas a 2-s pulse of PC light (1.5 W/cm^2) resulted in only minimal CaMPARI PC in unstimulated neurons, the same light exposure induced significant PC in field-stimulated neurons (Fig. 1, F to H), with a roughly linear correspondence between the frequency of field stimulation and the extent of CaMPARI PC (Fig. 1I). Stimulation of CaMPARI-expressing neurons without exposure to 405-nm light led to transient decreases of its green fluorescence (fig. S6), but with no conversion to the red form. We additionally depolarized neurons either by increasing extracellular potassium concentration or via pharmacogenetic activation of exogenously expressed P2X channels with adenosine 5'-triphosphate (ATP), both in concert with application of PC light. Cells were fixed with 4% paraformaldehyde (PFA) and colabeled with traditional antibody-staining techniques (Fig. 1, J and K). The green and red fluorescence of CaMPARI each decreased $\sim 50\%$ upon PFA fixation (fig. S7). Retention of the CaMPARI PC signal through fixation, permeabilization, and multicolor antibody labeling enables integrated Ca^{2+} concentrations within individual cells to be directly correlated to independent proteomic metrics typically used for post hoc estimation of cell-type identification and examination of a wide range of biochemical events related to plasticity and other key signaling cascades. We co-immunolabeled fixed neurons for P2X expression level (fig. S8, an indication of the magnitude of the exogenous pharmacogenetic manipulation) and phosphorylated nuclear cyclic adenosine 3',5'-monophosphate (cAMP)-responsive element-binding protein (pCREB), which increased with elevated intracellular calcium (Fig. 1L). CaMPARI signal after fixation was similar to that of conventional immunofluorescence and in situ hybridization markers, making it possible to image a direct measure of Ca^{2+} in parallel with proteomic markers that can only be accessed after fixation.

We next used CaMPARI to mark active neurons in vivo, during sensory stimuli or behavior, in four preparations of three model organisms: larval zebrafish and *Drosophila melanogaster* to demonstrate whole-brain and genetically targeted neural ensemble mapping during free behavior; mouse primary visual cortex (V1) for large-scale post hoc confirmation of known distributions of direction-selective cells in a mammalian brain; and adult *Drosophila* to highlight “labeled lines” of synaptically connected ensembles following naturalistic or optogenetic stimulation of sensory pathways. We chose calcium affinity variants (CaMPARI in mouse and adult

Howard Hughes Medical Institute, Janelia Farm Research Campus, 19700 Helix Drive, Ashburn, VA 20147, USA.

*These authors contributed equally to this work. †Present address: Department of Biochemistry and Molecular Biology, University of Chicago, Chicago, IL 60637, USA. ‡Corresponding author. E-mail: schreitere@janelia.hhmi.org

Drosophila; V398D, with about one-seventh the affinity for Ca^{2+} , in larval and adult *Drosophila*; W391F+V398L, with about one-half the affinity for Ca^{2+} , in larval zebrafish; fig. S3) based on performance of different GCaMP variants in these preparations, as well as literature estimates of intracellular calcium.

To demonstrate the utility of CaMPARI for whole-brain neural circuit marking in larval zebrafish (*Danio rerio*) during free behavior, we generated stable transgenic zebrafish expressing CaMPARI in all neurons from the *elavl3* promoter (16) (Fig. 2A). After exposure of larvae (4 to 5 days after fertilization) to 10 s of PC light (405-nm light-emitting diode array, 400 mW/cm², Fig. 2B), confocal stacks were acquired to generate a cellular-resolution snapshot of the calcium state of all neurons in the zebrafish brain (Fig. 2C and movie S1). Exposure of larvae anesthetized with tricaine methanesulfonate (MS-222) to PC light resulted in a lack of PC throughout the brain (Fig. 2C). Freely swimming fish with no additional stimulation showed a large amount of PC in the forebrain and habenula, but very little in the optic tectum. Additionally, patterns of hindbrain activity consistent with motor output for swimming (17, 18) were often observed. Treatment of larvae with proconvulsive compounds such as 4-aminopyridine (4-AP), exposure to noxious heat or cold stimuli (Fig. 2C), or exposure to turbulent water (fig. S9) during the PC light pulse resulted in qualitatively different patterns of CaMPARI PC throughout the brain, consistent with permanent marking of the subset of neurons activated by these stimuli. CaMPARI signals following each stimulus were consistent between fish (figs. S9 and S10) and showed clear cellular resolution (Fig. 2C, bottom panels).

Next, we tracked activity in a freely moving organism with CaMPARI expression isolated to a genetically specified subset of neurons. We expressed CaMPARI in peripheral sensory neurons (PSNs) of *Drosophila melanogaster* larvae using the P0163-Gal4 line (19). In third-instar larvae, CaMPARI fluorescence was clearly visible in PSN axonal projections in the ventral nerve cord (VNC) and could be segmented into proprioceptive, chordotonal, and nociceptive axon terminals (Fig. 2E). To highlight PSN responses to vibrational stimuli (20), we administered a single 5-s pulse of PC light to freely crawling larvae on an agar plate during presentation of a 1000-Hz tone delivered from a speaker below the plate (Fig. 2F). The vibration stimulus produced a twofold increase in green-to-red PC only within the axonal projections of chordotonal neurons, not the axons of proprioceptive or nociceptive neurons (Fig. 2G). The extent of CaMPARI PC within chordotonal axons increased in a dose-dependent manner with increasing amplitude of the vibration stimulus, with more sensitive responses in lateral compared with ventromedial axon terminals (Fig. 2H).

Within layer 2/3 of mouse V1, neurons responsive to different directions and orientations of moving bar gratings are interspersed throughout the tissue (21). CaMPARI was delivered to

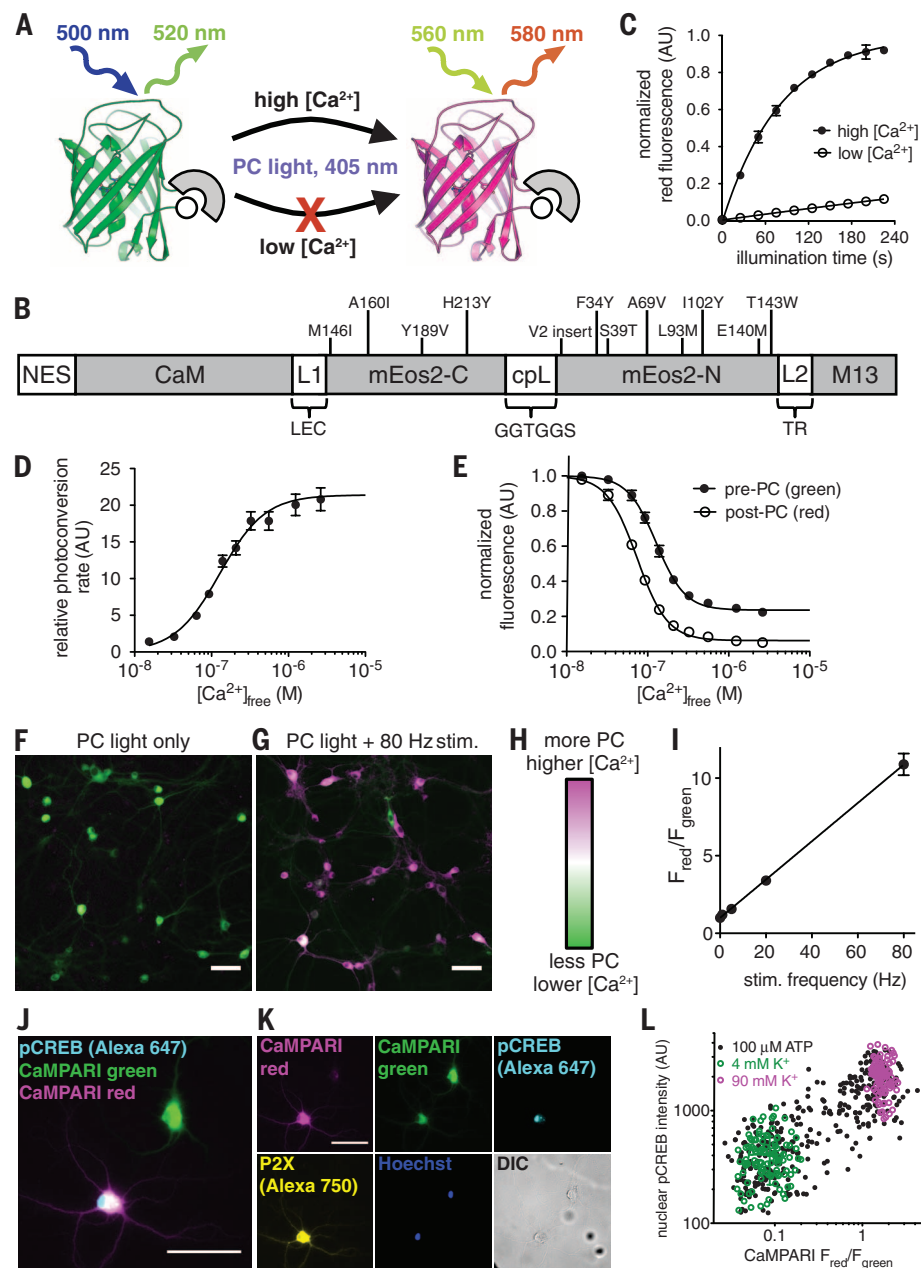


Fig. 1. CaMPARI engineering and in vitro characterization. (A) Schematic of CaMPARI function. (B) Primary structure of CaMPARI with mutations relative to mEos2. (C) Time course of red fluorescence appearance during exposure of CaMPARI to PC light. Lines represent single exponential fits to the PC time course. $n = 3$ measurements. All panels show means \pm SEM. (D) CaMPARI PC rate as a function of free Ca^{2+} . Black line represents a sigmoidal fit. $n = 3$ measurements. (E) Relative fluorescence of CaMPARI as a function of free Ca^{2+} concentration. Lines are sigmoidal fits to the data. $n = 3$ measurements. (F and G) Fluorescence of primary rat hippocampal neurons expressing CaMPARI after a 2-s PC light pulse without and with 80-Hz field electrode stimulation. (H) Color scale for composite micrographs of green and red CaMPARI fluorescence used throughout this work. (I) Quantitation of the red/green fluorescence ratio of neurons stimulated at different frequencies during PC light. Black line is a linear fit to the data. $n = 10$ measurements. (J) Fluorescence from two fixed, immunostained neurons. (K) Individual color channels from the same field of view as in (J). (L) Correlation between intensity of phospho-CREB staining and CaMPARI PC for high-potassium depolarization (90 mM K^+), controls (4 mM K^+), and P2X/ATP. A range of expression levels of P2X channels was present across neurons, resulting in the observed spread in activation upon 100 μM ATP stimulation. Scale bars: 50 μm in all panels.

layer 2/3 pyramidal cells with an adeno-associated virus 1 (AAV1)-*synapsin1* virus. Expression was bright and excluded from the nucleus (Fig. 3B). First, in vivo calcium imaging was performed through a cranial window by imaging two-photon excited CaMPARI fluorescence as moving gratings were presented to the contralateral eye (16) (Fig. 3A). This allowed generation of orientation-tuning maps of segmented cell bodies. After identification of cells responsive to specific orientations (Fig. 3C), the visual stimulus (a single direction—"northwest," preferred by cell 1 but not cell 2 in Fig. 3B) was replayed, and PC light was delivered through the cranial window in 500-ms pulses. After 20 PC pulses spaced 12 s apart, noticeable

red fluorescence was present in a subset of cells (cell 1, but not cell 2, in Fig. 3B and movie S2). Neurons responsive to the "northwest" moving grating direction (like cell 1 in Fig. 3) exhibited a red/green fluorescence ratio significantly higher than cells not responsive to that direction (like cell 2 in Fig. 3, fig. S11). We relocated the in vivo two-photon fields of view within fixed, sectioned tissue using a confocal microscope (Fig. 3, B and E, and fig. S12). The relative red/green ratio of cells was maintained after fixation (fig. S13), and we were additionally able to image the CaMPARI signal over a much larger volume (Fig. 3F) than would have been easily accessible through the cranial window

in vivo. When perfusion and fixation occurred 24 hours after PC, marked cells could still be easily distinguished in fixed sections with confocal microscopy (fig. S14).

Genetic tools in *Drosophila* do not include methods for trans-synaptic circuit tracing and whole-brain functional mapping. Although photoactivatable GFP (22) and optogenetics in combination with calcium imaging (23) have been employed to detect potential neuronal connections, these methods require knowledge of presynaptic neurons and operate on a limited field of view. We set out to test whether CaMPARI could provide a more comprehensive solution. We affixed intact flies with pan-neuronal expression

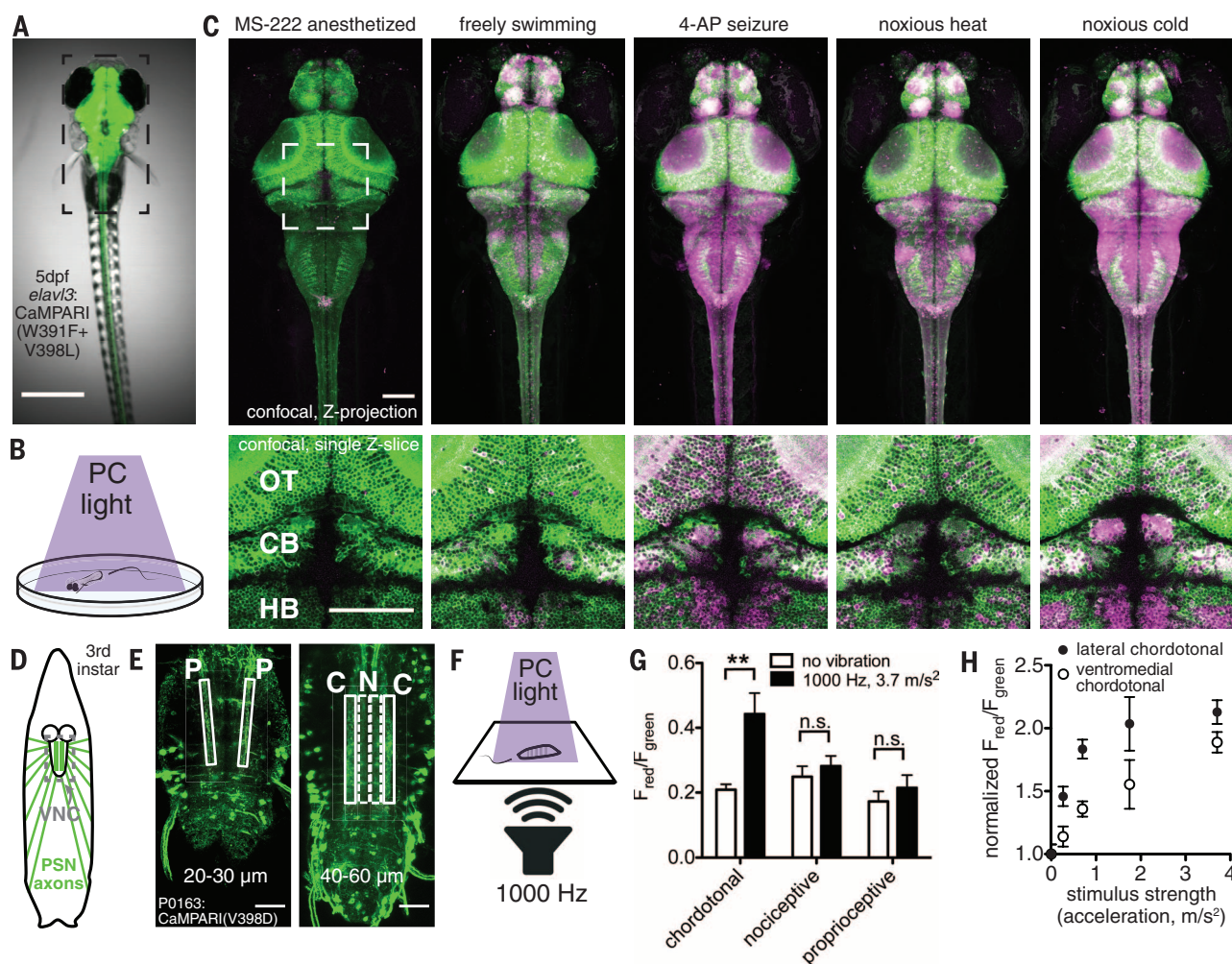


Fig. 2. Response in freely moving organisms. (A) CaMPARI expression in the Tg[*elav13*:CaMPARI(W391F+V398L)]^{if9} zebrafish. Dashed black rectangle represents the region displayed in the top panels of (C). (B) Schematic of experimental configuration. (C) Confocal images of zebrafish larvae (4 to 5 days after fertilization) after 10 s of PC light, applied during exposure to different conditions (labels above: MS-222 is tricaine, a sodium channel blocker; 4-AP is 4-aminopyridine, a potassium channel blocker; noxious heat is exposure to 45°C water; noxious cold is exposure to 4°C water). Top panels are maximum-intensity Z projections (MIPs) of the entire brain. Dashed gray box in the top left panel represents the region displayed in the bottom panels. Bottom panels are individual Z slices from the same fish, illustrating individual cells and neuropils within portions of the optic tectum (OT), cerebellum (CB),

and hindbrain (HB). (D) Schematic of labeled peripheral sensory neurons (PSNs) in a *Drosophila* larva. Axons (green lines) project from the body wall to the brain and branch along tracts within the VNC. Dashed gray box represents the region displayed in (E). (E) Confocal images of CaMPARI fluorescence in a subset of neurons in the VNC, driven by P0163-Gal4. Rectangles are segmented axonal tracts. P, proprioceptive; C, chordotonal; and N, nociceptive. (F) Schematic of the experimental setup. (G) Quantitation of the red/green CaMPARI fluorescence in sensory neuron projections. Mean \pm SEM from $n = 9$ larvae in each condition (** $P = 0.003$; n.s., not significant, $P > 0.4$; Student's t tests). (H) Dose response in chordotonal axons. Mean \pm SEM from $n = 6$ to 10 larvae in each condition. Scale bars: 500 μ m in (A), 100 μ m in (C), and 20 μ m in (E).

of low-affinity CaMPARI (V398D) to a physiology holder via the head cuticle and delivered PC light through a water-dipping objective while stimulating the animals with a panel of odors (Fig. 4A and fig. S15): (i) 3-octanol (3-Oct), which activates multiple glomeruli in the antennal lobe [AL; see (16) for a list of anatomical abbreviations used] (24); (ii) geosmin (Geo), an odorant that specifically activates the DA2 glomerulus (25); and (iii) phenylacetic acid (PAA), which strongly activates ionotropic receptor neurons projecting to the VL2a glomerulus (26). CaMPARI mapping confirmed the known neural representations of these odors in the antennal lobe (Fig. 4C, figs. S16 and S17, and movies S3 to S8). We also found additional, previously undescribed representations of some odors (Fig. 4, D and E). In the previous Geo study (25), a specific driver, GH146-Gal4, was used to express GCaMP3 in a limited subset of cells, facilitating segmentation of live-cell imaging data at the cost of ensemble undersampling. We similarly saw only the DA2 glomerulus activated when we drove CaMPARI expression with GH146-Gal4 (fig. S18), but additionally observed the DC1, VA1d, VA1v, and VM7 glomeruli (Fig. 4, D and E) with pan-neuronal CaMPARI. In the case of PAA, the original study (26) assessed odor responses using electrophysiology from specific Ir84a receptor neurons projecting to a single glomerulus (VL2a), rather than sampling the entire AL. When pan-neuronal CaMPARI was used, VL2a was the most salient responder, but weaker PC of VA1v and VM7 was also seen. Increasing the stimulation and PC time increased the overall red/green ratio without altering the relative amount of signal in different glomeruli (Fig. 4F).

Olfactory receptor neuron (ORN) responses likely contribute substantially to the activation patterns we observe in the AL with the broad R57C10-Gal4 driver. Although local neurons (LNs) likely contribute to AL labeling as well, we found evidence of projection neuron (PN) activation (fig. S19). The activation of these secondary neurons was clearer when we used the PN-specific GH146-Gal4 (figs. S18, S20, and S21). With GH146-Gal4, we also found photoconverted PN axons projecting to the mushroom body (MB) calyx (CA) and the lateral horn (LH) (figs. S20 and S21 and movie S6), confirming that CaMPARI enables trans-synaptic circuit mapping. The labeled axons in LH arborize primarily ventrally (fig. S21), consistent with previous reports (26). Thus, pan-neuronal expression enables large-scale unbiased ensemble mapping across the brain. Co-registration of active cells to standardized atlases or the use of specific drivers to identify activated neurons (27) could be a powerful strategy for mapping pathways involved in specific behaviors.

We reasoned that sensory-driven circuit mapping with CaMPARI could also be complemented by the use of optogenetic stimulation to activate circuits downstream of an arbitrary cellular point of entry. We expressed the red light-sensitive channelrhodopsin CsChrimson (28) in Ir84a receptor neurons (fig. S22) using a LexA driver while ex-

pressing CaMPARI pan-neuronally with a Gal4 driver. We then mapped active circuits throughout the brain during optogenetic stimulation of this single-receptor neuron type (Fig. 4G). In addition to the glomeruli in the antennal lobe, where axons of ORNs and dendrites of PNs synapse (Fig. 4H), we observed axons of PNs projecting to the posterior areas of the brain (Fig. 4, I to L). One axon commissure, the medial antennal lobe tract (mALT), targets both CA and LH (Fig. 4, I and K), whereas another commissure, the medial-lateral antennal lobe tract (mlALT), targets LH directly (Fig. 4, I to L). As with PAA odor-driven activation, photoconverted PN axons mostly target the ventral part of LH. In addition, we detected activity in the MB vertical lobe (VL, Fig. 4, J and L) and VLP (Fig. 4, I and K), which are putative postsynaptic partners of PNs (Fig. 4J and fig. S23). More specifically, the α' and β' MB lobes were more photoconverted than α and β (fig. S24, E, F, G, and I compared to D), consistent with previous reports (29, 30). Using the higher-affinity CaMPARI, we attempted to mark circuit components further downstream (Fig. 4, K and L, and fig. S25). Although we found similar patterns of active PNs and VLP neurons as before (Fig. 4K), we also found other putative downstream circuit components such as LH neurons (Fig. 4L, cyan arrows), mushroom body

output neurons (Fig. 4, J and L, and fig. S24), and descending neuron projections to the ventral nerve cord (fig. S25). Activation of deeper layers of the circuit suggests that CsChrimson may be able to drive the firing rates (and thus Ca^{2+} levels) of sensory neurons and downstream neurons more potently than natural stimuli.

In summary, CaMPARI was validated in four preparations in three organisms. Recording neural circuit activity free from restraint creates opportunities for studying complex behaviors such as social interaction, courtship, and so forth. In the case of direction-selective L2/3 pyramidal cells in mouse V1, CaMPARI labeling is consistent with results obtained from imaging of GECIs (12) and small-molecule dyes (31), as well as electrical recordings (21). In freely moving *Drosophila* larvae, vibration-evoked signals were restricted to chordotonal, but not proprioceptive or nociceptive, sensory neurons; the results show a functional difference in sensitivity of two distinct subtypes of chordotonal axons to vibration. In adult *Drosophila* brains, PC during both naturalistic and optogenetic stimulation of olfactory sensory pathways labeled activity in the expected OSN/PN circuit and, further, labeled PN projections to the LH and MB, and potential quaternary descending neurons in the VNC. In freely swimming zebrafish, activation patterns

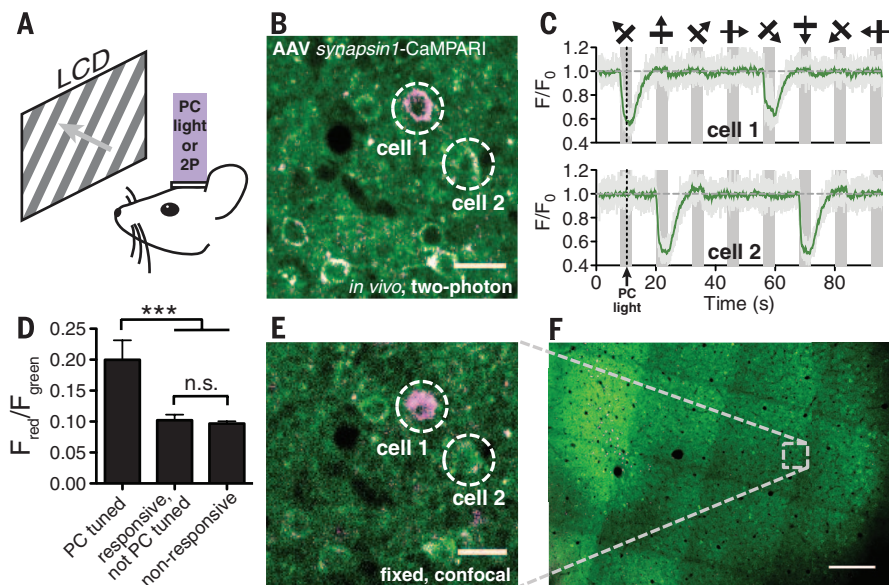


Fig. 3. Response in mouse primary visual cortex. (A) Schematic of experimental setup. (B) Two-photon fluorescence from cortical layer 2/3 of V1 after visual stimulus and PC light pulses. Two cells are circled and labeled for reference. (C) Calcium imaging fluorescence traces of the same two cells in response to different directions of drifting gratings (arrows and lines above traces). Average baseline-normalized green CaMPARI fluorescence (F/F_0) from five trials is in green; individual trial traces are light gray. Vertical gray bars represent periods of drifting grating visual stimulus. Vertical dashed lines show the timing of 500-ms PC light pulses during the “northwest” stimulus. (D) CaMPARI $F_{\text{red}}/F_{\text{green}}$ of cells according to functional properties identified by calcium imaging. “PC tuned”: cells with a significant (analysis of variance test, $P < 0.01$) calcium imaging response component to “northwest” gratings, ($n = 15$); “responsive, not PC tuned”: cells with a significant response to at least one direction, but no response to “northwest” ($n = 39$); “non-responsive”: no significant response during any grating orientation ($n = 248$) ($***P < 0.001$; n.s., not significant; $P = 0.13$; Mann-Whitney U tests). (E) Confocal image of fixed, sectioned tissue showing the same field of view as in (B). (F) Stitched composite confocal image of fixed, sectioned tissue. The region shown in (E) is outlined with a dashed gray box. Scale bars: 20 μm in (B) and (E), 200 μm in (F).

are consistent with hindbrain premotor and spinal cord motor output, as well as sensory modality-specific responses, which will be followed up experimentally. In all in vivo test cases, CaMPARI validates known results and offers extensions not otherwise possible: free movement, whole-brain activity mapping, a permanent signal compatible

with fixation, and follow-up experiments such as targeted electrical recordings, multichannel immunohistochemistry (allowing cell type identification), and isolation and genetic profiling of labeled cells. These properties facilitate “forward functional neuromics,” in which active neural populations are labeled during behav-

ior, drug treatment, sensory stimulation, and so forth in an unbiased fashion, with subsequent validation and characterization of labeled cells.

CaMPARI represents a new class of genetically encoded indicator that enables light-gated integration of Ca^{2+} flux in vivo with a time resolution of seconds to hours, specified by the user.

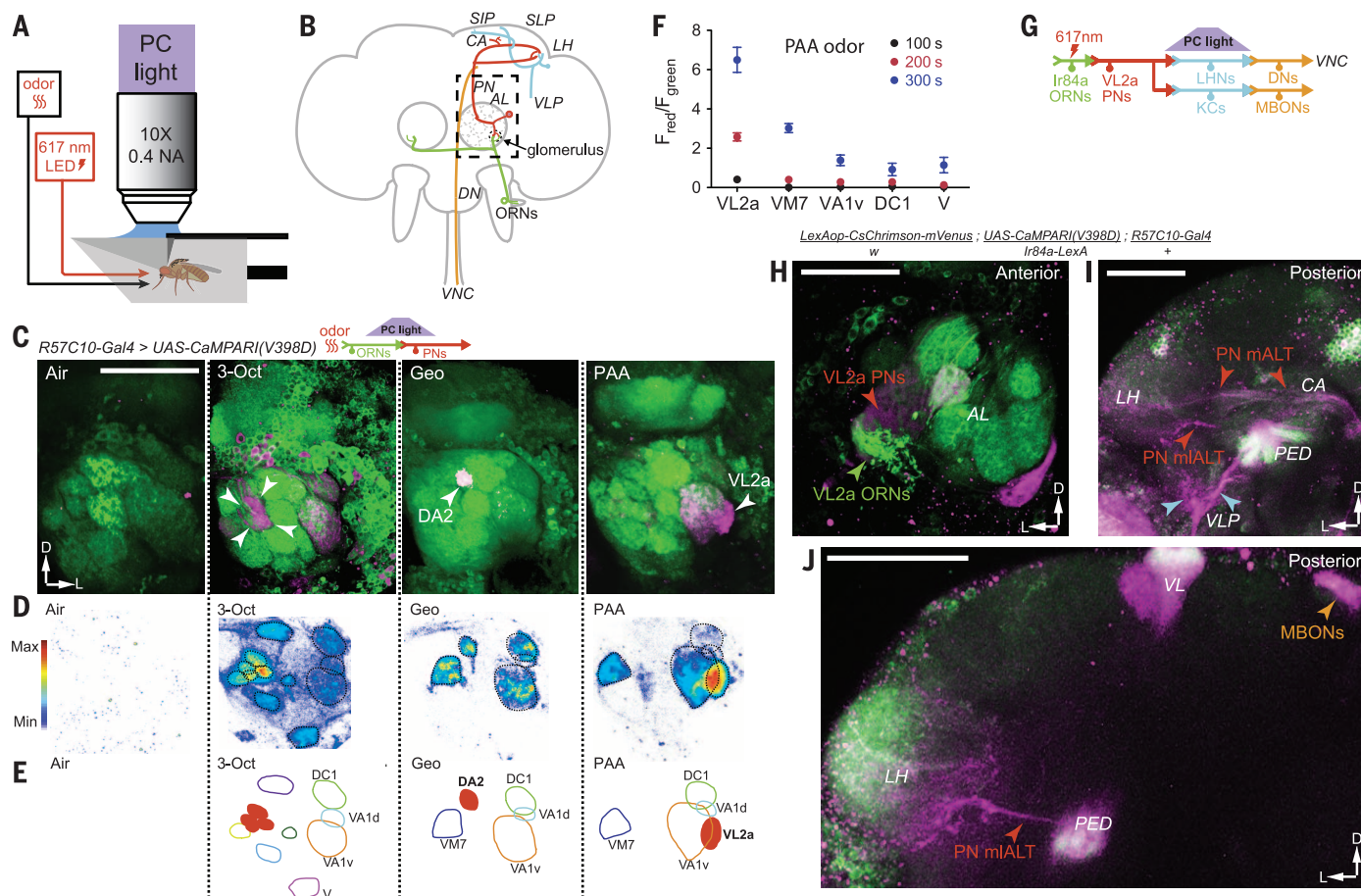


Fig. 4. Functional mapping and circuit tracing in adult *Drosophila*. (A) Schematic of experimental configuration. PC light is directed through an objective onto the head cuticle of a head-fixed adult fly during odor (C to F) or optogenetic (G to L) stimulation. (B) Schematic of olfactory circuitry targeted. The central brain of an adult fly is represented as a gray outline. ORNs [see (16) for a list of anatomical abbreviations used] (green) expressing specific receptors converge onto cognate glomeruli in the AL. PNs (red) from these glomeruli target the CA and LH. Putative tertiary neurons (cyan) then project to several areas including VL/SIP, SLP, VLP and finally to DN (orange), into the VNC. Dashed black box represents the area depicted in (C), (D), and (E). (C) MIPs of CaMPARI fluorescence from the left AL in response to indicated odors during PC. (D) MIP of red/green fluorescence ratios from (C). Dotted lines outline responsive glomeruli. (E) Maps of odor-response patterns in the AL. Each colored shape outlines one glomerulus from (C) and (D). Filled red glomeruli were previously reported in literature as responsive to that odor. Glomeruli that could be identified are labeled. (F) Comparison of glomerulus-specific responses to PAA at different PC and stimulation durations (100 s, $n = 4$; 200 s, $n = 4$; 300 s, $n = 3$). Means \pm SEM. (G to L) CsChrimson is expressed in specific ORNs while CaMPARI is expressed pan-neuronally. (G) Schematic showing the proposed connectivity of the olfactory circuit analyzed. (H) Response pattern in AL

shown with MIP; Ir84a ORNs are colabeled with mVenus. Ir84a-LexA:VP16 drives ORNs innervating ventromedial and dorsomedial glomeruli (see supplementary materials) that are photoconverted. (I) MIP of posterior sections showing marked PN axons targeting CA via the mALT bundle and LH through both the mALT and mALT bundles. Also shown are labeled putative tertiary neurons in VLP. (J) MIP of more medial sections [relative to (I), same brain] showing the mALT tract of PNs marked. (K and L) Experiments using high-affinity CaMPARI. (K) Similar to (H). (L) MIP of more medial sections [relative to (K), same brain] showing marked primary (ORNs, green arrows), secondary (PNs, red arrow), and putative tertiary (cyan arrows) neurons after optogenetic activation-PC. Scale bars: 25 μm in (C) and 50 μm in (H) to (L).

Converted signal is persistent, amenable to multitrail accumulation, and compatible with fixation for post hoc whole-brain (or targeted-area) activity reconstruction. CaMPARI signal is ratio-metric, correcting for expression-level differences. The protein engineering principles applied here could be extended to allow permanent marking of cell states or analytes other than Ca^{2+} by fusion of circularly permuted Eos variants to various ligand-binding or sensor domains, similar to previous GFP-based fluorescence intensity sensors (32–34).

REFERENCES AND NOTES

- P. F. Baker, A. L. Hodgkin, E. B. Ridgway, *J. Physiol.* **218**, 709–755 (1971).
- D. W. Tank, M. Sugimori, J. A. Connor, R. R. Llinás, *Science* **242**, 773–777 (1988).
- J. L. Chen, M. L. Andermann, T. Keck, N. L. Xu, Y. Ziv, *J. Neurosci.* **33**, 17631–17640 (2013).
- T. Riemensperger, U. Pech, S. Dipt, A. Fiala, *Biochim. Biophys. Acta* **1820**, 1169–1178 (2012).
- L. Tian, S. A. Hires, L. L. Looger, *Cold Spring Harbor Protoc.* **2012**, 647–656 (2012).
- E. Dreosti, B. Odermatt, M. M. Dorostkar, L. Lagnado, *Nat. Methods* **6**, 883–889 (2009).
- J. F. Guzowski et al., *Curr. Opin. Neurobiol.* **15**, 599–606 (2005).
- R. D. Fields, F. Eshete, B. Stevens, K. Itoh, *J. Neurosci.* **17**, 7252–7266 (1997).
- H. Z. Sheng, R. D. Fields, P. G. Nelson, *J. Neurosci. Res.* **35**, 459–467 (1993).
- R. Y. Tsien, *Proc. Natl. Acad. Sci. U.S.A.* **110**, 12456–12461 (2013).
- D. H. O'Connor, D. Huber, K. Svoboda, *Nature* **461**, 923–929 (2009).
- T. W. Chen et al., *Nature* **499**, 295–300 (2013).
- J. Akerboom et al., *J. Biol. Chem.* **284**, 6455–6464 (2009).
- J. Wiedenmann et al., *Proc. Natl. Acad. Sci. U.S.A.* **101**, 15905–15910 (2004).
- H. Hoi, T. Matsuda, T. Nagai, R. E. Campbell, *J. Am. Chem. Soc.* **135**, 46–49 (2013).
- Information on materials and methods is available on Science Online.
- J. Freeman et al., *Nat. Methods* **11**, 941–950 (2014).
- N. Vladimirov et al., *Nat. Methods* **11**, 883–884 (2014).
- T. Hummel, K. Krukkert, J. Roos, G. Davis, C. Klämbt, *Neuron* **26**, 357–370 (2000).
- T. Ohyama et al., *PLOS ONE* **8**, e71706 (2013).
- C. M. Niell, M. P. Stryker, *J. Neurosci.* **28**, 7520–7536 (2008).
- V. Ruta et al., *Nature* **468**, 686–690 (2010).
- Z. Yao, A. M. Macara, K. R. Lelito, T. Y. Minosyan, O. T. Shafer, *J. Neurophysiol.* **108**, 684–696 (2012).
- K. Ito et al., *Neuron* **81**, 755–765 (2014).
- M. C. Stensmyr et al., *Cell* **151**, 1345–1357 (2012).
- Y. Grosjean et al., *Nature* **478**, 236–240 (2011).
- A. Jenett et al., *Cell Reports* **2**, 991–1001 (2012).
- N. C. Klapoetke et al., *Nat. Methods* **11**, 338–346 (2014).
- G. C. Turner, M. Bazhenov, G. Laurent, *J. Neurophysiol.* **99**, 734–746 (2008).
- A. C. Lin, A. M. Bygrave, A. de Calignon, T. Lee, G. Miesenböck, *Nat. Neurosci.* **17**, 559–568 (2014).
- K. Ohki, S. Chung, Y. H. Ch'ng, P. Kara, R. C. Reid, *Nature* **433**, 597–603 (2005).
- J. S. Marvin et al., *Nat. Methods* **10**, 162–170 (2013).
- F. St-Pierre et al., *Nat. Neurosci.* **17**, 884–889 (2014).
- M. Tantama, J. R. Martínez-Francois, R. Mongeon, G. Yellen, *Nat. Commun.* **4**, 2550 (2013).

ACKNOWLEDGMENTS

This work was performed as part of the Janelia GENIE project. We thank L. Lavis, K. Svoboda, R. Kerr, J. Macklin, G. Jefferis, Y. Aso, S. Namikawa, A. Nern, J. Strother, and members of the Jayaraman lab, Looger lab, Zlatic lab, Svoboda lab, and GENIE project for discussions; A. Hu, B. Shields, and H. White for assistance with cell culture; J. Osborne, M. Peek, and T. Tabachnik for help with hardware design and fabrication; Janelia Fly Facility, especially K. Hibbard and B. Sharp for fly husbandry; Janelia Imaging Facility, especially P. Hulamm for support; Janelia Molecular Biology core for DNA sequencing and virus production;

G. Paez for DNA constructs; A. Wong for assistance with preliminary experiments in adult *Drosophila*; and T. Zhao for neuTube. The crystal structure of calcium-free CaMPARI has been deposited in the Protein Data Bank with the accession code 4OY4. DNA constructs, AAV particles, and transgenic *Drosophila* were deposited for distribution at Addgene (<http://www.addgene.org>), the University of Pennsylvania Vector Core (www.med.upenn.edu/gtp/vectorcore), and the Bloomington *Drosophila* Stock Center (<http://flystocks.bio.indiana.edu>), respectively. Please contact M. Ahrens (ahrensm@janelia.hhmi.org) for access to transgenic zebrafish.

SUPPLEMENTARY MATERIALS

www.sciencemag.org/content/347/6223/755/suppl/DC1
Materials and Methods
Supplementary Text
Figs. S1 to S35
Tables S1 to S3
References (35–65)
Movies S1 to S8

8 September 2014; accepted 16 January 2015
10.1126/science.1260922

MAMMALIAN EVOLUTION

Evolutionary development in basal mammaliaforms as revealed by a docodontan

Zhe-Xi Luo,^{1*} Qing-Jin Meng,^{2*} Qiang Ji,³ Di Liu,² Yu-Guang Zhang,² April I. Neander¹

A new Late Jurassic docodontan shows specializations for a subterranean lifestyle. It is similar to extant subterranean golden moles in having reduced digit segments as compared to the ancestral phalangeal pattern of mammaliaforms and extant mammals. The reduction of digit segments can occur in mammals by fusion of the proximal and intermediate phalangeal precursors, a developmental process for which a gene and signaling network have been characterized in mouse and human. Docodontans show a positional shift of thoracolumbar ribs, a developmental variation that is controlled by *Hox9* and *Myf5* genes in extant mammals. We argue that these morphogenetic mechanisms of modern mammals were operating before the rise of modern mammals, driving the morphological disparity in the earliest mammaliaform diversification.

Mammaliaforms consist of modern Mammalia and their fossil kin of the Mesozoic (1–3). We report a new Late Jurassic mammaliaform (Fig. 1) of the extinct docodontan clade that lived on Laurasia during the Mesozoic (2–6). It shows a reduction of segments in each digit and a positional shift in lumbar ribs, for which genetic mechanisms of morphogenesis have been characterized in modern mammals. This suggests that developmental mechanisms played a role in the evolution of disparate morphologies, which are associated with versatile functional adaptations and paleoecological diversities in docodontans.

Docofossor brachydactylus, gen. et sp. nov. (7), is preserved in part and counterpart (BMNH131735A and B) (Fig. 1 and fig. S1), with a skull length of 22 mm, a rostrum-pelvis length of 90 mm, and an estimated body mass of 13 to 17 g (7). It has a dentition of I4.C1.P3.M3/i4.c1.p3.m4 and shows mesiodistally short and transversely wide upper molar crowns known as “zalambdodont” (7) (Fig. 2). This is typical of mammals foraging underground, such as marsupi-

al moles, golden moles, some tenrecs (8, 9), and *Necrolestes* of the extinct meridiolestidans (9, 10). The rostrum has a complete premaxillary internarial process and septomaxillary bone, which are primitive features in early mammaliaforms, including other docodontans (2–4). Its protruding rostrum is common for fossorial mammals (11, 12).

Docofossor has many features indicative of scratch digging and subterranean living (7, 11–13), such as a hypertrophied olecranon process of the ulna (the olecranon-to-ulna length index is 47%) (11). It is similar to fossorial monotremes in possessing a sprawling posture of both limbs (Fig. 1) and a tibioastragalar (upper ankle) joint adapted for a habitually abducted foot (Fig. 3). In monotremes, the hindlimb shows a permanently flexed knee joint, which is constrained by the enlarged parafibula posterior to the knee. *Docofossor* likely had a similar sprawling posture constraint by the parafibula (Fig. 1C) (14, 15). The curved tibia has a pivotal tibioastragalar joint in which the tibial distal malleolus articulates with the medial concavity of the trochleated astragalus. The malleolus serves as a pivot around which the astragalus and the foot can rotate while the concave distal tibial facet glides over the medial trochlear crest of the astragalus (Fig. 3, F to H). This enables monotremes to habitually abduct their feet relative to the limb and allows a wider range of foot

¹Department of Organismal Biology and Anatomy, University of Chicago, Chicago, IL 60637, USA. ²Beijing Museum of Natural History, Beijing 100050, China. ³Institute of Geology, Chinese Academy of Geological Sciences, Beijing 100037, China.

*Corresponding author. E-mail: zxluo@uchicago.edu (Z.-X.L.); mengqingjin@bmnh.org.cn (Q.-J.M.)

Fig. 1. Mammaliaform *D. brachydactylus*.

(A) Holotype part (BMNH131735A) (the counterpart is in fig. S2). (B) Exposed skull of BMNH131735A. (C) Reconstruction of *Docofossor* as fossorial, with a sprawling posture and capable of digging (lateral view). (D) and (E) Antero-lateral views of limbs.

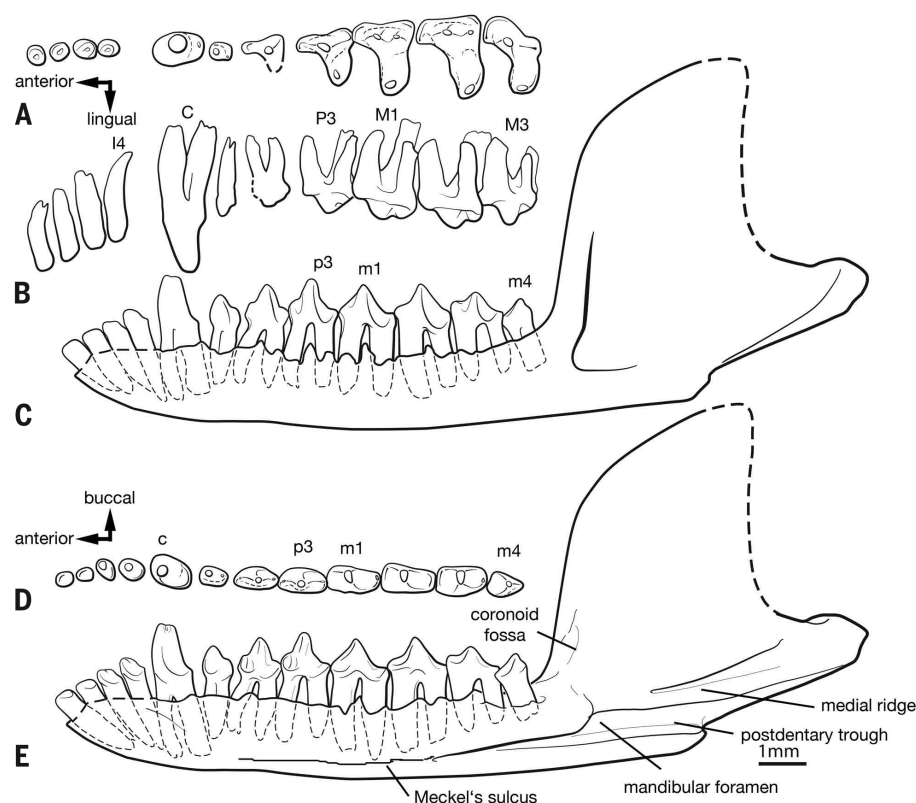
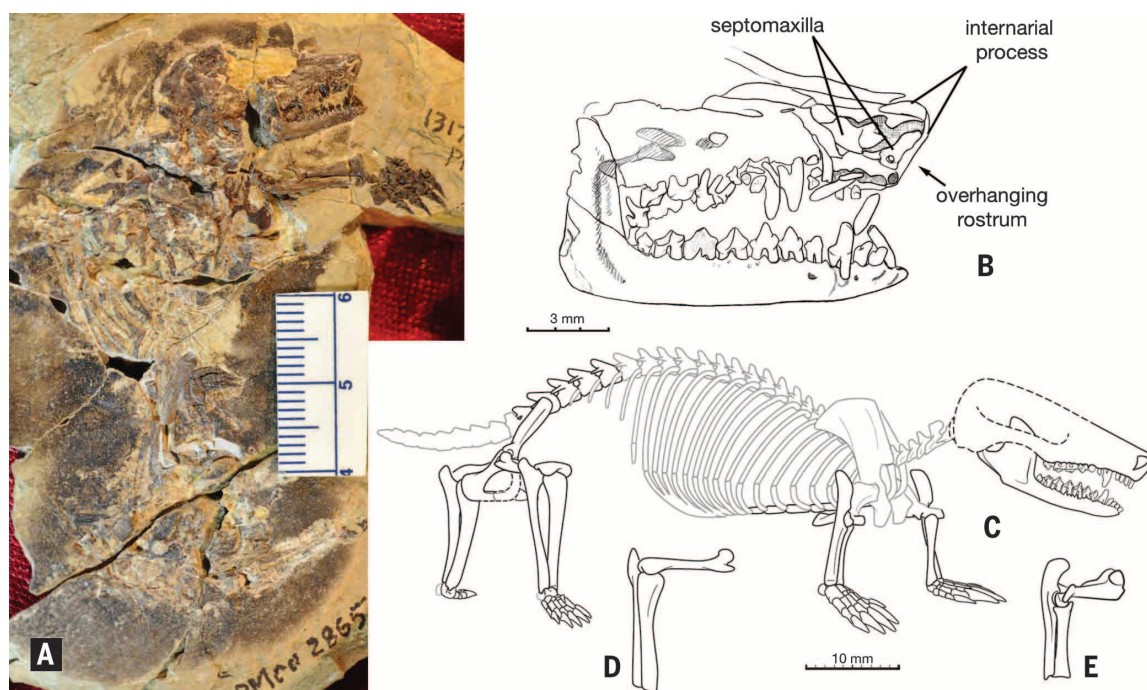


Fig. 2. Dentition of *Docofossor*. (A and B) Left upper dentition in occlusal and buccal views (M2 reconstructed from right). (C) Left lower teeth and mandible in buccal view. (D and E) Lower right teeth and mandible in occlusal and lingual view. More stereo images of teeth and mandibles are shown in fig. S3.

abduction (Fig. 3, F to H). *Docofossor* has a similar trochleate astragalus with a medial concavity (Fig. 3, A to D), thus a habitually abducted

foot capable of wide range of hyperextension and eversion, for monotreme-like pedal posture and movement (Fig. 3).

Docofossor has a reduced number of phalanges for hands (2-2-2-2-2) and feet (1-2-2-2-2), with only two segments in each digit of digit rays 2 to 5. Shovel-like terminal phalanges are dorsoventrally low but horizontally broad. Its dorsal surface projects posteriorly to form the bony stop against hyperextension, as in digging mammals (11). The flexor tubercle is massive and has a keyhole pit for the insertion of the flexor muscle. A single (not paired) enlarged sesamoid bone for the digital flexor muscle is preserved at the distal interphalangeal joints. Each digit ray has a single “middle” phalanx, and the metacarpal is shortened and wide, with combined length shorter than the terminal phalanx and strong hingelike joints, all typical of scratch-digging mammals (11, 12).

Extant mammals have conserved identities of the thoracic versus lumbar vertebrae (16). The thoraco-lumbar (T-L) transition, as marked by vertebral features and by the presence or absence of ribs, has functional implications for locomotion (17) and respiration (18). The T-L transition is usually distinctive, with several lumbar vertebrae lacking any ribs. These differences across the T-L transition are controlled by homeobox genes *Hox9* and *Hox10* (19). Ribs are developed from the lateral plate of mesoderm and are influenced both by these Hox genes and by myogenic factor (*Myf*) 5 and 6 down-cascade in the gene network from Hox genes (20).

The newly discovered *Agilodocodon* (21) and *Docofossor* reveal a positional shift of the lumbar ribs through the T-L transition among docodontans. *Docofossor* has relatively long lumbar ribs on three of the last four dorsal vertebrae (“lumbar”). Similarly, another docodont, *Castorocauda*, has lumbar ribs on the posterior dorsal vertebrae (“lumbar”) up to the ultimate dorsal (= dorsal 22) and a gradational reduction of rib lengths on

dorsals 18 to 22 (5). In contrast, *Agilodocodon* has no lumbar ribs on the four ultimate dorsal (“lumbar”) vertebrae, with a precipitous decrease in rib lengths on dorsals 16 to 18 and the posteriormost rib on dorsal 18 (fig. S2). Thus the T-L transition is more distinctive in *Agilodocodon*.

Eutriconodontans and spalacotherioids of crown mammals are already known for similar patterns in shifting T-L boundaries and in shifting lumbar rib positions (14, 22). However, docodontans are a stem clade outside the crown mammals (2–7). The positional shifting of lumbar ribs and T-L vertebral identities in docodontans show that the morphogenesis associated with the gene network of *Hox* 9–10 and *Mylf* 5–6 in extant mammals (19, 20) is operative not only in crown mammals but also in stem mammaliaforms, before the rise of modern mammals.

The phalangeal formula (number of segments in each of digit rays 1 to 5) of *Docofossor* is reduced to 2-2-2-2-2 for the manus and to 1-2-2-2-2 for the pes, which is different from the 2-3-3-3-3 formula for both hands and feet of the majority of mammaliaforms (including *Castorocauda* and *Agilodocodon*) and of advanced premammalian cynodonts (23–25). Golden moles of Africa (*Chrys-*

ochloridae), as an exception to most extant mammals, have reduced phalanges, and their manual formula is 2-2-1-2-0 for *Eremitalpa* and *Chrysothalpa*, and the pedal formula is 2-2-2-2-2 for *Eremitalpa* and *Chrysochloris* (25, 26), as reconfirmed by our analyses of computed tomography (CT) scans. Phalangeal reduction in golden moles is a striking parallel to phalangeal reduction in *Docofossor* within the docodont group (Figs. 3 and 4).

In synapsid evolution, the reduction of segments in a digit ray can occur by a loss of one or more ancestral segments, the fusion of ancestrally separate segments, or both (24). During development in extant mammals, segmental reduction can occur by two related processes: (i) a mesenchymal condensate precursor to a cartilaginous segment fails to develop, as in human brachydactyly (“short-fingeredness”) type A (BDA1), in which hypoplasia (underdevelopment) or aplasia (absence) of the intermediate phalangeal segment occurs across all five digits (27); or (ii) failure of the interzone—a region of flattened cells in higher density within the digit ray that is the precursor of the future joint. The interzone separates the presumptive segments during the

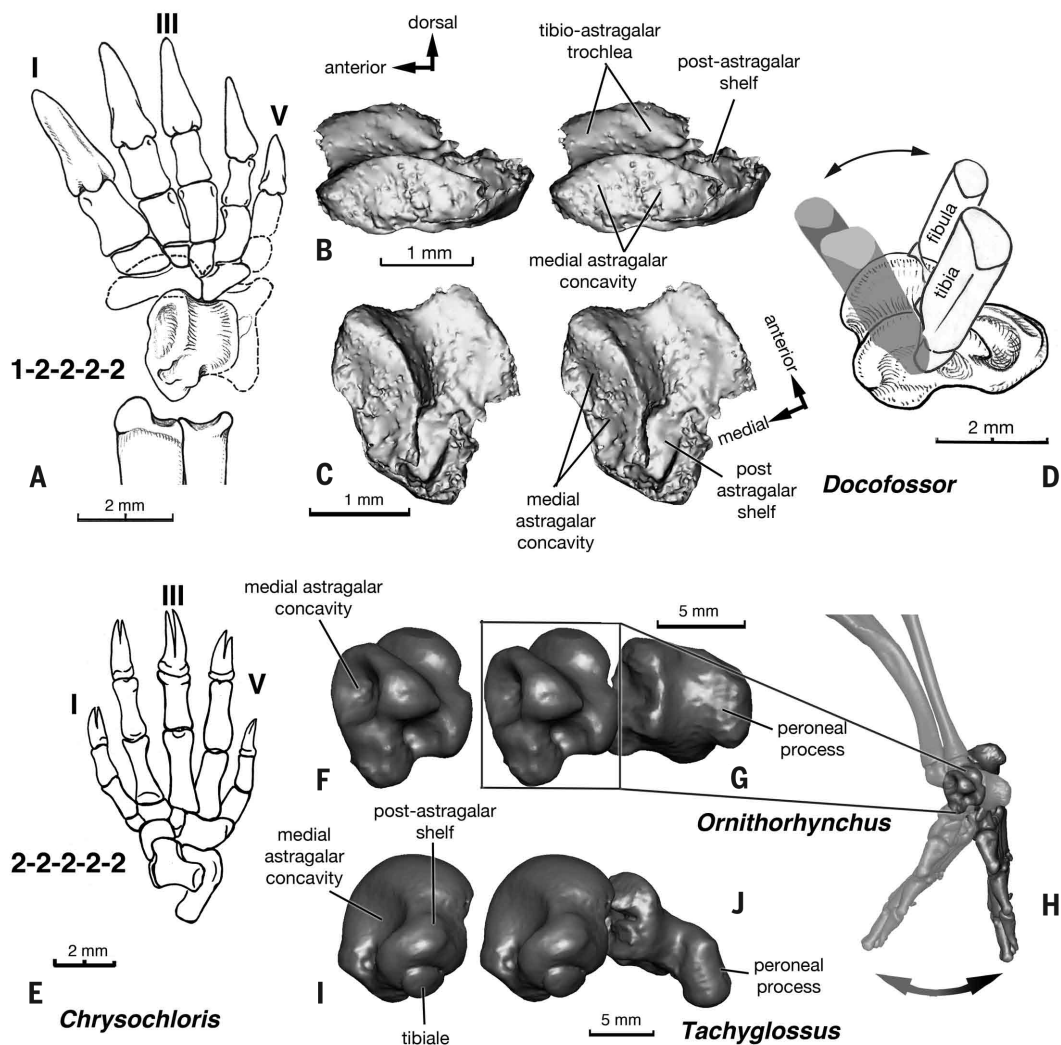
stage of condensation of phalangeal templates. Phalangeal reduction by an interzone failure is well characterized in symphalangism (“fused segments”) of human and mouse, in which the proximo-intermediate phalangeal joint is not developed because of the failure of the interzone to initiate or not to go through full differentiation (27, 28).

African golden moles, with a subterranean lifestyle and superb digging adaptation, are an example of brachydactyly as a result of symphalangism (26) (Fig. 4) (7): The early mesenchymal condensates are segmented in a digit ray. Digit rays 2 to 4 show three segments, starting variously at 9-, 10-, and 12-mm embryonic stages. However, the presumptive proximo-intermediate phalangeal joint fails to develop in later stages in these digits. As a result, the mesenchymal condensate segments become fused in later development, although developmental timing (stages) of this fusion can be different among digit rays. At the 19-mm stage, segments of digit rays 2 to 4 have reduced by fusing together the phalangeal segments that had been separate earlier (26).

The gene and signaling network for normal phalangeal development, which can also cause

Fig. 3. Foot of *Docofossor*. (A)

Reconstructed right foot (dorsal view) of phalangeal formula 1-2-2-2-2. (B and C) Right astragalus in the dorsomedial and dorsal views (stereo images from CT). (D) Fore-aft limb rotation to the trochleate ankle joint, with the tibial malleolus as a pivot in the medial concavity of the astragalus. (E) *Chrysochloris* right foot (dorsal view) with formula 2-2-2-2-2 by fusion of the proximo-intermediate phalanges of digit rays 2 to 5 (25). (F) and (G) *Ornithorhynchus* disassembled astragalus and calcaneus (posteromedial view). (H) Pivotal limb-foot rotation by the tibial malleolus in the medial concavity of the astragalus and tibio-astragalar joint as a gliding track. (I and J) *Tachyglossus* astragalus and calcaneus (posteromedial view). The pivotal tibio-astragalar joint of docodontans is similar to those of monotremes.



phalangeal reduction by mutation or other defects, has been characterized by developmental experiments on model mice and from genetic studies of abnormal development of phalanges in humans (27–30). The joint development is influenced by bone morphogenetic protein (BMP) 2 and growth and differentiation factor (GDF) 5, which positively regulate cell proliferation (29), and by Notch signaling limiting overgrowth of differentiated chondrocytes in the interzone or presumptive joint (27–30). The latter phenotype

structures become defective when mutations occur in genes encoding BMPs and GDF-5 (29); genes encoding the Wnt/ β -catenin pathway and Indian Hedgehog (*IHH*) (27) that are linked with BMPs and GDFs; the gene(s) for the transforming growth factor- β (TGF- β) receptor; TGF- β signaling is essential for interphalangeal joint development and operates upstream of BMPs/GDFs (28); or in *NOG*, which is antagonistic to BMPs, among other genes and signaling pathways. The shortening of phalangeal condensates also

leads to the failure of joint formation in distal segments (27).

These morphogenetic mechanisms also underlie the phalangeal embryogenesis for mammals as a whole, including the segmental reduction within each digit ray in golden moles. The single “middle” phalanx of *Docofossor* (Fig. 4) is similar to the single “middle” segment fused from the proximal and intermediate phalangeal precursors in the embryogenesis of golden moles (25, 26) (fig. S4). Given the similarity of golden moles and

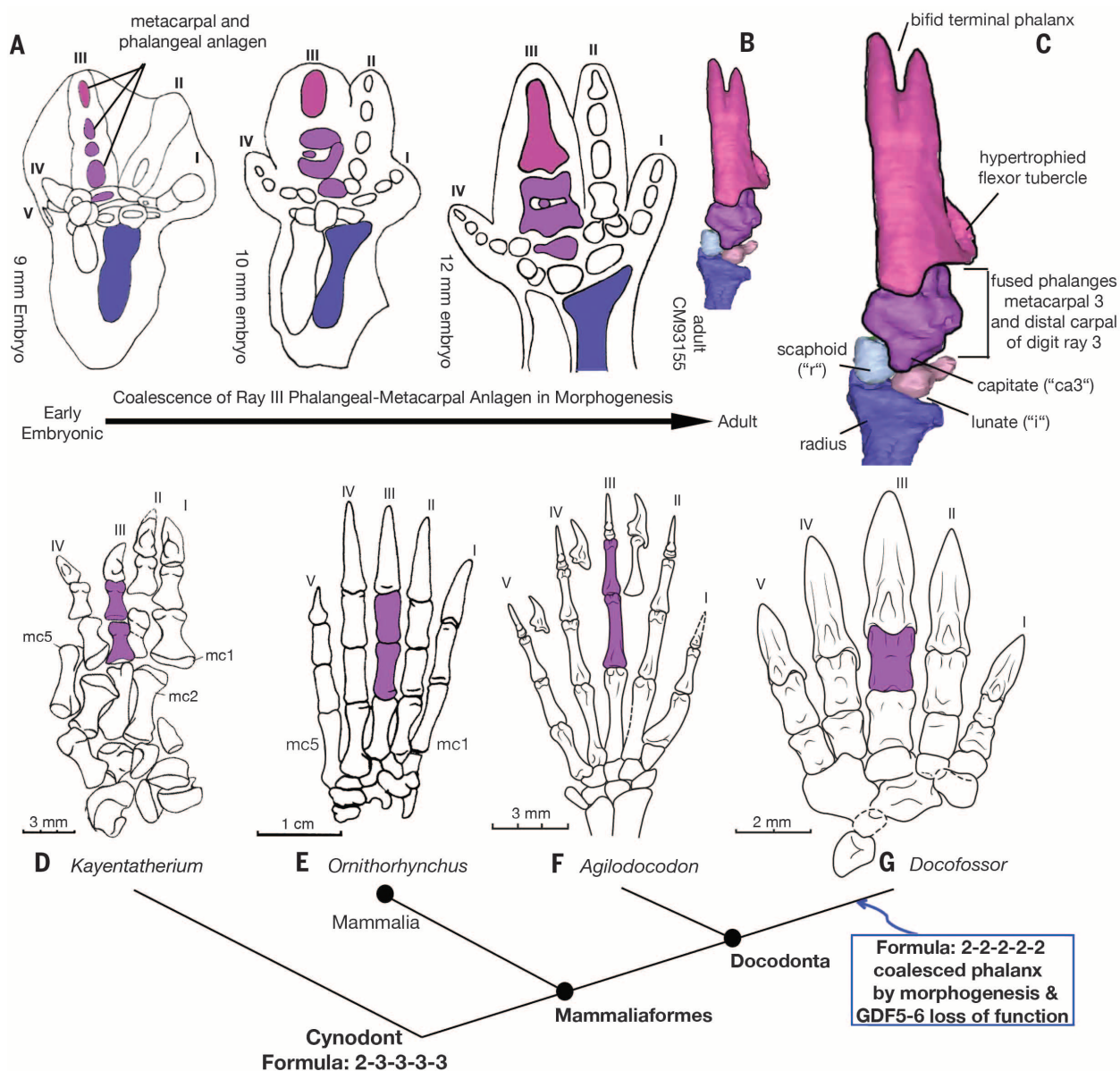


Fig. 4. Evolutionary development and morphological disparity of autopods of docodontans. (A and B) Fusion of phalangeal segments in the development of the golden mole *Eremitalpa*: anlagen of phalanges, metacarpal, and distal carpal of digit ray 3 are distinctive at the 9-mm embryonic stage and become fused in the 12-mm embryonic stage and adult (26). Shown is an adult from CT scanning of Carnegie Museum (CM) specimen 93155. (C) The digging “claw” of *Eremitalpa* is formed by a hypertrophied distal phalanx and the fusion of intermediate and proximal phalanges,

metacarpal, and the capitata (25, 26) (verified by CT scanning). (D) Cynodont *Kayentatherium* (23), (E) *Ornithorhynchus*, and (F) docodont *Agilodocodon* of ancestral phalangeal formula 2-3-3-3-3. (G) *Docofossor* with shortened phalanges of 2-2-2-2-2, convergent to some extant fossorial mammals. Embryogenesis of phalangeal joints in extant mammals is patterned by BMPs, GDF-5, and TGF- β (27–30). Mutation of these genes and signaling pathways can now be correlated with the shortening of digits (brachydactyly) by hypoplasia or aplasia of the middle phalanges in *Mus* knockouts (27).

Docofossor, we hypothesize that the gene and signaling pathways that control the morphogenesis of phalanges in extant mammals probably caused similar changes in *Docofossor*, significantly expanding the known morphological disparity of phalanges among the earliest mammaliaforms (Fig. 4), well before the rise of modern mammals.

The shortening and widening of digits and phalangeal reduction are major adaptations for digging and a subterranean lifestyle (11, 13, 25), which are common in mammals and clearly convey major evolutionary advantage (11, 12). The reduction of phalangeal segments by morphogenesis provides a mechanistic underpinning for the extensive convergent evolution of fossorial adaptation in fossil and extant mammaliaforms.

Evolutionary biologist Leigh Van Valen famously stated that “evolution is the control of development by ecology.” The new docodontan fossil reported here represents such an example of how developmental morphogenesis, which has become increasingly better understood in modern mammals, can be a driving mechanism of the evolution of lumbar vertebrae without ribs and the shortening and fusion of digital segments. Both features are significant for locomotion and ecological specialization during the earliest diversification of mammaliaforms.

REFERENCES AND NOTES

1. T. B. Rowe, T. E. Macrini, Z. X. Luo, *Science* **332**, 955–957 (2011).
2. Z. Kielan-Jaworowska, R. L. Cifelli, Z.-X. Luo, *Mammals from the Age of Dinosaurs: Origins, Evolution, and Structure* (Columbia Univ. Press, New York, 2004).
3. Z.-X. Luo, *Nature* **450**, 1011–1019 (2007).
4. J. A. Lillegraven, G. Krusat, *Contrib. Geol. Univ. Wyoming* **28**, 39–138 (1991).
5. Q. Ji, Z. X. Luo, C. X. Yuan, A. R. Tabrum, *Science* **311**, 1123–1127 (2006).
6. A. O. Averianov, A. V. Lopatin, S. A. Krasnoluski, S. V. Ivantsov, *Proceed. Zool. Institute RAS* **314**, 121–148 (2010).
7. See the supplementary materials.
8. R. J. Asher, I. Horowitz, T. Martin, M. R. Sánchez-Villagra, *Am. Mus. Novit.* **3546**, 1–40 (2007).
9. N. R. Chimento, F. L. Agnolin, F. E. Novas, *Revista Museo Argentino Ciencias Naturales* **14**, 261–306 (2012).
10. G. W. Rougier, J. R. Wible, R. M. Beck, S. Apesteguía, *Proc. Natl. Acad. Sci. U.S.A.* **109**, 20053–20058 (2012).
11. M. Hildebrand, in *Functional Vertebrate Morphology*, M. Hildebrand et al., Eds. (Belknap, Cambridge, MA, 1985), pp. 89–109.
12. N. J. Kley, M. Kearney, in *Fins into Limbs: Evolution, Development, and Transformation*, B. H. Hall, Ed. (Univ. of Chicago Press, Chicago, 2007), pp. 284–309.
13. Z.-X. Luo, J. R. Wible, *Science* **308**, 103–107 (2005).
14. M. Chen, Z.-X. Luo, *J. Mamm. Evol.* **20**, 159–189 (2013).
15. T. Martin, *Zool. J. Linn. Soc.* **145**, 219–248 (2005).
16. Y. Narita, S. Kuratani, *J. Exp. Zool. B* **304B**, 91–106 (2005).
17. F. Galis et al., *Proc. Natl. Acad. Sci. U.S.A.* **111**, 11401–11406 (2014).
18. E. A. Buchholtz, *Zoology* **117**, 64–69 (2014).
19. D. C. McIntyre et al., *Development* **134**, 2981–2989 (2007).
20. I. Guerreiro et al., *Proc. Natl. Acad. Sci. U.S.A.* **110**, 10682–10686 (2013).
21. Q.-J. Meng, Q. Ji, Y.-G. Zhang, D. Liu, D. M. Grossnickle, Z.-X. Luo, *Science* **347**, 764–768 (2015).
22. Z.-X. Luo, P. Chen, G. Li, M. Chen, *Nature* **446**, 288–293 (2007).
23. H.-D. Sues, F. A. Jenkins Jr., in *Amniote Paleobiology: Perspectives on the Evolution of Mammals, Birds, and Reptiles*, M. T. Carrano et al., Eds. (Univ. of Chicago Press, Chicago, 2006), pp. 114–152.
24. J. A. Hopson, *J. Verteb. Paleontol.* **15**, 615–639 (1995).
25. J. Lessertisseur, R. Saban, in *Traité de Zoologie. Tome XVI(I). Mammifères: Téguettes et Squelette*, P.-P. Grassé, Ed. (Masson, Paris, 1967), pp. 709–1078.
26. M. Kindahl, *Acta Zoologica* **30**, 133–152 (1949).
27. S. Stricker, S. Mundlos, *Dev. Dyn.* **240**, 990–1004 (2011).
28. A. Spagnoli et al., *J. Cell Biol.* **177**, 1105–1117 (2007).
29. E. E. Storm, D. M. Kingsley, *Dev. Biol.* **209**, 11–27 (1999).
30. L. J. Brunet, J. A. McMahon, A. P. McMahon, R. M. Harland, *Science* **280**, 1455–1457 (1998).

ACKNOWLEDGMENTS

We thank A. Tabrum and R. Masek for fossil preparation; R. Rudolph, B. Smith, and L. Leoni for CT scanning; L. Heaney and W. Stanley (Field Museum) and J. Wible and S. McLaren (Carnegie Museum) for collections access; T. Martin, J. Wible, A. Crompton, J. Hopson, and D. Grossnickle for discussion on the fossil; and M. Shapiro, K. Sears, and G. Wagner for discussion on development. Support was provided by the Beijing Science and

Technology Commission “Building of Innovative Team Plan Program,” 2014 First-Class Award In Science and Technology (Q.-J.M.), Ministry of Science and Technology of China 973 Project funding (Q.-J.), and the University of Chicago (Z.-X.L.). Full acknowledgement to colleagues is in the supplementary materials.

SUPPLEMENTARY MATERIALS

www.sciencemag.org/content/347/6223/760/suppl/DC1
Materials and Methods
Supplementary Text
Figs. S1 to S4
References (31–73)

5 September 2014; accepted 16 January 2015
10.1126/science.1260880

MAMMALIAN EVOLUTION

An arboreal docodont from the Jurassic and mammaliaform ecological diversification

Qing-Jin Meng,¹ Qiang Ji,² Yu-Guang Zhang,¹ Di Liu,¹
David M. Grossnickle,³ Zhe-Xi Luo^{3,4*}

A new docodontan mammaliaform from the Middle Jurassic of China has skeletal features for climbing and dental characters indicative of an omnivorous diet that included plant sap. This fossil expands the range of known locomotor adaptations in docodontans to include climbing, in addition to digging and swimming. It further shows that some docodontans had a diet with a substantial herbivorous component, distinctive from the faunivorous diets previously reported in other members of this clade. This reveals a greater ecological diversity in an early mammaliaform clade at a more fundamental taxonomic level not only between major clades as previously thought.

Docodontans are extinct early mammaliaforms without living descendants, but they were widespread and abundant in Laurasia during the Mesozoic (1–9). Mammaliaforms bear key evidence of the earliest evolution of mammalian characteristics (4, 10–12) and of the morphological disparity and functional diversification during the early evolution of mammaliaforms (4, 13–16). We report a new docodontan from the Middle Jurassic of China that has many skeletal features adapted for climbing (Fig. 1), different from the digging and swimming adaptations seen in other docodontans. Further, it shows dental features for a herbivorous diet including gum or sap, distinctive from the omnivorous to faunivorous diets of other docodontans (1). This species expands the ecological diversity known for the docodontan group and provides further evidence that adaptive diversification at the species level, as seen in the evolution of many extant mammal clades, occurred also within the earliest mammaliaform clades (17).

Agilodocodon scansorius, gen. et sp. nov. (18), is preserved in part and counterpart (BMNH001138A and B) (Fig. 1 and fig. S1), with a flattened skull (length at 27 mm) and a skeleton (estimated head-tail length at 140 mm). Its body mass is ~27 g, based on scaling of body mass to lengths of jaw and limb bones, but it may weigh up to 40 g (18). It has a dentition of incisors, canine premolars, and molars of I4.C1.P6.M4/i4.c1.p6.m4, and shows a typical diphyodont tooth replacement (Fig. 2 and figs. S2 and S3). *A. scansorius* has many docodontan synapomorphies (18) but differs from other docodontans in three unique molar characters: an enlarged prestylar wing anterior to cusp A, two stylar shelf ridges that extend from the apex of cusp A, and two ridges that extend from the apex of cusp C to the labial cingulum. On the basis of molar features, *Agilodocodon* is more similar to *Hutegotherium* (6), *Krusatodon*, *Borealestes* (3), and *Simpsonodon* (1) of the Middle Jurassic of Siberia and Europe. Although other docodontans have single-rooted, peglike lower incisors (1, 5, 9), *Agilodocodon* is unique in having incisors with incipiently divided roots. Their crowns are spatulate, mesiodistally broad, and have the shape of a broad spade on a wide base (Fig. 2). The incisors are convex on the labial side and concave on the lingual side with a low median ridge and a lingual cingulid (Fig. 2, G to H, and fig. S4) (18).

¹Beijing Museum of Natural History, Beijing 100050 China.

²Institute of Geology, Chinese Academy of Geological Sciences, Beijing 100037, China. ³Committee on Evolutionary Biology, The University of Chicago, Chicago, IL 60637, USA.

⁴Department of Organismal Biology and Anatomy, The University of Chicago, Chicago, IL 60637, USA.

*Corresponding author. E-mail: zxlue@uchicago.edu

This type of incisor is similar to the incisors of some extant New World monkeys. Specifically, the spade-shaped and spatulate lower incisors are known from small marmosets, spider monkeys (*Ateles*), and howler monkeys (*Alouatta*). The small anthropoid primates with this type of incisor use the incisors to gnaw into the bark of trees to feed on exudates, such as gum and sap (19). This type of incisor suggests that *Agilodocodon* had a similar component in its diet. This is the earliest-known evidence of gumnivorous feeding in mammaliaforms, which had evolved separately among docodonts,

and in convergence to those of extant primates. The crest pattern of the upper molars is analogous to those of galagid and some lorid primates that have a mixed diet of insects, other small animals, fruits, tree gums, and sap. The well-developed crests on the molars bear resemblance to those of lemurids, which have frugivorous-insectivorous diets.

Most docodontans have molars adapted for omnivorous-faunivorous diets (1) although *Castorocauda* has piscivorous (fish-eating) anterior molars and is large enough to feed on vertebrate prey (4). *Agilodocodon* diverged from previously

known docodontans in having an omnivorous diet with a significantly greater amount of plant food. The gumnivorous adaptation of its anterior lower teeth shows the versatility of feeding and dietary ecology at the species level of this mammaliaform clade in Middle Jurassic, akin to the dietary diversification of kuehneotheriid and morganucodont mammaliaforms during the Early Jurassic (16) and multituberculate mammals during the Late Cretaceous (20).

We hypothesize that *Agilodocodon* was likely a fully arboreal mammaliaform, or at least a scansorial mammaliaform, on the basis of its many skeletal features adapted for climbing and on its distinction from other Jurassic docodontans (4, 21) and mammaliaforms in the vertebral column, limbs, and digits (Figs. 3 and 4) (10, 22).

The shape and proportion of the hand, foot, and finger bones, as well as the horny claws, are informative about habits and the preference of substrate. In *Agilodocodon*, these bones are slender and gracile (Fig. 4 and figs. S4 to S6). The phalangeal slenderness ratio (PSR: lengths/widths \times 100) is 328% for all proximal phalanges and 210% for all intermediate phalanges (23). These values are well within the range of arboreal diprotodontian marsupials, but they are above (for proximal phalanges) or near the upper limit (for intermediate phalanges) of terrestrial diprotodontians (23).

In *Agilodocodon*, the phalanges are elongate relative to the metacarpals. The phalangeal index [PI: (combined length of proximal + intermediate phalanges)/(length of metacarpal \times 100)] is 137% for manual ray 3, typical of primates and arboreal marsupials, carnivorans, and rodents (24) but well above the range of this index for terrestrial mammals. Length ratios of the intermediate phalanx, proximal phalanx, and metacarpal of digit ray 3 are similar to those of primates (arboreal). The intrinsic proportions of hand bones of *Agilodocodon* (fig. S7) are closer in value to the arboreal than to the terrestrial marsupials and closer to the arboreal than to the terrestrial rodents (24).

In phalangeal morphology (Fig. 4), *Agilodocodon* is more similar to the arboreal flying lemur (Dermoptera: *Cynocephalus*) and the lemur (and other primates) than to the scansorial opossum (Marsupialia: *Didelphis*) and the terrestrial hedgehog (Lipotyphla: *Erinaceus*). By contrast, fossorial and subterranean docodontans, with their short proximal and intermediate phalanges but massive terminal phalanx are more comparable to the fossorial echidna (Monotremata: *Tachyglossus*) and the subterranean golden mole (Afrosoricida: *Eremitalpa*).

The terminal manual phalanges are bilaterally compressed, dorsoventrally deep with an arched dorsal margin (Fig. 3 and fig. S6). The flexor tubercles appear to be massive on the bilaterally compressed phalangeal body, which indicates the insertion of well-developed digit flexor muscles. The shape and proportion of phalanges are typical of arboreal or scansorial rodents, and they differ from terrestrial rodents (25, 26). Compared

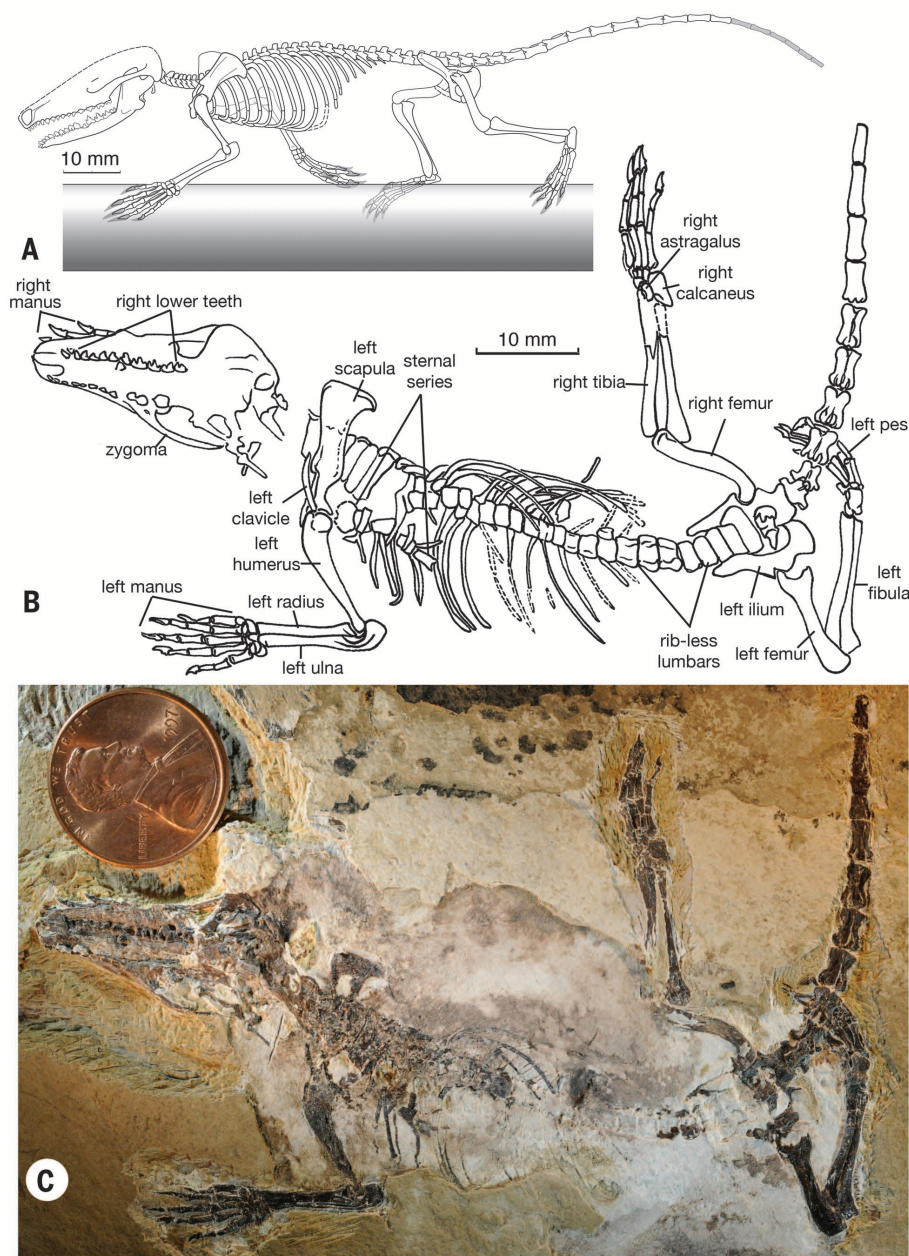


Fig. 1. Skeleton of the new docodont mammaliaform *Agilodocodon scansorius*. (A) Reconstruction of *Agilodocodon* as an arboreal mammaliaform. (B) Outline and (C) photo of the holotype main part of Beijing Museum of Natural History (BMNH) 001138A; counterpart BMNH001138B shown in fig. S1 (18).

with other docodontans, *Agilodocodon* is different from *Haldanodon* that has short, broad, and massive terminal phalanges for burrowing (or a semiaquatic lifestyle) (21), from the specialized swimming *Castorocauda* that has elongate, curved, but shallow, terminal phalanges (4), and from a new fossorial docodontan (BMNH131735) that has broad, flattened, and shovel-like terminal phalanges for digging in a subterranean niche (Fig. 4). The outline of horny claws is exquisitely preserved in organic residue (in distinctive white color) for several manual and pedal claws in *Agilodocodon*. Pedal horny claw 4 is twice as long as the terminal phalanx, laterally compressed, and strongly arcuate (Fig. 3). The horny claw of *Agilodocodon* is typical of mammals living on the tree or in the bushes. *Agilodocodon*, *Haldanodon*, *Castorocauda*, and the new docodont (BMNH131765) indicate a wide range of habits as evidenced by their diverse types of terminal phalangeal bones and claws.

The hypothesis that *Agilodocodon* is a climbing mammaliaform is supported further by features of the distal humerus and the proximal part of the ulna, the ankle joint, and the lumbar

and proximal caudal vertebrae (18). The distal humerus is gracile and narrow, in contrast to the robust and broad distal humeri associated with large muscles for burrowing and/or swimming in *Castorocauda* and *Haldanodon* (Fig. 3, H and I) (4, 21). The humerus has a small ectepicondylar shelf for the supinator and extensor muscles to rotate the radius relative to the ulna and for extensor muscles of the antebrachium and the wrist. The entepicondyle for flexor muscles of the wrist is also better developed in *Agilodocodon* than in the mammaliaform *Morganucodon* (27) (Fig. 3G). In didelphid marsupials (28) and tree shrew species (29), the supinator shelf and the entepicondyle tend to be better developed in species with better climbing capability than the terrestrial species of the same clades.

Agilodocodon has a greater range of ankle mobility than other mammaliaforms. The foot has a side-to-side juxtaposition of the astragalus and the calcaneus (Fig. 3) with a short, ventrally turned calcaneal tuber (fig. S7), which is also plesiomorphic in mammaliaforms *Morganucodon* and *Megaconus* (10, 27). However, the

distal parts of the calcaneus and the astragalus (defined as distal to their sustentacular facets) are more elongate in *Agilodocodon* (Fig. 3 and fig. S7) than in *Morganucodon* and *Megaconus*. This allows a wider movement of the distal end of the astragalus and the navicular, relative to the calcaneus and the cuboid, for better eversion, inversion, and flexion or adduction of pedes and greater abduction of the medial pedal digit(s) relative to the lateral digit(s) than in *Megaconus* (10).

The vertebral function of *Agilodocodon* is unique compared with mammaliaforms of the same Jurassic fauna that are terrestrial, fossorial, and swimming. The last four lumbar vertebrae ("posterior dorsals") have no lumbar ribs. The posterior dorsal vertebrae show a distinctive thoracolumbar transition, and a more distinctive transition corresponds to wider range of movement of the posterior vertebral column (30), as expected for a scansorial or arboreal mammaliaform living in bushes or on trees. Moreover, *Agilodocodon* differs from other mammaliaforms in the same paleoecological community (*Castorocauda*, *Megaconus*, and *Pseudotribos*) that show lumbar ribs and

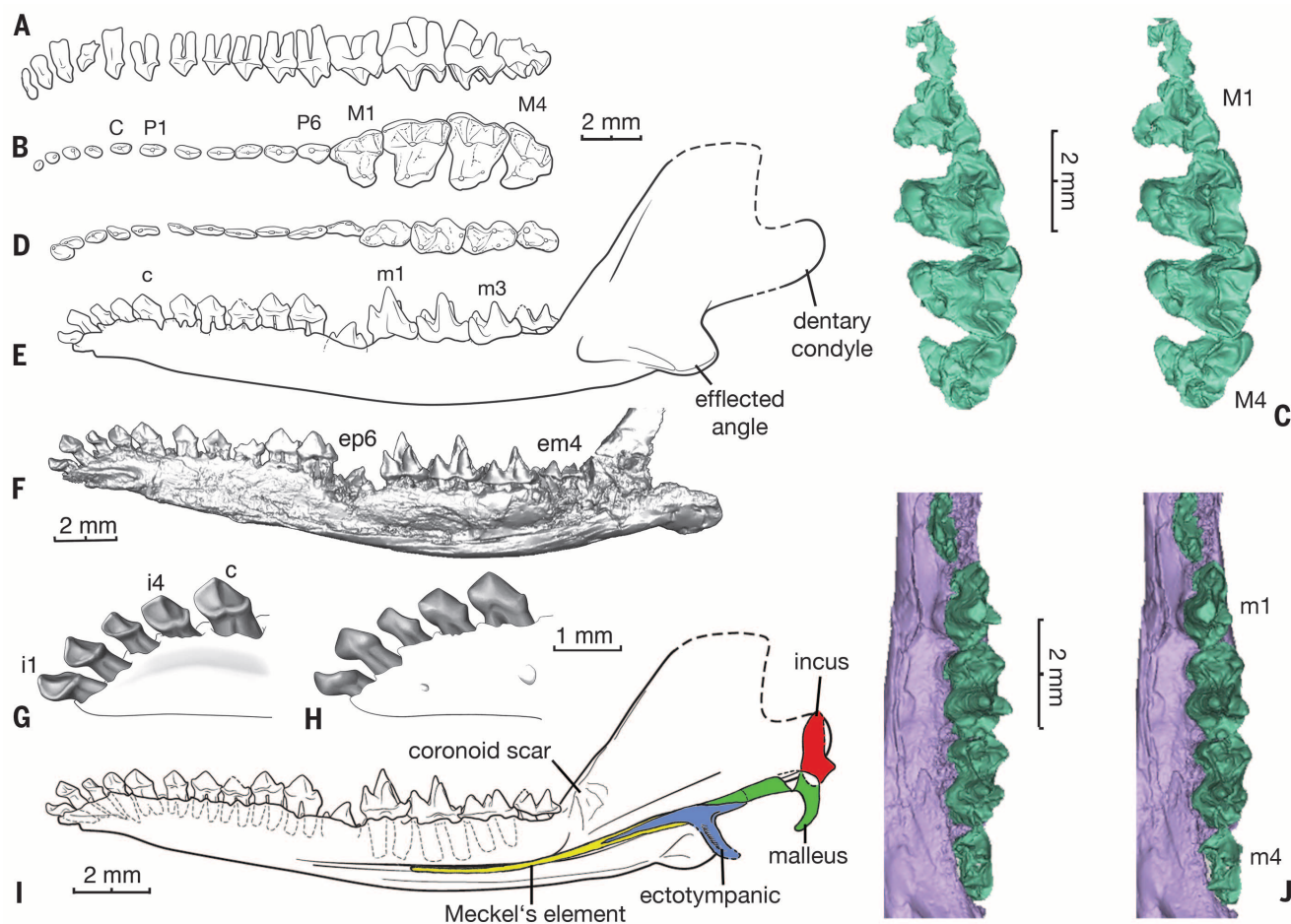


Fig. 2. Mandible and dentition of *Agilodocodon*. (A) and (B) Labial and occlusal views of left upper teeth in outline. (C) Left upper P6-M4 by stereoisimages rendered from CT scans. (D) Occlusal view of lower teeth. (E) Labial view of left mandible and teeth. (F) Lingual view of mandible (image rendered from CT scans, omitting middle ear elements). (G and H) Lingual and labial views of spatulate, spade-shaped incisors. (I) Reconstructed mandible and middle ear bones, additional details in fig. S4 (18). (J) Occlusal view of left lower p6-m4, stereo images rendered from CT. Abbreviations: ep6-erupting p6; em4-erupting m4.

gradational thoracolumbar transition (10, 22). *Castorocauda* also has partially overlapping and widened ribs of posterior dorsal vertebrae up to the pelvis. The distinction of the thoracolumbar transition suggests a major difference in vertebral function between *Agilodocodon* and *Castorocauda*, *Megacomus* and *Pseudotribos*. The first eight caudals of *Agilodocodon* are dorsoventrally flattened and transversely widened with prominent transverse processes, which indicate well-developed

vertebral extensor (epaxial) muscles. The proximal seven caudals have synovial surfaces in zygapophyses and were mobile relative to each other. The highly mobile and well-muscularized tail, by itself, does not necessarily indicate an arboreal habit but is consistent with the arboreal locomotor adaptation (30).

Agilodocodon is the first arboreal species among docodontans, and it differs in substrate preference from other terrestrial, digging, and

swimming forms, adding to the diversity of life styles of docodonts (Fig. 4). Its dietary adaptation includes a gumnivorous component, which is unique among mammaliaforms in the Jurassic fauna. The great range of ecological diversity of the docodontans provides further evidence that adaptive diversification at the species level, typical of many species of extant mammalian clades, also occurred within the earliest mammaliaforms (17).

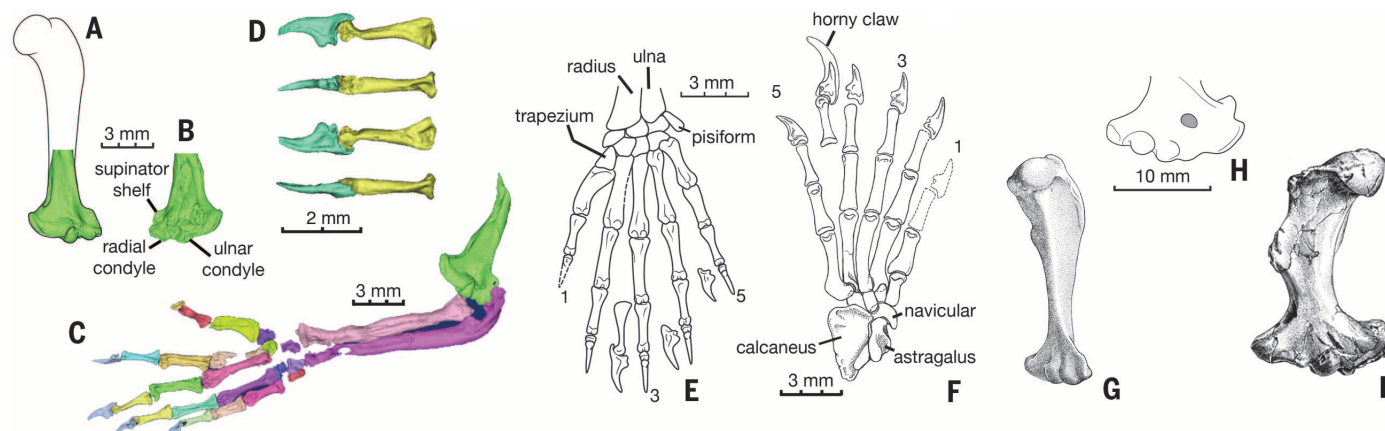


Fig. 3. Comparative morphology of forelimb of *Agilodocodon*. (A) and (B) Humerus (right, distal part) in posterior and anterior views. (C) Right forelimb and manus (humerus in posterior view; manus in palmar view). (D) The intermediate and terminal phalanges of digit ray 3 in medial, ventral, lateral, and dorsal views. (E) Reconstructed right manus in palmar view. (F) Left pes, dorsal view. (G) *Morganucodon* from (26). (H) Distal humerus of *Castorocauda*. (I) *Haldanodon* from (20).

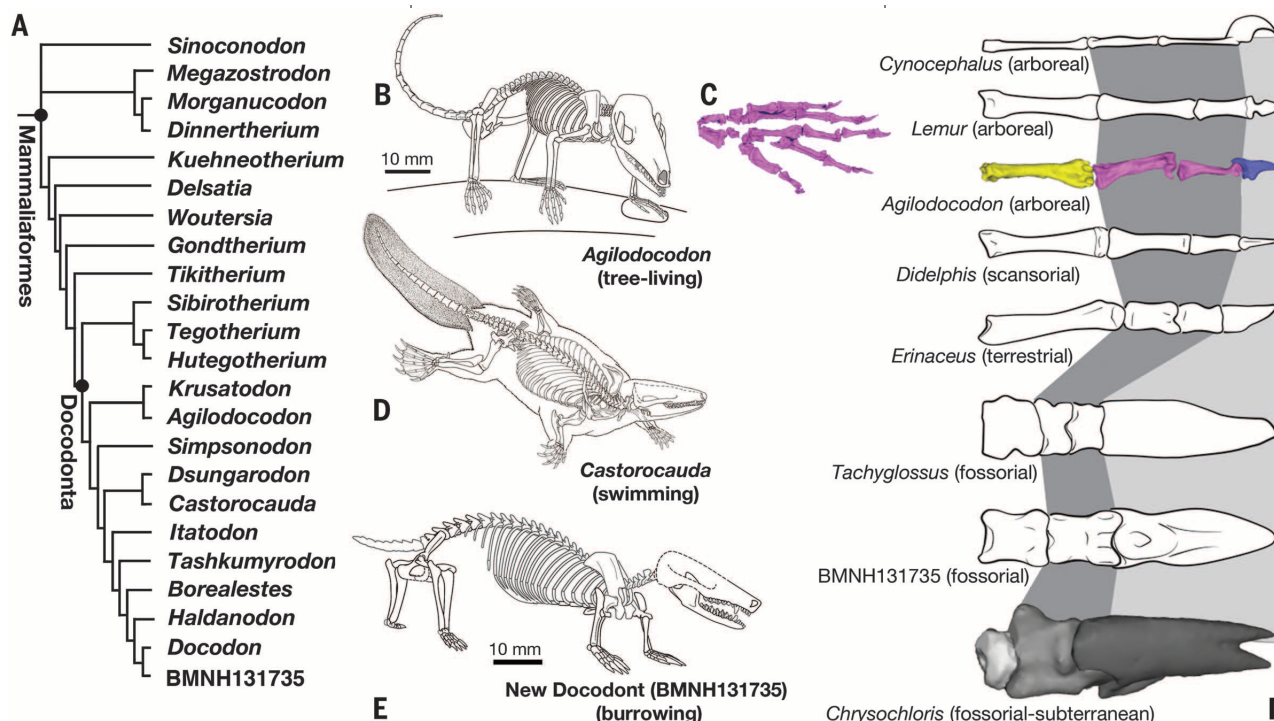


Fig. 4. Ecomorphological diversification of docodont mammaliaforms. (A) Phylogeny of docodontans—analysis presented in supplementary materials (18). (B) *Agilodocodon* as a tree-living mammaliaform. (C) Manus of *Agilodocodon*. (D) *Castorocauda* as a swimming mammaliaform. (E) Fossorial and subterranean docodont (BMNH131735) from Late Jurassic. (F) Phalangeal proportion of *Agilodocodon* compared with those of *Cynocephalus* (Dermoptera, arboreal), *Lemur* (Primates, arboreal), *Didelphis* [Didelphidae, scansorial according to (28)], *Erinaceus* (Eulipotyphla, terrestrial), *Tachyglossus* (Monotremata, terrestrial-fossorial), and *Chrysochloris* (Chrysochloridae, subterranean-fossorial).

REFERENCES AND NOTES

1. Z. Kielan-Jaworowska, R. L. Cifelli, Z.-X. Luo, *Mammals from the Age of Dinosaurs: Origins, Evolution, and Structure* (Columbia Univ. Press, New York, 2004).
2. J. A. Lillegraven, G. Krusat, *Rocky Mount. Geol.* **28**, 39–138 (1991).
3. D. Sigogneau-Russell, *Acta Palaeontol. Pol.* **48**, 357–374 (2003).
4. Q. Ji, Z. X. Luo, C. X. Yuan, A. R. Tabrum, *Science* **311**, 1123–1127 (2006).
5. Z.-X. Luo, T. Martin, *Bull. Carnegie Mus. Nat. Hist.* **39**, 27–47 (2007).
6. A. O. Averianov, A. V. Lopatin, S. A. Krasnolutskii, S. V. Ivantsov, *Proc. Zool. Inst. Russian Acad. Sci.* **314**, 121–148 (2010).
7. Y.-M. Hu, J. Meng, J. M. Clark, *Vertebr. Palasiat.* **45**, 173–194 (2007).
8. T. Martin, A. O. Averianov, H.-U. Pfretzschner, *Palaeobiodivers. Palaeoenviron.* **90**, 295–319 (2010).
9. G. W. Rougier, A. S. Sheth, K. Carpenter, L. Appella-Guiscafre, B. M. Davis, *J. Mamm. Evol.* (2014).
10. C.-F. Zhou, S. Wu, T. Martin, Z. X. Luo, *Nature* **500**, 163–167 (2013).
11. T. B. Rowe, T. E. Macrini, Z. X. Luo, *Science* **332**, 955–957 (2011).
12. Z.-X. Luo, *Annu. Rev. Ecol. Evol. Syst.* **42**, 355–380 (2011).
13. J. Meng, Y. Hu, Y. Wang, X. Wang, C. Li, *Nature* **444**, 889–893 (2006).
14. Z.-X. Luo, *Nature* **450**, 1011–1019 (2007).
15. G. W. Rougier, S. Apesteguía, L. C. Gaetano, *Nature* **479**, 98–102 (2011).
16. P. G. Gill et al., *Nature* **512**, 303–305 (2014).
17. M. Chen, Z.-X. Luo, *J. Mamm. Evol.* **20**, 159–189 (2012).
18. Materials and methods and supplementary text are available as supplementary materials on Science Online.
19. P. Hershkovitz, *New World Monkeys (Platyrrhini)* (Univ. Chicago Press, Chicago, 1977).
20. G. P. Wilson et al., *Nature* **483**, 457–460 (2012).
21. T. Martin, *Zool. J. Linn. Soc.* **145**, 219–248 (2005).
22. Z.-X. Luo, Q. Ji, C. X. Yuan, *Nature* **450**, 93–97 (2007).
23. V. Weisbecker, D. I. Warton, *J. Morphol.* **267**, 1469–1485 (2006).
24. E. C. Kirk, P. Lemelin, M. W. Hamrick, D. M. Boyer, J. I. Bloch, *J. Hum. Evol.* **55**, 278–299 (2008).
25. N. MacLeod, K. D. Rose, *Am. J. Sci.* **293** (A), 300–355 (1993).
26. Z. Kielan-Jaworowska, P. P. Gambaryan, *Fossils Strata* **36**, 1–92 (1994).
27. F. A. Jenkins Jr., F. R. Parrington, *Philos. Trans. R. Soc. Lond.* **273**, 387–431 (1976).
28. C. Argot, *J. Morphol.* **247**, 51–79 (2001).
29. E. J. Sargis, *Evol. Anthropol.* **13**, 56–66 (2004).
30. J. Lessertisseur, R. Saban, in *Traité de Zoologie. Tome XVI (Fascicule I). Mammifères: Téguments et Squelette*, P.-P. Grassé, Ed. (Masson, Paris, 1967), pp. 587–675.

ACKNOWLEDGMENTS

Research supported by Beijing Science and Technology Commission Grant, 2014 First-Class Award in Science and Technology to Q.-J.M., Ministry of Science and Technology of China 973 Project funding and Chinese Academy of Geological Science funding to Q.J., and the University of Chicago to Z.-X.L. We thank A. I. Neander for her superb graphics work. Full acknowledgment to colleagues for supporting our research is in SM (18). Full datasets are in SM (18).

SUPPLEMENTARY MATERIALS

www.sciencemag.org/content/347/6223/764/suppl/DC1
Materials and Methods
Supplementary Text
Figs. S1 to S8
Tables S1 to S3
References (31–80)

5 September 2014; accepted 16 January 2015
10.1126/science.1260879

MARINE POLLUTION

Plastic waste inputs from land into the ocean

Jenna R. Jambeck,^{1*} Roland Geyer,² Chris Wilcox,³ Theodore R. Siegler,⁴
Miriam Perryman,¹ Anthony Andrady,⁵ Ramani Narayan,⁶ Kara Lavender Law⁷

Plastic debris in the marine environment is widely documented, but the quantity of plastic entering the ocean from waste generated on land is unknown. By linking worldwide data on solid waste, population density, and economic status, we estimated the mass of land-based plastic waste entering the ocean. We calculate that 275 million metric tons (MT) of plastic waste was generated in 192 coastal countries in 2010, with 4.8 to 12.7 million MT entering the ocean. Population size and the quality of waste management systems largely determine which countries contribute the greatest mass of uncaptured waste available to become plastic marine debris. Without waste management infrastructure improvements, the cumulative quantity of plastic waste available to enter the ocean from land is predicted to increase by an order of magnitude by 2025.

Reports of plastic pollution in the ocean first appeared in the scientific literature in the early 1970s, yet more than 40 years later, no rigorous estimates exist of the amount and origin of plastic debris entering the marine environment. In 1975, the estimated annual flux of litter of all materials to the ocean was 6.4 million tons [5.8 million metric

tons (MT)], based only on discharges from ocean vessels, military operations, and ship casualties (1). The discharge of plastic from at-sea vessels has since been banned (2), but losses still occur. It is widely cited that 80% of marine debris originates from land; however, this figure is not well substantiated and does not inform the total mass of debris entering the marine environment from land-based sources.

Plastics have become increasingly dominant in the consumer marketplace since their commercial development in the 1930s and 1940s. Global plastic resin production reached 288 million MT in 2012 (3), a 620% increase since 1975. The largest market sector for plastic resins is packaging (3); that is, materials designed for immediate disposal. In 1960, plastics made up less than 1% of municipal solid waste by mass in the United States (4); by 2000, this proportion increased by an order of magnitude. By 2005, plastic made up at least 10% of solid waste by

mass in 58% (61 out of 105) of countries with available data (5).

Plastics in the marine environment are of increasing concern because of their persistence and effects on the oceans, wildlife, and, potentially, humans (6). Plastic debris occurs on coastlines, in Arctic sea ice, at the sea surface, and on the sea floor (7, 8). Weathering of plastic debris causes fragmentation into particles that even small marine invertebrates may ingest (9). Its small size also renders this debris untraceable to its source and extremely difficult to remove from open ocean environments, suggesting that the most effective mitigation strategies must reduce inputs.

We estimated the annual input of plastic to the ocean from waste generated by coastal populations worldwide. We defined mismanaged waste as material that is either littered or inadequately disposed. Inadequately disposed waste is not formally managed and includes disposal in dumps or open, uncontrolled landfills, where it is not fully contained. Mismanaged waste could eventually enter the ocean via inland waterways, wastewater outflows, and transport by wind or tides. Estimates of the mass of plastic waste carried by particular waterways range from <<1 kg per day (Hilo, HI) to 4.2 MT (4200 kg) per day (Danube River) (10, 11). Because of their dependence on local watershed characteristics, these results cannot be easily extrapolated to a global scale.

Here we present a framework to calculate the amount of mismanaged plastic waste generated annually by populations living within 50 km of a coast worldwide that can potentially enter the ocean as marine debris. For each of 192 coastal countries with at least 100 permanent residents that border the Atlantic, Pacific, and Indian oceans and the Mediterranean and Black seas, the framework includes: (i) the mass of waste generated per capita annually; (ii) the percentage of waste that is plastic; and (iii) the percentage of plastic waste that is mismanaged and,

¹College of Engineering, University of Georgia, 412 Driftmier Engineering Center, Athens, GA 30602, USA. ²Bren School of Environmental Science and Management, University of California, Santa Barbara, CA 93106, USA. ³Oceans and Atmosphere Flagship, Commonwealth Scientific and Industrial Research Organization, Castray Esplanade, Hobart, Tasmania 7000, Australia. ⁴DSM Environmental Services, Windsor, VT 05089, USA. ⁵Department of Chemical and Biomolecular Engineering, North Carolina State University, Raleigh, NC 27695, USA. ⁶Department of Chemical Engineering and Materials Science, Michigan State University, East Lansing, MI 48824, USA. ⁷Sea Education Association, Woods Hole, MA 02543, USA.

*Corresponding author. E-mail: jjambeck@uga.edu

therefore, has the potential to enter the ocean as marine debris (12) (data S1). By applying a range of conversion rates from mismanaged

waste to marine debris, we estimated the mass of plastic waste entering the ocean from each country in 2010, used population growth data

(13) to project the increase in mass to 2025, and predicted growth in the percentage of waste that is plastic. Lacking information on future

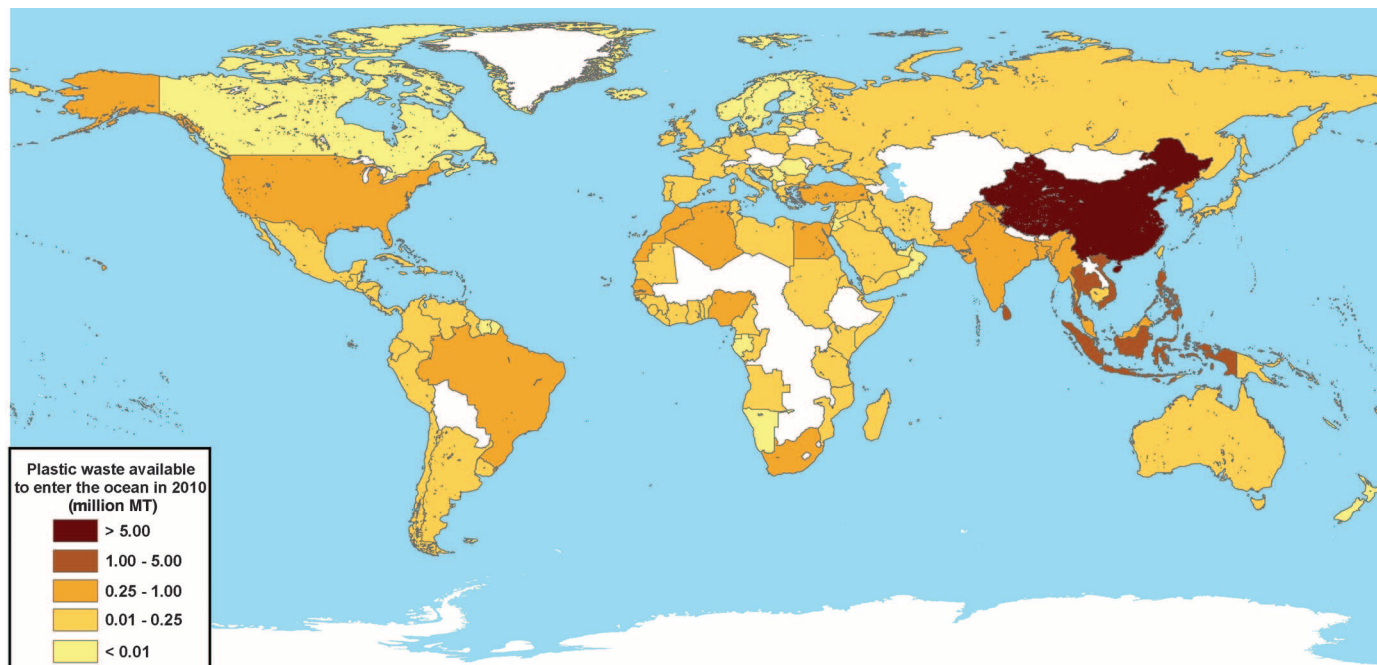


Fig. 1. Global map with each country shaded according to the estimated mass of mismanaged plastic waste [millions of metric tons (MT)] generated in 2010 by populations living within 50 km of the coast. We considered 192 countries. Countries not included in the study are shaded white.

Table 1. Waste estimates for 2010 for the top 20 countries ranked by mass of mismanaged plastic waste (in units of millions of metric tons per year). Econ. classif., economic classification; HIC, high income; UMI, upper middle income; LMI, lower middle income; LI, low income (World Bank definitions based on 2010 Gross National Income). Mismanaged waste is the sum of inadequately managed waste plus 2% littering. Total mismanaged plastic waste is calculated for populations within 50 km of the coast in the 192 countries considered. pop., population; gen., generation; ppd, person per day; MMT, million metric tons.

Rank	Country	Econ. classif.	Coastal pop. [millions]	Waste gen. rate [kg/ppd]	% plastic waste	% mismanaged waste	Mismanaged plastic waste [MMT/year]	% of total mismanaged plastic waste	Plastic marine debris [MMT/year]
1	China	UMI	262.9	1.10	11	76	8.82	27.7	1.32–3.53
2	Indonesia	LMI	187.2	0.52	11	83	3.22	10.1	0.48–1.29
3	Philippines	LMI	83.4	0.5	15	83	1.88	5.9	0.28–0.75
4	Vietnam	LMI	55.9	0.79	13	88	1.83	5.8	0.28–0.73
5	Sri Lanka	LMI	14.6	5.1	7	84	1.59	5.0	0.24–0.64
6	Thailand	UMI	26.0	1.2	12	75	1.03	3.2	0.15–0.41
7	Egypt	LMI	21.8	1.37	13	69	0.97	3.0	0.15–0.39
8	Malaysia	UMI	22.9	1.52	13	57	0.94	2.9	0.14–0.37
9	Nigeria	LMI	27.5	0.79	13	83	0.85	2.7	0.13–0.34
10	Bangladesh	LI	70.9	0.43	8	89	0.79	2.5	0.12–0.31
11	South Africa	UMI	12.9	2.0	12	56	0.63	2.0	0.09–0.25
12	India	LMI	187.5	0.34	3	87	0.60	1.9	0.09–0.24
13	Algeria	UMI	16.6	1.2	12	60	0.52	1.6	0.08–0.21
14	Turkey	UMI	34.0	1.77	12	18	0.49	1.5	0.07–0.19
15	Pakistan	LMI	14.6	0.79	13	88	0.48	1.5	0.07–0.19
16	Brazil	UMI	74.7	1.03	16	11	0.47	1.5	0.07–0.19
17	Burma	LI	19.0	0.44	17	89	0.46	1.4	0.07–0.18
18*	Morocco	LMI	17.3	1.46	5	68	0.31	1.0	0.05–0.12
19	North Korea	LI	17.3	0.6	9	90	0.30	1.0	0.05–0.12
20	United States	HIC	112.9	2.58	13	2	0.28	0.9	0.04–0.11

*If considered collectively, coastal European Union countries (23 total) would rank eighteenth on the list

global infrastructure development, the projection represents a business-as-usual scenario.

We estimate that 2.5 billion MT of municipal solid waste was generated in 2010 by 6.4 billion people living in 192 coastal countries (93% of the global population). This estimate is broadly consistent with an estimated 1.3 billion MT of waste generated by 3 billion people in urban centers globally (5). Approximately 11% (275 million MT) of the waste generated by the total population of these 192 countries is plastic. We expect plastic waste to roughly track plastic resin production (270 million MT in 2010) (3), with differences resulting from the time lag in disposal of durable goods (lifetime of years to decades), for example. Scaling by the population living within 50 km of the coast (those likely to generate most of the waste becoming marine debris), we estimate that 99.5 million MT of plastic waste was generated in coastal regions in 2010. Of this, 31.9 million MT were classified as mismanaged and an estimated 4.8 to 12.7 million MT entered the ocean in 2010, equivalent to 1.7 to 4.6% of the total plastic waste generated in those countries.

Our estimate of plastic waste entering the ocean is one to three orders of magnitude greater than the reported mass of floating plastic debris in high-concentration ocean gyres and also globally (14–17). Although these ocean estimates represent only plastics that are buoyant in seawater (mainly polyethylene and polypropylene), in 2010 those resins accounted for 53% of plastic production in North America and 66% of plastic in the U.S. waste stream (4, 18). Because no global estimates exist for other sources of plastic into the ocean (e.g., losses from fishing activities or at-sea vessels, or input from natural disasters), we do not know what fraction of total plastic input our land-based waste estimate represents.

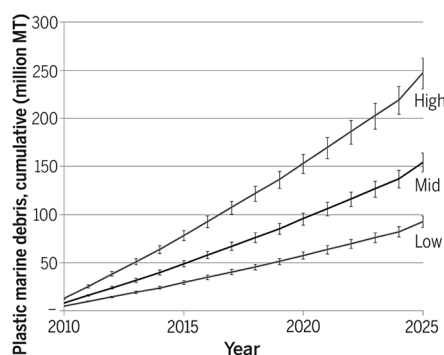


Fig. 2. Estimated mass of mismanaged plastic waste (millions of metric tons) input to the ocean by populations living within 50 km of a coast in 192 countries, plotted as a cumulative sum from 2010 to 2025. Estimates reflect assumed conversion rates of mismanaged plastic waste to marine debris (high, 40%; mid, 25%; low, 15%). Error bars were generated using mean and standard error from the predictive models for mismanaged waste fraction and percent plastic in the waste stream (12).

Our framework was designed to compute, from the best-available data, an order-of-magnitude estimate of the amount of mismanaged plastic waste potentially entering the ocean worldwide. It is also a useful tool to evaluate the factors determining the largest sources of mismanaged plastic waste. The amount of mismanaged plastic waste generated by the coastal population of a single country ranges from 1.1 MT to 8.8 million MT per year, with the top 20 countries' mismanaged plastic waste encompassing 83% of the total in 2010 (Fig. 1 and Table 1). Total annual waste generation is mostly a function of population size, with the top waste-producing countries having some of the largest coastal populations. However, the percentage of mismanaged waste is also important when assessing the largest contributors of waste that is available to enter the environment. Sixteen of the top 20 producers are middle-income countries, where fast economic growth is probably occurring but waste management infrastructure is lacking (the average mismanaged waste fraction is 68%). Only two of the top 20 countries have mismanaged fractions <15%; here, even a relatively low mismanaged rate results in a large mass of mismanaged plastic waste because of large coastal populations and, especially in the United States, high per capita waste generation.

Assuming no waste management infrastructure improvements, the cumulative quantity of plastic waste available to enter the marine environment from land is predicted to increase by an order of magnitude by 2025 (Fig. 2 and table S1). The predicted geographic distribution of mismanaged plastic waste in 2025 does not change substantially, although the disparity between developing and industrialized countries grows (table S2). For example, mismanaged plastic waste in the United States increases by 22%, whereas in the top five countries it more than doubles. The increase in these middle-income countries results from population growth, waste generation rates for 2025 that are consistent with economic growth (5), and a projected increase in plastic in the waste stream.

The analytical framework can also be used to evaluate potential mitigation strategies. For example, if the fraction of mismanaged waste were reduced by 50% (i.e., a 50% increase in adequate disposal of waste) in the 20 top-ranked countries, the mass of mismanaged plastic waste would decrease 41% by 2025. This falls to 34% if the reduction is only applied to the top 10 countries and to 26% if applied to the top 5. To achieve a 75% reduction in the mass of mismanaged plastic waste, waste management would have to be improved by 85% in the 35 top-ranked countries. This strategy would require substantial infrastructure investment primarily in low- and middle-income countries.

Alternatively, reduced waste generation and plastic use would also decrease the amount of mismanaged plastic waste. If per capita waste generation were reduced to the 2010 average (1.7 kg/day) in the 91 coastal countries that exceed it, and the percent plastic in the waste

stream were capped at 11% (the 192-country average in 2010), a 26% decrease would be achieved by 2025. This strategy would target higher-income countries and might require smaller global investments. With a combined strategy, in which total waste management is achieved (0% mismanaged waste) in the 10 top-ranked countries and plastic waste generation is capped as described above, a 77% reduction could be realized, reducing the annual input of plastic waste to the ocean to 2.4 to 6.4 million MT by 2025 (table S3).

Sources of uncertainty in our estimates result from the relatively few measurements of waste generation, characterization, collection, and disposal, especially outside of urban centers. Even where data were available, methodologies were not always consistent, and some activities were not accounted for, such as illegal dumping (even in high-income countries) and ad hoc recycling or other informal waste collection (especially in low-income countries). In addition, we did not address international import and export of waste, which would affect national estimates but not global totals. Although national estimates are somewhat sensitive to the model predicting the percentage of mismanaged waste, the global estimate and ranking of top countries are not. The long-term projections are also sensitive to the model predicting growth of plastic in the waste stream; historical growth may not be a good indicator of future trends (12). The inclusion of the economic cost of implementation, as well as socio-cultural, environmental, and other factors that affect infrastructure development or behavioral change, would improve the evaluation of mitigation strategies (19).

We will not reach a global “peak waste” before 2100 (20). Our waste will continue to grow with increased population and increased per capita consumption associated with economic growth, especially in urban areas and developing African countries (see supplementary materials). Historically, waste management by burying or burning waste was sufficient for inert or biodegradable waste, but the rapid growth of synthetic plastics in the waste stream requires a paradigm shift. Long-term solutions will likely include waste reduction and “downstream” waste management strategies such as expanded recovery systems and extended producer responsibility (21, 22). Improving waste management infrastructure in developing countries is paramount and will require substantial resources and time. While such infrastructure is being developed, industrialized countries can take immediate action by reducing waste and curbing the growth of single-use plastics.

REFERENCES AND NOTES

1. National Research Council (U.S.) Study Panel on Assessing Potential Ocean Pollutants, *Assessing Potential Ocean Pollutants: A Report of the Study Panel on Assessing Potential Ocean Pollutants to the Ocean Affairs Board, Commission on Natural Resources, National Research Council* (National Academy of Sciences, Washington, DC, 1975).
2. International Maritime Organization, “International Convention for the Prevention of Pollution from Ships (MARPOL), annex V prevention of pollution by garbage from ships”

- (International Maritime Organization, London, 1988); www.imo.org/Environment/mainframe.asp?topic_id=297.
3. "Plastics – the facts 2013" (PlasticsEurope, Brussels, Belgium, 2013); www.plasticseurope.org/Document/plastics-the-facts-2013.aspx?FolID=2.
 4. "Municipal solid waste generation, recycling, and disposal in the United States: Facts and figures for 2010" [U.S. Environmental Protection Agency (EPA), Washington, DC, 2011]; www.epa.gov/solidwaste/nonhaz/municipal/pubs/msw_2010_rev_factsheet.pdf.
 5. D. Hoornweg, P. Bhada-Tata, "What a waste: A global review of solid waste management" (The World Bank, Washington, DC, 2012); <https://openknowledge.worldbank.org/handle/10986/17388>.
 6. R. C. Thompson, C. J. Moore, F. S. vom Saal, S. H. Swan, *Philos. Trans. R. Soc. London Ser. B* **364**, 2153–2166 (2009).
 7. D. K. A. Barnes, F. Galgani, R. C. Thompson, M. Barlaz, *Philos. Trans. R. Soc. London Ser. B* **364**, 1985–1998 (2009).
 8. R. W. Obbard et al., *Earth's Future* **2**, 315–320 (2014).
 9. M. C. Goldstein, D. S. Goodwin, *PeerJ* **1**, e184 (2013).
 10. H. S. Carson et al., *Mar. Environ. Res.* **84**, 76–83 (2013).
 11. A. Lechner et al., *Environ. Pollut.* **188**, 177–181 (2014).
 12. Materials and methods are available as supplementary materials on Science Online.
 13. "Probabilistic projections of total population: Median and confidence intervals," (United Nations, Department of Economic and Social Affairs, New York, 2012); http://esa.un.org/unpd/ppp/Data-Output/UN_PPP2010_output-data.htm.
 14. K. L. Law et al., *Science* **329**, 1185–1188 (2010).
 15. K. L. Law et al., *Environ. Sci. Technol.* **48**, 4732–4738 (2014).
 16. A. Cözar et al., *Proc. Natl. Acad. Sci. U.S.A.* **111**, 10239–10244 (2014).
 17. M. Eriksen et al., *PLOS ONE* **9**, e111913 (2014).
 18. "2013 resin review" (American Chemistry Council, Washington, DC, 2013).
 19. R. E. Marshall, K. Farahbakhsh, *Waste Manag.* **33**, 988–1003 (2013).
 20. D. Hoornweg, P. Bhada-Tata, C. Kennedy, *Nature* **502**, 615–617 (2013).
 21. M. Braungart, *Nature* **494**, 174–175 (2013).
 22. T. Lindqvist, K. Lidgren, in *Ministry of the Environment, From the Cradle to the Grave - Six Studies of the Environmental Impact of Products* (Ministry of the Environment, Stockholm, Sweden, 1990), pp. 7–44.

ACKNOWLEDGMENTS

We thank M. A. Barlaz and N. Starr for critical discussions and L. Amaral-Zettler, M. G. Chapman, G. Leonard, and R. Williams for helpful reading of the manuscript. We also thank the anonymous reviewers for their constructive comments. This work was conducted within the Marine Debris Working Group at the National Center for Ecological Analysis and Synthesis, University of California, Santa Barbara, with support from the Ocean Conservancy. Our data and model can be found at <http://jambeck.engr.uga.edu/landplasticinput> and in the supplementary materials.

SUPPLEMENTARY MATERIALS

www.sciencemag.org/content/347/6223/768/suppl/DC1
Materials and Methods
Supplementary Text
Fig. S1
Tables S1 to S6
References (23–30)
Data S1

25 August 2014; accepted 16 January 2015
10.1126/science.1260352

VIRAL REPLICATION

Structural basis for RNA replication by the hepatitis C virus polymerase

Todd C. Appleby,^{1*} Jason K. Perry,¹ Eisuke Murakami,¹ Ona Barauskas,¹ Joy Feng,¹ Aesop Cho,¹ David Fox III,² Diana R. Wetmore,² Mary E. McGrath,¹ Adrian S. Ray,¹ Michael J. Sofia,¹ S. Swaminathan,¹ Thomas E. Edwards^{2*}

Nucleotide analog inhibitors have shown clinical success in the treatment of hepatitis C virus (HCV) infection, despite an incomplete mechanistic understanding of NS5B, the viral RNA-dependent RNA polymerase. Here we study the details of HCV RNA replication by determining crystal structures of stalled polymerase ternary complexes with enzymes, RNA templates, RNA primers, incoming nucleotides, and catalytic metal ions during both primed initiation and elongation of RNA synthesis. Our analysis revealed that highly conserved active-site residues in NS5B position the primer for in-line attack on the incoming nucleotide. A β loop and a C-terminal membrane-anchoring linker occlude the active-site cavity in the apo state, retract in the primed initiation assembly to enforce replication of the HCV genome from the 3' terminus, and vacate the active-site cavity during elongation. We investigated the incorporation of nucleotide analog inhibitors, including the clinically active metabolite formed by sofosbuvir, to elucidate key molecular interactions in the active site.

Hepatitis C virus (HCV) is a positive-sense, single-stranded RNA virus of the family *Flaviviridae* and genus *Hepacivirus* and is the cause of hepatitis C in humans (1). Long-term infection with HCV can lead to end-stage liver disease, including hepatocellular carcinoma and cirrhosis, making hepatitis C the leading cause of liver transplantation in the United States (2). Direct-acting antiviral drugs were approved in 2011, but they exhibited limited efficacy and had the potential for adverse side effects (3). The catalytic core of the viral replication complex, the NS5B RNA-dependent RNA

polymerase (RdRp), supports a staggering rate of viral production, estimated to be 1.3×10^{12} virions produced per day in each infected patient (4). Because the NS5B polymerase active site is highly conserved, nucleotide analog inhibitors offer advantages over other classes of HCV drugs, including activity across different viral genotypes and a high barrier to the development of resistance (5, 6). The nucleotide prodrug sofosbuvir was recently approved for combination treatment of chronic HCV (7, 8).

One substantial obstacle for the rapid discovery of effective nucleotide-based drugs for HCV was the lack of molecular detail concerning substrate recognition during replication. NS5B contains several noncanonical polymerase elements, including a C-terminal membrane anchoring tail and a thumb domain β -loop insertion (9–11), that are implicated in RNA synthesis initiation (12).

To gain insight into the mechanism of HCV RNA replication and its inhibition by nucleotide analog inhibitors, we determined atomic-resolution ternary structures of NS5B in both primed initiation and elongation states.

Because traditional approaches failed to yield ternary complexes (see the supplementary materials), we prepared multiple stalled enzyme-RNA-nucleotide ternary complex structures containing several designed features. First, we used NS5B from the JFH-1 genotype 2a isolate of HCV, which is extraordinarily efficient at RNA synthesis (13). Second, we exploited a conformational stabilization strategy that had been developed for structural analysis of G protein-coupled receptors (14). We hypothesized that a triple resistance NS5B mutant isolated under selective pressure of a guanosine analog inhibitor that exhibits 1.5 times the initiation activity of the wild type (15) might stabilize a specific conformational state along the initiation pathway. Indeed, this triple mutant exhibits a substantial structural rearrangement of the polymerase (15), which is consistent with the structural rearrangement observed in binary complexes of a β -loop deletion mutant bound to primer-template RNA (16). The triple mutant was able to incorporate native and nucleotide analog inhibitors with the RNA samples used in structure determination (fig. S1). The use of nucleotide diphosphate substrates rather than nucleotide triphosphates (fig. S2) generates stalled polymerase complexes in a catalytically relevant conformation. Ternary complexes could be obtained only with Mn^{2+} , which lowers the Michaelis constant (K_m) of the initiating nucleotide (17) and increases the activity of NS5B 20-fold relative to Mg^{2+} (18), and only with a nucleotide/ Mn^{2+} /double-stranded RNA ratio of 1.0/0.6/0.2. These approaches designed to stabilize the incoming nucleotide allowed for soaking experiments targeting several distinct assemblies.

Hepatitis C virus NS5B initiates RNA synthesis by a primer-independent mechanism. Two slow steps in the catalytic pathway have been identified, including the formation of an initial dinucleotide

¹Gilead Sciences, 333 Lakeside Drive, Foster City, CA 94404, USA. ²Beryllium, 7869 NE Day Road West, Bainbridge Island, WA 98110, USA.

*Corresponding author. E-mail: todd.appleby@gilead.com (T.C.A.); tedwards@be4.com (T.E.E.)

primer and the transition from the dinucleotide-primed state to a rapid, processive elongation state (19, 20). We obtained crystal structures of ternary complexes containing NS5B, two Mn^{2+}

ions, an RNA template, and a dinucleotide primer by soaking nucleic acid and manganese ions into a previously elucidated apo crystal form (15) (see supplementary materials). Stalled ternary

structures were obtained either with a 5'-pGG RNA primer and an incoming adenosine diphosphate (ADP) (2.2 Å resolution), cytidine diphosphate (CDP) (2.5 Å), or uridine diphosphate (UDP) (2.0 Å)

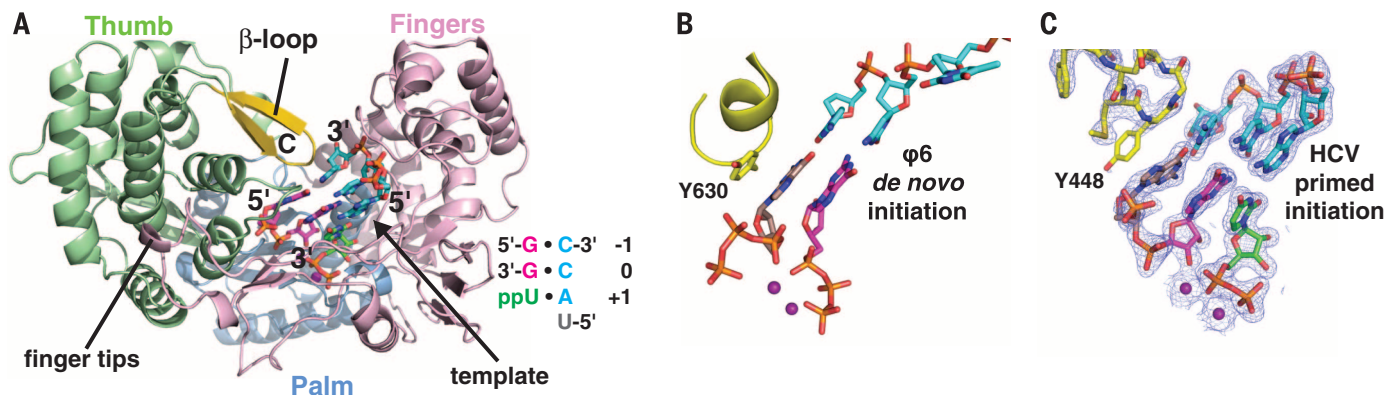


Fig. 1. NS5B primed initiation assembly. (A) Overall structure of the stalled NS5B ternary primed initiation complex. The protein is represented by ribbons and colored by subdomain (pink, fingers; light blue, palm; pale green, thumb), with the β loop highlighted in yellow and the position of the last visible residue at the C terminus labeled "C." The RNA template (5'-UACC; cyan carbons), 5'-pGG dinucleotide primer (magenta carbons), and incoming UDP nucleotide (green carbons) are represented by sticks and colored according to atom type (red, oxygen; blue, nitrogen; orange, phosphate). The two catalytic Mn^{2+} ions

are shown as purple spheres. (B) $\phi 6$ RdRp de novo initiation assembly, with the priming nucleotide colored by atom type with brown carbons, the incoming nucleotide colored by atom type with magenta carbons, and an active-site loop shown in yellow. (C) Primed initiation assembly of HCV, which is one catalytic step after the de novo initiation assembly. Thus, the dinucleotide primer is colored as in (B) after catalysis, with the next incoming nucleotide colored by atom type with green carbons. The $2|F_o| - |F_c|$ electron density map is contoured at 1σ and superimposed on the refined ligand and β -loop atoms.

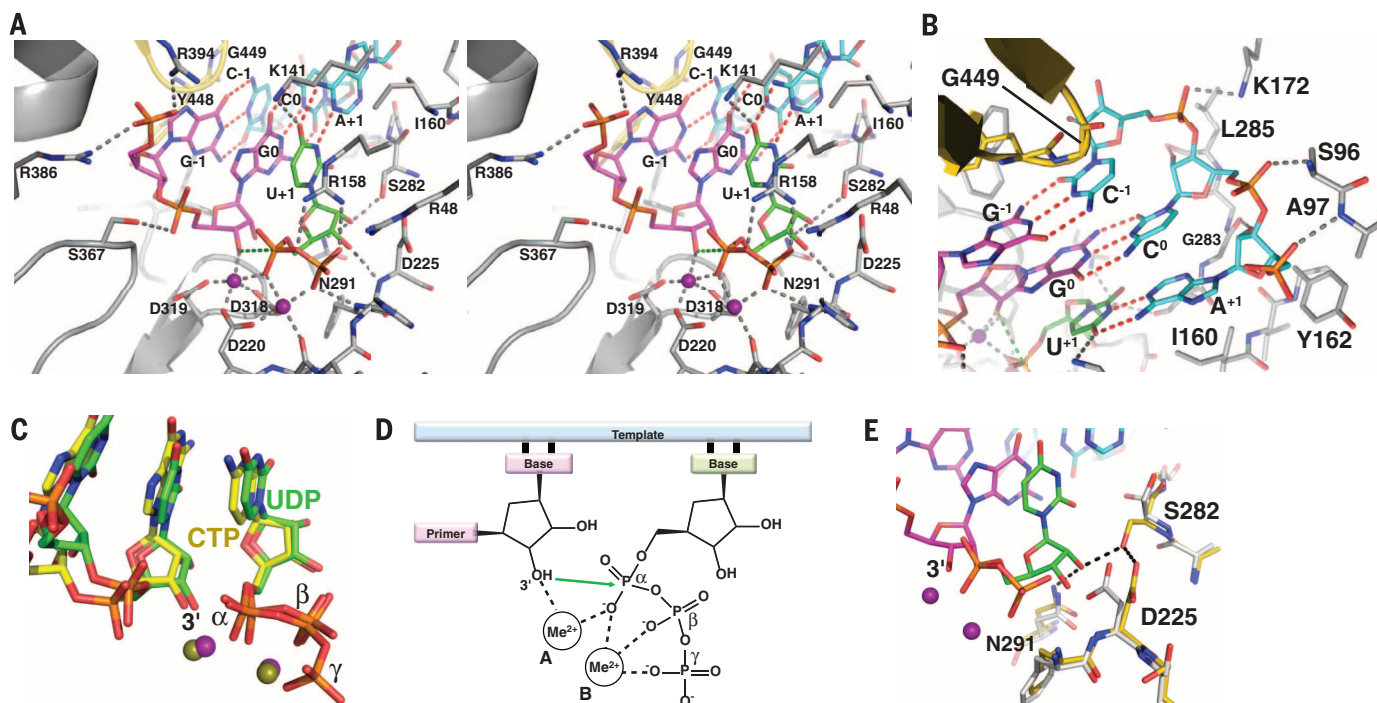


Fig. 2. Recognition of the incoming nucleotide. (A) Stereoscopic view of the NS5B active site during primed initiation. Select protein atoms are represented by sticks and are colored by atom type with gray carbons, except for the β -loop residues, which are highlighted in yellow. RNA bases are labeled according to standard polymerase numbering conventions. Protein-ligand hydrogen bonds are shown as gray dashed lines, whereas base-pair hydrogen bonds are shown as red dashed lines. The proposed path of in-line attack by the 3'-hydroxyl on the α phosphate of the incoming nucleotide is illustrated by a green dashed line. (B) Close-up view of the RNA template binding site. (C) Comparison of the 3' end of RNA primers, metal ions, and incoming nucleotides from the Norwalk virus

polymerase ternary complex containing cytidine triphosphate (CTP) as the incoming nucleotide [PDB ID: 3BSO (23)] and the NS5B ternary complex containing UDP as the incoming nucleotide. The Norwalk structure atoms are colored according to atom type with yellow carbons and gold metal ions, whereas the NS5B ternary complex atoms are colored by atom type with green carbons and purple metal ions. (D) Common chemical mechanism of polymerases (24). (E) Molecular mechanism for recognizing ribonucleotide substrates. Protein atoms of the apo enzyme are colored with gray carbons, whereas protein atoms of the substrate complex are colored with yellow carbons. Dashed lines represent the hydrogen bonding network formed upon binding to an incoming ribonucleotide.

molecular details of a platform for RNA synthesis in which the tip of the β loop now buttresses the end of the short RNA duplex. A similar global arrangement has been observed previously in the de novo initiation assembly of RNA bacteriophage $\phi 6$ RdRp (21) (Fig. 1B), which illustrates the catalytic event preceding the primed initiation state of HCV (Fig. 1C). These β -loop interactions appear critical for setting the register to ensure that the polymerase initiates transcription at the 3' end of the viral genome. In general, the β -loop residues exhibit increased temperature factors and contain weaker electron density compared with the apo enzyme, indicating that the β loop starts to become disordered during primed initiation (fig. S5). In addition to retraction of the β loop, the C terminus vacated the active-site cavity now occupied by nucleic acid and appeared disordered beyond residue T552 (22) in the primed assemblies. These movements generate space to accommodate only two Watson-Crick pairs upstream of the incoming nucleotide, suggesting that further conformational changes are required to accommodate additional phosphotransfer and translocation events. This includes, at a minimum, an opening of the thumb domain via reorientation of the β loop. Thus, these structures demonstrate the polymerase assembly before the second slow step in RNA replication (19).

Mutational analysis of NS5B revealed R386 of the primer grip motif to be important for dinucleotide-initiated RNA synthesis (12), and the primed-state assemblies show that both R386 and R394 of the primer grip helix form salt bridges with the 5'-phosphate of the dinucleotide primer (Fig. 2A). The conserved catalytic residues D220, D318, and D319 coordinate the two catalytic Mn^{2+} ions, which in turn coordinate the α and β phosphates of the incoming nucleotide. Conserved basic residues R48 and R158 coordinate the α and β phosphates opposite the metal ions. The incoming nucleotide forms a Watson-Crick interaction with the pairing residue of the template strand, which packs against conserved hydrophobic residues I160 and Y162 (Fig. 2B). The 3'-hydroxyl of the dinucleotide primer forms an inner-sphere coordination with a catalytic metal ion in an in-line conformation with the scissile bond of the incoming nucleotide, nearly identical to that observed for the Norwalk virus RdRp (23) (Fig. 2C). Thus, the nucleotide diphosphates exhibit enzymatically competent conformations consistent with the common polymerase mechanism (24) (Fig. 2D).

In HIV-1 reverse transcriptase, Y115 provides specificity for deoxynucleotide triphosphates by serving as a steric gate to prevent the binding of ribonucleotide triphosphates (rNTPs) (25), and it was predicted that the structurally homologous residue in HCV, conserved D225, would be involved in recognition of the 2'-hydroxyl of incoming rNTPs (9–11). In the NS5B ternary complexes, the main chain of conserved S282 flips, allowing its side chain to swing out and hydrogen bond with the 2'-hydroxyl of the substrate and the carboxylic acid of D225, which moves away from the

nucleotide substrate during binding (Fig. 2E). The 2'-hydroxyl of the incoming ribonucleotide also forms a direct hydrogen bond with the side chain amine of N291 on the opposite face of the ribose ring. This network of hydrogen bonds, together with complementary base-pairing to the template, provides the structural basis for recognition of the correct ribonucleotide substrate.

Crystal structures of a β -loop deletion construct of the HCV NS5B polymerase were solved as apo (2.5 Å resolution) or via soaking (see supplementary materials and methods) with a symmetrical RNA primer-template pair (16) and an incoming UDP (2.8 Å), CDP (2.75 Å), ADP (2.7 Å), or GDP (2.9 Å) (Fig. 3, figs. S6 to S8, and tables S4 to S6). These ternary complexes probably represent the highly processive elongation phase of viral genome replication after the transition from the primed state in the second slow step of polymerization (19). These high-resolution elongation state structures were obtained via soaking into the same crystal form as the triple-mutant structures with the intact β loop but could only be obtained with a construct containing both the triple mutant (15) and the β -loop deletion (16) (see supplementary materials). Overall, there is excellent overlap between the catalytic residues, the 3' end of the primer, and the incoming nucleotide when comparing the elongation complexes with the primed initiation assemblies, including the same in-line conformation of the 3'-hydroxyl of the primer with the scissile bond. The thumb domain moved away from the palm and fingers domains by an additional 1.5 Å for similar C α atoms, demonstrating a slightly more relaxed state of the polymerase during elongation. In addition, the C-terminal residues downstream of A534 have evacuated the RNA binding groove and become disordered, preventing overlap with the template strand. Thus, these structures provide further evidence for concerted movements of the β loop, the thumb domain, and the C terminus once RNA elongation begins. Moreover, they provide the structural basis for the hypothesis that these elements provide a "swinging gate" that allows the polymerase to initiate at the terminus of the RNA genome and then transition to a processive elongation state, thereby replicating the complete genome (12).

The crystal structures presented here lead us to propose a model of the structural events involved in HCV genome replication (Fig. 4). At the outset, the β loop and the C-terminal membrane-anchoring linker are buried within the encircled active-site cavity. In the first of two slow steps in HCV RNA replication (19), the 3' end of the viral RNA template and the incoming nucleotides enter the active site, possibly with accompanying conformational changes, and the initial phosphoryl transfer step generates a dinucleotide primer. This de novo initiation step immediately precedes the primed initiation assembly captured here. At this early stage, the complex remains unstable, which may account for the observed large quantity of two- to four-nucleotide-long abortive transcripts (26, 27). As the dinucleotide primer is extended by another one to three nucleotides, the

build-up of tension displaces the β loop and the remaining C-terminal residues, further opening the cavity and allowing the RNA duplex to exit during the second slow step in replication (19). With both the β -hairpin loop and the C terminus expelled from the active-site cavity, the polymerase transitions into the highly processive elongation mode also captured here.

By using an extensive hydrogen bond network to recognize the 2'-hydroxyl of the incoming nucleotide (Fig. 3C), HCV NS5B displays stringent selectivity for ribonucleotides. Consequently, 2'-deoxyribonucleotide chain terminators such as azidothymidine are ineffective against HCV, whereas 2'-modified nucleotides are effective HCV antivirals (6). The nucleotide analog inhibitor sofosbuvir is a 2'-F-2'-C-methyluridine monophosphate pro-drug (28–30) and is approved for the treatment of chronic HCV infection (7, 8). Efficacy of chain-terminating nucleotide analogs requires viral RdRps to recognize and successfully incorporate the inhibitors into the growing RNA strand. To gain insight into the molecular details of 2'-modified nucleotide analog recognition, we determined elongation-phase ternary complexes of both 2'-OH/2'-CH₃-UDP and 2'-F/2'-CH₃-UDP at 2.65 and 2.9 Å resolution, respectively (table S7). The stalled ternary complex with 2'-OH/2'-CH₃-UDP as the incoming nucleotide was essentially identical to the UDP-bound elongation assembly, with S282 undergoing the same conformational change to interact directly with the 2'-hydroxyl group and hydrogen bond with D225 (Fig. 3D). Although the addition of the 2'-C-methyl group of the inhibitor places it within 3.1 Å of the S282 O γ , previous biochemical studies using 2'-C-methyl nucleotides reveal that these analogs are readily incorporated into the growing chain with K_m values approaching those of the natural ribonucleotide substrates (31). In contrast, the trapped elongation assembly containing 2'-F/2'-CH₃-UDP (i.e., sofosbuvir diphosphate) as the incoming nucleotide reveals that the hydrogen bonding network is disrupted (Fig. 3E). D225 is oriented away from the incoming nucleotide, but S282 remains in the same conformation as in the apo enzyme. The loss of the hydrogen bonding network involving S282 results in a substantially higher K_m for 2'-F/2'-CH₃-modified nucleotides. Nevertheless, recognition of the 2'-F by N291 and Watson-Crick pairing with the template allow sofosbuvir to form the in-line conformation necessary for incorporation into the growing chain, thereby promoting non-obligate chain termination. Key contacts formed by S282 with the incoming nucleotide and the surrounding environment give insight into the in vitro selection of a threonine as a potential resistance mutation to some 2'-CH₃-modified nucleotides (32, 33), although S282→T282 has been infrequently observed in the clinic (34). In particular, a steric clash between the T282 side chain and the 2'-CH₃ would be predicted based on the structure determined with 2'-OH/2'-CH₃-UDP.

The results presented here define the structural requirements for HCV genomic replication from primed initiation to elongation and demonstrate the structural basis for inhibitor recognition. The

primed initiation state explains much of the known biochemistry behind the slow steps in the enzymatic pathway and highlights the differences between *Flaviviridae* RdRps and other polymerases. These structural and mechanistic differences have been exploited for the development of HCV nucleotide therapeutics that feature pangenomic activity and a high barrier to the development of drug resistance. Thus, they may provide an avenue for the development of therapeutics against related viruses.

REFERENCES AND NOTES

1. R. Bartenschlager, V. Lohmann, *J. Gen. Virol.* **81**, 1631–1648 (2000).
2. W. R. Kim et al., *Am. J. Transplant.* **14** (suppl. 1), 69–96 (2014).
3. F. Poordad, D. Dieterich, *J. Viral Hepat.* **19**, 449–464 (2012).
4. A. U. Neumann et al., *Science* **282**, 103–107 (1998).
5. S. Le Pogam et al., *J. Antimicrob. Chemother.* **61**, 1205–1216 (2008).
6. M. J. Sofia, *Adv. Pharmacol.* **67**, 39–73 (2013).
7. E. J. Kane et al., *N. Engl. J. Med.* **368**, 34–44 (2013).
8. R. S. Koff, *Aliment. Pharmacol. Ther.* **39**, 478–487 (2014).
9. H. Ago et al., *Structure* **7**, 1417–1426 (1999).
10. S. Bressanelli et al., *Proc. Natl. Acad. Sci. U.S.A.* **96**, 13034–13039 (1999).
11. C. A. Lesburg et al., *Nat. Struct. Biol.* **6**, 937–943 (1999).
12. Z. Hong et al., *Virology* **285**, 6–11 (2001).
13. P. Simister et al., *J. Virol.* **83**, 11926–11939 (2009).
14. R. Abrol, S. K. Kim, J. K. Bray, B. Trzaskowski, W. A. Goddard III, *Methods Enzymol.* **520**, 31–48 (2013).
15. A. M. Lam et al., *Antimicrob. Agents Chemother.* **58**, 6861–6869 (2014).
16. R. T. Mosley et al., *J. Virol.* **86**, 6503–6511 (2012).
17. C. T. Ranjith-Kumar et al., *J. Virol.* **76**, 12513–12525 (2002).
18. G. Luo et al., *J. Virol.* **74**, 851–863 (2000).
19. D. Harrus et al., *J. Biol. Chem.* **285**, 32906–32918 (2010).
20. N. Scrima et al., *J. Virol.* **86**, 7107–7117 (2012).
21. S. J. Butcher, J. M. Grimes, E. V. Makeyev, D. H. Bamford, D. I. Stuart, *Nature* **410**, 235–240 (2001).
22. Single-letter abbreviations for the amino acid residues are as follows: A, Ala; C, Cys; D, Asp; E, Glu; F, Phe; G, Gly; H, His; I, Ile; K, Lys; L, Leu; M, Met; N, Asn; P, Pro; Q, Gln; R, Arg; S, Ser; T, Thr; V, Val; W, Trp; and Y, Tyr.
23. D. F. Zamyatkin et al., *J. Biol. Chem.* **283**, 7705–7712 (2008).
24. T. A. Steitz, *Nature* **391**, 231–232 (1998).
25. H. Huang, R. Chopra, G. L. Verdine, S. C. Harrison, *Science* **282**, 1669–1675 (1998).
26. H. Dutartre, J. Boretto, J. C. Guillemot, B. Canard, *J. Biol. Chem.* **280**, 6359–6368 (2005).
27. W. Zhong et al., *J. Virol.* **74**, 9134–9143 (2000).
28. A. M. Lam et al., *Antimicrob. Agents Chemother.* **56**, 3359–3368 (2012).
29. E. Murakami et al., *J. Biol. Chem.* **285**, 34337–34347 (2010).
30. M. J. Sofia et al., *J. Med. Chem.* **53**, 7202–7218 (2010).
31. H. Dutartre, C. Bussetta, J. Boretto, B. Canard, *Antimicrob. Agents Chemother.* **50**, 4161–4169 (2006).
32. S. S. Carroll et al., *J. Biol. Chem.* **278**, 11979–11984 (2003).
33. A. M. Lam et al., *Antimicrob. Agents Chemother.* **54**, 3187–3196 (2010).
34. E. S. Svarovskaia et al., *Clin. Infect. Dis.* **59**, 1666–1674 (2014).

ACKNOWLEDGMENTS

We thank D. Smith at the Advanced Photon Source, Argonne National Labs, Life Sciences Collaborative Access Team (LS-CAT), for assistance in data collection, as well as our co-workers from Pharmasset, Beryllium, and Gilead Sciences, who have participated on the HCV polymerase collaboration. Coordinates and structure factors have been deposited with the Protein Data Bank under accession codes 4WT9, 4WTA, 4WTC, 4WTD, 4WTE, 4WTF, 4WTG, 4WTI, 4WTJ, 4WTK, 4WTL, and 4WTM. Expression plasmids are freely available from the authors. Gilead Sciences and the authors (T.E.E. and E.M.) have filed international patent application number PCT/US2013/021130, which relates to crystal structures of HCV polymerase complexes and their methods of use.

SUPPLEMENTARY MATERIALS

www.sciencemag.org/content/347/6223/771/suppl/DC1
Materials and Methods
Supplementary Text
Figs. S1 to S8
Tables S1 to S7
References (35–43)

25 July 2014; accepted 18 December 2014
10.1126/science.1259210

TIGHT JUNCTIONS

Structural insight into tight junction disassembly by *Clostridium perfringens* enterotoxin

Yasunori Saitoh,^{1,2*} Hiroshi Suzuki,^{1,*†} Kazutoshi Tani,^{1*} Kouki Nishikawa,¹ Katsumasa Irie,^{1,2} Yuki Ogura,³ Atsushi Tamura,³ Sachiko Tsukita,³ Yoshinori Fujiyoshi^{1,2,†}

The C-terminal region of *Clostridium perfringens* enterotoxin (C-CPE) can bind to specific claudins, resulting in the disintegration of tight junctions (TJs) and an increase in the paracellular permeability across epithelial cell sheets. Here we present the structure of mammalian claudin-19 in complex with C-CPE at 3.7 Å resolution. The structure shows that C-CPE forms extensive hydrophobic and hydrophilic interactions with the two extracellular segments of claudin-19. The claudin-19/C-CPE complex shows no density of a short extracellular helix that is critical for claudins to assemble into TJ strands. The helix displacement may thus underlie C-CPE-mediated disassembly of TJs.

Infection with *Clostridium perfringens* type A by eating contaminated food is a common cause of food poisoning in humans and animals. In the intestines, this bacterium produces *Clostridium perfringens* enterotoxins (CPEs) that trigger foodborne illness (1). Upon binding to their receptor, the complexes aggregate on the intestinal cell surface and form a large oligomer that inserts into the membrane and forms an ion pathway. The resulting Ca²⁺ influx triggers cell death (2, 3). The receptors for CPE, initially named CPE-R and RVP-1 (4, 5), were later recognized as claudin-4 and -3, respectively (6), based on their sequence simi-

larity with claudin-1 and -2, known constituents of cell-to-cell tight junctional complexes (7, 8). The carboxyl-terminal half of CPE (C-CPE) mediates the interaction with specific claudins (9, 10), which reversibly modulates the paracellular permeability of tight junctions (TJs), whereas its amino-terminal half is responsible for pore formation and thus for cellular cytotoxicity (11).

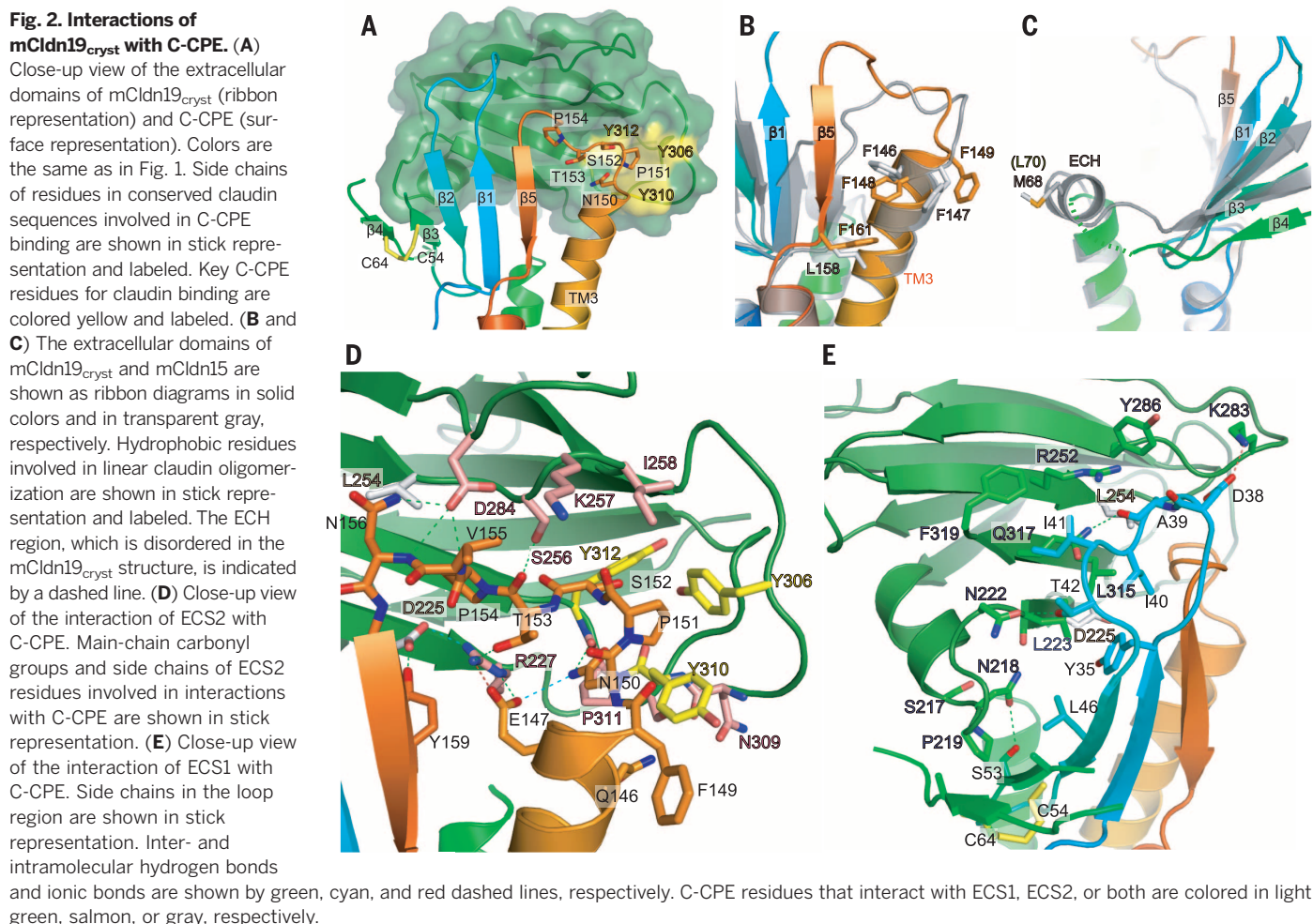
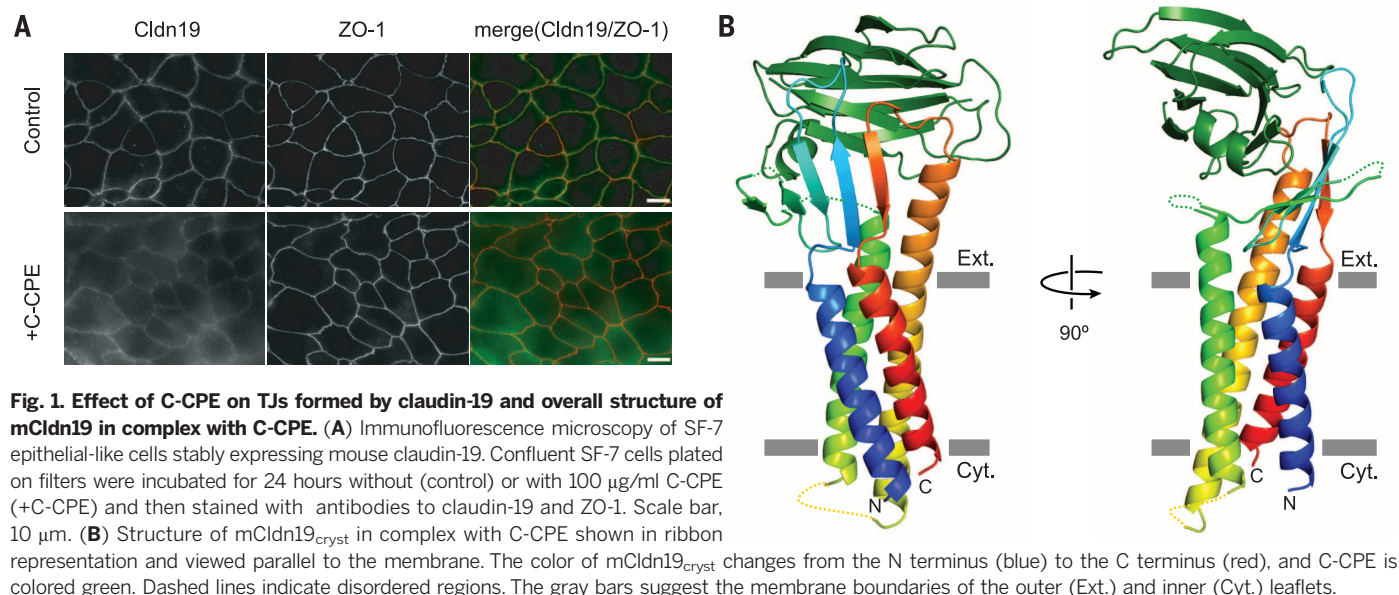
Claudins have a common structural topology consisting of four transmembrane (TM) segments; a large first extracellular segment (ECS1), which contains the claudin consensus motif; and a shorter second extracellular segment (ECS2)

(12–14). The adhesion and polymerization properties of claudins enable them to form linear polymers, called TJ strands, which connect adjacent cells and form the structural backbone of TJs (15). TJs serve mainly as barriers that restrict the diffusion of solutes through intercellular spaces in epithelial and endothelial cell sheets (16), thus separating internal tissue compartments from external environments to maintain the homeostasis of our bodies (8).

To understand the structural basis for how C-CPE recognizes specific claudins, we expressed all mouse claudin subtypes in Sf9 insect cells and assessed their capacity to bind C-CPE by using fluorescent-detection size-exclusion chromatography (FSEC) (17). Mouse claudin-19 showed considerable affinity for C-CPE (fig. S1A) (18). When expressed in a mammalian epithelial-like cell line, mouse claudin-19 formed TJs in the plasma membranes of cell-to-cell contact regions (Fig. 1A). Although a previous study reported that a synthetic ECS2 peptide of claudin-19 had no affinity for CPE (9), a 24-hour incubation with C-CPE resulted in a significant delocalization of the claudin-19 signal away from the junctional borders (Fig. 1A), suggesting that binding of C-CPE causes claudin-19 to dissociate from TJs. The disruption of TJs by incubating cells expressing

¹Cellular and Structural Physiology Institute, Nagoya University, Chikusa, Nagoya 464-8601, Japan. ²Department of Basic Medical Science, Graduate School of Pharmaceutical Science, Nagoya University, Chikusa, Nagoya 464-8601, Japan. ³Laboratory of Biological Science, Graduate School of Frontier Biosciences and Graduate School of Medicine, Osaka University, Suita, Osaka 565-0871, Japan.

*These authors contributed equally to this work. †Present address: Department of Cell Biology, Harvard Medical School, 240 Longwood Avenue, Boston, MA 02115, USA. ‡Corresponding author. E-mail: yoshi@cespi.nagoya-u.ac.jp



claudin-19 with C-CPE was also seen in freeze-fracture electron microscopy images (fig. S1, B and C). We used FSEC to quantify the affinity of C-CPE for claudin-19, as well as for claudin-3 and claudin-1 as positive and negative controls, respectively. Our analysis yielded the apparent dissociation constant ($K_{0.5}$) values for C-CPE binding of 240 ± 18 nM and 7.9 ± 0.2 nM for claudin-19 and -3, respectively, which is consistent with previous reports (11, 19), and we found only negligible binding for claudin-1 (fig. S2B).

For crystallization, we removed 26 residues from the C terminus of mouse claudin-19 and

substituted three membrane-proximal cysteines with alanines (fig. S3). After crystallization of this construct, mCldn19_{cryst}, in complex with C-CPE, the structure was determined at 3.7 Å resolution using the molecular replacement method (Fig. 1B, fig. S4, and table S1). Crystals of mCldn19_{cryst} with bound C-CPE contain two 1:1 claudin-toxin complexes per asymmetric unit (fig. S5), which, despite different crystal contacts, have almost identical conformations, with an average root mean square deviation (RMSD) between their $C\alpha$ atoms of 0.39 Å (fig. S5, B and C).

The overall structure of mCldn19_{cryst} is similar to that of mCldn15 (14), a CPE-insensitive claudin, with the four TM segments forming a typical left-handed bundle (Fig. 1B and fig. S6). In addition, the binding does not induce a conformational change in C-CPE (fig. S7). However, the two extracellular β -sheet segments of mCldn19_{cryst}, ECS1 and ECS2, are oriented differently compared with those of mCldn15 (Fig. 2, A to C, and fig. S6). In mCldn19_{cryst}, the loop between β 1 and β 2 (residues 35 to 42), which is disordered in the mCldn15 structure (fig. S6), is clearly resolved and makes contact with C-CPE

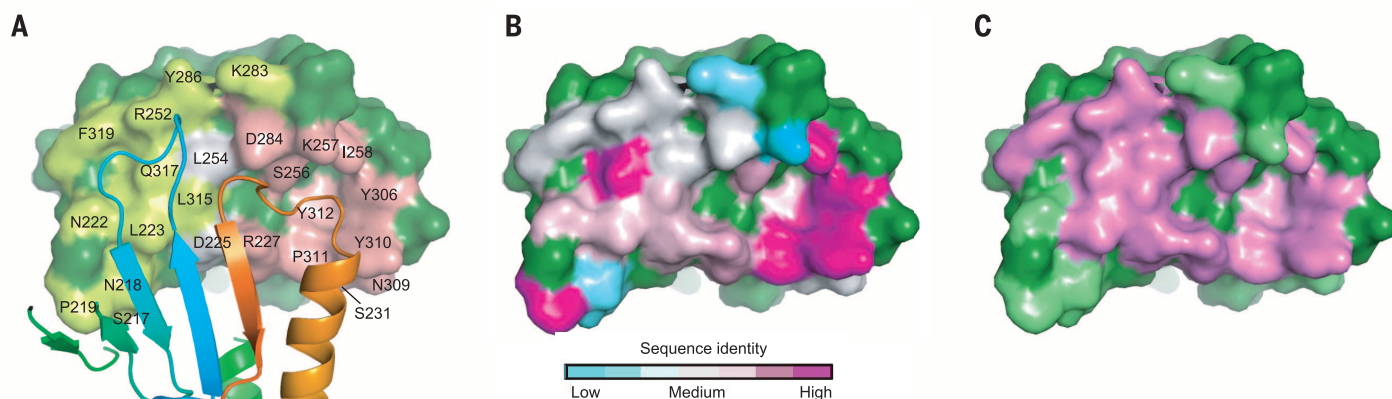


Fig. 3. The interface between mCldn19_{cryst} and C-CPE. (A) Surface representation of C-CPE with bound mCldn19_{cryst} shown in ribbon representation. C-CPE residues that interact with ECS1, ECS2, or both are labeled and colored in light green, salmon, or gray, respectively. (B and C) The surface of C-CPE that interacts with claudins viewed as in (A). (B) The C-CPE residues involved in the interaction with mCldn19_{cryst} are conserved and can thus mediate binding to all CPE-sensitive claudins. (C) Mapping of claudin-19 mutations that affect the binding affinity onto the surface of the interacting C-CPE residues. Violet indicates a significant reduction in binding affinity, and lime indicates a small reduction.

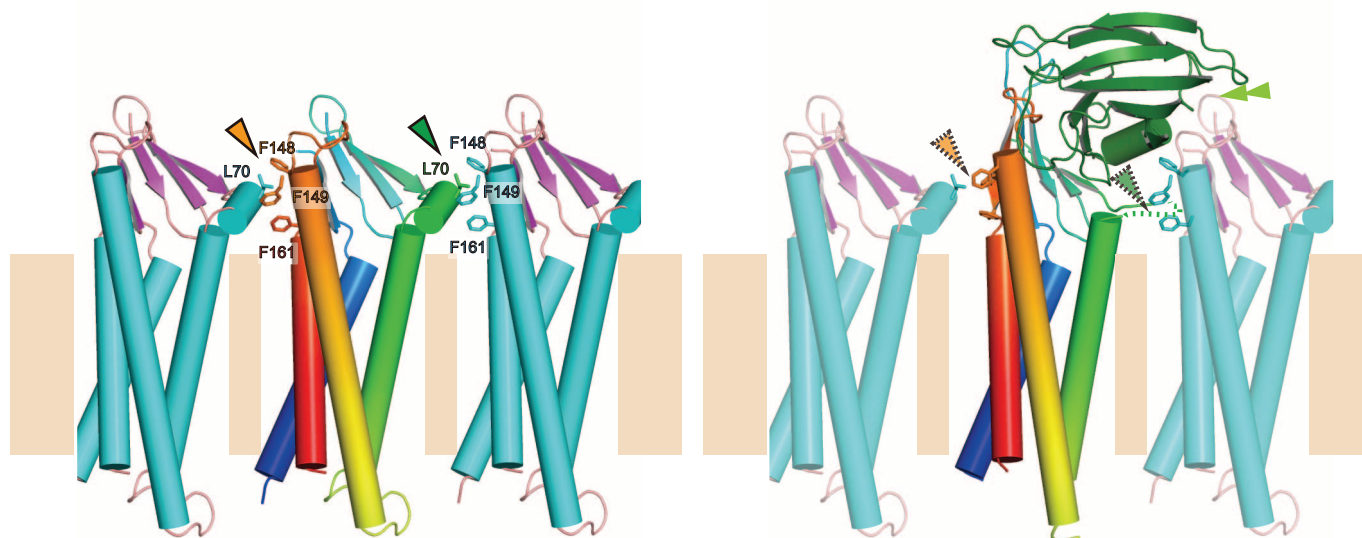


Fig. 4. Structural insights into the disassembly of a TJ strand induced by C-CPE binding. The linear arrangement of claudin-19 in a TJ strand is modeled based on the mCldn15 crystal structure. The hydrophobic residues involved in the linear interactions are shown in stick representation and indicated by arrowheads (left panel). Binding of C-CPE disrupts the hydrophobic interactions between neighboring claudin protomers (arrowheads) and also creates steric clashes (double arrowhead) that prevent interactions with neighboring claudin protomers as well as with claudin protomers from an adjoining cell.

(Fig. 2, A and E). Also, the $\beta 5$ strand in the loop connecting TM3 to TM4 is longer in mCldn19_{cryst} than in mCldn15 and can thus form more hydrogen bonds with the adjacent $\beta 1$ strand (Fig. 2B). In addition, whereas the disulfide bond between highly conserved cysteine residues at $\beta 3$ and $\beta 4$ (C54 and C64, respectively) is also apparent in the mCldn19_{cryst} structure, the loop between $\beta 3$ and $\beta 4$ seen in mCldn15 is disordered (Fig. 2A and fig. S3). Finally, the residues in ECS1 that connect $\beta 4$ to TM2 (residues 69 to 74) are disordered in mCldn19_{cryst}, whereas the corresponding region in mCldn15 forms a short extracellular helix (ECH) that is oriented almost parallel to the membrane surface (Fig. 2C and fig. S4C).

Experiments with ECS2-derived peptides suggested that the ECS2 region of claudins contains a toxin-binding motif, NP(V/L)(V/L)(P/A), that is responsible for CPE binding (3, 9). This toxin-binding motif is probably located in a hydrophobic cavity formed by three tyrosine residues in C-CPE, Y306^{CPE}, Y310^{CPE}, and Y312^{CPE} (throughout the text, CPE residues are indicated with superscripted CPE) (Fig. 2, A and D), thought to be a claudin-binding pocket (3, 9, 20). The ECS2 loop starting with a conserved asparagine residue, N150, stabilizes the complex with CPE by forming hydrogen bonds with the main chain carbonyl of P311^{CPE}, the side chain of the positively charged R227^{CPE} residue, and so on (Fig. 2D and fig. S4B). Recently, a structure was determined of full-length CPE bound to a short peptide with a modified sequence of the claudin-2 ECS2 (27). The ECS2 peptide was observed in the same hydrophobic cavity on C-CPE despite the differences in ECS2 sequences of claudin-2 and -19 (fig. S8).

Because previous biochemical studies suggested that only ECS2 is involved in CPE binding (10, 19), the observed interaction of ECS1 with C-CPE is unexpected. Although the sequences connecting the $\beta 1$ and $\beta 2$ strands in ECS1 (residues 32 to 48) differ among claudin subtypes, the residues in the middle of this region (residues 39 to 42) are more conserved (fig. S3). The motif (A/N/S)-I-(I/L/V)-(T/V) in the claudin-19 structure clearly interacts with the surface of C-CPE, whereas the corresponding region is disordered in the mCldn15 structure (Fig. 2E and fig. S6). To test the binding site observed in the structure of the complex, we introduced point mutations in both ECS1 and ECS2 of mCldn19 in the region where they make contact with C-CPE (Fig. 3). The affinity of the mutants for C-CPE in detergent solution was assessed using FSEC (18) (table S2 and figs. S9 and S10). The binding affinity for C-CPE was affected most by substitutions of residues in the putative binding motif in ECS2 (N150-P154; Fig. 2, A and D) and of the three successive residues forming the conserved motif in ECS1 (A39-I41; Fig. 2E). Mapping of these mutagenesis results onto the C-CPE surface (Fig. 3C) shows almost perfect agreement with the mapping of the sequence conservation in CPE-sensitive claudins (Fig. 3B). Thus, both ECS1 and ECS2 are involved in the physiological interaction with C-CPE.

The surface of C-CPE that interacts with the extracellular claudin domains is mainly composed of hydrophobic residues (fig. S11, A and B) but also contains residues that can form hydrogen or ionic bonds, especially with ECS2 (Fig. 2 and fig. S11C). The side chains of the residues forming the conserved motif in ECS2 (150N-P-S-T-P154 in mCldn19) extend toward C-CPE and fit snugly into the hydrophobic cavity formed by the tyrosine triplet of C-CPE (Y306^{CPE}, Y310^{CPE}, and Y312^{CPE}) (fig. S4B). Mutation of these residues to alanine reduced the binding of CPE to claudin-4 (22), and substitutions of S152 in ECS2 with hydrophobic residues resulted in mCldn19 variants with a higher affinity for C-CPE (table S2). Thus, the presence of a hydrophobic residue in ECS2 that can fit into the hydrophobic cavity may determine whether a claudin is sensitive to CPE or not. The size of the side chain of N150 and the hydrogen bonds it could form were also critical for CPE binding, and a negative charge at this position inhibited CPE binding even if the pI of the ECS2 region remains unchanged (for details, see the materials and methods and table S2). These results are consistent with the finding that it is predominantly hydrophobic and uncharged residues that form the claudin-toxin interface around the CPE tyrosine triplet (indicated by the dashed line in fig. S11). On the other hand, the residues of the conserved motif in ECS1 (39A-I-I41 in mCldn19) among all claudins were sensitive to the size of their side chains (table S2). Therefore, it seems to be predominantly ECS2 that determines the sensitivity of a claudin for CPE, whereas ECS1 contributes to the interaction simply by enlarging the hydrophobic contact area.

Structures of claudins with and without bound C-CPE could potentially provide insights into the disruption of TJ strands. The structure of mCldn15, which does not bind CPE, enables us to build a homology model for mCldn19 without bound C-CPE and thus to infer the conformational changes that may result from C-CPE binding (Fig. 4 and fig. S12). The claudin-CPE interaction would cause a disordering of the ECH region between $\beta 4$ and TM2 (fig. S4C and S6B). Because the ECH could form hydrophobic interactions with TM3 of the neighboring claudin protomer (14), it is conceivable that the movement of TM3 and the disordering of ECH induced by CPE binding destabilize the linear claudin polymer in the TJ strand. Furthermore, CPE binding would also interfere with the head-to-head interaction of claudin protomers in TJ strands in adjoining cells. Several studies support our insights (9, 23), but further experiments are needed to fully understand how CPE binding causes the disassembly of TJs.

Our structure and mutational analyses of the interaction of C-CPE with claudin-19 may help in the design of drugs or biomarkers that selectively target specific claudin subtypes, regardless of their sensitivity to CPE (24, 25). The molecular information on C-CPE-induced TJ disassembly may also be useful to design strategies aimed at increasing the permeability of drugs across TJs in the blood-brain barrier (26).

REFERENCES AND NOTES

- B. A. McCrane, *Toxicol.* **39**, 1781–1791 (2001).
- A. Veshnyakova et al., *Toxins* **2**, 1336–1356 (2010).
- L. A. Mitchell, M. Koval, *Toxins* **2**, 1595–1611 (2010).
- J. Katahira, N. Inoue, Y. Horiguchi, M. Matsuda, N. Sugimoto, *J. Cell Biol.* **136**, 1239–1247 (1997).
- J. Katahira et al., *J. Biol. Chem.* **272**, 26652–26658 (1997).
- K. Morita, M. Furuse, K. Fujimoto, S. Tsukita, *Proc. Natl. Acad. Sci. U.S.A.* **96**, 511–516 (1999).
- M. Furuse, K. Fujita, T. Hiragi, K. Fujimoto, S. Tsukita, *J. Cell Biol.* **141**, 1539–1550 (1998).
- S. Tsukita, M. Furuse, M. Itoh, *Nat. Rev. Mol. Cell Biol.* **2**, 285–293 (2001).
- L. Winkler et al., *J. Biol. Chem.* **284**, 18863–18872 (2009).
- J. Kimura et al., *J. Biol. Chem.* **285**, 401–408 (2010).
- N. Sonoda et al., *J. Cell Biol.* **147**, 195–204 (1999).
- A. Tamura, S. Tsukita, *Semin. Cell Dev. Biol.* **36C**, 177–185 (2014).
- D. Günzel, A. S. L. Yu, *Physiol. Rev.* **93**, 525–569 (2013).
- H. Suzuki et al., *Science* **344**, 304–307 (2014).
- E. E. Schneeberger, R. D. Lynch, *Am. J. Physiol. Cell Physiol.* **286**, C1213–C1228 (2004).
- D. W. Powell, *Am. J. Physiol.* **241**, G275–G288 (1981).
- T. Kawate, E. Gouaux, *Structure* **14**, 673–681 (2006).
- See supplementary materials on Science Online.
- K. Fujita et al., *FEBS Lett.* **476**, 258–261 (2000).
- C. M. Van Itallie, L. Betts, J. G. Smedley 3rd, B. A. McCrane, J. M. Anderson, *J. Biol. Chem.* **283**, 268–274 (2008).
- T. S. Yelland et al., *J. Mol. Biol.* **426**, 3134–3147 (2014).
- A. Takahashi et al., *Biochem. Pharmacol.* **75**, 1639–1648 (2008).
- M. Harada et al., *Biochem. Pharmacol.* **73**, 206–214 (2007).
- P. J. Morin, *Cancer Res.* **65**, 9603–9606 (2005).
- D. P. English, A. D. Santin, *Int. J. Mol. Sci.* **14**, 10412–10437 (2013).
- M. Kondoh et al., *Mol. Pharmacol.* **67**, 749–756 (2005).

ACKNOWLEDGMENTS

We thank M. Uji, Y. Yamazaki, and Y. Ito for technical support; K. Abe for calculation of affinity values; the beamline staff members at BL32XU, BL38B1, and BL41XU of SPring-8 (Hyogo, Japan) for technical help during data collection; and T. Walz for critical reading of the manuscript. The synchrotron radiation experiments were performed with the approval of the Japan Synchrotron Radiation Research Institute (proposal nos. 2013A1112, 2013B1178, 2013B1342, and 2014A1501). This research was supported by Grants-in-Aid for Scientific Research (S) (to Y.F.), (A) (to S.T.), and (C) (to K.T.); Grants-in-Aid for Scientific Research in Innovative Areas (to S.T.); and the Platform for Drug Discovery, Information, and Structural Life Science from the Ministry of Education, Culture, Sports, Science and Technology of Japan. This research was also supported by the Japan Science and Technology–Core Research for Evolutionary Science and Technology (to S.T.), the Japan New Energy and Industrial Technology Development Organization, and the National Institute of Biomedical Innovation (to Y.F.). Y.S., H.S., and A.T. screened claudin genes. Y.S. performed protein expression, purification, crystallization, and binding assays. K.I. assisted in crystallization. Y.S., H.S., and K.I. collected x-ray data. H.S. and K.T. processed diffraction data and solved and refined the structure. K.N. took electron microscopy images. Y.O. and A.T. collected fluorescence microscopy images. Y.S., H.S., K.T., S.T., and Y.F. wrote the manuscript, and all authors commented on the paper. S.T. and Y.F. supervised the research. The authors declare no competing financial interests. Coordinates and structure factors were deposited in the Protein Data Bank under accession number 3X29.

SUPPLEMENTARY MATERIALS

www.sciencemag.org/content/347/6223/775/suppl/DC1
Materials and Methods
Figs. S1 to S12
Tables S1 and S2
References (27–45)

29 September 2014; accepted 16 December 2014
10.1126/science.1261833

CHEMICAL BIOLOGY

A small-molecule inhibitor of the aberrant transcription factor CBF β -SMMHC delays leukemia in mice

Anuradha Illendula,^{1*} John A. Pulikkan,^{2*} Hongliang Zong,³ Jolanta Grembecka,⁴ Liting Xue,² Siddhartha Sen,³ Yunpeng Zhou,¹ Adam Boulton,¹ Aravinda Kuntimaddi,¹ Yan Gao,¹ Roger A. Rajewski,⁵ Monica L. Guzman,³ Lucio H. Castilla,^{2†} John H. Bushweller^{1†}

Acute myeloid leukemia (AML) is the most common form of adult leukemia. The transcription factor fusion CBF β -SMMHC (core binding factor β and the smooth-muscle myosin heavy chain), expressed in AML with the chromosome inversion inv(16)(p13q22), outcompetes wild-type CBF β for binding to the transcription factor RUNX1, deregulates RUNX1 activity in hematopoiesis, and induces AML. Current inv(16) AML treatment with nonselective cytotoxic chemotherapy results in a good initial response but limited long-term survival. Here, we report the development of a protein-protein interaction inhibitor, AI-10-49, that selectively binds to CBF β -SMMHC and disrupts its binding to RUNX1. AI-10-49 restores RUNX1 transcriptional activity, displays favorable pharmacokinetics, and delays leukemia progression in mice. Treatment of primary inv(16) AML patient blasts with AI-10-49 triggers selective cell death. These data suggest that direct inhibition of the oncogenic CBF β -SMMHC fusion protein may be an effective therapeutic approach for inv(16) AML, and they provide support for transcription factor targeted therapy in other cancers.

Acute myeloid leukemia (AML) is the most common form of adult leukemia (1). Long-term survival for AML remains poor and varies with the mutational composition of the leukemic cells. The transcription factor fusion CBF β -SMMHC (fusion of core binding factor β and smooth-muscle myosin heavy chain), expressed in AML with the chromosome inversion inv(16)(p13q22), cooperates with activating mutations in components of cytokine signaling pathways in leukemia transformation (2–5). CBF β is a component of the heterodimeric transcription factor core binding factor, where it binds to RUNX proteins and enhances their affinity for DNA (6), and the resulting complex plays a key role in regulating hematopoiesis (7). CBF β -SMMHC outcompetes CBF β for binding to RUNX1 (8), deregulates RUNX1 transcription factor activity in hematopoiesis, and induces AML. Current inv(16) AML treatment with nonselective cytotoxic chemotherapy results in a good initial response but limited long-term survival. Studies in mice and patient samples support the concept that inv(16) is a driver mutation that generates preleukemic progenitor cells that, upon acquisi-

tion of additional cooperating mutations, progress to leukemia (3, 4, 9–12).

To develop a targeted inhibitor of CBF β -SMMHC function, we used a previously described fluorescence resonance energy transfer (FRET) assay (13) with Venus-CBF β -SMMHC replacing Venus-CBF β (fig. S1) to screen the National Cancer Institute, NIH, Diversity Set for compounds that inhibit the binding of CBF β -SMMHC to the RUNX1 Runt domain. This screen identified the active compound AI-4-57 with a 50% inhibitory concentration (IC₅₀) of 22 μ M, whereas AI-4-88, a derivative lacking the methoxy functionality, is inactive (Table 1). Changes in the chemical shifts in a nuclear magnetic resonance (NMR) spectrum of a protein upon binding of a small molecule are a powerful method to confirm binding to a protein. We recorded two-dimensional 2D ¹⁵N-¹H heteronuclear single quantum coherence (HSQC) spectra and 1D saturation transfer difference (STD) NMR experiments of AI-4-57 with CBF β and the Runt domain. No interaction was observed for the Runt domain, but we can demonstrate chemical shift perturbations in the HSQC spectrum of CBF β upon addition of AI-4-57 (Fig. 1A) and no changes upon addition of the inactive derivative AI-4-88 (fig. S2), which establishes that the compound binds to CBF β . Chemical shift perturbations in the backbone and in two aromatic side chains [tryptophan at position 113 (W113) and tyrosine at position 96 (Y96)] indicate that the compound binds in a site spatially close to CBF β but not on the protein-protein interaction surface on CBF β , that is, it acts in an allosteric manner to inhibit binding (fig. S3).

We have shown that a reduced dosage of CBF β in the presence of a CBF β -SMMHC knockin al-

lele enhances leukemogenesis in mice (14) and argue that selectivity for CBF β -SMMHC versus CBF β is critical for in vivo utility. To achieve such specificity, we have taken advantage of the state of the two in solution: CBF β -SMMHC is oligomeric, whereas CBF β is monomeric (8, 15) and have applied the principles of polyvalency (16, 17) to develop derivatives of AI-4-57 with enhanced potency and selectivity (Fig. 1B). Substitutions at the five position of the pyridine ring do not affect activity (Table 1), so we have utilized polyethylene glycol-based linkers at this position to create bivalent derivatives with 5-, 7-, 10-, and 16-atom linker lengths (Table 1). Measurement of the IC₅₀ values with the FRET assay (Fig. 1C) shows that the five-atom linker compound has less activity, but the longer linker compounds show potent inhibition with the seven-atom linker inhibitor (AI-4-83) yielding a 350 nM IC₅₀, which corresponds to a 63-fold enhancement over the monovalent compound (Fig. 1D and Table 1). In addition, AI-4-83 achieves >10-fold dissociation of CBF β -SMMHC and RUNX1 Runt domain at saturating concentrations (Fig. 1D).

The activity of the bivalent inhibitors on cell growth was tested in three human leukemia cell lines [ME-1, inv(16) cell line; Kasumi-1, t(8;21) cell line; and U937, lymphoma cell line] by using a 3-(4,5-dimethylthiazol-2-yl)-2,5-diphenyltetrazolium bromide (MTT) conversion assay. Mimicking the results obtained with the FRET assay, even in terms of relative efficacy, growth of inv(16) cell line ME-1 was sensitive to compounds AI-4-71, AI-4-83, and AI-4-82 but not to AI-10-19 (Fig. 1E). In contrast, growth of non-inv(16) cell lines U937 and Kasumi-1 was unaffected over the same concentration range (fig. S4, A and B), which demonstrated a high degree of specificity and suggested that the activity of these bivalent compounds was on target.

Analysis of the pharmacokinetic properties of AI-4-57 showed that the compound has a short half-life ($t_{1/2}$ = 37 min) in mouse plasma (fig. S5) and that loss of the methyl group from the methoxy functionality is the primary metabolite. Trifluoromethoxy (CF₃O) substitutions have been shown to be less reactive (18, 19), so we synthesized AI-10-47 with this substitution. FRET measurements show that this substitution actually enhances the activity of the monovalent compound (Table 1). Measurements of stability in liver microsomes showed that AI-10-47 reduced the metabolic liability and so justified the synthesis of the bivalent derivative AI-10-49 (Table 1). AI-10-49 is potent (FRET IC₅₀ = 260 nM) (Table 1) [isothermal titration calorimetry (ITC) measurements yielded a dissociation constant (K_D) = 168 nM] (fig. S6), has improved in vivo pharmacokinetic properties ($t_{1/2}$ = 380 min) (fig. S5), and has enhanced inhibitory activity on ME-1 cell growth (IC₅₀ = 0.6 μ M) (Fig. 1F) compared with the parent protonated bivalent compound AI-4-83 (IC₅₀ of ~3 μ M) (Fig. 1E). Note that AI-10-49 showed negligible activity (IC₅₀ > 25 μ M) in normal human bone marrow cells (Fig. 1G), which indicated a robust potential therapeutic window. In a panel of 11 human leukemia cell lines, ME-1 cells were

¹Department of Molecular Physiology and Biological Physics, University of Virginia, Charlottesville, VA 22908, USA.

²Program in Gene Function and Expression, University of Massachusetts Medical School, Worcester, MA 01605, USA.

³Department of Medicine, Weill Medical College of Cornell University, New York, NY 10065, USA. ⁴Department of Pathology, University of Michigan, Ann Arbor, MI 48109, USA.

⁵Department of Pharmaceutical Chemistry, University of Kansas, Lawrence, KS 66045, USA.

*These authors contributed equally to this work. †Corresponding author. E-mail: jhb4v@virginia.edu (J.H.B.); Lucio.Castilla@umassmed.edu (L.C.)

the only cell line highly sensitive to AI-10-49 (fig. S7).

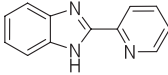
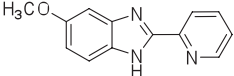
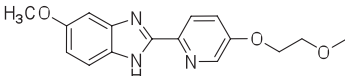
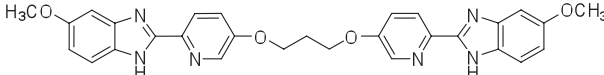
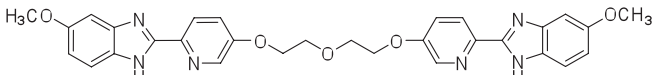
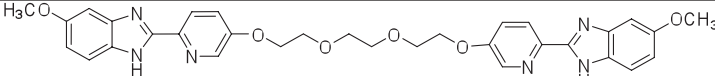
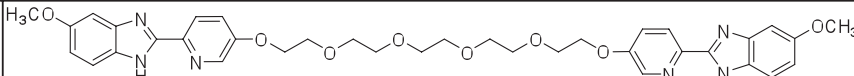
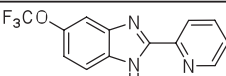
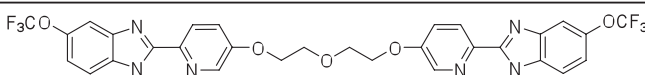
The specificity of AI-10-49 in disrupting endogenous RUNX1 binding to CBFβ-SMMHC versus CBFβ was assessed in ME-1 cells. AI-10-49 effectively dissociated RUNX1 from CBFβ-SMMHC, with 90% dissociation after 6 hours of treatment, whereas it had only a modest effect on CBFβ-RUNX1 association (Fig. 2A). The stability of RUNX1, CBFβ, and CBFβ-SMMHC was not affected by AI-10-49 (fig. S8A). Expression of the RUNX1-regulated genes *RUNX3*, *CSF1R*, and *CEBPA* is repressed by CBFβ-SMMHC in inv(16) AML (20–22). Previous studies have shown decreased RUNX1 binding to target genes in the presence of CBFβ-SMMHC (23, 24), which suggests that CBFβ-SMMHC represses RUNX1 target genes by blocking binding of RUNX1 to target DNA sites (Fig. 2B). Consistent with this model, chromatin-immunoprecipitation (ChIP) assays showed that treatment of ME-1 cells for 6 hours with AI-10-49 increased RUNX1 occupancy 8-, 2.2-, and 8-fold at the *RUNX3*, *CSF1R*, and *CEBPA* promoters, respectively, whereas no enrichment was observed at control loci (Fig. 2C and fig. S8, B and C). In accordance with this, treatment of ME-1 cells for 6 or 12 hours with AI-10-49 increased expression of *RUNX3*, *CSF1R*, and *CEBPA* but had no effect on control gene *PIN1* (Fig.

2D). Neither of these effects was observed in inv(16)-negative U937 cells. These data establish AI-10-49 selectivity in inhibiting CBFβ-SMMHC binding to RUNX1 and validate our approach of using bivalent inhibitors to achieve this specificity.

Up to 90% of inv(16) AML patients have cooperating mutations in components of the receptor tyrosine kinase pathway, including N-RAS and c-Kit (25). We have recently developed an efficient mouse model of inv(16) AML, by combining the conditional *Nras^{LSL-G12D}* and *Cbfb^{MYH11}* alleles (26). To test the effects of AI-10-49 administration in vivo, we transplanted mice with *Cbfb^{+/MYH11}; Ras^{+/G12D}* leukemic cells, waited 5 days for engraftment, and then treated mice with vehicle [dimethyl sulfoxide (DMSO)] or 200 mg/kg of body weight AI-10-49 for 10 days, and assessed the effect on disease latency. As shown in Fig. 3A, vehicle-treated mice succumbed to leukemia with a median latency of 33.5 days, whereas AI-10-49-treated mice survived significantly longer (median latency = 61 days; *P* = 2.7×10^{-6}). Thus, transient treatment with AI-10-49 reduces leukemia expansion in vivo. Although we have not assessed toxicity after long-term exposure, after 7 days of administration of AI-10-49, we observe no evidence of toxicity (figs. S9 to S11).

To test the potential utility of AI-10-49 for use in human inv(16) leukemia treatment, we evaluated the survival of four primary inv(16) AML cell samples treated for 48 hours with a dose range of monovalent AI-10-47 and bivalent AI-10-49. As shown in Fig. 3B, the viability of inv(16) patient cells was reduced by treatment with AI-10-49 at 5 and 10 μM concentrations (individual dose-response experiments are shown in fig. S12). Note that the bivalent AI-10-49 was more potent than the monovalent compound AI-10-47 and so recapitulated the effects observed in the human inv(16) cell line ME-1. In contrast, the viability of normal karyotype AML samples was not affected by AI-10-49 treatment (Fig. 3C). Analysis of an additional set of five AML samples revealed that AI-10-49 treatment specifically reduces the viability of inv(16) leukemic cells without having an apparent effect on their differentiation (fig. S13). AI-10-49 specificity was also evident when we assessed the ability of AML cells to form colonies by evaluating colony-forming units (CFUs) after compound exposure. The ability of inv(16) AML cells to form CFUs was selectively reduced by AI-10-49 when compared with normal karyotype and t(8;21) AML patient samples (Fig. 3D). This inhibitory effect was dose-dependent (40 and 60% at 5 and 10 μM, respectively) (Fig. 3E),

Table 1. Chemical structures and IC₅₀ values of AI-10-49 and related compounds, determined by using the FRET assay.

Compound Name	Compound Structure	FRET IC ₅₀ (μM)
AI-4-88		>240
AI-4-57		22 ± 8
AI-10-11		14 ± 4
AI-10-19		>2.5
AI-4-83		0.35 ± 0.05
AI-4-82		0.44 ± 0.07
AI-4-71		0.37 ± 0.07
AI-10-47		2.0 ± 0.3
AI-10-49		0.26 ± 0.01

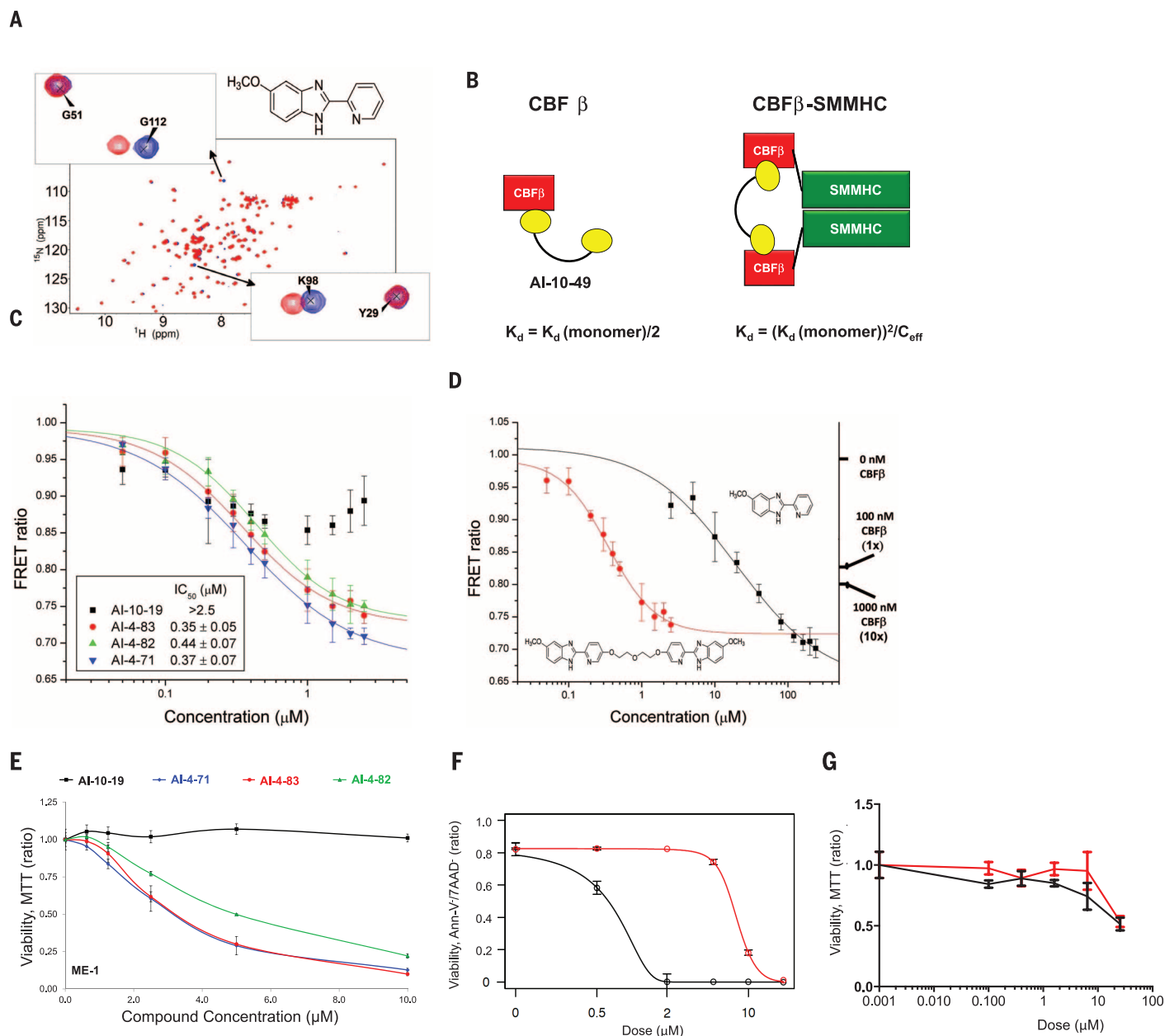


Fig. 1. Development of potent selective inhibitor of CBF β -SMMHC-RUNX binding. (A) ^{15}N - ^1H HSQC spectrum (peaks correspond to all NH moieties of protein) of CBF β alone (blue) and CBF β + AI-4-57 (red). (B) Schematic diagram for the application of polyvalency to develop a specific and potent inhibitor of CBF β -SMMHC-RUNX binding. Equations refer to predicted K_D values for a bivalent inhibitor binding to CBF β and CBF β -SMMHC. C_{eff} is the effective local concentration, which depends on the distance between CBF β domains in the oligomeric CBF β -SMMHC. (C) FRET assay measurements for bivalent inhibitors with varying linker lengths with 10 nM Cerulean-Runt domain and 10 nM Venus-CBF β -SMMHC. The y axis is the ratio of emission intensities at 525 and 474 nm. Three independent measurements were performed, and their average and standard deviation were used for IC_{50} data fitting. (D) FRET assay measurements of inhibition of CBF β -SMMHC-RUNX binding for AI-4-57 and AI-4-83 with 10 nM Cerulean-Runt domain and 10 nM Venus-CBF β -SMMHC. Data for AI-4-83 are the same as presented in (C). Data for these two compounds are presented separately for

clarity of comparison to one another. Left y axis is the ratio of emission intensities at 525 and 474 nm. Right y axis indicates the FRET ratios observed with addition of 100 nM and 1000 nM untagged CBF β , corresponding to roughly 1-fold and 10-fold dissociation of CBF β -SMMHC and Runt domain [CBF β -SMMHC binds with 7-fold the affinity of CBF β (8)]. Three independent measurements were performed, and their average and standard deviation were used for IC_{50} data fitting. (E) Dose-dependent effect of a 24-hour treatment of ME-1 cells with bivalent inhibitors with varying linker lengths measured by MTT assay and normalized to the DMSO-treated group. Each symbol represents the mean of triplicate experiments; error bars represent the SD. (F and G) Dose-dependent effect of AI-10-47 (red) and AI-10-49 (black) treatment for 48 hours; (F) ME-1 cells were assessed by annexin V and 7-amino-actinomycin (7AAD) viability staining, and (G) human bone marrow cells were assessed by MTT assay. The data were normalized to the DMSO-treated group. Each data point represents the mean of triplicate experiments; error bars represent the SD.

whereas there was no change in CFUs of AML cells treated with AI-10-47, AML cells with normal karyotype (Fig. 3F), or CD34+ cord blood cells (Fig. 3G). These studies show that AI-10-49 selectively inhibits viability and CFU capacity in *inv(16)* AML blasts, whereas it has negligible effects on AML blasts with normal karyotype or, importantly, on normal human hematopoietic progenitors.

Dysregulated gene expression is a hallmark of cancer and is particularly important for the maintenance of cancer stem-cell properties, such as self-renewal, which lead to relapse. As such, the targeting of proteins that drive transcriptional dysregulation, so-called “transcription therapy,” represents an avenue for drug development with immense potential. A number of fusion pro-

teins involving transcription factors have been identified as drivers of disease in leukemia (27); sarcoma (28); and, recently, in prostate cancer (29), which provide excellent targets for therapeutic intervention. Our results provide a proof-of-principle for this approach, as AI-10-49 specifically inhibits CBF β -SMMHC-RUNX binding and shows efficacy against CBF β -SMMHC-driven leukemia in mice with no obvious side effects. Specificity of action is a key component in the development of a targeted drug. Imatinib, for example, shows excellent specificity, and its efficacy in chronic myelogenous leukemia is clearly a result of effective inhibition of the BCR-ABL fusion protein that drives chronic myelogenous leukemia. However, even this highly selective agent inhibits both the BCR-ABL fusion protein, as well as wild-type ABL

The “Holy Grail,” as it were, of targeted therapy with fusion or mutated protein drivers of cancer is to achieve inhibition of the fusion or mutated protein with little to no effect on the wild-type protein. This study demonstrates that AI-10-49 represents an example of such selectivity for *inv(16)* leukemia, as it inhibits CBF β -SMMHC activity while having a minimal effect on CBF β function. There are relatively few examples of drugs targeting transcription factors. ATRA (*all-trans-retinoic acid*) for RAR (retinoic acid receptor) fusions in leukemia and MDM2-p53 inhibitors are successful examples; however, neither of these has the selectivity of AI-10-49. In addition, AI-10-49 has the key properties of a high-quality chemical probe recently outlined by Frye (30)—namely, a clear molecular profile of activity, mechanism of

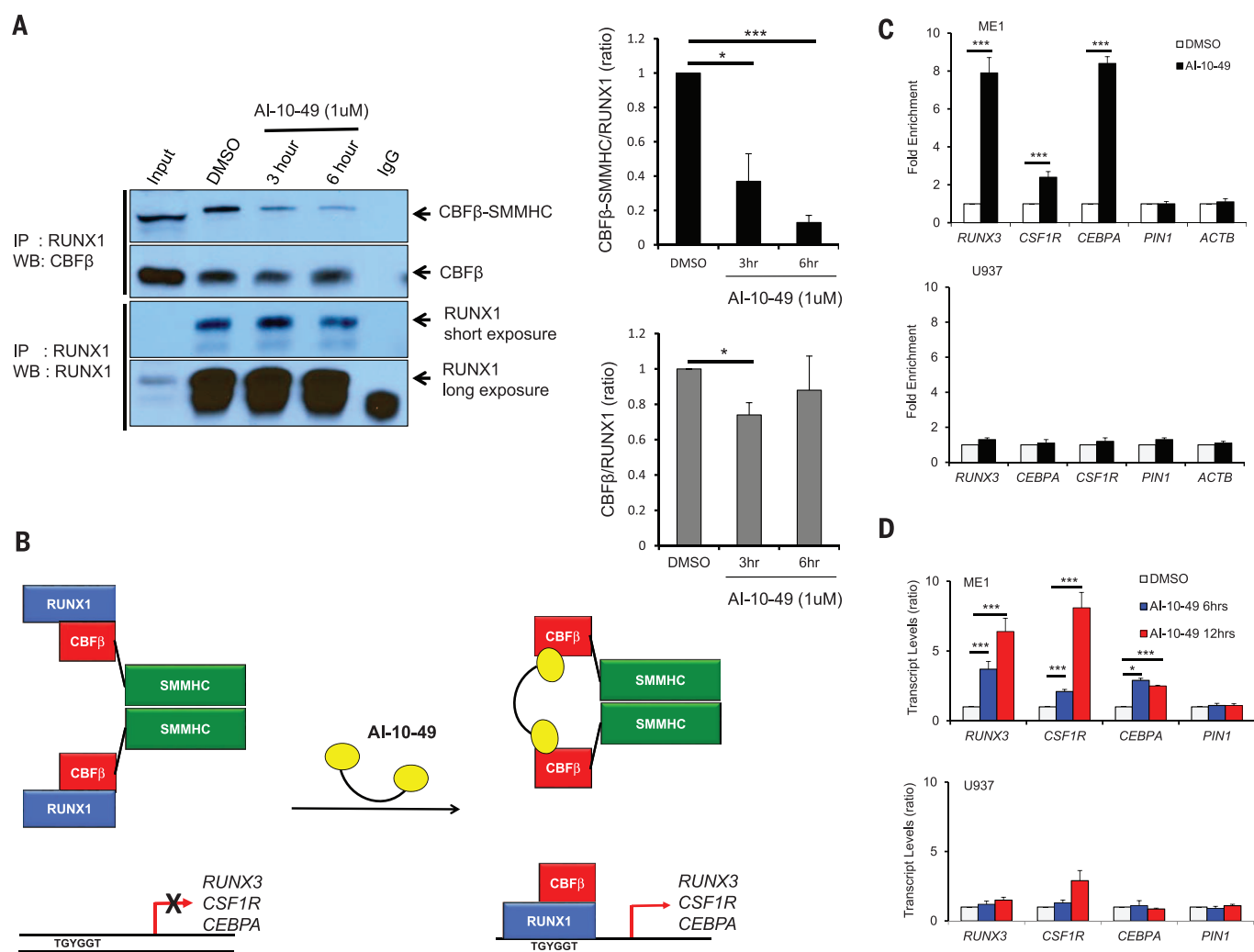


Fig. 2. Specificity of AI-10-49 activity on CBF β -SMMHC-RUNX1 binding. (A) Effect of 1 μ M AI-10-49 on CBF β -RUNX1 and CBF β -SMMHC-RUNX1 binding at 3 and 6 hours in ME-1 cells, measured by coimmunoprecipitation (quantification of three experiments is shown on the right). (B) Schematic of the effect of CBF β -SMMHC on RUNX1 occupancy and target gene expression and the effect of AI-10-49 on occupancy and expression. (C) Chromatin immunoprecipitation assay showing RUNX1 occupancy on *RUNX3*, *CSF1R*, and *CEBPA* in ME-1 and U937 cells treated with 1 μ M AI-

10-49 for 6 hours and represented as fold enrichment relative to DMSO-treated cells. Each symbol represents the mean of triplicate experiments; error bars represent the SD. (D) Relative expression (qRT-PCR) of *RUNX3*, *CSF1R*, and *CEBPA* in ME-1 and U937 cells treated with 1 μ M AI-10-49 for 6 and 12 hours, and normalized to the DMSO control group. Each symbol represents the mean of triplicate experiments; error bars represent the SD. For all panels, significance was calculated as unpaired *t*-test, **P* < 0.05, or ****P* < 0.001.

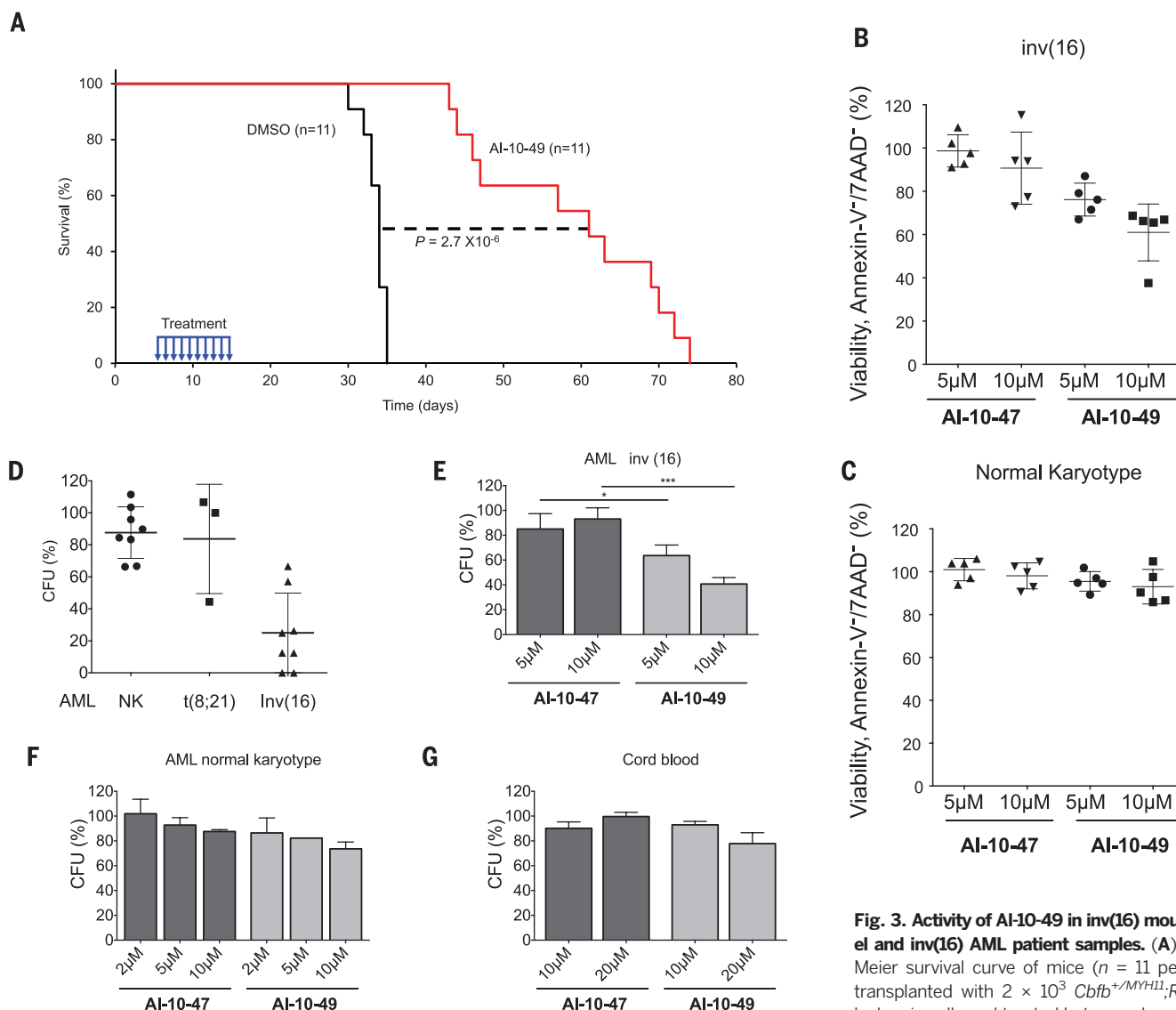


Fig. 3. Activity of AI-10-49 in *inv(16)* mouse model and *inv(16)* AML patient samples. (A) Kaplan-Meier survival curve of mice ($n = 11$ per group) transplanted with 2×10^3 *Cbfb*^{+/MYH11};*Ras*^{+/G12D} leukemic cells and treated between days 5 and 15 posttransplantation (blue arrows) with DMSO (black

line) or 200 mg/kg of body weight per day AI-10-49 (red line); Statistics described in the statistical methods section. (B) Percent viability (annexin V and 7AAD assay) relative to vehicle control (DMSO) for CD34⁺ purified primary human *inv(16)* AML samples treated for 48 hours with either AI-10-49 or AI-10-47 at the indicated concentrations. Each symbol represents the average for an individual sample from duplicate treatments. The line represents the mean; error bars represent the SD. (C) Percent viability (annexin V and 7AAD assay) relative to vehicle control (DMSO) for primary human AML samples with normal karyotype treated for 48 hours with either AI-10-49 or AI-10-47 at the indicated concentrations. Each symbol represents the average for an individual sample from duplicate treatments. The line represents the mean of all biological replicates; error bars represent the SD. (D) Percentage of colony-forming units (CFUs) after treatment with AI-10-49 relative to vehicle control (DMSO) for primary human AML cells. Each symbol represents the average for an individual sample from duplicate treatments; error bars represent the SD. (E) Percent CFUs to vehicle control (DMSO) for CD34⁺ purified primary human *inv(16)* AML samples treated with either AI-10-49 or AI-10-47 at the indicated concentrations. CFU assays were performed in triplicate. Error bars represent the SD. (F) Percent CFUs to vehicle control (DMSO) for CD34⁺ purified primary human AML samples with normal karyotype treated with either AI-10-49 or AI-10-47 at the indicated concentrations. CFU assays were performed in triplicate. Error bars represent the SD. (G) Percent CFUs to vehicle control (DMSO) for CD34⁺ purified primary CD34⁺ cord blood cells treated with either AI-10-49 or AI-10-47 at the indicated concentrations. Significance calculated as unpaired *t* test, * $P < 0.05$ or *** $P < 0.001$.

action, identity of active species, and proven utility. Development of agents, like AI-10-49, which can inhibit the driver mutation(s) in specific types of cancer, is essential for better therapeutic outcomes for patients.

In summary, AI-10-49 is a potent and specific first-generation CBF β -SMMHC lead compound that induces cell death in *inv(16)* leukemic cells. The work described here provides additional

evidence that transcription factor drivers of cancer can be directly targeted.

REFERENCES AND NOTES

- C. C. Kumar, *Genes Cancer* **2**, 95–107 (2011).
- P. Liu et al., *Science* **261**, 1041–1044 (1993).
- L. H. Castilla et al., *Nat. Genet.* **23**, 144–146 (1999).
- L. H. Castilla et al., *Proc. Natl. Acad. Sci. U.S.A.* **101**, 4924–4929 (2004).
- F. Ravandi, A. K. Burnett, E. D. Agura, H. M. Kantarjian, *Cancer* **110**, 1900–1910 (2007).
- N. Adya, L. H. Castilla, P. P. Liu, *Semin. Cell Dev. Biol.* **11**, 361–368 (2000).
- M. F. de Bruijn, N. A. Speck, *Oncogene* **23**, 4238–4248 (2004).
- S. M. Lukasik et al., *Nat. Struct. Biol.* **9**, 674–679 (2002).
- Y. H. Kuo et al., *Cancer Cell* **9**, 57–68 (2006).
- P. D. Kottaridis et al., *Blood* **100**, 2393–2398 (2002).
- L. Y. Shih et al., *Leukemia* **22**, 303–307 (2008).
- Y. Nakano et al., *Br. J. Haematol.* **104**, 659–664 (1999).
- M. J. Gorczyński et al., *Chem. Biol.* **14**, 1186–1197 (2007).

14. S. A. Heilman, Y. H. Kuo, C. S. Goudswaard, P. J. Valk, L. H. Castilla, *Cancer Res.* **66**, 11214–11218 (2006).
15. X. Huang, J. W. Peng, N. A. Speck, J. H. Bushweller, *Nat. Struct. Biol.* **6**, 624–627 (1999).
16. M. Mammen, S. K. Choi, G. M. Whitesides, *Angew. Chem. Int. Ed.* **37**, 2754–2794 (1998).
17. L. L. Kiessling, J. E. Gestwicki, L. E. Strong, *Angew. Chem. Int. Ed. Engl.* **45**, 2348–2368 (2006).
18. F. R. Leroux, B. Manteau, J. P. Vors, S. Pazenok, *Beilstein J. Org. Chem.* **4**, 13 (2008).
19. B. Manteau, S. Pazenok, J. P. Vors, F. R. Leroux, *J. Fluor. Chem.* **131**, 140–158 (2010).
20. C. K. Cheng et al., *Blood* **112**, 3391–3402 (2008).
21. H. Guo, O. Ma, N. A. Speck, A. D. Friedman, *Blood* **119**, 4408–4418 (2012).
22. D. E. Zhang et al., *Mol. Cell. Biol.* **14**, 8085–8095 (1994).
23. W. Cao et al., *Oncogene* **15**, 1315–1327 (1997).
24. J. Markus et al., *Cancer Res.* **67**, 992–1000 (2007).
25. C. Haferlach et al., *Leukemia* **24**, 1065–1069 (2010).
26. L. Xue, J. A. Pulikkan, P. J. Valk, L. H. Castilla, *Blood* **124**, 426–436 (2014).
27. A. T. Look, *Science* **278**, 1059–1064 (1997).
28. M. Ladanyi, *Diagn. Mol. Pathol.* **4**, 162–173 (1995).
29. D. Hessels, J. A. Schalken, *Curr. Urol. Rep.* **14**, 214–222 (2013).
30. S. V. Frye, *Nat. Chem. Biol.* **6**, 159–161 (2010).

ACKNOWLEDGMENTS

We thank P. Bradley for assisting in the linker-length analyses in cell lines, R. Delwel for providing patient AML cells, and L. Zhu for performing the statistical analysis of mouse transplantation studies. This work was supported by grants from the National Cancer Institute, NIH (R01 CA140398), to J.H.B., L.H.C., and R.A.R.; (R01 CA096983) to L.H.C.; and a Specialized Center of Research grant from the Leukemia and Lymphoma Society to J.H.B.

(SCOR 7006). L.H.C. is the recipient of a Scholar Award from the Leukemia & Lymphoma Society (grant 1334-08) and J.A.P. of a Scholar Award from the American Society of Hematology. M.L.G. is funded by the NIH through the NIH Director's New Innovator Award Program, 1 DP2 OD007399-01. J.H.B., A.I., and J.G. are coinventors on a U.S. patent (US8748618 B2) for AI-10-49 and related analogs. A patent application (10775546.4) has also been filed in Europe.

SUPPLEMENTARY MATERIALS

www.sciencemag.org/content/347/6223/779/suppl/DC1
Materials and Methods
Figs. S1 to S13
References (31–35)

9 October 2014; accepted 23 December 2014
10.1126/science.aaa0314

HUMORAL IMMUNITY

Apoptosis and antigen affinity limit effector cell differentiation of a single naïve B cell

Justin J. Taylor,^{1,2*} Kathryn A. Pape,¹ Holly R. Steach,² Marc K. Jenkins¹

When exposed to antigens, naïve B cells differentiate into different types of effector cells: antibody-producing plasma cells, germinal center cells, or memory cells. Whether an individual naïve B cell can produce all of these different cell fates remains unclear. Using a limiting dilution approach, we found that many individual naïve B cells produced only one type of effector cell subset, whereas others produced all subsets. The capacity to differentiate into multiple subsets was a characteristic of clonal populations that divided many times and resisted apoptosis, but was independent of isotype switching. Antigen receptor affinity also influenced effector cell differentiation. These findings suggest that diverse effector cell types arise in the primary immune response as a result of heterogeneity in responses by individual naïve B cells.

Antibody production results from a differentiation process that begins when the surface form of immunoglobulin (Ig) known as the B cell receptor (BCR) on a naïve B cell binds an antigen (1, 2). BCR signaling causes the B cell to migrate to the border of the T cell zone, where it receives signals from T cells (3, 4). These signals cause the B cell to proliferate and differentiate into several types of effector cells, including short-lived plasma cells, germinal center (GC) cells, and GC-independent memory cells (1, 2). GC cells then undergo somatic hypermutation in their Ig genes, and cells with mutations that improve BCR affinity for antigen are selected to become GC-dependent memory or plasma cells (1, 2).

Despite the importance of this process to immunity and vaccination, it is unclear how individual naïve B cells simultaneously produce all of the early effector cell types. Some studies suggest that different naïve B cell clones only produce a single ef-

fector subset, depending on BCR affinity for antigen (5–8) or intrinsic stochastic biases of the responding clonal population (9). Alternatively, each naïve B cell may produce all effector cell types, as suggested by recent work on naïve T cells (10–13).

We addressed these possibilities by tracking the fates of antigen-specific naïve B cells during the primary immune response to the protein antigen allophycocyanin (APC). Using a sensitive antigen-based cell enrichment method (14), we found that the spleen and lymph nodes of a C57BL/6 (B6) mouse contained about 4000 polyclonal APC-specific naïve B cells, which produced ~100,000 effector cells 7 days after immunization with APC in complete Freund's adjuvant (CFA) (Fig. 1, A and B). As expected, the effector cell population consisted of B220^{low} Ig^{high} antibody-secreting plasma cells, CD38⁺ GL7⁺ GC cells, CD38⁺ GL7⁺ memory cells, and a few remaining undifferentiated CD38⁺ GL7⁺ activated precursors (APs) (15) (Fig. 1, C and D, and fig. S1).

In vivo limiting dilution was used to assess the multipotentiality of a single APC-specific naïve B cell. Before limiting dilution could be achieved, it was necessary to determine the fraction of APC-specific naïve B cells that responded to immuni-

zation. Twenty million B cells from CD45.1⁺ mice that were never exposed to APC were labeled with the cell division-tracking dye carboxyfluorescein succinimidyl ester (CFSE) (16) and transferred into CD45.2⁺ recipients. Donor-derived APC-specific B cells were CFSE^{high} 7 days after immunization with CFA alone, which is indicative of cells that had not divided (Fig. 1E). After the injection of APC in CFA, most donor APC-specific B cells were CFSE^{low}, and the CFSE^{high} population was 33% smaller than in mice injected with CFA alone (Fig. 1, E and F). These results indicated that one in three APC-specific naïve B cells, or 1 in 60,000 total B cells, proliferated in mice immunized with APC. The 33% response frequency of APC-specific naïve B cells was not a limitation of the CFSE dilution assay, because 97 to 100% of naïve MD4 B cells proliferated (fig. S2) after the injection of hen egg lysozyme (HEL) or duck egg lysozyme (DEL), for which the MD4 BCR has a high or medium affinity, respectively (17). Thus, the 33% responder frequency was a feature of the polyclonal APC-specific B cell population under these immunization conditions.

Limiting dilution experiments were then performed, based on the above knowledge and the fact that $7.7 \pm 2.8\%$ ($n = 116$ recipients) of donor naïve B cells survive after transfer: 2×10^6 or 0.2×10^6 CD45.1⁺ B cells were transferred into CD45.2⁺ mice, with the expectation that an average of 3.3 or 0.33 APC-responsive CD45.1⁺ naïve B cells would survive per recipient. Seven days after APC immunization, mice that did not receive transferred B cells contained two or fewer CD45.1⁺ background events (Fig. 2A). All mice that received 2×10^6 B cells contained a defined population of CD45.1⁺ donor-derived APC-specific B cells that had proliferated in response to APC (Fig. 2, A and B). In contrast, 19% (74 out of 384) of mice that received the limiting number of 0.2×10^6 B cells contained donor-derived APC-responsive B cells (Fig. 2, B and C). Based on the Poisson distribution (18), over 91% of the donor-derived populations in this group were the progeny of a single naïve B cell.

Extensive effector cell heterogeneity was observed in the progeny of individual naïve B cells. Single naïve B cells produced between 4 and 957 progeny, with a median of 16 (Fig. 2C). The polyclonal naïve cell populations of recipient origin

¹Department of Microbiology, Center for Immunology, University of Minnesota Medical School, Minneapolis, MN 55455, USA.

²Vaccine and Infectious Disease Division, Fred Hutchinson Cancer Research Center, Seattle, WA 98019, USA.

*Corresponding author. E-mail: jtaylor3@fhcr.org

produced all effector cell subsets, but 35 of the 74 clonal populations (44%) contained only plasma cells, only GC cells, only GC-independent memory

cells, or only AP cells (Fig. 2, D and E). Four clonal populations contained all four subsets, and many contained two or three.

Large clonal populations were more likely to contain multiple subsets. The clonal populations that contained all four subsets had a median of

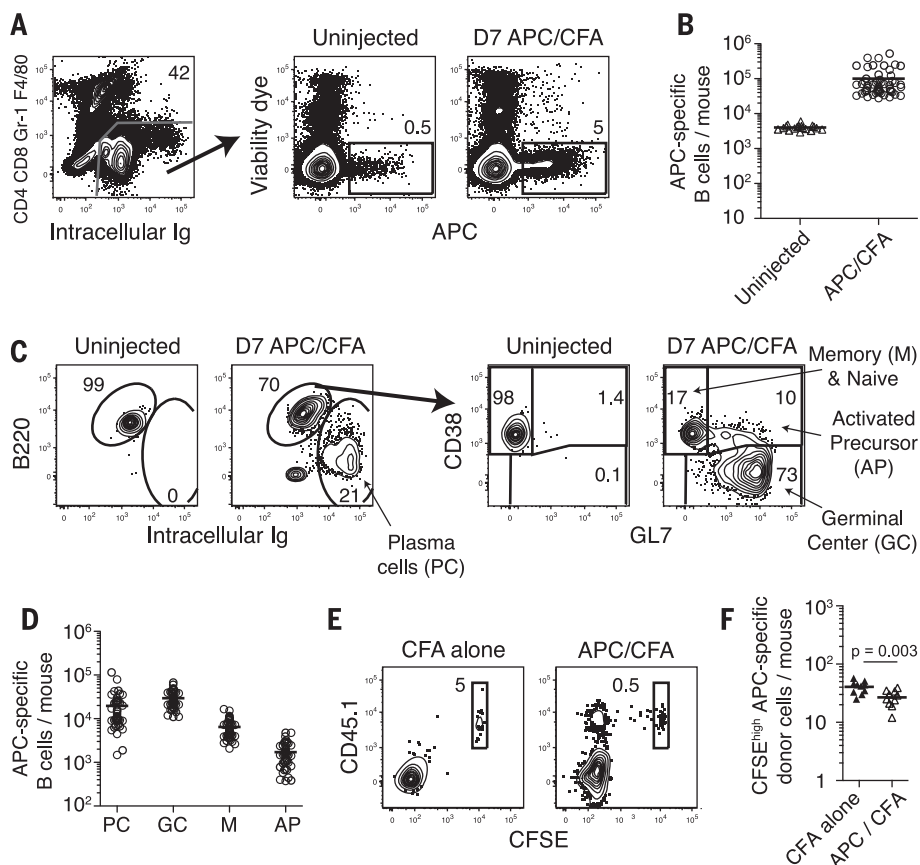


Fig. 1. Assessing the polyclonal APC-specific B cell response. (A) Detection and (B) quantitation of APC-specific B cells from pooled spleen and lymph node samples enriched using anti-APC microbeads from naïve mice ($n = 18$) or mice immunized with APC in CFA ($n = 45$) 7 days earlier. (C) Detection and (D) quantitation of APC-specific plasma cells (Ig^{high}), GC ($\text{Ig}^{\text{+}} \text{B220}^{\text{+}} \text{CD38}^{\text{+}} \text{GL7}^{\text{+}}$), naïve/memory (M) ($\text{Ig}^{\text{+}} \text{B220}^{\text{+}} \text{CD38}^{\text{+}} \text{GL7}^{\text{+}}$), and AP B cells ($\text{Ig}^{\text{+}} \text{B220}^{\text{+}} \text{CD38}^{\text{+}} \text{GL7}^{\text{+}}$). Memory B cells were quantitated by the increase in $\text{CD38}^{\text{+}} \text{GL7}^{\text{+}}$ cells over uninjected controls. (E) Detection and (F) quantitation of $\text{CFSE}^{\text{high}}$ $\text{CD45.1}^{\text{+}}$ APC-specific B cells from $\text{CD45.2}^{\text{+}}$ mice that received 2×10^7 donor $\text{CD45.1}^{\text{+}}$ B cells before immunization with APC in CFA, or CFA alone ($n = 10$). Numbers on the flow cytometry plots in (A), (C), and (E) reflect the percent of cells within the gated population. These percentages and knowledge of the total number of B cells in the enriched fraction were used to calculate the number of cells shown in (B), (D), and (F). The bars represent the mean and P values determined using an unpaired two-tailed Student's t test. Data points were combined from two to six experiments.

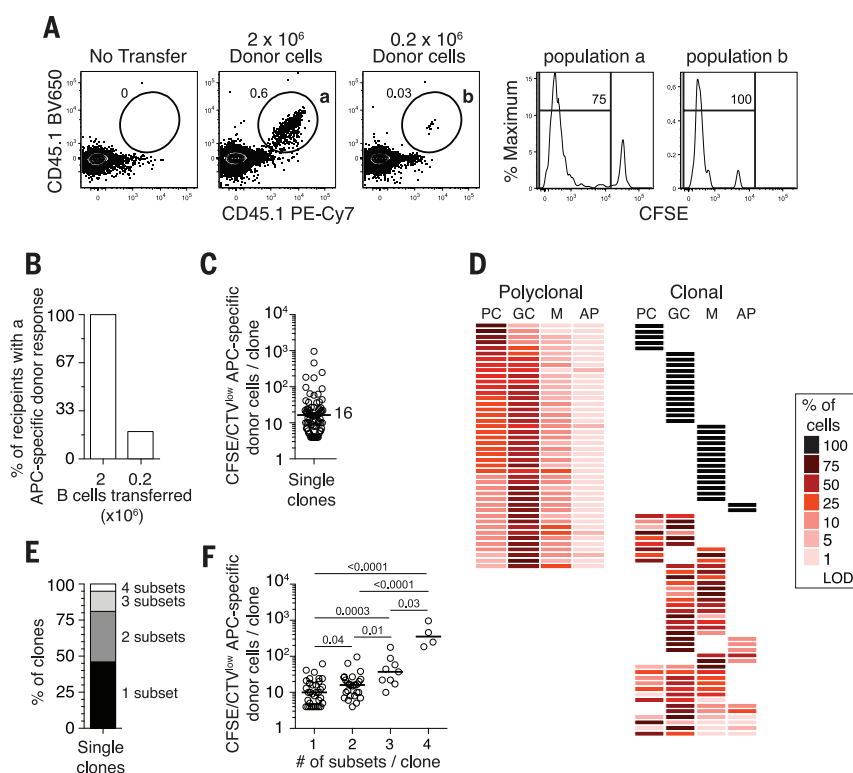


Fig. 2. Assessing the response of an individual naïve APC-specific B cell. (A) Detection of APC-specific donor cells from $\text{CD45.2}^{\text{+}}$ recipients that received 0.2 or 2×10^6 CFSE or Celltrace violet (CTV)-labeled $\text{CD45.1}^{\text{+}}$ B cells 1 to 3 days before immunization with APC in CFA. Samples were analyzed 7 days after immunization, after simultaneous CD45.1 and APC-based cell enrichment. The fourth and fifth plots show CFSE profiles for gated populations a and b from the second and third plots. Numbers on the plots reflect the percent of cells within the gated population. (B) Frequency of immunized recipient mice ($n = 6$ for mice that received 2×10^6 cells or $n = 384$ for those that received 0.2×10^6) containing an APC-specific $\text{CFSE/CTV}^{\text{low}}$ donor population above the limit of detection (LOD) of two cells. (C) Total number of cells in APC-specific clonal populations from 74 mice that received 0.2×10^6 cells and contained a population above the LOD. (D) Frequency of each subset within polyclonal or clonal APC-specific populations. Subsets are gated as shown in Fig. 1C, and each row depicts an individual clone ($n = 74$) or the entire APC-specific population from a mouse ($n = 45$). (E) Frequency of APC-specific clones generating one, two, three, or four subsets. (F) Total number of cells produced by each clone, separated into groups based on the number of subsets produced. A Mann-Whitney test was used to generate the P values. Bars in (C) and (F) represent medians. Data points were combined from 12 experiments.

352 cells, whereas the populations that contained only one had a median of 10 cells (Fig. 2F). No relationship was observed between the size of a clonal population and the frequency of cells in it that divided seven or more times (Fig. 3, A and B). This finding pointed toward cell death

as a basis for the differences in clonal population size. Consistent with the idea that cell death limits population size, most clonal populations contained less than 20% of the minimum number of daughter cells expected based on their CFSE profile (Fig. 3C). This effect was not uni-

form across all populations. Large clonal populations that contained all four subsets exceeded the expected minimum number of daughter cells, whereas the small populations that contained only one subset had a median of only 12% (Fig. 3D).

Fig. 3. Assessing proliferation and apoptosis of APC-specific clones. (A) Frequency of cells in each CFSE/CTV division bin (Div) in wild-type ($n = 74$) or Bim-deficient ($n = 34$) APC-specific clonal populations. Clones are displayed in the same order as in Fig. 2D. (B) Total number of cells detected for each wild-type (open circle) or Bim-deficient (black triangle) clone compared to the frequency of cells completing at least seven divisions. (C and D) Number of cells detected for each clone displayed as a percentage of the minimum number predicted based on CFSE/CTV dilution analysis, with the clones grouped in (D) based on the number of subsets produced. (E) Total number of cells produced by APC-specific Bim-deficient clones. (F and G) Frequency of clones that produced (F) the indicated number or types of subsets or (G) any of the indicated subset. The bars in (C) to (E) represent medians. P values were determined in (C) and (D) using a Mann-Whitney test and in (F) and (G) using Fisher's exact test. Data points were combined from 3 to 12 experiments.

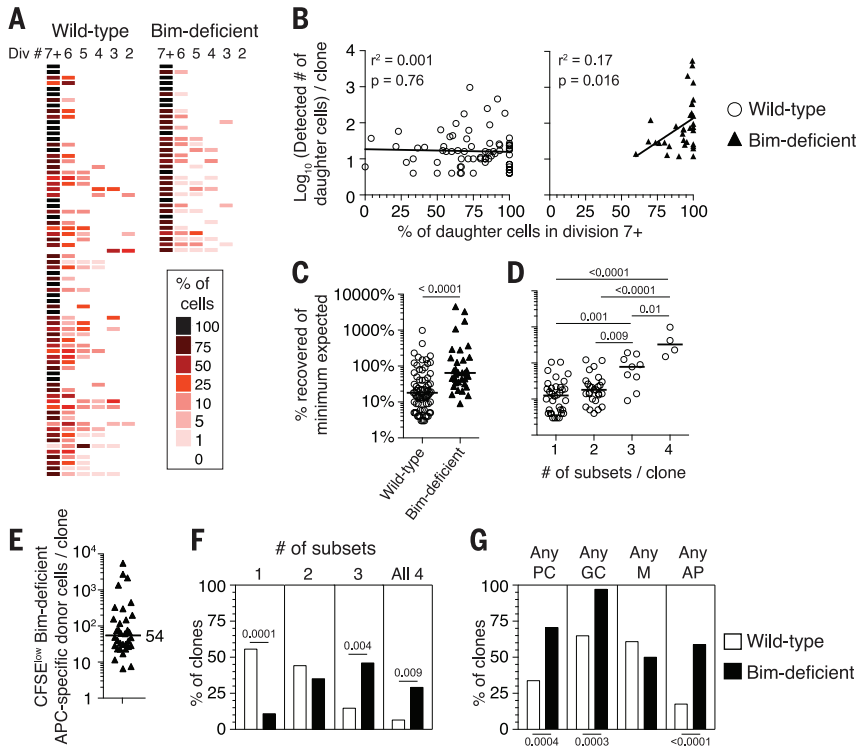
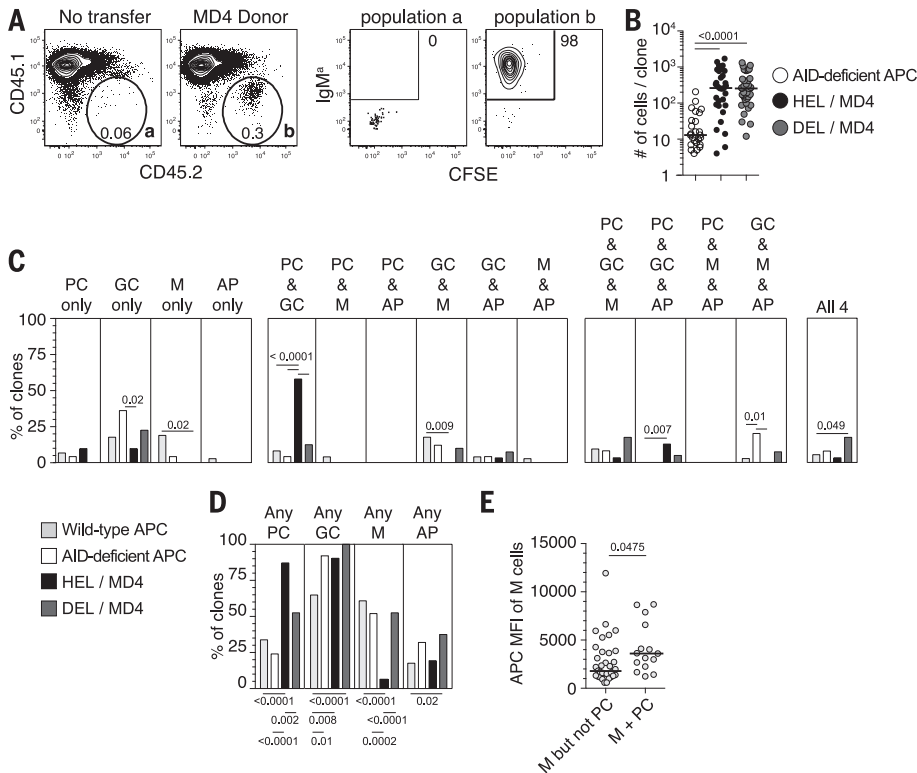


Fig. 4. Assessing the response of an individual BCR transgenic B cell. (A) Representative detection of CD45.2⁺ IgM^a CFSE^{low} donor cells from recipients of a limited number (5 to 15 cells) of MD4 *Rag1*^{-/-} B cells 1 to 3 days before immunization with HEL-OVA or DEL-OVA in CFA. Samples were analyzed 7 days after immunization after CD45.2-based cell enrichment. The second and third plots show gated populations a and b from the first and second plots. Numbers on the plots reflect the percent of cells within the gated population. (B) Total number of cells in HEL-stimulated MD4 (black circles, $n = 31$), MD4 DEL-stimulated (gray circles, $n = 40$), or AID-deficient APC-specific (white circles, $n = 27$) clonal populations generated by immunization. (C and D) Frequency of clones that produced (C) the indicated subset combinations or (D) any of the indicated subset. (E) Amount of APC staining of memory cells in clonal APC-specific populations that produced memory cells and plasma cells or memory cells but not plasma cells. The bars in (B) and (E) represent medians. P values were determined in (B) and (E) using a Mann-Whitney test and in (C) and (D) using Fisher's exact test. Data points were combined from 17 MD4 experiments, 3 AID-deficient experiments, and 12 wild-type experiments.



These results suggested that the multipotentiality of a single naïve B cell was related to the production of progeny resistant to cell death. This idea was tested using B cells lacking the proapoptotic mediator Bim (19). Bim-deficient and wild-type B cells fluxed calcium and proliferated equally in response to BCR signaling in vitro (fig. S3). Single Bim-deficient, APC-specific, naïve B cells, however, produced 3.4-fold more progeny than wild-type clones ($P < 0.0001$, compare Fig. 2C to Fig. 3E) in response to APC immunization. Bim-deficient clones were also more likely to produce multiple effector cell subsets (Fig. 3F), especially those containing plasma cells, GC cells, and AP cells (Fig. 3G). Unlike wild-type clones, Bim-deficient clonal populations showed a significant correlation between the number of cells and cell division (Fig. 3B), suggesting that they experienced less apoptosis. Consistent with apoptosis limiting population size, most Bim-deficient clones approached or exceeded the minimum number of daughter cells expected based on their CFSE profile (Fig. 3C). Thus, the capacity of a single naïve B cell to produce many effector cells and multiple subsets appears to be limited by Bim-mediated apoptosis, although suppression of proliferation by Bim could also contribute.

The multipotentiality of a single naïve B cell could also be influenced by BCR affinity for antigen. This was tested by comparing the response of single BCR transgenic MD4 B cells to high-affinity (HEL) or medium-affinity (DEL) antigens to that of activation-induced cytidine deaminase (AID)-deficient APC-specific B cells (Fig. 4, A and B), which like MD4 cells are unable to undergo class switching (20). Single AID-deficient APC-specific B cells produced a similar number (compare Fig. 2C to Fig. 4B) and diversity (Fig. 4C) of effector cells as their wild-type counterparts, indicating that class switching does not play a major role in differentiation at the early time point analyzed in these experiments. In contrast, single naïve MD4 cells stimulated with HEL or DEL produced more progeny than single APC-specific cells stimulated with APC (Fig. 4, A and B). 58% of HEL-stimulated single MD4 cells produced only plasma cells and GC cells, a combination

that occurred in few clonal APC-specific B cell populations (Fig. 4C). This idiosyncrasy was related to BCR affinity, because only 12.5% of single MD4 cells produced this pattern when stimulated with the lower-affinity antigen DEL (Fig. 4C). In addition, HEL-stimulated clones generated more plasma cells and fewer memory cells than DEL-stimulated clones (Fig. 4D), which is consistent with earlier work in the MD4 system (5, 8). The tendency of clones with higher-affinity BCRs to produce plasma cells was also observed in the polyclonal repertoire. BCR affinity for antigen was indirectly measured as the amount of APC bound to memory cells, which express BCR at levels similar to naïve cells (fig. S1A). Among the APC-specific clones that produced memory cells, those that also produced plasma cells bound more APC than those that did not (Fig. 4E). Together, these data indicate that BCR affinity for antigen influences the precise effector cell pattern produced by a naïve B cell.

Overall, our results demonstrate that individual naïve B cells vary greatly with respect to the number and types of effector cells generated early during the primary response, as reported for naïve T cells (10–13). Analogous to CD4⁺ T cells (12), the precise effector cell subset pattern produced by a single naïve B cell was influenced by BCR affinity for antigen. Unlike T cells, however, many individual naïve B cells only produced a single type of effector cell, which was associated with Bim-mediated apoptosis. This situation could come about because naïve B cells are biased toward the production of only one subset (9). The progeny of different clones may then experience different levels of trophic signals from T cells or cytokine receptors. Some clonal populations may prematurely stop receiving these trophic signals, resulting in apoptosis of some of their members and cessation of further differentiation. Other cells that continued to receive trophic signals may be protected by these signals from apoptosis, allowing further proliferation and the generation of additional effector cell subsets. Together, the combination of extrinsic heterogeneity in trophic signals and intrinsic heterogeneity in BCRs expressed

by the population of naïve B cells specific for an antigen ensures that a diverse set of effector cell types is produced during the primary response.

REFERENCES AND NOTES

1. J. J. Taylor, M. K. Jenkins, K. A. Pape, *Trends Immunol.* **33**, 590–597 (2012).
2. D. Zotos, D. M. Tarlinton, *Trends Immunol.* **33**, 281–288 (2012).
3. D. A. Fulcher *et al.*, *J. Exp. Med.* **183**, 2313–2328 (1996).
4. P. Garside *et al.*, *Science* **281**, 96–99 (1998).
5. D. Paus *et al.*, *J. Exp. Med.* **203**, 1081–1091 (2006).
6. B. P. O'Connor *et al.*, *J. Immunol.* **177**, 7723–7732 (2006).
7. T. A. Schwickert *et al.*, *J. Exp. Med.* **208**, 1243–1252 (2011).
8. K. Ochiai *et al.*, *Immunity* **38**, 918–929 (2013).
9. K. R. Duffy *et al.*, *Science* **335**, 338–341 (2012).
10. V. R. Buchholz *et al.*, *Science* **340**, 630–635 (2013).
11. C. Gerlach *et al.*, *Science* **340**, 635–639 (2013).
12. N. J. Tubo *et al.*, *Cell* **153**, 785–796 (2013).
13. C. R. Plumlee, B. S. Sheridan, B. B. Cicek, L. Lefrançois, *Immunity* **39**, 347–356 (2013).
14. K. A. Pape, J. J. Taylor, R. W. Maul, P. J. Gearhart, M. K. Jenkins, *Science* **331**, 1203–1207 (2011).
15. J. J. Taylor, K. A. Pape, M. K. Jenkins, *J. Exp. Med.* **209**, 597–606 (2012).
16. A. B. Lyons, C. R. Parish, *J. Immunol. Methods* **171**, 131–137 (1994).
17. T. B. Lavioie, W. N. Drohan, S. J. Smith-Gill, *J. Immunol.* **148**, 503–513 (1992).
18. C. Taswell, *J. Immunol.* **126**, 1614–1619 (1981).
19. P. Bouillet *et al.*, *Science* **286**, 1735–1738 (1999).
20. M. Muramatsu *et al.*, *Cell* **102**, 553–563 (2000).

ACKNOWLEDGMENTS

We thank J. Walter, A. Quade, K. Anderson, S. Voght, B. Debuysscher, the Jenkins Lab, and the University of Minnesota Flow Cytometry Resource for technical assistance and helpful discussions; M. Jankovic, M. Nussenzweig, D. Liao, and G. Kelsoe for providing AID-deficient cells; and L. Manlove, M. Farrar, S. Roepke, and M. Pric for providing Bim-deficient cells. The data presented in this manuscript are tabulated in the main paper and in the supplementary materials. This work was supported by the Irvington Fellowship Program of the Cancer Research Institute (J.J.T.), and the National Institutes of Health [P01AI035296, R01AI036914, and R37AI027998 (M.K.J.)]. The authors have no conflicting financial interests.

SUPPLEMENTARY MATERIALS

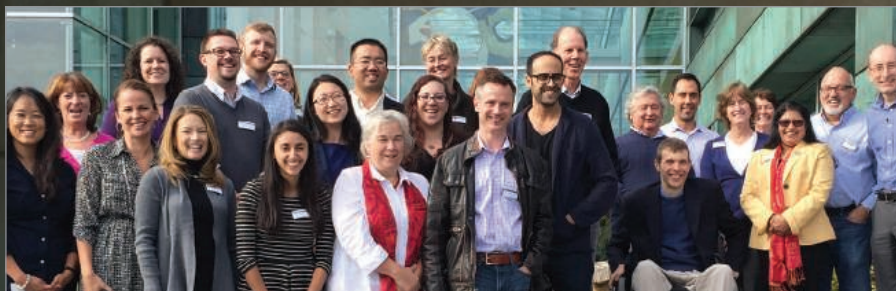
www.sciencemag.org/content/347/6223/784/suppl/DC1
Materials and Methods
Figs. S1 to S3
References (21, 22)

9 November 2014; accepted 14 January 2015
10.1126/science.aaa1342

CELEBRATING 40 YEARS OF PASSION IN SCIENCE

In celebration of our 40th anniversary, New England Biolabs recently introduced the Passion in Science Awards™, recognizing those within the scientific community working to solve many of today's challenges. Based on NEB's foundational values, the Passion in Science Awards were offered in four categories: Inspiration in Science, Humanitarian Duty, Environmental Stewardship and Arts and Creativity.

In October 2014, fifteen dedicated and compassionate scientists were chosen from around the world to participate in this first-of-its-kind event. Award winners visited NEB's campus in Ipswich, MA, for two days of discussions, presentations, tours and an awards celebration.



2014 Passion in Science Award winners pictured with their hosts outside New England Biolabs' facility in Ipswich, MA.



Learn more about our award winners and their inspiring projects
in our latest video at www.neb.com/PassionInScience

2015 (31th) Japan Prize Laureates

“Resources, Energy and Social Infrastructure” Field

Contribution to development of innovative concept on river basin management and reduction of water-related disasters.



Dr. Yutaka Takahasi
Japan

How they have contributed to Society through science and technology?



Dr. Theodore Friedmann, M.D.
USA



Prof. Alain Fischer, M.D.
France

“Medical Science and Medicinal Science” Field

Contribution to pioneering efforts of gene therapy and its clinical applications leading to the treatment of refractory diseases such as cancer and congenital disorders.

Japan prize selection criteria

The Japan Prize is awarded to scientists and engineers from around the world who are recognized as having achieved original and dramatic accomplishments that greatly enhance the progress of science and technology, thereby contributing to the peace and prosperity of mankind.



The logo for the AAAS 2016 Annual Meeting, featuring a stylized 'A' icon followed by the text 'AAAS 2016 ANNUAL MEETING' in a bold, sans-serif font.

**AAAS 2016
ANNUAL MEETING**

WASHINGTON, DC
FEBRUARY 11–15

Global Science Engagement

Science is a global endeavor that advances when knowledge is both generated and shared. Increasingly, scientists and engineers are working both within and outside of national boundaries on local and global issues.

Challenges necessitating innovation and international scientific collaboration are abundant in food and water security, sustainable development, infectious disease and health, climate change, natural disasters, and energy. Countries with varying levels of development, education, and scientific capacity may have different goals and expectations for international scientific engagement.

What elements make international collaboration successful and sustainable? What engagement opportunities are available, and what are the responsibilities of researchers, entrepreneurs, educators, and policymakers in global scientific endeavors?

Call for Symposium Proposals

Symposium proposals for the 2016 AAAS Annual Meeting are now being solicited. To submit a proposal, visit aaas.org/AM16. The deadline for submission is **April 24, 2015**.

aaas.org/AM16

A person wearing a bright yellow raincoat and blue jeans stands on a dark, wet beach, holding a smartphone to take a photo of a massive volcanic eruption in the background. The eruption features large, intense orange and red flames rising from dark, jagged rock formations. The foreground shows the dark, reflective surface of the beach and the turbulent, dark water of the ocean.

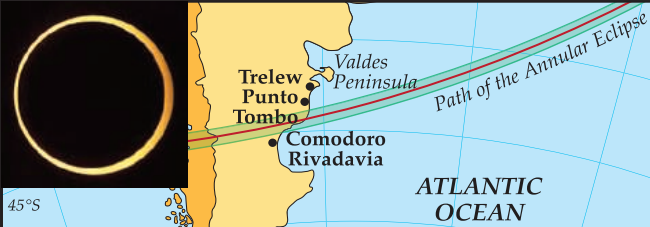
Open access. Open **for discovery**.

***Science Advances*, the new open-access journal from AAAS, is now available online.**

Featuring innovative, multidisciplinary articles, *Science Advances* offers the high quality, peer-reviewed research you expect from the publishers of *Science*—in an open, digital-only format. Read the latest findings and submit your research at **scienceadvances.org**.

ScienceAdvances

AAAS



45°S

Trelew
Punto Tombo
Comodoro Rivadavia

Valdes Peninsula

Path of the Annular Eclipse

ATLANTIC OCEAN

Discover Antarctica!
& the Annular Solar Eclipse
February 23–March 9, 2017

55°S

60°S

Drake Passage

Elephant Island

King George Island

Deception Island

Paradise Bay

Lemaire Channel

Peterman Island

Wilkins Ice Sheet


George VI Ice Sheet

Larsen C Ice Sheet

ANTARCTIC PENINSULA

AAAS Travels

For a detailed brochure, call (800) 252-4910

 **BETCHART EXPEDITIONS Inc.**
17050 Montebello Rd, Cupertino, CA 95014
Email: AAASInfo@betchartexpeditions.com
www.betchartexpeditions.com

©2015 Betchart Expeditions Inc.

"YOU ARE WATCHING THIS BEAUTIFUL ECOSYSTEM BE DEGRADED BY CLIMATE CHANGE OR HUMAN INTERACTION ... THEN YOU SORT OF PULL UP YOUR SOCKS AND GO SEE WHAT YOU CAN DO."


Marine conservationist and
Kenyan coral reef expert,
Tim McClanahan, AAAS Member



Every scientist has a *story*

Read his story at membercentral.aaas.org

 **AAAS**
MEMBERCENTRAL

In the Nation, exclusive discounts are just the beginning.



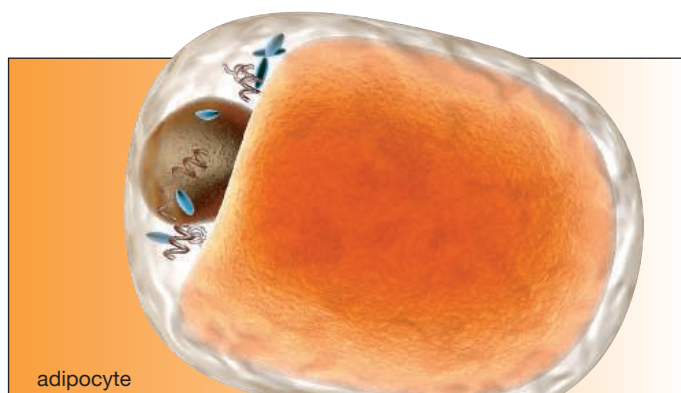
AAAS members are rewarded.

With Nationwide®, you get great protection for you, your loved ones and all you've worked for in life.

As a member of AAAS, you can save with special discounts on Nationwide auto insurance. In addition, when you add rewards like **Vanishing Deductible®**,* you can take \$100 off your deductible for every year of safe driving, for up to \$500 in savings.

Call 1-866-238-1426 or visit
nationwide.com/AAAS for
a quote today!





adipocyte

Greasing the Wheels of Lipidomics

Lipids have traditionally been among the hardest biomolecules to study, but new technologies and techniques are gradually revealing more of the lipidome. **By Alan Dove**

Biology is swaddled in lipids. Fats, oils, and waxes enclose cells and organelles, mediate vast networks of information flow, protect fragile tissues from hostile environments, and store essential energy for all kinds of organisms. Unfortunately, lipid structures don't rely on the sorts of well-defined building blocks and simple rules that govern DNA, RNA, and proteins. From the complete DNA sequences of the biosynthetic genes in a cell, for example, one can reliably predict the RNA transcripts likely to arise from those genes and the protein sequences they'll encode; the lipids synthesized by those proteins, though, will remain mostly mysterious.

This disjunction, between the relatively predictable patterns of nucleic acids and proteins and the largely inscrutable world of lipids, has skewed the progress of biochemistry for years. Genome sequencing technology and genomics quickly fed the rise transcriptomics and proteomics. As those fields charged ahead, amassing terabytes of data on the biology of RNA and proteins respectively, lipid biochemists felt largely left out.

That began to change in 2003, as a major National Institutes of Health (NIH)-funded effort set out to establish the field of lipidomics. In the ensuing decade, researchers and equipment makers have developed several new techniques and tools for analyzing these challenging molecules.

The fat of the land

"In 2002 ... there were no publications using the word 'lipidomics,'" says Edward Dennis, Ph.D., professor of chemistry, biochemistry, and pharmacology at the **University of California**

in San Diego. That year, Dennis proposed a project to create the field, and the NIH's National Institute of General Medical Sciences (NIGMS) agreed to fund it. The result was the 10-year, \$73 million Lipid Metabolites and Pathways Strategy (Lipid MAPS) effort, which Dennis oversaw.

Dennis started by recruiting five other researchers at institutions across the country, each an expert on a particular type of lipid. The scientists began developing techniques to isolate and quantify their assigned lipid categories from biological samples, but they ran into a major problem immediately. "We came to realize that there was no classification for lipids that was suitable for the bioinformatics age," says Dennis, adding that "you need a taxonomy to classify them and ... store all the billions of bits of information we were intending to get."

To answer that need, the team invented a new classification scheme, dividing all lipids into eight major categories, six of which are found in mammals. The group also revised the nomenclature for lipid structures and developed a standardized system for drawing them. The Lipid MAPS website now features a searchable database with more than 40,000 structures, all classified and drawn using the new system, which researchers worldwide have also adopted. "I would say virtually everybody in the world today who talks about a lipid uses this structural representation," says Dennis.

With the taxonomy in place, the Lipid MAPS researchers focused on lipidomics protocols. All of the labs began with identical equipment, based on the **AB Sciex** QTRAP 4000 Liquid Chromatography/Mass Spectrometry (LC/MS) system that was then considered the state of the art. Each scientist optimized fractionation methods to isolate one specific category of lipids, then added radioactively labeled standard compounds before performing mass spectrometry. The combination of fractionation and mass spectrometry identified the lipids in the sample, and the internal standards allowed precise quantitation of them. Combining the data from all six labs produced complete lipidomic profiles of some samples that answered specific biological questions. Lipid MAPS also discovered a number of novel lipids, though that wasn't their primary goal.

In an era when genomics tools are a mouse-click away and most major universities run dedicated core labs for proteomics, the scale and intensity of the six-facility Lipid MAPS approach may seem out of reach for nonspecialists. It probably is. "It would be very expensive to set it up from scratch," Dennis concedes. With the conclusion of the Lipid MAPS project, though, many of the individual participants have continued to keep their doors open. Dennis's group, for example, offers its lipidomics services to other researchers through collaborative grants or recharge funding.

The techniques and technologies for lipidomics both evolved during the decade-long project. Dennis's lab now uses an **AB Sciex** QTRAP 6500M—the successor to the 4000—combined with an Acquity ultrahigh-performance liquid chromatography

Upcoming Features

Cell Culture—March 13 ■ **Proteomics—April 17** ■ **Microscopy—June 15**



(UPLC) system from **Waters** in Milford, Massachusetts. Other Lipid MAPS groups, and the growing population of lipidomics researchers outside the project, have adopted other strategies and tools depending on the types of experiments they pursue.

Wax on, wax off

"There isn't one method that people are using everywhere," says Ruth Welti, Ph.D., director of the lipidomics core facility at **Kansas State University** in Manhattan, Kansas. One reason for the diversity of techniques is that lipidomics researchers fall into two separate camps: high precision and high throughput. High-precision projects, most notably, focus on obtaining accurate measurements of the levels of specific types of lipids. High throughput experiments, in contrast, tend to process large numbers of samples looking for relative changes in lipid levels, "sort of more like a gene expression analysis, where the absolute amounts aren't so important but the comparison across the samples is important," says Welti.

Welti is a practitioner of the high throughput approach. Instead of fractionating samples and looking for specific types of lipids in each fraction, she and her colleagues infuse crude samples directly into a Waters triple-quadrupole mass spectrometer. That allows the team to analyze thousands of samples for a single experiment, a useful capability for Welti's large-scale studies on agriculturally important plant phenotypes.

Besides enabling higher throughput, direct infusion also mitigates one of the drawbacks of LC-coupled MS. Lipids in a sample can affect one another's ionization in the mass spectrometer. By separating the sample into distinct groups of lipids, LC sends particular subsets of molecules into the mass spectrometer in distinct pulses. "If you use LC, then at some points the percentage of particular lipids that are ionized might relate to what other lipids they're going in with," says Welti. By sending the entire sample through without fractionation, the concentrations of all of the lipids remain constant relative to each other.

Direct infusion has its own weaknesses, of course, and researchers using the technique have to take steps to address them. For example, most high throughput experiments need quality control samples made from a pool of all of the samples being analyzed. The pooled sample contains all of the lipids that could show up in any experimental sample. "A big problem with mass spec in general is normalization of data across time on the same mass spec, across different machines, across different labs, so having reference standards that contain all of the compounds that are in your samples is really helpful and can



"Even if you're not an expert in lipid analysis, the way lipids fragment and the way that you measure them and detect them is quite defined."

increase the precision of the data a lot," says Welti.

Lipidomics in general, and direct infusion in particular, can also be a messy business. "There isn't any instrument that doesn't need to be cleaned a lot if you're [studying] lipids by direct infusion," says Welti.

Despite using different approaches, Welti and Dennis agree on the need for specialized lipidomics facilities. The combination of technical complexity and often high instrument maintenance causes many core

facilities to avoid lipidomics. As a result, Welti estimates that her group has collaborated with about 400 other laboratories in the past decade. "It's a big need and people don't have this kind of thing available to them," she says.

In addition to academic facilities such as Welti's, at least one company, Avanti Polar Lipids in Alabaster, Alabama, also offers lipidomics services to the scientific community. Avanti worked on the Lipid MAPS project and now makes its facilities available for a fee.

Don't fear the hydrophobes

As more researchers discover the potential of lipidomics, though, some are starting to do the work themselves rather than collaborate with a dedicated lipid facility. "It's not only the Ed Dennises of the world who are doing lipidomics today," says Fadi Abdi, Ph.D., senior global market manager for lipidomics, metabolomics, and imaging at AB Sciex in Framingham, Massachusetts. Abdi adds that "there's a transition in the market from the proteomics side to the metabolomics and lipidomics side."

Indeed, all of the major mass spectrometer makers now offer products specifically for lipidomics. At AB Sciex, that means catering to both the high throughput and high-precision markets with different mass spectrometry systems. For high throughput survey experiments, the company sells triple time-of-flight mass spectrometers that provide accurate mass information very quickly. "That allows us to do discovery type of work for lipids. At the same time, we have another set of products, which are the QTRAP platforms, which allows us to do more targeted types of work," says Abdi.

A few miles away in Waltham, Massachusetts, **Thermo Scientific** now offers several lipidomics systems built around the company's Orbitrap mass spectrometry technology. Meanwhile **Bruker**, in Billerica, Massachusetts, caters to the lipidomics market with a unique combination of mass spectrometers, thin layer chromatography, and nuclear magnetic resonance (NMR) instruments. **continued>**



The diversity of technology on the market reflects the unusual challenges of lipidomics. Unlike proteins and nucleic acids, lipids in cells often come in different isomeric forms, with identical compositions and molecular weights but different structures. Even a perfectly accurate mass measurement can't distinguish between isomers, so high-precision lipidomics studies often have to rely on additional analytical techniques. Separating the samples by UPLC before the mass spectrometer, or analyzing them with methods such as NMR afterward, may help fill gaps in the data.

Besides learning about the strengths and limitations of the many equipment configurations, researchers considering taking up lipidomics should ask companies about training and user-friendliness. Most are happy to guide newcomers. "Even if you're not an expert in lipid analysis, the way lipids fragment and the way that you measure them and detect them is quite defined," says Baljit Ubhi, Ph.D., staff scientist in metabolomics and lipidomics applications at AB Sciex. Ubhi adds that "we have predefined methods [and] application specialists who are experts in that field who can get a user up and running fairly quickly."

Mass spectrometers inevitably come with software as well. In addition to the applications that run the machine, most manufacturers include data analysis packages with varying degrees of sophistication and flexibility. Software optimized for proteomics or metabolomics may be useless for lipidomics, so scientists who want a complete system should look for lipidomics-specific data handling options. Advanced systems either include their own databases of lipids, or tie into the Lipid MAPS database to identify specific lipid species in a sample.

Apps for fats

Many lipidomics researchers use the software that came with their mass spectrometers only for initial data collection, preferring to export the data to another program for analysis. For some experimenters, that means transferring it into a common spreadsheet program such as Microsoft Excel. Dedicated lipidomics specialists, however, often prefer to develop their own software.

Christer Ejsing, Ph.D., associate professor in the department of biochemistry and molecular biology at the **University of Southern Denmark** in Odense, Denmark, is one of the scientists who chose to write his own data analysis program. "If you have several hundreds of injections on your instrument and you

Featured Participants

AB Sciex
www.absciex.com

Bruker
www.bruker.com

Kansas Lipidomics Research Center
www.k-state.edu/lipid/lipidomics

Premier Biosoft
www.premierbiosoft.com

Thermo Scientific
www.thermoscientific.com

University of California, San Diego
www.ucsd.edu

University of Southern Denmark
www.sdu.dk/en

Waters
www.waters.com

Additional Resources

Lipid MAPS
www.lipidmaps.org

MetaboLights
www.ebi.ac.uk/metabolights/about

Plant/Eukaryotic and Microbial Systems Resource
metnetdb.org/pmr

want to organize the data, you don't want to do that in Excel," says Ejsing.

As a result, Ejsing and his colleagues created the Analysis of Lipid Experiments (ALEX) software package, which is specifically designed for the type of high-precision lipidomics Ejsing's lab pursues. Ejsing uses a small script to export data from his mass spectrometry software into a database format, then uses Tableau, a data visualization language originally developed for the banking industry, to create graphs. Typical of most software

from academic researchers, ALEX is open source, free for other scientists to download, use, and modify.

For those pursuing high throughput lipidomics, Welte's software project, LipidomeDB, may be more useful. LipidomeDB is a web-based system that takes Microsoft Excel files of mass spectrometry data as inputs and exports data in the same format. The freely accessible system has been quite popular with Welte's collaborators. "A lot of people use it, if we run samples for people, [they] have the option of processing it themselves or having us process it for them," she says.

Several other lipidomics labs have developed their own analysis software as well. Each program is optimized for the lab that created it, but most are freely available to other researchers. At least one company, **Premier Biosoft** in Palo Alto, California, has also released a commercial stand-alone lipidomics data analysis application.

The wide selection of data analysis tools is both a blessing and a curse. While researchers can likely find a ready-built application that will fit their own needs, there's no standardization across the systems to ensure that they'll handle data consistently. As a result, scientists working in lipidomics often like to export their raw mass spectrometer data to outlets such as the European Molecular Biology Laboratory's MetaboLights database or Iowa State University's Plant/Eukaryotic and Microbial Systems Resource. That allows other scientists to reanalyze the data with their own applications to make comparisons across systems.

Analyzing lipids may never be as straightforward as studying nucleic acids or proteins, but lipidomics is clearly off to a strong start. A recent search of PubMed revealed nearly a thousand publications using the term—not bad for a field that didn't exist 12 years ago.

Alan Dove is a science writer and editor based in Massachusetts.

DOI: 10.1126/science.opms.p1500091



High Throughput Lipid Analysis

A novel high throughput Shotgun Lipidomics technology has been designed based on the Hamilton STARlet platform in combination with a mass spectrometer and the proprietary software, LipotypeXplorer. The platform allows comprehensive and absolute quantitative lipidomics analysis from different types of up to 96 clinical or biological samples in three hours. The system is designed in a way that allows an easy adaption to various extraction procedures. All kinds of organic solvents for the lipid extraction can be handled in a reliable way using Hamilton's Anti Droplet Control technology. All liquid transfer steps are checked for accuracy and reproducibility using a balance to determine the real pipetted volume. The complete method validation included extraction of 90 copies of the same sample arrayed together on a single plate. Three independently prepared replicates of such plates were independently processed and analyzed on three consecutive days to check intraday and interday variation.

Hamilton Robotics

For info: 800-648-5950
www.hamiltonrobotics.com

Metabolomics/Lipidomics Analyses Software

Progenesis QI Version 2.0 is the next generation of liquid chromatography-mass spectrometry (LC-MS) software for small molecule 'omics data analysis. This software complements the earlier introduction of Progenesis QI for proteomics Version 2.0 for large molecule 'omics data analysis. Both Progenesis QI and Progenesis QI for proteomics software take LC-MS data analysis to new levels of speed and sophistication, enabling users to rapidly quantify and identify the significantly changing small molecule, lipid compounds, and proteins in samples. The new features of Progenesis QI Version 2.0 include Pathway Mapping, which facilitates the process of placing discoveries into a biological context, extracting maximum value from 'omics data; workflow automation, which enables the software to move through multiple processing stages without user intervention; improved access to compound databases; and seamless integration with the extended statistics functionality in EZInfo 3.0, with two-way dataflow to allow for flexible data mining through a single, menu-driven command.

Waters Corporation

For info: 800-252-4752
www.waters.com

qTOF Mass Spectrometers

The maxis line of ultrahigh resolution quadrupole time-of-flight (UHR-qTOF) mass spectrometers brings industry-leading resolution and mass accuracy to the liquid chromatography, time-of-flight MS market space. The system is designed to deliver outstanding resolution and mass accuracy that, for example, allows for unambiguous identification of the mono-isotopic mass peak of both the light and heavy chains of monoclonal antibodies. In addition, this level of performance also provides scientists confident detection and identification of modifications hard to detect at the protein level, such as deamidation. The maxis II system delivers the fastest time-to-success for life science researchers and across a broad range of applications from the in-depth identification and characterization of biopharmaceuticals and small molecule pharmaceuticals to bottom-up proteomics and proteoform screening.

Bruker

For info: 978-663-3660
www.bruker.com



Glycan Quantitation Analysis

Enterprise Edition of SimGlycan v. 5.0 is a comprehensive high throughput tool that provides support for glycan quantitation using Thermo Scientific aminoxy-TMT for MS/MS glycan data analysis workflows. Additionally, it can be used for processing of liquid chromatography/mass spectrometry (LC-MS) data for peak detection, peak picking, and alignment of glycans based on retention time, precursor m/z values, and observed intensities across multiple samples. The Thermo Scientific aminoxyTMT reagents are designed to provide efficient relative quantitation of carbohydrates, improve labeled-glycan ionization efficiency, and increase analytical throughput. These reagents can be used for quantitative analysis of native N-glycans by direct or LC-coupled ESI-MS. Using SimGlycan, glycans are quantified by measuring reporter ion peak intensities from the corresponding MS/MS spectra. Various charts are provided to facilitate visualization of either the quantity of each glycan in different TMT channels or relative change in abundance of glycans across samples.

Premier Biosoft

For info: 888-847-7494
www.premierbiosoft.com

Lipid Analysis Software

Complementing Protein Metrics' advanced Byonic protein identification engine, Lipify software makes structural identifications across an expanding list of lipids (>20,000), covering many lipid subclasses, to provide automated processing of high throughput liquid chromatography-tandem mass spectrometry (LC-MS/MS) data. Lipify provides structural characterization as part of the identification process. This unique tool can even characterize lipids

that have never been observed before, opening the door to new biological and medical discoveries. The Lipify software offers a friendly graphical user interface to allow scientists to interact with results and provide intuitive views of analyzed data that aids manual verification of identifications. Its algorithms are sensitive and efficient, with a typical search of 26,000 lipid targets completed in less than 15 seconds. Results can be readily exported for reporting and publication.

Protein Metrics

For info: 650-412-4210
www.proteinmetrics.com

Electronically submit your new product description or product literature information! Go to www.sciencemag.org/products/newproducts.dtl for more information.

Newly offered instrumentation, apparatus, and laboratory materials of interest to researchers in all disciplines in academic, industrial, and governmental organizations are featured in this space. Emphasis is given to purpose, chief characteristics, and availability of products and materials. Endorsement by *Science* or AAAS of any products or materials mentioned is not implied. Additional information may be obtained from the manufacturer or supplier.

want new technologies?

antibodies

apoptosis

biomarkers

cancer

cytometry

data

diseases

DNA

epigenetics

genomics

immunotherapies

medicine

microbiomics

microfluidics

microscopy

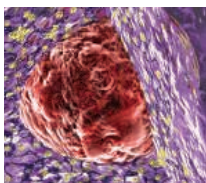
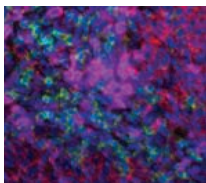
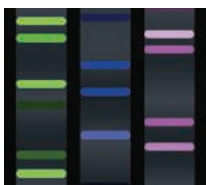
neuroscience

proteomics

sequencing

toxicology

transcriptomics



watch our **webinars**

Learn about the latest breakthroughs, new technologies, and ground-breaking research in a variety of fields. Our expert speakers explain their quality research to you and answer questions submitted by live viewers.

VIEW NOW!

webinar.sciencemag.org

Science
AAAS

Brought to you by the *Science*/AAAS
Custom Publishing Office



@SciMagWebinars

Your Most Trusted Cell Viability Assay— **Now in 3D**

CellTiter-Glo® 3D Cell Viability Assay

Validated for 3D microtissue culture and based on the same reliable chemistry as the classic CellTiter-Glo® Assay, the CellTiter-Glo® 3D Cell Viability Assay Reagent has increased lytic capacity for penetrating large spheroids—allowing more accurate determination of viability compared to other assay methods.

- ***Accurate 3D Cytotoxicity Determination***
- ***Easy Assay Implementation***
- ***Simple, 30-Minute Protocol***

To learn more and request a **FREE SAMPLE**, visit:

www.promega.com/TryGlo3D



*Scan QR code to
directly access the
free sample form.*



High Throughput Lipid Analysis

A novel high throughput Shotgun Lipidomics technology has been designed based on the Hamilton STARlet platform in combination with a mass spectrometer and the proprietary software, LipotypeXplorer. The platform allows comprehensive and absolute quantitative lipidomics analysis from different types of up to 96 clinical or biological samples in three hours. The system is designed in a way that allows an easy adaption to various extraction procedures. All kinds of organic solvents for the lipid extraction can be handled in a reliable way using Hamilton's Anti Droplet Control technology. All liquid transfer steps are checked for accuracy and reproducibility using a balance to determine the real pipetted volume. The complete method validation included extraction of 90 copies of the same sample arrayed together on a single plate. Three independently prepared replicates of such plates were independently processed and analyzed on three consecutive days to check intraday and interday variation.

Hamilton Robotics

For info: 800-648-5950
www.hamiltonrobotics.com

Metabolomics/Lipidomics Analyses Software

Progenesis QI Version 2.0 is the next generation of liquid chromatography-mass spectrometry (LC-MS) software for small molecule 'omics data analysis. This software complements the earlier introduction of Progenesis QI for proteomics Version 2.0 for large molecule 'omics data analysis. Both Progenesis QI and Progenesis QI for proteomics software take LC-MS data analysis to new levels of speed and sophistication, enabling users to rapidly quantify and identify the significantly changing small molecule, lipid compounds, and proteins in samples. The new features of Progenesis QI Version 2.0 include Pathway Mapping, which facilitates the process of placing discoveries into a biological context, extracting maximum value from 'omics data; workflow automation, which enables the software to move through multiple processing stages without user intervention; improved access to compound databases; and seamless integration with the extended statistics functionality in EZInfo 3.0, with two-way dataflow to allow for flexible data mining through a single, menu-driven command.

Waters Corporation

For info: 800-252-4752
www.waters.com

qTOF Mass Spectrometers

The maXis line of ultrahigh resolution quadrupole time-of-flight (UHR-qTOF) mass spectrometers brings industry-leading resolution and mass accuracy to the liquid chromatography, time-of-flight MS market space. The system is designed to deliver outstanding resolution and mass accuracy that, for example, allows for unambiguous identification of the mono-isotopic mass peak of both the light and heavy chains of monoclonal antibodies. In addition, this level of performance also provides scientists confident detection and identification of modifications hard to detect at the protein level, such as deamidation. The maXis II system delivers the fastest time-to-success for life science researchers and across a broad range of applications from the in-depth identification and characterization of biopharmaceuticals and small molecule pharmaceuticals to bottom-up proteomics and proteoform screening.

Bruker

For info: 978-663-3660
www.bruker.com



Glycan Quantitation Analysis

Enterprise Edition of SimGlycan v. 5.0 is a comprehensive high throughput tool that provides support for glycan quantitation using Thermo Scientific aminoxy-TMT for MS/MS glycan data analysis workflows. Additionally, it can be used for processing of liquid chromatography/mass spectrometry (LC-MS) data for peak detection, peak picking, and alignment of glycans based on retention time, precursor m/z values, and observed intensities across multiple samples. The Thermo Scientific aminoxyTMT reagents are designed to provide efficient relative quantitation of carbohydrates, improve labeled-glycan ionization efficiency, and increase analytical throughput. These reagents can be used for quantitative analysis of native N-glycans by direct or LC-coupled ESI-MS. Using SimGlycan, glycans are quantified by measuring reporter ion peak intensities from the corresponding MS/MS spectra. Various charts are provided to facilitate visualization of either the quantity of each glycan in different TMT channels or relative change in abundance of glycans across samples.

Premier Biosoft

For info: 888-847-7494
www.premierbiosoft.com

Lipid Analysis Software

Complementing Protein Metrics' advanced Byonic protein identification engine, Lipify software makes structural identifications across an expanding list of lipids (>20,000), covering many lipid subclasses, to provide automated processing of high throughput liquid chromatography-tandem mass spectrometry (LC-MS/MS) data. Lipify provides structural characterization as part of the identification process. This unique tool can even characterize lipids

that have never been observed before, opening the door to new biological and medical discoveries. The Lipify software offers a friendly graphical user interface to allow scientists to interact with results and provide intuitive views of analyzed data that aids manual verification of identifications. Its algorithms are sensitive and efficient, with a typical search of 26,000 lipid targets completed in less than 15 seconds. Results can be readily exported for reporting and publication.

Protein Metrics

For info: 650-412-4210
www.proteinmetrics.com

Electronically submit your new product description or product literature information! Go to www.sciencemag.org/products/newproducts.dtl for more information.

Newly offered instrumentation, apparatus, and laboratory materials of interest to researchers in all disciplines in academic, industrial, and governmental organizations are featured in this space. Emphasis is given to purpose, chief characteristics, and availability of products and materials. Endorsement by *Science* or AAAS of any products or materials mentioned is not implied. Additional information may be obtained from the manufacturer or supplier.



There's only one **Science**

Science Careers Advertising

For full advertising details, go to ScienceCareers.org and click For Employers, or call one of our representatives.

Tracy Holmes
Worldwide Associate Director
Science Careers
Phone: +44 (0) 1223 326525

THE AMERICAS

E-mail: advertise@sciencecareers.org
Fax: 202 289 6742

Tina Burks
Phone: 202 326 6577

Nancy Toema
Phone: 202 326 6578

Marci Gallun
Sales Administrator
Phone: 202 326 6582

Online Job Posting Questions
Phone: 202 312 6375

EUROPE / INDIA / AUSTRALIA / NEW ZEALAND / REST OF WORLD

E-mail: ads@science-int.co.uk
Fax: +44 (0) 1223 326532

Axel Gesatzki
Phone: +44 (0) 1223 326529

Sarah Lelarge
Phone: +44 (0) 1223 326527

Kelly Grace
Phone: +44 (0) 1223 326528

JAPAN

Katsuyoshi Fukamizu (Tokyo)
E-mail: kfukamizu@aaaas.org
Phone: +81 3 3219 5777

Hiroyuki Mashiki (Kyoto)
E-mail: hmashiki@aaaas.org
Phone: +81 75 823 1109

CHINA / KOREA / SINGAPORE / TAIWAN / THAILAND

Ruolei Wu
Phone: +86 186 0082 9345
E-mail: rwu@aaaas.org

All ads submitted for publication must comply with applicable U.S. and non-U.S. laws. *Science* reserves the right to refuse any advertisement at its sole discretion for any reason, including without limitation for offensive language or inappropriate content, and all advertising is subject to publisher approval. *Science* encourages our readers to alert us to any ads that they feel may be discriminatory or offensive.

Science Careers
FROM THE JOURNAL SCIENCE 

ScienceCareers.org

ONLINE CAREER FAIR

March 4, 2015 | 10:00 AM – 4 PM EST



Register now for this exciting virtual career fair and engage, screen, and recruit hundreds of targeted candidates.

HOW THE EVENT WILL WORK

Employers receive a fully customized “booth” tailored to meet their recruiting needs. This landing page can include open positions, company information, testimonials and branding videos.

During the live event, candidates browse your booth and then choose to chat one-on-one. The conversations are timed to allow companies to meet as many candidates as possible.

BENEFITS OF EXHIBITING

- Connect with candidates from the comfort of your own desk
- Showcase your employer brand online to your target audience
- No travel or accommodation costs
- Get access to resumes to build your talent community
- Candidate information is displayed during the chat
- Powerful follow up tools to move top candidates through the hiring process
- Screen candidates with pre-qualifying questions to connect with the most relevant candidates

Book your booth today!

For more information, please visit:
ScienceCareers.org/onlinecareerfairemployers

SCIENCECAREERS.ORG

Science Careers

FROM THE JOURNAL SCIENCE 

VAN ANDEL RESEARCH INSTITUTE IS RECRUITING



FIVE NEW FACULTY AND FOUR VAN ANDEL FELLOWS

Van Andel Research Institute is continuing its rapid growth and is seeking to build on recent additions of internationally recognized experts, outstanding experienced scientists and exceptional new investigators. With the aim of establishing the Institute as a globally recognized research hub for the study of epigenetics, cancer, neurodegenerative diseases and skeletal diseases, we are further expanding the Center for Epigenetics, the Center for Neurodegenerative Science and the Center for Cancer and Cell Biology. All faculty positions come with 100 percent support for faculty salary and benefits.

PROFESSOR AND ASSISTANT PROFESSOR IN NEUROEPIGENETICS

Please direct questions about the Center's research to:

Peter Jones, Ph.D., D.Sc.
*Research Director and Chief Scientific Officer
Co-leader, VARI-SU2C Epigenetics
Dream Team*

Patrik Brundin, M.D., Ph.D.
*Associate Director of Research
Director, Center for Neurodegenerative Science*

PROFESSOR IN TRANSLATIONAL PARKINSON'S DISEASE RESEARCH

Please direct questions about the Center's research to:

Patrik Brundin, M.D., Ph.D.
*Associate Director of Research
Director, Center for Neurodegenerative Science*

PROFESSOR OR ASSOCIATE PROFESSOR IN SKELETAL DISEASE BIOLOGY

Please direct questions about the Center's research to:

Bart Williams, Ph.D.
Director, Center for Cancer and Cell Biology

ASSISTANT PROFESSOR IN EPIGENETICS

Please direct questions about the Center's research to:

Peter Laird, Ph.D.
*Search Chair
Professor*
Peter Jones, Ph.D., D.Sc.
*Research Director and Chief Scientific Officer
Co-leader, VARI-SU2C Epigenetics Dream Team*
Stephen Baylin, M.D.
Co-leader, VARI-SU2C Epigenetics Dream Team

VAN ANDEL FELLOWS

We are recruiting four exceptional early career scientists for interdisciplinary postdoctoral training under the mentorship of two or more VARI principal investigators, with the goal of providing fellows with a clear path to a faculty position at a top academic institution.

Van Andel Fellows receive a highly competitive salary that exceeds the national average for postdoctoral fellows, full benefits and funding for research projects.

ABOUT VAI

Van Andel Institute (VAI) is an independent biomedical research and science education organization committed to improving the health and enhancing the lives of current and future generations. Established by Jay and Betty Van Andel in 1996 in Grand Rapids, Michigan, VAI has grown into a premier research and educational institution.



Learn more about Van Andel Research Institute and the open positions at www.vai.org/vari

VAI is an equal-opportunity/affirmative action employer and encourages all qualified individuals to apply. Qualified applicants should apply online at <https://vai-openhire.silkroad.com/> epostings. Review of applications will begin at the end of February 2015 and will continue until the positions are filled.

CARNEGIE INSTITUTION

At the Frontiers of Science

Deep-Time Data Infrastructure—Project Science Manager

The W. M. Keck Foundation has announced a 3-year project to understand Earth's changing near-surface oxidation state and the rise of oxygen through deep time. Central to this objective is creation of an open-access Deep-Time Data Infrastructure (DTDI). The DTDI Project Science Manager (PSM) will coordinate and integrate the efforts of a team of Earth, life, and data scientists from 6 nodes. The PSM's responsibilities will include:

- Maintaining regular contact with teams from all 6 nodes (Harvard, Rutgers, Johns Hopkins, University of Arizona, RPI, and Carnegie);
- Organizing annual meetings of all co-investigators;
- Coordinating the development of varied data resources and ensuring that these resources are integrated into a user-friendly open-access interface;
- Overseeing project budgets and expenditures and preparing regular progress reports and briefing materials;
- Communicating with the press and engaging potential scientist users of the DTDI;
- Serving as liaison with the National Science Foundation (especially EarthCube), related data infrastructure efforts at other institutions, and professional societies;
- Exploring other funding opportunities, especially for the sustained maintenance and operations of the DTDI beyond the initial 3-year period of Keck support;
- Engaging in active research related to the development and implementation of the DTDI.

The PSM must have a Ph.D. in Earth Sciences with at least one year of program management experience, as well as expertise in geobiology, geochemistry, and mineralogy/petrology. She/he must be familiar with concepts of Earth's changing near-surface environments in deep time. Programming skills are not required, but familiarity with database development, management, and use are desirable. The full-time, 2.5-year position will be based at the Carnegie Institution's Broad Branch Road campus in Washington, DC. Interested applicants should submit a CV and cover letter stating interest in the position by **March 6, 2015**. Finalists will be notified by **March 13, 2015**.

To view the complete job listing or apply, please visit <https://jobs.carnegiescience.edu/jobs/deep-time-data-infrastructure-project-science-manager/>. Only complete applications submitted via the website will be considered.

The Carnegie Institution of Washington is an Equal Opportunity Employer.



**Shriners Hospitals
for Children™**

Assistant Corporate Director of Research Shriners Hospitals for Children International

Shriners Hospitals for Children (SHC) invites applications for Assistant Corporate Director of Research Programs, at its headquarters in Tampa, Florida.

The applicant will assist in the management of an extensive program in basic, translational, and clinical research in pediatric congenital orthopedic diseases, spinal cord injury and burns at its 22 hospitals and eight Research Centers, with an annual departmental budget exceeding \$32 million. Responsibilities include organizing peer review of grant applications, grants administration, site visit reviews of Research Centers, budget and program planning and evaluation, and research facilities development.

The applicant must have a Ph.D., M.D., or highest degree in a professionally related field, a track record of scholarly productivity, including publications and federal grants in biomedical/clinical research and knowledge of grant and research administration.

Applications should include a curriculum vitae, a letter summarizing professional accomplishments, and detailing administrative and management experience and philosophy, and the names and contact information of three potential references, and be submitted to: shrinerhqemployment@shrinenet.org

Worcester Polytechnic Institute

Assistant/Associate/Full Professor, Biochemistry

Worcester Polytechnic Institute (WPI) invites applications and nominations of candidates for the Richard T. Whitcomb Professorship in Biochemistry. The appointment will be made in the Department of Chemistry and Biochemistry (CBC), within Arts and Sciences at WPI. The Department offers undergraduate and graduate (MS and PhD) degrees in Chemistry and Biochemistry. CBC is integral to WPI's ongoing major life science research initiative and five new faculty at the assistant, associate and full professor level were recently hired.

This Professorship offers a generous start-up package, continued financial support for research and substantial laboratory space in the recently built, state-of-the-art Life Sciences research facility.

The holder of the Whitcomb chair will be a dynamic scholar and teacher, with a strong track record of creativity and an internationally highly visible research program, studying biochemical systems at the molecular level. The successful candidate will have a strong record of continued funding, high impact publications, and a solid presence in the scientific community. The ideal candidate for the Whitcomb Professorship will have a strong interest in collaborative research and is expected to provide leadership in new or established research areas at the interface of Chemistry and Biology.

To apply, visit: <http://apptrkr.com/571605>



WPI

To enrich education through diversity,
WPI is an affirmative action, equal opportunity employer.



The 2015 (31st) International Prize for Biology

Calling for Nominations

This year's research field:

Cell Biology

Please access at: <http://www.jsps.go.jp/english/e-biol>

Deadline: April 15, 2015

- The International Prize for Biology was established in 1985 to commemorate the 60-year reign of Emperor Showa and his longtime devotion to biological research.
- The Prize is awarded each year to an individual who has made an outstanding contribution to the advancement of basic research in a field of biology.
- The Prize shall consist of a medal and a prize of 10-million yen.

Recent Years Prize Winners



2014
Prof. Sir Peter Crane FRS
(Systematic Biology and
Taxonomy)



2013
Dr. Joseph Felsenstein
(Biology of Evolution)



2012
Dr. Joseph Altman
(Neurobiology)



UC San Diego

Assistant, Associate, Full Professor, Child Neurology (10-917)

(Ladder Rank, In Residence, Adjunct,
Clinical X, HS Clinical)

School of Medicine - Neurosciences

The Department of Neurosciences (<http://neurosciences.ucsd.edu/>) at the University of California San Diego is committed to academic excellence and diversity within the faculty, staff, and student body.

We seek an outstanding Developmental Neuroscientist for the neurology unit at UCSD/Rady Children's Hospital San Diego. The successful candidate will be a neurologist-neuroscientist who is Board Certified in Child Neurology. The successful candidate will have a distinguished research program and be clinically active. We expect to appoint an individual who is currently at the Assistant, Associate, or Professor level.

To view the full ad posting/application visit: apptkr.com/578125

AA-EOE: The University of California is an Equal Opportunity/Affirmative Action Employer. All qualified applicants will receive consideration for employment without regard to race, color, religion, sex, national origin, disability, age or protected veteran status.



生物膜与膜生物工程国家重点实验室
State Key Laboratory of Biomembrane & Membrane Biotechnology



The State Key Laboratory of Biomembrane and Membrane Biotechnology Recruitment of Outstanding Young professors (Beijing China)

The State Key Laboratory of Biomembrane and Membrane Biotechnology (LBM), at the Institute of Zoology (IOZ), Chinese Academy of Sciences (CAS), invites applications from qualified individuals for 3~5 faculty positions at the level of Full-time Professor.

Directions: Cell Biology, Developmental Biology, Genetics, Cancer Biology and related fields.

Requirement and treatment: Candidates should receive a doctor degree abroad with a research experience abroad over 3 years or a doctor in China with a research experience overseas over 5 years. All candidates should not be older than 40 years, and will serve as an independent group leader. Successful candidates will be recommended to apply for "National Thousand Young Talents Program" and will receive competitive start-up packages. In addition, there is a strong institutional commitment to core facilities, graduate programs, and an interdisciplinary environment.

Contacts: Applicants should submit your application materials in one package including (1) a cover letter, including your research achievements and future plan, (2) curriculum vitae, (3) reprints of major publications, (4) three letters of recommendation, solicited by the applicant. Please send application materials to **Ms. Fan Lihua** (1-5 Beichen West Road, Chaoyang District, Beijing 100101, P.R., China. Email: fanlh@ioz.ac.cn; Telephone/Fax: +86-10-64807313. Further information is available at <http://www.biomembrane.ioz.ac.cn>).

Review of applications will begin **Feb 15, 2015**, and will continue until the positions are filled.



Fundamental Immunology & Its Therapeutic Potential

April 14 - 18, 2015

Poster abstract deadline February 28



Organizers

James Allison, Eric Pamer, Fiona Powrie, Stephen Smale

Topics

- Fundamental Mechanisms of Immunity
- Cancer Immunotherapy
- Anti-Microbial Immunity
- Autoimmunity
- Inflammatory Disorders
- Transplant Immunology

Invited Speakers

Rafi Ahmed, David Artis, Rosa Bacchetta, Yasmine Belkaid, Lisa Coussens, Mark Davis, Joel Ernst, Richard Flavell, Thomas Gajewski, Philip Greenberg, Gillian Griffiths, Jose-Carlos Gutierrez-Ramos, Kenya Honda, Lora Hooper, Michael Karin, Bart Lambrecht, Antonio Lanzavecchia, Ming Li, Dan Littman, Michel Nussenzweig, Bali Pulendran, Nicholas Restifo, Alexander Rudensky, Michael Sadelain, Federica Sallusto, Robert Schreiber, Ton Schumacher, Padmanee Sharma, Jedd Wolchok, Kathryn Wood, Cassian Yee

Other CSHL Spring 2015 Meetings

RNA & Oligonucleotide Therapeutics April 8 - 11

The Ubiquitin Family April 21 - 25

Telomeres & Telomerase April 28 - May 2

Biology and Genomics of Social Insects May 2 - 5

The Biology of Genomes May 5 - 9

The Biology of Cancer: Microenvironment,

Metastasis & Therapeutics May 12 - 16

Retroviruses May 18 - 23

80th Symposium: 21st Century Genetics -

Genes At Work May 26 - 31

Cold Spring Harbor Laboratory - Meetings & Courses
www.cshl.edu/meetings

POSITIONS OPEN

UNIVERSITY OF SOUTH ALABAMA College of Medicine Department of Physiology and Cell Biology

The Department of Physiology and Cell Biology at the University of South Alabama College of Medicine is seeking to fill two research-intensive tenure-track **ASSISTANT/ASSOCIATE PROFESSOR** positions. Existing departmental research interests include cardiovascular, pulmonary, neural, and mitochondrial biology, biomedical imaging, mechanics, and modeling. Successful candidates will have research programs that complement these ongoing efforts, and will contribute to the college's graduate and medical education mission. We are seeking individuals who are highly engaged and collaborative, with exceptional written and oral communication skills. Competitive applicants must have a Ph.D. and/or M.D. degree, postdoctoral experience, and demonstrated success in securing extramural grant support. Review of applications will begin immediately and continue through the application deadline of April 1, 2015. Interested candidates must e-mail an application packet, including an introductory letter, complete curriculum vitae, summary of research and teaching interests (one-page limit), and contact information of three references to the Search Committee at e-mail: pcbsearch@southalabama.edu.

Equal Opportunity Employer—Minorities/Females/Veterans/Persons with Disabilities.

Your career is our cause.

Get help from the experts.

ScienceCareers.org

- Job Postings
- Job Alerts
- Resume/CV Database
- Career Advice
- Career Forum

ScienceCareers
FROM THE JOURNAL SCIENCE 

☒ More scientists agree—we are the most useful website.

ScienceCareers.org

Download your free copy today.

ScienceCareers.org/booklets



From technology specialists to patent attorneys to policy advisers, learn more about the types of careers that scientists can pursue and the skills needed in order to succeed in nonresearch careers.

ScienceCareers
FROM THE JOURNAL SCIENCE 



Learn more and avoid driving your job search around in circles.

- Search thousands of job postings
- Create job alerts based on your criteria
- Get career advice from our Career Forum experts
- Download career advice articles and webinars
- Complete an individual development plan at “myIDP”

Target your job search using relevant resources on **ScienceCareers.org**.

ScienceCareers

FROM THE JOURNAL SCIENCE  AAAS

By Eli Kintisch

The science of schmoozing

Watching Hugues Lantuit work the cocktail hour at Arctic Change, a Canadian research conference held in Ottawa in December, is a master class in networking. He's gracious. ("It is very nice to meet you," he tells a graduate student, shaking with two hands.) He's self-deprecating. ("I'm sure I have no shot at that job.") He's a little coarse. ("I tried for half an hour to tie this f***ing bow tie; can you help me?") He is constantly introducing one person to another. "Ah, you work at the Yukon Research Centre," he says to the stranger he's persuaded to tie his bow tie, as a crowd forms. "We are actually collaborating on a multimillion-dollar grant proposal. So if we get it, I will remember this moment as a formative step." Laughter all around.

In the burgeoning world of Arctic research, nearly everyone knows Lantuit, a professor at the Alfred Wegener Institute (AWI) in Potsdam, Germany. At age 37, he's leveraged his deep network of contacts to build an impressive career. In 2006, he co-founded the Association of Polar Early Career Scientists (APECS), which now has more than 5000 members. Five years later, he became co-principal investigator on a 5-year, €9 million project to study permafrost in the Arctic. He serves on major international research committees. The research program he manages, on Herschel Island in the Canadian Beaufort Sea, is at an important site for monitoring erosion of Arctic permafrost coasts, which make up a third of Earth's shores. "He's the man," says colleague Paul Overduin, a geoscientist at AWI. "He puts us on the map in a lot of ways."

As early as graduate school, Lantuit says, he was "genuinely interested in bringing people together." As a master's student at McGill University in 2002, he founded the Geography Graduate Society and became a key assistant on an international permafrost-mapping project. The experience taught him lessons about networking in science that have subsequently shaped his career.

First, he says, what matters isn't how impressive the title on a business card is—it's the role you play in projects or initiatives. Second, while wearing a welcoming face never hurts, it's what you offer scientifically that turns conversations into scientific opportunities.

Lantuit got connected early on, but he found few resources to help other young Arctic scientists do the same. So he and Jenny Baeseman, a microbial biologist, created APECS, which runs workshops that bring together young



"He's just someone who's constantly connecting his peers."

and established scientists to explore publishing, fieldwork, funding, and career advancement. His reputation as a connector grew as he matched colleagues with opportunities—including helping Baeseman, who was focused on Antarctica, join a project in the Arctic. "He's just someone who's constantly connecting his peers," Baeseman says.

They connect him in return: Lantuit's CV lists the myriad partnerships, international research projects, journal special issues, panels, and conferences he's created or run. All that connecting takes time away from research, he acknowledges. "There are scientists who will publish 50 papers in *Nature* in their career. I won't. I'm fine with that." Yet, none of this would be possible if he hadn't published well-regarded papers on erosion on Arctic coasts. "I

tell my [Ph.D.] students, you need to deliver scientifically," he says. Several of them wanted to attend the Ottawa meeting, but Lantuit said no. "Their dissertations are late."

Lantuit's appetite for new projects and partnerships remains voracious. Managing his various ongoing efforts taxes his phone's scheduling app, which lists a relentless string of meetings, dinners, sessions, and cocktail hours for the 5-day meeting. "I have this inner drive to connect," he says as he gets up to walk to the conference's gala dinner. He has assembled a colorful table of heavy hitters: influential scientists, well-known administrators, and funders. These are useful people to know, but it's clear he genuinely likes each one. "It's fun," he says, and heads for the ballroom. ■

Eli Kintisch is a contributing correspondent for Science. For more on life and careers, visit www.sciencemag.org. Send your story to SciCareerEditor@aaas.org.